Characterisation of the Human Two-Pore Channels



Timothy Michael Funnell

Department of Pharmacology

University of Oxford

A thesis submitted for the degree of

DPhil in Pharmacology

Trinity term 2011

Characterisation of the Human Two-Pore Channels

A thesis submitted for the degree of
DPhil in Pharmacology

Abstract

The Ca^{2+}-mobilising messenger NAADP has been shown to play a key role in the regulation of mammalian physiology. Recently, the two-pore channels (TPCs) have been proposed as an NAADP-gated Ca^{2+} channel.

Chapter 1 introduces the TPCs as the major candidates in governing NAADP-mediated Ca^{2+}-release from acidic stores. **Chapter 2** explains the methodologies developed and used.

Chapter 3 demonstrates the successful immunopurification of HsTPC2 and its incorporation into an artificial lipid bilayer. K^+ and Ca^{2+} currents were seen in response to nM - µM concentrations of NAADP; with the open probability (P_o) fitting a bell-shaped concentration-response curve. Ligand sensitivity was shown to be regulated by luminal $[Ca^{2+}]$, whereby a 20-fold increase in $[Ca^{2+}]_{lumen}$ (10 µM to 200 µM) caused a 100-fold reduction in the EC_{50} from $\approx$ 500 nM to 5 nM. Furthermore, a reduction in luminal pH from 7.2 to 4.8 reduced the P_o by 10-fold. Partial agonist properties were shown for Ned-19 (a structural analogue of NAADP) with nM concentrations increasing channel P_o but 1 µM Ned-19 inhibiting all channel activity.

Chapter 4 investigates the *in situ* properties of HsTPC2 by the purification and patch clamp of intact lysosomes from cells overexpressing HsTPC2. Three methods of purification were compared: differential centrifugation, whole lysosome immunoprecipitation and magnetic chromatography. Techniques involving lysosomal swelling and whole cell homogenisation were also optimised to ensure minimal contamination by non-lysosomal proteins. Whole lysosome patch clamping revealed NAADP-induced, Ca^{2+}-specific currents in response to NAADP, but not cADPR, IP_3 or Ned-19. High concentrations of NAADP (mM) and Ned-19 (µM) showed prolonged ($\approx$ 5 minutes) inhibition of channel activity.

Chapter 5 explores the protein-protein interactions of the purified HsTPC2 and identifies a heterodimeric interaction between HsTPC1 and HsTPC2 was further dissected by coimmunoprecipitation, colocalisation and FRET studies. Despite clear evidence that both isoforms independently form homodimers, it is likely that heterodimerisation is a dynamic interaction only seen in a subset of the channel population.

Chapter 6 discusses the results obtained in the wider context of cell physiology.

Timothy Funnell
New College

Trinity Term 2011

Publications

M Ruas, K Rietdorf, A Arredouani, L C Davis, E Lloyd- Evans, H Koegel, **T Funnell**, A J Morgan, J A Ward, K Watanabe, X Cheng, G C Churchill, M X Zhu, F M Platt, G M Wessel, J Parrington, and A Galione. *Purified TPC Isoforms Form NAADP Receptors with Distinct Roles for Ca2+ Signaling and Endolysosomal Trafficking.* Curr Biol, volume 20, issue 8, 703 - 709. Mar 2010.

S J Pitt*, **T Funnell***, M Sitsapesan, E Venturi, K Rietdorf, M Ruas, A Ganesan, R Gosain, G C Churchill, M X Zhu, J Parrington, A Galione, and R Sitsapesan. *TPC2 is a novel NAADP-sensitive Ca^{2+}-release channel, operating as a dual sensor of luminal pH and Ca^{2+}.* J Biol Chem, 285, 35039 - 35046. Aug 2010.

(∗ Joint first authors)

Presentations

Tim Funnell, Samantha Pitt, Margarida Ruas, Katja Rietdorf, Rebecca Sitsapesan, Antony Galione. *Purification of Human TPC2 and its incorporation into a planar lipid bilayer.*

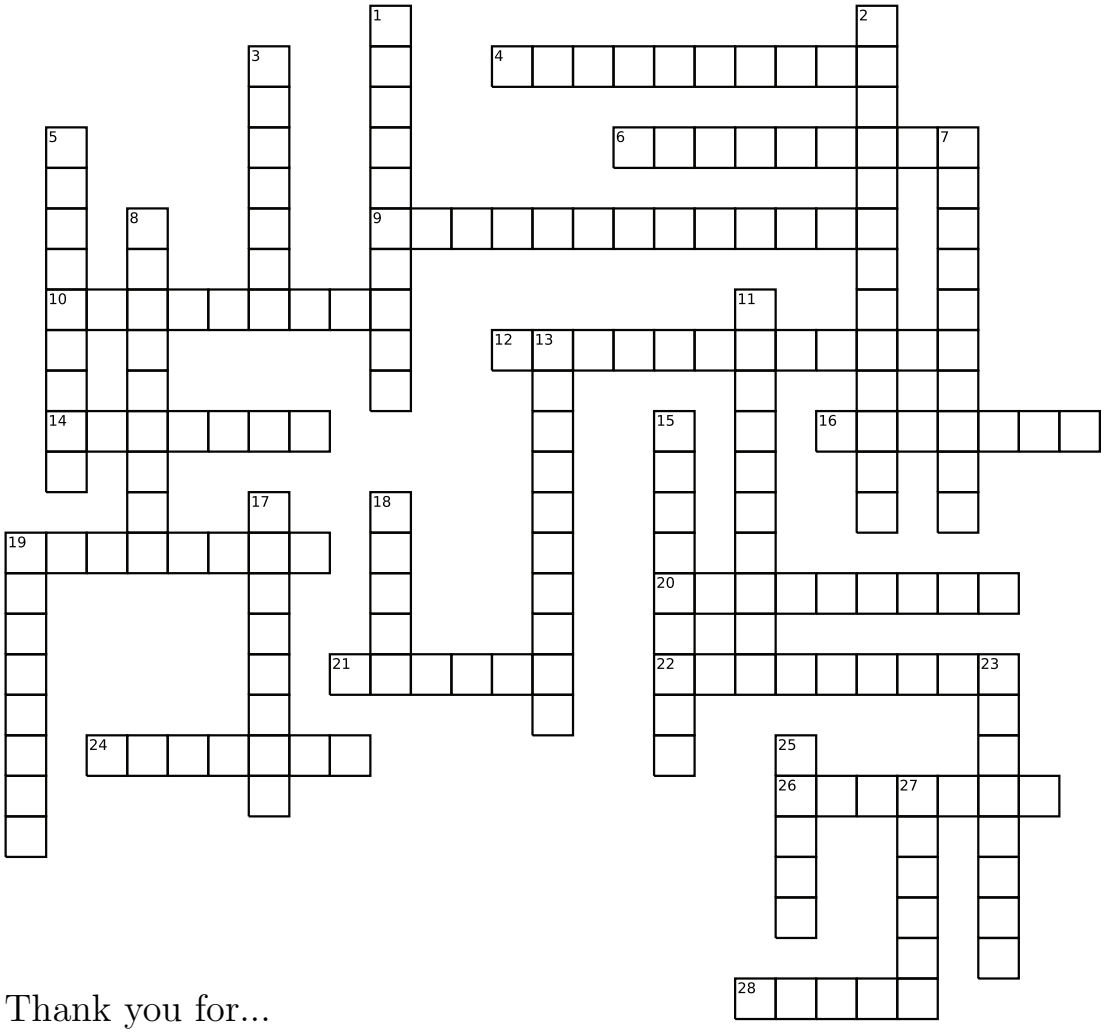
Abstract accepted for poster presentation

Gordon research conference - Calcium signalling
Lucca, Italy. June 2009

Awards

A. J. Clark Scholarship	2007 - 2010	British Pharmacological Society
Schatcher Award	Summer 2008	British Pharmacological Society

My deepest thanks to the individuals below:



Thank you for...

Across

4 Everything I know
6 Teaching me how to cheat
9 Powers of distraction
10 Americanisms
12 Trips to Bristol
14 My alter ego
16 Scholarly guidance and edification
19 Emphasising my faults
20 Constructive decimation
21 Leading me astray
22 Mass spectrometry assistance
24 Mirthful cynicism
26 His eponymous scholarship
28 Patience and tolerance

Down

1 A roof over my head and meals on the table
2 Unparalleled friendship
3 Electrophysiological knowhow
5 Pharmacological insights
7 Being better than me
8 Giving me the boot
11 Nothing
13 Being there to the end
15 Teaching me tolerance
17 German efficiency
18 Paving the way
19 Trust and understanding
23 A great two years
25 Prodigious kindness and excellent advice
27 Unwavering encouragement

Contents

List of Abbreviations **xvii**

1 Introduction **1**

1.1 Calcium - Ca^{2+} . . . 1

1.1.1 Ca^{2+} - the messenger . . . 1

1.1.2 Ca^{2+} efflux . . . 2

1.1.2.1 Ca^{2+} translocation across the plasma membrane . . . 2

1.1.2.2 Ca^{2+} translocation across intracellular membranes . . . 3

1.1.3 Ca^{2+} release . . . 4

1.1.3.1 Plasma membrane Ca^{2+} entry . . . 4

1.1.3.2 Ca^{2+} release from intracellular stores . . . 6

1.1.4 Ca^{2+} homeostasis . . . 6

1.1.5 Spatial and temporal attributes . . . 8

1.2 Intracellular second messengers . . . 10

1.3 IP_3-gated Ca^{2+} release . . . 10

1.3.1 The IP_3 receptor family . . . 11

1.3.2 IP_3R channel function . . . 11

1.3.3 IP_3R channel regulation . . . 12

1.4 cADPR-gated Ca^{2+} release . . . 12

1.4.1 RyR channel function . . . 12

1.4.2 RyR channel regulation . . . 13

1.5 NAADP-gated Ca^{2+} release . . . 14

1.5.1 Production of NAADP . . . 14

1.5.2 Breakdown of NAADP . . . 16

1.5.3 Endogenous NAADP . . . 16

1.5.4 Discovery of NAADP . . . 17
1.5.5 NAADP targeting to acidic stores . . . 18
1.5.6 NAADP receptor properties . . . 20
1.5.7 Self-desensitisation of NAADP . . . 22
1.5.8 The effect of cytoplasmic Ca^{2+} on NAADP binding. . . . 23
1.5.9 Antagonism of the NAADP response . . . 23
1.6 Summary of NAADP characteristics . . . 27
1.7 The NAADP receptor . . . 28
1.8 Candidate NAADP receptors . . . 30
1.8.1 TRPML1 . . . 30
1.8.2 TRPM2 . . . 31
1.8.3 P2X and P2Y receptors . . . 31
1.8.4 RyR . . . 32
1.8.5 The Two-Pore Channels (TPCs) . . . 34
1.9 The Two-Pore Channels . . . 35
1.9.1 Discovery . . . 35
1.9.2 Eligibility . . . 35
1.9.3 Structure . . . 37
1.9.4 Homology across species . . . 38
1.9.5 Plant TPC1 . . . 41
1.9.6 Sea urchin TPCs . . . 42
1.9.7 Human TPCs . . . 43
1.10 The TPCs as the NAADP receptor . . . 46
1.11 The aims of this thesis . . . 48

2 Materials and Methods **49**
2.1 Materials . . . 49
2.2 Bioinformatics . . . 49
2.2.1 Sequence alignments . . . 49
2.2.2 Phylogenetic analysis . . . 49
2.2.3 Protein sequence analysis . . . 50
2.2.4 Hydropathy plot . . . 50
2.3 Expression and extraction of HsTPC proteins . . . 50

2.3.1 Cell culture . . . 50
2.3.2 Stable HEK293 cell lines . . . 51
2.3.3 Long-term cell storage . . . 51
2.3.4 Membrane preparation . . . 51
2.3.5 Removal of sugar groups . . . 52
2.3.6 Solubilisation of the membranes . . . 52
2.4 Protein quantification . . . 52
2.4.1 Bicinchoninic acid assay . . . 52
2.4.2 EZQ protein quantification . . . 53
2.4.3 Spectrophotometer . . . 53
2.5 Protein electrophoresis and blotting . . . 54
2.5.1 SDS PAGE . . . 54
2.5.2 PFO PAGE . . . 54
2.5.3 Protein staining . . . 55
2.5.4 Western Blotting . . . 55
2.5.5 Stripping membranes . . . 56
2.6 Gel filtration . . . 56
2.7 Antibody generation and purification . . . 58
2.8 Immunoprecipitation . . . 58
2.8.1 Covalently coupling antibodies to beads . . . 58
2.8.2 Immunoprecipitation of TPC protein complex . . . 59
2.8.3 Dialysis . . . 59
2.9 Radioligand binding . . . 60
2.9.1 Saturation binding . . . 60
2.10 Incorporation of HsTPC2 into bilayers . . . 60
2.10.1 Forming the bilayer . . . 61
2.10.2 Channel incorporation . . . 61
2.10.3 Data acquisition and analysis . . . 61
2.11 Lysosomal swelling . . . 63
2.11.1 Confocal microscopy of swollen lysosomes . . . 63
2.12 Purification of lysosomes . . . 64
2.12.1 Differential centrifugation . . . 64
2.12.2 Lysosome immunoprecipitation . . . 64

2.12.3 Magnetic chromatography 65
2.12.4 Light microscopy of lysosomes 66
2.12.5 Homogenisation techniques 67
2.13 Organelle assays 68
2.13.1 Lysosomes - β-Galactosidase 68
2.13.2 Plasma membrane - alkaline phosphatase 68
2.13.3 Golgi - α-Mannosidase 69
2.13.4 ER - β-Glucuronidase 69
2.13.5 Mitochondria - PMS/MTS 70
2.14 Automated patch clamp studies 70
2.14.1 Flyion 70
2.14.2 Port-a-patch 71
2.15 Mass spectrometry 72
2.15.1 Tryptic digest 72
2.15.2 MALDI TOF MS 73
2.15.3 LCMS 73
2.15.4 Peptide comparison software 73
2.16 Cloning techniques 74
2.16.1 Subcloning 74
2.16.2 Primer design 74
2.16.3 Polymerase chain reaction for DNA amplification 75
2.16.4 Synthesis and annealing of oligonucleotide tags 75
2.16.5 Restriction digest 76
2.16.6 Agarose gel electrophoresis 76
2.16.7 Purification of DNA from agarose gel 76
2.16.8 Dephosphorylation of 5' phosphate group 77
2.16.9 Ligation 77
2.16.10 Preparation of chemically-competent bacteria 77
2.16.11 Transformation of bacteria by heat-shock 77
2.16.12 Homologous recombination 78
2.16.13 Small scale preparation of plasmid DNA (Minipreps) 78
2.16.14 Large scale preparation of plasmid DNA (Maxipreps) 79
2.16.15 DNA quantitation 79

2.16.16 DNA sequencing . . . 80
2.17 Adhering cells to cover slides . . . 80
2.18 Transient transfection . . . 80
2.18.1 Calcium phosphate . . . 80
2.18.2 jetPEI . . . 81
2.19 Localisation . . . 81
2.19.1 Immunofluorescent staining . . . 81
2.19.2 Image capture . . . 82
2.20 FRET . . . 82
2.20.1 Sensitised FRET . . . 82
2.20.2 FRET acceptor photobleach . . . 83
2.21 Statistical analysis . . . 83
2.22 List of Primers . . . 84

3 Results - Channel properties of purified TPC2 89
3.1 Summary . . . 89
3.2 Glycosylation of HsTPC proteins . . . 91
3.3 Solubilisation of HsTPC2 by the detergent CHAPS . . . 95
3.4 Gel filtration . . . 97
3.5 Immunoprecipitation of HsTPC2 via an HA-tag . . . 99
3.5.1 Optimising the HA immunoprecipitation . . . 103
3.5.2 Quantification of the purification from western blot analysis . . . 105
3.5.3 Radioligand binding to HA-immunopurified samples . . . 105
3.5.4 Incorporation of the HA-immunopurified protein into a lipid bilayer 110
3.6 Immunoprecipitation of HsTPC2 by polyclonal anti-TPC2 antibodies . . . 111
3.6.1 Radioligand binding to HsTPC2-immunopurified samples . . . 113
3.7 Incorporation of the TPC2-immunopurified protein into a lipid bilayer . . . 114
3.7.1 K^+ permeability of HsTPC2 and gating by NAADP . . . 114
3.7.2 Sub-conductance state . . . 115
3.7.3 Coupled gating . . . 115
3.7.4 K^+ conductance . . . 118
3.7.5 Ca^{2+} permeability . . . 118
3.7.6 NAADP concentration-response relationship . . . 120

3.7.7 Regulation by luminal [Ca^{2+}] . . . 122
3.7.8 Regulation by luminal pH . . . 125
3.7.9 Partial agonist properties of Ned-19 . . . 127
3.7.10 Synergy between NAADP and Ned-19 . . . 129
3.8 Discussion . . . 132
3.8.1 Immunoprecipitation as a purification technique . . . 132
3.8.2 Protein yield . . . 133
3.8.3 Monovalent cation conductance . . . 133
3.8.4 Ion selectivity . . . 135
3.8.5 Divalent cation conductance . . . 137
3.8.6 Coupled gating . . . 137
3.8.7 Voltage sensitivity . . . 138
3.8.8 NAADP sensitivity . . . 139
3.8.9 The effects of luminal pH . . . 140
3.8.10 The effects of luminal Ca^{2+} . . . 141
3.8.11 Gating by Ned-19 . . . 142
3.8.12 Channel modulation by accessory proteins . . . 142
3.9 Conclusions . . . 144
3.10 Future prospects . . . 144

4 Results - Patch clamp of purified lysosomes 149
4.1 Summary . . . 149
4.2 Lysosome purification by differential centrifugation . . . 151
4.2.1 Lysosome enrichment by differential centrifugation . . . 152
4.2.2 Contamination by ER . . . 157
4.2.3 Contamination by mitochondria . . . 158
4.2.4 Contamination by PM and Golgi . . . 160
4.2.5 The purity of the lysosome pellet . . . 161
4.3 Purification by immunoprecipitation . . . 163
4.3.1 Lysosomal enrichment by immunoprecipitation . . . 166
4.3.2 Contamination by ER and mitochondria . . . 167
4.4 Magnetic chromatography of iron-containing lysosomes . . . 168
4.4.1 Enrichment of lysosomes by magnetic chromatography . . . 168

4.4.2 Contamination by other organelles . . . 171
4.5 Lysosomal swelling as a cause of contamination . . . 174
4.6 Purification of sucrose-swollen lysosomes . . . 177
4.7 Optimisation of homogenisation . . . 179
4.7.1 Lysosome recovery by Balch homogenisation . . . 179
4.7.2 Organelle recovery by Balch homogenisation . . . 182
4.8 Magnetic chromatography of the Balch supernatant . . . 188
4.8.1 The purity of the lysosomal preparation . . . 192
4.9 Electrophysiological recordings by Flyion . . . 193
4.9.1 Flyion - non-swollen lysosomes . . . 193
4.9.2 Flyion - sucrose-swollen lysosomes . . . 195
4.10 Electrophysiological recordings by Port-a-patch . . . 199
4.10.1 Seal formation on Port-a-patch . . . 199
4.10.2 Recording conventions . . . 200
4.10.3 Ion composition of the luminal buffer . . . 202
4.11 NAADP-induced current in HsTPC2 overexpressing lysosomes . . . 203
4.12 Effects of IP_3 and cADPR on channel activity . . . 206
4.13 NAADP concentration response relationship . . . 207
4.14 1 mM NAADP channel block . . . 207
4.15 100 µM Ned-19 channel block . . . 210
4.16 Discussion . . . 212
4.16.1 The optimal lysosomal purification . . . 212
4.16.2 Patch clamp on subcellular organelles . . . 213
4.16.3 The physiological significance of lysosomal swelling . . . 216
4.16.4 Patch clamp devices and seal formation . . . 218
4.16.5 Lysosomal resting potential . . . 219
4.16.6 Ionic composition of the lysosomal lumen . . . 220
4.16.7 Whole lysosome conductance . . . 223
4.16.8 Channel density prediction . . . 223
4.16.9 Second messenger distinctions . . . 224
4.16.10 Response to NAADP . . . 225
4.16.11 Desensitisation by mM NAADP . . . 226
4.16.12 Antagonism by Ned-19 . . . 226

4.16.13 Channel conductance and ion selectivity . . . 227
4.16.14 Whole lysosome patch vs. lipid bilayer studies . . . 228
4.17 Conclusions . . . 231
4.18 Future prospects . . . 231

5 Results - Protein-protein interactions of HsTPCs 233
5.1 Summary . . . 233
5.2 Presence of other putative NAADP receptors . . . 234
5.3 Mass spectrometry analysis of immunoprecipitated complexes . . . 236
5.3.1 Coimmunoprecipitated proteins in the anti-HA preparation . . . 236
5.3.2 Coimmunoprecipitated proteins in the anti-HsTPC2 preparation 241
5.4 Coimmunoprecipitation of HsTPCs . . . 245
5.4.1 Endogenous HsTPC1 coimmunoprecipitation with HA.HsTPC2 . 245
5.4.2 HA.HsTPC2 coimmunoprecipitation with endogenous HsTPC1 . 245
5.4.3 HsTPC1.His coimmunoprecipitation with endogenous HsTPC2 . 248
5.4.4 Endogenous HsTPC2 coimmunoprecipitation with HsTPC1.His . 248
5.4.5 Antibody limitations . . . 250
5.5 HsTPC constructs created for further analysis . . . 252
5.6 Validating serum specificity . . . 253
5.6.1 Dimerisation of cotransfected constructs. . . . 255
5.7 Dissecting the HsTPC western blot . . . 259
5.8 Subcellular localisation of HsTPCs . . . 262
5.9 Colocalisation of HsTPCs . . . 266
5.10 FRET . . . 268
5.10.1 The orientation of dimerisation . . . 269
5.10.2 Localisation of CFP and YFP constructs . . . 270
5.10.3 Sensitised FRET . . . 270
5.10.4 HsTPC homodimers . . . 276
5.10.5 HsTPC heterodimers . . . 277
5.10.6 Potential pitfalls . . . 278
5.11 Acceptor photobleaching FRET . . . 279
5.11.1 CFP photobleaching . . . 279
5.11.2 HsTPC dimers . . . 281

5.11.3 Controls and concerns . . . 283
5.12 Discussion . . . 285
5.12.1 Homodimerisation . . . 285
5.12.2 Heterodimerisation . . . 286
5.12.3 Orientation of interaction . . . 287
5.12.4 HsTPC-HsTPC interaction . . . 288
5.12.5 Dynamic assembly . . . 289
5.12.6 Biological relevance of heterodimers . . . 289
5.12.7 Other interactions . . . 290
5.13 Conclusions . . . 292
5.14 Future prospects . . . 292

6 Discussion **295**
6.1 HsTPCs as NAADP-gated Ca^{2+} channels . . . 295
6.2 Interaction with other Ca^{2+}-signalling pathways . . . 297
6.3 HsTPCs and the ER . . . 298
6.3.1 HsTPC2-mediated trigger . . . 298
6.3.2 HsTPC1-mediated trigger . . . 300
6.3.3 Trigger zones . . . 301
6.4 HsTPCs and the plasma membrane . . . 302
6.5 HsTPCs in lysosomal function . . . 303
6.5.1 HsTPCs in autophagy . . . 304
6.6 HsTPCs in endosomal function . . . 305
6.7 HsTPCs in lysosome-related organelles . . . 306
6.8 HsTPCs in disease . . . 306
6.9 Final conclusions . . . 308

Appendices **311**

A Supplementary figures **311**

B Methods tables **315**

C Calculations **319**

References **327**

List of Abbreviations

4MU	4-methylumbelliferone
ADP	Adenosine diphosphate
AM	Acetoxymethyl ester
ARC	ADP-ribosyl cyclase
BAPTA	1,2-bis(o-aminophenoxy)ethane-N,-N,N',N'-tetraacetic acid
BCA	Bicinchoninic acid
bp	Base pairs
BSA	Bovine serum albumin
cADPR	Cyclic ADP ribose
CatSper	Cation channel of Sperm
CCK	Cholecystokinin
CFP	Cyan fluorescent protein
CHAPS	3-[(3-Cholamidopropyl)dimethyl-ammonio]-1-propanesulfonate
CHO	Chinese hamster ovary cell line
CICR	Calcium-induced calcium release
CNG	Cyclic nucleotide gated
d.p.m.	Disintegrations per minute
DAG	Diacylglycerol
DMEM	Dulbeccos modified Eagle medium
DMSO	Dimethyl sulfoxide
DMT	Dimethyl pimelimidate
dNTP	Deoxyribonucleotide triphosphate
DTT	Dithiothreitol
EC_{50}	Half maximal effective concentration
ECL	Enhanced chemiluminescence
EDTA	Ethylene diamine-tetraacetic acid
EEA1	Early endosome antigen 1
EGTA	Ethylene glycol-bis (2-amino-ethylether)-N,N,N',N'-tetraaceticacid
ER	Endoplasmic reticulum
ExPASY	Expert protein analysis system
FBS	Foetal bovine serum
FCCP	Carbonyl cyanide-p-trifluoro-methoxyphenylhydrazone
FKBP	FK506 binding protein
FPLC	Fast protein liquid chromatography
FRET	Fluorescence resonance energy transfer
GPCR	G protein-coupled receptor
GPN	Glycylphenylalanine 2-naphthylamide
HA	Hemagglutinin
HEK	Human embryonic kidney cell line
HNR	Heterogenous nuclear ribonucle-arprotein
HPLC	High performance liquid chroma-tography
HRP	Horseradish peroxidase
Hs	*Homo sapiens* - Human
IC_{50}	Half maximal inhibitory concentra-tion
IgG	Immunoglobulin G
IMAGE	Integrated molecular analysis of genomes and their expression
IP	Immunoprecipitation

IP_3R	IP_3 Receptor
IP_3	Inositol 1,4,5-trisphosphate
IRBIT	IP_3R binding protein
IRS	Insulin receptor substrate
IV	Current-voltage
kDa	Kilo Daltons
KDEL	lys-asp-glu-leu - ER marker
KLH	Keyhole limpet haemocyanin
LAMP	Lysosomal-associated membrane protein
LB	Luria broth
LCMS	Liquid chromatography mass spectrometry
LSD	Lysosomal storage disorder
M_w	Molecular weight
MALDI	Matrix-assisted laser desorption ionization
ML	Mucolipin
Mm	*Mus musculus* - mouse
MTS	(3-(4,5-dimethylthiazol-2-yl)-5-(3-carboxymethoxyphenyl)-2-(4-sulfophenyl)-2H-tetrazolium
NAADP	Nicotinic acid adenine dinucleotide phosphate
NADP	Nicotinamide adenine dinucleotide phosphate
NCX	Na^+/Ca^{2+} exchanger
NPC1	Niemann-Pick disease, type C1
OAc	Acetate anion (CH_3COO^-)
P_o	Channel open probability
PAGE	Polyacrylamide gel electrophoresis
PBS	Phosphate-buffered saline
PBST	PBS, 0.5 % (v/v) Tween-20
PCR	Polymerase chain reaction
PFA	Paraformaldehyde
PFO	Perfluoro-octanoic acid
pI	Iso-electric point
PIP_2	Phosphotidylinositol 4,5,bisphosphate
PLC	Phospholipase C
PM	Plasma membrane
PMCA	Plasma membrane Ca^{2+} ATPase
PMS	Phenazine methosulfate
PNGaseF	Peptide N-glycosidase F
PPADS	Pyridoxal-phosphate-6-azophenyl-2',4'-disulfonate
PVDF	Polyvinylidene fluoride
RT-PCR	Reverse transcription PCR
RyR	Ryanodine Receptor
S.D	Standard deviation
S.E.M	Standard error of the mean
SDS	Sodium dodecyl sulphate
SERCA	Endo(sarco)plasmic reticulum calcium ATPase
shRNA	Short hairpin RNA
SOC	Store operated channel
Sp	*Strongylocentrotus purpuratus* - sea urchin
SPCA	Secretory pathway Ca^{2+} ATPase
STIM	Stromal interaction molecule
SV	Slow vacuolar (current)
T_m	Primer melting temperature
TAE	Tris-acetate, EDTA buffer
TEMED	Tetramethylethylenediamine
TfR	Transferrin receptor
TM	Transmembrane
TOF	Time of flight

TPC Two-pore channel

TRP Transient receptor potential

UV Ultra violet

VGCC Voltage-gated calcium channels

YFP Yellow fluorescent protein

YVC Yeast vacuolar channel

Chapter 1

Introduction

1.1 Calcium - Ca^{2+}

Calcium is the most abundant metal in the human body. However, it is very unevenly distributed, with 99.9 % being locked up as mineral salts of calcium phosphate and sulphate which act as the structural support in bone and calcified cartilage (59). These calcium salts are poorly soluble so much of this calcium is biologically unavailable. Even so, the tiny amounts ($<$ 10 g) of soluble Ca^{2+} ions that do escape play a vital role in the majority of physiological processes (62).

1.1.1 Ca^{2+} - the messenger

Free calcium ions can be extremely toxic as Ca^{2+} has a high affinity for phosphate and carbonate ions and can cause these vital salts to precipitate out of solution. Prolonged levels of high Ca^{2+} also activate Ca^{2+}-dependent proteases and nucleases which result in cell death. Thus eukaryotic cells have evolved a variety of techniques to maintain a very low cytoplasmic Ca^{2+} concentration.

In a resting cell the intracellular concentration of Ca^{2+} is maintained at between 20-100 nM by a variety of ATP-dependent Ca^{2+} pumps and ion exchangers which transport Ca^{2+} across the plasma membrane or into intracellular stores, such as the endoplasmic reticulum (ER). This results in a concentration gradient as levels in these stores or the extracellular space can reach 2 mM (30). These values are only approximate predictions as Ca^{2+} ions are also buffered by Ca^{2+} binding proteins such as calretinin, calbindin and calsequestrin (82).

Most intracellular signalling messengers are small molecules or steroids, which can be synthesised and degraded by enzymes. Ca^{2+} ions, however, cannot be created or destroyed, so their regulation relies fully on transport or buffering mechanisms.

1.1.2 Ca^{2+} efflux

To rid the cytoplasm of Ca^{2+} ions the cell must translocate Ca^{2+} ions across a phospholipid membrane, where the high charge density of Ca^{2+} prevents significant re-entry by diffusion through the hydrophobic bilayer. However, this translocation against the electrochemical gradient requires an energy input, either from ATP or by coupling Ca^{2+} transport to an energetically favourable ion exchange down the electrochemical gradient, usually Na^+ ions or H^+ ions. The activity of these Ca^{2+} efflux mechanisms is tightly controlled and whilst some are constitutively active, others can respond to high levels of Ca^{2+} and have a high capacity to reduce the cytoplasmic concentration rapidly (30).

1.1.2.1 Ca^{2+} translocation across the plasma membrane

The plasma membrane Ca^{2+} ATPase (PMCA) is present in almost every cell type (411). It is crucial in maintaining the resting Ca^{2+} at very low concentrations and although PMCA has quite a low capacity for Ca^{2+} translocation, the high affinity for Ca^{2+} ions (K_m of 100 - 200 nM) allows efficient efflux in a resting cell. PMCA is a member of the P-type ATPases and forms an energetically unstable intermediate upon phosphorylation by ATP, as this reverts back to a stable state once Ca^{2+} is translocated, giving a stoichiometry of one Ca^{2+} ion per molecule of ATP (58). PMCA is constitutively active but during periods of elevated $[Ca^{2+}]$, the rate of translocation is increased 10-fold and also the affinity of the PMCA for Ca^{2+} is enhanced, these changes are in response to calmodulin regulation of PMCA (61, 461).

Despite this ability to up-regulate Ca^{2+} translocation, the PMCA still remains relatively ineffective when there is a large influx of Ca^{2+} ions. Thus to complement the PMCA the plasma membrane hosts a low affinity, high capacity Na^+/Ca^{2+} exchanger (NCX). This antiporter protein couples the flow of Na^+ ions down their electrochemical gradient to the efflux of Ca^{2+}. NCX is electrogenic as it requires the translocation of three Na^+ ions into the cell to transport one Ca^{2+} ion out (463). Although this is very energetically expensive, the low affinity of the NCX dictates that it is only effective

when the cytoplasmic concentration of Ca^{2+} is high (> 1 µM). When active, the NCX can transport up to five thousand Ca^{2+} ions per second (62). This high capacity means that Ca^{2+} is removed from the cytoplasm quickly which prevents excitotoxic levels of Ca^{2+} accumulating during stimulus.

1.1.2.2 Ca^{2+} translocation across intracellular membranes

As Ca^{2+} is highly buffered within the cytoplasm, diffusion rates are slow and the ions often remain localised, thus not all Ca^{2+} ions are accessible to the transporters localised to the plasma membrane. Hence cells express an array of transporters which remove Ca^{2+} ions by sequestering them into membrane bound organelles. Of all the organelles the endoplasmic/sarcoplasmic reticulum (ER/SR) has the largest capacity for Ca^{2+} storage but the mitochondria also play a role, as do acidic organelles, the nuclear envelope and the Golgi apparatus (31).

Homologous to the PMCA is the sarco/endoplasmic reticulum Ca^{2+} ATPase (SERCA) which acts with a high affinity yet low capacity to actively transport Ca^{2+} into the lumen of the SR/ER (428). To increase the storage capability of the lumen, Ca^{2+}-buffering proteins such as calsequestrin effectively remove the ions from solution, this assists SERCA by reducing the concentration gradient against which it is pumping.

The mitochondria play a more ephemeral role in Ca^{2+} sequestration, acting more like cytoplasmic Ca^{2+} buffers rather than permanent stores. A Ca^{2+} uniporter on the inner-mitochondrial membrane responds to high Ca^{2+} concentration in the cytoplasm, Ca^{2+}-uptake is driven by the mitochondrial membrane potential and the uniporter has a vast capacity for Ca^{2+} transport into the matrix (220). However, the mitochondria have a constitutively active Na^+/Ca^{2+} antiporter which facilitates Ca^{2+} release from the matrix coupled to the inward movement of two Na^+ ions. Equilibrium is achieved at $\approx$ 100 nM Ca^{2+}, which allows a net uptake when cytoplasmic Ca^{2+} levels are high effectively buffering the Ca^{2+} ions and releasing them slowly again when the cell returns to a resting state (293).

As with the efflux pathways in the plasma membrane, the intracellular sequestration of Ca^{2+} facilitates both the efficient, high-affinity, low capacity removal of Ca^{2+} from the cytoplasm when the cell is resting together with a rapid, high-capacity, low-affinity removal when levels are elevated on stimulation.

Relative newcomers to the field of intracellular Ca^{2+} storage are the acidic organelles which constitute the endo-lysosomal pathway. These are ubiquitous organelles, responsible for the degradation and recycling of defunct cellular constituents. Lysosomes in particular have been suggested as Ca^{2+} stores because their rupture by the lysomotropic agent glycyl-L-phenylalanine 2-naphthylamide (GPN) causes an increase in cytoplasmic Ca^{2+} (171). As endosomes mature into lysosomes the pH within the organelle drops; this is achieved by the activity of a V-type ATPase which couples the transport of protons to the hydrolysis of ATP (60). Blockade of this pump causes a depletion of Ca^{2+} within these stores, suggesting the presence of an H^+/Ca^{2+} antiporter which utilises the H^+ gradient to sequester Ca^{2+} from the cytoplasm (80). It is also thought that the lysosomal membrane contains Ca^{2+}-ATPases homologous to SERCA (76, 257, 407).

Other intracellular stores can influence the cellular homeostasis of Ca^{2+} ions, for example the Golgi complex seems to have a luminal Ca^{2+} concentration similar to those of the ER/SR (345). This Golgi Ca^{2+} may be sequestered by the secretory pathway Ca^{2+}-ATPase (SPCA) pumping Ca^{2+} into the Golgi lumen (294). The nuclear envelope has also been shown to efflux Ca^{2+} in response to intracellular stimuli (344), probably via IP_3R and RyR due to a high interconnectivity with the ER/SR (111).

1.1.3 Ca^{2+} release

The large Ca^{2+} concentration gradient formed by the cell to prevent Ca^{2+} toxicity has evolved and been harnessed into a sophisticated signalling mechanism, whereby a range of stimuli act upon an array of Ca^{2+} channels to allow an influx of Ca^{2+} down its electrochemical gradient, from intracellular stores or from the extracellular millieu back into the cytoplasm. This constitutes a Ca^{2+} signal and depending on the cell type and stimulus this results in reactions ranging from muscle contraction and neurone excitation to regulation of gene expression and neurotransmitter release (31).

1.1.3.1 Plasma membrane Ca^{2+} entry

At the level of the plasma membrane the fastest influx of Ca^{2+} ions is mediated by the voltage-gated channels (VGCCs - subtypes L, T, N, P, Q and R) which are activated by depolarised transmembrane potentials (30). Despite large functional differences between the subtypes, the VGCCs have a homologous structure of 24 putative transmembrane (TM) segments which is schematically depicted in figure 1.1. Based on homology

with the voltage-gated K^+ channels, it is thought that there are 4 repeating domains of 6-TM segments, with a voltage-sensing region on S4, composed of a repeating arginine residue on the alpha helices. Using the established structure of KcsA as a framework, the pore is predicted to be formed by a re-entry loop between S5-S6 on each domain (63, 64).

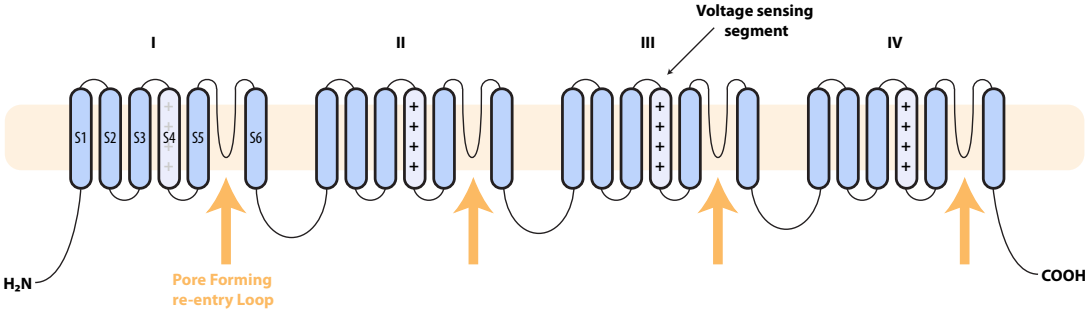


Figure 1.1: The common structure of VGCC. Comprised of 24-TM domains, in four homologous domains, each with a voltage sensing S4 segment and re-entry loop thought to form the pore between S5-S6.

Also present in the plasma membrane are ligand-gated Ca^{2+} channels (LGCCs). LGCCs respond to various hormones, growth factors and neurotransmitters. As the ligand binds the channel, this subsequently induces a conformational change to open the channel pore and allow Ca^{2+} ions to flow into cytoplasm. This process means that the LGCCs have a much slower onset than the voltage-gated channels.

Some members of the transient receptor potential (TRP) family are present in the plasma membrane and contribute to Ca^{2+} entry. The TRPs are a diverse family of receptors activated by a huge repertoire of external stimuli ranging from light, pH, mechanical stress and heat (83). There are more than 30 channels within the TRP family, which are classified into eight main subfamilies based on their homology. The TRP channels each contain 6 putative transmembrane domains, which tetramerise to form the familiar 24-TM channel as represented by the VGCC structure in figure 1.1. Most TRPs show Ca^{2+} permeability but many are not overly selective and allow other cations through the pore.

The plasma membrane also hosts the store-operated Ca^{2+} channels (SOC) which open in response to depleted levels of Ca^{2+} in the ER. Members of the TRP family were

implicated as providing this channel activity, but recently a sophisticated interaction between two proteins STIM1, on the ER membrane and Orai1 on the plasma membrane explains this form of influx (419).

1.1.3.2 Ca^{2+} release from intracellular stores

In contrast to the LGCCs, activation of plasma membrane G protein-coupled receptors (GPCRs) by extracellular ligands results in a Ca^{2+} signal not by influx across the plasma membrane, but by Ca^{2+} release from intracellular stores via second messenger pathways.

Ca^{2+} signals can originate from, or be augmented by, these Ca^{2+} reserves stored within intracellular organelles of which the ER is the largest, most active and best characterised.

Two major players have been identified as the Ca^{2+} release channels in the ER: the inositol-1,4,5-trisphosphate (IP_3) receptors (isoforms IP_3R1-3) (126) and the ryanodine receptors (isoforms RyR1-3) (405). Both of these channels are gated by endogenous messengers IP_3 and cADPR respectively. These channels also demonstrate the phenomenon that an increase in cytoplasmic [Ca^{2+}] can induce further Ca^{2+} release via these channels. This feed-forward process allows the propagation of local Ca^{2+} signals (Ca^{2+} sparks) to form global Ca^{2+} changes (Ca^{2+} waves).

The Golgi apparatus and the nuclear envelope have both been shown to respond to IP_3 and result in Ca^{2+} release (345, 476).

A final aspect of cellular Ca^{2+} release, which is still yet to be fully understood, is that which originates from the lysosome-related acidic stores in response to the novel second messenger Nicotinic Acid Adenine Dinucleotide Phosphate (NAADP).

1.1.4 Ca^{2+} homeostasis

A summary of the various Ca^{2+} efflux and influx pathways is shown in figure 1.2. The significance of each pathway varies between cell types with muscle cells relying on VGCCs and SR Ca^{2+} release to cause muscle contraction, whereas neurones respond to a host of Ca^{2+}-activating ligands at the synapse and secretory cells, like the pancreatic acinar cell, have developed finely-tuned differential Ca^{2+} release from intracellular organelles in response to certain extracellular ligands.

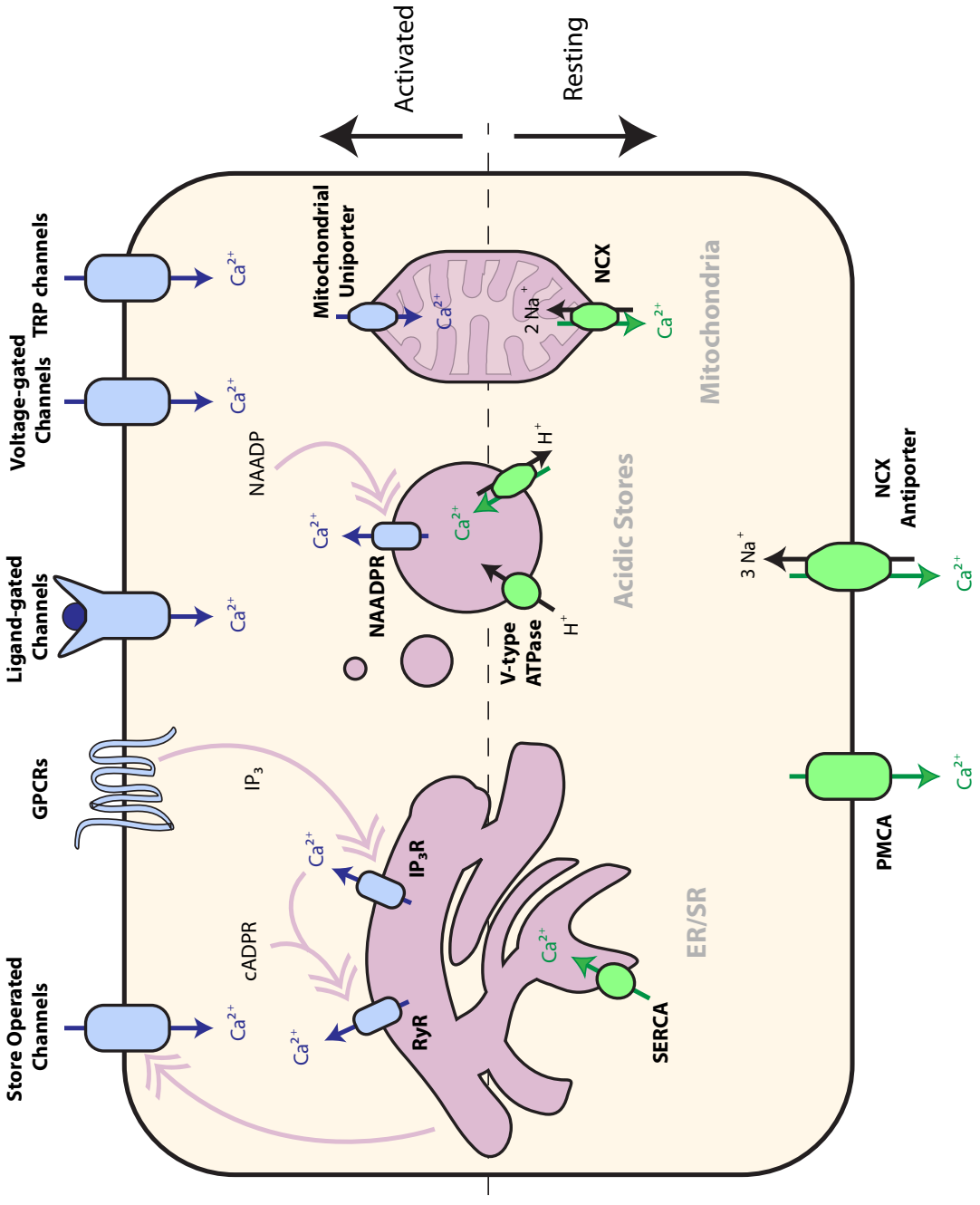


Figure 1.2: Schematic diagram of Ca^{2+} homeostasis. Simplified compilation of the various mechanisms involved in the influx/release (blue arrows) and subsequent removal (green arrows) of Ca^{2+} ions to and from the cytoplasm.

1.1.5 Spatial and temporal attributes

It is difficult to see how a simple change in Ca^{2+} concentration can play host to such a wide range of cellular responses, from the concerted contraction of muscle cells to the highly precise up-regulation of gene expression. The specificity of these responses is achieved by varying the localisation and the timing of the Ca^{2+} signals.

There are many levels at which a Ca^{2+} signal can be generated. A weak stimulus can result in a single channel responding, but these elementary events: Ca^{2+} blips (IP_3Rs) (329) or quarks (RyRs) (253) rarely result in a cellular response. With a slightly stronger stimulus, Ca^{2+} puffs from multiple IP_3Rs (328) or sparks from many RyRs can raise cytoplasmic Ca^{2+} levels in a limited spatial region (2 - 6 µm)(70). Due to the phenomenon of calcium-induced calcium release (CICR) whereby Ca^{2+} can diffuse and activate neighbouring channels, these Ca^{2+} puffs/sparks can propagate and form global intracellular Ca^{2+} waves (328). These waves can spread even further if cells are connected via gap junctions then a signal can stimulate neighbouring cells to result in an intercellular Ca^{2+} wave (79, 234, 367, 477). Figure 1.3 depicts this channel interplay.

The duration of the Ca^{2+} response also determines the response it elicits. Local transients can generate fast events such as exocytosis, synaptic transmission or cardiac contraction, in the timescale of micro to milliseconds (30). Longer transients lasting from seconds to minutes can mediate the up-regulation of receptors or enzymes and elicit metabolic responses, whereas prolonged stimulation results in oscillating Ca^{2+} release and removal which can be modulated by frequency and amplitude. Oscillations can last from minutes to hours, with both frequency and amplitude affecting the responses to these signals (31).

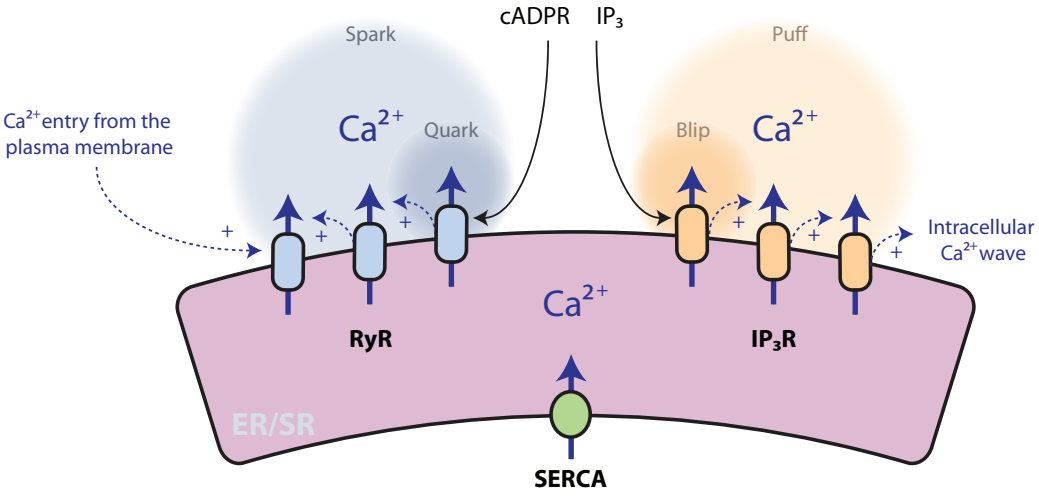


Figure 1.3: Ca^{2+} signals from the ER. IP_3R and RyR channels positioned on the ER membrane respond to their cognate ligand: IP_3 and cADPR respectively. Ca^{2+} ions further activate channels in Ca^{2+} induced Ca^{2+} release (CICR) which can propagate and augment the initial signal.

1.2 Intracellular second messengers

As briefly mentioned, extracellular ligands can stimulate Ca^{2+} release from intracellular stores via second messenger pathways. It is worth introducing the characteristic properties of the two most established second messengers, IP_3 and cADPR and their cognate receptors before introducing the less characterised NAADP-gated Ca^{2+} release and the putative NAADP receptor which will be the focus of this thesis. Although these three pathways produce disparate responses, parallels can be drawn in their underlying mechanisms.

1.3 IP_3-gated Ca^{2+} release

In order for an extracellular stimulus to transduce a signal via Ca^{2+} release, it must promote the synthesis of an intracellular second messenger, the synthesis of which and subsequent binding to its respective receptor results in Ca^{2+} release from intracellular stores.

The first Ca^{2+}-mobilising second messenger to be discovered was inositol-1,4,5-trisphosphate (IP_3) - this molecule is the archetypal second messenger with tightly regulated synthesis and degradation together with a high affinity and efficacy for its target channel, the IP_3R.

IP_3 is generated by the receptor-mediated activation of a membrane-bound Phospholipase C (PLC; $\beta, \gamma, \delta, \epsilon$, η and ζ), each isoform is coupled to a specific receptor pathway: PLCβ is activated by the conformational change within GPCRs ($G_{q/11}$); PLCγ responds to receptor tyrosine kinases; PLCδ responds to elevated cystosolic Ca^{2+} concentrations; PLCϵ is coupled to Ras/Rho GTPase activation; PLCη is a neurone-specific isoform that may be important in neuronal networking (193); and finally PLCζ is activated upon sperm contact with the egg (30). Activated PLC catalyses the hydrolysis of phophatidylinositol-4,5-bisphosphate (PIP_2) into the water soluble IP_3 and the membrane-bound diacylglycerol (DAG). Most PLC isoforms are localised on the cytoplasmic face of the plasma membrane, however activity has been seen in subcellular regions including the cytoplasm, nucleus and the ER (32, 89, 446).

IP_3 binding to its cognate receptor releases Ca^{2+} from the ER where the IP_3R is most abundantly expressed, however IP_3-induced Ca^{2+} release has also been seen from the Golgi apparatus and the nucleus (345, 476). There is also some evidence that IP_3

can induce Ca^{2+}entry across the plasma membrane, this may be due to direct activation of IP_3R in the plasma membrane (104, 105) or indirectly by a close coupling to the intrinsic plasma membrane Ca^{2+} channels such as TRP3 (222).

1.3.1 The IP_3 receptor family

IP_3 binds to a large tetrameric receptor complex ($\approx$ 1 MDa) composed of homo- or heteromers of three isoforms of the IP_3 receptor (IP_3R 1, 2 & 3). Most cells express at least two isoforms at significant levels but IP_3R1 is especially prevalent in the brain (312, 420).

Variation in the expression levels of each isoform affects the sensitivity of the IP_3 response as the three subtypes have different affinities for IP_3 with IP_3R2 being the highest (14 nM) > IP_3R1 (50 nM) > IP_3R3 (160 nM) (200, 420).

The isoforms also vary in the extent of their post-translational modifications (*e.g.* glycosylation or phosphorylation) and subcellular localisation. Accessory proteins such as Ca^{2+}/CaM-dependent kinase and protein kinase C also regulate the IP_3R channel function (82), together with adaptor proteins such as IRBIT (8) and RACK1 (334) which further modulate ligand sensitivity. These variations allow a versatility in the generation of IP_3-induced Ca^{2+} signals, which can be tuned to produce a specific cellular response (420).

1.3.2 IP_3R channel function

The flow of Ca^{2+} through the IP_3Rs depends on the channel Ca^{2+} conductance and the amount of time the channel remains open. To determine these properties electrophysiological studies have investigated the detailed permeability and gating properties of the IP_3Rs.

The first demonstration of IP_3-gated Ca^{2+} release used tracer Ca^{2+} flux through IP_3R from cerebellar membranes, reconstituted into liposomes (125). Subsequent studies examined purified channels reconstituted into planar lipid bilayers (38, 267) or direct patch clamp on isolated nuclear membranes (268, 269) (which are highly contiguous with the ER (111)). From these studies IP_3Rs were shown to be permeable to monovalent cations (Cs^+/K^+) with a large slope conductance (320 - 500 pS) (129). However, the permeability ratios with various different ions showed a preference for divalent cations and especially Ca^{2+} with a $P_{Ca}/P_K \approx 5$ - 10, suggesting that Ca^{2+} ions enter

the pore more readily than K^+ ions (129). These techniques also allowed investigation into the gating properties of the IP_3Rs and their regulation by cytoplasmic Ca^{2+} ions.

1.3.3 IP_3R channel regulation

The binding of IP_3 alone is not sufficient to stimulate channel opening, there is a requisite cytoplasmic Ca^{2+} concentration range between which the IP_3 receptor shows a bell shape activation curve (38). This is because Ca^{2+} ions can be both stimulatory and inhibitory, the extent of this effect varies between the IP_3R isoforms. In general, low concentrations of Ca^{2+} (100 - 300 nM) are stimulatory, but above 300 nM Ca^{2+} becomes inhibitory. Two Ca^{2+} binding sites, stimulatory and inhibitory, have been proposed to account for this regulation. Binding of IP_3 is thought to mask the inhibitory site and allow Ca^{2+} to bind to the stimulatory site which thus increases the channel open probability. For this reason IP_3 is considered a secondary activator (38, 127, 208).

1.4 cADPR-gated Ca^{2+} release

Another key second messenger involved in Ca^{2+} release from the ER is the NAD^+ metabolite, cyclic ADP-ribose (cADPR). This was shown to cause Ca^{2+} release in an IP_3 independent manner which was blocked by the known RyR antagonists: ruthenium red and high concentrations of ryanodine (136, 161) which suggests that it is acting on the RyRs. No direct evidence demonstrating an interaction between the cADPR and the channel has been shown, and most of the evidence suggest that it acts via an accessory protein (242, 398). Initial studies with radio-labelled [^{32}P]-cADPR in sea urchin egg homogenates showed cADPR binding to intermediate proteins, distinct from RyR (444). These intermediates have since been identified as the FK506-binding proteins (FKBP 12/12.6) which can bind to the RyRs to regulate Ca^{2+} release (91, 315, 424).

1.4.1 RyR channel function

As with the IP_3R, the first studies in RyR permeability were conducted using radioactively labelled ions to detect flux through SR-derived vesicles (286). Incorporation of cardiac (374) and skeletal (400) muscle SR vesicles incorporated into a planar lipid bilayer allowed precise measurements of ion flow. However, due to the presence of SR

K^+ and Cl^- channels which co-incorporate in these preparations, more reliable data were obtained from CHAPS-purified skeletal muscle RyR (228, 229).

Similar to the IP_3Rs, these channels are cation-specific and showed large conductances with monovalent (Na^+: 600 pS, K^+: 750 pS (287)) and divalent cations (Ca^{2+}: 100-150 pS) with a selective permeability to Ca^{2+} ($P_{Ca}/P_K \approx 6$) (228, 229, 400). These permeability properties are conserved across the RyR isoforms from many species, suggesting a highly conserved pore forming region (287).

1.4.2 RyR channel regulation

The ryanodine receptor derives its name from the plant alkaloid ryanodine, which was shown to specifically bind to and antagonise an ER/SR-derived Ca^{2+} channel (204). There are three isoforms of ryanodine receptor (RyR: 1, 2 & 3), the predominant form is the skeletal RyR1, whilst RyR2 is localised mainly to the heart and RyR3 has low levels of ubiquitous expression. Like the IP_3R, these proteins tetramerise to form large channel complexes ($\approx$ 2.2 MDa) composed of four identical subunits ($\approx$ 565 kDa).

RyRs are localised to the ER membrane where they open in response to elevated Ca^{2+}, like the IP_3Rs this Ca^{2+} regulation has both stimulatory and inhibitory properties to produce a bell-shaped concentration-response relationship. RyRs are activated by µM $[Ca^{2+}]$ but inhibited when the concentration increases to mM levels. This regulation by Ca^{2+} also implicates RyRs as a major player in CICR.

It is well established that cADPR sensitises RyRs to cytoplasmic Ca^{2+}, which results in receptors that are more likely to be activated by Ca^{2+} and thus give CICR. In addition to cADPR, RyRs are regulated by protein-protein interactions such as conformational coupling in skeletal muscle with VGCCs ($CaV_{1.1}$, $CaV_{1.2}$) and accessory proteins like Calmodulin (CaM), calsequestrin (Ca^{2+} buffer in SR), FK506-Binding Protein 12 and 12.6, as well as modulation by ATP, Mg^{2+} ions, kinase phosphorylation (PKA, and CAMKII), and reactive oxygen and nitrogen species (233).

1.5 NAADP-gated Ca^{2+} release

A relative newcomer to the scene of intracellular Ca^{2+} release is Nicotinic Acid Adenine Dinucleotide Phosphate (NAADP). This is the most potent of the Ca^{2+} mobilising messengers, with picomolar concentrations eliciting a Ca^{2+} response in sea urchin egg preparations (243). Mammalian smooth muscle has been shown to respond to concentrations of NAADP as low as 10 nM (46).

The characteristic properties of NAADP and its putative Ca^{2+}-channel receptor form the basis of this thesis.

1.5.1 Production of NAADP

The enzymes responsible for the endogenous synthesis of NAADP remain to be clearly defined (324). It has long been thought that enzymes of the ADP-ribosyl cyclase (ARC) family were responsible, as when purified from *Aplysia* or the human ecto-enzyme CD38 heterologously expressed, these enzymes were capable of synthesising NAADP *in vitro* (242). CD38 is widely expressed throughout mammals, and is implicated in cell proliferation (242) and social behaviour (274). These *in vitro* assays show that depending on the substrate and pH, CD38 can catalyse the synthesis of both second messengers, cADPR and NAADP (244). The base exchange reaction to form NAADP occurs preferentially at pH 4 - 5, producing NAADP from β-NADP and nicotinic acid (243). NAADP can also be synthesised by the oxidation of NAADPH or the phosphorylation of NAAD. However, only the base exchange reaction has been shown to be physiologically relevant (figure 1.4).

Notwithstanding this *in vitro* evidence, there is dispute over the role of CD38 as the catalyst for *in vivo* synthesis of NAADP. Two papers in favour of CD38-mediated synthesis have shown disrupted NAADP signalling in $CD38^{-/-}$ knock-out mice. One group prepared lymphokine-activated killer (LAK) cells from wild type and $CD38^{-/-}$ knock-out mice, and upon stimulation by IL-8, only the wild type cells synthesised NAADP (359). Cancela *et al.* showed a similar result in the well studied pancreatic acinar cell, demonstrating that the cholecystokinin (CCK) response requires the presence of CD38 to produce the NAADP-induced Ca^{2+} signal from the acid stores (93). Others showed contradictory evidence where NAADP signals were seen in $CD38^{-/-}$ knock-out mice in response to stimulation by Glucagon-like peptide-1 (217) or histamine (402),

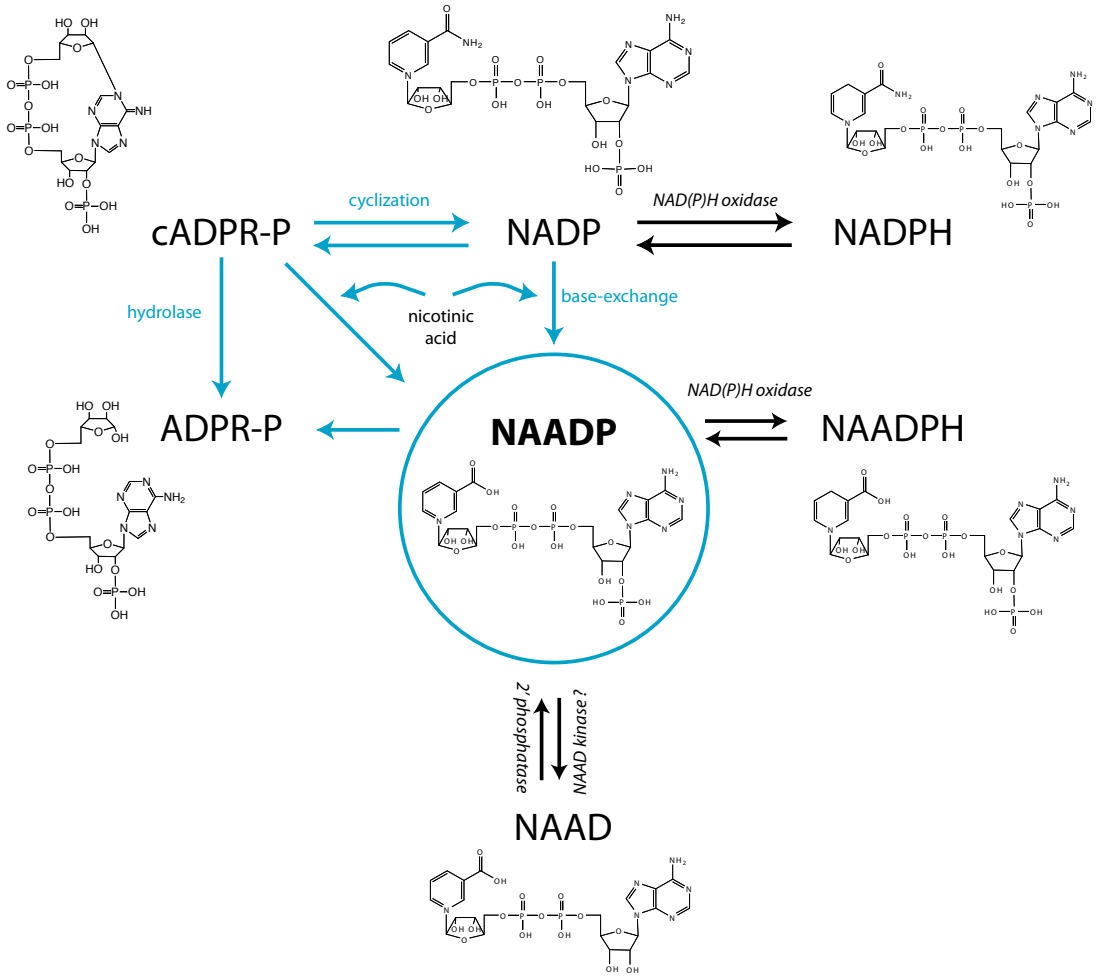


Figure 1.4: The putative metabolism and catabolism of NAADP. NAADP could be synthesised from a number of starting molecules through base exchange, phosphorylation or oxidation reactions. Many of these reactions are reversible, those with blue arrows can be catalysed by ARC enzymes.

suggesting that CD38 is not needed. It is possible that there are additional enzymes responsible for the synthesis of NAADP or that remodelling of the $CD38^{-/-}$ knock-out mice compensated for the physiological role of CD38.

To add one further piece of confounding evidence, the catalytic domain of CD38 is exposed at the cell surface, suggesting that the enzyme is producing these messengers extracellularly (93). All NAADP induced Ca^{2+} signals shown to date have been due to cytoplasmic stimulation of the receptor yet NAADP is a charged molecule and cannot diffuse through the plasma membrane, which would suggest that if it is synthesised outside the cell its uptake must be facilitated. A slight mitigation of this paradox could lie in a small proportion of intracellular CD38 localised on endosomal vesicles during stimulation (93), together with the optimal catalytic activity occurring at a low pH, it may be feasible that the NAADP is produced within the lumen of these acidic organelles. Even so, there would need to be a mechanism of NAADP release from the lumen, or a NAADP binding site on the receptor that faces inwards.

1.5.2 Breakdown of NAADP

Very little is known about the metabolism of NAADP. A potential pathway has been identified in the brain, involving the dephosphorylation of NAADP to NAAD by a 2'-specific Ca^{2+}-dependent phosphatase (28). The dependence on Ca^{2+} is supported in CCK-stimulated pancreatic acinar cells, as chelation of free Ca^{2+} by BAPTA prevents NAADP breakdown (249). This behaviour would result in a negative feedback mechanism with Ca^{2+} release promoting NAADP breakdown, whereas for IP_3 and RyR Ca^{2+} often results in the positive feedback of CICR.

Two other enzymes have been shown to catabolize NAADP. CD38 shows hydrolase activity *in vitro* converting NAADP to 2'ADPR-phosphate (160) this is shown in figure 1.4. Meanwhile the enzyme glucose-6-phosphate dehydrogenase, which usually reduces NADP to NADPH in the pentose-phosphate pathway, is also capable of reducing NAADP to NAADPH, which has no Ca^{2+}-evoking properties (42).

1.5.3 Endogenous NAADP

It has been difficult to directly measure the endogenous concentration of NAADP within the cytoplasm. One method allowed approximate quantification by comparing the level of competition the cell lysate presents to the robust radiolabelled NAADP binding assay

in sea urchin eggs (41). This assay was first used to measure changing NAADP levels in sea urchin sperm during activation before fertilisation (81). Since then, changes in NAADP levels have been shown in pancreatic β cells in response to glucose (282), smooth muscle cells in response to endothelin-1 (218), pancreatic acinar cells in response to CCK (459), human myometrial cells with histamine (402) and glutamate in neurones (326).

1.5.4 Discovery of NAADP

NAADP was first discovered as a trace contaminant in a commercial preparation of the co-enzyme NADP. This contamination is not surprising as the structure of these two compounds is almost identical. Figure 1.5 highlights the minor difference where an -NH_2 group in NADP is substituted for an -OH group to form the nicotinic acid group in NAADP. This alteration has very little bearing on the steric structure of the molecule, however the deprotonated acid allows additional electrostatic interactions which could explain why NAADP is a potent Ca^{2+}-releasing messenger, while NADP remains inactive.

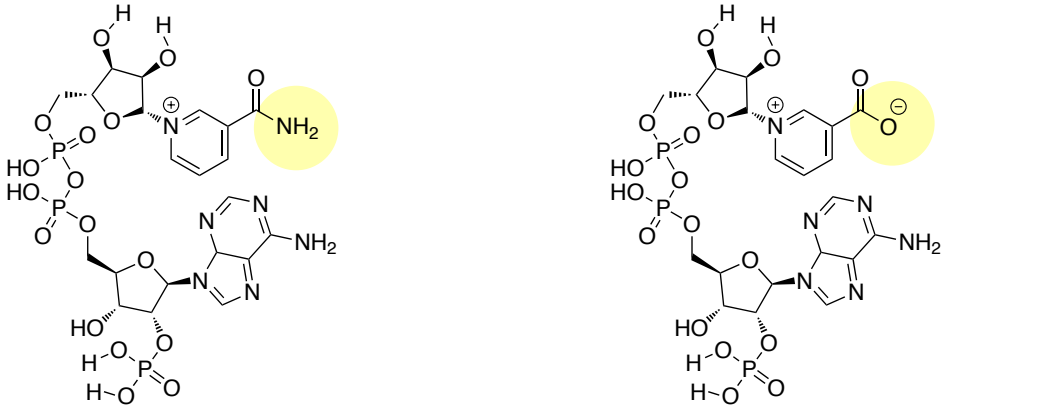


Figure 1.5: The structures of NADP and NAADP. The almost identical structure of these two compounds is displayed with the difference on the nicotinic group highlighted. NAADP (right) contains the hydroxy moiety which forms a carboxylic acid group, compared to the amide in NADP (left).

This serendipitous discovery was made in 1987 when Clapper *et al.* were investigating the Ca^{2+}-releasing properties of various pyridine nucleotides in sea urchin homogenate (87). Since then, the sea urchin preparation has become a model system for investigating Ca^{2+}-release mechanisms and was used to show that NAADP releases Ca^{2+} from acidic stores via a novel receptor, independently of IP_3 and cADPR (244).

1.5.5 NAADP targeting to acidic stores

Even before the NADP-contaminant was identified as NAADP by Aarhus and Lee in 1995 (244), differences were seen in the organellar target of this compound as it did not conform to the paradigm of ER derived Ca^{2+}-release. This was first shown by subcellular fractionation of sea urchin egg homogenate in a percoll gradient, where a Ca^{2+}-store which was sensitive to NAADP could be partially separated from the IP_3- and cADPR-sensitive microsomes (87).

This finding was confirmed in intact sea urchin eggs. These normally spherical cells elongate under gentle centrifugation, this causes stratification of the organelles which migrate to different poles of the cell. IP_3 and cADPR mobilised Ca^{2+} from the the nuclear pole, which contains the ER, whereas NAADP elicited responses from the opposite mitochondrial pole (245).

Pharmacological tools allowed further dissection. The SERCA-blocker, thapsigargin, prevents Ca^{2+} uptake into the ER (369), the store is depleted via inherent Ca^{2+} leak and the empty store no longer reponds to IP_3 and cADPR. In sea urchin egg homogenate treated with thapsigargin, NAADP still caused Ca^{2+} release, with an example trace shown in figure 1.6, this suggested that NAADP was accessing an undepleted store distinct from the ER (148). Intact sea urchin eggs showed similar properties where the responses from photolysis of caged derivatives of IP_3 and cADPR were abolished by pretreatment with thapsigargin whereas caged-NAADP responses persisted (78, 148).

The first hint that NAADP targets acidic stores was again seen in the stratified sea urchin egg. LysoTracker^{TM} is a fluorescent dye which preferentially localises to acidic stores, and in the stratified sea urchin eggs stained the non-ER pole where NAADP was shown to act (80). This study also showed that a host of pharmacological agents known to abolish a proton gradient could be used to abrogate NAADP-induced Ca^{2+} release. These agents included: the protonophore FCCP (carbonyl cyanide p-(trifluoromethoxy) phenylhydrazone); the K^+/H^+ ionophore nigericin; and the membrane-permeant weak

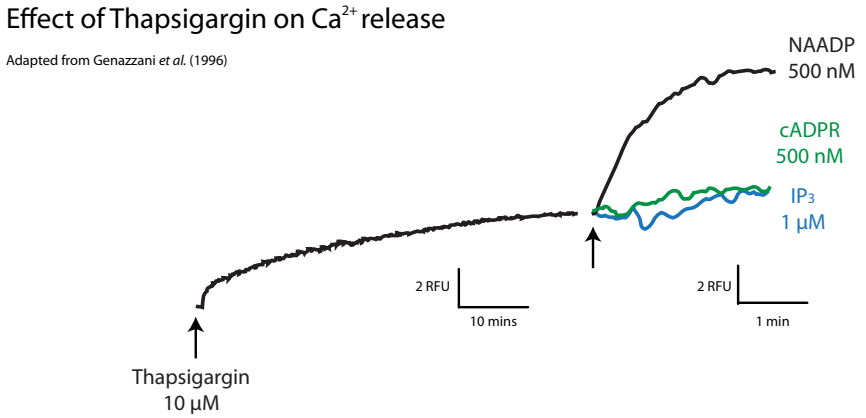


Figure 1.6: NAADP responses remain unaffected by ER depletion. Overlayed Ca^{2+} release traces from sea urchin egg homogenate. Thapsigargin inhibited the SERCA pump and prevented refilling of the ER Ca^{2+} stores. IP_3 and cADPR showed no Ca^{2+} release, whilst NAADP responses were unaffected (148).

base NH_3 (80). Furthermore, bafilomycin A1 which acts as an inhibitor of the vacuolar H^+ pump also abolished NAADP responses (80). This evidence strongly implicated acidic organelles as the elusive NAADP-sensitive store.

Another useful tool was added to the pharmacological armoury, the lysomotropic agent GPN. This is a membrane-permeant agent that is broken down by cathepsins into a membrane-impermeant product. Acid organelles contain high levels of cathepsins, so these products accumulate, cause osmotic swelling and eventually organelle lysis (454). GPN treatment of intact eggs resulted in brief localised Ca^{2+} release flashes, and also reduced the fluorescent staining by LysoTracker. Addition of GPN to the bath solution surrounding the sea urchin eggs caused the abolition of NAADP-induced Ca^{2+} release whereas IP_3 and cADPR remained effective (80).

NAADP-evoked Ca^{2+} release has now been shown in various mammalian systems and even in plants (137). These higher organisms also show a functional localisation of NAADP-induced Ca^{2+} release from acidic stores, in a range of tissues for example, pancreatic acinar cell (458), smooth muscle (218) and neurones (48).

Whilst these studies show that NAADP induces Ca^{2+} release from a distinct organelle, further work was required to show that this was due to a novel receptor.

1.5.6 NAADP receptor properties

Early studies in the the sea urchin egg homogenate showed that IP_3, cADPR and NAADP could independently induce homologous desensitisation of their target mechanisms without affecting the response of the other two mechanisms. This was seen in whichever order the messengers were added (244). Figure 1.7 demonstrates this specificity by separately desensitising each messenger in the same homogenate sample (149). The complete independence of these mechanisms suggests that they act on separate receptors.

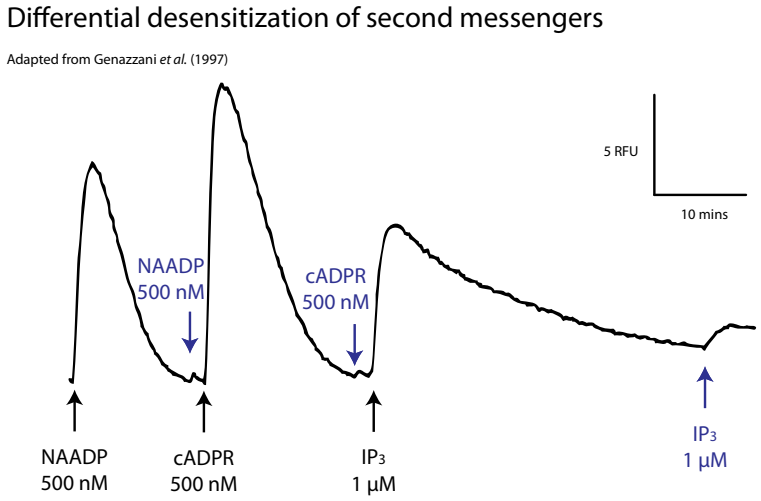


Figure 1.7: Homologous desensitisation by NAADP, IP_3 and cADPR. Representative Ca^{2+}-release trace from sea urchin egg homogenate treated with sequential additions of NAADP, cADPR and IP_3. Homologous desensitisation was seen for each messenger with no cross talk between receptors (149).

The use of pharmacological agents further supported this conclusion. Antagonists of the RyR (ryanodine and 8-NH_2-cADPR) and of the IP_3R (heparin) had no impact on the NAADP-induced Ca^{2+} release (149, 244). Traces in figure 1.8 represent these experiments. Microinjection of heparin into intact sea urchin eggs abolished Ca^{2+} release by IP_3 and had no affect on the NAADP response (341). Similarly ryanodine, which blocks RyR and induces ER depletion of Ca^{2+}, abrogated responses by both IP_3 and cADPR, but NAADP still induced Ca^{2+} release (138).

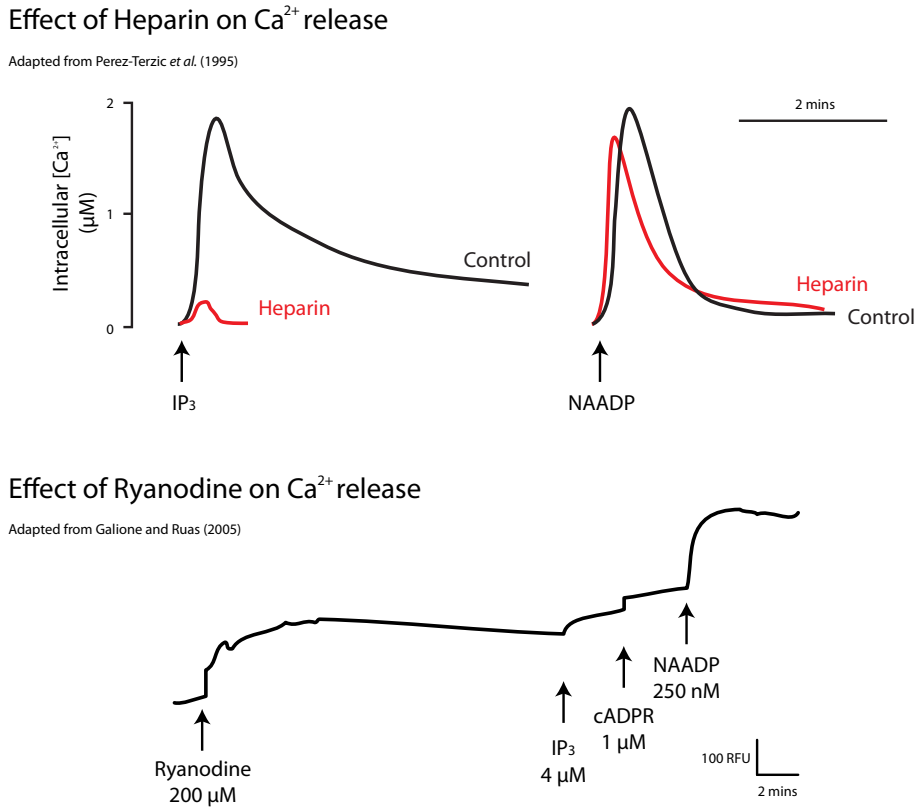


Figure 1.8: NAADP responses remain unaffected by IP_3R and RyR antagonists. Top: Representative Ca^{2+}-release traces from intact sea urchin eggs. Microinjection of the IP_3 antagonist heparin (500 µg) abolished the IP_3 (100 - 200 nM final concentration) response (left) but not the NAADP response ($\approx$ 20 nM final concentration) (right) (341). **Bottom:** Representative trace of Ca^{2+} release in sea urchin egg homogenate. Ryanodine induced the emptying of the ER Ca^{2+} stores which prevented Ca^{2+} release by cADPR and IP_3. NAADP was still effective at inducing Ca^{2+} release (138).

1.5.7 Self-desensitisation of NAADP

Investigation into the desensitisation properties of NAADP showed a unique concentration-response relationship. In sea urchin egg homogenate, pre-treatment with sub-threshold concentrations of NAADP can abolish Ca^{2+} release from subsequent additions of normally maximal concentrations of NAADP, despite causing no detectable release themselves (1, 147). This remarkable property is shown by the trace in figure 1.9.

This sub-threshold desensitisation was slow to develop ($\approx$ 3 minutes) and seemed to be essentially irreversible in egg homogenate as no recovery has ever been reported. These experiments have been replicated in intact urchin eggs, which show consistent sub-threshold desensitisation of NAADP-induced Ca^{2+}-release. However, in these experiments eggs fully restored their sensitivity to NAADP after about 20 minutes (149).

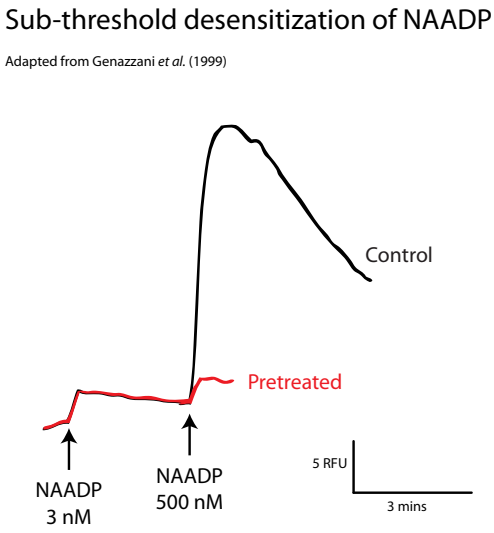


Figure 1.9: Sub-threshold inactivation of the NAADP response. Representative Ca^{2+} trace in sea urchin egg homogenate. Pretreatment with sub-threshold concentrations (3 nM) of NAADP prevented Ca^{2+} release by subsequent addition of activating concentrations (500 nM) (146).

This binding of such low concentrations suggests a high affinity NAADP-binding site. Experiments conducted with various analogues of the NAADP-antagonist Ned-19, propose that the NAADP receptor has two binding sites: one high affinity inhibitory site, and one activating site with a lower affinity (370).

Similar studies show sub-threshold densitisation in other tissues: plants (309), brain (14) and liver (276). However this phenomenon is not universal, with many human tissues only showing desensitisation by high concentrations of NAADP: pancreatic cells (acinar (57) and β (202, 282)); myoblasts (4); human T-lymphocytes (25); cardiac myocytes (266); bladder (431); and uterus (5). These cells and tissues give a bell-shaped concentration-response curve with nM activating concentrations and µM inhibitory concentrations (304).

1.5.8 The effect of cytoplasmic Ca^{2+} on NAADP binding.

A final distinctive feature of NAADP-evoked Ca^{2+} release is the lack of Ca^{2+}-feedback as both the IP_3R and RyR are biphasically modulated by cytoplasmic Ca^{2+}. It was first demonstrated by Ca^{2+}-release assays in sea urchin egg homogenate that the NAADP response remained unaffected over a range of $[Ca^{2+}]_{cytoplasm}$ (0 - 1 mM) (74). This was later supported in rat brain microsomes which demonstrated robust NAADP binding that was unaltered by changes to cytoplasmic Ca^{2+} concentrations (14). A more recent study also showed that changes to the luminal Ca^{2+} concentration of the organelles in sea urchin egg homogenate did not affect the affinity of NAADP binding (13).

Furthermore, variations in cytoplasmic Mg^{2+} and Sr^{2+} concentration also had no regulatory effect on NAADP-mediated Ca^{2+}-release (148).

These studies focused on ligand binding and Ca^{2+} release assays, however Ca^{2+} may play a localised regulatory role in the channel gating and this will be discussed in chapter 3.

1.5.9 Antagonism of the NAADP response

Direct pharmacological intervention to block the NAADP response allowed predictions as to the structure of its putative receptor.

Agents have been identified which selectively block the NAADP response without affecting either the IP_3R or RyR. These included the VGCC blockers - the dihydropryidines (149) and diltiazem. Figure 1.10 shows the inhibitory effect of diltiazem on NAADP-induced Ca^{2+} release in the urchin homogenate (147). The TRPC blocker SKF96365 (297) also antagonised the NAADP response. These molecules block homologous channels, the TRPs and VGCCs which are part of the same protein lineage, this suggests that the putative NAADP receptor may also be part of this family.

In contrast to this theory, the P2-purinoreceptor antagonist PPADS (Pyridoxal-phosphate-6-azophenyl-2',4'-disulfonate) has been shown to selectively antagonise NAADP induced Ca^{2+}-release in the sea urchin homogenate with an IC_{50} of 20 µM (40).

As interest in NAADP signalling grew, a deliberate attempt to create pharmacological agents yielded the compound Ned-19. This is a novel membrane permeant analogue of NAADP, modelled to resemble the 3-dimensional structure of the agonist (310). It showed NAADP-specific antagonism as depicted by the traces in figure 1.10. NAADP-evoked Ca^{2+} release from the sea urchin egg homogenate, usually seen at nanomolar concentrations, was totally abolished in the presence of Ned-19, whereas cADPR and IP_3 responses were unaffected.

The specificity of Ned-19 makes it a useful tool in studying the properties of NAADP-induced Ca^{2+} release and this compound is utilised throughout this thesis.

The pharmacology of the acidic store and the NAADP receptor are summarised in the schematic shown in figure 1.11.

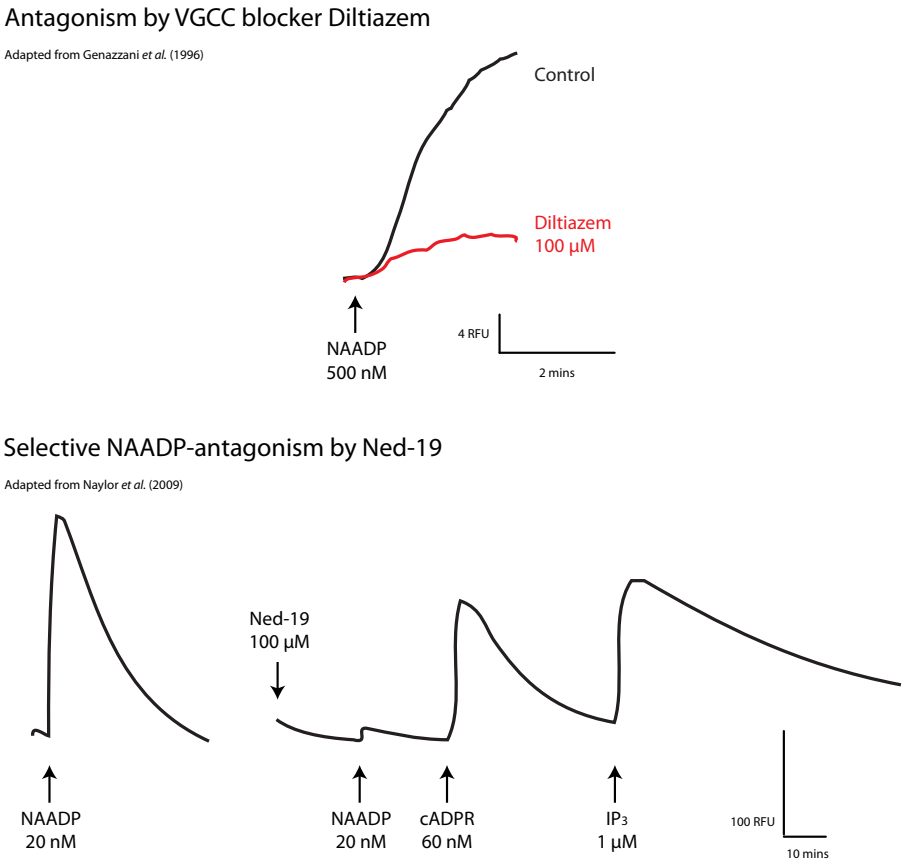


Figure 1.10: Diltiazem and Ned-19 are known NAADP antagonists. Top: Representative trace of Ca^{2+} release in sea urchin egg homogenate. Reduced Ca^{2+} release is seen when the channel blocker diltiazem is present (147). **Bottom:** NAADP-induced Ca^{2+} release is abolished in the presence of Ned-19, whereas IP_3 and cADPR responses are unaffected (310).

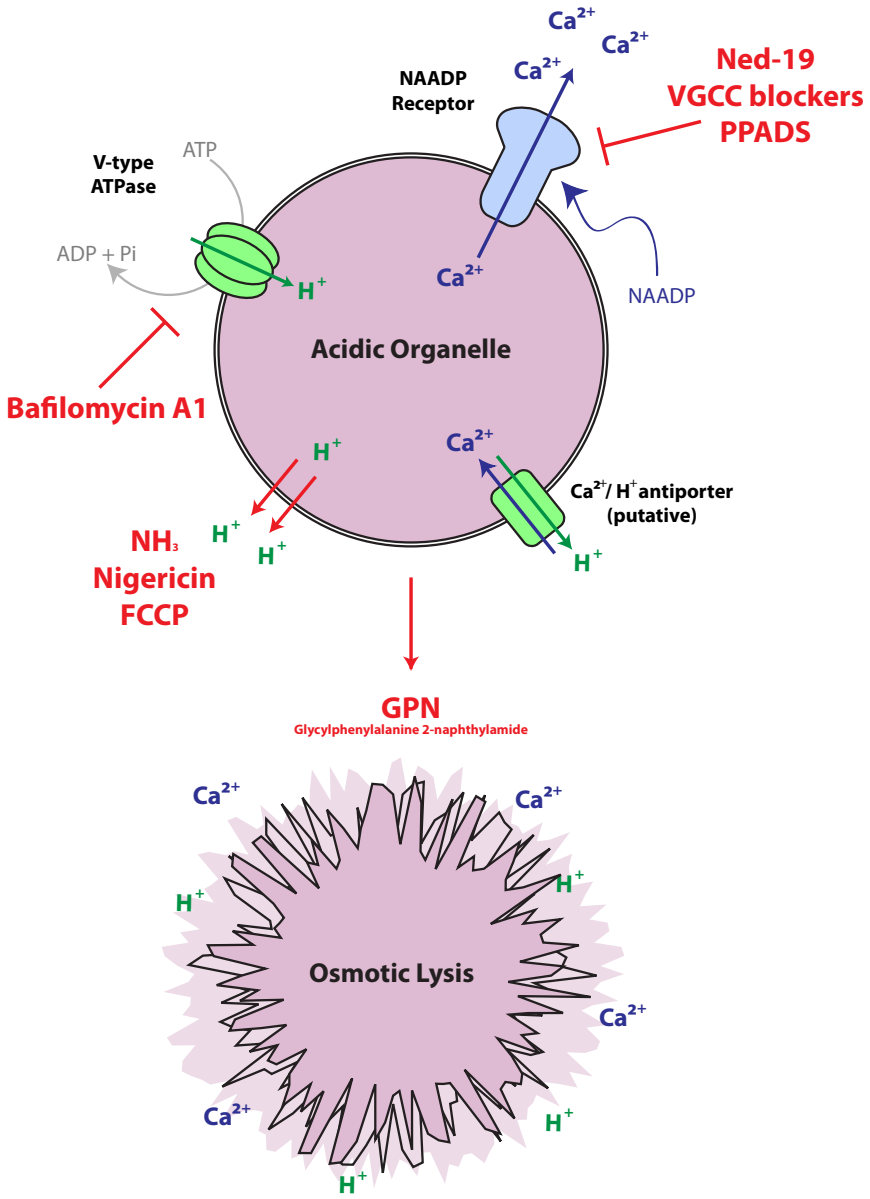


Figure 1.11: The acidic store and its pharmacology. A simplified model lysosome depicting H^+ uptake by the V-type ATPase and putative Ca^{2+} uptake by a Ca^{2+}/H^+ antiporter. This physiology can be disrupted by bafilomycin A1 which inhibits proton-pumping, proton ionophores such as FCCP and nigericin, which dissipate the proton gradient and GPN which causes osmotic lysis of the lysosome. The more specific antagonists of the NAADP receptor are also shown: Ned-19, VGCC blockers and PPADS.

1.6 Summary of NAADP characteristics

As has been shown, NAADP-evoked Ca^{2+} signals display distinctly different properties from those of IP_3 or cADPR. These unique features will be important in future discussion when the effects of NAADP on its cognate receptor are investigated in chapters 3 & 4. A brief outline of these properties is summarised here:

- NAADP is the most efficacious of the Ca^{2+} second messengers, evoking a response at low nM concentrations as opposed to the higher µM concentrations required for cADPR and IP_3 (57).
- NAADP mobilizes Ca^{2+} from an acidic store, unlike IP_3 and cADPR which act at the SR/ER (47, 52, 80, 458).
- In mammalian cells, NAADP self-inactivates with high concentrations which desensitise the channel to give a bell-shaped concentration-response relationship (4, 5, 282, 304, 431).
- Changes to cytoplasmic and luminal [Ca^{2+}] do not regulate NAADP-binding (13, 14).
- NAADP signalling is unaffected by well established antagonists of RyR and IP_3R, but is completely abolished by Ned-19 (310), as well as VGCC and TRP channel blockers (149).

1.7 The NAADP receptor

The major question in the field of NAADP signalling was the identity of the cognate NAADP receptor. From the properties discussed above it is possible to outline the key criteria and unique properties that the putative receptor must display:

Localisation to an acidic organelle. From all the sea urchin homogenate experiments above, pharmacological disruption and subcellular fractionation support the predominant NAADP-mediated Ca^{2+}-release emanating from the acidic stores. This has also been shown in mammalian systems. The NAADP-sensitive channel must be localised in the lysosomal/late endosomal membrane to allow Ca^{2+} release from these stores.

Consistent Pharmacology. The known NAADP antagonists (section 1.5.9) must show interaction and blockade of any channel activity. Due to the sensitivity of the NAADP response to the known VGCC blockers, the dihydropyridines and SKF96365, it is likely that the NAADP-sensitive Ca^{2+} channel has a homologous structure which allows these compounds to bind. The VGCC family is large with many subgroups containing the 6-TM motif and the pore forming region (figure 1.12).

Molecular weight $\approx$ 120 kDa. Berridge *et al.* determined the mass of the NAADP-binding protein complex (29). Radio labelling of crudely purified sea urchin egg membranes revealed a single NAADP-binding protein on native gel electrophoresis. However, as protein migration is affected by inherent charge as well as protein mass this method could not determine protein size. So the NAADP-bound protein was further purified by using gel-filtration and predicted a protein around 470 kDa. To confirm this result a parallel purification using a sucrose gradient was conducted but gave a significantly smaller protein around 120 kDa. It was suggested that a multimeric channel with monomeric subunits of 120 kDa could form a tetramer around 470 kDa, would explain this discrepancy between the two results. This size is notably smaller than the monomers of IP_3R (260 kDa), RyR (550 kDa) and plasma membrane VGCC (α subunit $\approx$ 210 kDa) which supports the hypothesis of a novel receptor. (29).

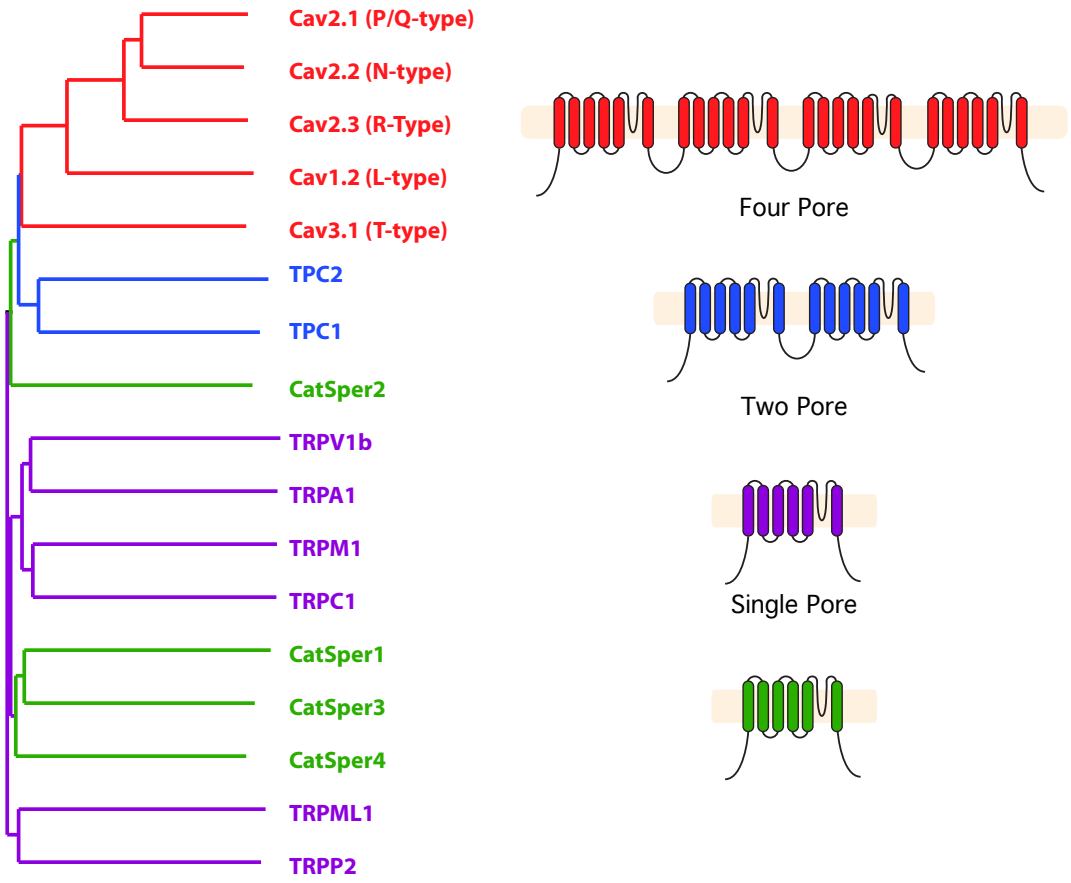


Figure 1.12: The voltage-gated Ca^{2+} channel family. Phylogenic tree of human proteins closely related to the VGCCs, sequences of known related proteins were compared using ClustalW2 (72) and plotted using a Neighbour-Joining algorithm. A structural schematic for each group is also shown. The 24-TM four pore channels are known to be functional as monomers, whereas the single pore TRP channels tetramerise. This suggests a common structural arrangement requiring four repeating domains of 6-TM.

1.8 Candidate NAADP receptors

Whilst this thesis will eventually focus on a single protein, it is worth considering all those proteins which have been implicated as potential candidates for the role of NAADP receptor.

1.8.1 TRPML1

Based on the criteria above, one of the most obvious protein families to focus on were the well characterised cation channels TRP mucolipins (TRPMLs). These were known to localise within lysosomes as mutations in the isoform TRPML1 resulted in the lysosomal storage disease mucolipidosis IV (18). TRPML1 is the most understood isoform of the three TRPMLs present in mammals (TRPML1 - 3) and has been shown to localise to late endosomes as well as lysosomes (278). With the characteristic TRP structure of 6-TM domains and a propensity to tetramerise into the familiar structure of the VGCCs (86), TRPML1 has been shown to be permeable to Ca^{2+} ions, but confusion has arisen as other studies show that it is also a H^{+} channel (406) and more unsuspected still permeable to Fe^{2+} ions (112).

TRPML1 meets many of the criteria established for the NAADP-receptor and it is thus not surprising that groups have focused on this candidate. Li *et al.* coalesced lysosomes purified from rat liver with an artificial lipid bilayer and conducted electrophysiological recordings (465, 466). NAADP elicited channel activity that was lost when preparations were treated with an antibody targeted against the C-terminus of TRPML1 (466). Activity was also lost when the lysosome preparation was depleted of TRPML1 via immunoprecipitation, and reduced when the cells were pretreated with siRNA against TRPML1 (466).

The same group also implicated TRPML1 as the endogenous effector using coronary aterial myocytes (CAMs), which have been shown to release Ca^{2+} from acidic stores in response to endothelin-1 (ET1). Knock-down of the TRPML1, again by siRNA, gave a reduction in this ET1 response of nearly 50 % of the local Ca^{2+} release and 70 % of the global Ca^{2+} wave (465). Taking this further, Zhang *et al.* showed that TRPML1$^{-/-}$ human fibroblasts did not respond to NAADP (0.01 - 1 µM), but NAADP-induced Ca^{2+} release was seen by transient transfection of TRPML1 back into this cell line (467).

The role of TRPML1 as the NAADP receptor has been disputed based on evidence that overexpression of TRPML1 has no effect on NAADP-induced Ca^{2+} release (457) in HEK293 cells. Similarly the expression of a dominant negative TRPML1 mutant (D471K) did not alter endogenous NAADP responses (457) and finally NAADP-evoked Ca^{2+} oscillations were identical in wild type and TRPML1$^{-/-}$ pancreatic acinar cells (457).

This last evidence has seriously weakened the candidacy of TRPML1, but due to their lysosomal localisation and Ca^{2+} permeability the TRPMLs are likely to affect NAADP signalling via ion homeostasis and lysosomal trafficking (113).

1.8.2 TRPM2

A very close relation of the TRPMLs is TRPM2, it has a similar structure and has been shown to be a non-selective Ca^{2+}-permeable ion channel (343). TRPM2 is implicated as a potential NAADP-receptor because it has been shown to localise to lysosomal membranes in β cells, and in studies investigating oxidative cell death TRPM2 was activated by ADP-ribose, a nucleotide very similar to NAADP (231).

Although TRPM2 is principally gated by ADP-ribose (342) this is not specific and TRPM2 shows polymodal activation responding to oxidants such as H_2O_2 (172), Ca^{2+} ions (284) and also cADPR (224). One study has shown direct activation of TRPM2 by NAADP, however the concentrations used were much higher than in any other study (EC_{50} = 730 µM (21), this concentration is normally considered inhibitory in mammalian systems (135)).

Considering that most of this evidence is based on conjecture and measurements made under unphysiological conditions, more direct data would be required to strengthen the candidacy of this protein.

TRPV2 is another member of the TRP family which has shown localisation to endosomes (378), it shows the same hallmarks of a Ca^{2+} channel and potential for nucelotide binding (441), however there not yet evidence showing NAADP-binding or channel activation.

1.8.3 P2X and P2Y receptors

The purinergic receptors are a family of of cation-permeable ligand gated ion channels that open in response to the binding of extracellular adenosine 5'-triphosphate (ATP).

Usually they are located to the plasma membrane, however one isoform, P2X4, has been shown in the lysosomal membrane (358). These channels are implicated in NAADP signalling due to the pharmacology of the P2-purinoreceptor antagonist, PPADS, which seems to competitively antagonise the NAADP-elicited Ca^{2+}-release in sea urchin egg homogenates (40). NAADP has also been shown to activate recombinant P2Y11 in human astrocytoma cells (302). One *non-sequitur* regarding these receptors is that if their topology at the plasma membrane is maintained in the lysosome, the known nucleotide-binding site would be facing the lumen of the store (358), if these proteins are indeed the NAADP receptor then there would need to be a separate cytoplasmic binding site.

1.8.4 RyR

There are numerous reports suggesting a role for the RyRs in NAADP signalling (150, 187, 298, 408).

The most direct evidence was demonstrated on purified RyR1 which had been incorporated into a lipid bilayer and showed an increase in channel open probability (P_o) in the presence of NAADP (187). However these findings have been disputed as they could not be repeated, NAADP did not activate purified rabbit skeletal RyR1 or sheep cardiac RyR2 when they were incorporated into a lipid bilayer under identical conditions (347). Furthermore, NAADP failed to significantly increase the P_o of RyR in SR-enriched microsomes when they were reconstituted into lipid bilayers (468).

It has been suggested that a subset of the RyRs are localised on the acidic store where they act directly as the NAADP receptor. Evidence for this comes from the inhibition of NAADP-mediated Ca^{2+} signals in Jurkat T-lymphocytes by the RyR antagonist ruthenium red (408) and knock-down of RyR (232). There is also evidence of RyRs present on acidic secretory vesicles involved in insulin secretion in MIN6 cells (a pancreatic β cell line) (295). A contradiction which needs to be resolved is the fact that RyR activity has been shown to be inhibited by a low luminal pH, with most channels inactive at pH 5.5 (238), which would make RyR an inappropriate candidate for an acidic store Ca^{2+}-release channel.

Involvement of the RyRs may be explained by the trigger hypothesis whereby a relatively small amount of Ca^{2+} release induced by NAADP triggers the activation of RyRs through CICR (figure 1.13) (57). Studies have shown that knocking out the ER

response either by the IP_3R/RyR blockers or by thapsigargin, dramatically reduced the amplitude of the NAADP response but did not totally abolish all Ca^{2+} release like the lysosome-targeted agents bafilomycin A1 or GPN (47, 140, 266, 288).

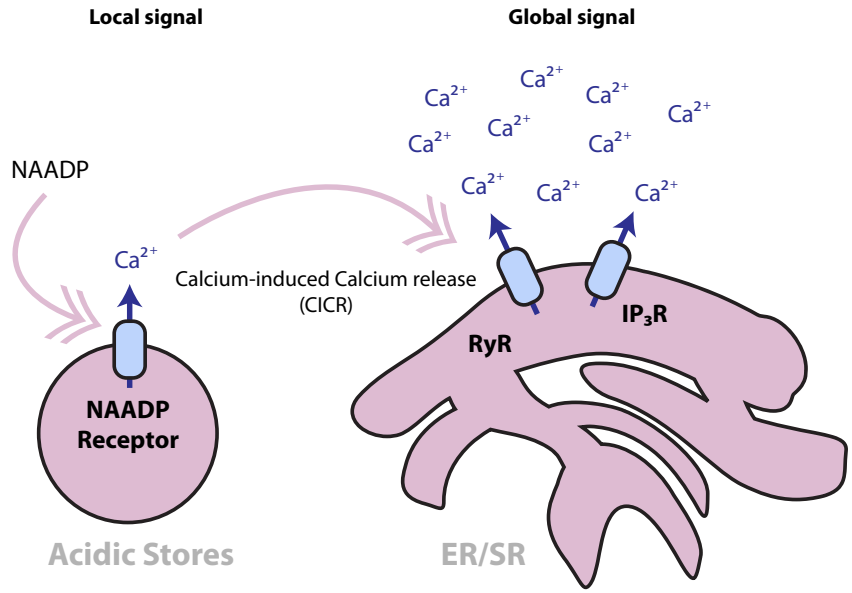


Figure 1.13: NAADP can trigger global signals. NAADP-induced Ca^{2+} release from acidic stores is a relatively small and localised signal. By coupling this Ca^{2+} release close to the ER, this signal can induce further Ca^{2+} release by CICR from RyRs and IP_3Rs similar to propagation of Ca^{2+} signals seen in excitation-contraction coupling of VGCC channels and the ER in cardiac muscle.

This would require a subcellular architecture that allows a close coupling of these receptors to enable local Ca^{2+} signals from lysosomes to reach the ER membranes where they are subsequently amplified. Early evidence from immunofluorescence staining in arterial smooth muscles indicates the presence of lysosome-sarcoplasmic reticulum junctions of less than 100 nm (218, 219), these may constitute a "trigger zone" reminiscent of a nerve synapse.

This hypothesis does not rule out RyRs as the direct NAADP receptor but can explain the observed pharmacology given a more likely candidate.

1.8.5 The Two-Pore Channels (TPCs)

The TPCs are novel members of the superfamily of voltage-gated cation channels more closely related to the VGCCs than the TRP channels (135). Figure 1.12 showed the extent of homology in a sequence alignment tree together with a schematic representation of their common structure. TPCs have recently been implicated as acting as the NAADP receptor by three separate laboratories (47, 55, 478). As these proteins are the main focus of this thesis their eligibility as the candidate will be discussed more fully in the next section.

1.9 The Two-Pore Channels

1.9.1 Discovery

TPCs were first predicted to be involved in Ca^{2+} signalling at the turn of the millenium when the first isoform was cloned from rat kidney (199). By sequence homology this novel protein was predicted to dimerise to form a Na^+/Ca^+ channel closely related to the VGCC family. However, the first empirical evidence of TPC Ca^{2+} channel activity was shown in the plant cell vacuole (132) (an acidic Ca^{2+} store (352)) with channel opening in response to elevated cytoplasmic $[Ca^{2+}]$. The eventual association of the TPCs with NAADP signalling was made almost a decade later (55).

1.9.2 Eligibility

Two major streams of evidence suggested that the TPCs could be involved in NAADP signalling and these converged from two distinct fields, the TRP channels and plant electrophysiology. The first clue was presented by the Mike Zhu laboratory who were searching for novel members of the TRP family and cloned the human isoform of TPC2. Heterologous expression of this protein in HEK293 cells showed a predominant colocalisation with LAMP1 in the lysosomal membrane (47, 55, 333). The second clue came from the association of plant TPC1 with the slow vacuolar (SV) current in plants, and their localisation to the plant cell vacuole, an acidic organelle (336). The localisation of the TPCs to acidic organelles together with their homology with VGCC made these proteins a credible candidate as the NAADP receptor.

The subcellular localisation of the TPCs was further dissected with both human isoforms, HsTPC1 and HsTPC2, which both showed localisation to the endo-lysosomal system with no apparent localisation to the ER, mitochondria, Golgi apparatus or plasma membrane. HsTPC2 consistently localised to the lysosome whereas HsTPC1 showed a more disparate localisation with only a sparse overlap with lysosomal markers (47, 55).

Overexpression of HsTPC2 correlated with an increase in the specific binding of ^{32}P-radiolabelled NAADP in HEK293 membranes and this could be depleted by removing HsTPC2 by immunoprecipitation (55). The binding affinity of the membranes correlated with values seen in endogenous mouse liver membranes, a model tissue for

[^{32}P]NAADP binding which also shows a particularly high level of TPC expression (478).

NAADP-evoked Ca^{2+} responses were also seen to be augmented by overexpression of HsTPC2. Photolysis of caged NAADP in patched wild type HEK293 cells elicited a small Ca^{2+} response, whereas similar treatment of HsTPC2 overexpressing cells gave a large biphasic Ca^{2+} response, with a small increase in local Ca^{2+} followed by a subsequent rapid global Ca^{2+} release. Preincubation with bafilomycin abolished both phases of the Ca^{2+} response, whereas the IP_3R antagonist, heparin, ablated the large global response without affecting the initial phase of Ca^{2+} release. This was hypothesised to represent an initial lysosomal response elicited by NAADP, followed by the larger ER response activated by CICR (55). Wild type cells did show an NAADP response, however they did not show this biphasic release and required higher concentrations of NAADP to activate, suggesting that this response was probably mediated by the low levels of endogenous TPC expression (55).

The concentration-response relationship between NAADP and Ca^{2+} release in these cells showed the characteristic mammalian bell-shaped curve, with maximal release occurring between 1 nM - 1 µM, concentrations $>$ 1 mM gave no response (55, 478).

Further association was proved by knock-down of the HsTPC2 by shRNA, which abolished the NAADP response in the overexpressing cell line and the native response in a human hepatoblastoma cell line (55, 478). This requirement for TPC2 is also seen in mouse pancreatic β cells. Wild type β cells showed the activation of a non-selective cation current upon application of NAADP, however this response was not seen in cells prepared from *Tpc2* knock-out mice (55).

Electrophysiological studies by three independent groups have shown NAADP-gated Ca^{2+} channel activity from TPC2. Firstly, immunopurified HsTPC2 was incorporated into an artificial lipid bilayer, both K^+ and Ca^{2+} currents were seen and the channel open probability (P_o) increased upon addition of NAADP in a dose dependent relationship. Luminal Ca^{2+} and pH also were shown to regulate the channel activity (chapter 3) (347).

Meanwhile, Biel *et al.* isolated lysosomes from cells overexpressing MmTPC2 (387), they detected current activity using an automated patch-clamp device and showed NAADP-induced Ca^{2+} selective currents, which were abolished by mutations in the

putative pore region of the TPC. Preliminary experiments on lysosomes purified from HsTPC2-overexpressing cells (chapter 4) confirm many of their findings.

Finally, a mutated HsTPC2, with a truncated N-terminal tail, was shown to be redirected to the plasma membrane. This allowed patch clamp recordings in the whole-cell configuration and resulted in NAADP-gated Ca^{2+} flux through the mutated HsTPC2 (50). A further point mutation in the putative pore region reduced Ca^{2+} conductance in response to NAADP, further confirming that HsTPC2 was the pore-forming subunit of an NAADP-gated channel (50).

TPC1 has also been implicated as an NAADP-gated Ca^{2+} channel. HsTPC1 transiently transfected into the human breast cancer cell line, SKBR3, gave robust Ca^{2+} responses when the cells were microinjected with 10 nM NAADP (47). Knock-down of HsTPC1 in this cell line attenuated NAADP-induced Ca^{2+} signals as did the overexpression of a non-functional HsTPC1 which had been mutated at a conserved residue in the pore region (47). In general, HsTPC1 was only shown to produce localised signals as opposed to the amplified global signals triggered by HsTPC2 (47). This may be due to the endosomal localisation of HsTPC1 which lack the close apposition and coupling to the ER thus making CICR less likely (260).

1.9.3 Structure

As mentioned above, the TPCs sit within the family of the VGCCs. Hydropathy analysis of the primary sequence predicts 12 transmembrane spanning domains (figure 1.14), which are divided into two repeats of the ubiquitous 6-TM domains with pore-forming re-entry loop between S5 and S6. The name two-pore channel is derived from these two 6-TM repeats each with a pore forming loop. However, this is not to be confused with the two-pore potassium channels, which have two repeats of a 2TM domain which are homologous to S5/S6.

In terms of sequence homology the TPCs are very closely related to the 24-TM voltage-gated Ca^{2+}/Na^{+} channels as well as the single domain 6-TM TRP channels and the CatSpers (Cation Channels of Sperm). This suggests that the TPCs are an evolutionary intermediate between the two groups (figure 1.12). Given that the single domain channels are known to tetramerise to form a pseudo-24-TM channel, it is likely that the TPCs need to form dimers to complete the channel pore. A summary of the predicted structure of the TPCs is shown in figure 1.15.

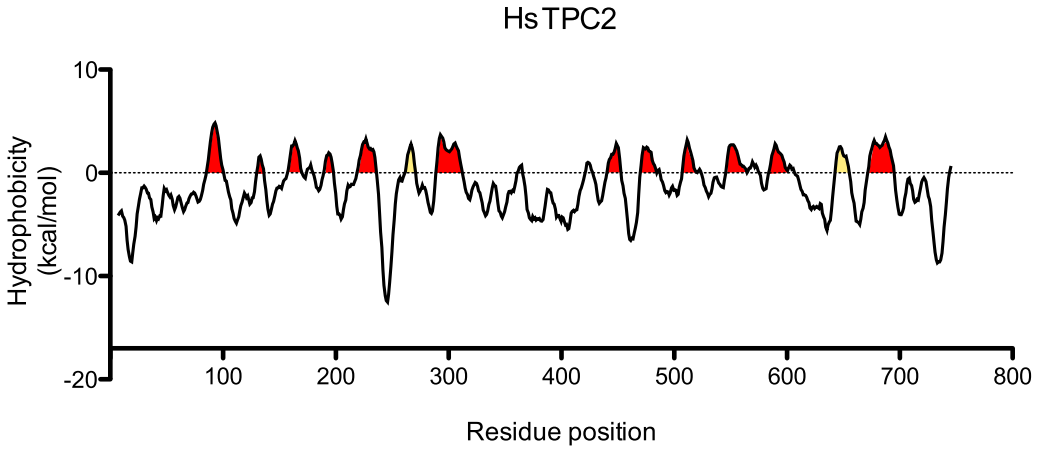


Figure 1.14: Hydrophobicity plot of HsTPC2. The predicted transmembrane domains in the HsTPC2 protein are highlighted in red, the putative re-entry loop highlighted in yellow. The online prediction software was provided by the TMHMM server (CBS, Denmark), and was conducted with a window size of 9 amino acids.

1.9.4 Homology across species

Angiosperms, such as the thale cress (*Arabidopsis thaliana*), in which the TPCs were first discovered, wheat (*Triticum aestivum*) and rice (*Oryza sativa*) have just a single gene, TPC1. Some higher plants such as tobacco (*Nicotiana tabacum*) have a duplicate TPC with 97 % homology, whereas mosses have up to 9 TPC genes (55).

In animals there are 3 known isoforms (TPC1 - 3), but even here the distribution is not straightforward. The TPCs are absent in two of the most widely used model organisms, the nematode (*Caenorhabditis elegans*) and the fruit fly (*Drosophila melanogaster*), however in the deuterostome lineage, all the TPC isoforms seem to have been retained in most organisms. Importantly for Ca^{2+} studies, sea urchins (*Strongylocentrotus purpuratus*) have the full armoury of TPCs, as do the majority of chordates: frogs (*Xenopus tropicalis*), fish (*Danio rerio*) and birds (*Gallus gallus*). Mammals begin to show a divergence and redundancy of the TPC3 isoform, whilst it is present in cows (*Bos taurus*) and horses (*Equus caballus*), it is absent in rats (*Rattus norvegius*), mice (*Mus musculus*) and, significantly, humans (*Homo sapiens*). Thus the TPCs have undergone both expansion and loss in a lineage specific manner. A summary of isoform distribution is shown in figure 1.16 (55).

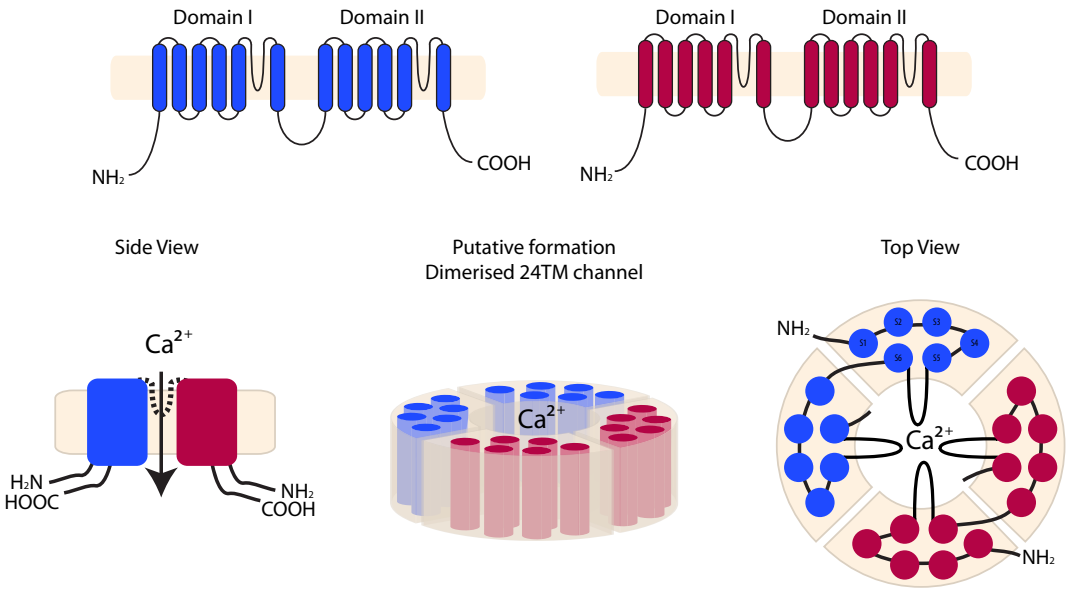


Figure 1.15: Predicted structure of the TPC protein. Based on the homology of voltage-gated Ca^{2+}/K^{+} channels, the TPCs are likely to dimerise to form the common 24-TM motif around a central pore.

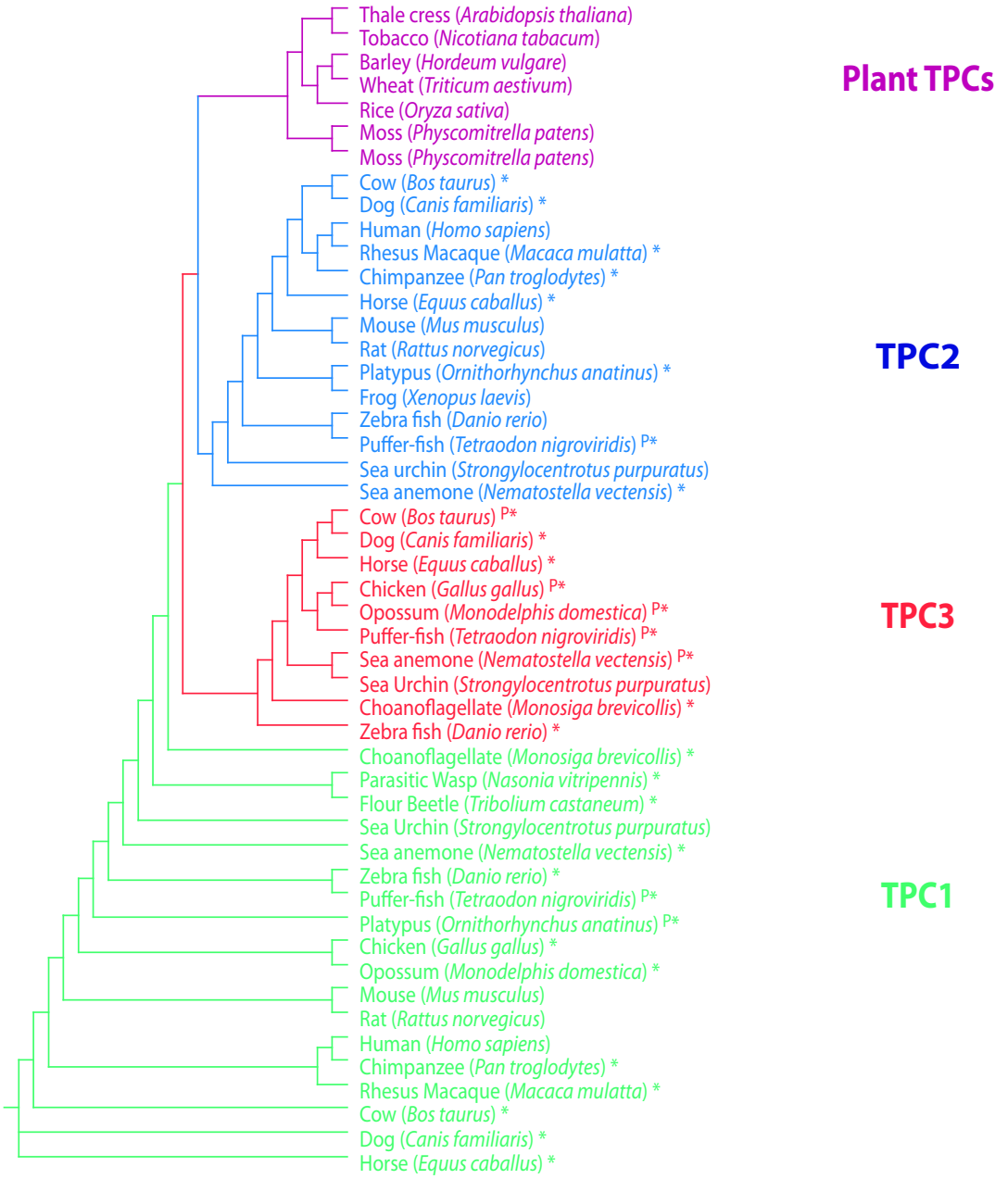


Figure 1.16: Comparison of TPCs across multiple species. All currently known TPC sequences were compared using ClustalW2 (72) and plotted using a Neighbour-Joining algorithm to produce this phylogenic tree. For some TPCs, lengthy and non-homologous N-terminal sequences were not included. $*$ Corrections were made to these sequences based on multi-sequence alignments. P - Only partial sequences were available.

1.9.5 Plant TPC1

The most extensively studied TPC is the isoform found in plant cells, often referred to as TPC1, however as shown in figure 1.16 this isoform shows more homology with the TPC2 isoforms found in animals.

Plant TPCs have been implicated in providing the Slow Vacuolar (SV) current, which consists of flow of Ca^{2+} ions from the plant cell vacuole, the main acidic organelle (352). This current is activated in response to H_2O_2 (207) or sucrose (132) and has a role in regulating stomatal movement and germination (336). Overexpression of AtTPC (*Arabidopsis thaliana*) gave an increased cytoplasmic Ca^{2+} response upon stimulation with both sucrose and H_2O_2 (214), whilst its suppression by antisense RNA prevented sucrose-induced Ca^{2+} release (132). Aluminium has also been shown as an inhibitor of the SV/TPC current (214).

One controversial paper shows that whilst knock-out of AtTPC does abolish the SV current, this in fact has negligible impact on the overall cytoplasmic Ca^{2+} homeostasis (361), this suggests that there are other vacuolar Ca^{2+} channels compensating for TPC action.

Plant TPCs have the same homologous voltage-sensing region on S4 as the voltage-gated Ca^{2+} channels, and have shown an element of voltage-gating but seemingly at non-physiological potentials (289). Current consensus is that the plant TPC is more likely to function as a Ca^{2+}-gated channel rather than a voltage-gated channel (176). A recent study investigated the effect of known Ca^{2+}-signalling molecules on the SV current, Ca^{2+}, calmodulin and nucleotides all caused Ca^{2+} release (351); disappointingly, NAADP was not amongst the compounds studied.

The Ca^{2+}-dependence of plant TPCs is further supported by evidence that SV/TPC channels show CICR (340). Analysis of the amino acid sequence reveals the presence of two EF-hand motifs located on the cytoplasmic loop between the two domains (336). Despite these EF-hands being highly conserved amongst plant TPCs, sequence alignments of the cytoplasmic loop of animal TPCs predicts that they do not have the same Ca^{2+} sensing capabilities as the EF-hands are absent (333).

1.9.6 Sea urchin TPCs

As much of the seminal work on the pharmacology of NAADP was conducted on sea urchin egg homogenates, the TPCs from *Strongylocentrotus purpuratus* were some of the first to be fully investigated.

The sea urchin has three isoforms of TPC (SpTPC1, SpTPC2 & SpTPC3), all of which possess distinctive properties attributed to the putative NAADP receptor, namely: NAADP binding, localisation to acidic organelles and a correlation with increased Ca^{2+} signals in response to NAADP.

NAADP binding was shown by immunoprecipitation of endogenous TPCs from sea urchin egg homogenates, the immunopurified complexes showed nM affinity for NAADP in a radioligand binding assay (375).

The subcellular localisation of SpTPCs has been investigated by heterologous expression in various systems: *Xenopus* oocytes, mammalian cell lines (SKBR3 & HEK293) and oocytes from the closely related starfish *Asterina miniata*. All three isoforms tended to show a punctate subcellular distribution across all systems. This could attributed to acidic stores in SKBR3 cells due to partial colocalisation with LysoTracker red (49) and to cortical granules (acidic vesicles) in the starfish. More detailed dissection of SpTPC localisation was conducted in the HEK293 cells revealing that whilst SpTPC2 showed a strong lysosomal localisation, there was a more disparate distribution of SpTPC1 and SpTPC3 as these colocalised with markers for late and recycling endosomes (375).

The overexpression of SpTPCs in mammalian cell lines also correlated with augmented Ca^{2+} signals in response to NAADP delivered by microinjection (49) or NAADP-AM (a membrane permeant ester which is broken down by cytoplasmic esterases to release NAADP) (375). Furthermore, this NAADP-evoked Ca^{2+} release could be inhibited by pre-treatment with bafilomycin A1, Ned-19 and sub-threshold concentrations of NAADP, which conforms with the pharmacology predicted from the sea urchin homogenate.

Whilst all current studies concur as to the role of SpTPC1 and SpTPC2 in augmenting NAADP-mediated Ca^{2+} release, the function of SpTPC3 is still under dispute (49, 375). Overexpression of SpTPC3 reduced basal levels of NAADP-evoked Ca^{2+} release in wild type HEK293 cells, and inhibited the increase attributed to SpTPC2 when both isoforms were coexpressed (375). However, in SKBR3 cells, SpTPC3 showed

an augmented Ca^{2+} signal in response to NAADP albeit smaller than SpTPC1 and SpTPC2 (49).

Although these studies have further associated TPCs in NAADP-mediated Ca^{2+} signalling, the heterologous overexpression of sea urchin proteins in mammalian cell lines may not yield physiological results. In fact, the overexpression of SpTPCs in HEK293 cells was shown to dramatically alter lysosome morphology and endolysosomal trafficking (375), more akin to the pathophysiology of lysosomal storage disorders such as Niemann-Pick C1 (254) (see section 6.8).

The human TPCs have also been implicated in pathophysiological conditions.

1.9.7 Human TPCs

Homo sapiens express both TPC1 and TPC2, encoded by the genes *TPCN1* (chromosome 12q24.13) and *TPCN2* (chromosome 11q13), respectively. Since their initial cloning of TPC1 from rats by Ishibashi *et al.* in 2000 (199) very little work has been conducted on mammalian TPCs. The human isoform of TPC1 has not been implicated in anything other than NAADP signalling. However, TPC2 has appeared in three very disparate fields and shown an association in cancer pathology (190), hereditary deafness (216) and hair pigmentation (413).

The chromosomal region upon which *TPCN2* is situated (11q13) is amplified in a wide variety of tumours, including 50 % of human oral carcinomas and 20 % of other organs such as esophageal, breast, lung, bladder and pancreatic cancers (109, 141, 157, 354, 417). *TPCN2* has been identified as one of three genes on the 11q13 amplicon, suggesting that TPC2 overexpression may contribute to accelerated growth and metastatic potential of cancer cells (190). The mouse equivalent, the 7F5 amplicon also contains the *Tpcn2* gene (190). Despite this conserved link, it is thought that it is the concerted overexpression of all the genes on the 3.6 Mb 11q13 amplicon rather than any individual gene that results in the carcinoma.

Another pathological link has been shown between *TPCN2* and hereditary hearing impairment in certain families: one Turkish (209) and four Pakistani (216). They show autosomal recessive nonsyndromic deafness which correlates with differences on chromosome 11q13.2-q13.4. *TPCN2* was one of 13 candidate genes within this region but as there were no mutations in the genes from affected individual it suggests that this defect is due to a different expression level or splicing alterations. Indeed the Turkish

family revealed five exonic and four intronic TPC2 variants (209). Hearing impairment is a known symptom of several lysosomal storage disorders (210), and thus abnormal lysosomal Ca^{2+} release by a dysfunctional TPC2 is a plausible cause of deafness.

A slightly less detrimental role of *TPCN2* is hair colour determination. The gene has been directly implicated in human pigmentation of Scandinavians from a genome-wide association study (413). Four single nucleotide polymorphisms (SNPs) in *TPCN2* were associated in defining hair colour in a > 5000 Icelandic population, these resulted in two TPC2 variants which were distinct in blond and brown haired individuals. These results were confirmed in a follow up study involving a population of > 1000 Dutch people (413). A link between hair pigmentation and Ca^{2+} transporters has been reported in two other genes, both are $Na^+/K^+/Ca^{2+}$ exchangers encoded by the genes SLC24A4 (414) and SLC24A5 (230). These are both thought to be localised within an intracellular membrane, likely to be the melanosome or a precursor (230). The melanosomes are small lysosome-related organelles which produce and release the pigment melanin to keratinocytes. Melanosomes are derived from similar precursors to lysosome (362), therefore it is not unlikely that melanosomal membranes may contain TPC2.

When TPC2 was first linked to the NAADP signalling pathway its expression levels in various human organs was determined by Northern blotting. A ubiquitous expression was seen but particularly distinct were the higher levels present in the kidney and the liver (figure 1.17) (55). This localisation is similar to previous studies of TPC1 rat tissues (199). The liver and the kidneys have myriad roles in controlling metabolic and homeostatic functions in the body, the prevalence of TPCs in these organs emphasises their potential role in the tight regulation of Ca^{2+} homeostasis and intracellular signalling.

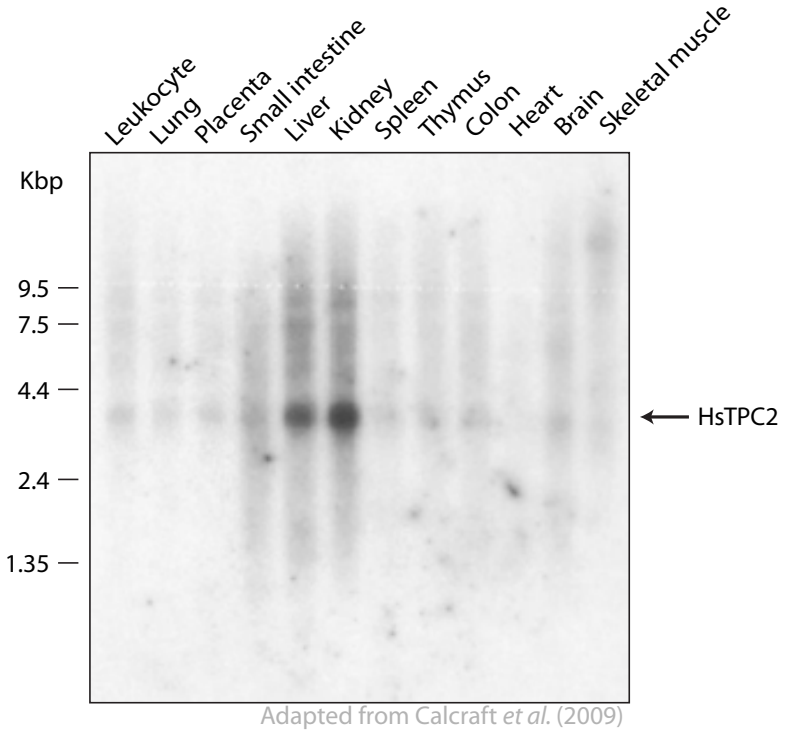


Figure 1.17: Northern blot analysis of endogenous TPC2 expression in human tissues. The 3.2 kbp band is seen across all tissues. The highest expression was seen in kidney and liver tissue (55).

1.10 The TPCs as the NAADP receptor

This previously uncharacterised family of ion channels has met the defined criteria: their homology to known Ca^{2+} channels, the defined pharmacological properties together with their localisation to lysosomes and predicted molecular mass implicate TPCs as the long sought-after NAADP receptor.

By establishing this crucial relationship, one of the major questions in the field of NAADP signalling has been resolved. However this presents a host of new questions which to answer will require a huge collaboration across the many fields of biology.

To begin on the molecular scale, the biochemistry of the channel protein, its structure and quaternary interaction with other proteins needs investigating as this may give clues towards how this channel functions. A crucial question is in the multimerisation of TPCs due to the predicted homology with the VGCCs it is likely that TPCs form dimers to assemble to 24-TM domain channel pore, whether these are homo- or heterodimers may govern ligand binding and Ca^{2+} conductance.

With this in mind, the electrophysiological characteristics of the TPCs including the ion selectivity, conductance, voltage sensitivity and channel gating still need to be determined. Traditional patch clamp methodologies suitable for plasma membrane channels would be inappropriate for these intracellular channels, so the precedent set by the RyR and IP_3R of single channel recordings in a lipid bilayer would provide a means of establishing these biophysical properties.

Considering the extensive pharmacology conducted on the NAADP signalling pathway, the mechanisms of action are still yet to be associated with the TPC protein. Identification of the NAADP binding site(s), and how analogues interact with the TPCs would unequivocally confirm this protein as the receptor; however, the possibility of accessory binding proteins such as the FKBPs in RyRs should not be discounted. The mechanisms behind the characteristic desensitisation also need dissecting and further resolution is also required of the interactions by TPCs with the ER Ca^{2+} channels and plasma membrane receptors.

On the larger scale, the roles that the TPCs play in the whole organism and in knock-out animals are still unresolved and more connections with aberrant TPC function resulting in disease are likely to be found. Already studies linking abnormal Ca^{2+} signals in the regulation of autophagy and defects in the endolysosomal pathway (159)

implicate a potential role of TPCs in cell wounding, plasma membrane repair and organelle-trafficking pathophysiology.

Finally the genetics of this family of proteins require investigation. Whilst the position of the TPCs as evolutionary intermediates between the VGCCs and the TRP channels seems likely, the variation in isoform expression across the species varies wildly, with an explosion of plant isoforms and yet the redundancy of TPC3 in primates and other mammals.

1.11 The aims of this thesis

This thesis aims to tackle some of the fundamental molecular characteristics of the human TPC isoforms. Building on the properties of NAADP signalling as discussed in this introductory chapter and by analogy with the established IP_3R and RyR, this thesis will investigate the following questions:

What are the channel properties of HsTPC2? As TPC2 was initially postulated as the most likely candidate for the NAADP receptor, this thesis begins by discussing the purification of HsTPC2 from an overexpressing cell line and its reconstitution into a lipid bilayer. The resulting single channel recordings establish HsTPC2 as a K^+/Ca^{2+}-permeable NAADP-gated cation channel. The channel regulation by luminal $[Ca^{2+}]$ and luminal pH will also be shown. Furthermore, the pharmacology of HsTPC2 channel activity is consistent with NAADP signalling seen in the sea urchin homogenate and mammalian systems.

How does HsTPC2 behave in a native lysosomal membrane? This next question will be answered by the purification of lysosomes for direct patch clamp studies. This methodology allows measurement of NAADP-induced Ca^{2+}-currents from a population of HsTPC2 channels within the native lysosomal environment. The dose-response relationship of NAADP, together with preliminary pharmacology conform to predicted models, those discrepancies that are seen are discussed.

What is the native configuration of the HsTPC channel? Finally the protein interactions within a TPC complex will be investigated by mass spectrometry. Clarification will also be sought regarding the putative dimerisation of the two HsTPC isoforms by coimmunoprecipitation, immunofluorescence and FRET. The tendency for hetero-/homodimerisation and the orientation of the interaction are investigated and discussed.

Overall, this thesis attempts to combine the biochemistry and electrophysiology of the HsTPC proteins and put them in the context of NAADP and Ca^{2+} signalling mechanisms.

Chapter 2

Materials and Methods

2.1 Materials

All chemicals were purchased from Sigma-Aldrich unless otherwise stated. The country of origin is only mentioned for companies which do not have registered UK subsidiaries.

2.2 Bioinformatics

Sequences for the HsTPCs were obtained from the NIH National Center for Biotechnology Information (NCBI) server, which currently lists 13 protein entries for TPC1 (TPCN1) and 9 entries for HsTPC2 (TPCN2). The sequences chosen were those cloned by Zhu *et al.* first published in Calcraft *et al.* (55).

HsTPC1: Accession number AY083666
HsTPC2: Accession number AY029200

2.2.1 Sequence alignments

The amino acid sequences for the VGCC family and TPC isoforms across species were compared by constructing a multiple sequence alignment using CLUSTALW (422).

2.2.2 Phylogenetic analysis

The aligned sequences were converted into phylogenic trees on the basis of the proportion of amino acids that differed between isoforms using the neighbour-joining method

carried out by the software programme Treeview X (323).

2.2.3 Protein sequence analysis

General analysis of amino acid sequences were conducted by online software provided by many academic institutions, compiled on ExPASY (143). These included cDNA-translations (144) and predictions of molecular weight (M_w), iso-electric point (pI) (43) and post-translational modifications (166).

2.2.4 Hydropathy plot

Various providers of online prediction software were used to analyse the HsTPC sequence and predict topology based on hydropathy predictions. The programmes used are listed below:

- DAS - dense alignment surface method (98);
- HMMTOP - prediction of transmembrane helices and topology of proteins (433);
- PredictProtein - prediction of transmembrane helix location and topology (372);
- TMHMM - prediction of transmembrane helices in proteins (300);
- TMPred - prediction of transmembrane regions and protein orientation (185); and
- TopPred - topology prediction of membrane proteins (88).

All programmes were set to consider a 9 amino acid window size for transmembrane domains. Predictions were compared and the final representative prediction used was provided by the TMHMM server (CBS, Denmark).

2.3 Expression and extraction of HsTPC proteins

2.3.1 Cell culture

Wild type HEK293 cells were maintained in Dulbecco's modified Eagle medium (DMEM) supplemented with 10 % (v/v) fetal bovine serum (FBS, Biosera), 2 mM glutamine (Invitrogen) as well as antibiotics 100 U/ml penicillin (Invitrogen) and 100 µg/ml streptomycin (Invitrogen). Cells were kept at 37 °C in a humidified culture incubator supplied

with 5 % (v/v) CO_2. After reaching confluency, cells were partly digested with 0.05 % trypsin (Invitrogen) to give a cell suspension, diluted in desired medium and propagated in new flasks.

2.3.2 Stable HEK293 cell lines

Stable clones of HEK293 cells over-expressing HsTPC1 with a C-terminal hexa-histidine (His_6) tag or HsTPC2 with an N-terminal hemagglutinin (HA) tag were generated in Dr Mike Zhu's group (Ohio State University, US). Details of how these cells were generated are included in Calcraft *et al.* (55); briefly the HA epitope and HsTPC2 cDNA were subcloned into pIRESneo vector (BD Biosciences), whereas the His_6 epitope and HsTPC1 cDNA were subsubcloned into the pIREShyg2 vector (BD Biosciences). Cells were transfected with Lipofectamine 2000 (Invitrogen) following the manufacturers protocol. Monoclonal cell lines were generated via limiting dilution under selective conditions. Cells were cultured as described above, however to maintain selectivity the cell culture medium contained selective antibiotics: 100 µg/ml hygromycin (Invitrogen) for HsTPC1 and 200 µg/ml geneticin (Invivogen) for HsTPC2.

2.3.3 Long-term cell storage

Stocks of each cell line were maintained in a liquid nitrogen cell bank at −195 °C. Cells were prepared for storage as a single-cell suspension in a freezing medium of FBS with 10 % (v/v) DMSO which was cooled slowly to −80 °C in an isopropanol cooling chamber, before transfer to the cell bank.

2.3.4 Membrane preparation

To crudely purify cell membranes, confluent cells were harvested in ice-cold phosphate-buffered saline (PBS) and washed twice by centrifugation at 1500 xg for 3 minutes at 4 °C. To aid lysis, the cells were osmotically swollen by a 30 minute incubation on ice with hypotonic buffer (20 mM HEPES, 1 mM EDTA; pH 7.2 supplemented with a cocktail of protease inhibitors (Roche)). Lysis was completed by mechanical disruption using a Dounce tissue homogeniser and a tight pestle for 15 strokes on ice (other methods of homogenisation are discussed in section 2.12.5). Cell lysis could be observed under a light microscope. Nuclei and unbroken cells were pelleted during a

centrifugation at 1500 xg for 3 minutes at 4 °C. Crude membranes were pelleted from the supernatant by ultra-centrifugation at 100,000 xg for 1 hour in a vacuum at 4 °C. The pellet was resuspended and either used directly or snap frozen in liquid nitrogen and stored at −80 °C.

2.3.5 Removal of sugar groups

To remove the sugar residues and determine the intrinsic molecular weight of the HsTPC1 and HsTPC2 proteins, the enzyme Peptide N-Glycosidase F (New England BioLabs) was used according to the manufacturer's guidelines. Briefly, 20 µg total membrane protein was incubated with a denaturing buffer (provided) and protease inhibitors (Roche) for 30 minutes at room temperature. 2 µl of enzyme mixture (500 U/µl) was added with the buffer provided and NP40 as a detergent and incubated for 1 hour at 37 °C. The sample was then mixed with a reducing SDS PAGE loading buffer (Sigma) ready for analysis.

2.3.6 Solubilisation of the membranes

Membranes were resuspended to a concentration of 1 mg/ml in IP buffer (150 mM NaCl, 20 mM HEPES; pH 7.2) containing 1 % CHAPS, a zwitterionic detergent. After incubation for 1 hour at 4 °C with agitation the mixture was ultra-centrifuged at 50,000 xg for 30 minutes at 4 °C to pellet all insoluble contaminants. Solubilised membranes were used as a starting material for further purification.

2.4 Protein quantification

2.4.1 Bicinchoninic acid assay

Solubilised protein was diluted in 100 mM NaOH to a ratio of 1 : 50. 20 µl samples were plated in triplicate into 96-well clear bottomed microplate wells. Along side 20 µl of bovine serum albumin (BSA) standards (0 - 1500 µg/ml) in 100 mM NaOH were also plated in triplicate.

To each well 200 µl of reagent (3.2 mM $CuSO_4$ in bicinchoninic acid (BCA)) was added. The plate was incubated at 37 °C for 1 hour and the absorbance measured at 562 nm on a Novostar plate reader (BMG LABTECH). The BSA standard curve of

$A_{562\ nm}$ was plotted (Microsoft Excel) as a linear relationship and interpolated for each unknown sample.

2.4.2 EZQ protein quantification

The EZQ protein quantititation kit (Invitrogen) was used following the manufacturer's instructions to determine the protein concentration of samples which contained chemicals incompatible with the BCA assay, or for quantitation of antibody concentration or where sample volume was low. Briefly, 1 µl of ovalbumin (chicken egg) protein standard (prepared in 100 mM NaOH) or 1 µl of sample (diluted in 100 mM NaOH) was applied to the assay paper in triplicate and allowed to air-dry. The protein was fixed and contaminating substances (e.g. reducing agents and salts that might be present) removed by incubating the assay paper in methanol for 5 minutes at room temperature with gentle agitation. The assay paper was air-dried and incubated with the EZQ protein quantitation reagent at room temperature, agitated gently on an orbital shaker for 30 minutes. After staining, the assay paper was rinsed for 1-2 minutes in 10 % (v/v) methanol, 7 % (v/v) acetic acid for a total of three washes, and imaged using a Typhoon 9400 imager (GE Healthcare) using 457 nm excitation and a 610 nm emission filter. A standard curve was plotted (Microsoft Excel) for fluorescence values of the standards versus the corresponding protein concentration and the experimental protein concentration of samples determined from the standard curve.

2.4.3 Spectrophotometer

A rapid protein concentration was determined by UV absorbance at 280 nm on a nanospectrophotometer (Implen). Due to strong nucleotide absorbance at 280 nm, the absorbance was also measured at 260 nm. Using the established absorbance constants for protein and nucleotides at these wavelengths the nanospectrophotometer automatically calculated the protein concentration by the Warburg equation (448):

$$\text{Protein (mg/ml)} = (1.55 \times A_{280}) - (0.76 \times A_{260})$$

This method gave a quick and approximate estimate of protein concentration but was not as accurate as those assays detailed above.

2.5 Protein electrophoresis and blotting

2.5.1 SDS PAGE

Sodium dodecyl-sulphate (SDS) polyacrylamide gel electrophoresis (PAGE) separates denatured proteins by molecular weight. Typically, SDS-PAGE was performed using Mini-PROTEAN 3 vertical electrophoresis system (Bio-Rad). Resolving gels (8.6 × 7.3 × 0.1 cm) of 8 % to 12 % were prepared by diluting 30 % (v/v) 37.5 : 1 acrylamide : bis-acrylamide (National Diagnostics) in 400 mM Tris-HCl pH 8.8, 0.1 % (w/v) SDS, 0.1 % (w/v) ammonium persulphate and 0.1 % (v/v) Tetramethylethylenediamine (TEMED). Cast resolving gels were overlaid with H_2O-saturated butanol and allowed to polymerise for at least 15 minutes. This was surmounted by a stacking gel comprising of 4 % (v/v) acrylamide, 125 mM Tris-HCl pH 6.8, 0.1 % (w/v) SDS, 0.1 % (w/v) ammonium persulphate and 0.1 % (v/v) TEMED, into which a comb (1 mm thick) was placed to generate wells, again this was left to polymerise for ≈ 15 minutes.

Protein standards were loaded in one of the wells (PAGEruler Plus, Fermentas). Electrophoresis was performed at 100 V in running buffer: 25 mM Tris-base, 192 mM glycine and 0.1 % (w/v) SDS; pH 8 at room temperature.

In some experiments precast 8 % - 12 % acrylamide gels were used (Precise, Pierce). These required a running buffer of: 100 mM Tris, 100 mM HEPES, 3 mM SDS; pH 8.

Protein samples (50 µg, unless otherwise stated) were prepared in Laemmli buffer (62.5 mM Tris-HCl, 2 % (v/v) SDS, 10 % (v/v) glycerol, 0.02 % (w/v) bromophenol blue; pH 6.8) and reduced by the addition of 10 mM Dithiothreitol (DTT) or 2 % (v/v) β-mercaptoethanol. Samples were not boiled, as boiling was shown to increase hydrophobic aggregation.

2.5.2 PFO PAGE

Native gel, perfluoro-octanoic acid (PFO) PAGE as described in (360) separates proteins by molecular mass without disrupting multimeric interactions. Gels were prepared as in section 2.5.1 however the SDS was omitted. The running buffer for electrophoresis was 25 mM Tris, 192 mM glycine, 0.5 % (w/v) PFO; pH 8.5. Electrophoresis was run at 100 V at 4 °C.

2.5.3 Protein staining

To ubiquitously stain all proteins within a gel, the gel was first washed 3 times for 5 minutes in distilled, deionised water. The gel was then treated with a coomassie dye or, for greater sensitivity, stained by silver precipitation.

To stain using a dye, the gel was submerged in a commercial solution which contained coomassie brilliant blue R-250 (Imperial Blue, Pierce) and left to incubate for 1 hour at room temperature with agitation. The gel was then washed repeatedly with distilled, deionised water until bands could be resolved. This took between 1 hour and overnight, depending on protein concentration.

The silver stain was conducted following the manufacturer's recommendations (Pierce silver stain kit). Briefly, the proteins were first fixed by submerging the gel in a mixture of acetic acid and ethanol, then was washed twice with 10 % ethanol and the gel was incubated in the silver stain for 30 minutes at room temperature with agitation. This was subsequently washed away with distilled, deionised water and replaced with a developer solution which caused the precipitation of silver in the presence of protein. Once bands were resolved, the reaction was quenched by 5 % acetic acid.

The gels were scanned using a flat-bed scanner (Epson Perfection 3490).

2.5.4 Western Blotting

Once proteins had been resolved by SDS PAGE, the gel was blotted onto a non-reactive Polyvinylidene Fluoride (PVDF) membrane (0.45 µm pore size, GE Healthcare) submerged in a transfer buffer (25 mM Tris-base, 192 mM glycine; pH 8.2) cooled with an ice pack, and held under a constant current of 300 mA for 1 hour. Protein transfer was confirmed with Ponceau S staining solution (0.2 % (w/v) Ponceau S in 3 % (v/v) acetic acid), which is washed from the membrane in ultrapure water.

Non-specific antibody interactions were blocked by pretreating the blotted membrane with a high protein solution, either 1 % (w/v) Bovine Serum Albumin (BSA) or more usually 5 % (w/v) skimmed milk powder (Marvel) dissolved in PBS, 0.5 % (v/v) Tween-20 (PBST), for 1 hour at room temperature. The choice of blocking solution depended on the chemiluminescent reagent, for a more sensitive western blot BSA was used as milk proteins gave a higher level of background.

Antibodies (Table B.3) were diluted in blocking buffer (PBST, 5 % milk powder) and incubated with the membrane for 1 hour at room temperature or overnight at 4 °C. Membranes were washed 5 times for 10-15 minutes with PBST. The horseradish peroxidase (HRP) conjugated secondary antibody was diluted in blocking solution, incubated and washed as before. To visualise the presence of the HRP, the membranes were treated with the chemiluminescent ECL reagent (Pierce) for 1 minute, or Supersignal Pico (Pierce) for 5 minutes. The treated membrane was then exposed to Blue-Sensitive (Cole-Parmer) autoradiography film. The film was then fixed and developed (Xograph film processor) to reveal the specific bands.

2.5.5 Stripping membranes

To re-probe membranes with a different primary antibody the membranes were stripped by treatment with stripping buffer (62.5 mM Tris.HCl, 2 % (w/v) SDS, 100 mM β-mercaptoethanol; pH 6.7) for 40 minutes at 60 °C. The membrane then needed to be re-blocked before antibodies were added.

2.6 Gel filtration

To separate all soluble proteins by size, a Superdex 200 HR 10/30 column with a 25 ml bed volume (GE Healthcare) was connected to an AKTA Fast Protein Liquid Chromatography (FPLC) Chromatographic System (GE Healthcare). All apparatus was cooled to 4 °C. The column was equilibrated with the the cell lysate buffer (150 mM NaCl, 20 mM HEPES; pH 7.2) and 1 % CHAPS for more than two bed volumes before loading samples.

To determine the separation parameters of the column, several protein standards of varying molecular weight (see figure 2.1) were added to the column and their efflux measured by UV absorption at 280 nm at the base of the column. Each run was prepared with the same parameters: 1 mg protein, flow rate 0.5 ml/min, running buffer 150 mM NaCl, 20 mM HEPES, 1 % CHAPS; pH 7.2. A standard curve showing the molecular weights against the elution volumes is shown in figure 2.1.

To separate membrane proteins, 250 µl of solubilised sample (up to 5 mg total protein) were loaded onto the column. The separation was performed with a flow

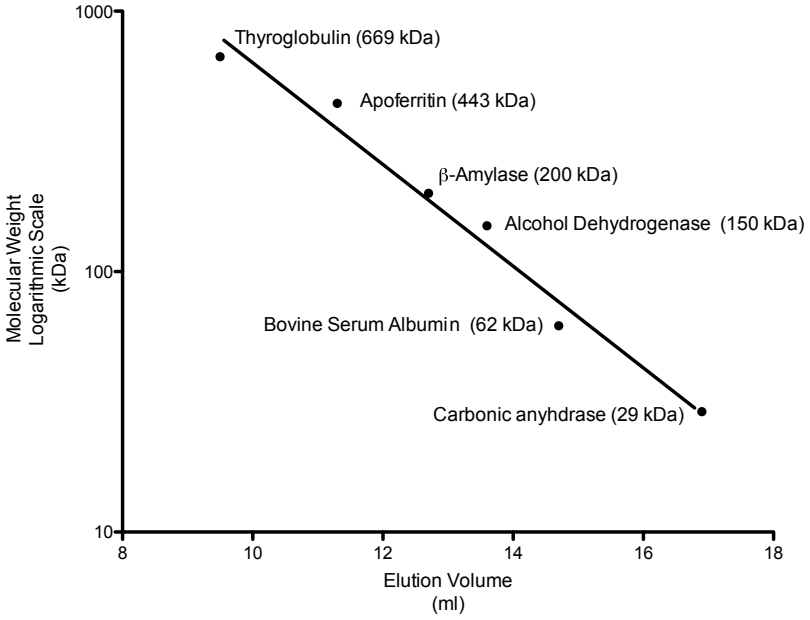


Figure 2.1: Protein standards with known molecular weights (indicated in brackets) were loaded onto the Superdex 200HR 10/30 column for gel filtration with IP buffer and 1 % CHAPS. The elution volumes were plotted against the molecular weights of the standards proteins. The curve was analysed with linear regression in Prism (GraphPad, $r^2 = 0.97$).

rate of 0.5 ml/min. Fractions were collected (2 ml each) via an automated collector controlled by the system.

2.7 Antibody generation and purification

Antibodies specific for HsTPCs were raised commercially (Eurogentec) by immunizing rabbits simultaneously with two specific peptides derived from the protein sequences coupled to keyhole limpet haemocyanin (KLH) as a carrier. HsTPC1: peptide a - IQEWYEEHAREQEQQR ; peptide b - APAAQQPPGSRQRSQTVT. HsTPC2: peptide a - GGKQDDGQDRERLTY; peptide b - VKEHPPRPEYQSPFL. Specific antibodies could not be purified using these peptides due to the lack of necessary cysteine residues required, hence new peptides were synthesised HsTPC1: peptide a - CIQWEYEEHAREQEQQR ; peptide b - CAPAAQQPPGSRQRSQTVT. HsTPC2: peptide a - CGGKQDDGQDRERLTY; peptide b - CVKEHPPRPEYQSPFL. These were conjugated to Sulfo-link agarose (Pierce) according to the manufacturers' instructions. Specific antibodies were purified form the immunized rabbit serum and eluted in 0.1 M glycine.HCl; pH 2.5, the eluate was neutralised with 1.5 M TRIS; pH 8.8. Antibody-containing fractions were determined by absorbance at 280 nm and were dialysed into PBS, 50 % glycerol, to be stored at 4 °C.

2.8 Immunoprecipitation

The human TPCs were purified from the solubilised crude membrane by specific antibodies bound to a solid substrate of Sepharose beads (GE Healthcare).

2.8.1 Covalently coupling antibodies to beads

To avoid antibody contamination in the final protein sample, the antibody and the solid substrate were covalently linked. Sepharose beads (GE Healthcare) were washed three times with PBS and incubated with depleted serum or purified antibodies for 1 hour at room temperature. If using serum, carrier protein antibodies had been depleted from the serum by incubation with KLH or BSA coupled agarose for 1 hour at room temperature.

The beads were then washed twice with 10 volumes of 0.2 M $Na_2B_4O_7$ (pH 9.0) to remove the excess antibodies and to create the alkaline environment required for optimal coupling efficiency. The coupling reagent, dimethyl pimelimidate (DMT) was added to a final concentration of 20 mM in 0.2 M $Na_2B_4O_7$. The mixture was incubated at room temperature for 30 minutes, for the reaction to complete. To stop the reaction, the slurry was washed once with 0.2 M ethanolamine (pH 8.0) and then left for 2 hours in 0.2 M ethanolamine with mixing at room temperature. Finally the beads were washed twice with PBS and stored at 4 °C in PBS with 0.05 % azide.

2.8.2 Immunoprecipitation of TPC protein complex

Sepharose beads coupled to antibodies (see section 2.8.1) were washed twice with cold PBS and once with IP buffer (150 mM NaCl, 20 mM HEPES; pH 7.2) containing 1 % CHAPS. The beads were then added to samples of solubilised membranes which had been pre-cleared by addition of non-immune control serum coupled covalently to Protein-A Sepharose for 1 hour at 4 °C with constant agitation. The ratio used was 100 µl of bead bed volume per mg of total protein. The immunoprecipitation was incubated with continual mixing for 1 hour at room temperature or overnight at 4 °C.

Once the proteins had bound, the beads were pelleted by centrifugation at 1000 xg for 2 minutes. Following removal of the supernatant, the beads were washed once with IP buffer containing 1 % CHAPS, followed by two washes containing 0.1 % CHAPS. The immunoprecipitated protein complexes were eluted from the beads by incubation with the peptides used to raise the antibody, at a concentration of 50 µg/ml in 0.1 % CHAPS and 0.05 % phosphatidylcholine for 4 hours at 4 °C with constant agitation. For direct analysis by western blotting the protein was eluted by 5 minute incubation with Laemmli denaturing buffer (62.5 mM Tris-HCl, 2 % (v/v) SDS, 10 % (v/v) glycerol, 0.02 % (w/v) bromophenol blue; pH 6.8).

2.8.3 Dialysis

If the purified TPC protein complex was destined for functional analysis in the lipid bilayer, the detergent (0.1 % CHAPS) was dialysed from the solution. The elution from the immunoprecipitation was added to a 20 kDa molecular-weight cut-off dialysis chamber (Slide-A-Lyzer MINI, Pierce) which was floated in a solution of: 100 mM NaCl, 25 mM PIPES, 0.15 mM $CaCl_2$, 0.1 mM EGTA; pH 7.4. The buffer was 1000

times the volume of the sample and was changed at least every 4 hours. The dialysis was conducted at 4 °C over 36 hours. After dialysis an equal volume of 0.5 M sucrose was added to the sample and this mixture was left to equilibrate for 30 minutes at 4 °C. The stabilised complex was snap frozen in liquid nitrogen and stored at −80 °C.

2.9 Radioligand binding

2.9.1 Saturation binding

Immunoprecipitated proteins were eluted from the beads as above. 100 µl samples were mixed with radiolabelled NAADP (synthesised in house (249)) to give a final concentration of 0.2 nM [^{32}P]NAADP in 250 µl. The reaction was incubated for 1 hour at room temperature, in the presence or absence of 100 µM unlabelled NAADP. All NAADP solutions were in a binding buffer of 140 mM KOAc, 20 mM HEPES; pH 7.2.

To precipitate the solubilised proteins, 50 µl of γ-globulins (10 mg/ml) were added alongside 300 µl of 30 % poly(ethylene glycol) (PEG, average M_n) in binding buffer and incubated on ice for 30 minutes. The precipitate was pelleted by centrifugation at 14,000 xg for 5 minutes and the supernatant aspirated and disposed. The pellet was washed with 500 µl of 15 % PEG, which was promptly aspirated and disposed. 1 ml of distilled, de-ionised water was used to resuspend the pellet.

The suspension was then vacuum filtered through GF/B filters (Whatman) on a cell harvester (Brandel) or a smaller manifold with a lower vacuum pressure. The filters were washed three times with approximately 3 ml of wash buffer (20 mM HEPES; pH 7.2) Filters were exposed to a phosphor screen (Amersham Biosciences) overnight and this was analysed on a Typhoon 9400 Phosphor Imager (GE Healthcare) at a resolution of 100 microns. The resulting image was analysed using ImageQuant software (GE Healthcare). The specific binding was determined by subtracting non-specific binding (seen in the presence of unlabelled NAADP) from total binding. The results plotted with Prism (Graphpad) alongside a positive control of solubilised mouse liver.

2.10 Incorporation of HsTPC2 into bilayers

The purified TPC2 complex was incorporated into planar lipid bilayers under voltage-clamp conditions as described in (396).

2.10.1 Forming the bilayer

The neutral phospholipid Phosphatidylethanolamine (Avanti PolarLipids) was dissolved in decane (30 mg/ml) and this solution was painted across a 150 µm diameter aperture in a teflon cup which separated two fluid-filled compartments; the *cis* (0.5 ml) and *trans* (1 ml) chambers. As the painted lipid thinned to form a bilayer, the capacitance across the aperture dropped, a good bilayer had a capacitance around 80 - 120 pF.

2.10.2 Channel incorporation

HsTPC2 vesicles were added to the *cis* chamber where they incorporated into the bilayer in a fixed orientation so that the *cis* chamber corresponded to the cytosolic space and the *trans* chamber to the lysosomal lumen. This fixed orientation has previously been reported in SR vesicles (292, 426). The *trans* chamber was clamped at ground, whilst the *cis* chamber was clamped at various potentials relative to ground. The electrodes used were Ag-AgCl with 2 % agar, 3 M LiCl bridges. All current measurements across the bilayer were converted by an operational amplifier (291).

Current fluctuations were measured at room temperature, with either Ca^{2+}or K^{+} as the permeant ion.

2.10.3 Data acquisition and analysis

Current recordings were filtered at 800 Hz (-3 dB) and digitized at 20 kHz (ITC-18, Instrutech Corporation) with WinEDR v2.5.9 (Strathclyde University) or Pulse (HEKA, Germany). Measurements of single-channel current amplitudes were made using the single-channel analysis software WinEDR V2.5.9 (Strathclyde University). The closed and open current levels were assessed manually using cursors. Amplitude histograms were obtained from single-channel data using Clampfit version 10.2 (Molecular Devices, USA) and fitted with Gaussian curves. In all records, amplitude histograms were best fit with a single Gaussian function representing the main conductance level. Sub-conductance state gating was too brief to be detected by this method of analysis. The channel open probability (Po) was determined over 3 minutes of continuous recording, using the method of 50 % threshold analysis (396). Concentration-response curves were fit using a four parameter logistical equation in Prism (Graphpad). The

Table 2.1: Solutions used in lipid bilayer studies. Ion composition of solutions, pH was titrated with 1 M acetic acid or 1 M KOH. Sucrose was used to adjust osmolarity.

Conducting ion	***cis* chamber**	***trans* chamber**
Ca^{2+}	250 mM HEPES 80 mM Tris 15 µM free Ca^{2+}	10 mM HEPES 250 mM glutamic acid 50 mM free Ca^{2+}
	Both chambers pH 7.2	
K^+	**Symmetrical**	
	210 mM KCl 10 mM HEPES 50 mM free Ca^{2+} Both chambers pH 7.2	
$K^+_{\text{Low pH}}$	***cis* chamber**	***trans* chamber**
	250 mM HEPES 80 mM Tris 15 µM free Ca^{2+} pH 7.2	10 mM HEPES 210 mM KOAc 15 µM free Ca^{2+} pH 4.8

The free $Ca^{2+}$of all solutions was measured using a Ca^{2+}electrode (Thermo Orion, USA).

Ca^{2+}/K^+ permeability ratio ($P_{Ca^{2+}}/P_{K^+}$) was calculated using the equation given by Fatt and Ginsborg (123):

$$P_{Ca^{2+}}/P_{K^+} = \frac{[K^+]_e}{(4.[Ca^{2+}]_i)}.e^{(\frac{E_{rev}F}{RT})}.(1 + e^{(\frac{E_{rev}F}{RT})})$$

Where: F is the Faraday constant; R is the gas constant; the value of RT/F was based on the recording temperature of 22 °C and was considered constant at 25.4 mV; E_{rev} is the reversal potential; $[K^+]_e$ is the activity of K^+ in the external solution; and $[Ca^{2+}]_i$ is the activity of Ca^{2+}in the internal solution. The activity coefficients $\gamma_{Ca^{2+}}$ and γ_{K^+} were: 0.5 and 0.75, respectively.

The zero current reversal potential (E_{rev}) was obtained under bi-ionic conditions (210 mM KCl, 20 mM HEPES, pH 7.2 *cis*: 210 mM $CaCl_2$, 20 mM HEPES, pH 7.2 *trans*) and represented the point where no current could be detected.

2.11 Lysosomal swelling

Lysosomes to be used for patch clamp experiments were induced to swell as the enlarged diameter of the lysosomes increased the likelihood of giga-ohm seal formation. Lysosomal swelling was induced by treatment with the small chemical vacuolin or by prolonged sucrose treatment.

As published in Cerny *et al.* (66) vacuolin can induce homotypic fusion of endosomes and lysosomes, HEK293 cells were treated with 1 µM vacuolin in wild type cell culture medium, for 2 hours under normal cell culture conditions (37 °C, 5 % CO_2, humidified).

Lysosome swelling was also induced by overnight incubation of cells in wild type medium containing 0.05 M Sucrose. As sucrose is not metabolised it accumulated in the lysosome and caused osmotic swelling (103).

2.11.1 Confocal microscopy of swollen lysosomes

To determine lysosomal swelling and Dextran localisation, cells were loaded for 15 minutes with 200 nM LysoTracker Green (Invitrogen) in imaging buffer (121 mM NaCl, 5.4 mM KCl, 0.8 mM $MgCl_2$, 1.8 mM $CaCl_2$, 6 mM $NaHCO_3$, 5.5 mM D-glucose, 25 mM HEPES; pH 7.4) at room temperature. Cells had been loaded with 0.5 mg/ml Rhodamine B isothiocyanate Dextran for 12 hours followed by a 24 hour chase period during which the lysosomes were swollen with sucrose or vacuolin (see section 2.11).

Live cells were viewed on a Zeiss 510 Meta confocal laser scanning microscope with a 40x oil immersion objectives (NA 1.3) and images collected with a digital zoom in the Multitrack mode which alternates laser lines to reduce bleed through. Excitation/emission (nm): green (Argon 488/ Bandpass 505-530), red (HeNe 543/ Longpass > 560).

2.12 Purification of lysosomes

Swollen or non-swollen lysosomes were purified from HEK293 cells stably expressing HsTPC2 and control HEK293 cells, which was achieved by three different methods: differential centrifugation, magnetic chromatography, or organelle immunoprecipitation.

For all these techniques the purity of the lysosome was assessed for different organelle markers by western blots (section 2.5.4) and enzyme assays (section 2.13).

2.12.1 Differential centrifugation

The following purification was based on the preparation of microsomes by Schenkman and Cinti (383) which was utilised by Schieder *et al.* to purify lysosomes for patch clamp studies (387).

HEK293 cells were grown to 80 % confluency they were either treated by vacuolin, sucrose or left to grow untreated. The cells were washed once with PBS and then scraped from the cell culture dish. After centrifugation at 2000 xg for 3 minutes the cells were then resuspended in a buffer containing 0.25 M sucrose, 10 mM Tris-Cl ; pH 7.4 supplemented with a protease inhibitor cocktail (Roche) and homogenised in a Dounce homogeniser with a tight fitting pestle to obtain whole cell lysates. The lysates were centrifuged at 14,000 xg for 15 minutes at 4 °C and the supernatant recovered. Lysosomes were induced to aggregate by the addition of 8 mM (final concentration) $CaCl_2$. A final centrifugation step at 25,000 xg for 15 minutes pelleted the lysosomal aggregates, the purified lysosomes were resuspended in 150 mM KCl, 10 mM Tris-Cl; pH 7.4 and used directly for analysis.

2.12.2 Lysosome immunoprecipitation

As the HA-tagged HsTPC2 spans the membrane and topological homology predicts the tag to be expressed on the cytoplasmic side of the membrane, the lysosomes were

purified using an anti-HA antibody coupled to magnetic beads.

1.25 µg of anti-HA antibody (Roche 3F10 rat monoclonal) was incubated with 50 µl bed volume of MACS anti-Rat magnetic beads and the mixture was incubated on ice for 30 minutes. The beads were washed once with buffer (80 mM KCl, 6 mM $Mg(OAc)_2$, 1 mM DTT, 10 mM HEPES; pH 7.4) then they were added to a postnuclear supernatant as prepared for the Fe-Dextran preparation below (section 2.12.3). After a 1 hour incubation on ice, the mixture was allowed to flow through a MACS LS column (Miltenyi Biotec, CA) contained in a magnetic sleeve at 4 °C. The column had been pre-equilibrated with 500 µl of 0.5 % bovine serum albumin in PBS to prevent nonspecific binding of organelles to the column. The column was washed twice with PBS containing 0.5 % bovine serum albumin. To elute the purified lysosomes, the column was removed from the magnet and 1 ml of PBS allowed to elute under gravity flow, the eluate was then added back to the column and forced through the matrix with the plunger provided.

2.12.3 Magnetic chromatography

Isolation of magnetically labelled lysosomes was first developed by Diettrich *et al.* (110); this procedure was based on modifications made by Duvvuri and Krise (117).

HEK293 were incubated with 40,000 kDa Dextrans coupled to Fe_2O_3 (Fe-Dextran) at a concentration of 2 mg/ml overnight ($8 - 10$ hours) at 37 °C in wild type medium to allow for endocytic uptake. The medium was removed and the cells were washed thoroughly with PBS (4 washes), then left in dextran-free medium for 24 hours to allow accumulation of the Fe-Dextran in the lysosomes. At the end of this chase period, cells were washed twice with ice-cold PBS and homogenised in a hypotonic buffer (15 mM KCl, 1.5 mM $Mg(OAc)_2$, 1 mM DTT, and 10 mM HEPES; pH 7.4 supplemented with a protease inhibitor cocktail (Roche) and 5 mg/ml DNase I). Cells were homogenised either with a Dounce homogeniser (15 strokes) using the loose fitting pestle, or by a Balch homogeniser (6 strokes) with an 18 µm gauge. Salt levels were restored to the solution by the addition of 375 mM KCl, 22.5 mM $Mg(OAc)_2$, 1 mM DTT, and 10 mM HEPES; pH 7.4 to 20 % (v/v) of the homogenate volume. The mixture was centrifuged at 700 xg for 10 minutes to pellet nuclei and unbroken cells. The postnuclear supernatant was passed through a midiMacs LS column (Miltenyi Biotec, USA) contained in a magnetic sleeve at 4 °C. The column had been pre-equilibrated with 500 µl of 0.5 %

bovine serum albumin in PBS as above. Solutions were allowed to clear by gravity flow and the column was then washed twice with chilled PBS containing 0.5 % bovine serum albumin and 0.5 mg/ml DNase I. An incubation period of 10 minutes in the presence of the DNase I helped to break up any organelle agglomerates formed during homogenisation. The column was washed twice more with PBS containing 0.5 % bovine serum albumin. To elute the purified lysosomes, the column was removed from the magnet and 1 ml of PBS allowed to elute under gravity flow, the elutate was then added back to the column and forced through the matrix with the plunger provided.

Lysosomes were then pelleted at 15,000 xg for 10 minutes and resuspended in a cytoplasmic buffer (50 mM KCl, 10 mM NaCl, 60 mM KF, 20 mM EGTA, 10 mM HEPES; pH 7.2).

2.12.4 Light microscopy of lysosomes

To assess the recovery of lysosomes, their size, distribution and whether they were damaged, a sample from each preparation was viewed under a light microscope.

Purified lysosomes were mixed in a 50 : 50 ratio with 0.4 % trypan blue which is excluded by intact vesicles. This mixture was loaded onto a Neubauer haemocytometer and brightfield images were taken by DFC300FX microscope (Leica) with a 40x air objective facilitated by QWinV3 software (Leica).

2.12.5 Homogenisation techniques

As a means of optimising lysosomal purity various forms of cell homogenisation were investigated:

Dounce

A loose fitting glass pestle and accompanying mortar (Wheaton) were cooled on ice and cells were homogenised with 20 full strokes. For immunoprecipitation experiments cells were swollen with hypotonic buffer (20 mM HEPES, 1 mM EDTA; pH 7.2) for 30 minutes before homogenisation.

Potter

Cells were kept on ice and experienced 5x 30 second pulses with an ULTRA-TURRAX® electric homogeniser.

Freeze-thaw

Cells were placed in −20 °C freezer for 30 minutes or until the solution was frozen solid, this was left to thaw slowly on ice. This was repeated three times.

Needle trituration

Cells were kept on ice and passed through a 25G needle (BD Microlance) 10 times.

Sonication

Cells were kept on ice and experienced 5x 30 second pulses with a Vibra cell sonicator (Jencons).

Balch

The Balch homogeniser (Isobiotech, Germany) was pre-cooled on ice, cells were loaded into a 2 ml Luer-lock syringe and passed through the ball-bearing chamber 6 times in each direction (figure 4.20, page 180).

2.13 Organelle assays

A series of assays were used to detect specific activity which would determine the presence of major organelles within various fractions of the lysosomal preparation.

2.13.1 Lysosomes - β-Galactosidase

The integrity of lysosomal fractions was verified by β-Galactosidase assay.

$$4MU{-}\beta{-}Galactose + Lysosomes \Longrightarrow 4MU_{(\mathrm{Free})} + Galactose$$

Esters of the group 4-methylumbellifery (4MU) do not fluoresce unless the free fluorophore is cleaved. As 4MU-β-Galactose is hydrolysed by the lysosomal galactosidase, the 4MU fluorophore emits light at 460 nm when excited by 365 nm light. The assay is buffered to pH 4.3 so only the lysosomal galactosidase will be active.

20 µl samples were plated into a 96-well clear-bottomed microplate, alongside a negative control of distilled water and a positive control of 40 µM $4MU_{(\mathrm{Free})}$. To each well an equal volume of substrate (1 mM 4MU-β-Galactose, 0.2 M NaOAc, 100 mM NaCl; pH 4.3) was added and the reaction incubated at 37 °C for 1 hour. The reaction was quenched by addition of 200 µl of 500 mM Na_2CO_3; pH 10.7 (alkalisation increases 4MU fluorescence). The fluorescence was determined by measuring emission filtered at 460-10 (450 nm - 470 nm) after excitation at 360-10 (350 nm - 370 nm) on a Novostar plate reader (BMG LABTECH).

2.13.2 Plasma membrane - alkaline phosphatase

Contamination by plasma membrane in various samples was assessed by the Quanti-Chrom alkaline phosphatase assay (Gentaur) according to the manufacturer's instructions.

$$p{-}nitrophenylphosphate + membrane \Longrightarrow p{-}nitrophenol + phosphate$$

p-nitrophenol is a yellow coloured product with a maximal absorbance at 405 nm, however it is colourless when bound as an ester. Hydrolysis of the p-nitrophenyl phosphate substrate by plasma membrane alkaline phosphatase results in dephosphorylation and release of free p-nitrophenol at a rate directly proportional to enzyme activity.

20 µl samples were plated into a 96-well clear-bottomed microplate, alongside a negative control of distilled water and a positive control of 47 µM tartrazine (a stable yellow azo-dye). A working solution was prepared from 200 µl assay buffer, 5 µl $Mg(OAc)_2$, 2 µl p-nitrophenyl phosphate liquid substrate (10 mM stock). 180 µl of working solution was added to each well and the $OD_{405\ nm}$ was directly measured (t = 0) on a Novostar plate reader (BMG LABTECH). The plate was incubated at room temperature for 5-15 minutes and the $OD_{405\ nm}$ was measured again.

2.13.3 Golgi - α-Mannosidase

Contamination by Golgi apparatus in various samples was assessed by an α-Mannosidase assay.

$$p{-}nitrophenylmannose + Golgi \Longrightarrow p{-}nitrophenol + mannose$$

20 µl samples were plated into a 96-well clear-bottomed microplate, alongside a negative control of distilled water and a positive control of 47 µM tartrazine (a stable yellow azo-dye). A working solution was prepared (5.5 mM p-nitrophenyl mannose, 0.1 M K_3PO_4; pH 7.2) and 80 µl added to each well and the $OD_{405\ nm}$ was directly measured (t = 0) on a Novostar plate reader (BMG LABTECH). The plate was incubated at room temperature for 5 - 15 minutes and the $OD_{405\ nm}$ was measured again.

2.13.4 ER - β-Glucuronidase

Contamination by endoplasmic reticulum (ER) in various samples was verified by a β-Glucuronidase assay.

$$4MU{-}\beta{-}Glucuronide + ER \Longrightarrow 4MU_{(\mathrm{Free})} + Glucuronide$$

20 µl samples were plated into a 96-well clear-bottomed microplate, alongside a negative control of distilled water and a positive control of 40 µM $4MU_{(Free)}$. To each well an equal volume of substrate (1 mM 4MU-β-Glucuronide (Invitrogen), 10 mM HEPES; pH 6.8) was added and the reaction incubated at 37 °C for 1 hour. The reaction was quenched by addition of 200 µl of 500 mM Na_2CO_3, alkalisation increases 4MU fluorescence. The fluorescence was determined by measuring emission filtered at 460-10 after excitation at 360-10 on a Novostar plate reader (BMG LABTECH).

2.13.5 Mitochondria - PMS/MTS

Contamination by mitochondria in various samples was verified by an assay designed to detect cell death, CellTiter 96 AQ_{ueous} Non-radioactive Cell Proliferation Assay (Promega). The assay is composed of a novel tetrazolium compound MTS [3-(4,5-dimethylthiazol-2-yl)-5-(3-carboxymethoxyphenyl)-2-(4-sulfophenyl)-2H-tetrazolium, inner salt)] together with an electron coupling reagent PMS (phenazine methosulfate). MTS is reduced in the presence of mitochondrial dehydrogenases to a formazan which is highly absorbent of light at 490 nM. The assay was conducted according to the manufacturer's instructions.

20 µl samples were plated into a 96-well clear-bottomed microplate, alongside a negative control of distilled water. To each well an equal volume of substrate (PMS/MTS solution provided) was added and the reaction incubated at 37 °C for 1 hour. $OD_{490\ nM}$ was measured on a Novostar plate reader (BMG LABTECH).

2.14 Automated patch clamp studies

Rather than using conventional patch clamp methods to measure currents in lysosomal membranes, two methods of automated patch clamping were tested. These two techniques were predicted to provide more support for a patched lysosome, as it had been reported that lysosomal integrity was compromised in conventional patch (387).

2.14.1 Flyion

Lysosomes were purified by the Fe-Dextran method (section 2.12.3) and resuspended in 1 ml cytoplasmic buffer (50 mM KCl, 10 mM NaCl, 20 mM EGTA, 10 mM HEPES; pH 7.2) the bath solution represented the lysosomal lumen (140 mM KOAc, 114 mM Acetic acid, 1 mM $CaCl_2$; pH 4.8). Lysosomes were maintained at room temperature with constant agitation during the experiment.

The Flyion technique works on a 'flip-the-tip' technology whereby lysosomes were loaded within the glass micro-pipette and forced towards the bath solution. As the lysosomes were pushed firmly into the tip, seals would form between the membrane and the glass. A vacuum pulse was applied from the bath to break open the membrane and achieve whole-lysosome recordings. Figure 4.30, page 194 depicts the principles behind Flyion.

The lysosome handling was controlled by the FlyScreen 8500 robot and software suite (Flyion, Tübingen, Germany). Currents were recorded using an EPC-10 patch clamp amplifier (HEKA, Germany) and PatchMaster acquisition software (HEKA, Germany). Data were digitized at 25 µs and filtered at 2.8 kHz. Fast and slow capacitative transients were cancelled by the compensation circuit of the EPC-10. Membrane potentials were corrected for liquid junction potential which was calculated by pClamp 10 (Molecular Devices, USA).

2.14.2 Port-a-patch

Lysosomes were purified by the Fe-Dextran method (section 2.12.3) and resuspended in 50 µl of cytoplasmic buffer (50 mM KCl, 10 mM NaCl, 20 mM EGTA, 10 mM HEPES; pH 7.2). Lysosomes were maintained on ice until they were needed. The composition of solutions used during recordings are listed in table 2.2.

Table 2.2: Solutions used in planar patch clamp. Ion composition of Port-a-patch solutions. OAc refers to the acetate ion (CH_3COO^-). Solutions titrated with 1 M acetic acid or 1 M KOH. Sucrose was used to adjust osmolarity.

Cytoplasmic solution		**Intralysosomal solution**	
60 mM	KOAc	70 mM	KOAc
60 mM	KF	60 mM	$Ca(OAc)_2$
2 mM	$Ca(OAc)_2$*	2 mM	$Mg(OAc)_2$
10 mM	HEPES	60 mM	AcOH (acetic acid)
	pH 7.2		pH 4.6

* $Ca(OAc)_2$ was added immediately before use to prevent precipitation of CaF_2.

Port-a-patch represents a planar patch clamp system, where lysosomes are attached to a small aperture (< 1 µm) in a microstructured planar borosilicate chip. 5 µl of lysosomal suspension was pipetted over the aperture and gentle suction was applied, after seal formation a vacuum pulse was applied from the bath to break open the membrane and achieve whole-lysosome recordings. Figure 4.34, page 199 depicts the principles behind Port-a-patch.

Currents were recorded using an EPC-10 patch clamp amplifier (HEKA, Germany) and PatchMaster acquisition software (HEKA, Germany). Data were digitized at 25 µs

and filtered at 2.8 kHz. Fast and slow capacitative transients were cancelled by the compensation circuit of the EPC-10. Membrane potentials were corrected for liquid junction potential which was calculated by pClamp 10 (Molecular Devices, USA). For all experiments Ag-AgCl pellets were used to connect the bath solutions, the cytoplasmic electrode was clamped at ground, whilst the lysosomal lumen electrode was clamped at various potentials relative to ground.

All experiments were conducted at room temperature. The membrane potential was established and held at +40 mV. Voltage ramps lasting 500 ms from +100 mV to -100 mV were applied every 5 seconds. Compounds were added to the cytoplasmic face by completely exchanging the cytoplasmic solution in a series of 5 µl washes. The current in the absence of a compound was subtracted from the current in the presence of the compound to dissect out $I_{compound}$. Maximal currents at -100 mV were extracted from ramp data to compare current amplitudes under different conditions.

Reverse potentials were calculated for Ca^{2+} and K^+ using the Nernst equation:

$$E = \frac{RT}{zF} \times ln \frac{[ion]_{outside}}{[ion]_{inside}}$$

Where R is the universal gas constant (R = 8.314 J K^{-1} mol^{-1}), T is the temperature of the system (°K), z is the charge on the ion (Ca^{2+} = 2, K^+ = 1), F is the Faraday constant (F = 96485 × 10^4 C mol^{-1}). $[ion]_{outside}$ refers to the ion concentration in the cytoplasmic buffer, $[ion]_{inside}$ is the concentration in the luminal buffer.

2.15 Mass spectrometry

The mass-charge ratio of digested fragments of immunopurified HsTPC2 (section 2.8) was analysed by mass spectrometry which allowed prediction of proteins that may interact within the HsTPC2 complex. These reactions were carried out at the Oxford University's central proteomics facility.

2.15.1 Tryptic digest

Proteins were run on a denaturing SDS-gel and stained with coomassie blue as above (section 2.5.3), the bands were excised and diced. The gel was washed twice for 30 minutes in 25 mM ammonium bicarbonate, 50 % (v/v) acetonitrile to remove contamination of the stain. The gel was then dehydrated by washing in 100 % acetonitrile and dried

by evaporation. 100 µl of 55 mM iodoacetamide was incubated with the gel pieces in the dark for 1 hour, the wash and dehydration procedure was repeated. 20 µl of trypsin (Promega sequencing grade modified) in 25 mM ammonium bicarbonate solution was added to the gel pieces and left over night at 37 °C. The digestion was stopped by the addition of 1 µl of formic acid. The supernatant containing peptide fragments was removed. The gel was resuspended in 50 µl 25 % (v/v) acetonitrile and 50 % (v/v) formic acid and incubated for 30 minutes to extract all remaining peptides. The supernatant from this step was taken and pooled with the rest of the peptide solutlion.

2.15.2 MALDI TOF MS

Matrix-assisted laser desorption/ionization (MALDI) time of flight (TOF) mass spectrometry uses soft ionisation to protect biological molecules. Peptide fragments were co-precipitated with a solid-state matrix which absorbs UV light. This complex was irradiated by a laser pulse for a nanonsecond, but as the matrix absorbed most of the energy this prevented unwanted fragmentation.

The ionised peptides were accelerated in an electric field towards the flight tube, where they are sorted by their charge to mass ratio and reach the detector at differing times. As the time of flight depends entirely on the charge-mass of a fragment, the primary amino acid structure can be deduced.

2.15.3 LCMS

Liquid chromatography mass spectrometry was used to provide greater sensitivity and resolution on very low concentration samples. The digested peptide fragments were initially separated by size via liquid chromatography, before being ionised by electrospray and analysed by time-of-flight recordings as above.

2.15.4 Peptide comparison software

All data analysis was conducted using software provided by Oxford University's Central Proteomics Facility Pipeline, hosted by its Computational Biology Research Group. The pipeline makes heavy use of the Trans Proteomic Pipeline (TPP) tools, developed at Seattle Proteome Center (2). Peptide spectra were collated and identified via three algorithms:

- Mascot (Matrix Science, London)
- X!Tandem kscore (215)
- Open Mass Spectrometry Search Algorithm (OMSSA) (145)

These searched known *Homo sapiens* protein libraries and their results were combined in a meta-search. Control and immunoprecipitate sample results were compared using a false discovery rate of 1 %. Proteins seen in the control were discounted from the immunoprecipitate and those remaining were ranked by the number of unique peptide matches.

2.16 Cloning techniques

2.16.1 Subcloning

IMAGE cDNA clones were obtained for both TPC human isoforms, details shown in table 2.3 (247).

Table 2.3: HsTPC IMAGE cDNA.

	HsTPC1	**HsTPC2**
IMAGE #	40148827	5214862
Genebank Accession	BC150203	NP620714.2
Vector	pCMVSPORT6	pCMVSPORT6

The TPC cDNAs were excised from the library vector by a double restriction digest and ligated into an expression vector. Unless otherwise stated the expression vector used was always the hygromycin resistant tetracycline regulated pcDNA5/TO (Invitrogen).

2.16.2 Primer design

To clone the cDNA from the library-vector, primers were designed against the 3' and 5' ends of the clone. Each primer was designed to incorporate a restriction enzyme binding site appropriate to those in the target expression vector. The primers also included a

Kozak site at the 3' end to aid expression and often mutation to knock-out the stop codon at the 5' end, as reporter genes such as the red fluorescent protein mCherry, or the small peptide sequence hemagglutinin (HA) were used to tag the protein.

Primers were synthesised by Invitrogen and a full list can be seen in section 2.22.

2.16.3 Polymerase chain reaction for DNA amplification

The coding regions were amplified from the library-vector using the High Fidelity PCR Master system (Roche) as per the manufacturer's instructions. This involved the downstream and upstream primers being mixed to 300 nM with 2 - 10 µg of template DNA in PCR grade water (DNase/RNase free) followed by the addition of the Master mix provided in a 1 : 1 ratio. The master mix contained the active Taq polymerase enzyme and free dNTPs in the appropriate buffer. The sample was then subjected two rounds of thermal-cycling as summarised in table 2.4.

Table 2.4: Thermal cycling conditions for PCR.

	Cycles	**Time**	**Temperature**
Denaturation	1	2 minutes	94 °C
Denaturation	10	10 seconds	94 °C
Annealing		70 seconds	45 °C to 65 °C*
Elongation		2 minutes	72 °C
Denaturation	20	15 seconds	94 °C
Annealing		30 seconds	45 °C to 65 °C*
Elongation		2 minutes	72 °C
		+ 5 seconds per cycle	
Elongation	1	7 minutes	72 °C

* The annealing temperature was usually 2 °C lower than the lowest melting temperature (T_m) of the primer pair.

2.16.4 Synthesis and annealing of oligonucleotide tags

Small peptide tags: 2x HA and His_6 (see section 2.22) were synthesised *de novo* (Invitrogen). These oligonucleotides were synthesised with a 5' base modified by the addition of

a phosphate group which allowed direct insertion into the vector. The oligonucleotides were annealed together at 25 µM once dissolved in buffer (10 mM Tris, 50 mM NaCl, 1 mM EDTA; pH 7.5) and subjected to a temperature ramp from 2 minutes at 92 °C, dropping 0.1 °C every second to 4 °C.

2.16.5 Restriction digest

DNA digestion was always conducted with excess restriction enzyme (1 U enzyme/1 µg DNA) at 37 °C for 2 hours in a reaction containing the appropriate restriction buffers (as recommended by manufacturer). Enzymes which were available as FastDigest (Fermentas) were used at room temperature for 5 - 30 minutes in a universal buffer. Successful digestion was confirmed by analysing the resulting fragments by agarose gel electrophoresis (section 2.16.6).

2.16.6 Agarose gel electrophoresis

DNA samples were mixed with DNA loading buffer (2 % (v/v) glycerol, 0.1 % (v/v) SDS, 0.0005 % (w/v) bromophenol blue, 10 mM EDTA; pH 8.0) and analysed using horizontal 1 % to 1.5 % (w/v) agarose gels in TAE buffer (40 mM Tris-acetate, 5 mM sodium acetate, 1 mM EDTA; pH 7.6) containing ethidium bromide (0.5 µg/ml) and were electrophoresed at 100 V in TAE buffer. A DNA ladder which ranged from 250 - 10000 bp (Generuler from Fermentas) was used to provide size markers. DNA was visualized using an UV transilluminator and when required, fragments of interest were excised for further purification.

2.16.7 Purification of DNA from agarose gel

Electrophoresed DNA was purified from agarose using QIAquick spin columns (QIAGEN) using the buffers provided, as per the manufacturer's instructions. Briefly, a gel slice containing the DNA fragment of interest was solubilised and applied to a silica-gel membrane of the spin column. DNA was adsorbed to the silica-membrane in the presence of high salt whilst agarose and other contaminants passed through the column. Bound DNA was washed and then eluted in distilled, deionised water.

2.16.8 Dephosphorylation of 5' phosphate group

To prevent re-circularisation of the vector, the 5' ends were dephosphorylated by 1 U rAPid alkaline phosphatase (Roche) in 0.5 M Tris/HCl, 1 mM EDTA; pH 8.5 for 15 minutes at 37 °C. The enzyme was inactivated at 75 °C for 2 minutes.

2.16.9 Ligation

Digested and dephosphorylated vector arms (up to 1 µg) were diluted in a 5x DNA dilution buffer (Roche), insert DNA was added to a molar ratio of 1 vector : 3 insert. T4 DNA Ligase (Roche) was added to a final concentration of 5 U together with the appropriate ligation buffer supplied with the enzyme (Roche). The reaction was incubated at room temperature for 15 minutes. Ligated DNA was either used to directly transform chemically competent bacteria or frozen at −20 °C.

2.16.10 Preparation of chemically-competent bacteria

Escherichia coli were used to propagate vectors, to increase transformation efficiency the bacteria underwent chemical manipulation to make them chemically-competent. A single colony from a non-selective agar plate was picked and cultured (5 ml) overnight in Luria broth (LB: 10 g/L Tryptone, 5 g/L Yeast extract, 10 g/L NaCl) shaken at 37 °C. This preculture was used to inoculate 500 ml of LB which was incubated until the *E. coli* were dividing exponentially ($OD_{600\ nm}$ = 0.4 - 0.6). The bacteria were pelleted by centrifugation for 10 minutes at 5,000 xg in a SLA-1500 rotor which had been pre-cooled to 4 °C. The pellet was washed once by resuspension in 100 ml ice cold 0.1 M $CaCl_2$ followed by another 10 minute centrifugation. After resuspension in 5 ml of ice cold 0.1 M $CaCl_2$, 15 % glycerol (v/v) the cells were incubated on ice for 30 minutes and then aliquoted into 100 µl samples to be stored at −80 °C.

2.16.11 Transformation of bacteria by heat-shock

100 µl of chemically-competent bacteria were thawed on ice. Typically, 10 µl of ligated DNA or 1 µl of plasmid DNA (prepared by Maxiprep, section 2.16.14) was then added and the mixture incubated on ice for 20 minutes. Ligated DNA was introduced into bacteria via heat-shock by placing the mixture in a water bath set at 42 °C for 30 seconds, immediately followed by re-placing on ice for 5 minutes. Transformed bacteria

were diluted with LB and directly plated out on LB-agar containing the antibiotic selection for the plasmid, typically this was ampicillin at 25 µg/ml for the pcDNA5/TO expression vector. If a poor yield was expected or kanamycin (50 µg/ml) was used as the antibiotic, transformed bacteria were pre-incubated at 37 °C for 1 hour in super optimal broth (SOC) before plating, as this allowed 3 rounds of cell division under non-selective conditions. Agar plates were incubated overnight at 37 °C to allow colonies to form.

2.16.12 Homologous recombination

The In-Fusion PCR cloning kit (Clontech) was used to insert HsTPC cDNA into the pcDNA5/TO expression vector. This kit was designed to join multiple pieces of DNA which have 15 base pairs of homology at their linear ends. Hence primers were designed to amplify HsTPC cDNA by PCR and to incorporate homologous sequences from the regions flanking the site of insertion in the vector, these are listed below in section 2.22.

The PCR product was purified as above (section 2.16.7) and combined with the linearised vector (digested with appropriate restriction enzymes) as per the manufacturer's instructions. The samples were incubated for 15 minutes at 37 °C to allow the exonuclease activity of the enzyme provided to induce homologous recombination. This method guaranteed the insertion of the cDNA in the correct orientation. The enzyme was inactivated by incubation for 15 minutes at 50 °C.

The resulting construct was diluted in water and transformed into chemically competent bacteria (section 2.16.11).

2.16.13 Small scale preparation of plasmid DNA (Minipreps)

Plasmid DNA was prepared using the QIAprep Miniprep system (QIAGEN) following the manufacturer's instructions and using the solutions provided. Successfully transformed bacterial colonies were cultured overnight in 5 ml LB containing the selective antibiotic. The bacteria were pelleted and subsequently lysed under alkaline conditions. Upon neutralisation, genomic DNA, proteins and lipids were precipitated and the lysates were cleared by centrifugation. The resulting supernatant was run through a silica-gel membrane QIAprep column. DNA was adsorbed onto the silica under the high salt composition of the buffers, all other contaminants were washed through. Salt

was removed by washing the column with 80 % (v/v) ethanol. The purified plasmid DNA was then eluted from the QIAprep column with distilled, deionised water.

2.16.14 Large scale preparation of plasmid DNA (Maxipreps)

Large scale purification of plasmid DNA was performed using the HiSpeed Plasmid Maxi Kit (QIAGEN), according to the manufacturer's instructions and using the solutions provided. Briefly, pelleted bacteria from a 250 ml overnight culture were lysed under alkaline conditions. Upon neutralisation, genomic DNA, proteins and lipids were precipitated and the lysates were cleared manually using a QIAfilter cartridge. The filtered cell lysate was loaded onto a QIAGEN-tip and passed by gravity flow. The plasmid DNA was adsorbed to the anion-exchange resin of the QIAGEN tip under low salt conditions, whilst contaminants ran through during a subsequent wash step. The DNA was eluted by a high salt buffer which saturated the resin, the eluted DNA was desalted and concentrated by isopropanol precipitation and washed with 70 % (v/v) ethanol. The purified plasmid DNA was redissolved in distilled, deionised water. All plasmids were stored at −20 °C.

2.16.15 DNA quantitation

The plasmid concentration was determined on a nano-spectrophotometer (Implen) which measured the intensity of absorbance of the DNA solution at wavelengths 260 nm and 280 nm. DNA absorbs UV light at 260 and 280 nm, however aromatic proteins absorb UV light at 280 nm. The ratio between the two absorbance intensities was calculated to give an approximate prediction of DNA concentration.

The more precise Quant-iT PicoGreen DNA assay (Invitrogen) was frequently used to confirm concentrations. Quant-iT PicoGreen reagent and the sample DNA were diluted 200-fold into 10 mM Tris, 1 mM EDTA; pH 7.5. These were then mixed in a ratio of 1 : 1 in a 96-well clear-bottomed microplate and incubated for 3 minutes at room temperature, protected from light. Samples were excited at 488 nm and the fluorescence emission intensity measured at 520 nm using a Typhoon 9400 imager (GE Healthcare). Fluorescence emission intensity was plotted versus DNA standard concentration (0.01 - 1.0 µg/ml) and unknown sample DNA concentration calculated from the standard curve.

2.16.16 DNA sequencing

All new plasmid constructs were confirmed by sequencing a DNA sample, which was conducted by GATC using an automated Sanger method (379). All sequences returned were analysed using web-based sequence software. The CAP3 sequence assembly program (191) was used to compile a contiguous sequence by comparing the sequenced sense and antisense fragments. This compilation was analysed by eye to check for mutations or changes to the open reading frame, compared to the original cDNA of the IMAGE clone.

2.17 Adhering cells to cover slides

Glass coverslides were washed in 100 % alcohol and allowed to air dry. 100 µg/ml Poly-D lysine was used to treat the glass surface to allow cells to adhere. For a Ø = 16 mm coverslide 100 µl of Poly-D lysine was added and incubated for 1 hour at 37 °C. The solution was removed and the coverslides air dried either to be used directly or kept at 4 °C in the dark. To adhere the cells, the coated coverslides were warmed to 37 °C and a cell suspension (see section 2.3.1) was added onto the coated region.

2.18 Transient transfection

In summary, HEK293 cells were plated on cell culture dishes (Greiner) or glass coverslides coated with poly-D lysine as above (section 2.17). When the cells reached 50 % confluency the transfection reagent was added, cotransporting the DNA construct into the cell. HEK293T cells expressing the large T-antigen from the SV40 virus were frequently used rather than the wild type HEK293 cells as they have a greater transfection efficiency of the pcDNA5/TO expression vector. Specific transfection techniques are listed below.

2.18.1 Calcium phosphate

Transfection was carried out using the CAPHOS transfection kit (Sigma), according to the manufacturer's recommendations. Purified DNA plasmid was diluted to 80 µg/ml in 250 mM $CaCl_2$. This solution was added dropwise to an equal volume of 2x HEPES buffered saline (50 mM HEPES, 280 mM NaCl, 1.5 mM Na_2HPO_4; pH 7.05) with

vigorous agitation. The mixture was incubated at room temperature for 30 minutes to allow formation of $Ca_3(PO_4)_2$/DNA precipitate, which was then distributed gently over the cells. For a 10 cm diameter cell culture dish 1.2 ml of $Ca_3(PO_4)_2$/DNA (5 µg DNA) was used in 15 ml of cell culture medium. Typically the cells were incubated with the calcium phosphate transfection agent for 24 hours before harvesting. If required, the medium was changed 12 hours after transfection.

2.18.2 jetPEI

As calcium phosphate precipitate can obscure cells under a microscope, linear polyethylenimine (PEI) was used as an alternative transfection reagent. The commercial preparation JetPEI (Qbiogene) was used according to the manufacturer's instructions. Briefly, purified DNA plasmid was diluted to 20 µg/ml in 150 mM NaCl, to this an equal volume of 1 % (v/v) jetPEI in 150 mM NaCl was added. After vigorous mixing the solution was incubated for 30 minutes at room temperature and added dropwise to the cell culture medium. For a 10 cm diameter cell culture dish 1 ml of JetPEI/DNA mixture (10 µg DNA) was used in 15 ml of cell culture medium. Typically the cells were incubated with the transfection agent for 24 hours before harvesting.

2.19 Localisation

To determine the sub-cellular localisation of the TPC isoforms, HEK293 cells were transfected with various combinations of the HsTPC proteins and organelle markers. Cells were adhered to coverslips (section 2.17) and permeabilised (section 2.19.1) to allow sequential labelleling of specific primary antibodies followed by fluorescently-labelled secondary antibodies which were visualised under a confocal microscope.

2.19.1 Immunofluorescent staining

The adhered cells were washed three times with cold PBS and immersed in fixation buffer (2 % (w/v) paraformaldehyde in PBS; pH 7.3) for 15 minutes. After another three washes, the cells were permeabilised in 0.2 % (v/v) Triton X-100 in PBS for 15 minutes at room temperature. Non-specific protein binding sites were blocked by incubating the permeabilised cells for 1 hour in a blocking buffer of 5 % (v/v) goat serum in 0.1 % Triton X-100/PBS. Meanwhile the primary antibody was diluted in blocking

buffer and this was used to immerse the cells overnight at 4 °C, or 1 hour at room temperature. The cells were washed by several changes of 0.1 % Triton X-100/PBS over the course of 1 hour. Fluorescently labelled secondary antibodies were diluted in blocking buffer and added to the cells for 1 hour at room temperature, whilst being protected from light. Excess antibody was removed by 1 hour of repeated washes in 0.1 % Triton X-100/PBS, finally 2 washes in PBS alone. Excess liquid was removed and the coverslides were mounted onto glass microscope slides with ProLong Gold Antifade mounting solution (Invitrogen). The mounted coverslides were left overnight at room temperature to set firm in the dark.

2.19.2 Image capture

As in section 2.11.1, immunofluorescence was viewed on a Zeiss LSM510 META confocal laser scanning microscope with 40x and 63x oil immersion objectives (NA 1.3 and 1.4 respectively) and images collected with 2 - 5x digital zoom in the Multitrack mode. Excitation/emission (nm): green (Argon 488/ Bandpass 505-530), red (HeNe 543/ Longpass > 560).

2.20 FRET

In all cases, adhered HEK293T cells were cotransfected with CFP/YFP constructs (see table B.2) with jetPEI as above (section 2.18.2). The cells were then incubated for 24 hours and fixed to the coverslide with (2 % (w/v) paraformaldeyhde to prevent fluorescence recovery after photobleaching, this also allowed the cells to be stored at 4 °C for future use.

2.20.1 Sensitised FRET

Cells were examined with the setup used for immunofluorescence (Zeiss LSM510 META confocal laser scanning microscope - section 2.19.2) and all images were taken with the 40x oil immersion objective (NA 1.3) - digital zoom varied between images. Laser lines and filter sets used for each channel recording are summarised in table 2.5.

Data analysis was conducted in MetaFluor imaging software (Molecular Devices, USA) to calculate mean pixel intensity per cell. Further analysis was done manually in Excel (Microsoft) and Prism (Graphpad).

Table 2.5: Zeiss confocal settings for FRET. Laser lines and filter sets used to distinguish FRET signals between CFP/YFP tagged HsTPCs.

Channel	Excitation laser	Emission detection filter
CFP	457 nm	Metahead 473 - 612 nm
YFP	514 nm	Bandpass 530 - 600 nm
FRET	457 nm	Longpass > 505 nm

2.20.2 FRET acceptor photobleach

The instrumentation was used as with sensitised FRET. The acceptor photobleach regime consisted of 100x 10 ms pulses at 100 % laser power of the Argon 514 nm line. This procedure bleached the YFP signal by an average of 92.6 ± 5.3% (n = 88).

2.21 Statistical analysis

All values are given as mean ± S.E.M. unless otherwise stated. n is the number of experiments. An unpaired t test was performed for the comparison between two groups. The scientific significance was assumed at $P < 0.05$. Statistical analysis was performed using Prism (GraphPad).

2.22 List of Primers

All primers were synthesised by Invitrogen unless otherwise stated. Primers were stored at −20 °C at 200 µM in distilled, deionised water.

Hemagglutinin Tag

Oligonucleotitdes were designed to introduce 2x HA tag at a NotI (3, 3, 2) site - destroying the site at the 5' end and introducing a Kozak sequence.

```
GGCCATGGGGTACCCTTACGACGTGCCCGACTACGCCGGGTATCCCTATGATGTACCGGACTATGCGGC
    TACCCCATGGGAATGCTGCACGGGCTGATGCGGCCCATAGGGATACTACATGGCCTGATACGCCGCCGG
```

The second HA contains different codons for the same amino acids to prevent the *E. coli* recognising and excising repeated DNA.

5' — 3'
Forward Oligonucleotide
`GGCCATGGGGTACCCTTACGACGTGCCCGACTACGCCGGGTATCCCTATGATGTACCGGACTATGCGGC`
Reverse Oligonucleotide
`GGCCGCCGCATAGTCCGGTACATCATAGGGATACCCGGCGTAGTCGGGCACGTCGTAAGGGTACCCCAT`

PCR forward primer to detect presence of HA tag

Successful insertion of the HA oligonucleotide could not be determined by digestion as the tag was too small to be resolved on an acrylamide gel. Thus to confirm insertion a forward primer was designed to complement the tag, this was used in a PCR reaction with a reverse primer complementary to the downstream cDNA depending on the construct.

PCR forward primer
`GACTACGCCGGGTATCCCTAT`

His_6 Tag

Oligonucleotides which introduce six Histidines to form a tag which could be inserted between the restriction sites AflII and HindIII (2, 3, 1) and introduced a Kozak sequence.

```
TTAAGGCCATGGGGCATCATCACCATCACCACA
    CCGGTACCCCGTAGTAGTGGTAGTGGTGTTCGA
```

5' — 3'
Forward Oligonucleotide
TTAAGGCCATGGGGCATCATCACCATCACCACA
Reverse Oligonucleotide
AGCTTGTGGTGATGGTGATGATGCCCCATGGCC

mCherry Tag

Primers to clone mCherry from preexisting vector which could be inserted between the restriction sites AflII and HindIII (2, 3, 1) and included a Kozak sequence. The stop codon was deleted from the 3' end and an additional nucleotide (G) added to preserve the reading frame.

5' — 3'	Annealing Temperature
Forward Oligonucleotide	
GATCCTTAAGGCCATGGTGAGCAAGGGCGA	57.0 °C
Reverse Oligonucleotide	
GATCAAGCTTGCTTGTACAGCTCGTCCATGC	56.4 °C
PCR product size:	724 bp

RT-PCR cloning of TRP-ML1

These primers were designed to conduct RT-PCR of Human TRP-ML. The optimal combination of primers was calculated by the web-based software Primer3Plus (434) using the mRNA sequence of Mucolipin 1 from the PubMed Gene database (NCBI Reference Sequence: NG_015806.1) .

5' — 3'	Annealing Temperature
Forward primer	
GACATTCCGGGAAGAGAACA	60 °C
Reverse primer	
GGAAGACACTGGGGTGCTTA	60.1 °C
PCR product size:	599 bp

Primers for HsTPC1 insertion into pcDNA5/TO by In-Fusion

Primers to introduce HsTPC1 into pcDNA5/TO.HA between the restriction sites BamHI and NotI (3,3,2), the stop codon was deleted from the 3' end.

5' — 3'	Annealing Temperature
Forward primer	
TACCGAGCTCGGATCCATGGCTGTGAGTTTGGATGA	55.8 °C
Reverse primer	
TAAGGGTACGCGGCCGCGGTAACGGTCTGGGAGCG	58.4 °C
PCR product size:	2.45 kbp

Primers for HsTPC2 insertion into pcDNA5/TO by In-Fusion

Primers to introduce HsTPC2 into pcDNA5/TO.mCherry between the restriction sites BamHI and NotI (3,3,2), the stop codon was deleted from the 3' end.

5' — 3'	Annealing Temperature
Forward primer	
TACCGAGCTCGGATCCACCATGGCGGAACCCCAGGC	63.4 °C
Reverse primer	
TTGCTCACCGCGGCCGCCCTGCACAGCCACAGGTGC	62.8 °C
PCR product size:	2.26 kbp

Primers for HsTPC1 insertion into Clontech CFP/YFP vectors

Primers to introduce HsTPC1 into pECFP/pEYFP clontech vector both C/N terminal forms. HsTPC1 was inserted between the restriction sites HindIII (2, 3, 1) and EcoRI (2, 3, 1), the stop codon was deleted from the 3' end.

5' — 3'	Annealing Temperature
Forward primer	
TCGAGCTCAAGCTTCCATGGCTGTGAGTTTGGATGA	55.8 °C
Reverse primer	
GTCGACTGCAGAATTCTGGTAACGGTCTGGGAGCG	58.4 °C
PCR product size:	2.45 kbp

Primers for HsTPC2 insertion into Clontech CFP/YFP vectors

Primers to introduce HsTPC2 into pECFP/pEYFP clontech vector both C/N terminal forms. HsTPC2 was inserted between the restriction sites HindIII (2, 3, 1) and EcoRI (2, 3, 1), the stop codon was deleted from the 3' end.

5' — 3'	Annealing Temperature
Forward primer	
TCGAGCTCAAGCTTCCAATGGCGGAACCCCAG	57.9 °C
Reverse primer	
GTCGACTGCAGAATTCTCCTGCACAGCCACAGGTG	58.1 °C
PCR product size:	2.26 kbp

Primers for DNA sequencing

HsTPC1

Based on cDNA sequence from IMAGE clone # 40148827

5' — 3'	
Forward primers	Reverse primers
GGTGCTGGTGGTGCAGTTT	TGGGAGTCGTGGATGGCAT
CTTCCAGTATTTCATGTAC	AAGCAGGTTCATGATGAAA
TCACCCTTGAGAAGGAAAT	GCGAAGGAGTAGTAAAAGA

HsTPC2

Based on cDNA sequence from IMAGE clone # 5214862

5' — 3'	
Forward primers	Reverse primers
CTGAGTCTCGTGTGTCATG	TCCCTGTCCTGCCCATCAT
CTGGCAAACCTGGTGTCCA	ATCTCCAAAACCAGCAGGA
CAGAGGCCACCTACCAGAT	

Chapter 3

Results - Channel properties of purified TPC2

3.1 Summary

Two precedents have paved a clear methodology in validating a receptor as a second messenger-gated Ca^{2+} channel; the IP_3R (416) and RyR (195, 196). In both these cases membranes were crudely purified from tissues abundantly expressing the protein, these membranes were detergent-solubilised and the protein was purified by affinity chromatography against a compound known to tightly associate with the receptor, heparin and ryanodine respectively.

Since the discovery of NAADP as a Ca^{2+}-mobilising second messenger, the identity of the receptor has been a key question. With such well characterised binding properties (39, 331) which were shown to be maintained for the solubilised receptor (29) the triumphant publication of the identity of the NAADP receptor ought to have swiftly followed.

Despite many attempts made to purify the NAADP receptor by affinity chromatography none have been successful. A number of factors may explain why in the case of NAADP the identification of the receptor has not been straightforward. Firstly, it is likely that the receptor abundance is very low because of the small amplitude of NAADP-mediated Ca^{2+} currents which rapidly desensitise, suggesting a small channel population. Secondly, the chemistry of NAADP may be inhibitory for this type of purification because there are few active sites available to couple NAADP to a solid

support, and those are likely to destroy the three dimensional structure which has been shown to be essential in binding (310). Finally, slow dissociation of NAADP from its receptor would make it difficult to recover significant quantities of the native receptor from the column once it has been bound.

Recent evidence has proposed TPC2 as the NAADP receptor (55, 387), and a potential role for HsTPC1 (47). With a candidate in mind it is possible to work backwards to prove its role in NAADP-induced Ca^{2+} release. Therefore the purification of HsTPC2 and its response to NAADP was the main focus of this chapter.

This was conducted by the immunoprecipitation of HsTPC2 from an overexpressing cell line and its reconstitution into a lipid bilayer. As will be shown, this system allowed single channel recordings of current through the HsTPC2 protein, which demonstrated a non-selective permeability for both K^+ and Ca^{2+}. NAADP increased the open probability (P_o) of the channel in a dose dependent manner to give the characteristic mammalian bell-shaped curve. Therefore this chapter provides the first direct evidence that HsTPC2 mediates NAADP-evoked Ca^{2+} release.

The pharmacology of the channel will also be discussed. Channel activity was regulated by luminal [Ca^{2+}] which altered the sensitivity to NAADP, and luminal pH whereby an acidic lumen reduced the P_o and changed the ligand binding properties, to allow reversible NAADP binding. Ned-19, the NAADP antagonist, increased P_o of HsTPC2 at low concentrations, therefore implying that this compound acts as a partial agonist, and these effects seemed to originate from a separate binding site from NAADP. These interesting properties will be put in the context of NAADP signalling and the biophysical properties of HsTPC2 compared to related Ca^{2+} channels.

3.2 Glycosylation of HsTPC proteins

It is worth introducing a few of the protein characteristics of the HsTPCs and the overexpressing cell lines before proceeding with the purification procedure.

Due to the low levels of endogenous TPC expression in human cell lines, HEK293 cells had been stably transfected to overexpress HsTPC1 or HsTPC2 (Mike Zhu laboratory, Ohio State University, US). Small peptide tags had been added to each protein for easier analysis: the HsTPC1 was tagged at the carboxy-terminus with six histidine residues (His_6), whilst HsTPC2 was tagged at the amino-terminus with two repeats of the influenza Haemagglutinin (HA) sequence. These tags provided very specific epitopes to which commercially-available antibodies could bind with a high affinity, therefore allowing identification and purification of HsTPCs via these HA or His tags.

As HsTPCs are situated in subcellular organelle membranes, a crude purification of total cell membranes provided a means of concentrating HsTPC protein and removing any soluble contaminants. Therefore membranes from the overexpressing cell above were prepared according to the schematic in figure 3.1

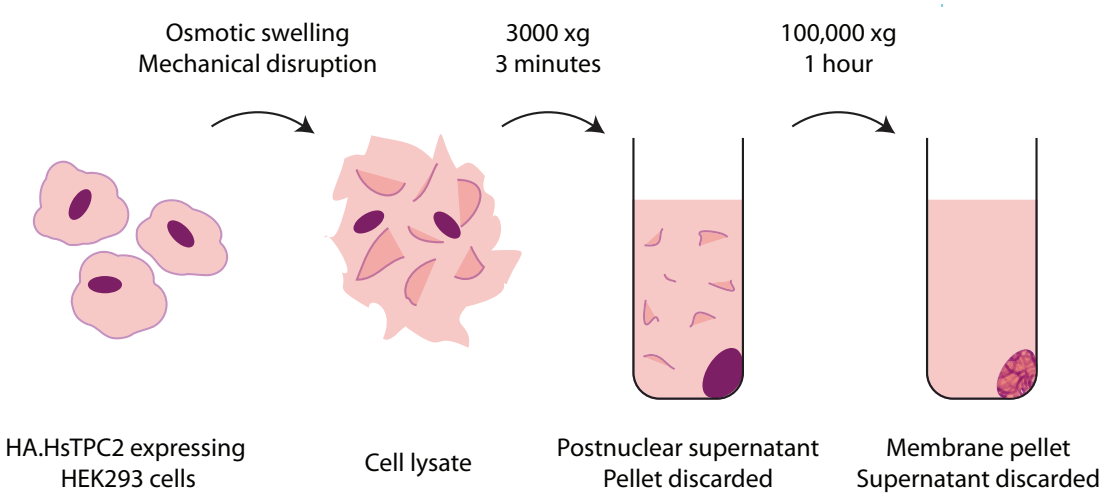


Figure 3.1: Schematic methodology of a membrane preparation. Membranes were crudely purified from HsTPC expressing cells by centrifugation of cell homogenate. Cells were swollen with hypotonic buffer and homogenised, the resulting lysate was cleared of unbroken cells and nuclei by an initial centrifugation step. Membranes were then separated from soluble proteins by powerful centrifugation at 100,000 xg for 1 hour. The resulting pellet was resuspended in a suitable buffer for the experiment.

The anticipated molecular weight of HsTPC1 and HsTPC2 can be predicted from their primary amino acid sequence. HsTPC1 is predicted to be 94.16 kDa and HsTPC2 85.26 kDa. However, analysis of the protein sequences also revealed 3 putative N-glycosylation sites (Asn - Xxx - Ser/Thr), which could contain asparagine (N)-linked oligosaccharides groups which will affect the mass of the native protein. These have been mapped onto the predicted topology of the TPC proteins in figure 3.2. All sugar groups face the lysosomal lumen according to hydropathy plots. There were no O-glycosylation sites predicted.

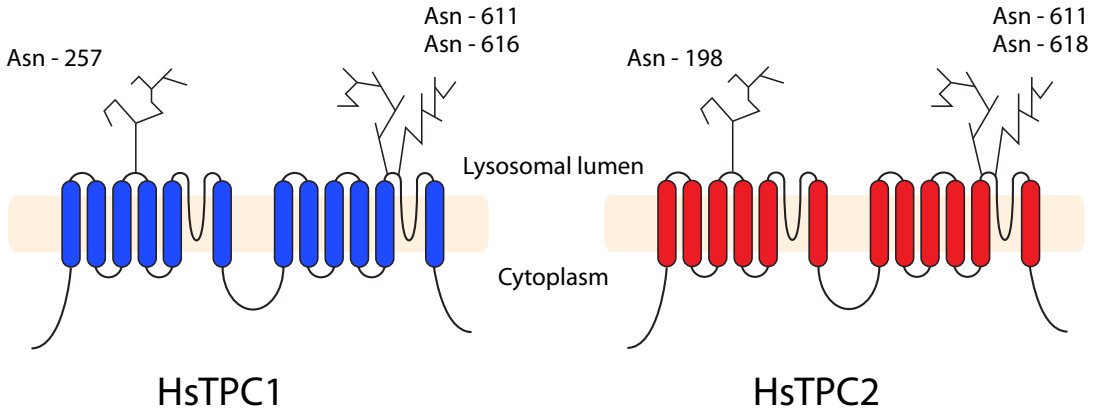


Figure 3.2: Schematic depicting the predicted position of glycosylated arginine residues. Both HsTPC1 and HsTPC2 are predicted to contain 3 N-glycosylation sites by the web-based software NetNGlyc 1.0 (166). These map accordingly to regions facing the lysosomal lumen: the loop between S3 and S4 on domain I and two sites before the S5/S6 re-entry loop on domain II.

To determine the level of protein expression in these cell lines and the native size of the HsTPC protein, purified membranes were run on SDS PAGE and western blots. Antibodies directed against the His/HA peptide tags or the TPC protein themselves were used to probe the western blots. Furthermore to gauge the extent of protein glycosylation, samples from the same membrane preparation were treated with the glycoaminidase PNGase F which causes cleavage of the link between asparagine and N-acetylglucosamines, this yielded non-glycosylated proteins which were also investigated by western blot. Figure 3.3 combines these western blots.

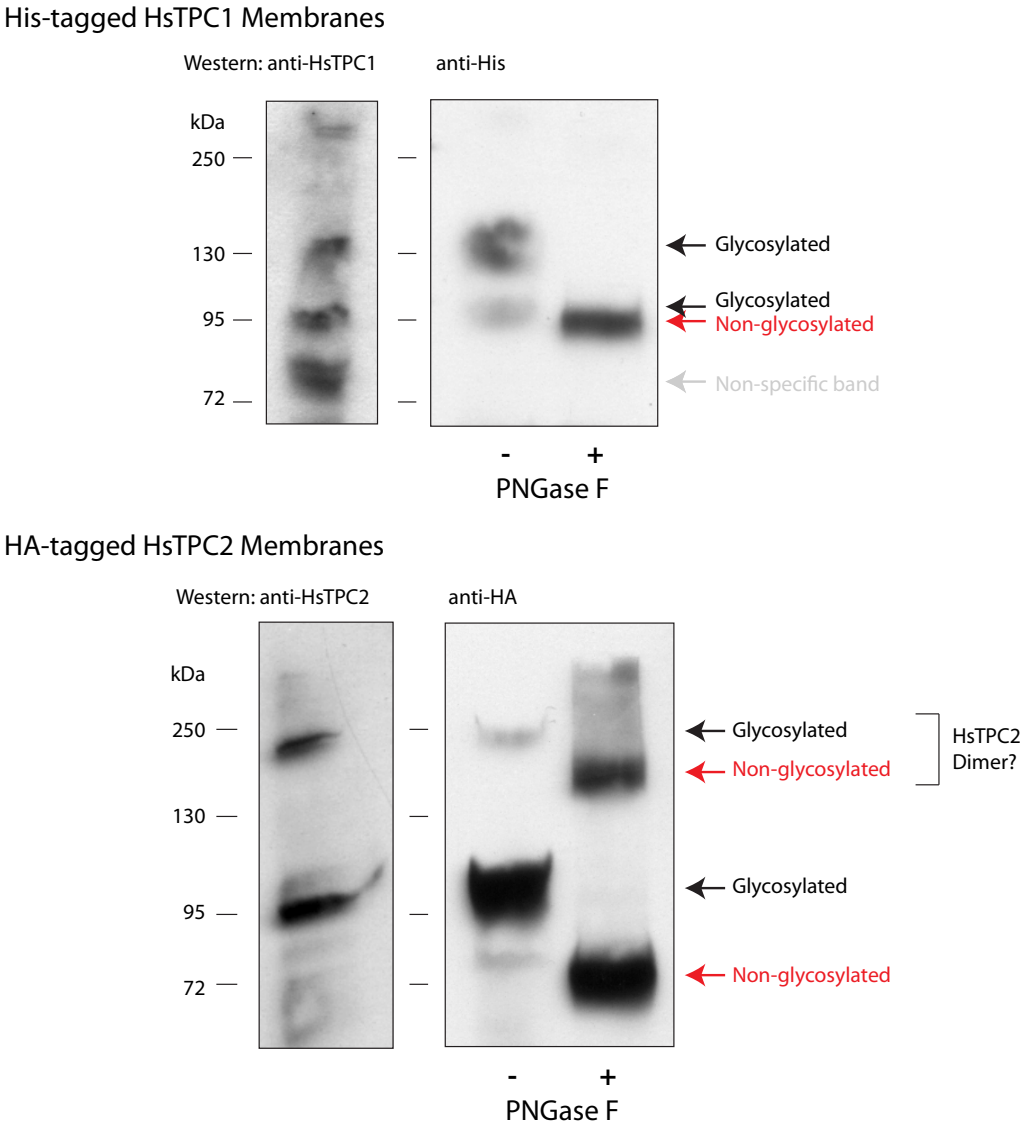


Figure 3.3: Western blots of membranes prepared from overexpressing HEK293 cells. Top: His-tagged HsTPC1 detected by anti-HsTPC1 and anti-His antibodies. **Bottom:** HA-tagged HsTPC2 detected by anti-HsTPC2 and anti-HA antibodies. PNGase F treated membranes show predicted M_w of non-glycosylated HsTPC proteins.

Two distinct HsTPC1 bands were seen on both the anti-HsTPC1 and anti-His western blots, one at around 95 kDa and one at 130 kDa. This doublet was abolished by PNGase F treatment to give one band around the predicted mass of HsTPC1. This result suggests that there are two glycoprotein variants with differing degrees of N-glycosylation: a heavily glycosylated form which runs at 130 kDa, and a less glycosylated form which is only marginally heavier than the predicted mass.

HsTPC2 also showed two bands at 95 kDa and 250 kDa. However, treatment of these membranes with PNGase F revealed two non-glycosylated proteins that run at a reduced molecular mass, one around the predicted molecular weight of HsTPC2 (85 kDa). This implies that the difference between the two bands is intrinsic to the protein rather than due to differences in sugar groups. Whilst the lower band can be assumed to be the HsTPC2 monomer, the top band could either be due to a tight HsTPC2 dimer, which resists SDS denaturation and reducing conditions, or simply due to a non-specific hydrophobic aggregate of HsTPC2 protein. The potential dimerisation of HsTPCs is discussed in chapter 5.

Thus HsTPCs exist as glycoproteins with sugar residues adding 20 - 40 kDa to their molecular mass. These sugar groups are known to protect proteins from protease degradation (26), whilst the topology of the HsTPCs already demonstrates that very little of the protein is exposed on the lumenal loops, further protection by large oligosaccharides would make the HsTPCs more resilient. This is likely to be important as they are localised in highly proteolytic endolysosomal vesicles. HsTPC2 has been shown to be expressed in the lysosome, whereas HsTPC1 has a more dynamic localisation and is seen in endosomes and lysosomes (47, 55). The disparate localisation of HsTPC1 may explain the different glycoslyation regimes seen, with different organelles requiring different sugar arrays.

Glycosylation may also be essential for correct HsTPC protein folding. The sugar groups are expressed on the small hydrophilic loops between the transmembrane segments, this positioning may prevent excessive folding and non-specific hydrophobic interactions by reducing protein flexibility (393). Removing these sugar groups by PNGase F hydrophobic makes aggregation more likely, therefore the increased intensity of the top HsTPC2 band after PNGase F treatment supports the suggestion that this is due to non-specific aggregation.

3.3 Solubilisation of HsTPC2 by the detergent CHAPS

For SDS PAGE the membranes had to be treated with a denaturing detergent (SDS) which solubilised the hydrophobic proteins. However, to purify the TPCs in their native configuration a non-denaturing detergent is required. The zwitterionic agent 3-[(3-Cholamidopropyl)dimethylammonio]-1-propanesulfonate (CHAPS) is an efficient non-denaturing detergent commonly used to solubilise membrane proteins. It has been previously used in radioligand binding studies and did not disrupt NAADP binding to its receptor (29).

Detergents are most efficient at solubilising proteins when they are evenly dissolved amongst the buffer because if the concentration is too high then the detergent assembles to form micelles. The critical micellular concentration of CHAPS is dependent on buffer salt concentration, and thus it was necessary to optimise solubilisation conditions with this detergent (68). As the HsTPC2 isoform was the first to be associated with NAADP signalling (55), optimisation was first carried out with this protein. Membranes were prepared as in figure 3.1 from HEK293 cells overexpressing HsTPC2 with the HA tag. The membranes were then solubilised with various concentrations of CHAPS. Figure 3.4 shows a western blot against the HA tag of HsTPC2 of samples of equal protein content from both the solubilised fraction or the insoluble pellet treated with Laemmli (SDS) buffer.

When no detergent was present all the HsTPC2 remained insoluble and within the pellet fraction. As the concentration of detergent was increased a greater proportion of HsTPC2 was solubilised into the supernatant up to a maximal solubilisation at 1 %. However, at the even higher CHAPS concentration of 2 %, the efficiency was reduced, this may be due to the the independent formation of micelles by detergent molecules which would impair solubilisation.

From figure 3.4 it was decided that the optimal concentration of CHAPS under these experimental conditions was 1 % (w/v).

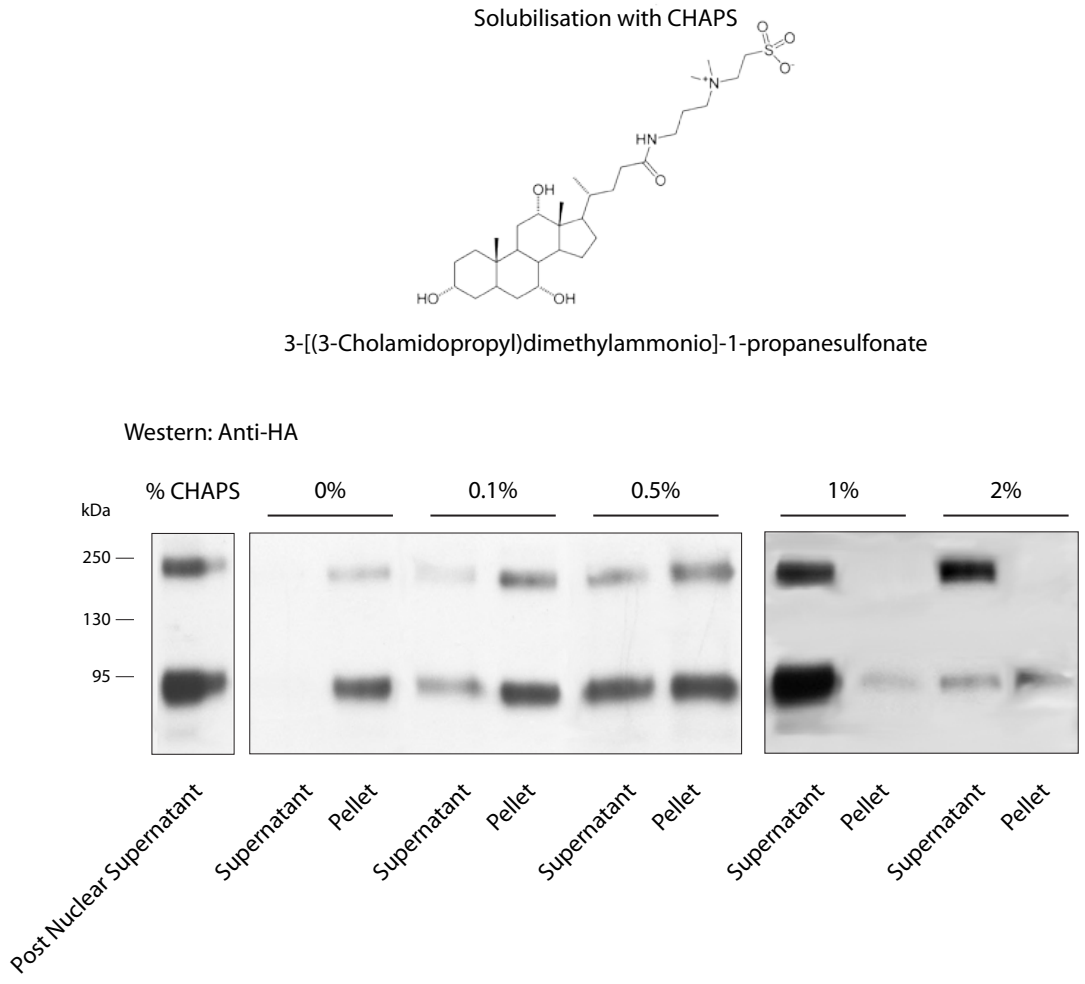


Figure 3.4: HsTPC2 solubility with CHAPS. CHAPS the zwitterionic detergent is pictured above. Cell membranes were treated with various concentrations and centrifuged to pellet insoluble material. 25 µg of the supernatant and resuspended pellet fractions from each solubilisation were loaded on SDS PAGE and blotted with anti-HA antibodies. The post nuclear supernatant presents a positive control demonstrating the presence of HsTPC2 before solubilisation. The same amount of total protein (50 µg) was loaded per lane. The greatest HsTPC2 recovery in the supernatant fraction was with 1 % CHAPS.

3.4 Gel filtration

In an attempt to further isolate HsTPC2 from the solubilised membrane mixture, and to remove contaminating proteins, fast protein liquid chromatography (FPLC) was used to separate proteins by gel filtration. This is a widely used method for the fractionation and purification of proteins, including the purification of IP_3Rs and RyRs (195, 416).

Gel filtration fractionates a sample simply based on the molecular weight of the component proteins. In these experiments a Superdex 200 HR 10/30 column packed with Superdex 200 matrix was used to separate HsTPC2 from a sample of solubilised membranes. The range of this column is suitable for fractionating proteins with a molecular weight ranging from 10 to 600 kDa, the HsTPC2 protein at 85 kDa fits within this range.

Solubilised HsTPC2 membranes were added to the column to a maximum of 5 mg of protein. Purification was performed with the same parameters as shown with the standard proteins in chapter 2 and 2 ml fractions were collected. These were then run on a western blot and probed for the HA tag. The protein $UV_{280\ nm}$ absorbance trace is aligned with the anti-HA western blot in figure 3.5.

HsTPC2 eluted the column in the major peak at around 8 ml (n = 3). This correlates with the void volume of the column (Blue Dextran M_w = 20,000 kDa elutes at 7.9 ml), which means that HsTPC2 is too large (> 600 kDa) for the column to resolve. This suggests that HsTPC2 may be eluted as a complex with tightly bound accessory proteins. Initial purifications of RyR and IP_3R eluted at larger molecular masses than expected, and were shown to exist as multimers (194, 416) and bound to accessory proteins (168, 470). Previous purifications of the NAADP receptor from sea urchin egg homogenate revealed complexes > 670 kDa (71) and 400 kDa (29). If these are indeed TPCs then these discrepancies would need to be investigated. They could be due to differences in experimental conditions or the composition of any complex could vary between isoforms.

There is also again the possibility that these signals are due to hydrophobic aggregates of HsTPC2 when it is removed from the membrane. However, these aggregates seem to be broken when the fractions are run on SDS PAGE where bands were seen at 90 kDa and 250 kDa.

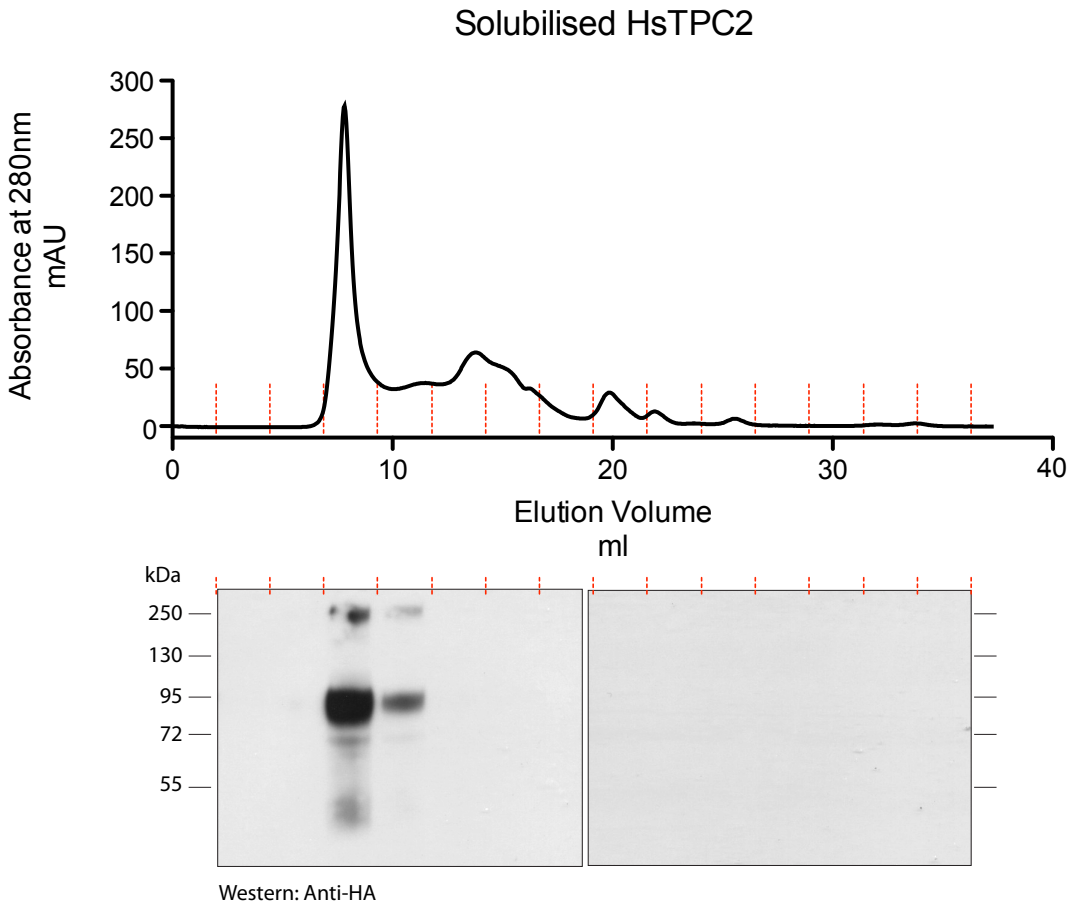


Figure 3.5: HsTPC2 separation by gel chromatography. The trace above shows the $UV_{280\ nM}$ absorbance at the base of the Superdex 200HR 10/30 column of 5 mg of solubilised HsTPC2 membrane proteins with the elution volume required for gel filtration with IP buffer containing 1 % CHAPS. The red lines indicate 2 ml fraction divisions. Aligned to these divisions the anti-HA western blot depicts the presence of HsTPC2 in fractions 3 and 4. This corresponds to the largest elution peak.

It would be possible to run these samples on a column with a higher protein range, for example the Sephacryl S- 400 HR (average particle size of 50 µm) which is able to separate proteins with molecular weight ranging 20 - 8,000 kDa, and was used in the purification of the IP_3R (416). However, this would require larger quantities of protein and buffer and would result in substantial dilution of HsTPC2, which would then need to be extracted from the solution, so further gel filtration was not conducted.

Overall, gel filtration did not prove a worthwhile procedure in the purification of HsTPC2. The fractions of interest were still contaminated by all proteins > 600 kDa and the additional manhandling of the protein solution, together with the time and materials required, outweighed the benefits of this procedure. Therefore, purification was conducted directly from solubilised membrane preparations.

3.5 Immunoprecipitation of HsTPC2 via an HA-tag

The technique chosen to purify native HsTPC2 from the solubilised membranes was immunoprecipitation. This is a highly specific purification, whereby antibodies against the protein are coupled onto a solid support. This effectively brings the protein out of solution as it binds the antibody and the solid support is pelleted by centrifugation. The HA tag on HsTPC2 provides a very specific target as this small peptide is highly antigenic and many anti-HA antibodies are commercially available.

Whilst HA-immunoprecipitation is a common procedure and ready-made anti-HA matrices are available, they have a low specific antibody concentration. This section will discuss that despite the additional cost and experimental steps, antibodies coupled to beads in-house were proved to be more efficient at HsTPC2 purification.

The coupling procedure used, together with the immunoprecipitation protocol and final elution of HsTPC2 are summarised by the schematics in figure 3.6.

Commercially available anti-HA antibodies were compared for their ability to immunoprecipitate HsTPC2. The Roche monoclonal high-affinity clone 3F10 was obtained both pre-coupled to an agarose matrix by the manufacturer or as free antibody in solution to be coupled to protein G sepharose in house. Two Sigma anti-HA antibodies were also compared: the mouse monoclonal (clone HA-7) pre-coupled to agarose, and the rabbit polyclonal antibody raised against HA-KLH which was coupled in-house to protein A sepharose. These antibodies are summarised in table 3.1.

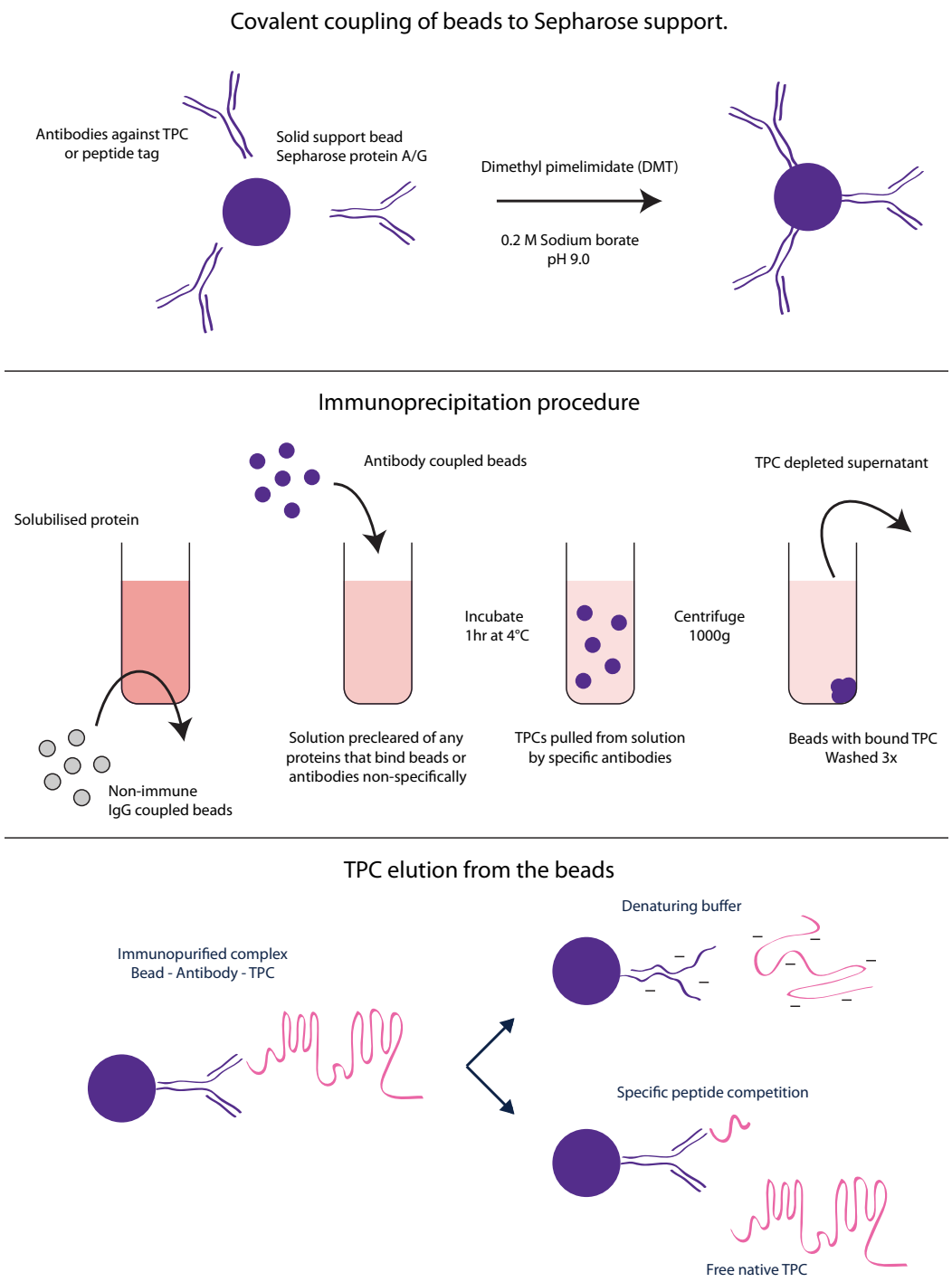


Figure 3.6: Schematic methodology of immunoprecipitation techniques. Top: Antibodies bound to a solid-support matrix of Sepharose via protein A/G interactions covalently coupled with the compound dimethyl pimelimidate (DMT). **Middle:** Solutions precleared with non-immune antibodies before incubation and centrifugation of specific beads. **Bottom:** Proteins eluted from the solid support by denaturing SDS solution or specific epitope peptides to outcompete HsTPC binding.

Table 3.1: Anti-HA antibodies.

	Manufacturer	Species	Epitope	Coupled to
A	Roche	Rat	HA monoclonal (clone 3F10)	Protein G sepharose 25 mg/ml
B	Roche	Rat	HA monoclonal (clone 3F10)	Coupled to bead by Manufacturer 3.5 mg/ml
C	Sigma	Mouse	HA monoclonal (clone HA-7)	Coupled to bead by Manufacturer 20 mg/ml
D	Sigma	Rabbit	HA polyclonal	Protein A sepharose 25 mg/ml

When the antibodies were coupled in-house (A & D) the specific antibody concentration was always 25 mg/ml of bead resin, the commercially available beads have lower concentrations (see table 3.1). Solubilised membranes from cells overexpressing the HsTPC2 were diluted to a protein concentration of 1 mg/ml and once this had been precleared with the relevant non-immune IgGs, samples were treated with 10 % (v/v) anti-HA beads. The purified immunocomplex was eluted from the beads by 10 µg/ml HA peptide, then subsequently with denaturing Laemmli buffer to remove what was remaining. Both the elutions and a sample of the depleted supernatant were run on an anti-HA western blot. As a positive control 10 µg sample of the input solubilised protein was run on the gel alongside the same volume of the solution that had been precleared with non-immune rat IgGs (rabbit IgG precleared solution not shown).

The anti-HA western blot in figure 3.7 demonstrates that each antibody could successfully purify the HsTPC2 protein to some extent. All results were compared to the positive control of the input which shows the expression of the typical two HsTPC2 bands ($\approx$ 85 kDa & 200 kDa). These are not substantially diminished by the preclearing step. A negative control experiment with beads coupled to non-immune rat IgG did not show these bands confirming that the HsTPC2 interaction with anti-HA beads is specific (data not shown).

Of all the antibodies tested, the most efficient was the Roche rat monoclonal coupled to the sepharose beads in house (A) (figure 3.7), this is based on the large recovery of protein seen in the peptide elution. The peptide elutions are the most important

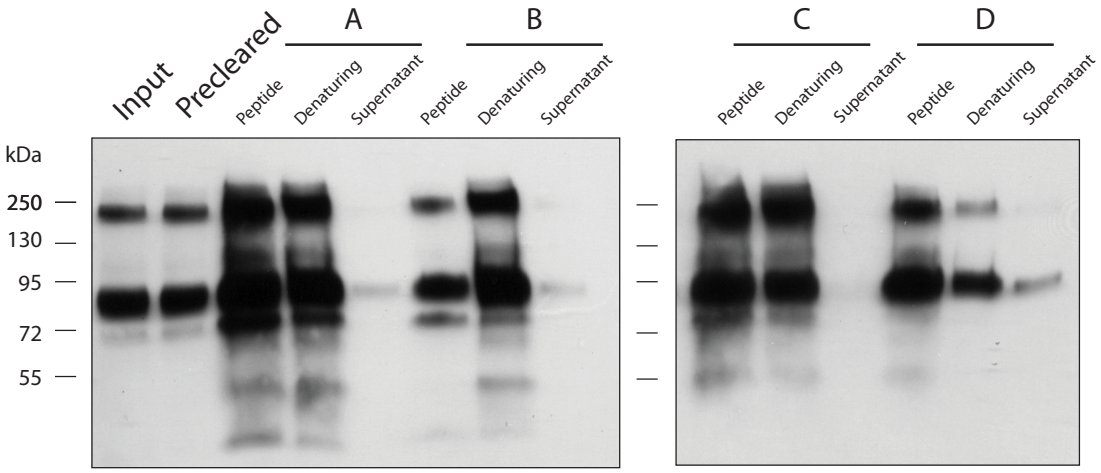


Figure 3.7: Immunoprecipitation of HsTPC2 by commercially available HA antibodies. Anti-HA western blot depicting the results of four anti-HA immunoprecipitation experiments with different antibody-beads. The input of solubilised HsTPC2-expressing membranes acts as a positive control and the precleared lane shows that treatment with rat IgG does not substantially affect levels of HsTPC2. All antibodies tested are listed in table 3.1. 'Peptide' refers to elution with 10 µg/ml HA peptide, 'Denaturing' refers to a subsequent elution with SDS containing Laemmli buffer. 'Supernatant' is the supernatant remaining once the beads have been removed.

bands, as ultimately the purified HsTPC2 will be analysed to detect functional Ca^{2+} conductance and need to remain in their native state. The other anti-HA antibodies show a good level of HsTPC2 purification but to a lesser extent.

From this analysis, the in house coupling of the Roche anti-HA monoclonal (A) was chosen as the methodology used in all future HA-immunoprecipitations.

3.5.1 Optimising the HA immunoprecipitation

A noticeable feature of the immunprecipitation is that there remained a large amount of HsTPC2 bound to the bead after the HA-peptide competition, which was only recovered by a the harsh denaturing elution which disrupts protein structure. A simple solution to this problem was to optimise the effect of increased HA-peptide concentration during the elution step.

The immunoprecipitation with the chosen beads (A - Roche anti-HA coupled in house) was repeated as above, however, two higher HA peptide concentrations were tried at elution: 25 µg/ml and 50 µg/ml. Figure 3.8 illustrates that higher concentrations were more efficient at competing the HsTPC2 from the antibody, with the 50 µg/ml eluting nearly all the protein bound.

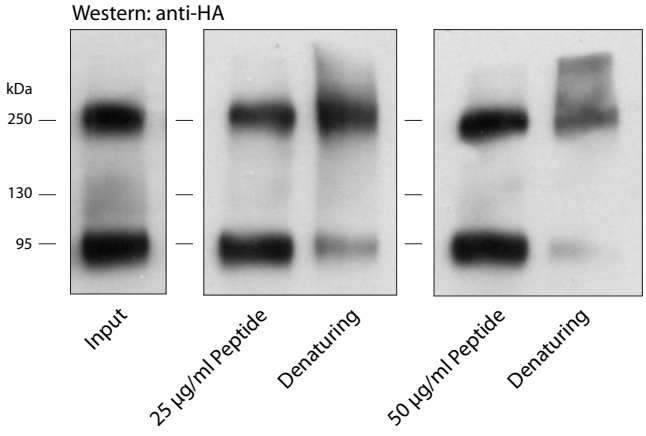


Figure 3.8: Elution of HsTPC2 with higher peptide concentrations. Anti-HA western blot depicting two anti-HA immunoprecipitation reactions. The input lane refers to solubilised membranes expressing HsTPC2. The HA peptide concentrations use to elute the proteins are labelled. A subsequent elution with an SDS containing Laemmli buffer is labelled 'Denaturing'.

The reverse experiment was performed to verify the affinity of the HA antibody. Samples of beads were pre-incubated with a range of HA-peptide concentrations for 1 hour before the solubilised membranes containing HsTPC2 were added and the immunoprecipitation was then conducted as before and the anti-HA western blot shown in figure 3.9.

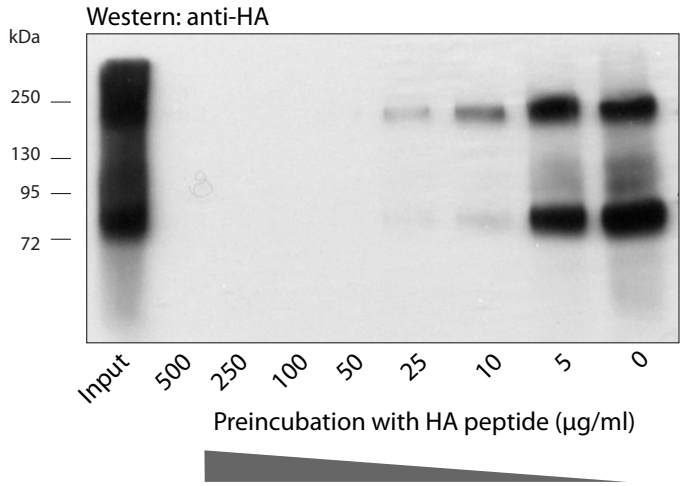


Figure 3.9: Preincubation with specific peptide prevents immunoprecipitation. Anti-HA western blot depicting 8 anti-HA immunoprecipitation reactions, each set of beads had been preincubated for 1 hour with the concentration of HA peptide labelled. Input refers to a sample of solubilised membranes expressing HsTPC2.

This long exposure makes it impossible to resolve the two HsTPC2 bands in the positive control input lane, however, it is clear that there was a high level of HsTPC2 present. Where the beads had been incubated with a high HA peptide concentrations, the immunoprecipitation was unsuccessful. The range at which the HsTPC2 began to compete with the HA-peptide correlates nicely with the elution experiment above. Whilst 50 µg/ml of peptide entirely prevented HsTPC2 binding, 25 µg/ml allowed a small extent of immunoprecipitation. HsTPC2 recovery increased as the peptide concentration was further reduced.

From these results all subsequent immunoprecipitations were eluted with 50 µg/ml of peptide. Higher concentrations may have yielded a marginally better elution, but this was considered negligible when compared to the cost of increasing the concentration further. A higher peptide concentration may also have further affected buffer osmolarity

and pH. The isoelectric point (pI) of the HA peptide is 3.56, which means it acts as a weak acid.

3.5.2 Quantification of the purification from western blot analysis

Unlike the purification of enzymes, where protein yield can be quantified by assaying catalytic activity, HsTPC2 has no quantifiable characteristics. To gauge the extent of purification an analysis of several western blots provided a rough estimate of how much HsTPC2 protein was being eluted.

Total protein of solubilised membrane was loaded alongside the same volume of precleared solution. The immunoprecipitate elutions and the depleted supernatants were also analysed. The western blot was probed with an anti-HA antibody and the band intensities were analysed and normalised to the input (n = 5).

Figure 3.10 aligns the intensities of both bands with an example anti-HA western blot. The analysis shows that the preclearing step removed a proportion of HsTPC2, however, approximately 85 % of solubilised membrane HsTPC2 remained after preclearing. The immunoprecipitation with anti-HA beads recovered the majority of the 90 kDa band, but significantly less of the high molecular weight band. The solution was not saturated with antibody-coupled beads because some HsTPC2 remained in the supernatant. The rat IgG control was very clean within minimal levels of contamination, however, the reduced levels of HsTPC2 in the supernatant suggests that the immunoprecipitation procedure depleted the solution of HsTPC2 perhaps due to non-specific interactions with the beads or plasticware.

Therefore this shows a immunoprecipitation yield of $> 80\,\%$, demonstrating the high affinity of the anti-HA monoclonal and optimal purification conditions. However, for future functional single-channel analysis in the lipid bilayer, yield is not important, it is the functionality of the channel which is essential.

3.5.3 Radioligand binding to HA-immunopurified samples

One functional assay would be the binding of radiolabelled NAADP to the purified samples. Previous studies have shown that levels of ^{32}P-labelled NAADP binding are increased in cells overexpressing HsTPC2 and that this binding is lost when HsTPC2 is removed from the solution (55). However, in these experiments levels of binding are very low (167 - 300 d.p.m.) compared to background (100 d.p.m.) (55).

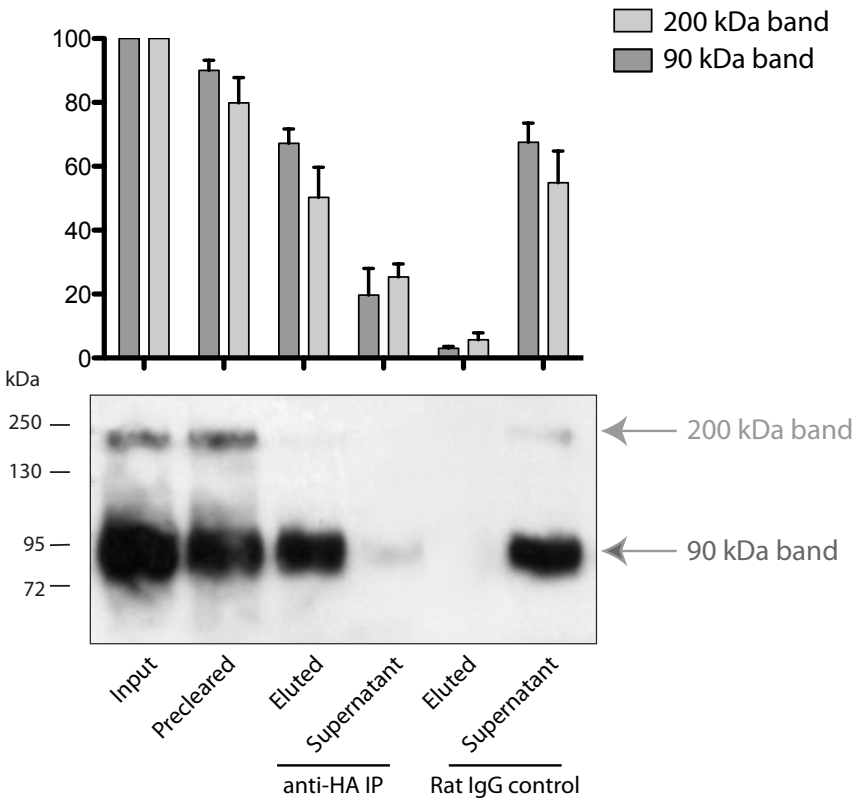


Figure 3.10: Percentage recovery of HsTPC2 in the immunoprecipitate. Histogram depicting mean band intensities from anti-HA western blots (n = 5) normalised to solubilised membrane input. An example blot is aligned below. Solubilised membranes from HEK293 cells overexpressing HsTPC2 are the loading control. Membranes precleared with rat IgG beads are the input for the immunoprecipitation. Anti-HA immunoprecipitation yields the eluted sample (HA Eluted) and a depleted solution (HA supernatant). The equivalent from the non-immune IgG control immunoprecipitation acts as a negative control. The two bands labelled were analysed separately.

Radioligand binding also provides an ideal method of further quantifying HsTPC2 purity and yield, as this was employed in purifying RyR and IP_3R (195, 416).

Under the assumption that HsTPC2 acts as the NAADP receptor, a simple radioligand binding assay was conducted to determine the extent of ^{32}P-labelled NAADP binding seen in samples of solubilised membranes and immunoprecipitated HsTPC2.

Specific binding was ascertained by comparing the total binding seen when radiolabelled NAADP was added to the sample, to non-specific binding determined with sample pre-blocked in the presence of 100 µM NAADP as depicted in the schematic figure 3.11. This high pre-blocking concentration saturates all specific binding sites preventing the radioligand binding, therefore all binding seen with a pre-blocked sample is due to non-specific interactions with the plasticware or other contaminants. Non-specific binding can be subtracted from the total binding and the resulting difference therefore corresponds to the specific binding.

Mouse liver membranes solubilised in 1 % CHAPS were used as as a positive control because this tissue has been shown to bind NAADP with a high affinity (55).

Solubilised membranes and eluted samples from anti-HA and IgG control immunoprecipitations were either preincubated with 100 µM NAADP (unlabelled) or the same volume of buffer for 1 hour. ^{32}P-labelled NAADP was added to both tubes to a final concentration of 0.2 nM and further incubated for an hour. The proteins were precipitated and filtered from the solution to be analysed for the presence of ^{32}P. Figure 3.12 summarises the data normalised to the solubilised liver membrane input (n = 3). All experiments were validated by western blotting and each showed HsTPC2 presence in the HA-IP sample but not the control.

As has previously been shown by Calcraft *et al.* there was a large difference in the extent of NAADP binding between the human protein and mouse liver samples, with the HsTPC2 giving considerably lower signals than the mouse liver control (55). Here even input membranes represented just 5.6 ± 1.2 % of the positive control. Thus in the immunoprecipitation samples background noise swamped much of the signal and the error bars show large variation in results. Overall, there was no difference in the extent of binding in the specific IP elution and the control. This lack of NAADP binding could be due to insufficient protein levels, which would result in the very low signal to noise ratio seen.

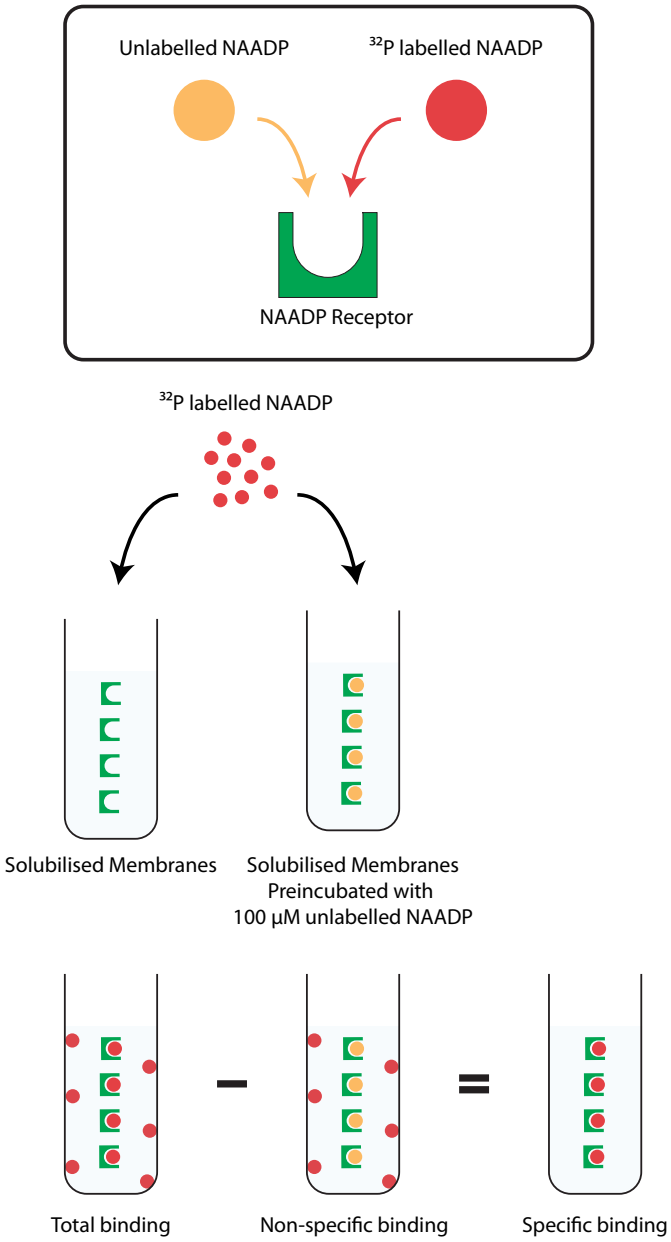


Figure 3.11: Schematic methodology of radioactive ligand binding assay. ^{32}P-labelled NAADP competes with unlabelled NAADP at any given binding site. Specific binding sites will be blocked if solubilised membranes are preincubated with unlabelled NAADP. Addition of ^{32}P-labelled NAADP to blocked membranes will bind non-specifically. Non-specific binding can be subtracted from total binding to deduce the extent of specific binding.

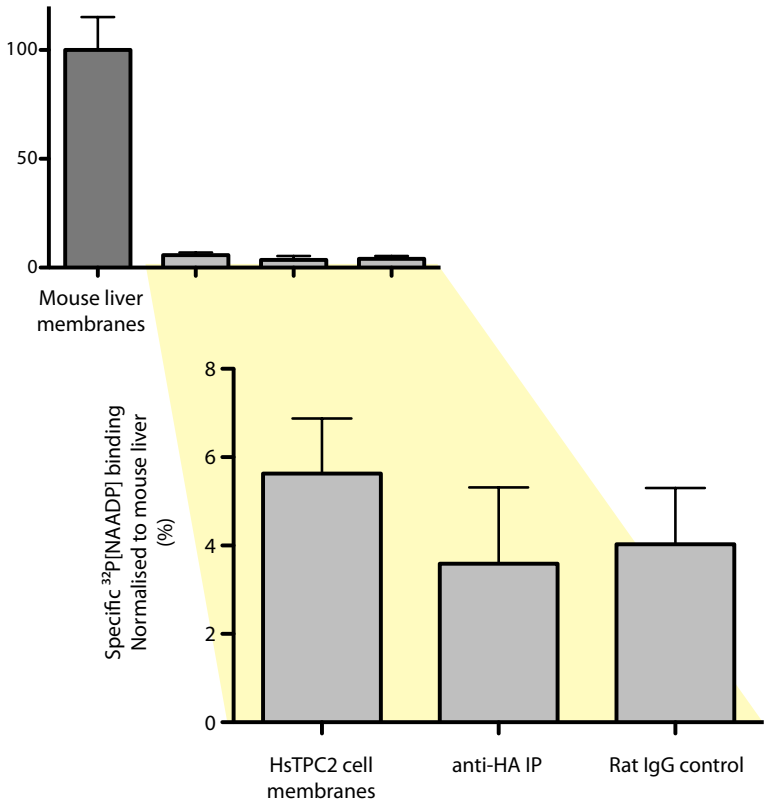


Figure 3.12: Specific ^{32}P-NAADP binding on HA immunoprecipitate. Extent of ^{32}P-NAADP specific binding normalised to solubilised mouse liver membranes. Solubilised membranes from HEK293 cells overexpressing HsTPC2 ("HsTPC2 cell membranes") were the input for the immunoprecipitation. Anti-HA IP was the eluted complex from the specific immunoprecipitation, Rat IgG control was the eluted complex from non-immune IgG immunoprecipitation. Samples were validated by western blotting (n = 3).

This result may even suggest that HsTPC2 is not the NAADP binding protein itself, but associates with an accessory protein which binds NAADP and is coupled to HsTPC2 channel gating. However, if this accessory protein is not coimmunoprecipitated with HsTPC2 then binding would not be seen. A similar phenomenon is currently being investigated whereby the RyR accessory protein, FK-506 binding protein 12.6, may act as an intermediary which binds cADP-ribose and causes a shift in RyR gating (418, 449).

3.5.4 Incorporation of the HA-immunopurified protein into a lipid bilayer

The impetus for HsTPC2 purification was to develop a functional assay to measure the channel properties of the protein. Artificial bilayers provide a model membrane into which channel proteins can be incorporated and single-channel currents measured. Most of the knowledge regarding RyR electrophysiological properties has been gathered using this technique (449).

The immunopurified complex was dialysed to remove detergent and was reconstituted into planar lipid bilayers in collaboration with Rebecca Sitsapesan's laboratory at the University of Bristol. Electrophysiological recordings were taken under voltage clamp conditions, with the *trans* chamber held at a fixed potential and the *cis* chamber held at various potentials relative to ground as shown in the schematic figure 3.13. Compounds such as NAADP could be added to either chamber and currents through the bilayer were measured.

Incorporation of the HA.HsTPC2-immunopurified complex into an artificial bilayer gave no current activity in the presence or absence of NAADP (n = 8, data not shown) suggesting that either HsTPC2 is not the NAADP-gated Ca^{2+}-channel, or that this purification technique was damaging the complex.

In an attempt to reconcile this dilemma, immunoprecipitation was conducted via a different antibody and this approach to purify the native HsTPC2 had more success functionally, as will be shown.

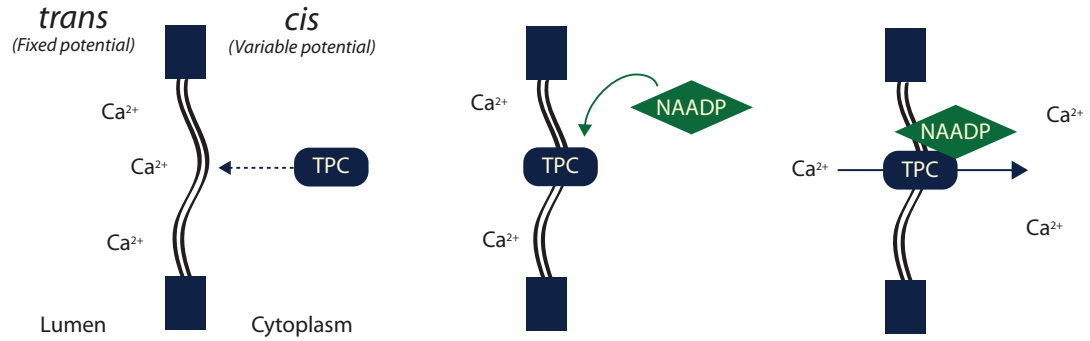


Figure 3.13: Schematic representation of HsTPC2 incorporation into an artificial bilayer. A planar phosphatidylethanolamine bilayer was painted across a teflon aperture separating two chambers: *cis* and *trans*. Channel complexes were added to the *cis* chamber and incorporation was seen by increased current activity due to sporadic constitutive channel openings. Compounds could be added to both chambers and channel activity recorded as the permeant ion traversed down its electochemical gradient.

3.6 Immunoprecipitation of HsTPC2 by polyclonal anti-TPC2 antibodies

To purify the HsTPC2 protein directly (*i.e.* not via tags), custom antibodies were raised against peptide residues which topology analysis predict to be exposed on the cytoplasmic loops between S5/S6 and between the two 6-TM domains. The epitope positions are mapped in the schematic figure 3.14.

The resulting polyclonal rabbit serum was used to produce anti-HsTPC2 beads, by covalently coupling the whole serum to protein A sepharose beads with DMT as shown in figure 3.6. Immunoprecipitations were conducted with these coupled beads using the same protocol as with the anti-HA beads.

Polyclonal antibodies can often result in multiple non-specific interactions but this serum gave a very clean signal, with an anti-HA western blot (figure 3.15) showing a successful immunoprecipitation of HsTPC2. The characteristic two bands of HsTPC2 are present in the anti-HsTPC2 lane whilst the rabbit IgG control remains negative. This purification could be blocked by pre-incubation with 50 µg/ml of both specific epitope peptides.

This showed that HsTPC2 could be successfully purified by this method.

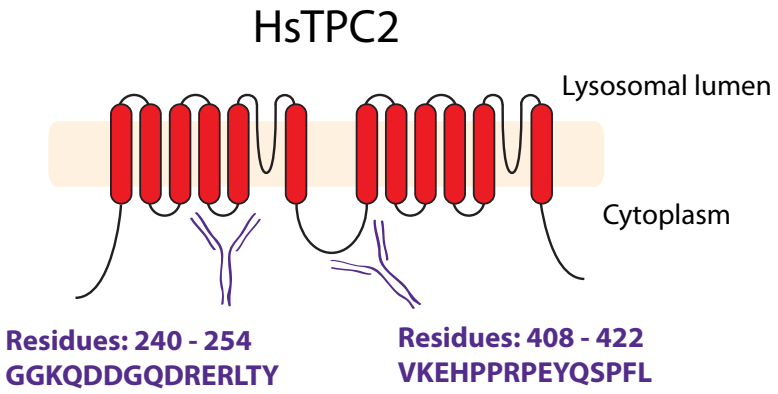


Figure 3.14: Diagram depicting the predicted position of the antigenic peptides. Two regions of HsTPC2 were targeted, the cytoplasmic loop between S4/S5 and the interdomain loop. The peptides used to generate the antibody are listed with their primary position within the HsTPC2 sequence.

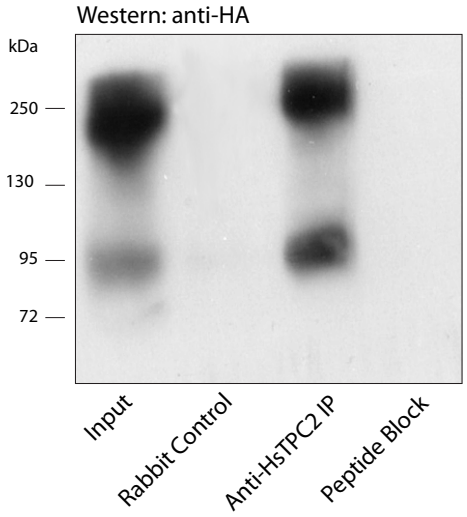


Figure 3.15: Immunoprecipitation of HsTPC2 with polyclonal serum. Anti-HA western blot depicting the successful immunoprecipitation of HsTPC2. The input lane acts as a positive control as it corresponds to solubilised membranes before immunoprecipitation, the two characteristic HsTPC2 bands at $\approx$ 250 kDa and $\approx$ 90 kDa are detected. The Rabbit control lane contains the negative control immunoprecipitation elution from beads coupled to non-immune rabbit serum. The anti-HsTPC2 lane contains the immunoprecipitation elution from beads coupled to anti-HsTPC2 serum. Peptide block refers to immunoprecipitation with anti-HsTPC2 beads which had been preincubated for 1 hour with 50 µg/ml of both HsTPC2 epitope peptides.

3.6.1 Radioligand binding to HsTPC2-immunopurified samples

Radioligand binding experiments were conducted on these samples of HsTPC2 purified by anti-HsTPC2 immunoprecipitation to determine whether they contained a functional NAADP-binding protein. Once again, the signal to noise ratio was very low and no difference was seen between the specific immunoprecipitation and the rabbit IgG control (figure 3.16).

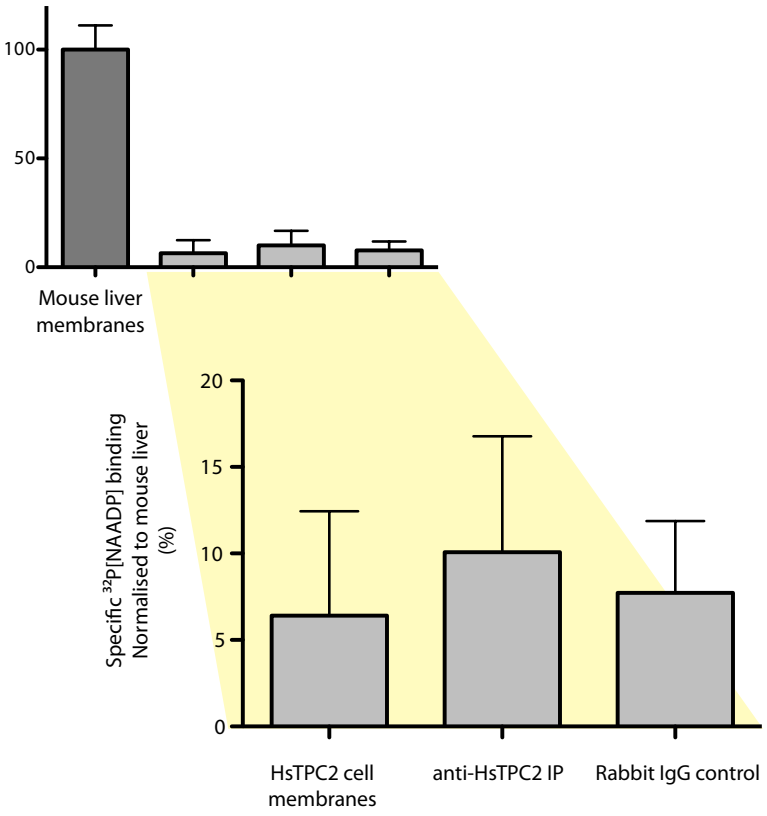


Figure 3.16: Specific ^{32}P-NAADP binding on HsTPC2 immunoprecipitate. Extent of ^{32}P-NAADP specific binding normalised to solubilised mouse liver membranes. Solubilised membranes from HEK293 cells overexpressing HsTPC2 ("HsTPC2 cell membranes") were the input for the immunoprecipitation. Anti-HsTPC2 IP was the eluted complex from the specific immunoprecipitation. Rabbit IgG control was the eluted complex from non-immune IgG immunoprecipitation. Samples were validated by western blotting. (n = 2)

This again suggests that the protein concentration in the eluted samples was too low to detect NAADP binding. However, as will be seen in subsequent experiments, the protein purified by this technique responded to NAADP in a dose-dependent manner which suggests that the NAADP-binding protein was present in these samples.

3.7 Incorporation of the TPC2-immunopurified protein into a lipid bilayer

As before, the channel function of the purified HsTPC2 was determined by incorporation into an artificial bilayer with the Sitsapesan laboratory in Bristol.

This alternative immunoprecipitation using the polyclonal serum directed against HsTPC2 itself resulted in a complex which gave measurable single current recordings. The difference between the two procedures may be due to the HA-antibody damaging protein folding, or interfering with the binding site of an accessory protein. Another alternative is that the overexpressed HA.HsTPC2 protein is not functional as a Ca^{2+}-channel and the currents seen are due to the anti-HsTPC2 serum immunoprecipitating the low levels of endogenous HsTPC2.

The next sections discuss the findings made from these single channel recordings and reveal many of the biophysical properties of the channel which provide some evidence of how HsTPC2 might behave in the cellular environment. The raw data in these sections were generated in Bristol by Dr Samantha Pitt, using protein purified in Oxford. Experimental planning and interpretation of the results were also collaborative.

3.7.1 K^+ permeability of HsTPC2 and gating by NAADP

As a preliminary investigation, the K^+ permeability of HsTPC2 was investigated in the presence and absence of NAADP. Despite predictions that HsTPC2 is a Ca^{2+} channel, K^+ ions were initially used based on analogy with IP_3R (118) and RyR (400) channels which are non-selective and show higher current amplitudes with K^+, rather than Ca^{2+}, as the conducting ion. Therefore it was not unreasonable to assume a K^+ permeability for HsTPC2 which would give a higher signal to noise ratio.

Purified HsTPC2 was incorporated into a lipid bilayer which separated *trans/cis* chambers containing symmetrical 210 mM KCl; pH 7.2 and held at +20 mV. Repre-

sentative examples of HsTPC2 single channel currents in the presence and absence of NAADP are shown in figure 3.17.

In the absence of NAADP occasional channel openings were observed, these were too brief to resolve and occurred with an open probability (P_o) of 0.0005.

Addition of NAADP to the *trans* chamber made no impact on channel opening (n = 5). However, NAADP addition to the *cis* chamber produced a substantial increase in the channel P_o (n = 101). This suggests that HsTPC2 incorporates into the bilayer in a fixed orientation such that the *cis* chamber corresponds to the cytoplasmic face of the channel, which is responsive to NAADP action whereas the *trans* chamber represents the lysosomal lumen. The basis for this topological bias is unknown but is also reported with other purified ion channels including RyR2 (397) and TRIC-A (348).

To ensure that channel activity was indeed due to HsTPC2 action, proteins immunoprecipitated with the non-immune rabbit IgG coupled beads were incorporated into the bilayer under identical conditions and no currents were seen in the presence or absence of NAADP (n = 20). Example traces are shown in figure 3.18. This evidence directly links the NAADP-induced channel activity with HsTPC2 protein.

3.7.2 Sub-conductance state

An intriguing discovery was that the HsTPC2 channel often enters a sub-conductance state at approximately 70 % of the full open channel level, this distinctive feature is magnified in figure 3.17. Subconductance states have been seen in RyRs (3, 469) and whilst their physiological relevance is still unknown, it may give an additional layer of gating control. Alternatively, this could simply be an artefact due to channel damage during purification.

3.7.3 Coupled gating

Another observation of note was that multiple channels appeared to open and close concomittently in a synchronised or coupled fashion. Figure 3.19 shows an example of 4 channels which opened simultaneously.

This phenomenon has also been observed in RyRs where multiple RyR channels were shown to open and close in synchrony. This was termed 'coupled gating' when it was first described (281) and although the mechanism is yet to be elucidated, it is ligand-dependent (FKBP-dependent) similar to the effect seen in HsTPC2. Coupled

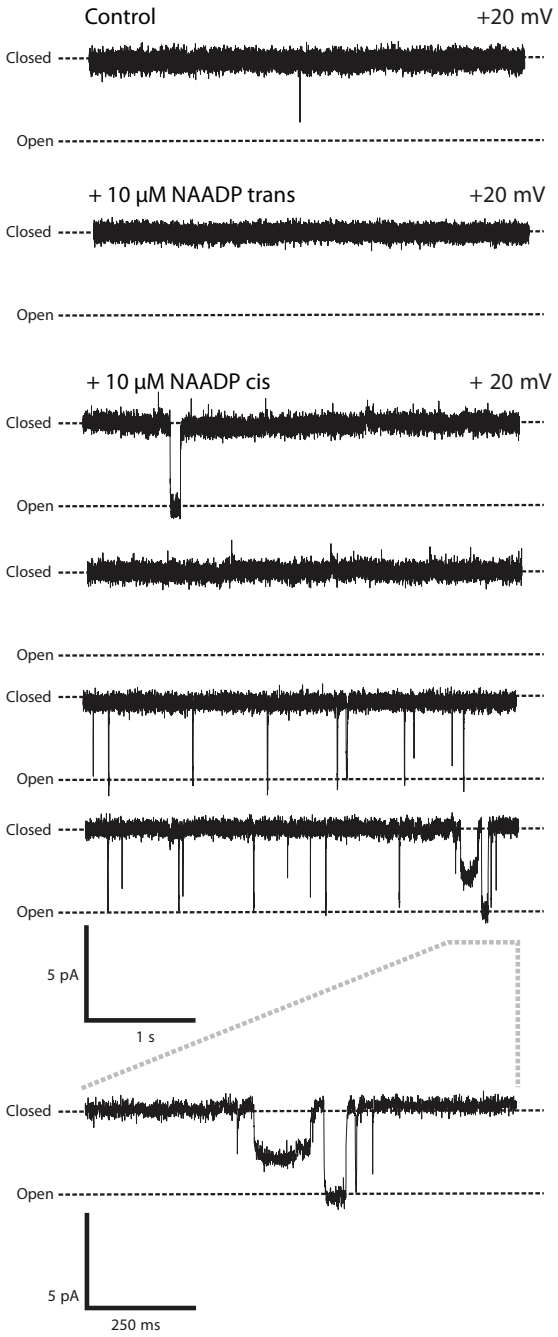


Figure 3.17: Representative traces with K^+ as the permeant ion. Example of single-channel HsTPC2 currents in the presence of 10 µM NAADP. Both chambers contained 210 mM KCl; pH 7.2. The control trace shows basal HsTPC2 activity in the absence of NAADP. Addition of 10 µM NAADP to the *trans* chamber had no effect on the P_o. Addition of 10 µM NAADP to the *cis* chamber increased channel activity considerably (n = 101). The bottom panel magnifies the trace to demonstrate the presence of a sub-conductance state.

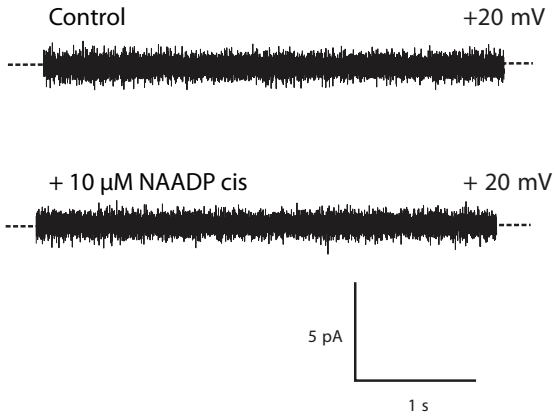


Figure 3.18: Control IgG immunoprecipitate does not respond to NAADP. Example of current recordings with elutates from the non-immune rabbit IgG immunoprecipitation control. Both chambers contained 210 mM KCl; pH 7.2. No basal activity was seen and addition of 10 µM NAADP to the *cis* chamber did not induce channel-like events (n = 20).

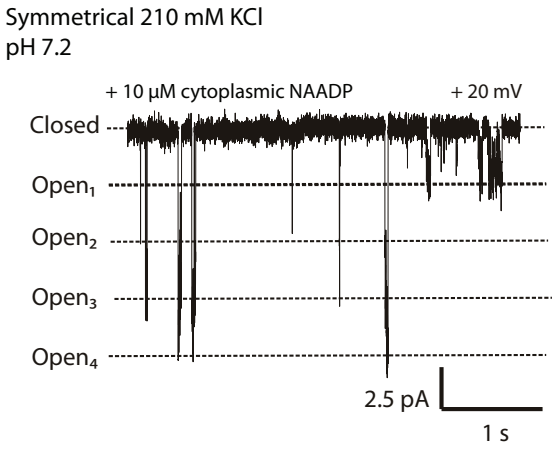


Figure 3.19: Episodic gating of HsTPC2 channels. Representative trace depicting the simultaneous opening of multiple channels, demonstrating coupled gating of HsTPC2 in the presence of 10 µM NAADP. Four distinct open states can be seen. Both chambers contained 210 mM KCl; pH 7.2 (n = 7).

gating would enable the small conductance seen from a single channel to be amplified by recruiting surrounding channels to open simultaneously and thus produce larger Ca^{2+} signals.

3.7.4 K^+ conductance

The channels, once incorporated, were held at various holding potentials and total current was measured, these were compiled and a current voltage relationship was determined (appendix figure A.1). The gradient of this relationship under symmetrical 210 mM KCl represents the channel K^+ conductance, here 300 ± 6 pS (n = 5). In gradient KCl (210 mM *trans*: 510 mM *cis*) the current voltage relationship was shifted to the left, however, the conductance was not altered. The reversal potential was - 20.5 mV which would suggest a channel selective for cations.

3.7.5 Ca^{2+} permeability

As HsTPC2 has been predicted to be an NAADP-activated Ca^{2+}-permeable channel, experiments were conducted where Ca^{2+} was the conducting ion. NAADP action remained *cis*-specific with 15 µM Ca^{2+} in the *cis* (cytoplasmic) chamber and 50 mM Ca^{2+} in the *trans* (luminal) chamber (complete solutions shown in table 2.1) (n = 5). Representative traces are shown in figure 3.20. Addition of 10 µM NAADP to the *trans* chamber did not illicit channel opening, whereas when added to the *cis* chamber NAADP induces sustained channel opening.

This was the first evidence that HsTPC could act as a Ca^{2+}-permeable channel.

A current voltage relationship (appendix figure A.2) reveals a Ca^{2+} conductance of 15 ± 1.5 pS (n = 5). This conductance is very small in comparison with RyR2: 120 pS (425) and IP_3: 53 pS (37, 118) recorded under identical conditions.

The relative permeability of HsTPC2 to monovalent and divalent cations was measured by monitoring conductance with 210 mM K^+ *cis* and 210 mM Ca^{2+} *trans*. Under these conditions a Ca^{2+}/K^+ permeability ratio (P_{Ca}/P_K) of 2.6 was obtained. Thus like the known Ca^{2+} releasing channels IP_3R and RyR the HsTPC2 is selective for cations but lacks strong discrimination between monovalent and divalent cations (37, 252, 425).

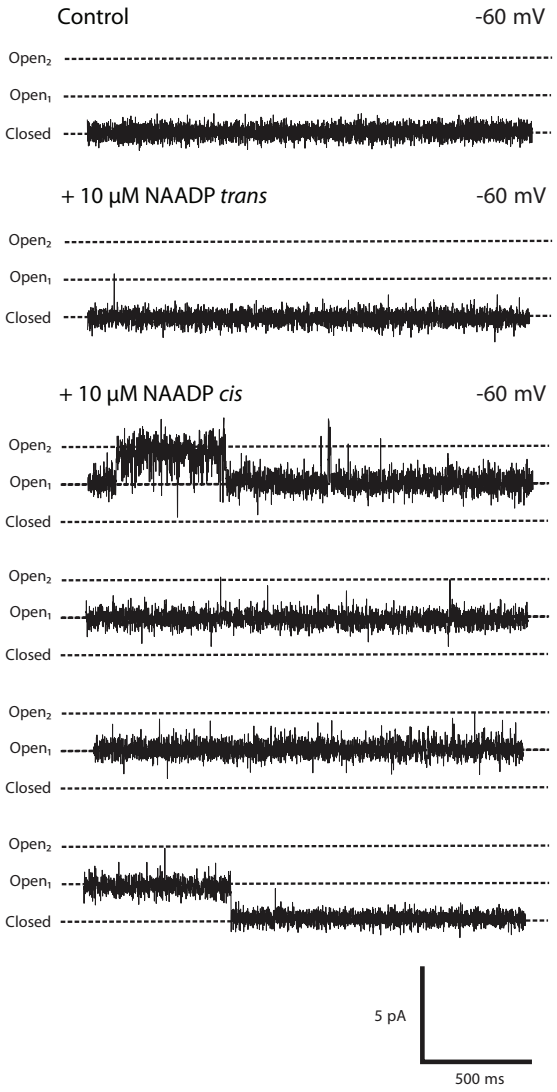


Figure 3.20: Representative traces with Ca^{2+} as the permeant ion. Example of single-channel HsTPC2 currents in the presence of 10 µM NAADP. The *cis* chamber (cytoplasmic) had 15 µM free Ca^{2+}; the *trans* chamber (luminal) had 50 mM free Ca^{2+}. Both chambers were at pH 7.2. The control trace shows basal HsTPC2 activity in the absence of NAADP. Addition of 10 µM NAADP to the *trans* chamber had no effect on the P_o. Addition of 10 µM NAADP to the *cis* chamber increased channel activity (n = 5).

3.7.6 NAADP concentration-response relationship

The pharmacology of HsTPC was investigated using K^+ as the conducting ion as the current amplitudes seen were much larger and suffered less noise interference. Figure 3.21 shows representative traces of HsTPC2 K^+ currents induced by various concentrations of NAADP. The concentration of NAADP applied to the cytoplasmic face was incremented in a cumulative fashion; each NAADP addition correlated with an increase in P_o up to a concentration of 1 µM where the activity plateaued and further addition of NAADP had no effect. However, if 1 mM NAADP was applied directly to the channel, without pre-treatment with activating concentrations, the channels immediately shut and no activity was seen (appendix figure A.3).

The final trace in figure 3.21 shows channel activity after the *cis* chamber had been perfused in the absence of NAADP. This washout did not diminish HsTPC2 activity which demonstrates that NAADP binds irreversibly on this time scale, under these conditions.

These experiments reveal a low affinity of HsTPC2 for NAADP, this data is summarised in figure 3.22 which plots the concentration-response curve for NAADP from which the EC_{50} value can be deduced. This value was unexpectedly high at around 500 nM compared to the K_d reported for NAADP binding to cells overexpressing HsTPC2 (5 nM) or membranes isolated from mouse liver (6.6 nM) (55). This also contradicts experiments which observe a physiological release of intracellular Ca^{2+} in response to low nM concentrations of NAADP (57, 275, 304).

The low affinity observed prompted investigation into physiological environmental factors that may affect HsTPC2 sensitivity to NAADP.

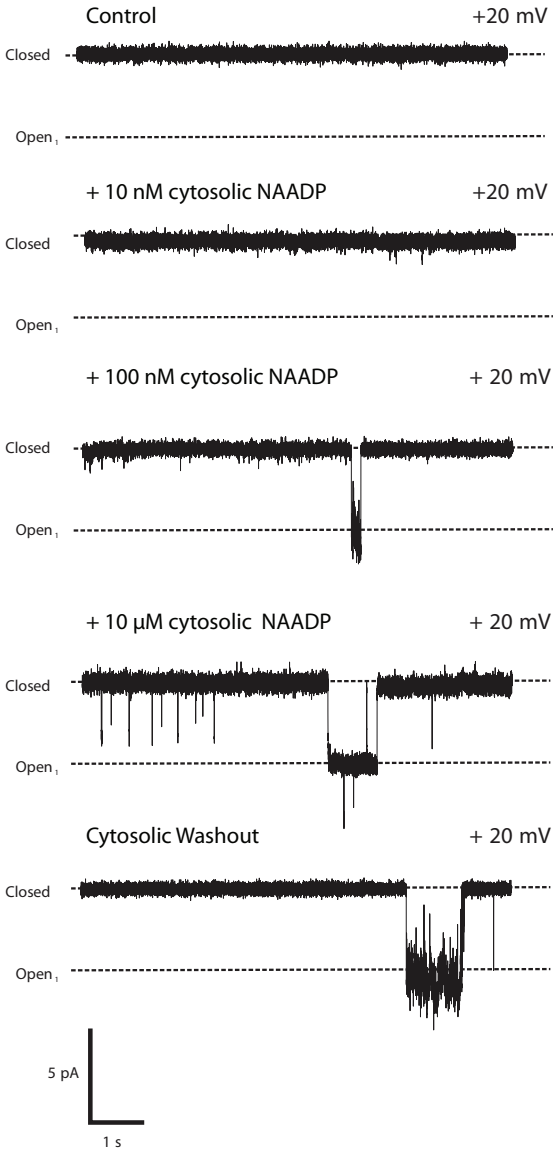


Figure 3.21: Effects of NAADP concentration of HsTPC2 channel gating. Representative traces of single channel HsTPC2 currents in response to sequential increments in NAADP concentration. Final concentrations are labelled above each trace. The control trace depicts basal channel activity. Cytosolic washout refers to total perfusion of the *cis* chamber in the absence of NAADP. K^+ was the conducting ion; both chambers were symmetrical at pH 7.2 and 10 µM Ca^{2+} (n = 3).

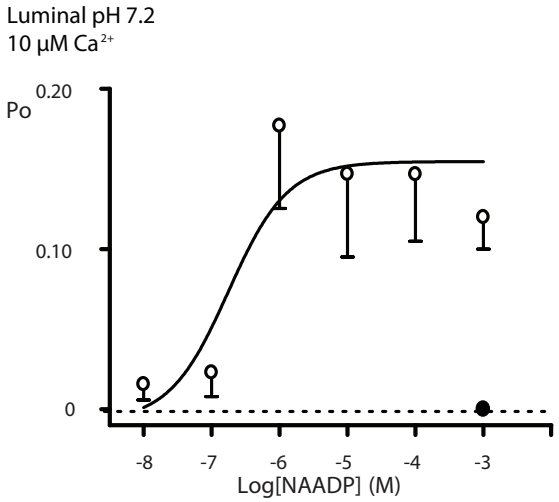


Figure 3.22: NAADP concentration-response relationship. The sigmoid relationship between mean P_o values induced by incrementally increasing concentrations of NAADP. K^+ was the conducting ion; both chambers were at pH 7.2. Data are mean values (n = 3, S.D.) The addition of 1 mM NAADP without pre-treatment with activating concentrations is showed by the filled circle (n = 4).

3.7.7 Regulation by luminal [Ca^{2+}]

Both IP_3R and RyR are reported to be sensitive to luminal levels of Ca^{2+} in the endoplasmic reticulum (37, 259, 397). To investigate the effects of luminal Ca^{2+} on HsTPC2 activity, the Ca^{2+} concentration in the *trans* chamber was raised. Previously with a luminal concentration of 10 µM Ca^{2+}, 10 nM NAADP had negligible effect on HsTPC2 P_o (figure 3.21), however, in figure 3.23 when the luminal Ca^{2+} concentration was raised to 200 µM the same concentration of 10 nM NAADP was optimally efficacious.

The free [Ca^{2+}] of the lysosomal lumen is a contentious issue which is further discussed in section 4.16.6, however, predicted values centre around 200 µM, so these experiments could be considered to be more physiologically relevant than those conducted with 10 µM luminal Ca^{2+}.

Channel activity was measured in the presence of various concentrations of NAADP and the resulting concentration-response relationship is plotted in figure 3.24. The solid line represents the relationship with 200 µM luminal Ca^{2+}, the dashed line depicts the relationship with 10 µM luminal Ca^{2+} as in figure 3.22 for comparison. With this 20-fold increase in luminal [Ca^{2+}] the NAADP concentration-response relationship is

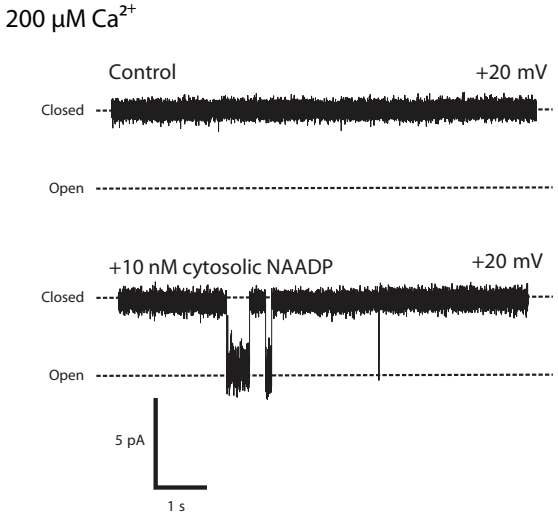


Figure 3.23: Example trace depicting increased NAADP sensitivity with 200 µM luminal Ca^{2+}. Single channel currents with K^+ as the conducting ion; both chambers pH 7.2, showing that previously inactive concentrations of NAADP (10 nM) open HsTPC2 when the *trans* chamber (lumen) contains 200 µM Ca^{2+} (n = 3).

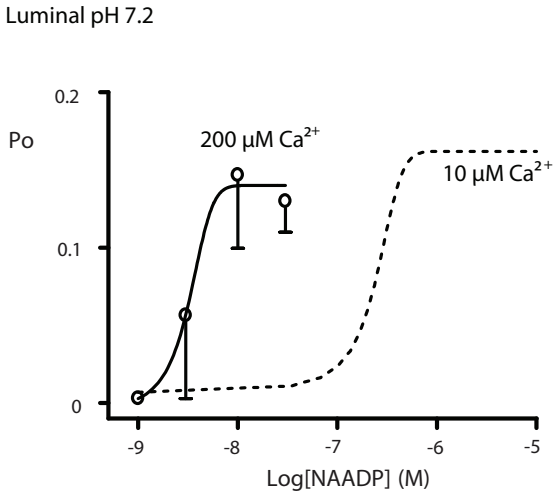


Figure 3.24: Concentration-response relationship for NAADP action on HsTPC2 P_o with 200 µM luminal Ca^{2+}. The sigmoid relationship between mean P_o values induced by incrementally increasing concentrations of NAADP with a high *trans* chamber Ca^{2+} concentration (200 µM). K^+ was the conducting ion; both chambers were at pH 7.2. Data are mean values (n = 3, S.D.) The dashed curve shows data from figure 3.22 for comparison.

shifted to the left with the consequence of a 100-fold reduction in the EC_{50} to 5 nM, this is comparable to previously observed K_d values in HsTPC2 overexpressing cells (55).

The relationship between luminal Ca^{2+} concentration and HsTPC2 P_o was measured in the presence of 10 nM NAADP (appendix figure A.4). The range of Ca^{2+} concentrations used covered the predicted luminal Ca^{2+} concentrations within lysosomal stores (10 µM - 1 mM) (254) and within this range the higher the luminal Ca^{2+} concentration the higher the P_o, with mM luminal Ca^{2+} giving a value of around 40 % open probability.

The ER/SR Ca^{2+} release channels are known to be very sensitive to luminal Ca^{2+} (252, 259, 397). RyR receptors from the SR in ventricular myocytes show an increased P_o with elevated luminal Ca^{2+} (259). The IP_3R is sensitive to the relative Ca^{2+} concentration between lumen and the cytoplasm, a high luminal Ca^{2+} concentration and low cytoplasmic Ca^{2+} concentration causes the receptor P_o to increase (182, 189). HsTPC2 responded by increasing NAADP sensitivity with high luminal Ca^{2+}, which results in a higher P_o at a fixed concentration. This suggests that lysosomal Ca^{2+} content plays a crucial role in channel regulation *in situ*. Depletion of the Ca^{2+}-stores below a threshold level could close HsTPC2 channels and prevent further Ca^{2+} flux, even in the continued presence of NAADP. This mechanism would allow the stores to refill until the threshold Ca^{2+} concentration was reached, which would lead to Ca^{2+} oscillations characteristic of NAADP signalling in physiological systems (55, 57, 246).

The regulation of ligand sensitivity by luminal Ca^{2+} shows how important a physiological recording environment can be. Considering the lysosomal localisation of HsTPC2, another crucial parameter to investigate was the effect of pH on channel activity.

3.7.8 Regulation by luminal pH

The lysosome is normally acidic with a pH < 5.5 (106) but is reported to alkalinise upon NAADP-induced Ca^{2+} release (303). Therefore, to investigate how this dynamic pH range affects the HsTPC2 function the *trans* chamber was acidified from pH 7.2 to pH 4.8.

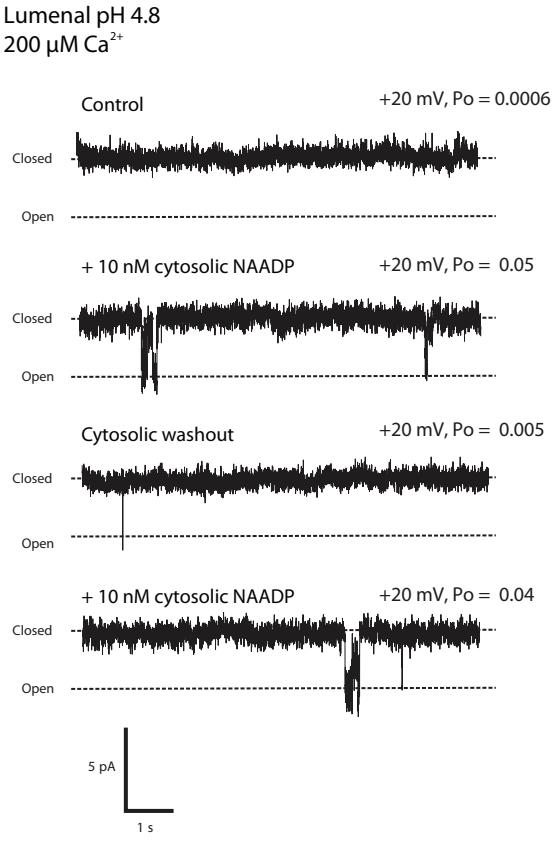


Figure 3.25: Example traces depicting the effect of lowering luminal pH. A typical experiment illustrating HsTPC2 activity in response to NAADP (10 nM) with low luminal pH (4.8). The *trans* chamber (lumen) was acidifed using an acetate buffer with 'high' Ca^{2+} concentration (200 µM). K^+ was the conducting ion; the *cis* chamber remained at pH 7.2. NAADP (10 nM) activates the channel (second trace), however, perfusion of the *cis* chamber reverses this activation, suggesting reversible NAADP binding under these conditions (n = 3). Reapplication of NAADP (10 nM) causes channel opening as before (bottom trace).

Figure 3.25 shows example traces of NAADP induced single channel activity with the luminal pH at 4.8, clearly demonstrating that HsTPC2 is still an active channel under these conditions. Averaging the results of P_o at various NAADP concentrations gives the concentration-response relationship as depicted in figure 3.26. These data demonstrate that HsTPC2 remains sensitive to low concentration of NAADP (EC_{50} = 5.5 nM), although with the lower luminal pH although the P_o levels are significantly decreased. Noticeably, as shown by the washout in figure 3.25, NAADP activation is reversible which results in the the concentration-response curve becoming bell-shaped (figure 3.26), which correlates with observed NAADP-induced Ca^{2+} fluxes in mammalian cells (57).

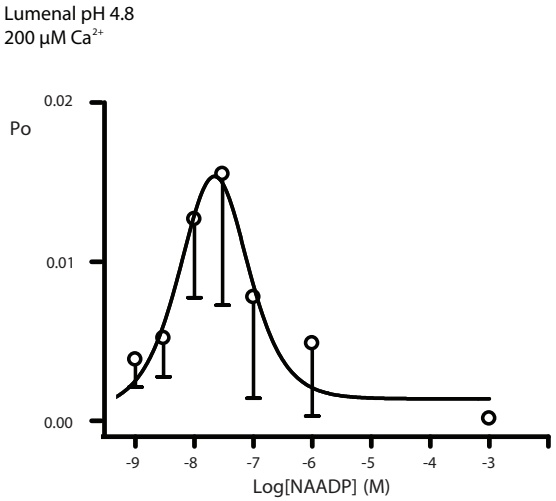


Figure 3.26: Concentration-response relationship for NAADP action on HsTPC2 P_o at luminal pH 4.8. The bell-shaped relationship between mean P_o values induced by incrementally increasing concentrations of NAADP with the *trans* chamber (lumen) acidifed to pH 4.8 and in the presence of 200 µM Ca^{2+}. K^+ was the conducting ion; the *cis* chamber remained at pH 7.2. Data are mean values (n = 3, S.D.)

Luminal pH may be governing the conformation of the NAADP binding site to allow dissociation of NAADP from HsTPC2. Considering the phenomenon shown by Morgan *et al.* whereby lysosomal pH increased upon NAADP activated Ca^{2+} flux (303), this suggests that under normal circumstances NAADP binding is reversible, but a prolonged NAADP signal which results in the lumen alkalinising would cause the binding site to clamp shut and prevent NAADP dissociation. Combined with the luminal Ca^{2+}

threshold, under continuous NAADP stimulation this would result in Ca^{2+} oscillations.

The luminal pH of 4.8 dramatically reduces the P_o of HsTPC2. Thus the final P_o induced by NAADP is a function of both luminal pH and luminal free Ca^{2+} concentration. These two interconnected modes of regulation reflect feedback from the lysosomal environment on NAADP signalling.

3.7.9 Partial agonist properties of Ned-19

In order to further investigate the pharmacology of HsTPC2, the effects of the antagonist Ned-19 were measured.

Ned-19 is a structural analogue of NAADP and has been shown to block Ca^{2+} release with high specificity and affinity in sea urchin homogenates and cell lines (310, 370, 375).

However, Ned-19 seemed to act as a partial agonist in this system, with a dose dependent increase in P_o at low concentrations. Figure 3.27 shows a series of typical experiments where HsTPC2 was activated by 10 nM NAADP. Ned-19 was added incrementally in the continual presence of NAADP and at nanomolar levels acted as an agonist which stimulated further channel openings. Concentrations of 1 µM antagonised HsTPC2 activity and shut the channel (mean data shown in figure 3.28).

Washout of both NAADP and Ned-19 (bottom trace, figure 3.27) reversed the inhibitory effects of Ned-19, but not the activation by NAADP. This simple observation suggests that the Ned-19 was not binding to the NAADP activation site and thus supports work by Rosen *et al.* who have proposed two sites of action for NAADP; one with a high affinity and one with a low affinity (370).

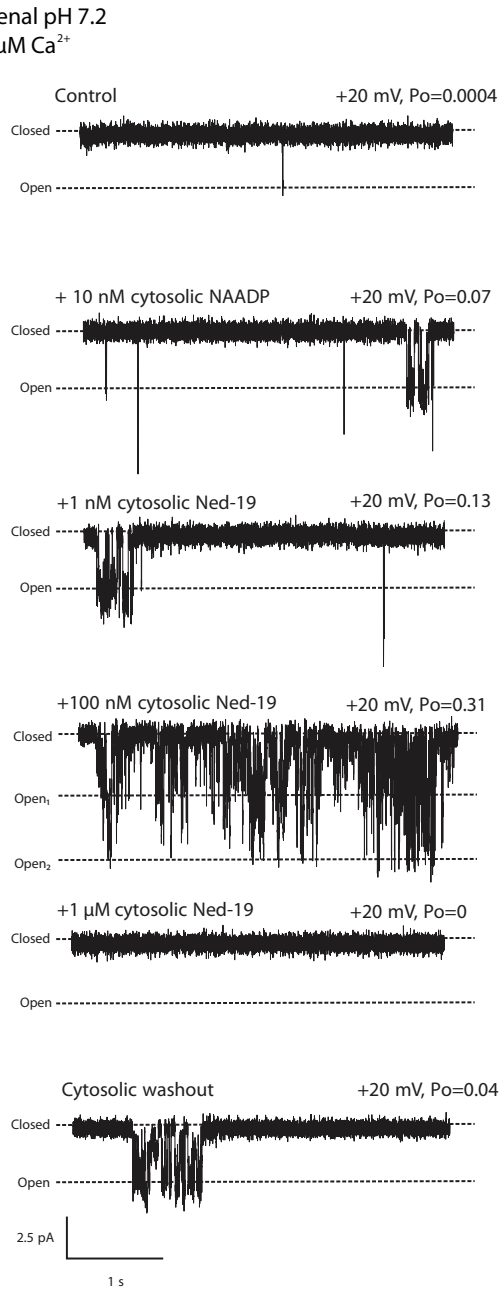


Figure 3.27: Example traces depicting effects of Ned-19 on HsTPC2. A typical experiment illustrating HsTPC2 activity in response to increasing concentrations of Ned-19. K^+ was the conducting ion; pH 7.2. The *trans* chamber (lumen) contained 200 µM Ca^{2+}. Compounds were applied to the *cis* (cytosolic) chamber, NAADP (10 nM) followed by sequential increments of Ned-19 as indicated above each trace. Cytosolic washout refers to a complete pefusion of the *cis* chamber in the absence of both compounds. The effects of Ned-19 were removed, but NAADP induced activity remained (n = 3).

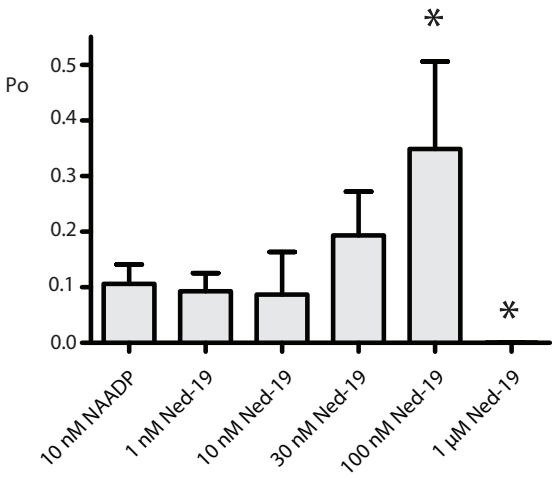


Figure 3.28: Concentration-response relationship for Ned-19 action on HsTPC2 P_o. Histogram showing the mean P_o of HsTPC2 with K^+ as the conducting ion, 200 µM luminal Ca^{2+}; pH 7.2 in the continued presence of NAADP (10 nM) and increasing concentrations of Ned-19 ($* p < 0.05$, n = 3).

3.7.10 Synergy between NAADP and Ned-19

Given that Ned-19 does not directly compete with NAADP it was investigated whether nanomolar concentrations of Ned-19 can still activate HsTPC2 even in the absence of NAADP. Figure 3.29 shows that 100 nM Ned-19 stimulated channel activity. Subsequent addition of NAADP in the continued presence of Ned-19 (100 nM) caused further channel activation. Mean population data shown in figure 3.30 demonstrates that Ned-19 and NAADP synergise to give a greater response than the sum of their individual responses, this again suggests separate modes of action.

These two streams of evidence combined strengthen claims that Ned-19 is a non-competitive antagonist as was reported by Naylor *et al.* (310). Again there are parallels seen in the other intracellular Ca^{2+} channels as both RyR and IP_3R possess various binding sites for a wide range of ligands, and this enables fine-tuning of channel activity to deliver complex but flexible systems of Ca^{2+}-release governing a range of biological processes.

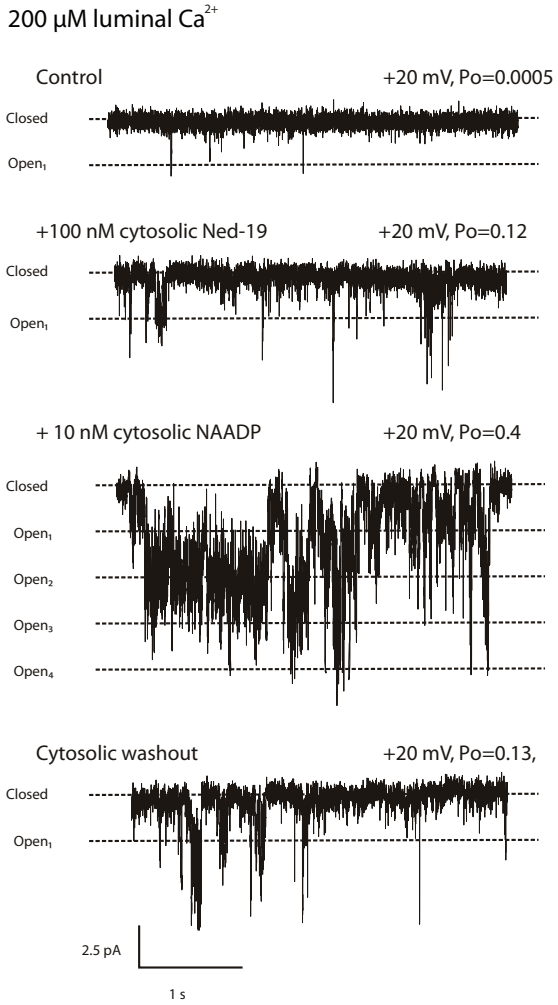


Figure 3.29: Example traces of the synergy between Ned-19 and NAADP. Representative traces depict Ned-19 (100 nM) activating HsTPC2 in the absence of NAADP. K^+ is the conducting ion, 200 µM luminal Ca^{2+}; pH 7.2. Subsequent addition of NAADP (1 nM) potentiates the effect of Ned-19 activation (n = 3). Washout of the *cis* chamber results in a lower P_o but to a level higher than the control. This is due to irreversible binding by NAADP and reversible binding by Ned-19.

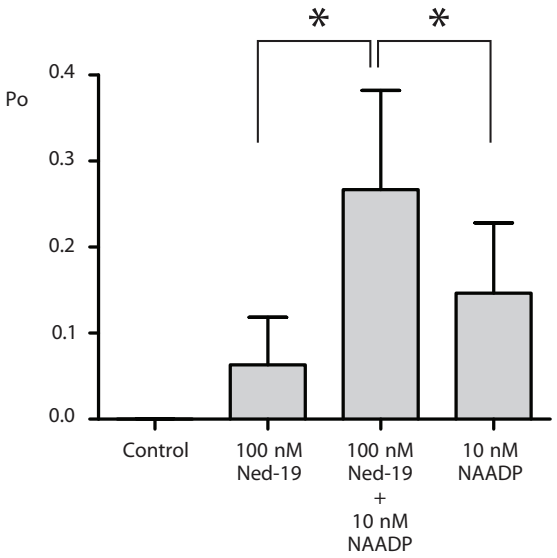


Figure 3.30: Ned-19 potentiates the effects of NAADP on HsTPC2. Histogram showing the mean P_o of HsTPC2 with K^+ as the conducting ion, 200 µM luminal Ca^{2+}; pH 7.2 in the presence of NAADP (10 nM) and Ned-19 (100 nM) either added individually or simultaneously ($* \ p < 0.05$, n = 3). The control is basal HsTPC2 P_o before compound addition.

3.8 Discussion

This is the first study to have associated HsTPC2 as a ligand-gated ion channel. This chapter was modelled on two seminal publications which reported the purification and reconstitution of the two archetypal intracellular Ca^{2+}-release channels: RyR (229) and IP_3R (37), which were both purified and characterised by reconstitution into a lipid bilayer. These channels also act as a useful comparison for the biophysical properties seen in HsTPC2.

3.8.1 Immunoprecipitation as a purification technique

Initial studies on intracellular channel electrophysiology were conducted by fusing ER-derived microsomes with lipid bilayers (400). Whilst this technique allowed measurements to be made, this could not be directly attributed to the RyR/IP_3R as other proteins would be present in the microsomal membrane. The RyR was first to be resolved by the solubilisation of membranes and further purification by molecular-size separation on a sucrose gradient (229). RyR was detected using a radioligand binding assay and proved to be 98 % pure (229).

Here, immunoprecipitation was used to purify HsTPC2. This is the most specific form of protein purification currently known as it directly targets epitopes on the desired protein. Although immunoprecipitation is a standard technique which is logically and procedurally simple, many variables affect the success of purification and conditions need to be optimised hence the extensive controls conducted here. However, immunoprecipitation requires multiple steps with heavy protein manipulation and this may have been the reason why the HA-purified protein was not functional in the lipid bilayer.

Alternatively the difference in functionality between HA-purified and polyclonal-purified channels could be due to the requirement of accessory proteins in channel function. The different epitopes used for the polyclonal antibody may allow coimmunoprecipitation of essential proteins whereas the HA-antibodies could interfere with these interactions, which may suggest that the N-terminal tail of HsTPC2 is crucial for protein-protein interactions (like in the TRP family (248)). Western blots only confirm the presence of HsTPC2 in the final preparation, but cannot rule out that other

proteins may be affecting the channel properties. The purified complex is analysed in more detail in chapter 5.

3.8.2 Protein yield

A hampering factor in this study has been the lack of a quantifiable assay to determine HsTPC2 yield and purity. Western blotting provided a highly useful means of detecting the presence of the tagged protein and allowed a rough comparison between samples, however, the fact that binding activity was never immunoprecipitated is a cause for concern. Previous studies on intracellular Ca^{2+} channels used [^{3}H]ryanodine to asses RyR yield (229) and [^{3}H]IP_3 for the IP_3R (416), however, here [^{32}P]NAADP binding was never above background for either immunoprecipitation procedure. This could be due to the small amounts of proteins used in the immunoprecipitation, usually 1 - 2 mg total protein starting material and undetectable ($<$ 8 ng) concentrations eluted from the beads; this is compared to final yields of 25 µg RyR (229) and 5 µg of IP_3R (416). Large scale immunoprecipitations were prohibitively expensive.

Another conclusion from these findings is that the HsTPC2 is not the direct binding protein of NAADP; an accessory protein may be required as an intermediate to bind NAADP and gate HsTPC2 channel activity. This scenario would be similar to the hypothesis whereby FKBP12.6 binds cADPR to gate RyRs (315). Two studies address NAADP binding to TPC complexes (55, 375) and the authors of these papers are currently investigating potential binding partners of the TPCs that may be involved in NAADP binding.

Thankfully HsTPC2 purified with polyclonal rabbit serum either coimmunoprecipitated the binding protein, or if HsTPC2 is the direct binding protein, even with such low protein yielded enough channels for one to incorporate into the lipid bilayer to give detectable NAADP-evoked currents.

3.8.3 Monovalent cation conductance

The human channel HsTPC2 investigated here showed a K^+ conductance of 300 $\pm$ 6 pS. The most direct comparison for this result is that of Cs^+ conductance shown in a HsTPC2 mutant functionally expressed at the plasma membrane (50). In this system the mistargetted HsTPC2 was stimulated by 500 nM intracellular NAADP and recordings made by plasma membrane patch clamp. A unitary Cs^+ conductance of 128 $\pm$ 4 pS

was shown, this was much smaller than the conductance detected in the bilayer. Whilst one cannot accurately compare conductances of different ions, estimates can be made. As a guideline, Cs^+ currents through the ryanodine receptor are only 60 % as large as those carried by K^+ (251), if selectivity is similar in HsTPC2 then the conductances seen for HsTPC2 in these two studies become more comparable.

A major problem when comparing the single channel conductances of the same protein are the variations in experimental conditions between laboratories. This is highlighted when comparing conductances seen in the plant TPC1 where K^+ conductances of the same isoform vary from between 20 pS up to 400 pS with most values centring around 100 pS (see Hedrich & Marten for a recent review (176)). Whilst these studies were conducted under the same concentrations of K^+ ions, variations in plant species, pH buffers and ion concentrations (including Ca^{2+} and Mg^{2+}) on either side of the membrane were shown to drastically affect channel conductance.

Notwithstanding these concerns, a good reference point upon which to base the results of HsTPC2 single channel recordings is the protein TRPML1, due to its structural similarity to the TPCs and its lysosomal localisation. Three electrophysiological studies have investigated the conductance properties of this channel. Firstly, a K^+ conductance of 130 - 150 pS was shown in endosomal vesicles containing wild-type TRPML1 which had been reconstituted into a lipid bilayer (363). This was supported by TRPML1 cDNA expressed in *Xenopus* oocytes under patch clamp conditions giving a K^+ conductance of 80 - 100 pS (235). Finally, purified lysosomes reconstituted in lipid bilayers gave a single channel K^+ conductance of 145 $\pm$ 35.5 pS (465). Whilst these values are lower than the K^+ conductance seen in HsTPC2, they are of the same scale of magnitude which substantiates the recordings made here.

Comparisons can also be made to the RyR and IP_3R, which both show monovalent cation permeability with unusually large conductances (287). Firstly the RyRs, which under comparable conditions CHAPS-purified RyR from rabbit skeletal (400), canine cardiac (7) and vascular smooth muscle (180) gave a main conductance of 700 - 800 pS for K^+.

Whilst this is the main RyR conductance, these channels also show multiple sub-conductance states which are thought to correlate to their tetrameric structure. Three distinct conductance states were seen that corresponded to $\frac{1}{4}$, $\frac{1}{2}$ and $\frac{3}{4}$ of the main

conductance level (400). It was proposed that this was either due to each subunit containing an individually conducting pore, or a single central pore sensitive to discrete changes in the subunit structure (400). Similar quaternary subconductance states were also seen in TRPML1 bilayer studies, again hinting towards a tetrameric structure (363).

Here, HsTPC2 shows just one subconductance state at 70 % of the main conductance level. If this phenomenon is determined by the subunit composition of a channel, this data supports predictions that the HsTPCs form dimers with each subunit governing a proportion of the total channel conductance (see chapter 5).

Whilst subconductance states have been observed in IP_3R, these are relatively rare (< 1 % of open transitions) and assumed to be due to channel damage as they are not as uniform as those seen in other channels (129). An undamaged IP_3R has a large monovalent K^+ conductance in mammalian systems around 350 pS. This is a similar magnitude to the K^+ conductance of HsTPC2.

Investigation into the monovalent conductances of Ca^{2+} channels can hint towards unsuspected roles. Previous reports have shown an importance of K^+ influx pathways in the ER that are coupled to Ca^{2+} release as part of a highly cooperative ion exchange mechanism (313, 322). These counter-currents are essential in maintaining electroneutrality of the ER membrane during Ca^{2+} release and similar currents have been shown to exist in the lysosomal membrane (409). The RyR has been shown to mediate its own counter current (153) and given the large non-rectifiying K^+ conductance of HsTPC2, it is likely that some of the lysosomal counter-current is carried through the HsTPC2 pore.

3.8.4 Ion selectivity

The relative ion permeability of channels can be estimated by the reversal potentials and by bi-ionic recordings. This value represents the relative ease of an ion to enter the pore and cross the membrane. Both the RyRs and IP_3Rs show a divalent-cation selectivity, allowing a greater flux of Ca^{2+}/Mg^{2+} ions than $Na^+/K^+/Cs^+$ and this selectivity is well conserved across the isoforms from different species. Variations exist between experimental procedures but in general, for both RyR and IP_3R the Ca^{2+}/K^+ selectivity $P_{Ca}/P_K = 5$ - 8. This can be interpreted that for every 1 K^+ ion crossing the membrane 5 - 8 Ca^{2+} ions also cross.

The permeability ratio of HsTPC2 was measured in the lipid bilayer under bi-ionic conditions and was shown to be less discriminating with $P_{Ca}/P_K = 2.6$. However, a study on patched lysosomes overexpressing the mouse isoform, MmTPC2, showed $P_{Ca}/P_K > 1000$, which shows that this channel is effectively K^+ impermeable. Site directed mutagenesis directed against the putative pore region dramatically reduced this ion selectivity to give $P_{Ca}/P_K = 8$ (387). This impermeability is supported by data in chapter 4, where similar experiments on lysosomal membranes overexpressing HsTPC2, show negligible K^+ flux through the human isoform in the native lysosomal membrane.

This major difference could be an artefact of the purification procedure, which may have damaged the selectivity filter in the bilayer recordings or it could be a technical issue, whereby the lower resolution of whole lysosome recording compared to single channel makes it difficult to determine whether a channel is open but impermeable to K^+ or shut due to a gating mechanism (129).

A complete impermeability to K^+ would not be surprising given the fact that the related voltage-gated Ca^{2+} channels show very high Ca^{2+}/Ba^{2+} selectivity (65) and whilst there is a large variation in permeabilities in the TRP family, TRPV5,6 have a $P_{Ca}/P_{Na} > 100$ (314). Unfortunately permeability ratios have not been calculated for the lysosomal TRPML1, however, as was shown above, this channel can conduct monovalent cations and may have a similar selectivity filter to the IP_3R and RyR.

Plant TPC1 has been shown to conduct monovalent K^+, Na^+, and NH_4^+ and divalent Ca^{2+} and Mg^{2+}. However, comparison of permeability ratios is difficult because vacuolar luminal Ca^{2+} does not simply act as a permeant ion, but regulates channel activity. As luminal $[Ca^{2+}]$ increases the activation potential of TPC1 is shifted to more positive voltages; this effectively limits Ca^{2+} flux and as a result K^+ ions are more permeable due to channel gating rather than a selectivity filter (176). One study contradicts this and proposes a $P_{Ca}/P_{Na} = 3$ (447).

Such disparate selectivities in supposedly similar channels makes it difficult to predict the physiologically relevant HsTPC2 selectivity. It is more closely related to the VGCC and TRP family than the RyR and IP_3R families which may suggest that a high P_{Ca}/P_K is more likely. However, the current data give opposing theories with the bilayer showing large K^+ conductance and whole lysosome patch clamping suggesting

a large selectivity to Ca^{2+}. More data will need to be gathered, preferably by different laboratories, before a consensus can be reached.

3.8.5 Divalent cation conductance

Whilst most of the data presented in this chapter uses K^+ as the permeant ion, it is worth emphasising that this study was the first to show that HsTPC2 is permeable to Ca^{2+} ions, which is of great importance as the aim of this work was to characterise a putative NAADP-gated Ca^{2+}-release channel.

The Ca^{2+} conductance shown here was relatively low with the IV slope value at 15 ± 1.5 pS. A higher value was reported in mutated HsTPC2 mistargeted to the plasma membrane, which gave a Ca^{2+} conductance of 40 ± 1.3 pS (50). However, the lower value is more likely to be physiologically relevant as this is within a comparable range seen in the VGCCs, with the α_1 of $Ca_V3.1$ showing a Ca^{2+} conductance of 7.5 pS and up to ≈ 20 pS for the Ca_V2 subtypes (65). Plant TPC1 also shows a Ca^{2+} conductance of ≈ 16 pS (447).

Studies purporting to record a TRPML1 current in lysosomes which had been coalesced with a lipid bilayer claim to have seen Ca^{2+} currents with a conductance of ≈ 145 pS (465) however, channel stability was too low for extensive characterisation. The ER channels do not even give Ca^{2+} conductances this large, with the RyR isoforms between 100 - 150 pS (287) and the $IP_3Rs \approx 50$ pS (129).

In general, the conductances seen in HsTPC in the lipid bilayer conform with values predicted from those of similar channels reported, this gives a greater confidence that the recordings are derived from an undamaged channel and made under the appropriate conditions.

3.8.6 Coupled gating

The synchronous opening and closing of HsTPC2 channels strongly resembles the phenomenon of coupled gating often seen in RyR (321). It is hypothesised that this mechanism is important in providing a robust termination of the RyR signal, which is intrinsically regenerative with CICR and feed forward regulation (133). Coupled gating was first shown in RyR1 channels isolated from rabbit skeletal muscle (281) and subsequently RyR2 from canine cardiac muscle (321) and the main requirement for both isoforms was a close apposition of the channels within the membrane. Electron

micrograph images and density gradient centrifugation shows an interaction of two to four RyR in 10 % of channels which suggests a direct physical coordination of channel gating. Furthermore coupled gating in RyRs is dependent on the allosteric modulation of the RyR binding protein FKBP and also luminal [Ca^{2+}] (133).

For HsTPC2 there seemed to be no major effect of luminal [Ca^{2+}] however, the coupled gating was ligand-dependent occurring only in the presence of NAADP or nM concentrations of Ned-19. This mechanism increases the flexibility of NAADP-mediated Ca^{2+} signals and may explain the potency of this second messenger as the stimulation of just one channel allows recruitment of other channels to amplify a signal. The predicted involvement of HsTPC2 in triggering CICR may also explain the need for such tight coordination of channel activity, whereby synchronous closing of all channels provides a definitive end to Ca^{2+} release.

3.8.7 Voltage sensitivity

The lysosomal membrane potential is still undefined (see chapter 4) and thus the requirement for voltage gating in TPCs is unclear. Whilst the archetypal intracellular channels, IP_3R and RyR do not show voltage sensitivity, the close relationship of the TPCs to the VGCCs and presence of the highly conserved voltage sensing domain on the two S4 transmembrane segments of every isoform suggest that TPCs are capable of voltage-gating.

So far, only the plant TPC1 has shown any voltage sensitivity and even then the interaction is not straightforward because the ionic gradients of Ca^{2+}, Na^+ and K^+ ions regulate the activating voltage range. A rise in cytosolic Ca^{2+} shifts the voltage-activation curve towards a negative potential which favours channel opening by physiological vacuole potentials. Conversely a rise in luminal Ca^{2+} has the opposite effect and reduces the likelihood of channel opening. Thus the ratio between cytosolic and luminal [Ca^{2+}] acts as a secondary trigger at a given potential, which is similar to the Ca^{2+} regulation of the IP_3Rs under a given concentration of IP_3. Na^+ ions are less efficacious but produce the same regulatory effects as Ca^{2+}; however, K^+ ions have the reversed regulatory role with a cytosolic-decrease/luminal-increase stimulating channel opening.

Characterisation of currents through TRPML1 show that this channel is also voltage-insensitive, despite containing the S4 domains, and that it is outwardly rectifying

(221, 235, 363). This would suggest that TRPML primarily conducts ions into the lysosomal lumen which further disqualifies this protein as a candidate as the NAADP receptor.

In the bilayer experiments conducted here on HsTPC2 as well as experiments on whole lysosomes expressing MmTPC2 (387), and later expressing HsTPC2 (chapter 4) the currents were not voltage sensitive and were non-rectifying. Similarly the mutated HsTPC2 at the plasma membrane did not show signs of voltage-gating but with Cs^+ as the permeant ion the current was inwardly rectifying (50). This inward rectification suggests that when present in the lysosomal membrane HsTPC2 primarily conducts ions from the lysosomal lumen into the cytosol, as would be predicted.

3.8.8 NAADP sensitivity

Returning again to the main aims of this work, it is important to remember that this channel is gated by its ligand NAADP. Thus the efficacious concentrations of this ligand must be taken into consideration. Here a concentration-response curve under the most physiological conditions (acidic lysosomal lumen with high $[Ca^{2+}]$) has shown a bell-shaped activation in response to nM - µM concentrations of NAADP, with an $EC_{50} = 5.5$ nM. This value correlates well with values seen in other mammalian systems (5, 57, 202, 282).

Most other studies investigating the channel properties of TPCs have used a single concentration to open the channel. In the plasma membrane study with mistargeted HsTPC2, 500 nM NAADP was microinjected into the cytoplasm to stimulate channel opening (50), which had a rapid onset and was reversible. In whole lysosome patch of MmTPC2 60 nM NAADP was efficacious whereas 5 µM NAADP failed to open the channels. This was a selective effect as NADP did not cause openings at the same concentrations (387). Both these studies use concentrations within the range predicted to evoke Ca^{2+} release and while not being the optimally efficacious concentration, both would activate HsTPC2 in the lipid bilayer.

Another study has shown bell-shaped concentration-response relationship for NAADP in purified lysosomes which had been coalesced into a lipid bilayer (465, 467). This was within a similar range to the data shown here but with a higher $EC_{50} \approx 100$ nM. Whilst the authors of this work claim to be recording the activity of TRPML1 which could be knocked-down by siRNA or immunoprecipitations against TRPML1, endogenous TPCs

would be present in the lysosomal membrane and could be accounting for this channel activity. The recordings presented actually resemble more characteristics of TPCs than TRPML1; this is seen by the magnitude of the conductance and the lack of outward rectification.

RyRs have also been implicated in NAADP-evoked currents, with the most convincing evidence shown in lipid bilayers (150, 187, 298, 408). Purified RyR1 from rabbit skeletal muscle, reconstituted into a lipid bilayer, responded to NAADP with a sigmoidal concentration-response relationship similar to the data shown here with symmetrical K^+, however, they do report that in some recordings concentrations of NAADP $>$ 200 nM began to reduce the open probability, which would suggest a bell-shaped curve (187). The $EC_{50} = 31.2 \pm 6.9$ nM, and current activity was blocked by Ruthenium red and ryanodine. This study is made more convincing by the magnitude of the conductances seen ($\approx$ 530 pS) with Cs^+ as the permeant ion, which are too large to be derived from potential TPC contaminants (187). However, the notion of RyRs being the NAADP receptor is seriously hampered by the fact that RyR is inactive at a low pH, as is discussed below.

3.8.9 The effects of luminal pH

The study on patched lysosomes with MmTPC2 reported that a neutral pH on the luminal face resulted in total inactivation of MmTPC2 activity (387). Whilst this was not seen in the HsTPC2 bilayer work presented here nor in the plasma membrane patch of HsTPC2 (50), luminal pH was shown here to have a dramatic effect on channel function. As was shown earlier in this chapter, acidification of the *trans* chamber from pH 7.2 to pH 4.8 resulted in a $\approx$ 10-fold reduction in the open probability of HsTPC2, effectively inhibiting channel activity. Acidification also enabled the reversible binding of NAADP to give the characteristic bell-shaped curve. As these channels reside in the lysosomal membrane which is predicted to have a luminal pH $\approx$ 5 (303) this activity should be considered more physiologically relevant.

NAADP-evoked Ca^{2+} release has been shown to cause an alkalinisation of the lysosomal lumen, this mechanism may play a feedforward role where ligand binding relieves pH-induced inhibition and increases HsTPC2 activity to amplify the signal.

RyR channels are inhibited by a luminal low pH, with most channels inactive at pH 5.5 (238). It has been shown that lowering the pH diminished Ca^{2+} binding to

calsequestrin, which ultimately reduced RyR channel activity (114). However, pH may also directly affect channel conformation. In TRPML1, which is also inhibited by a reduction in pH, atomic force microscopy of channel clusters has shown that the quaternary interaction between channel subunits is reduced at low pH (363). Clustering alterations have also been seen in IP_3R in response to changes in pH (395).

3.8.10 The effects of luminal Ca^{2+}

In data shown here, an increase in luminal [Ca^{2+}] from 10 µM to 200 µM increased the sensitivity of HsTPC2 to NAADP by 100-fold, thus increasing the likelihood of channel opening with low concentrations of NAADP.

Luminal [Ca^{2+}] in the ER also has a stimulatory role in regulating RyR activity. This has been traced to the presence of a luminal Ca^{2+} binding site which was identified by the loss of Ca^{2+} regulation upon a tryptic digestion of the luminal face. Before the digestion, an increase in luminal [Ca^{2+}] from 10 µM to 1 mM resulted in a higher open probability of the channel, whereas after the digestion the same increase in luminal [Ca^{2+}] gave a reduced open probability (73). These regulatory sites have since been confirmed by mutagenesis studies and their mechanisms of action modelled (237). The increase in luminal [Ca^{2+}] is thought to relieve inhibition by Mg^{2+} ions through competitive binding at the inhibitory site (239), however, other studies also implicate the accessory proteins calsequestrin, triadin, and junctin in conferring RyR responsiveness to luminal Ca^{2+} (167).

The IP_3R also shows increased activity with high luminal concentrations of divalent ions. Ba^{2+} gives a 10-fold increase in the open probability of IP_3R1 compared to K^+ (279). However, more importantly, luminal Ca^{2+} inhibits IP_3R activity, with channel P_o elicited by optimal cytoplasmic concentrations of IP_3 and Ca^{2+} reducing by 66 % when luminal [Ca^{2+}] was raised from 3 µM to 10 mM (37).

Plant TPC1 shows a similar feature of inhibition by increased luminal [Ca^{2+}], as was described above (section 3.8.7), this shifts the voltage-activation curve to more positive potentials which makes the channel less likely to open to physiological voltages (36, 351, 352).

The mode of luminal Ca^{2+} regulation varies across the channels studies and thus no consensus can be made for HsTPC2 without further studies of the TPC family and also the TRPMLs.

3.8.11 Gating by Ned-19

This work has also helped further characterise the novel pharmacological agent Ned-19, which has been confirmed as an NAADP antagonist at high concentrations. This study was the first to show that at the nM range Ned-19 acts as a partial agonist opening the HsTPC2 channel. This was further shown to synergise with NAADP to augment Ca^{2+} release which confirms that the HsTPC2 must have multiple binding sites as these two agents seem to be able to act independently of each other. Rosen *et al.* have proposed that the NAADP receptor contains two binding sites, one which is stimulatory and one which is inhibitory (370), the synergism shown here suggests that both sites could have a stimulatory effect.

The only other electrophysiological study to investigate Ned-19 was the plasma membrane patch clamp of the mutated HsTPC2, where 100 nM Ned-19 totally abolished NAADP-induced Cs^{+} currents (50). This presents a discrepancy as this concentration was stimulatory for purified HsTPC2 in the bilayer, yet inhibitory to the truncated HsTPC2 in the plasma membrane. It is difficult to say with certainty how this compound may affect the activity of HsTPC2 *in vivo* as both these studies are conducted under unphysiological conditions. There is also the possibility that the truncation of the N-terminal tail may affect Ned-19 action.

3.8.12 Channel modulation by accessory proteins

All known Ca^{2+}channels are regulated to some degree by accessory/modulatory proteins. One of the major disadvantages of studying purified HsTPC2 in the lipid bilayer is that unless an accessory protein was very tightly bound to the channel, it would have been washed away during the immunoprecipitation. A good example of how this can affect channel function can be seen in comparisons between electrophysiological results obtained from native RyRs in SR vesicles, compared to purified RyRs in bilayers: luminal Ca^{2+} regulation is not seen in the bilayer but is very distinct in the SR vesicles, suggesting the loss of an accessory protein (calsequestrin, triadin, and junctin) during the purification procedure (167). Solubilisation can also dissociate channel complexes, again this is seen in RyRs whereby CHAPS treated channels were no longer sensitive to cytosolic Ca^{2+} (236).

Preliminary attempts towards identification of HsTPC2 accessory proteins are discussed in chapter 5, however, the full characterisation of accessory proteins is beyond the scope of this thesis and will hopefully be followed-up with further research.

3.9 Conclusions

Until now, all studies on the role of HsTPCs in NAADP signalling have been based on incidental evidence, there have been no direct studies on purified HsTPCs. Work shown here proves that HsTPC2 behaves as a functional ion-channel which is Ca^{2+} permeable and responsive to NAADP. The distinct characteristics of NAADP signalling seen *in vitro* and *in vivo* were also replicated in this system including the extreme sensitivity to low concentrations of NAADP, the inhibition by high concentrations of NAADP and channel antagonism by 1 µM Ned-19.

This study also revealed subtle channel gating properties involving the concerted opening of multiple channels in response to a NAADP signal, as well as the presence of a subconductance state, where a channel is only partially open. The mechanisms behind these properties and their physiological relevance is still speculative, but this work proposes another layer of channel regulation to further differentiate these signals.

The most exciting discoveries were those regarding the control of HsTPC2 activity by the luminal environment, with both the lysosomal Ca^{2+} concentration and pH affecting the activity of this channel. Figure 3.31 tries to compile these different regulatory mechanisms into a predictive model.

3.10 Future prospects

Findings in this chapter hopefully represent the emergence of a new field regarding the electrophysiological properties of HsTPC2. Following the example of the RyR and IP_3R there are many more questions that need to be asked of the TPC proteins to clarify their role in Ca^{2+} signalling.

Considering the variation in the intrinsic single channel conductances and selectivity reported on HsTPC2, the amino acids responsible and the putative pore region require further investigation. Site directed mutagenesis provides an excellent means of dissecting the pore structure and function of TPCs and two studies have already begun work in this area. Brailoiu *et al.* have shown that a truncation of the N-terminus of HsTPC2 mistargets the protein to the plasma membrane, to give Cs^+ currents as discussed above (50), a subsequent point mutation of a conserved residue in the putative pore forming region (L265P) resulted in a $\approx$ 15-fold reduction in Cs^+ conductance, suggesting an essential role for this residue in maintaining channel function. Furthermore

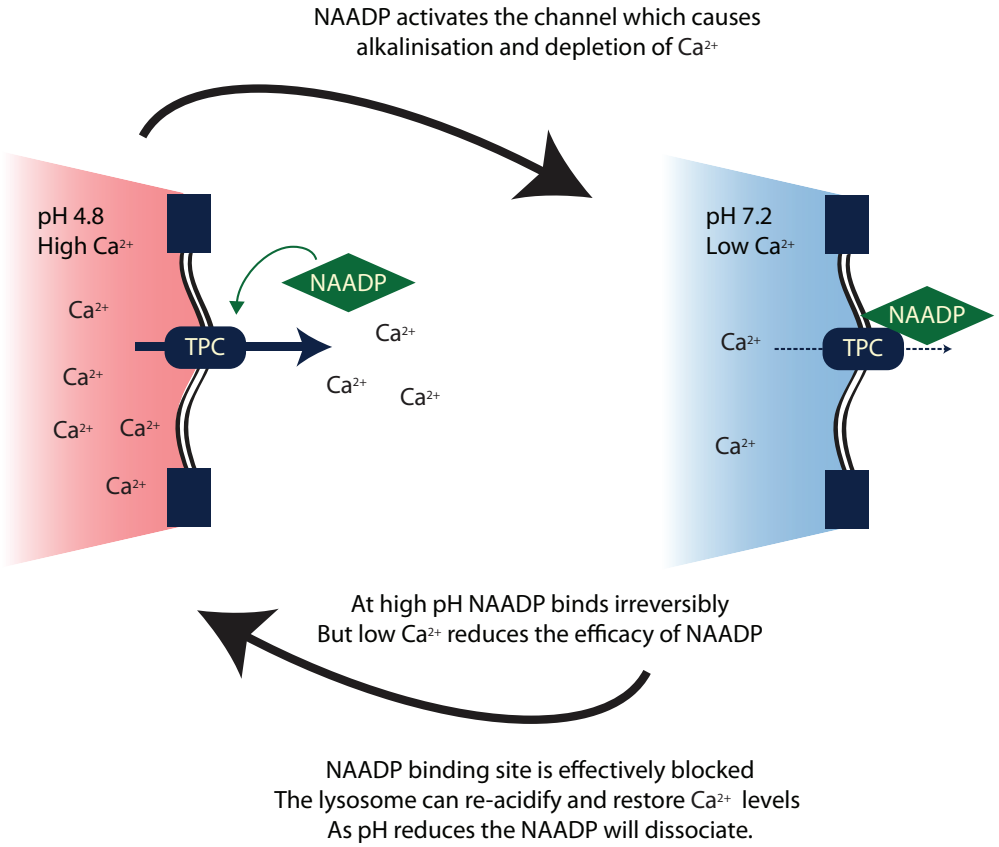


Figure 3.31: Model mechanism of HsTPC2 regulation by luminal conditions. Left: A resting lysosomal lumen predicted to have an acidic pH and high [Ca^{2+}], In the absence of activating ligands HsTPC2 has a low basal activity. Low concentrations of NAADP activate the channel which results in the depletion of the lysosomal Ca^{2+}-store and an increase in pH. **Right:** The high pH slows the rate of NAADP dissociation, but the channel is effectively desensitised as the concentrations of NAADP present which were activatory at high $[Ca^{2+}]_{luminal}$ become below the gating-threshold with low $[Ca^{2+}]_{luminal}$. This allows the stores to replenish Ca^{2+} and reacidify. Once a low pH is regained the NAADP can dissociate.

similar mutations, this time in the mouse MmTPC2 pore forming region, were used to alter ion selectivity (387). The mutations were based on homology with TRPV5,6 where a particular acidic residue had been shown to confer Ca^{2+}/Mg^{2+} selectivity on pore loop II. As MmTPC2 has two repeated domains, two residues could provide this selectivity and hence both were mutated to alanine. Whilst one mutation produced a non-functioning channel, E643A reduced the P_{Ca}/P_K from > 1000 to 8, thus removing the major Ca^{2+} selectivity filter. The reverse potential and channel conductance were unchanged. These mutations should be replicated in HsTPC2 and it would be interesting to see whether similar alterations to conductance (L265P) and selectivity (E643A) would be altered in the lipid bilayer.

The pharmacology of the HsTPC2 protein also needs further work, the properties of two most specific pharmacological effectors of HsTPC2 (NAADP and Ned-19) were shown above however, bilayer studies are required to investigate the effect of a range of NAADP antagonists on HsTPC2 such as the VGCC-blockers: diltiazem, D600, verapmil and SKF96365, also the P2-purinoreceptor antagonist PPADS. Their modes of action may enable a further dissection of channel properties, structure and function. It would also be worth confirming that effectors of the known Ca^{2+}-releasing channels, cADPR and IP_3 have no effect on HsTPC2. A further control on the purified protein would be to ensure that agents which were thought to inhibit NAADP responses by interruption of lysosomal physiology have no effect in the bilayer, these would include the SERCA-blocker thapsigargin, V-type ATPase blocker bafilomycin A1 and the lysomotropic agent GPN.

Throughout this discussion comparisons have been drawn between the human TPC2 and the mouse TPC2, this provided a useful guideline upon which to base results, however, species variation can give dramatically different results as was seen in the conductances of the plant TPC1 (176). Purification of the mouse TPC2 and its incorporation into a bilayer would allow a direct comparison between species. Taking this further, as the majority of initial characteristics of NAADP signalling were deduced in the sea urchin egg homogenate, it would be useful to assess the differences in function between the mammalian and sea urchin TPC2 proteins, especially considering the sub-threshold desensitisation to NAADP which is seen in sea urchin preparations but not mammals (1, 147).

Whilst not elaborated here, the RyRs and IP_3R show quite substantial differences in isoform function. With this in mind, HsTPC1 isoform should be investigated to determine the channel functions of this isoform and how it differs from HsTPC2. One study has already implicated HsTPC1 as a component in NAADP-evoked Ca^{2+} release. This was shown by enhanced NAADP-mediated Ca^{2+} signals seen in cells overexpressing HsTPC1, attenuation by HsTPC1 knockdown and also single-point mutation within a putative pore region which abrogated Ca^{2+} release (47). Preliminary work on purified HsTPC1 incorporated into a lipid bilayer has already begun and basal activity of HsTPC1 shows a similar K^+ conductance to HsTPC2 and also a degree of voltage sensitivity (Bristol & Oxford). These differences may be due to the subcellular localisation of HsTPC1, which is more disparate than HsTPC2 and can be found in endosomes and lysosomes (47, 55).

Finally, given the level of protein-protein interactions seen in the VGCCs, RyRs and IP_3R for channel regulation it is likely that accessory proteins interact with HsTPC2 to govern the channel gating. The next chapter in this thesis looks at channel activity in purified lysosomes overexpressing HsTPC2, this more physiological environment ought to ensure that a greater proportion of these interactions are maintained. Chapter 5 then will look back at the immunoprecipitated complexes discussed here in an attempt to identify any interacting proteins.

Chapter 4

Results - Patch clamp of purified lysosomes

4.1 Summary

Purification and reconstitution of the HsTPC2 protein into artificial bilayers allowed intricate investigation of the physical channel properties, however such extreme isolation and incorporation into an intrinsically artificial environment introduces many potential risk factors.

Crucial components of the lysosomal membranes such as the complex composition of glycolipids and a host of membrane proteins will not be present in a homogenous decane bilayer. These may interact with HsTPC2 *in vivo* and their absence could affect the protein folding and stability. Additionally, weakly interacting modulatory/accessory proteins may have been lost during the purification resulting in anomalous channel regulation.

As will be discussed in chapter 5 the immunopurified HsTPC2 complex consisted of many additional proteins. If these co-purified proteins were non-specific contaminants of the complex they could either have interfered with channel activity or produced additional ion pores which casts doubt on the current recordings. Therefore the main focus of this chapter is the purification of lysosomes and direct patch clamp recordings of lysosomal channel activity in response to NAADP.

The purification procedure based on previously published methodologies gave lysosomal preparations heavily contaminated with ER, mitochondria, plasma membrane

and Golgi apparatus (387). Many of the steps required to prevent this contamination are discussed. The optimised method involved cell homogenisation with a Balch homogeniser followed by magnetic chromatography of iron-loaded, sucrose-swollen lysosomes.

Patch clamp recordings will be shown which demonstrate a population of NAADP-sensitive channels on the HsTPC2-overexpressing lysosomal membrane. These channels responded with a bell-shaped curve in relation to NAADP concentration. Furthermore, channel activity could be inhibited by Ned-19 and high concentrations of NAADP (1 mM). Lysosomes purified from wild type cells did not show this activity.

These results will be discussed in context with other patched-organelles and the physiological relevance of the recordings technique. The relative merits of this method are compared to those of the lipid bilayer.

4.2 Lysosome purification by differential centrifugation

Most previous works attempting the purification of lysosomes have been based on differential centrifugation techniques, whereby the small buoyant lysosomes are separated from other organelles using sucrose or percoll gradients (162, 258, 455). Lysosomes are particularly difficult to distinguish from mitochondria and peroxisomes as these organelles have a similar size and weight. Chemical perturbations have been used to increase the density of lysosomes (*e.g.* loading with dextran) to give a cleaner preparation (10).

Furthermore, most studies involving purified lysosomes aimed to investigate lysosomal enzyme activity where small amounts of contamination is less critical. However, for electrophysiological recordings the lysosome preparation must be very pure to ensure that measurements were not due to channels from the ER or PM. Removal of the ER is especially important in this study due to claims of NAADP-evoked ER-derived Ca^{2+} release (150, 187, 298, 408).

Differential centrifugation also presents the problem that lysosomes are recovered in a sucrose/percoll solution, which would be unsuitable for electophysiological recordings. Further purification of the lysosomes from this solution into a suitable buffer would be difficult without potentially damaging ultracentrifugation.

Successful lysosomal purification and electrophysiological recordings by planar patch clamp were shown by Schieder *et al.* in 2010 (387). This group purified lysosomes based on evidence that homotypic aggregation and fusion of lysosomes is induced by raised intracellular $[Ca^{2+}]$ (15). Addition of 8 mM $CaCl_2$ to a cell lysate, caused the lysosomes to form dense clusters which could be centrifuged from the solution. A small proportion of lysosomes may not only aggregate but begin to fuse, although this would not be detrimental as an increase in the size of the lysosomes would be beneficial for patch clamp studies.

Patch clamping of lysosomes is technically very difficult due to their small size (0.5 - 1 µm diameter). The two successful reports of lysosomal patch clamp (112, 387) both used the chemical vacuolin to swell the lysosomes to a size of around 5 µm diameter. Vacuolin has been shown to affect lysosome morphology and whilst some defects in lysosomal trafficking have been reported after vacuolin treatment (66) this has been disputed and may be cell type dependent (192).

The methods used by Schieder *et al.* (387), involving Ca^{2+}-induced aggregation of lysosomes and subsequent centrifugation, were used as a model protocol and lysosomes from HEK293 cells overexpressing the HA-tagged HsTPC2 were purified according to the schematic in figure 4.1.

4.2.1 Lysosome enrichment by differential centrifugation

The resulting lysosomes were resuspended from the pellet by repeated pipette aspiration, however once the lysosomes had been induced to aggregate by Ca^{2+} and centrifuged at high speed, the lysosomes could not be released into the single-organelle suspension necessary for successful patch clamp. Figure 4.2 shows a light microscope image of the purified lysosomes which has been vigorously resuspended. This image clearly shows clusters of spherical membrane bound vesicles that exclude trypan blue. The few solitary vesicles range in size from 2 - 5 µm diameter.

To determine the extent of lysosome enrichment, assays were conducted on the lysosome pellet and compared to the input of postnuclear cell lysate and to the depleted supernatant. Two assays were performed against well established lysosomal markers: β-galactosidase and LAMP2. The enzyme activity of β-galactosidase under acidic conditions is specific to the lysosomal isoform (435). Whilst the epoynmous lysosomal location of LAMP2 - Lysosome Associated Membrane Protein 2 - is widely accepted (277).

The enzyme assay against β-galactosidase provided a quantitive assessment of lysosomal purification whilst the western blot gave a more sensitive, but less easily quantified confirmation of the presence of lysosomes.

Figure 4.3 contains the results of the lysosomal β-galactosidase assay which demonstrates that $45 \pm 35\,\%$ ($n = 3$) of β-galactosidase activity was recovered from the total activity present in the cell lysate. If this is normalised to the total protein concentration this results in a roughly 11-fold enrichment.

The western blot against the LAMP2 also demonstrates that the pellet contained lysosomes.

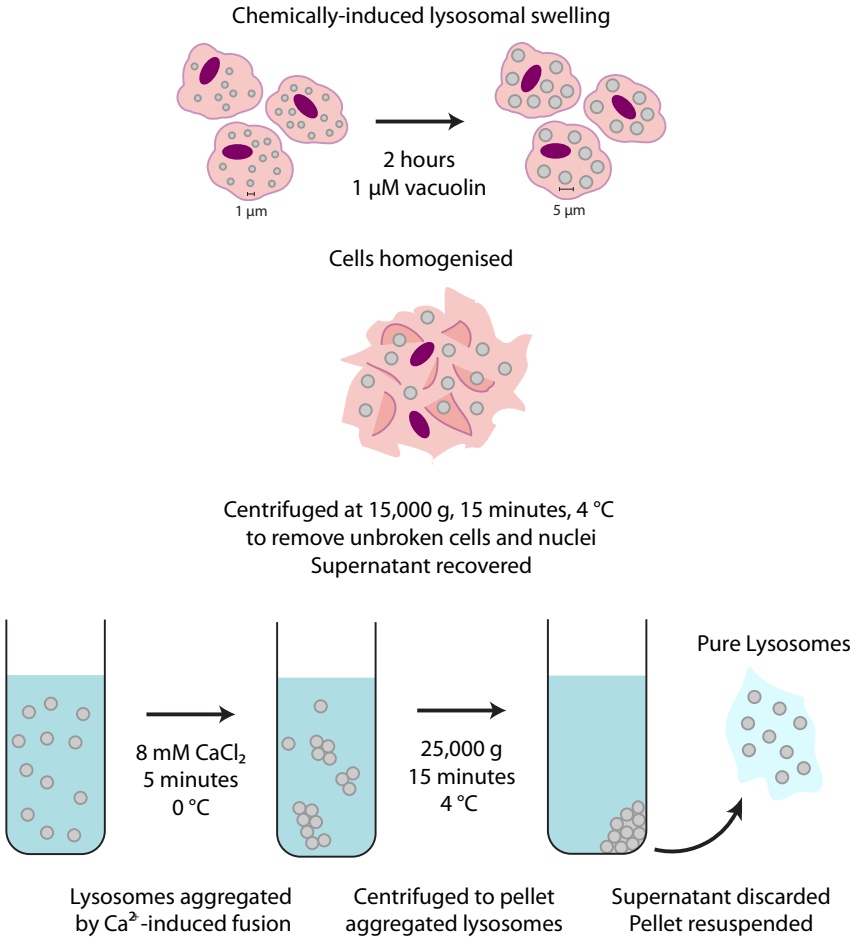


Figure 4.1: Schematic workflow of lysosomal preparation by Ca^{2+}-induced aggregation. Lysosomes were artificially swollen by 2 hour treatment with 1 µM vacuolin, cells were lysed by Dounce homogenisation and cleared of nuclei by centrifugation. Lysosomes were induced to aggregate by addition of 8 mM $CaCl_2$, the aggregates were pelleted by centrifugation

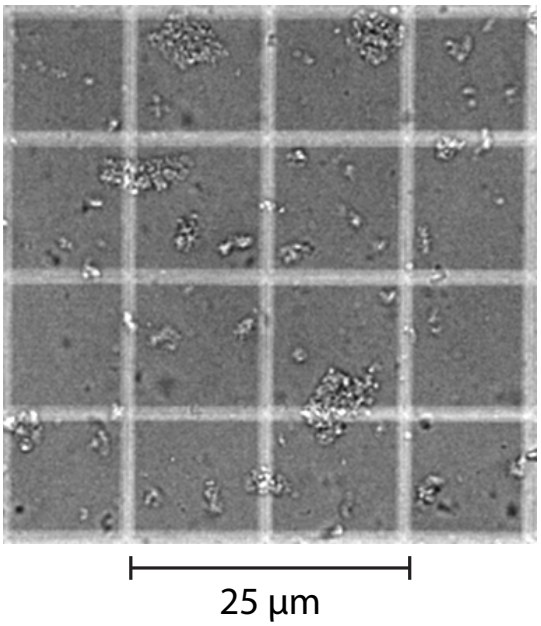


Figure 4.2: Light microscope image of resuspended lysosomes purified by centrifugation. Lysosomes purified by Ca^{2+}-induced aggregation and centrifugation viewed with a 40x air objective. 10 µl of resuspended lysosomes mixed with 10 µl 0.4 % trypan blue counted on a haemocytometer

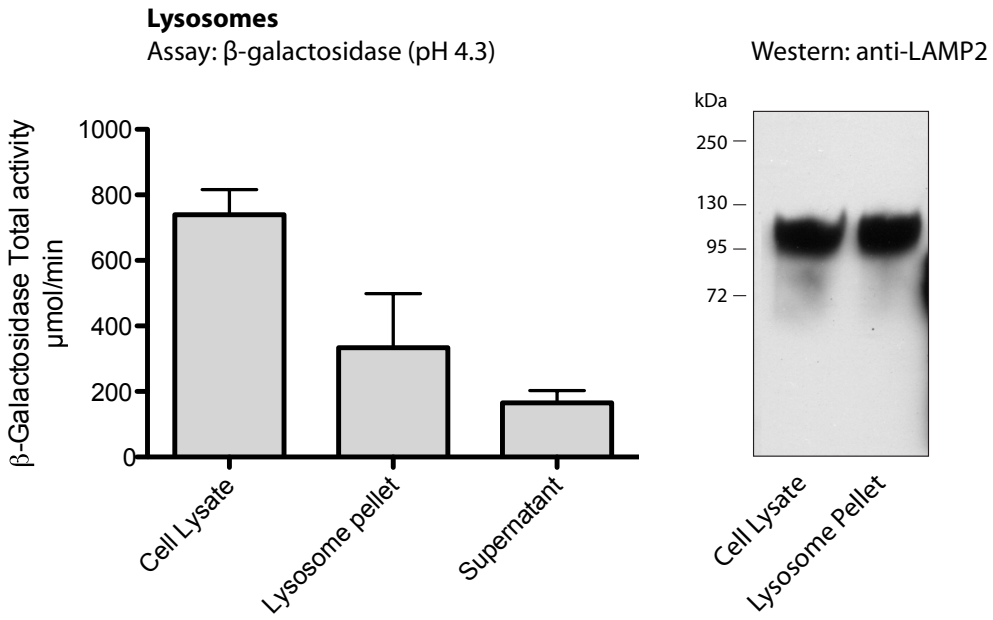


Figure 4.3: LAMP2 is present in the lysosomal pellet. Left: Total activity of lysosomal β-galactosidase in whole cell lysate compared to the purified lysosomal pellet and the depleted supernatant. **Right:** Anti-LAMP2 western blot depicting the presence of LAMP2 in the whole cell lysate and the purified lysosome pellet.

As the ultimate aim of the purification is to detect the activity of the *in situ* HsTPC2, a western blot against the N-terminal HA-tag on the HsTPC2 was conducted and the result is shown in figure 4.4. This western blot not only confirmed the successful enrichment of lysosomes but also that those lysosomes expressed HsTPC2 channels.

Having affirmed the enrichment of lysosomes by this method, their purity was assessed by assays (enzyme and western blot) against other organelles, namely: ER, mitochondria, plasma membrane (PM) and Golgi apparatus.

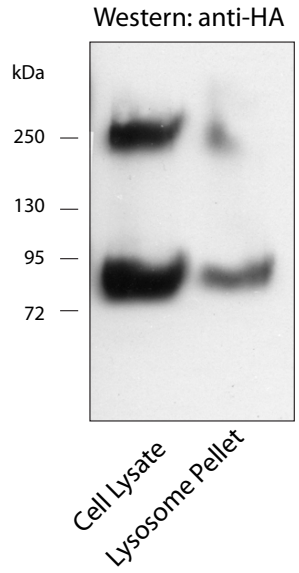


Figure 4.4: Western blot showing presence of HA tag in lysosomal pellet. Anti-HA western blot depicting the presence of HA.HsTPC2 in the whole cell lysate and the purified lysosome pellet.

4.2.2 Contamination by ER

Figure 4.5 contains the results of two assays against the ER. The enzyme β-glucuronidase was used as an ER marker due to its high activity and the availability of a well established fluorescence assay. Whilst this enzyme is present in the ER (97, 473), a lysosomal isoform also exists. However, the lysosomal isoform works optimally under acidic conditions and by conducting the assay at a neutral pH this isoform shows negligible activity (290). As can be seen in figure 4.5 the lysosome pellet contained a substantial proportion of the β-glucuronidase activity, which suggests that there was contamination by ER-derived material.

The western blot shown in figure 4.5 was probed against the membrane protein calnexin, this is a 90 kDa integral protein of the ER which is responsible for protein folding. A strong signal was detected for calnexin in the lysosomal pellet, which further confirms that the lysosomes were contaminated with ER-derived membranes.

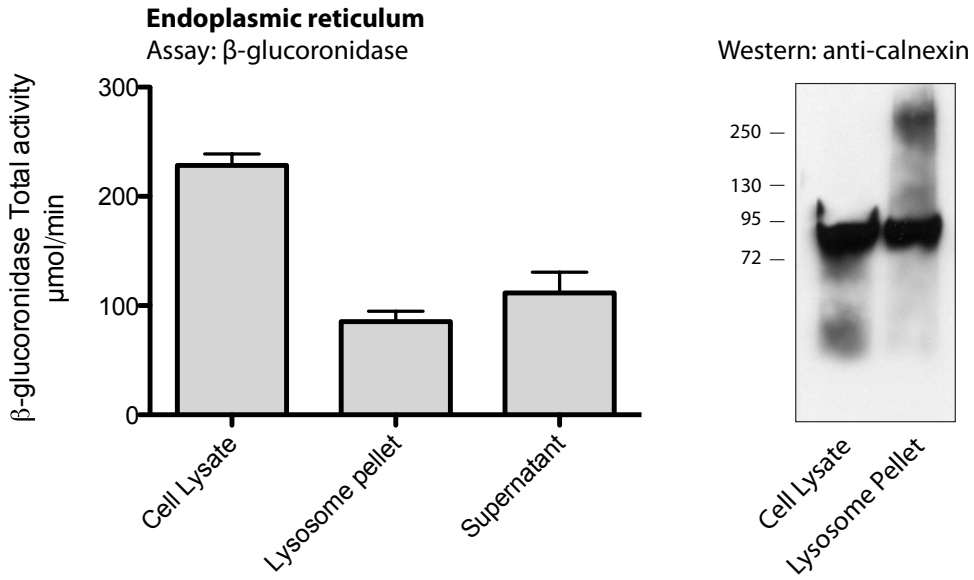


Figure 4.5: ER proteins present as contaminants in the lysosomal pellet. Left: Total activity of ER β-glucuronidase in whole cell lysate compared to the purified lysosomal pellet and the depleted supernatant. **Right:** Anti-Calnexin western blot depicting the presence of this integral ER protein in the whole cell lysate and contaminating the purified lysosome pellet.

The presence of ER contamination seen in figure 4.5 was most likely due to contamination during the Ca^{2+}-induced aggregation step. The method used by Schieder *et al.* was based on work by Scehnkman and Cinti who reported a protocol optimised to purify ER derived microsomes, which were also known to aggregate under conditions of high [Ca^{2+}] (383, 387). This suggests that microsomes formed during homogenisation would also aggregate and would pellet with the lysosomes. Furthermore, reports of heterotypic fusion of endosomes with lysosomes where membrane fusion is dependent on Ca^{2+} and calmodulin (261, 263, 356), may suggest heterotypic fusion events between lysosomes and microsomes which would bring ER proteins into the lysosomal membranes.

4.2.3 Contamination by mitochondria

Further analysis of the lysosomal fraction suggested contamination by mitochondria. A combination of both an enzyme assay against mitochondrial dehydrogenase enzymes and a western blot against prohibitin-1, an inner mitochondrial membrane protein, demonstrated the presence of mitochondria. The PMS/MTS assay is usually used to assess cell viability and proliferation based on dehydrogenation of oxidizable substrates coupled with the reduction of the tetrazolium dye, formazan which can be detected by its distinctive absorbance. It indirectly measures the number of viable cells by quantifying the amount of mitochondrial dehydrogenase present in the samples. Here this assay was used as a direct measure of mitochondrial activity.

Figure 4.6 shows that about half of the mitochondrial dehydrogenase activity was present in the lysosomal pellet. The western blot confirms the contamination by mitochondria in the lysosomal pellet, as a major signal was seen against prohibitin.

The Schieder methodology is based on the assumption that the preclearing centrifugation step at 15,000 xg removes all contaminating organelles, including the mitochondria (386). Whilst during the second centrifugation at 25,000 xg only the aggregated lysosomes will be pelleted. However, the result presented suggests that mitochondria remained in the supernatant and were pelleted by the higher centrifugal conditions.

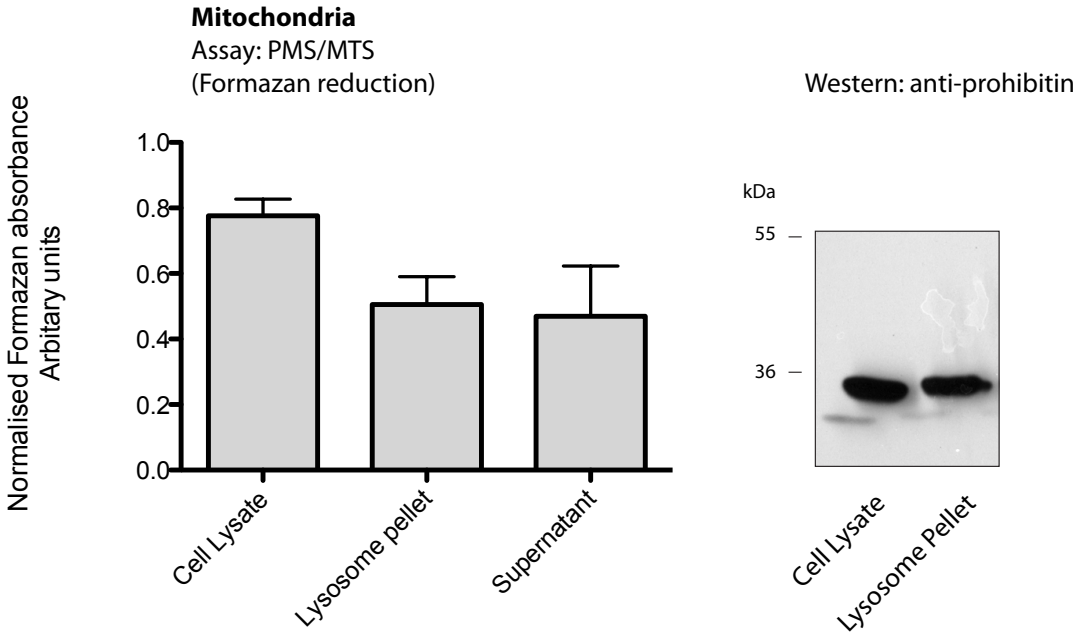


Figure 4.6: Mitochondrial proteins present as contaminants in the lysosomal pellet. Left: Mitochondrial reductase activity in whole cell lysate compared to the purified lysosomal pellet and the depleted supernatant, measured by formazan absorption which correlates to enzyme activity as MTS is reduced in the presence of PMS. **Right:** Anti-prohibitin western blot depicting the presence of this integral mitochondrial protein in the whole cell lysate and contaminating the purified lysosome pellet.

4.2.4 Contamination by PM and Golgi

In addition, assays were conducted against the PM and the Golgi, both known to interact closely with the endolysosomal pathway. Alkaline phosphatase has been shown by subcellular fractionation and electron microscopic histology to be associated with the PM (250, 399). Whilst α-mannosidase is a well established enzyme situated in the membrane of the Golgi (107, 432).

Figure 4.7 shows that enzymatic markers of the PM and the Golgi were more prevalent in the lysosomal fraction than the depleted supernatant.

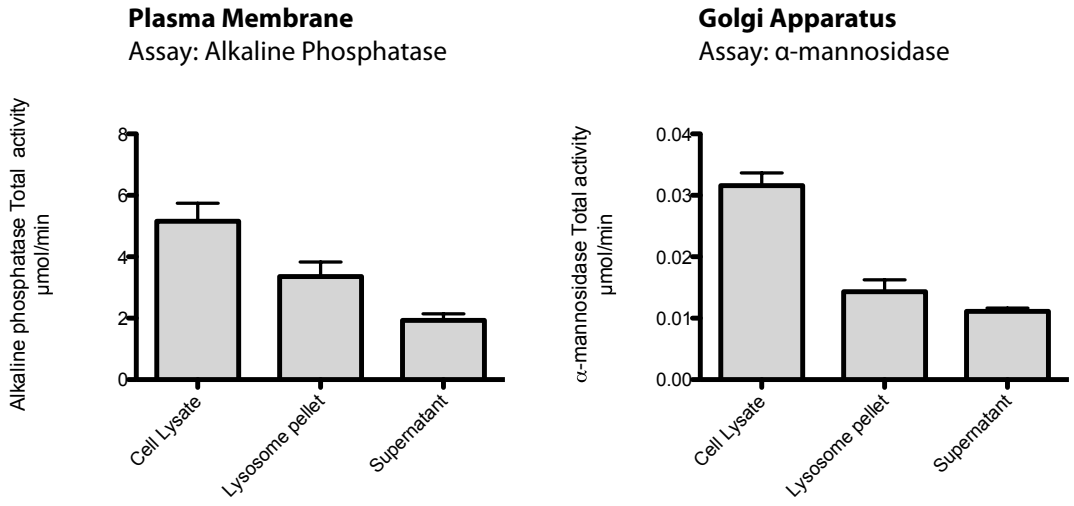


Figure 4.7: Lysosomal pellet contaminated with active enzymes from the Golgi and the PM. Left: Total activity of PM alkaline phosphatase in whole cell lysate compared to the purified lysosomal pellet and the depleted supernatant. **Right:** Total activity of Golgi α-mannosidase in whole cell lysate compared to the purified lysosomal pellet and the depleted supernatant.

Western blots were not conducted against these organelles due to a lack of effective antibodies available.

The contamination of the lysosomal pellet by markers of these organelles was expected due to the close interaction between these organelles and lysosomes. Lysosomal membranes may still contain enzymes from the Golgi from which many lysosomal

membrane proteins are trafficked, or from the PM after endocytosis. Purification by centrifugation cannot distinguish between lysosomes at different stages of the maturation pathway and thus the pellet would contain the immature and dynamic lysosomes which are more likely to contain proteins from other organelles.

Furthermore, lysosomes have been shown to fuse with the PM in response to a rise in cytosolic Ca^{2+} concentration, as part of the membrane repair mechanism (262). Fragments of PM could therefore be induced to aggregate by the addition of high Ca^{2+} to the cell lysate. This would encourage precipitation upon centrifugation and contamination of the lysosomal pellet.

4.2.5 The purity of the lysosome pellet

Throughout these assays the total enzyme activity in the lysosomal pellet has been compared to the total starting activity in the cell lysate, this can be expressed as a percentage recovery and has been plotted for each organelle in figure 4.8.

A surprisingly large proportion of all enzymatic activity is found in the lysosomal pellet, which suggests that this method of purification is not specific for lysosomes. This would cast doubt on the results generated by Schieder *et al.* as the currents measured from lysosomes purified by this method, could have arisen from contaminating membranes from any of the major organelles.

Such a high level of contamination was unacceptable for electrophysiological recordings and thus other methods of lysosomal purification were developed.

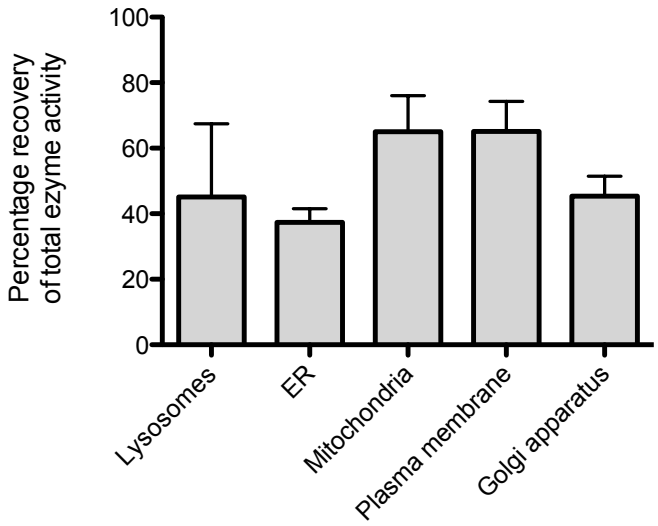


Figure 4.8: Centrifugation recovers a greater proportion of contaminating organelles than lysosomes. Enzyme activity seen in the lysosomal pellet as a percentage of total starting activity of each organelle assay seen in the cell lysate.

4.3 Purification by immunoprecipitation

To circumvent non-specific Ca^{2+}-induced aggregation and aggressive centrifugation, a protocol was developed building on the success of the clean HA.HsTPC2 protein immunoprecipitation (chapter 3). Whole lysosomes were recognised by an the anti-HA antibody coupled to a solid support which could be isolated from the solution.

The HA tag of the HsTPC2 is located on the extreme N-terminus of the protein which, from hydropathy plots and topological studies (188), is predicted to be exposed to the cytoplasm, whilst the HsTPC2 remains anchored in the lysosomal membrane. Anti-HA beads coupled to superparamagnetic beads allowed separation of lysosomes from a cleared cell lysate by immobilising them within a magnetic field as depicted in schematic figure 4.9.

An additional incubation with the enzyme DNase I was also included to break down any DNA ruptured from the nucleus on homogenisation which can cause agglomeration of organelles. This was hoped to prevent contamination and to limit lysosomal aggregation.

Light microscopy images of the resulting lysosomal elution showed a single-lysosomal suspension of vesicles around 5 µm in diameter. An example image is shown in figure 4.10. However, as can be seen by the dark blue staining of the lysosomes, those lysosomes recovered did not exclude trypan blue which suggests that the lysosomal membrane was damaged during this procedure.

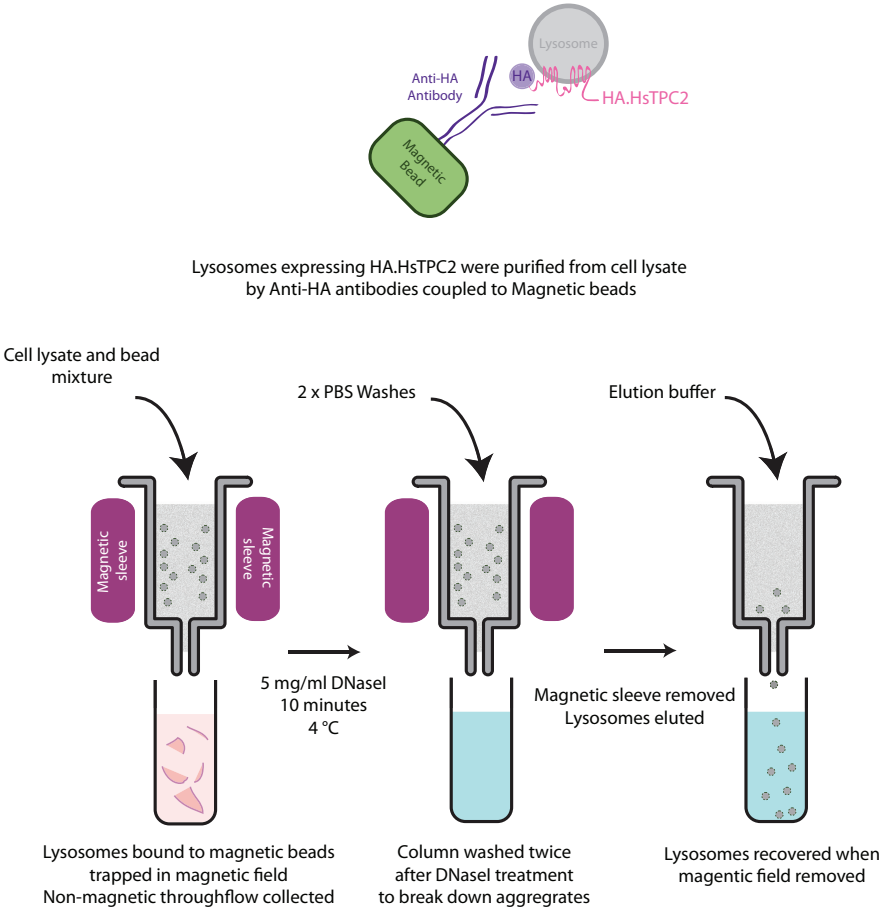


Figure 4.9: Schematic workflow of lysosomal preparation by anti-HA magnetic immunoprecipitation. Magnetic beads coupled to an anti-HA monoclonal antibody were used to bind the cytosolic HA-tag of heterologous HsTPC2 from a cell lysate (Dounce homogenised). The bead mixture was loaded onto a column held within a magnetic field and washed with a solution of 5 mg/ml DNAase I and twice with PBS. The beads were eluted by removal of the magnetic field.

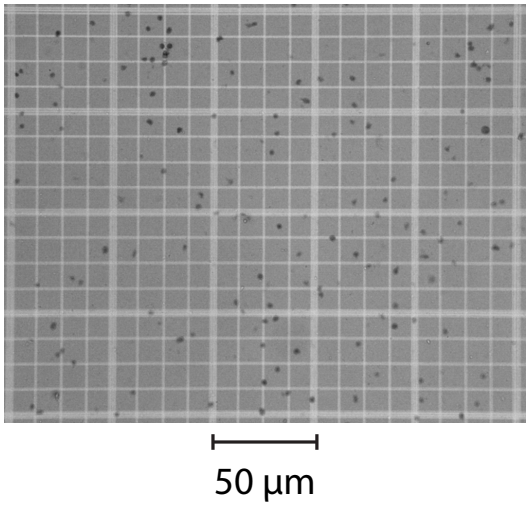


Figure 4.10: Light microscope image of resuspended lysosomes purified by immunoprecipitation. Lysosomes purified by Ca^{2+}-induced aggregation and centrifugation viewed with a 40x air objective. 10 µl of resuspended lysosomes mixed with 10 µl 0.4 % trypan blue counted on a haemocytometer.

4.3.1 Lysosomal enrichment by immunoprecipitation

Figure 4.11 shows the presence of lysosomal markers throughout the various stages in the immunoprecipitation by analysing the β-galactosidase activity and detecting the presence of the HA.HsTPC2. Both assays show that whilst a significant proportion of the lysosomes are purified by this method ($46 \pm 5.9\,\%$ [n = 6]) the majority pass through the column unhindered by the magnetic field.

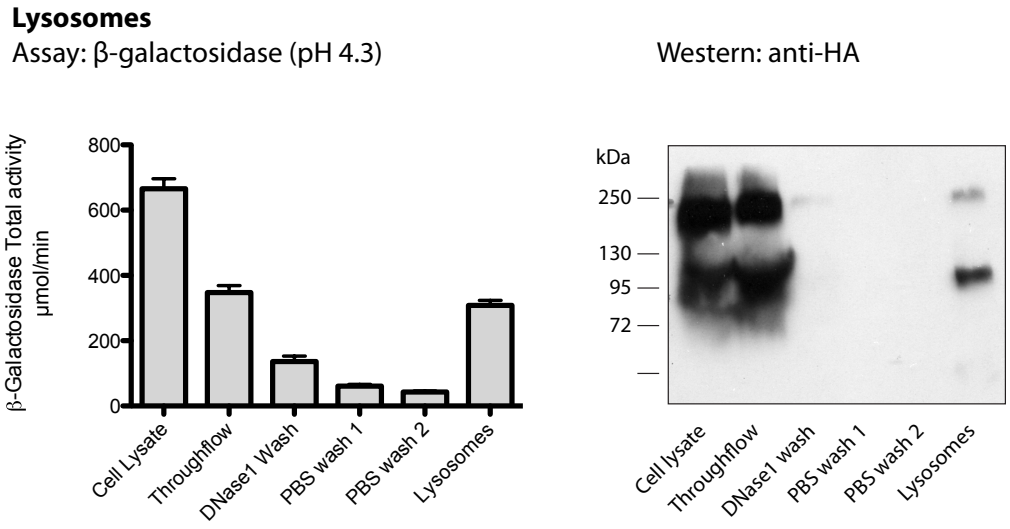


Figure 4.11: Determination of Lysosome recovery by anti-HA magnetic immunoprecipitation. Top left: Total activity of lysosomal β-galactosidase in each fraction eluted from the column. Cell lysate refers to the sample before the beads were added, throughflow refers to the initial output of the column depleted of beads. Each subsequent wash step was collected and these were compared to the final lysosomal elution. **Top right:** Anti-HA western blot against these fractions to determine the presence of HA.HsTPC2.

The lack of retention may be due to the insufficient density of beads to enable magnetic isolation. Despite overexpression of HsTPCs, there may not be a high enough exposure of the HA-tag on the surface of the lysosome for sufficient antibody binding. Also, given the size of the magnetic beads ($\approx$ 50 nm diameter) they may become sterically hindered and unable to fit around the lysosome to bind the HA tag with a high enough affinity.

4.3.2 Contamination by ER and mitochondria

Despite a poor yield, the purity of the lysosomal elution was assessed by western blot against calnexin (ER) and prohibitin (mitochondria). As shown in figure 4.12 both these proteins were present. To fully quantify the level of contamination an enzyme assay would be required thus with only the western blot it is impossible to accurately predict the purity of the lysosomal elution from this method.

Whilst the immunoprecipation did not improve lysosome yield or eliminate contamination from other organelles, it proved a useful negative control which suggested that the Ca^{2+}-induced aggregation was not the only cause of this contamination.

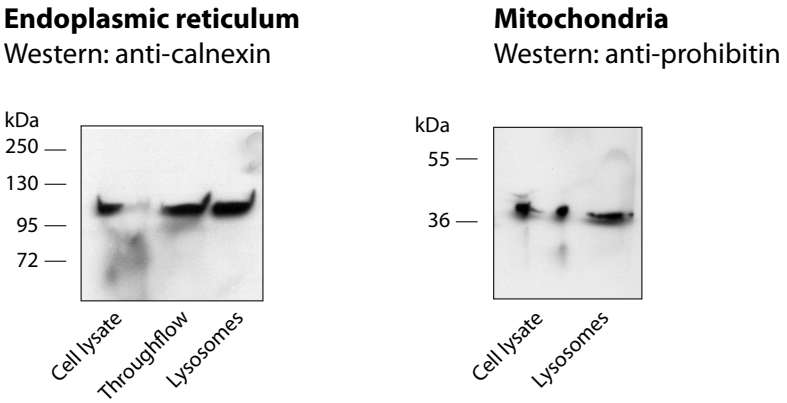


Figure 4.12: Contamination of the lysosomal elution by proteins from the ER and mitchondria. Left: Anti-calnexin western blot against cell lysate, depleted throughflow and lysosomal elution shows presence of ER membrane in lysosomal elution. **Right:** Anti-prohibitin western blot against the cell lysate input and lysosomal elution shows presence of mitochondria in lysosomal elution.

Therefore a method was used whereby the lysosomes were loaded with iron oxides and purified by magnetic chromatography in an attempt to isolate a purer preparation of lysosomes.

4.4 Magnetic chromatography of iron-containing lysosomes

Differential centrifugation and immunopreciption both require intensive manipulation of the cell lysate, vigorous centrifugation steps and lengthy incubation periods. To reduce these potentially disruptive steps, a more direct protocol was developed based upon previous studies involving the isolation of phagolysosomes from *Dictyostelium* by Rodriguez-Paris *et al.* (368). Particles of superparamagnetic colloidal iron coated with 40,000 M_w dextran (Fe-dextran) were endocytosed and transported to the lysosomes. Iron-containing lysosomes were then separated by magnetic chromatography. The schematic in figure 4.13 demonstrates how this methodology was adapted for HEK293 cells.

This method has the added benefit that cell lines incubated with large dextrans have been reported to show a dramatic increase in the size and quantity of lysosomes as they accumulate non-degraded material (75, 443). This phenomenon would result in an increased yield and the larger lysosomes are more likely to form high-resistance seals in patch clamp studies.

All light microscopy images of iron-containing lysosomes showed membrane bound vesicles ranging between 1 - 3 µm diameter, similar to those shown in figure **??**, **??**.

4.4.1 Enrichment of lysosomes by magnetic chromatography

The lysosomal assays shown in figure 4.14 show a better recovery of lysosomes than the immunoprecipitation with a yield of 66 ± 6.7 % (n = 3) based on the β-galactosidase assay. When normalised to protein concentration this equates to roughly 69-fold enrichment. The anti-HA western blot used to confirm presence of the HsTPC2 showed a high level of lysosome recovery.

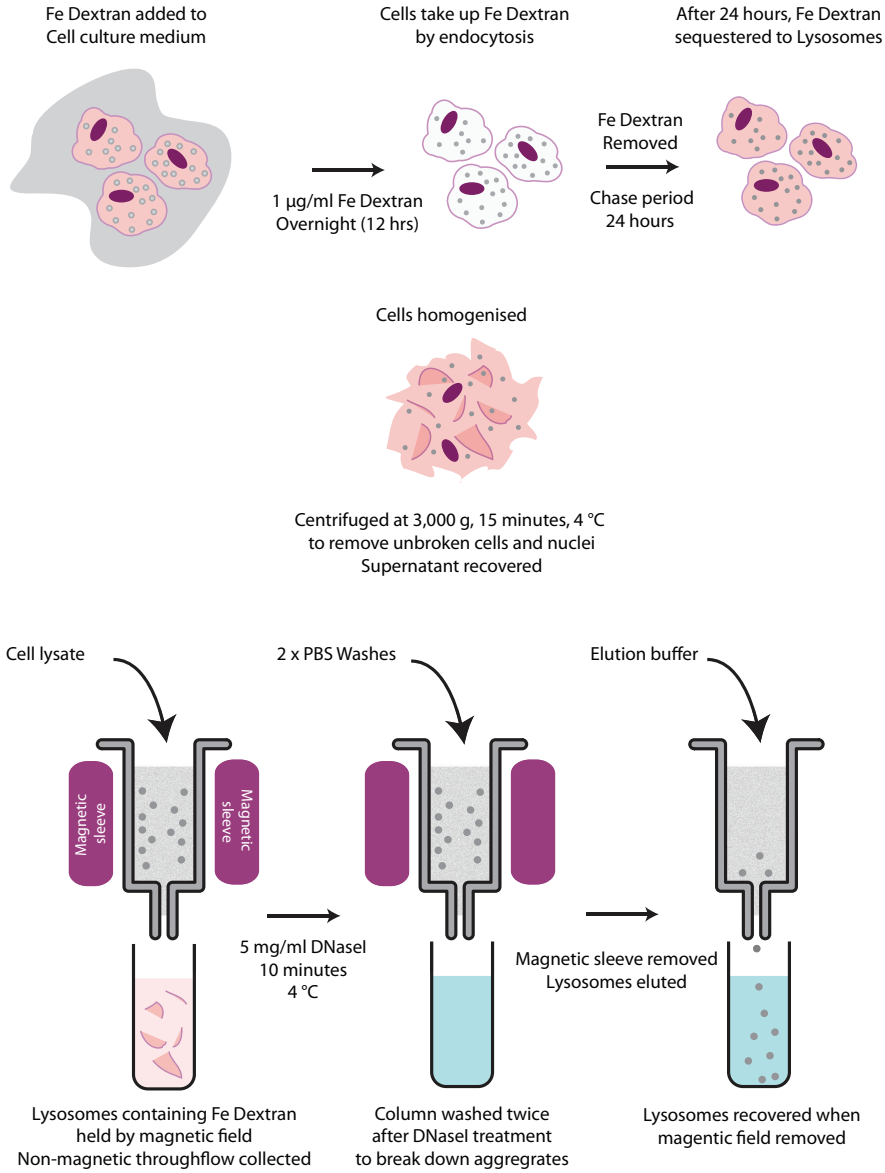


Figure 4.13: Schematic workflow of lysosomal preparation using iron dextran. Cells were grown for 8 hours in a medium containing 1 mg/ml iron-coupled dextran, after a 24 hour chase period to sequester the dextran to the lysosomes the cells were lysed and cleared of nuclei. The lysate was loaded onto a column held within a magnetic field and incubated with 5 mg/ml DNase I then washed twice with PBS. The lysosomes were eluted from the column by the removal of the magnetic field.

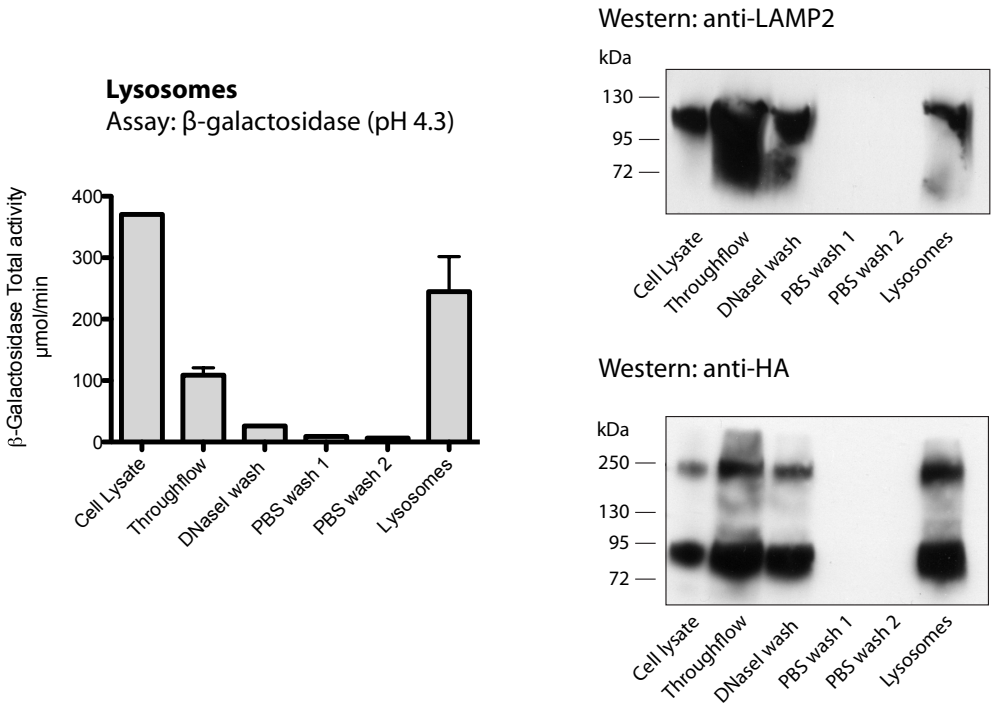


Figure 4.14: A high yield of lysosomes was purified by magnetic chromatography. Left: Total activity of lysosomal β-galactosidase in whole cell lysate, subsequent wash steps and the lysosomal pellet. **Top Right:** Anti-LAMP2 western blot depicting the presence of LAMP2 in the whole cell lysate and the purified lysosome pellet. **Bottom Right:** Anti-HA western blot depicting the presence of the HA tagged HsTPC2 in various fractions of the purification. Presence of HsTPC2 correlates with the lysosomal elution.

4.4.2 Contamination by other organelles

Infuriatingly, these preparations were still contaminated by proteins from all the organelles assayed. Figure 4.15 compiles the combined results of the enzyme assays and western blots which all show the continued presence of contamination.

As before, an overview of the recovery of each of the major organelles assayed is compiled. Figure 4.16 represents the total enzyme activity found in the lysosomal elution as a percentage of total enzyme activity seen in cell lysate.

Although the samples prepared by magnetic chromatography could not be used for patch clamping, due to he contamination seen, this technique did give promising results. Particularly encouraging was the increased level of lysosomal enrichment compared to the differential centrifugation and immunoprecipitation preparations (66% > 45/46%). Moreover, whilst the levels of ER and Golgi contamination were comparable between purification techniques, magnetic chromatography reduced mitochondrial contamination by over half compared to differential centrifugation (29 % < 65 %). This improvement may have been facilitated by the addition of DNase I which prevents organelle aggregation. Furthermore, PM contamination was reduced by $\approx$ 10 % in comparison to differential centrifugation (51 % < 65 %), potentially due to the omission of the Ca^{2+}-induced aggregation required for differential centrifugation which may have incorporated PM-derived microsomes into the lysosomal fraction.

Despite these improvements, this preparation is still too heavily contaminated to be of use, especially by ER which may interfere with Ca^{2+} current recordings. A major concern was that the ER was an inherent contaminant because of the chemically-induced enlarging of lysosomes by vacuolin. Therefore other methods of lysosomal swelling were investigated.

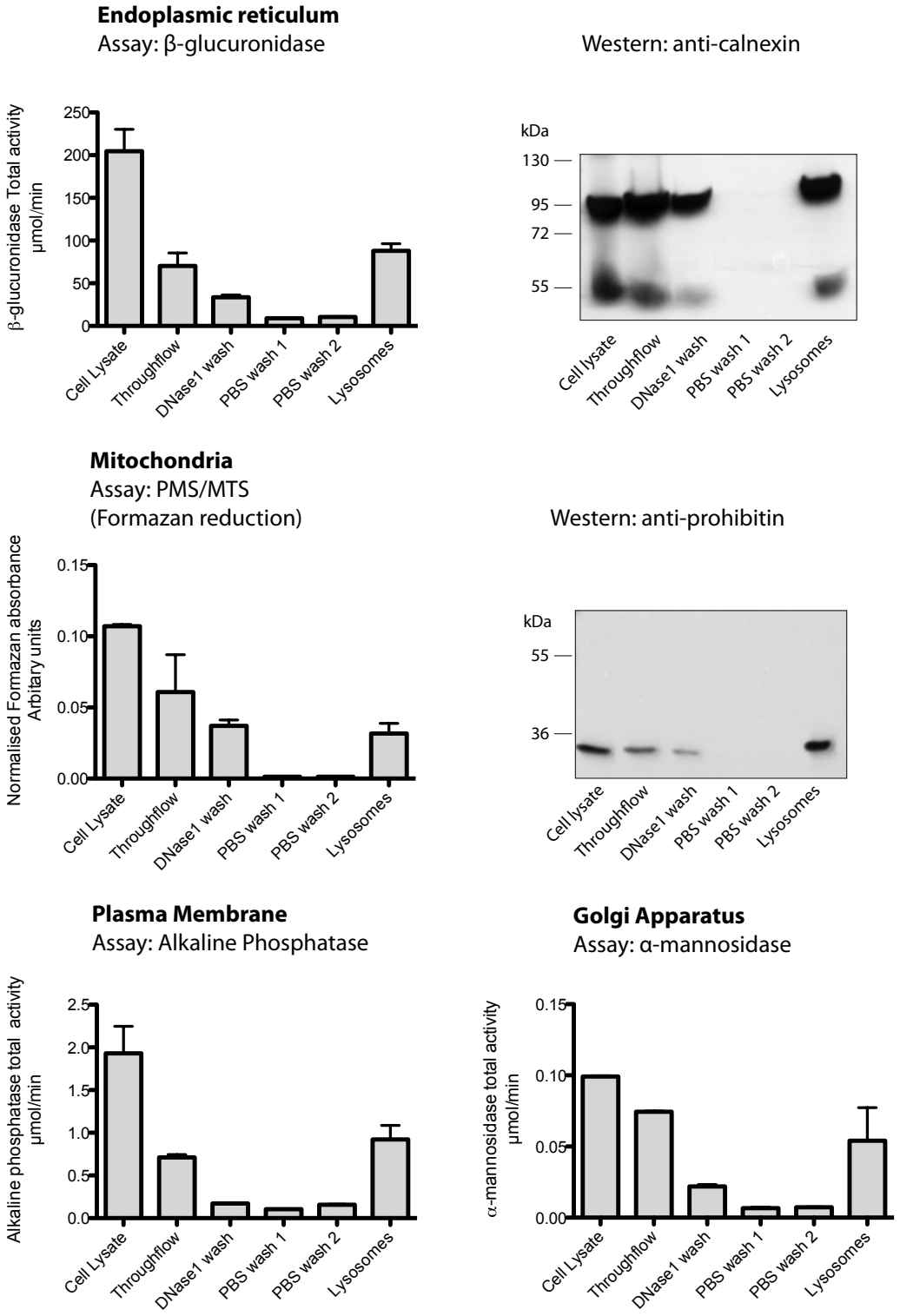


Figure 4.15: Magnetic chromatography did not eliminate contamination. Enzyme assays depicting the total activity of organelle markers together with western blots against ER and mitochondrial markers. All assays show the presence of contaminating organelles in the lysosomal pellet.

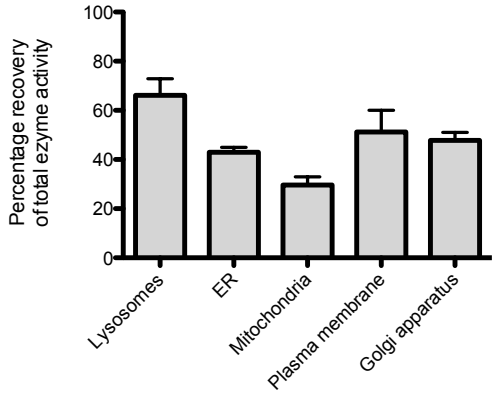


Figure 4.16: Magnetic chromatography yields a high proportion of lysosomes but with significant organelle contamination. Enzyme activity seen in the lysosomal pellet as a percentage of total activity seen in the cell lysate for each organelle assay.

4.5 Lysosomal swelling as a cause of contamination

The magnitude of vacuolin-induced swelling over such a short time scale is thought to be due to homotypic fusion of lysosomes and endosomes (66, 192). However, if vacuolin induced heterotypic fusion this may explain the consistent contamination of ER, Golgi and PM in lysosomes purified by different methods. Mitochondria have been shown to be tethered to ER by the adaptor protein mitofusin 2 (102); a close interaction may explain the level of mitochondrial contamination.

An alternative form of lysosomal swelling could be induced by sucrose. This is a well established phenomenon first shown in mouse macrophages by Cohn and Ehrenreich in 1969 (90), and was shown to be effective in cultured cells (124) and results in the specific swelling of mature lysosomes (103). Sucrose is endocytosed but not metabolised by the cell, and this is thought to induce osmotic swelling over 8 - 12 hours. The slower swelling would allow the cell time to synthesise the additional lipids and proteins required rather than importing them from foreign organelles by fusion.

Figure 4.17 shows HEK293 cells stained with LysoTracker green. Control cells were grown under normal conditions, whilst lysosomes were swollen either by vacuolin for 2 hours or by sucrose overnight. Both vacuolin and sucrose seemed to increase the number of vacuoles (Mean number of lysosomes per cell: wild type = 24.3 ± 6.1, vacuolin = 33.1 ± 8.0, sucrose = 37.8 ± 11.1) and their size from around 0.5 µm to roughly 2 - 3 µm.

For lysosomal purification, it was necessary to determine whether the sucrose swollen vacuoles were still capable of dextran sequestration. As Fe-dextran cannot be easily visualised, cells were loaded with the fluorescent Texas-Red dextran for 12 hours. It was assumed that this dextran would behave equivalently to the Fe-dextran as both dextrans are of similar large molar mass (40,000 g/mol) which would render the additional mass of iron negligible. Loading was followed by a 24 hour chase period during which the lysosomes were induced to swell by vacuolin or sucrose. Lysosomes were then labelled with LysoTracker green. Figure 4.18 shows an example cell for each treatment.

In all cases, localisation of dextran partially correlated with the presence of LysoTracker. The extent of colocalisation was determined by Pearson's coefficient, with control cells showing the highest level of overlap at 0.80 ± 0.02. Swollen lysosomes did show reduced colocalisation with vacuolin swollen cells at 0.62 ± 0.05 and sucrose

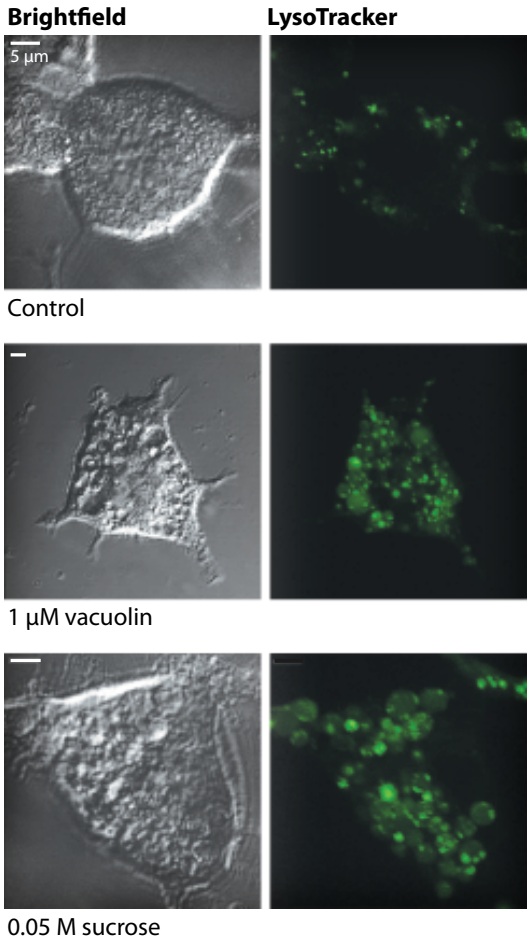


Figure 4.17: Both vacuolin and sucrose cause lysosome swelling. Confocal microscopy images of HEK293 cells treated with LysoTracker Green. Control cells were grown under normal conditions. Lysosomal swelling was induced by two chemicals: 1 µM vacuolin was added to the medium for 2 hours before imaging or 0.05 M sucrose added overnight. Scale bars are all 5 µm. A brightfield image of each cell is displayed on the left.

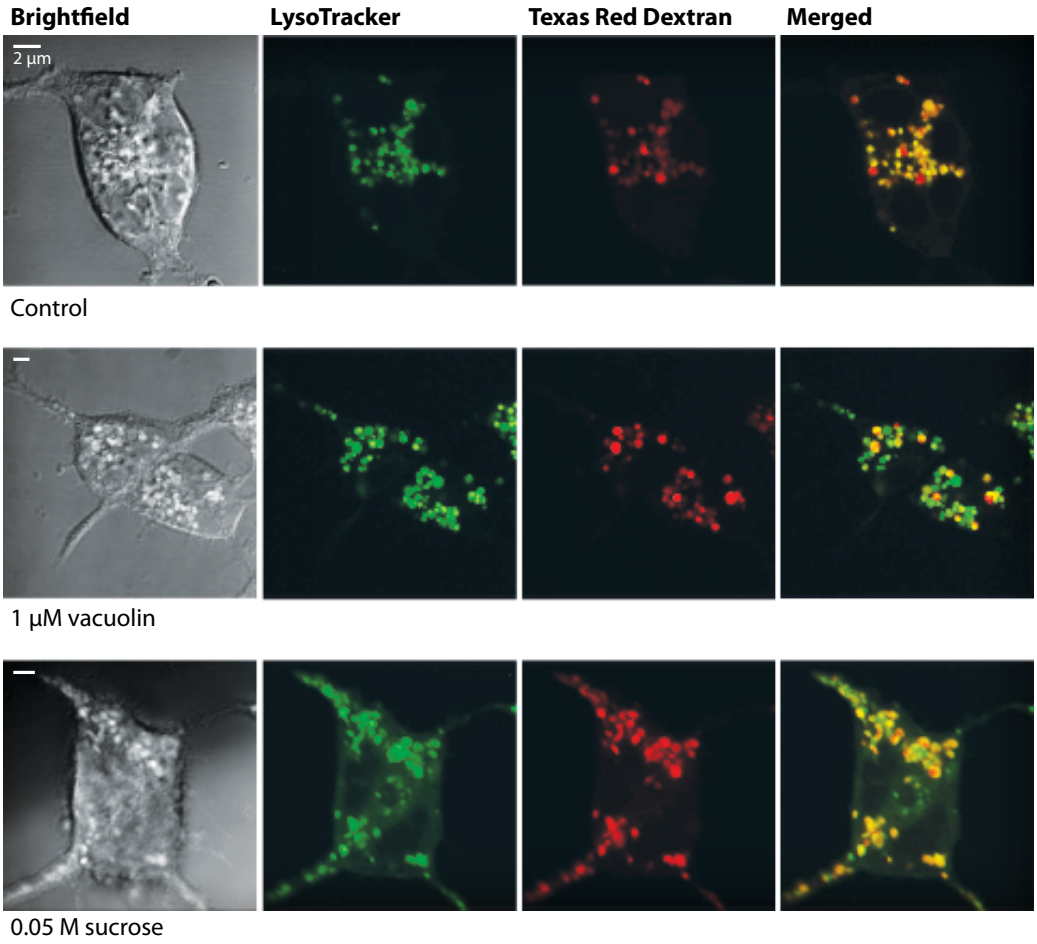


Figure 4.18: Dextrans accumulated in the lysosome are not displaced by swelling. Confocal microscopy images of HEK293 cells treated with LysoTracker green and Texas-Red dextran. Texas-Red dextran was added to cell culture medium for 12 hours and chased for 24 hours. Lysosomes were swollen with vacuolin or sucrose. Co-localisation of LysoTracker and dextran is depicted in yellow. Scale bars are all 2 µm.

swollen cells 0.68 ± 0.03. This partial localisation seen may be due to the fact that dextran accumulation after 36 hours would be mainly localised to the mature lysosome, whereas LysoTracker labelled all acidic organelles including late endosomes and immature lysosomes. These results suggest that although neither vacuolin- nor sucrose-induced swelling prevented dextran accumulation, the altered morphology caused by vacuolin seemed to reduce colocalisation to a greater extent than sucrose. Furthermore, the localisation of Texas-Red dextran in sucrose-treated cells was predominantly in the swollen lysosomes, whereas in vacuolin-treated cells presence of dextran was seen across a range of vesicle sizes. Therefore sucrose was used as the preferred swelling agent as this seemed less physiologically disruptive and more likely to yield uncontaminated lysosomes.

4.6 Purification of sucrose-swollen lysosomes

Iron-containing sucrose-swollen lysosomes were purified by magnetic chromatography as this seemed the most successful technique. A high yield of lysosomes was recovered, as shown by the anti-LAMP2 and anti-HA western blots in figure 4.19. It is impossible to calculate a precise percentage recovery from a western blot, but a crude analysis of the band intensity, normalised to loading concentrations suggests an approximate recovery of 60 % (HA: ≈ 70 %, LAMP2: ≈ 55 %).

However, calnexin (ER) and prohibitin (mitochondria) still contaminated the sample at around 20 % and 12 % of cell lysate levels respectively. Again these are very crude measurements based on non-linear band intensity measurements.

Despite the cleaner swelling methodology and the gentler purification procedure, contamination was still a major problem preventing the use of these lysosomes for electrophysiological studies. Reviewing the methods used, contamination was neither due to the purification procedure nor chemical disruption and thus must be due to an underlying feature common to all preparations. The mode of cell homogenistation was therefore investigated.

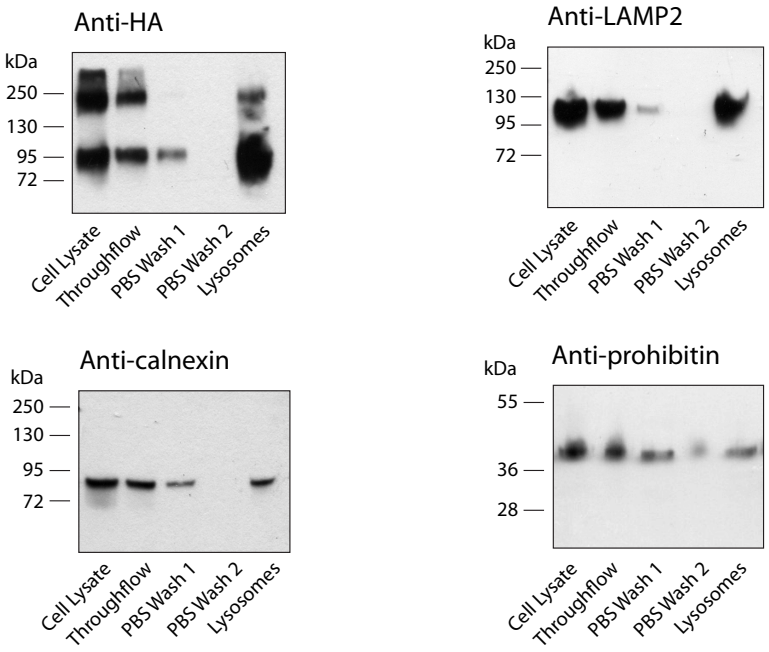


Figure 4.19: Purified sucrose-swollen lysosomes contain ER and mitochondrial proteins. Western blots against various organelle markers for each fraction of the magnetic chromatography purification of sucrose-swollen lysosomes. The lysosomal fraction is positive for all organelles tested.

4.7 Optimisation of homogenisation

Excessive homogenisation can cause formation of microsomes from the PM / ER that contaminate vesicular fractions. This factor had been considered and a loose fitting glass dounce homogeniser had been used for all purifications, as this is reported to be one of the gentlest forms of homogenisation (19, 101, 335); however, as has been shown in previous sections, it was evidently proving too damaging to these preparations.

A range of homogenisation techniques was assayed by measuring specific activity of marker enzymes in a postnuclear supernatant after homogenisation. Freeze-thaw, potter homogenisation and sonication were tried but gave higher levels of microsome formation or lower lysosome recovery than dounce (data not shown).

The three best forms of homogenisation will be compared in this section: needle trituration, dounce and Balch. The Balch homogeniser works by subjecting cells to constant pressure as they pass through a restricted chamber (16). Shear and compression forces create small ruptures in the PM but do not fully disrupt the cell structure (152). Small vesicular organelles can pass through the gaps in the PM during centrifugation whilst nuclei and large reticular organelles remain encased and sediment. As schematically outlined in figure 4.20 the Balch homogeniser consists of a tungsten-carbide ball-bearing that sits within a stainless steel chamber. The extent of homogenisation can be altered by varying the size of the ball bearing.

In these experiments, four differently sized ball bearings were tested, therefore varying the gauge width between the ball bearing and the chamber wall. A HEK293 cell is roughly 30 - 50 µm diameter, and they were subject to gauge widths of 6 - 18 µm. Dounce homogenisation and needle trituration were compared as controls.

Once the cells were homogenised, they were centrifuged for 10 minutes at 1000 xg, to pellet the ruptured cells. The supernatant would be used for further purification whilst the pellet would be discarded. Various assays were conducted to determine the presence of the major organelles in each fraction.

4.7.1 Lysosome recovery by Balch homogenisation

As the lysosomes are such small organelles they were not pelleted by the 1000 xg centrifugation step, even the most aggressive homogenisation resulted in a high yield of lysosomes in the supernatant. Freeze thaw was the only method which gave a low

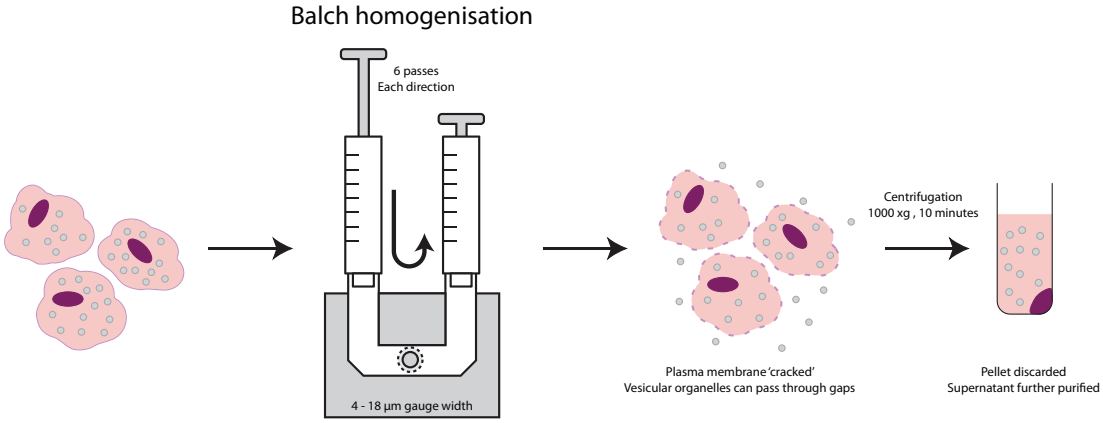


Figure 4.20: Schematic workflow of PM rupture by Balch homogenisation. Cells were passed under constant pressure through a narrow chamber containing a finely machined tungsten-carbide ball bearing, this was optimised to cause PM rupture but not full cell lysis. Centrifugation removed unbroken cells and debris. Lysosomes were purified from the supernatant.

lysosome yield. Figure 4.21 shows a combination of lysosome assays which demonstrate a similar level of lysosome recovery from the dounce, needle and all the Balch gauges.

A quick note regarding the units of enzyme activity is required. During the purification of lysosomes in the last sections, total enzyme activity was recorded, this was due to the different volumes eluted from the columns. The lack of normalisation to protein concentration allowed comparison between elutions and prevented misleading activities being shown for the PBS wash steps. Here however, specific activity was used as this is the more conventional unit of enzyme activity and is appropriate as all samples contained comparable protein concentrations.

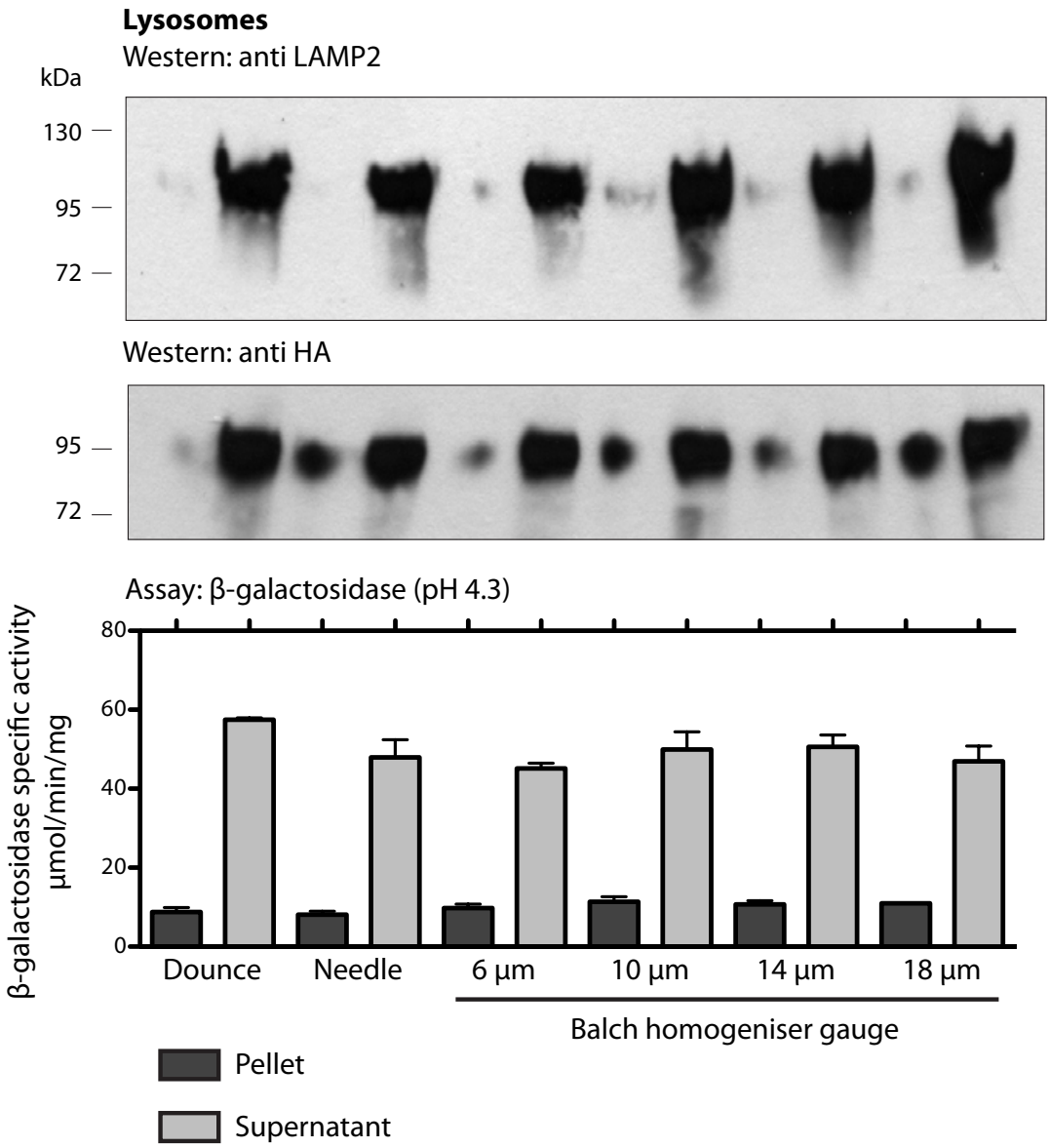


Figure 4.21: Lysosome recovery is similar for all homogenisation techniques. Samples of HA.HsTPC2 expressing cells were homogenised by 3 different techniques. A loose fitting pestle in a dounce homogeniser, a fine gauge needle (25G), or a Balch homogeniser with various gauge diameters. After a 1000 xg centrifugation step the pellet and supernatant were assayed for lysosomal proteins. **Top:** Anti-LAMP2 western blot depicting higher levels of this lysosomal protein in the supernatant than pellet. **Middle:** Anti-HA western blot confirming the presence of HA.HsTPC2 correlates with LAMP2. **Bottom:** Total activity of lysosomal β-galactosidase.

4.7.2 Organelle recovery by Balch homogenisation

ER recovery

The reticular structure of the ER makes it particularly vulnerable during homogenisation and once the ER membrane breaks to form microsomes, these can be indistinguishable from lysosomes. Intact ER would be expected to pellet with the cell debris at 1000 xg, however smaller microsomes would remain in the supernatant.

Homogenisation techniques, such as the dounce and the needle, fully lysed the cells and subjected the ER to relatively large mechanical forces. The resulting microsome formation can be seen in figure 4.22 as both calnexin and β-glucuronidase activity show higher levels in the supernatant.

The Balch homogeniser, which applies a constant pressure to the cell, does not show such high levels of ER-enzyme activity in the supernatant as the ER remained encased within the cell and fewer microsomes were formed. The largest gauge ball-bearing (18 µm) gave the best result with minimal levels of ER in the supernatant.

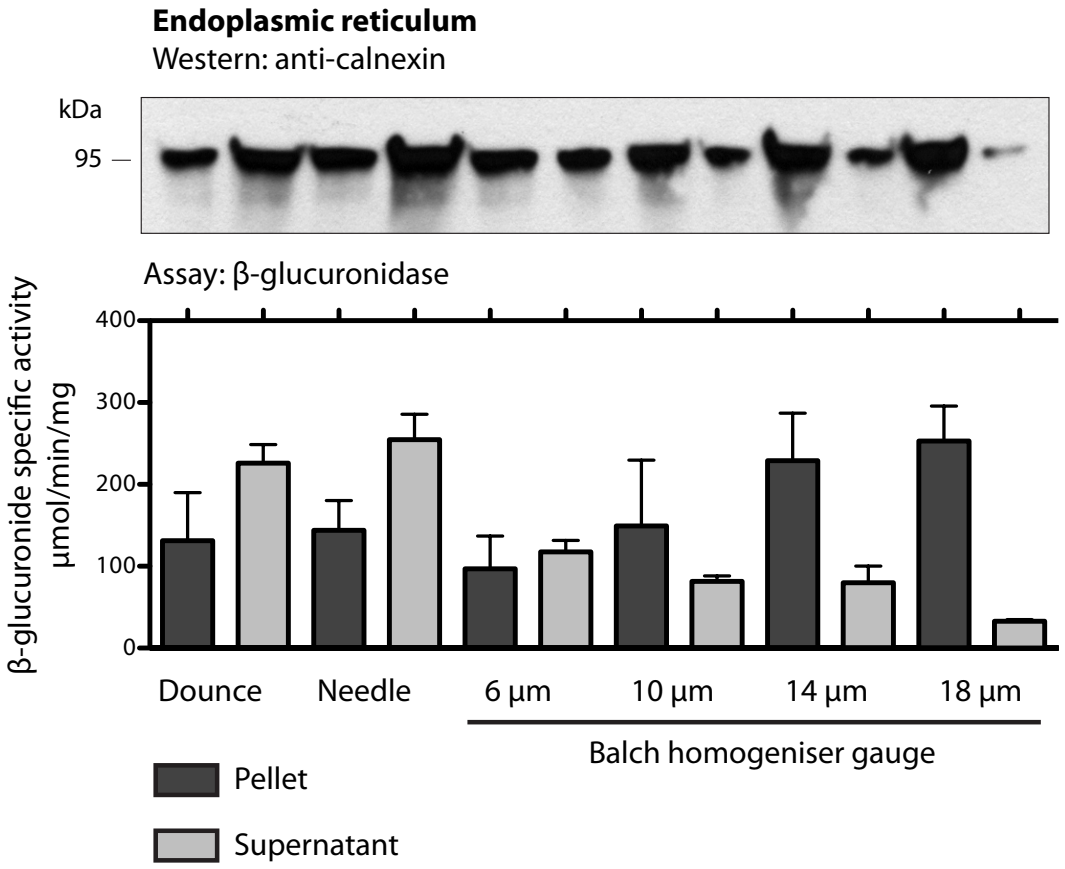


Figure 4.22: Balch homogenisation reduces ER contamination. Post-homogenisation analysis of different homogenisation techniques to detect presence of ER proteins **Top:** Anti-calnexin western blot shows ER contamination in all samples. Least ER contamination is seen using the 18 µm Balch gauge. **Bottom:** Total activity of ER β-glucuronidase.

Mitochondria recovery

Mitochondria are approximately 1 - 5 µm in diameter, and would not be pelleted by the 1000 xg centrifugation if they were released from the cell. Homogenisation techniques which fully lyse the cells, such as the dounce and the needle, show a high presence of mitochondria in the supernatant as shown by dehydrogenase activity in the PMS/MTS assay and anti-prohibitin western blot in figure 4.23.

Given their small size it was assumed that mitochondria would also be able to escape through the PM ruptured by the Balch homogeniser. Using a large ball bearing and thus a small gauge (6 to 10 µm) the cells seemed to rupture sufficiently that most mitochondria were found in the supernatant, however homogenisation with the larger gauge resulted in most of the mitochondria being pelleted as though they remained trapped within the cell (figure 4.23 - gauge 18 µm). This is a very beneficial result as it prevents excessive mitochondrial contamination of the input material, and thus reduces the chances of contamination in the final preparation.

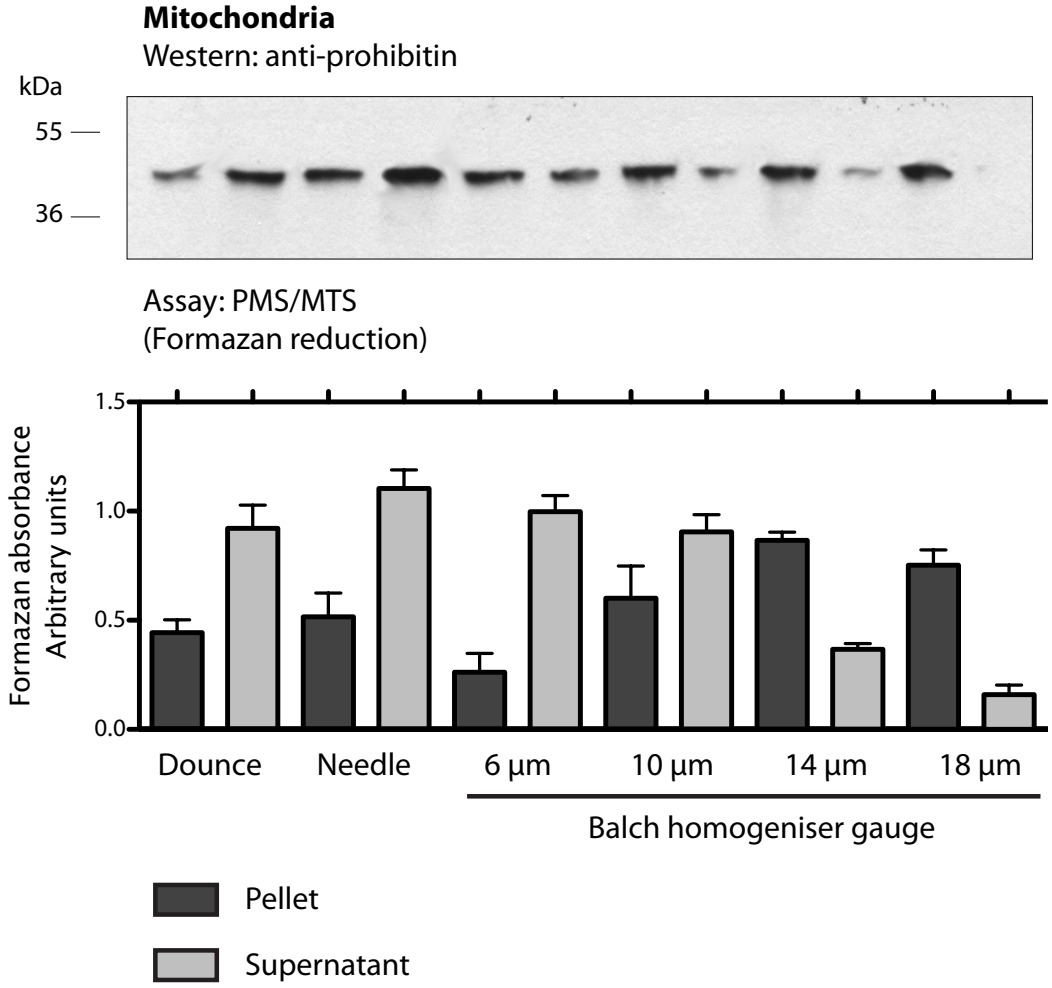


Figure 4.23: Balch homogenisation reduces mitochondrial contamination. Post-homogenisation analysis of different techniques to detect presence of mitochondrial proteins **Top:** Anti-prohibitin western blot shows mitochondrial contamination in all samples. Least mitochondrial contamination is seen using the 18 µm Balch gauge. **Bottom:** Mitochondrial reductase activity in each sample measured by formazan absorption which correlates to enzyme activity as MTS is reduced in the presence of PMS

PM recovery

Balch homogenisation was first designed to prevent PM contamination of cell lysates. Whilst this seems very true for the larger gauge setups, with the 18 µm showing little alkaline phosphatase activity in the supernatant, the smaller gauge setups seem to cause more extensive disruption of the PM. Figure 4.24 demonstrates specific enzyme activity after each homogenisation. A high level of enzymic activity suggests small fragments of PM were released into solution and were not pelleted with the larger cell debris during centrifugation.

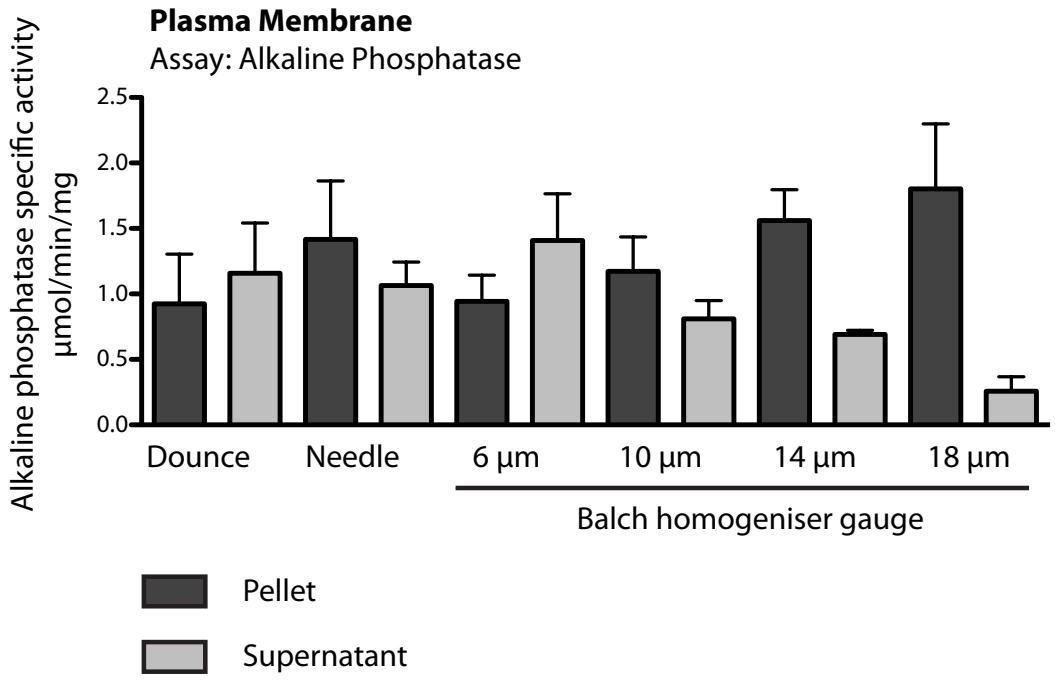


Figure 4.24: Balch homogenisation reduces PM contamination. Total activity of PM alkaline phosphatase in each homogenised sample.

Golgi recovery

The Golgi has a similar reticular structure to the ER and was assumed to behave in the same manner during homogenisation. However, as shown in figure 4.25 the Golgi enzyme α-mannosidase seems to be released into the supernant by all homogenisation techniques. This may be due to the presence of this enzyme in small Golgi-derived vesicles which would not be pelleted during centrifugation as they could migrate through the ruptured PM.

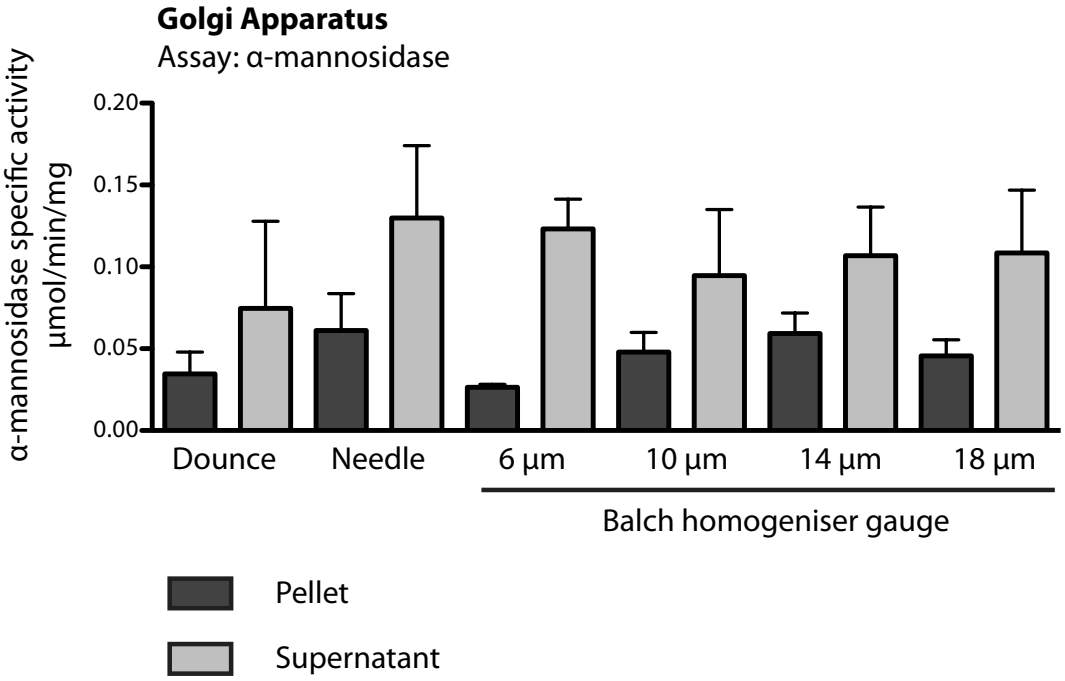


Figure 4.25: Golgi contamination is similar for all homogenisation techniques. Total activity of Golgi α-mannosidase in each homogenised sample.

This optimisation proved that the Balch homogeniser (18 µm gauge) yielded a far purer starting material of small vesicular organelles with less contamination from the ER, PM and mitochondria. The lysosomal content of the supernatant was similar to that of the dounce homogenisation which had previously been used. The only concern is high level of Golgi-derived contamination, but given the close association of the Golgi apparatus with early endosomes and immature lysosomes, some element of Golgi-derived material would always have contaminated any lysosomal preparation (261, 263).

Only those lysosomes that sequester the Fe-dextran would be purified by magnetic chromatography and these would tend to be the mature lysosomes.

4.8 Magnetic chromatography of the Balch supernatant

Therefore, the final protocol combined elements of each optimisation stage mentioned in this chapter. Cells were loaded as before with Fe-dextran for 12 hours followed by a 24 hour chase period to clear the Fe-dextran to the lysosomes. During this time the lysosomes were induced to swell with sucrose. The cells were then homogenised with a Balch homogeniser with an 18 µm gauge and the lysosomes were purified using the magnetic column as in figure 4.13. Figure 4.26 shows a light microscope image of the resultant lysosomes in single-organelle suspension diluted 50 % in trypan blue. The purified lysosomes had an average diameter of ≈ 2 - 3 µm.

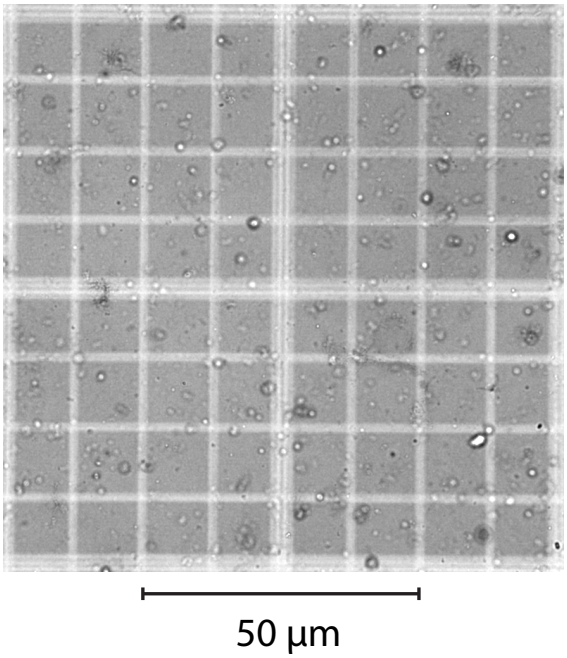


Figure 4.26: Light microscope image of lysosomes purified by Fe-dextran from Balch homogenate. Lysosomes eluted from the column viewed with a 40x air objective. 10 µl of resuspended lysosomes mixed with 10 µl 0.4 % trypan blue mounted on a haemocytometer.

Figure 4.27 shows a compilation of assays depicting a high level of lysosomal recovery. The β-galactosidase assay suggests a recovery of nearly 80 % of the lysosomes from the starting supernatant which when normalised to protein concentration accounts for a 71-fold enrichment. Western blots against both LAMP2 and the HA tag of HsTPC2 show a saturating level of protein, which demonstrates how highly concentrated the lysosomal preparation is compared to the cell lysate input.

Very low levels of ER were detected in this lysosomal preparation, this was aided by the fact that very little ER was present in the starting material ($\approx$ 40 µmol/min compared to $\approx$ 200 µmol/min in the dounce homogenate, page 172). Figure 4.28 shows the combined enzyme assays and western blots for each organelle and this shows that minimal levels of β-glucuronidase activity were in the lysosomal pellet confirmed by undetectable levels of calnexin in the western blot.

Similarly, due to the reduced level of mitochondria in the starting material, there was a dramatic reduction in the amount contaminating the lysosome elution. There was a low level of dehydrogenase activity and undetectable levels of prohibitin on the western blot.

The level of PM alkaline phosphatase activity was largely depleted by the Balch homogenisation step (figure 4.24, page 186) and whilst a small amount is seen in the lysosome fraction, this could be due to minor phosphatase activity in the lysosomal membrane.

The Golgi α-mannosidase assay shows a relatively high level of recovery in the lysosomal elution, which shows there is still some contamination. This raises concerns for potential electrophysiological recordings, as the Golgi has been shown to be a Ca^{2+} store which is sensitive to IP_3 (345). However, this is not a major worry as some contamination was always predicted because the Golgi membrane is constantly in flux with the early endosomes and lysosomes, as lysosomal proteins are trafficked from the trans-Golgi network (262). Another reason for the contamination may even be due to a subset of α-mannosidase localised to the lysosomal membrane (20).

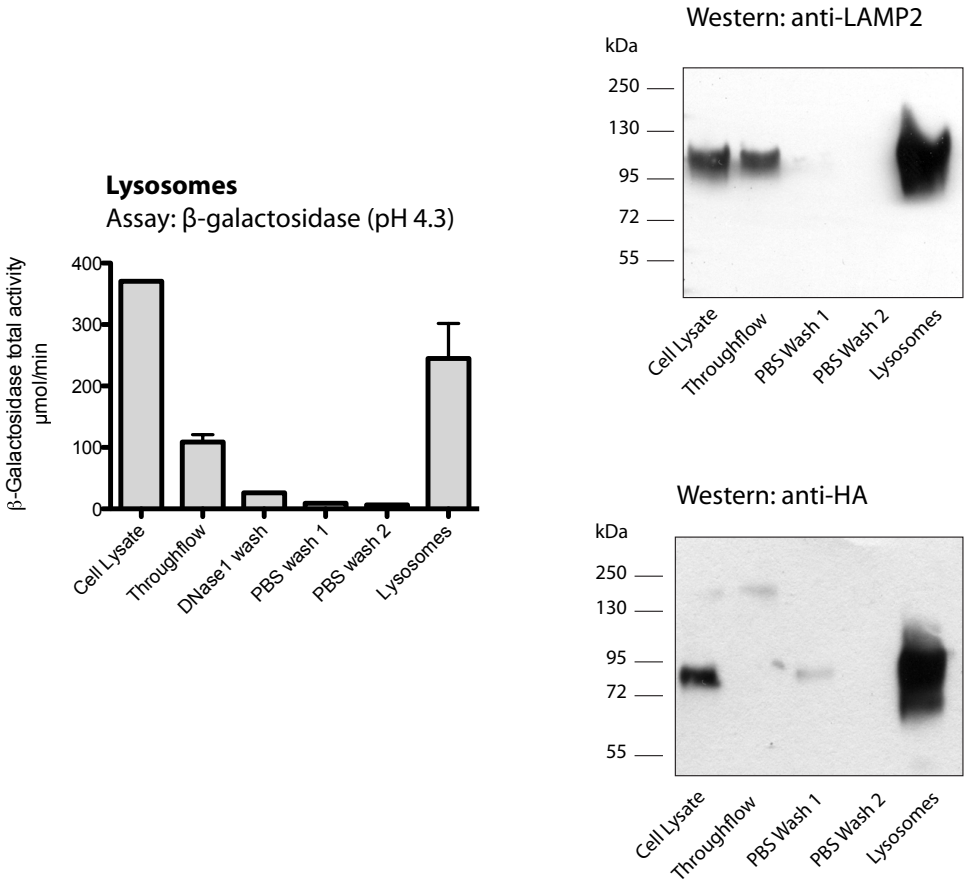


Figure 4.27: A high yield of lysosomes purified from Balch homogenised cells. Left: Total activity of lysosomal β-galactosidase in whole cell lysate, subsequent wash steps and the lysosomal elution. **Top right:** Anti-LAMP2 western blot depicting the presence of LAMP2 in the whole cell lysate and the purified lysosome pellet. **Bottom right:** anti-HA western blot depicting the presence of the HA tagged HsTPC2. Presence of HsTPC2 correlates with the lysosomal elution.

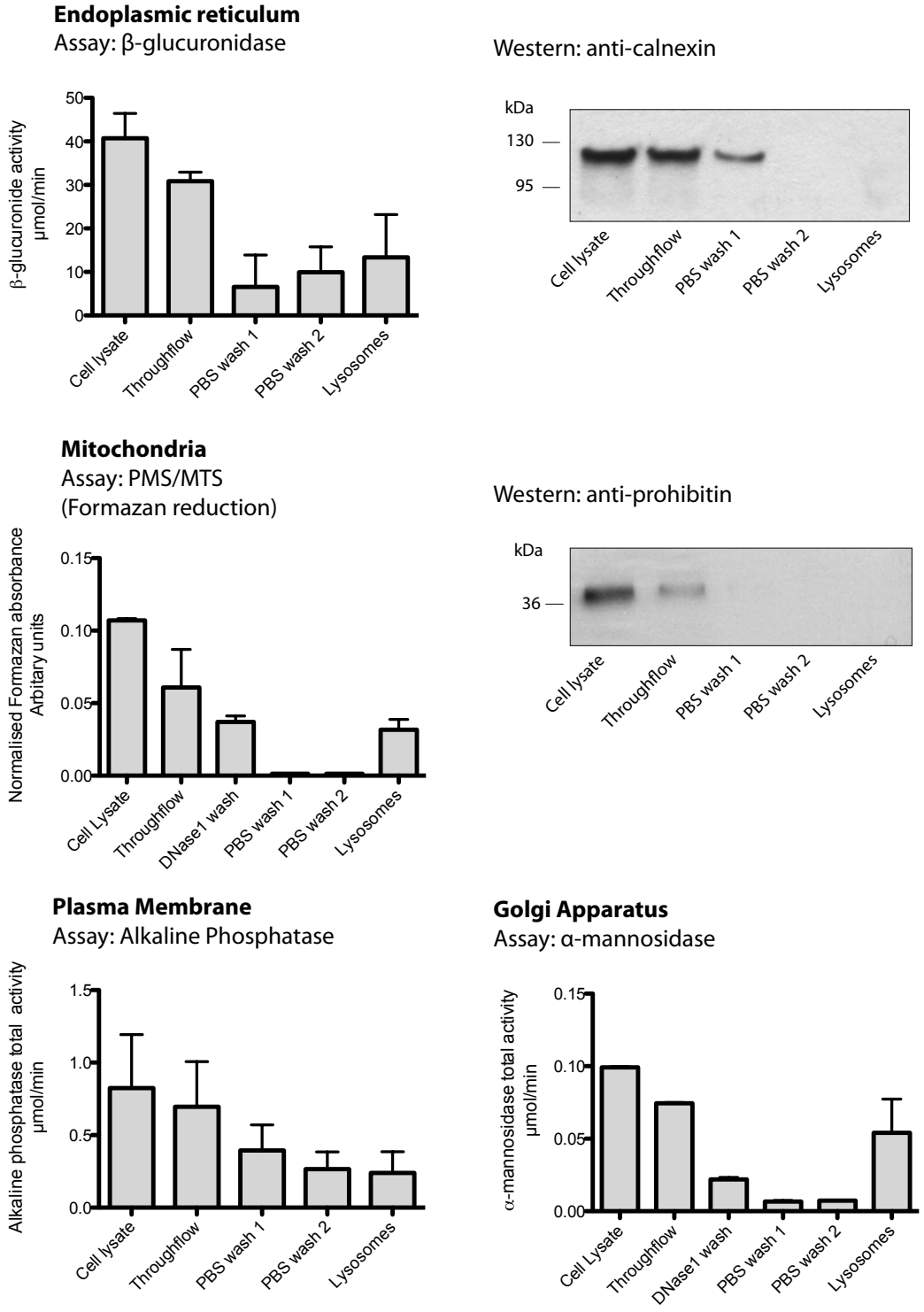


Figure 4.28: Negligible levels of organelles contamination in lysosomes purified by magnetic chromatography from Balch homogenised cells. Enzyme assays depicting the total activity of organelle markers together with western blots against ER and mitochondrial markers. All enzyme assays show the some low-level presence of contaminating organelles in the lysosomal pellet, although mitochondrial/ER contamination cannot be seen by western blot.

4.8.1 The purity of the lysosomal preparation

The individual assays discussed give a clear picture that lysosomes prepared by magnetic chromatography from Balch homogenised cells result in a higher yield and of greater purity than by the other protocols discussed. For consistency, figure 4.29 depicts the percentage recovery of enzymatic activity for the organelle markers investigated. Lysosomes show a high yield as discussed, however this graph suggests high levels of ER and PM contamination. This is misleading and is due to the fact that levels of these organelles was very low in the starting cell lysate from the Balch homogeniser. The low levels of activity seen in the lysosomal elution thus represent a reasonably high percentage recovery. In general, as enzyme levels decrease these assays become less reliable and error increases. The western blots provide a good confirmation that contamination had been eliminated.

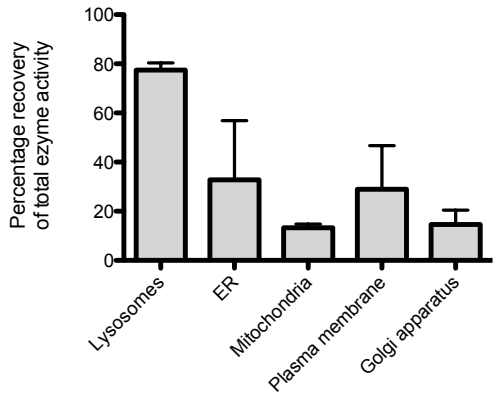


Figure 4.29: Magnetic chromatography yields high levels of lysosomes with negligible contaminants. Enzyme activity seen in the lysosomal pellet as a percentage of total activity seen in the cell lysate for each organelle assay.

4.9 Electrophysiological recordings by Flyion

Whilst it has been shown that swollen lysosomes can be patched directly for electrophysiological recordings (112) using conventional patch clamp methodology, this requires great technical dexterity and expertise. New technologies have been developed which claim to reduce the need for painstaking accuracy and patience. In addition, they claim the ability to patch small organelles such as lysosomes. One such technology developed by Flyion (Tüebingen, Germany) works on a "Flip-the-tip" concept and is depicted in the schematic in figure 4.30. Rather than patching a lysosome onto the end of a glass micro-pipette as in conventional patch clamp, the lysosomes are fed from inside the pipette and a seal forms as a lysosome is sucked into the tip. The solutions and holding potential are reversed. Flyion has been successfully demonstrated on whole cells (155), and narrow-tip pipettes (< 1 µm diameter) have been developed in order to patch clamp organelles, such as lysosomes. This technology is also fully automated which prevents user error and allows a high throughput of channel recordings (155).

4.9.1 Flyion - non-swollen lysosomes

Lysosomes prepared by Balch homogenisation and Fe-dextran magnetic chromatography were loaded onto the Flyion. Firstly, it was investigated whether this technology would be able to patch non-swollen lysosomes as these would be less physiologically altered. Figure 4.31 shows example traces of Flyion experiments. The majority of these lysosomes (37 out of 48) did not form a seal with the pipette tip, even with a generous definition of a seal being > 100 MΩ. Those few lysosomes which did form a weak seal were automatically treated with 100 nM NAADP. However, due to such wild current fluctuations, any effect of this addition was lost. Figure 4.31 shows the pipette resistances commonly seen with these lysosomes: either nothing at all, or a weak seal in the hundred MΩ range. This figure also shows the wild current fluctuations seen in a weak seal and that the addition of NAADP made no effect as there was no significant difference between average current before addition compared to average current after addition.

It is difficult to measure the tip width of the micro-pipettes, but this experiment suggests that it is probably around 1 µm diameter, with most non-swollen lysosomes

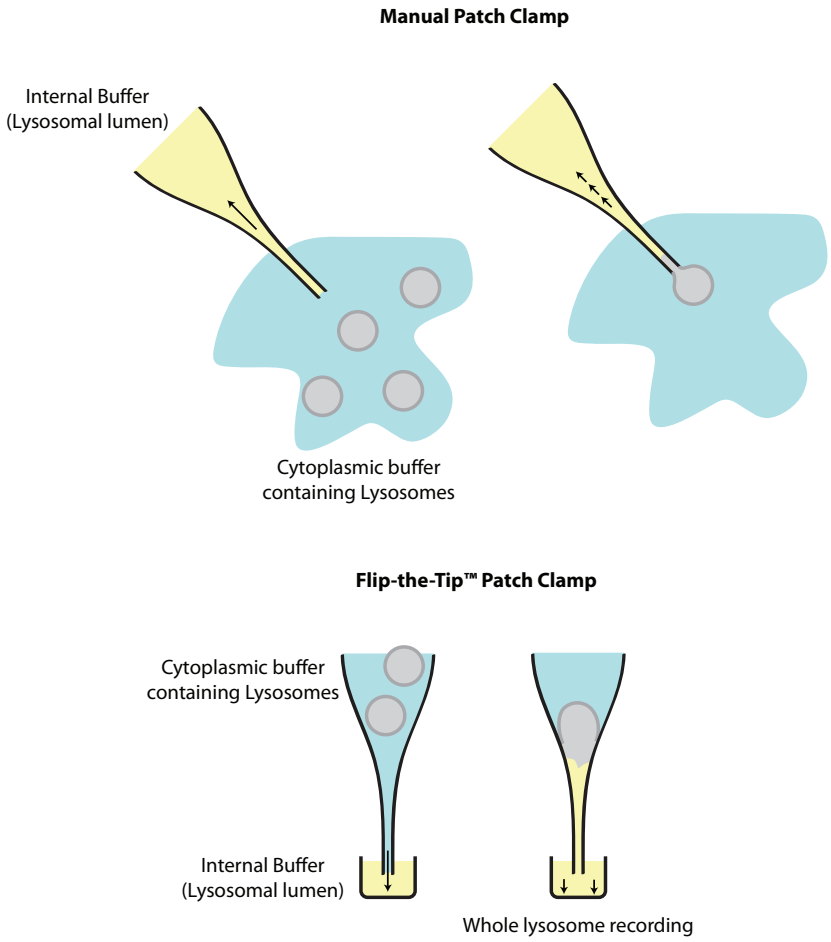


Figure 4.30: Schematic of Flyion technology. In conventional patch clamp lysosomes are sealed to the tip of a pipette from the bath solution. Flyion technology inverts this patching, lysosomes are added from within the pipette.

slipping through and only a few of the larger lysosomes remaining trapped at the pipette tip.

4.9.2 Flyion - sucrose-swollen lysosomes

Lysosomes that had been swollen with sucrose were purified using the Fe-dextran method and loaded onto Flyion. There was a greater success rate in formation of seals, however very few were in the optimum giga-Ω range. Example traces are shown in figure 4.32. Weak seals showed large fluctuations in current measurements and no significant change in current activity upon the addition of 100 nM NAADP. Trace C in figure 4.32 does seem to show an increase in average current after NAADP addition however, this was the only trace that showed this phenomenon and could not be repeated (n = 24). On two occasions giga-Ω seals were recorded, this resulted in a more stable current measurement, however NAADP addition made no significant difference to the average current.

Limitations of this technology prevented further studies. The Flyion machinery is fully automatic and does not allow experimenter manipulation. Large volumes of lysosomal preparations were required and these were passed through multiple syringes and lengths of tubing. Analysis of lysosomes that were reaching the tip showed aggregated and damaged lysosomes, as shown by the light microscope image in figure 4.33.

Due to the nature of this technology, aggregated lysosomes could simply block the tip of the pipette which could result in high resistance which was mistaken for a weak seal.

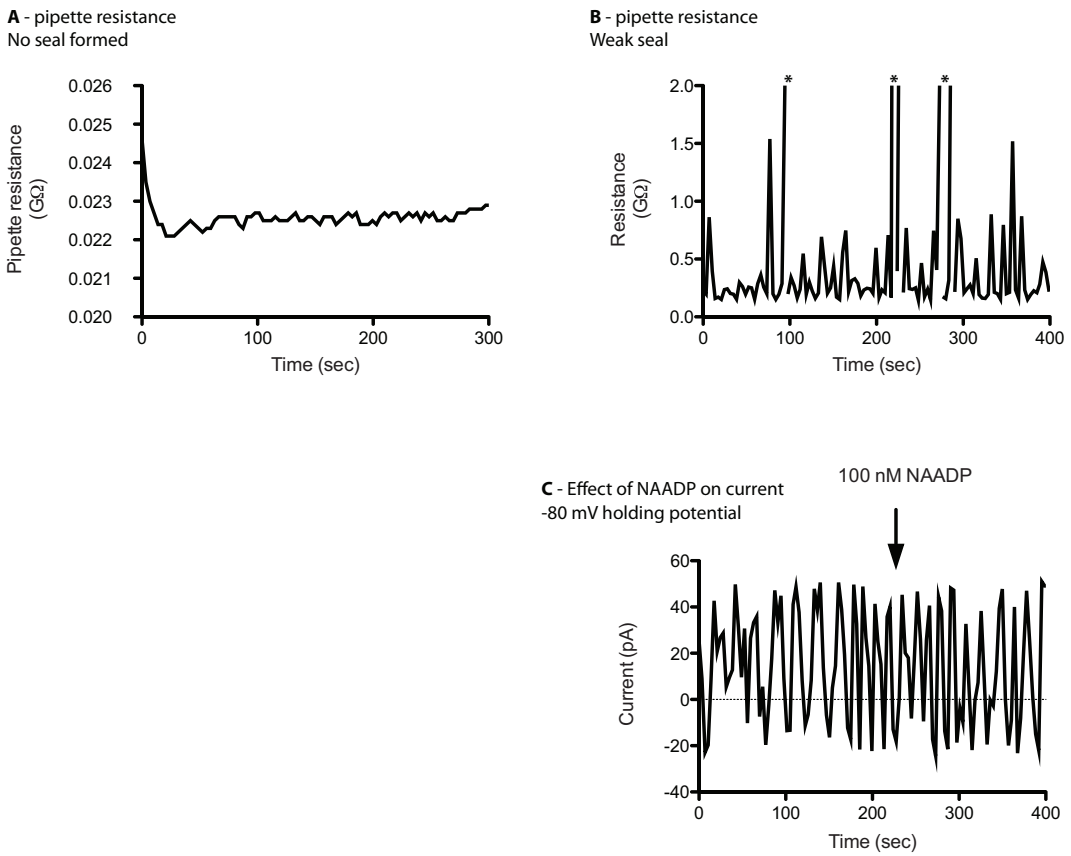


Figure 4.31: Example traces of attempted lysosomal patching with Flyion - non-swollen lysosomes. **A**: Trace depicting pipette resistance during the course of an experiment where no seal was formed, resistance remained < 100 MΩ . **B**. Trace depicting pipette resistance during the course of an experiment where a weak seal (≈ 500 MΩ) was formed ($*$ labels truncated data). **C**: Current measurements across the patched lysosome in B. 100 nM NAADP was added at 225 seconds. All lysosomes were from HsTPC2 overexpressing cells that had not been treated to swell lysosomes. Holding potentials were maintained at -80 mV throughout.

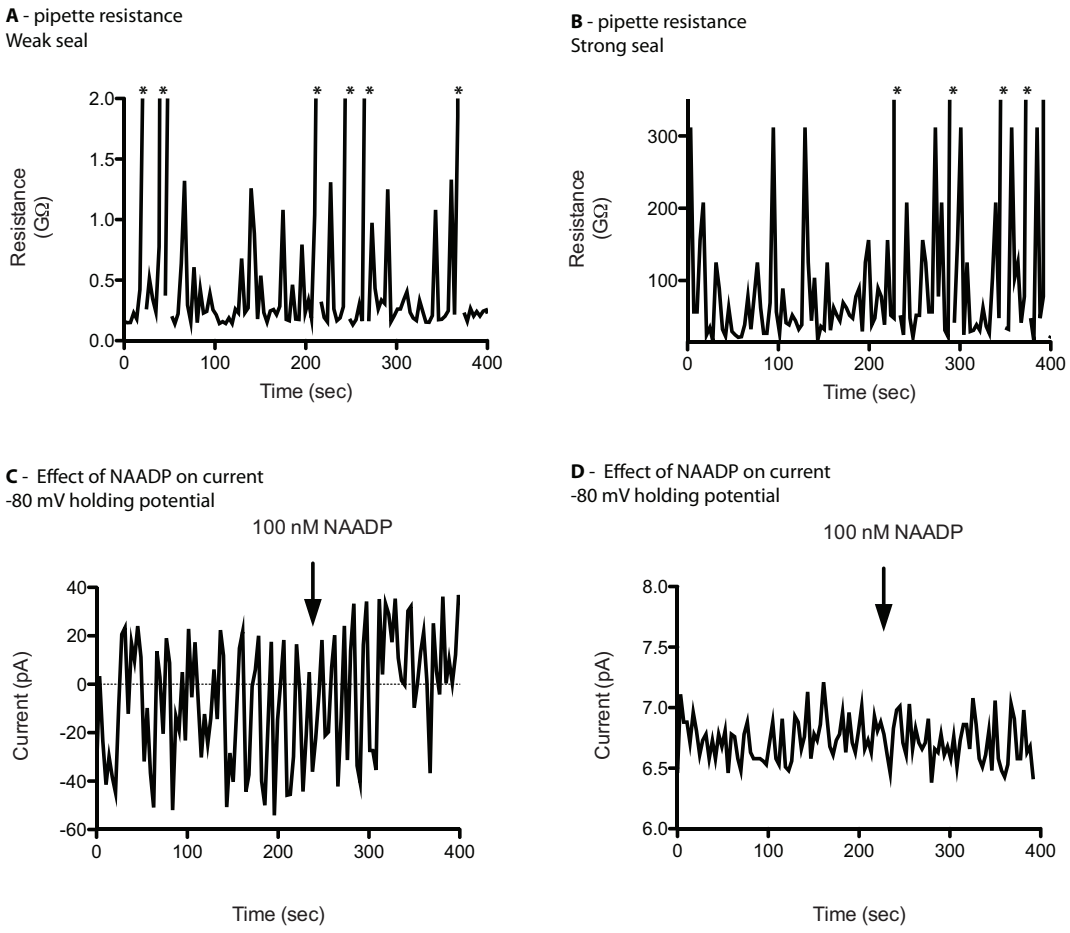


Figure 4.32: Example traces of attempted lysosomal patching with Flyion - sucrose-swollen lysosomes. **A**: Trace depicting pipette resistance during the course of an experiment where a weak seal ($\approx$ 200 MΩ) was formed. **B**. Trace depicting pipette resistance during the course of an experiment where a strong seal was formed, resistance reached $>$ 10 GΩ and was maintained ($*$ labels truncated data). **C & D**: Current measurements across the patched lysosomes in A and B respectively. 100 nM NAADP was added at 225 seconds. All lysosomes were swollen overnight by 0.05 M sucrose. Holding potentials were maintained at -80 mV throughout.

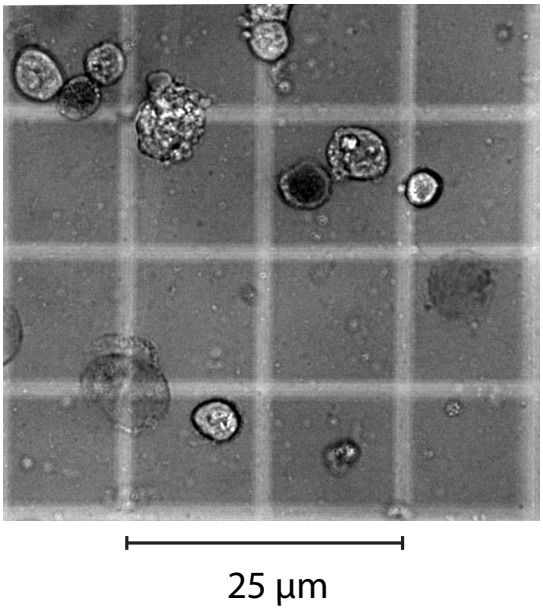


Figure 4.33: Light microscope image of Flyion-damaged lysosomes. Lysosomes recovered from Flyion tip viewed with a 40x air objective. 10 µl of resuspended lysosomes mixed with 10 µl 0.4 % trypan blue mounted on a haemocytometer.

4.10 Electrophysiological recordings by Port-a-patch

A less disruptive technology is the Port-a-patch (Nanion Technologies, Munich, Germany) (387), which works by patch clamping the lysosome on a thin layer of borosilicate glass with a laser cut pore (≈ 1 µm diameter) on an NPC-1 'Chip', the principals are shown in the schematic in figure 4.34. The Port-a-patch had many advantages over the Flyion technology. Firstly, it allowed much more user control over the sample, with lysosomes added directly to the glass surface, whereas in Flyion the lysosomes were pumped to the pipette tip through plastic tubing. Secondly, this also allowed more concentrated samples of lysosomes as very small volumes were required of both lysosomal preparation and buffers. Finally and most importantly, this technology had already been proven to patch lysosomes successfully (386).

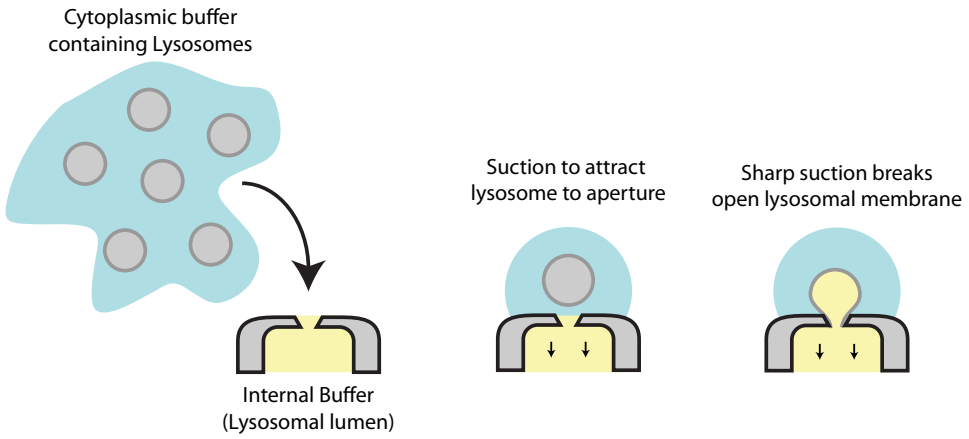


Figure 4.34: Schematic of Port-a-patch technology. Planar patch clamping. Lysosomes were added to the top of a thin layer of borosilicate with a laser-cut aperture. Negative pressure from below attracted single lysosomes to fuse with the borosilicate. Lysosome recordings were made once the lysosomal membrane was broken. Extra-lysosomal cytoplasmic buffer was maintained at ground; the relative potential of the internal buffer could be varied.

4.10.1 Seal formation on Port-a-patch

Fe-dextran purified, sucrose-swollen lysosomes (5 µl) were added to the Port-a-patch chip which had been primed with internal and external buffers (for buffer composition see table 4.2). The chip pore had an intrinsic resistance of 10 - 15 MΩ. Chips that were

damaged or had clogged pores were discarded. The system automatically subtracted liquid junction potentials and confirmed the chip pore resistance was within range. Negative pressure drew lysosomes to the pore and seals rapidly formed (< 30 seconds).

Lysosomes were never seen to enter 'lysosome-attached' mode, as the fragile lysosome membrane spontaneously broke open upon interacting with the pore. Therefore all recordings were made in the whole-lysosome configuration.

Seal formation was defined as when the resistance across the pore was greater than 600 MΩ, this was determined by 50 µs pulses at 50 mV. Successful seals were achieved with just 30.2 % of HsTPC2-overexpressing cells (39 successful seal from 129 attempts). However, the wild type lysosomes seemed to be more amenable to seal formation with 72.2 % of lysosomes samples added to the chip forming a stable seal. Despite this discrepancy, once the seals were formed there was very little difference in the quality of the seals, with lysosomes from cells overexpressing HsTPC2 averaging a seal of 2.84 ± 0.57 GΩ (n = 39) whilst wild type cells tended to give marginally stronger seals with a mean of 2.98 ± 0.57 GΩ (n = 12).

Seals were formed in the presence of high concentration of fluoride (60 mM) on the cytoplasmic face of the lysosome and high concentration of calcium (60 mM) on the intralysosomal face. Whilst the mechanism of this effect is unknown, this configuration has been shown to stabilise membranes in patch clamp studies and increase seal quality (225). Once the seals were formed they were remarkably stable with recordings lasting up to an hour with multiple buffer exchanges.

4.10.2 Recording conventions

Before proceeding with results, it is worth clarifying some nomenclature and electrophysiological convention, currents through the lysosomal membrane are treated as for conventional patch clamp. All currents are relative to the cytoplasm; where an inward current in conventional patch refers to one flowing from the extracellular space to the cytoplasm, and an inward current also refers to ions flowing from the lysosome into the cytoplasm (34). This is based on the assumption that the organelle lumen is functionally equivalent to the extracellular space and that organelle channel topology is homologous with channels in the PM. Figure 4.35 attempts to demonstrate that in order to comply by these conventions the axes on an average recording need to be inverted. This is equivalent to 'inside-out' patch clamp studies.

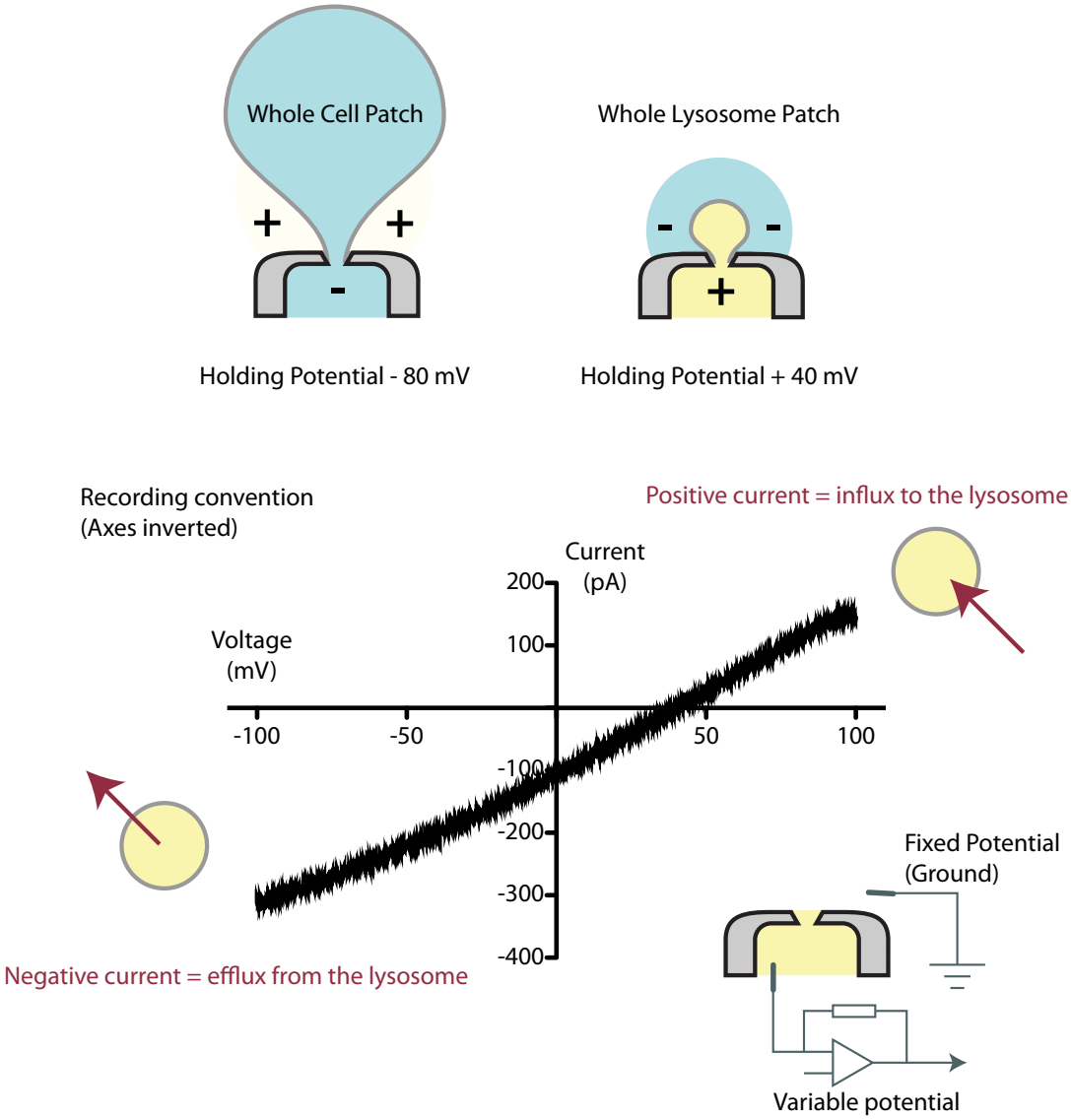


Figure 4.35: Predictions and assumptions in lysosomal potentials. Top: Comparison of configuration in whole cell patch clamping against whole lysosome patch clamping, with predicted resting potentials. **Bottom:** Example change in current during a voltage ramp after addition of 100 nM NAADP, subset with a diagrammatic representation of the planar patch clamp method. Both the variable potential and current are inverted to follow recording convention relative to the cytoplasm.

However, whilst the lysosomal lumen may be thought to be functionally equivalent to the extracellular milieu, they are chemically quite different. This is an important consideration before embarking on electrophysiological recording as it is necessary to determine a holding potential that would be physiologically relevant for the lysosomal membrane. The two previous lysosomal patch clamp studies have assumed the potential to be the same magnitude as the PM (80 mV) (112, 387). This assumption has no physiological basis, as although the potential difference is still disputed in the literature, none of the studies so far suggest a difference this large. Table 4.1 summarises a range of potentials predicted for the lysosomal membrane and related organelles.

Table 4.1: Resting potentials in acidic organelles. Compiled results of the observed membrane potentials of lysosomal-like organelles.

Organelle	Cell type	Resting value	Method	Ref.
Lysosome	Rat liver	+ 20 to 40 mV	diS-C_3-(5)	(319)
Lysosome	Rat kidney	+ 33 mV	S[^{14}C]CN^-	(174)
Lysosome ∗	RAW264.7	+ 19 mV	$DiBAC_4$ Rh-PE FRET	(223)
Phagosome	RAW264.7	+ 27 mV	$DiBAC_4$ DACCA FRET	(410)
Endosome	Rat liver	+ 6 - 42 mV	[^{14}C]methylamine and $^{36}Cl^-$	(436)
Recycling endosome	Rat liver	+ 1 - 69 mV	[^{14}C]methylamine and $^{36}Cl^-$	(436)

∗ Published 6th May 2011 - therefore not available when planning these experiments.

Preliminary experiments were conducted to empirically investigate the most stable holding potential for the lysosome. Membranes held at presumably unphysiological potentials show weaker seals which break more easily (299). Lysosomes were clamped during seal formation at -80, -40, 0, +40, +80 mV. Whilst only a few lysosomes were tested for each potential, only those with positive potentials formed stable seals and those at +40 mV formed the fastest and seemed most stable. This result also agrees most closely with the predicted potentials for the lysosome.

4.10.3 Ion composition of the luminal buffer

To allow direct comparison of results the intralysosomal buffers used in these experiments were based upon those used by Schieder *et al.* (386) with the notable exception that chloride is replaced by the acetate ion in all buffers, this is to eliminate the intrinsic chloride current seen in their studies. These buffers do fall within the range of

predicted concentrations for K^+ ions, however Ca^{2+} gradients were largely exaggerated with 60 mM in the intralysosomal buffer and 2 mM in the cytoplasmic buffer. Sodium was not included in any buffers.

The composition of solutions used during recordings are listed in table 4.2.

Table 4.2: Solutions used in planar patch clamp. Ion composition of Port-a-patch solutions. OAc refers to the acetate ion (CH_3COO^-). Solutions titrated with 1 M acetic acid or 1 M KOH. Sucrose was used to adjust osmolarity.

Cytoplasmic solution		**Intralysosomal Solution**	
60 mM	KOAc	70 mM	KOAc
60 mM	KF	60 mM	$Ca(OAc)_2$
2 mM	$Ca(OAc)_2$*	2 mM	$Mg(OAc)_2$
10 mM	HEPES	60 mM	AcOH (acetic acid)
	pH 7.2		pH 4.6

* $Ca(OAc)_2$ was added immediately before use to prevent precipitation of CaF_2.

4.11 NAADP-induced current in HsTPC2 overexpressing lysosomes

Once a successful seal was formed, the patched HsTPC2-expressing lysosomes were clamped at a holding potential of +40 mV. To determine voltage-sensitivity a voltage ramp (+100 mV to -100 mV) was passed over the membrane. A non-voltage dependent, non-rectifying current was seen which gave a reversal potential of 39.8 ± 6.0 mV. A voltage ramp applied in the opposite direction from -100 mV to +100 mV resulted in an identical current-voltage relationship.

In this system chloride salts were replaced with acetate salts in all buffers and the reversal potential of this current suggests that it is Ca^{2+} selective as it closely matches the calculated reversal potential for Ca^{2+} in these solutions is 43.2 mV.

Thus this current could be due to basal channel activity of HsTPC2 which has been shown to have a low basal open probability (figure 3.17, page 116) or indeed any other lysosomal Ca^{2+} channel. If a quotient of this channel is due to Cl^- ions, it could perhaps be due to Cl^- leeching from the AgCl pellet electrodes. Otherwise this could be a leak

in the membrane through a non-specific pore. Whatever the origins of this current, it was reproducible and could be considered the baseline from which current fluctuations could be measured.

To investigate the effect of NAADP on channel activity 100 nM NAADP was added to the cytoplasmic solution. This resulted in an immediate increase in current. The I/V plot shown as the top trace in figure 4.36 depicts both the basal current and the effect of addition of NAADP. To dissect out the NAADP-induced current, the trace obtained in the absence of NAADP was subtracted from the trace in the presence of NAADP; the result of this can be seen in the lower trace in figure 4.36. The NAADP-specific current shows no rectification and has a reverse potential of 42.9 ± 5.1 mV (n = 6), which again correlates with the calculated reverse potential for Ca^{2+} (43.2 mV) suggesting that the increased current is carried by Ca^{2+} alone.

One slight concern is the fact that the E_{rev} is not altered upon addition of NAADP. This implies that the basal conductance is carried entirely by Ca^{2+} perhaps via sporadic openings of HsTPC2, which seems unlikely considering the large K^+ concentrations in these solutions and the number of other channels present in the lysosomal membrane. A way to investigate whether this phenomenon is simply an artefact of the recording technique would be to include a K^+ ionophore, such as valinomycin, which will to shift the E_{rev} to more negative values, and act independently of NAADP-induced currents.

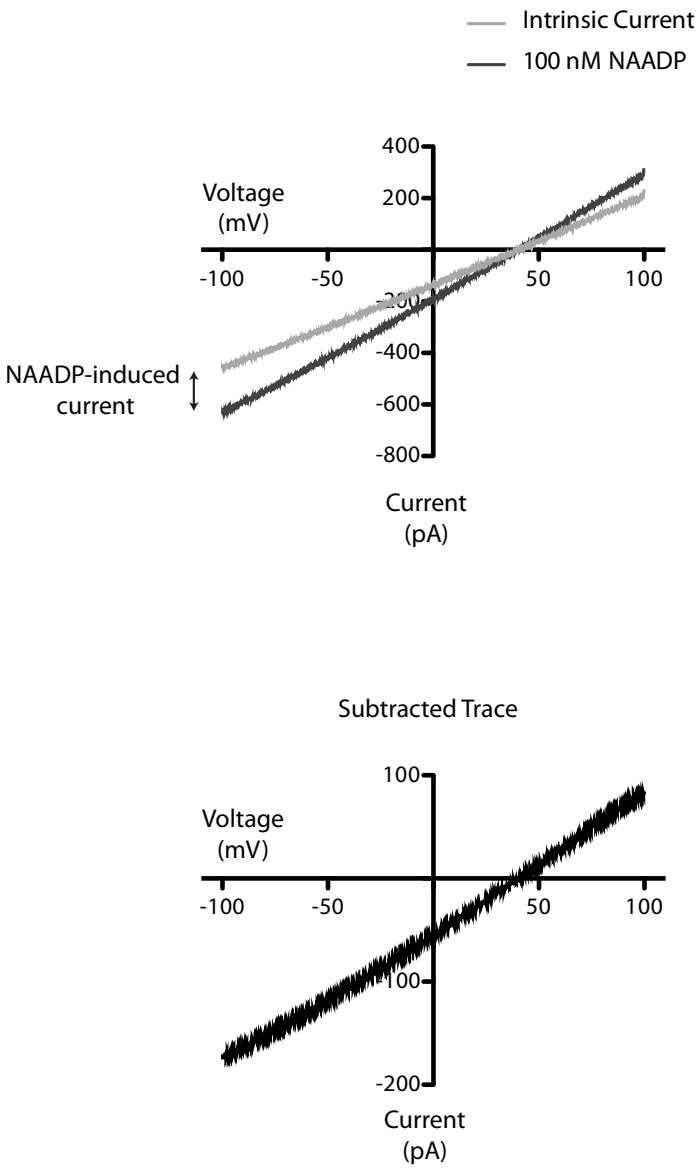


Figure 4.36: Example traces of lysosomal current recordings. Top: The intrinsic current-voltage (I/V) relationship of the HsTPC2 expressing lysosome (Grey trace). Addition of 100 nM NAADP caused an increased conductance (Black trace). The membrane potential was held at +40 mV and 500 ms ramps from +100 mV to -100 mV were applied every 5 s. The average reverse potential for this instrinsic current was 39.8 ±6.0 mV (n = 8). **Bottom:** Current-voltage relationship in the presence of 100 nM NAADP with the endogenous current subtracted. All currents were recorded in standard solutions (table 4.2, page 203).

4.12 Effects of IP_3 and cADPR on channel activity

Having ensured that the Fe-dextran lysosome preparation had minimal ER contamination, currents via the known Ca^{2+} channels of ER-derived IP_3R or RyR were very unlikely. This was confirmed by the addition of 100 µM cADPR and 100 µM IP_3 to patched lysosomes. The mean current amplitudes at -100 mV from individual traces are shown in figure 4.37. This shows that whilst NAADP invokes a large current, neither cADPR or IP_3 stimulate significant channel activity in these preparations.

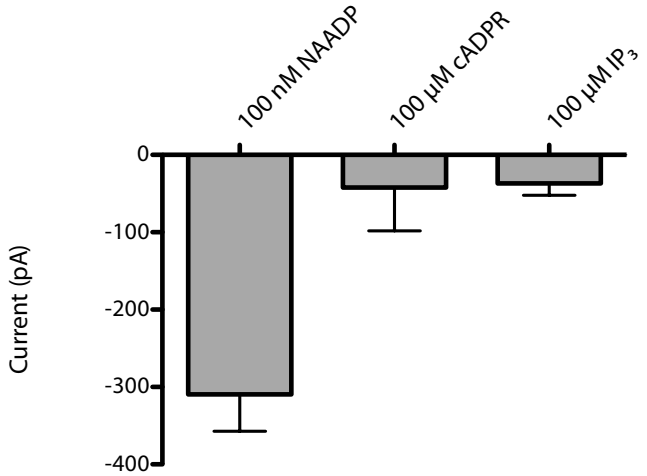


Figure 4.37: cADPR and IP_3 give negligible responses. Population data for current amplitudes at -100 mV obtained from individual subtracted traces (NAADP: n = 7, cADPR: n = 6, IP_3: n = 4). Negative currents are those that flow from the lysosomes into the cytosol. All experiments were conducted on HsTPC2 overexpressing lysosomes.

4.13 NAADP concentration response relationship

In mammals, one of the characteristic properties of the NAADP signal is the bell shaped concentration-response relationship whereby high concentrations begin to inhibit channel opening (25, 282). Purified HsTPC2 has been shown to reproduce this bell-shaped relationship in bilayers (with luminal pH 4.8) as shown in chapter 3, figure 3.25. To determine whether this characteristic is still seen with *in situ* HsTPC2 in the lysosomal membrane, whole-lysosome patches were treated with incremental concentrations of NAADP separated with a 2 minute wash.

Figure 4.38 shows the mean currents induced by each concentration of NAADP, both as full current-voltage relationship traces and the maximal current amplitude. HsTPC2-expressing lysosomes show large currents with 100 nM giving the largest response. There was significant variation between lysosomes, but it is clear that the concentration-response relationship follows the bell-shaped predictions with a stimulatory EC_{50} = 11 nM. This is comparable to the results seen in the lipid bilayer where the EC_{50} was 5.5 nM.

Wild type lysosomes still express endogenous levels of HsTPC2, however when lysosomes from wild type cells were patched and treated to the same incremental concentration gradient they did not show a measurable response relationship.

4.14 1 mM NAADP channel block

Another characteristic property of NAADP-induced Ca^{2+} release is the desensitisation of the channel by a high concentration of NAADP. This was investigated in patched lysosomes overexpressing HsTPC2 by first establishing a robust response with 100 nM NAADP, followed by a non-responsive and desensitizing concentration of 1 mM NAADP. Subsequent addition of 100 nM NAADP no longer evoked increased channel activity. Figure 4.39 shows an example trace combined with population data of current amplitudes at -100 mV.

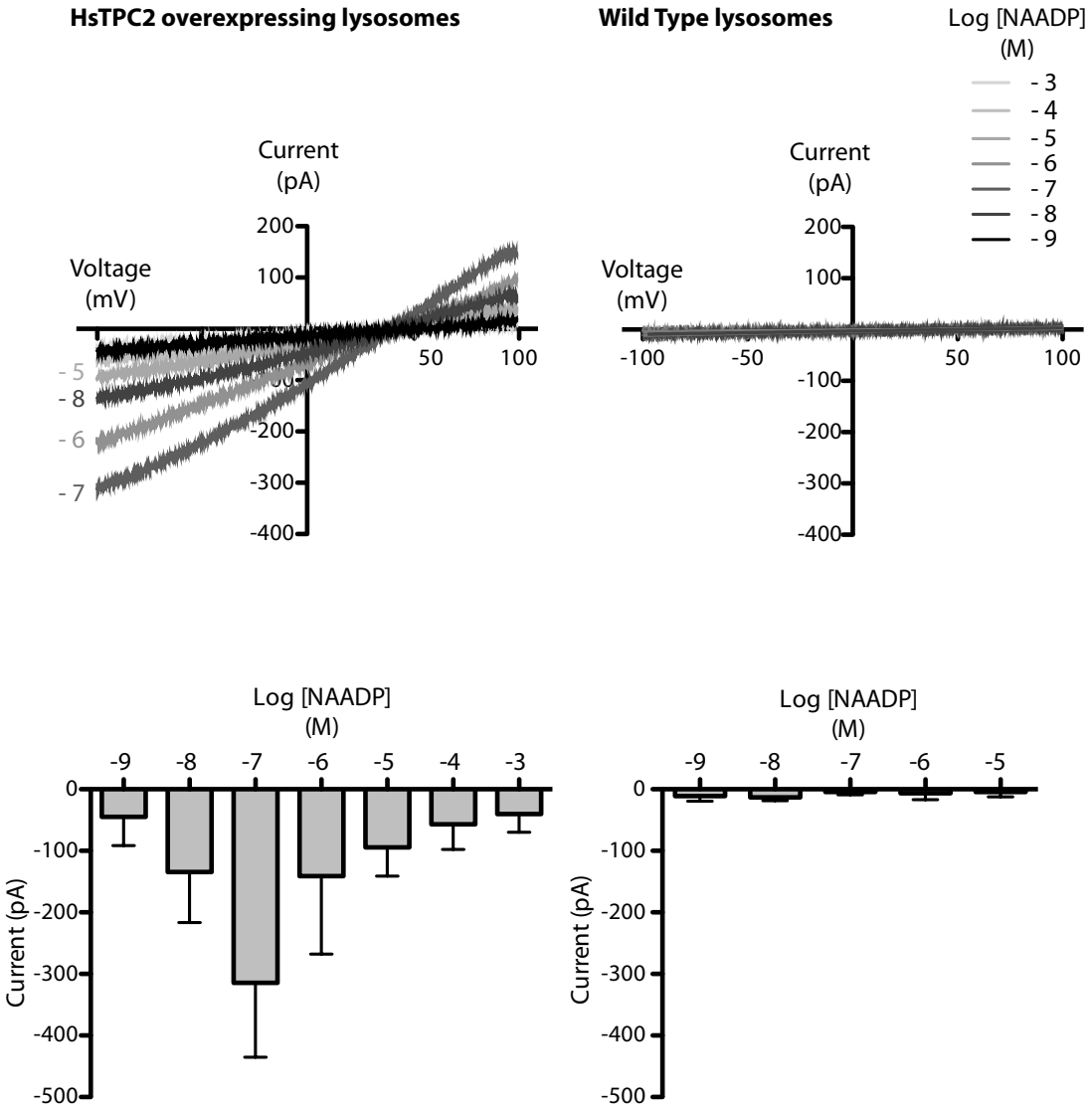


Figure 4.38: NAADP gives a bell-shaped concentration-response relationship in HsTPC2 overexpressing lysosomes. Top: Mean current-voltage relationship traces for NAADP over a range of concentrations, (n = 4) **Bottom:** Population data showing the concentration-response relationship of maximal NAADP-induced current measured at -100 mV. Left hand traces were conducted on HsTPC2 overexpressing lysosomes, right hand traces were conducted on wild type lysosomes.

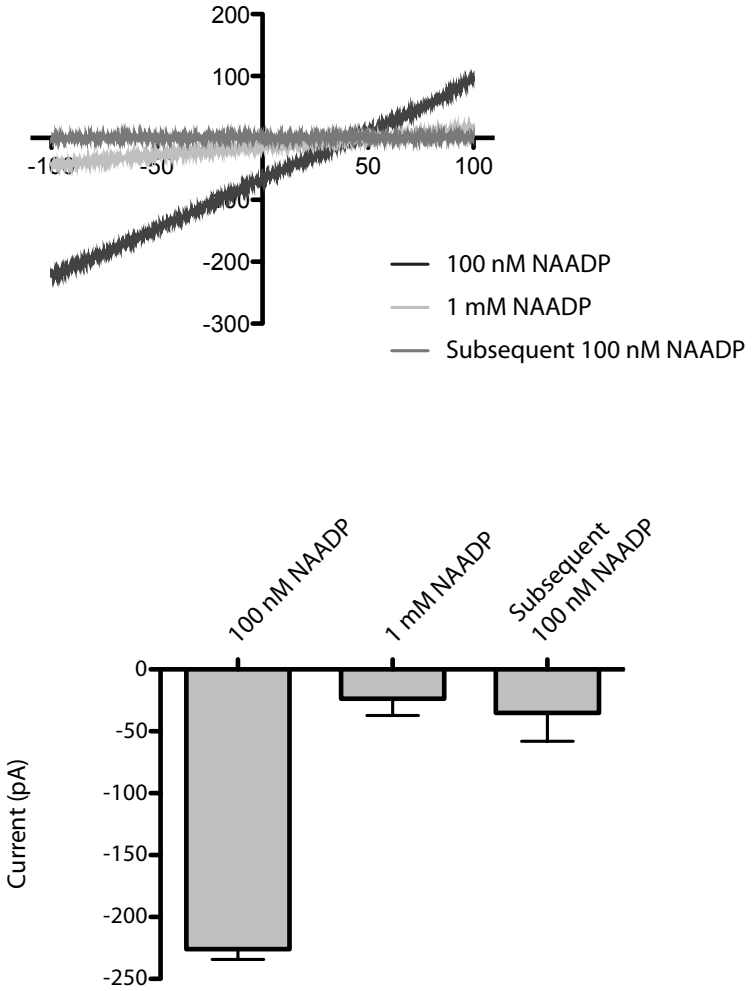


Figure 4.39: Pretreatment with 1 mM NAADP inhibits further NAADP-induced currents. Top: The current-voltage relationship trace induced by 100 nM NAADP (Black). After washing 1 mM NAADP was added (Light grey). A subsequent concentration of 100 mM NAADP was added after another wash but no current was seen (Mid-grey). **Bottom:** Population data of mean current amplitude at -100 mV (n = 4).

4.15 100 µM Ned-19 channel block

A final confirmation that these currents are indeed consistent with known NAADP pharmacology was conducted by using the selective antagonist Ned-19. In a similar experiment to the high NAADP desensitisation, a control concentration of 100 nM NAADP was added to validate that the lysosome would respond to NAADP, this was followed by addition on 100 µM Ned-19. Any further addition of NAADP was antagonised by the Ned-19 and no responses were seen. Figure 4.40 shows an example trace combined with population data of current amplitudes at -100 mV.

Controls conducted with DMSO (the solvent used to deliver Ned-19) did not show any significant block of the subsequent 100 nM NAADP signal (n = 3).

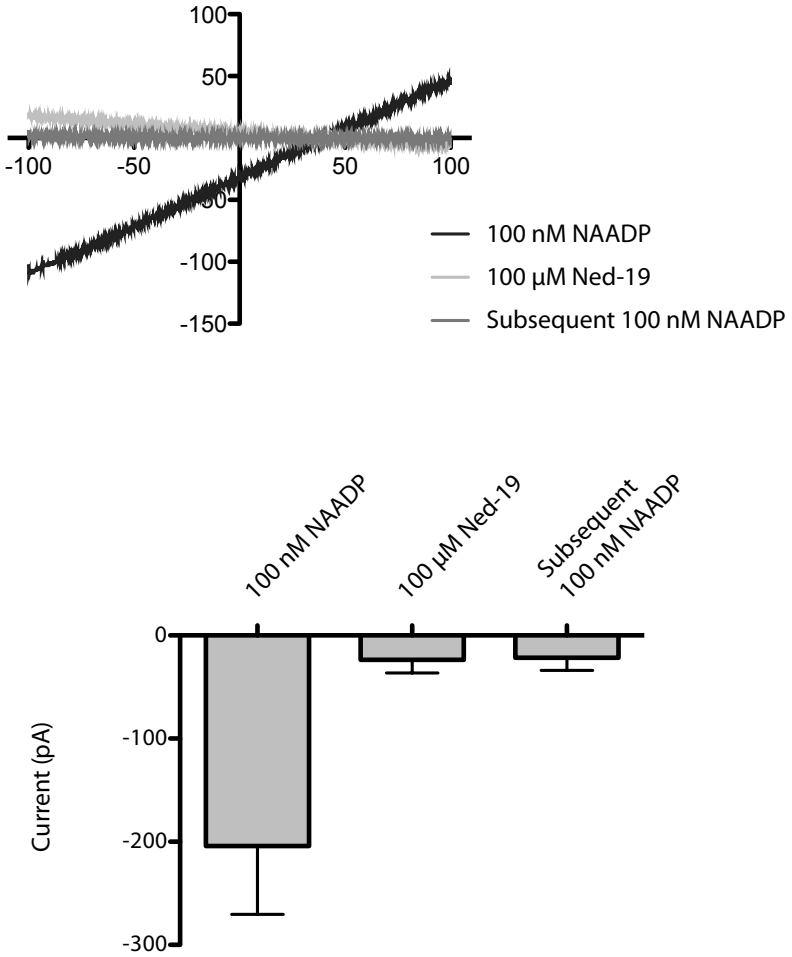


Figure 4.40: Addition of Ned-19 abolishes NAADP induced currents. Top: The current-voltage relationship trace induced by 100 nM NAADP (Black). After washing 100 μM Ned-19 was added (Light grey). A subsequent concentration of 100 nM NAADP was added after another wash but no current was seen (Mid-grey). **Bottom:** Population data of mean current amplitude at -100 mV (n = 4).

4.16 Discussion

The aim of this chapter was to investigate the channel activity of HsTPC2 *in situ* in the lysosomal membrane via organelle patch clamp and this is the first study to show NAADP-evoked currents in very pure lysosomes overexpressing HsTPC2. Whilst a methodology had already been published for lysosomes overexpressing MmTPC2 (386), this chapter investigated the optimisation of lysosomal purification and allowed a direct comparison of TPC2 electrophysiology between species. It also allows comparison of the two techniques used to measure HsTPC2 currents: lipid bilayer and lysosomal patch clamp.

4.16.1 The optimal lysosomal purification

Repeating the published techniques of lysosomal purification by differential centrifugation (Schieder *et al.* (386)) revealed that the final samples were heavily contaminated with ER, mitochondria, PM and Golgi. This either means their experiments were not conducted with the appropriate controls for organelle markers or that contaminations were introduced because of differences in laboratory equipment and experimental procedures.

Experiments in section 4.7 showed that Balch homogenisation of whole cells gave the optimal yield whilst still giving uncontaminated samples. Once the purification had been optimised using sucrose as a swelling agent and magnetic chromatography to separate lysosomes, further troubleshooting was not required. However, it would have been interesting to return to the differential centrifugation procedure with lysate prepared from the Balch homogeniser to see whether contamination still persisted.

A further reason for returning to a purification based upon centrifugation arises over concerns that the Fe-dextran may interfere with conductances seen. The lysosomal protein TRPML1 has been shown to be an iron (Fe^{2+}) release channel (112) so any leeching of free Fe^{2+} from the luminal Fe-dextran complex would add to currents seen through the lysosomal membrane. However, this was not a concern in experiments shown here for multiple reasons. Firstly, as soon as the whole lysosome patch was formed, the luminal contents of the lysosome became negligible due to exchange with the internal buffer which has a much greater volume. Secondly, recordings were made by subtracting the current seen before addition of NAADP from the current after addition;

therefore, assuming the Fe^{2+}-conductance of TRPML1 is not affected by NAADP, contributions to lysosomal currents by TRPML1 would have been removed. Thirdly, the magnetic particles used in the Fe-dextran preparation were mainly composed of iron-oxides (365) which are insoluble in water and even the weak acid conditions of the lysosome (pH $\approx$ 5), thus the concentrations of Fe^{2+} in solution would have been very small. A subtle addition to this point is that although Fe(III)oxide is more soluble than Fe(II)oxide, contamination by Fe^{3+} would not have affected the currents as TRPML1 was shown to be highly selective for Fe^{2+} ions and impermeable to Fe^{3+} (112). Finally, the group which published this result have acknowledged that TRPML1 is more likely to be a Ca^{2+}-permeable channel under physiological conditions, with Fe^{2+}-conductance being an ancillary feature (113).

Nonetheless, the presence of Fe-dextran in the lysosomal lumen may be altering the physiology of the lysosome and if differential centrifugation could produce a preparation of lysosomes free of contamination from other organelles then this technique ought to be favoured.

The other technique used to extract lysosomes was by immunoprecipitation, which should have resulted in a highly specific purification. However, this not only gave a poor yield but the lysosomes were damaged by the procedure. Further optimisation of buffering conditions and wash steps may be able to increase the yield seen but would not be worthwhile as this technique is expensive due to the large volume of antibodies required. Moreover, if purification was via immunoprecipitation of the HA-tag, then wild-type lysosomes could not be purified as a control.

4.16.2 Patch clamp on subcellular organelles

Because intracellular membranes *in situ* are not accessible to patch pipettes most channels localised to subcellular organelles have been studied by purification and incorporation into a lipid bilayer or the mistargetting of channels to the PM. However, as was discussed in the previous chapter both these techniques can result in unphysiological recordings due to the entirely different ionic and membrane composition, hence techniques have been established to employ patch clamp on native membranes.

As very little work has been published on the patch clamp of lysosomes, it is worth introducing the electrophysiological recordings made on analogous organelles such as the plant and yeast vacuole, and the ER.

Patch clamp of plant vacuoles

The forerunners in organelle patch clamp studies were the large vacuoles seen in plants and later in yeast. These organelles are analogous to the lysosome as they are both known to be acidic Ca^{2+} stores (332).

The isolation of the plant vacuole was relatively simple and could easily be performed by slicing tissue in an iso-osmotic buffer and washing the surface to liberate vacuoles into the recording chamber where they could be directly patched (95, 177). Using this technique the initial discoveries regarding vacuole physiology were determined; these included the identification of a K^+-permeable channel (175), the vacuolar proton pump (175), and the slow vacuolar current (177). More sophisticated isolation techniques involving the gentle lysis of plant protoplasts gave more stable vacuolar recordings (264, 265) by which it was later shown that the SV current was associated with plant TPC1 (336). This was demonstrated by direct patch clamp studies on vacuoles isolated from wild type, tpc1 knock-out mutants and cells overexpressing TPC1 protein. Many of the properties of the plant TPC1 channel were compared with HsTPC2 in the discussion in chapter 3; these characteristics were determined by direct patch recordings of the lysosome with the plant TPC1 *in situ*.

Patch clamp recordings on isolated vacuoles have also shown that both IP_3 and cADPR release Ca^{2+} from the plant vacuole (6, 241). However, the site of action for these messengers is unknown as the plant genome contains neither gene for the RyR or IP_3R. Further studies would be required to determine which channels are mediating this Ca^{2+} release.

Patch clamp of yeast vacuoles

Yeast vacuoles have also been widely investigated by patch clamp as these can be easily isolated and are inherently large enough to patch ($\approx$ 5 µm diameter), although many studies use enlarged vacuoles (308, 421, 453). Initial patch clamp studies on yeast vacuoles investigated proton currents through the V-type ATPase in response to ATP (33) but since then a host of channels has been identified on the vacuolar membrane (421), the most relevant of which is the yeast vacuolar channel 1 (YVC1) which is homologous to the mammalian TRP family and thus related to TPCs (325). YVC1 was

shown to be voltage-dependent, cation-selective and Ca^{2+}-activated by a series of gene-deletion and re-expression studies with direct patch clamp of the vacuolar membrane (325).

A major project within this DPhil was the stable expression of HsTPC1 and HsTPC2 in *Saccharomyces cerevisiae* (data not shown) as this species provides a null background because TPCs are absent from the yeast genome. The expression of the TPCs was inducible under the control of the Lac-operon, but even low levels of HsTPC2 expression dramatically impaired yeast viability with negligible growth upon induction; which may suggest that HsTPC2 expression had a detrimental effect on Ca^{2+} homeostasis and prevent cell growth. HsTPC1 expression was more successful with preliminary localisation studies showing a sub-cellular localisation. Isolated vacuoles were prepared by osmotic extrusion of protoplasts, but successful seals were never obtained on either Flyion or Port-a-patch. Bertl *et al.* discuss some of the difficulties in yeast vacuole seal formation in their seminal paper (33). However, the most likely reason for this lack of success from the HsTPC1 overexpressing yeast was the small size of vacuoles seen (1 - 2 µm diameter).

Patch clamp of the ER

The first mammalian organelle to be investigated was the ER. However, due to its fragile reticular structure, the ER cannot be purified and instead recordings were made by patch clamping isolated nuclei. The theory behind this was based on the fact that the ER is continuous with the nuclear envelope outer membrane (111), therefore a subset of the ER-localised channels such as RyR and IP_3R were expected to be present in the nuclear envelope. Single IP_3R channels were recorded in this native membrane by patch clamping isolated nuclei from a variety of cells: *Xenopus* oocytes (212), Sf9 insect cells (197) and various cell lines (CHO, COS-7, DT40 and HeLa (129)). Despite the high density of nuclear pores in the outer membrane of the nuclear envelope (156), the prerequisite GΩ seals were formed with relative ease, suggesting that these pores were closed or impermeable during patch clamp studies.

Of major relevance to the HsTPC2 studies shown in this thesis, the IP_3R has been studied in both artificial lipid bilayers and native membranes by patch clamp. However, the biophysical properties of IP_3R vary significantly and numerous studies have shown that IP_3R channels behave more robustly in native membranes with a higher P_o and

more consistent results (44, 44, 45, 270, 271, 272, 273, 460) compared to the bilayer. They also showed different pharmacological responses to ligands and gating kinetics which seem more physiologically relevant compared to those observed in reconstitution studies (129).

Patch clamp of lysosomes

The direct patch clamp of lysosomes has recently been achieved by two different methods. The first to be published involved the swelling of lysosomes by vacuolin, the rupture of the cell membrane and the direct patching of the liberated lysosomes, these were identified by the expression of EGFP-tagged LAMP1 (112). This study was investigating the properties of TRPML1 and concluded it was an Fe^{2+}-release channel present in the lysosomal membrane. A further study by this group using the same techniques showed that the endolysosomal phosphoinositide PI(3,5)P(2) evoked Ca^{2+} release via TRPML1 which played a role in the endolysosomal trafficking (113).

The other methodology has already been mentioned and will be discussed throughout the next few sections. This involved the direct planar patch clamp of vacuolin-swollen lysosomes overexpressing MmTPC2. Experiments were conducted using the Port-a-patch system as used here. In fact, the electrophysiological protocols in this chapter emulated the published results of this group (386, 387) and the results obtained for HsTPC2 can be directly compared to those seen with MmTPC2.

4.16.3 The physiological significance of lysosomal swelling

A major technical problem in organelle patch clamp is the small size (< 5 µm diameter) of the target membrane. Plant vacuoles and nuclei tend to be large enough to patch without unphysiological manipulation but with yeast vacuoles and lysosomes swelling is often required. The previous studies, above which have successfully patched whole lysosomes, used the small chemical vacuolin to produce abnormally large lysosomes which can be more easily manipulated (112, 386). As was discussed earlier this was thought to be due to homotypic fusion of lysosomes and endosomes (66, 192) which occurred on a short timescale of ≈ 2 hours.

However, reports have shown that vacuolin does not only affect the morphology of the lysosome but also affected the trafficking within the endolysosomal pathway and prevented Ca^{2+}-dependent lysosomal exocytosis (66). Experiments in mast cells

also showed that vacuolin may not be as specific to endolysosomes as first thought. Lysosomes were prelabelled with fluorescently-tagged dextran or a LysoTracker dye and the cells were treated with vacuolin. Large 'vacuoles' were produced but both the dextran and the LysoTracker remained localised to the smaller endolysosomal vesicles (391). A similar result was seen with vacuolin in the figures shown earlier (4.18 & 4.19), whereby LysoTracker and Texas-Red dextran remained in smaller non-swollen vesicles.

The mechanism of vacuolin action is still unknown, with attempts at the pharmacological inhibition of the effect proving largely unsuccessful. Antagonists of kinases associated with the endolysosomal system (PKC, PI3K, Src and Syk) together with blockers of K^+ and Cl^- channels had no effect (391). The only exception was Bafilomycin A1, the inhibitor of V-type ATPase, suggesting a role of the proton gradient in vacuolin-induced enlargement (391). In this regard vacuolin resembles the VacA toxin produced by the gastric ulcer bacteria *Helicobacter pylori*, which mediates the influx of anions into endosomes to cause osmotic swelling, but this effect can be blocked by Bafilomycin A1 (94, 327). This would lead to the conclusion by analogy that vacuolin could enhance the influx of anions into the lysosomes to cause them to osmotically swell. If this is the case, vacuolin-treated lysosomes may have an affected anion permeability which may alter the conductance properties in patch clamp studies.

An alternative to inducing lysosomal swelling chemically would have been to use a cell line which shows abnormally large lysosomes. An example of this was shown by using swollen early endosomes to determine TRPV2 currents by patch clamp, these endosomes were inherently enlarged in hydrolysis-deficient SKD1/VPS4B mutant in HEK293 cells (378). To investigate lysosomes, there is a cell line associated with Chediak-Higashi Syndrome (CHS), which is an autosomal recessive disease affecting late endosomes and lysosomes. In CHS fibroblasts, acidic organelles are (> 4 µm) and clustered in the perinuclear area (54). Although the mutation clearly causes mislocalization of these organelles, it appears to have very little effect on their endocytic and degradative functions (54) and is thought to cause enlargement by excessive fusion. Purification of lysosomes from this cell line would allow patch clamping on a physiologically unaltered system, however as this thesis was looking at the effects of HsTPC2, the stable cell line of HEK293 cells overexpressing HsTPC2 was used, and swelling was achieved by prolonged exposure to 0.05 M sucrose.

Sucrose endocytosis provided a slower and less physiologically disruptive technique of lysosomal swelling than vacuolin. This technique has been shown to cause a prolonged osmotic gradient and thus a swelling of the lysosomes over a timescale which would allow synthesis of additional lysosomal lipids and proteins. Sucrose-induced swelling has also been shown to be highly specific for mature lysosomes (103), whereas vacuolin cannot discriminate between endosomes and lysosomes (192). All studies on sucrose-swollen lysosomes seemed to show normal lysosomal function (103, 124, 429).

Therefore all patch clamp experiments in this chapter were conducted on sucrose swollen lysosomes.

4.16.4 Patch clamp devices and seal formation

To obtain reliable electrophysiological recordings a strong seal ($> G\Omega$) is required. The Flyion automated patch device rarely obtained, and never maintained, seals of a good enough quality. Where a few brief periods of high resistance ($\approx$ 1 - 2 GΩ) were seen, these probably reflect sequential seals as lysosomes reached the tip of the pipette but due to their small size simply fell through the end. The other scenario seen whereby seals of $>$ 100 GΩ were formed, which is far higher than a single vesicle could create, must be due to aggregated lysosomes blocking the pipette tip.

Flyion was designed as a high-throughput system to automatically patch whole cells quickly and reliably. In theory, the same principles should allow patching of organelles with an appropriately scaled pipette tip. However, this assumes that organelles such as the lysosome behave as though they were miniature whole cells and ignores differences in membrane fragility and inter-organelle interactions. Hence the rough mechanics of the Flyion procedure damaged the lysosomes and prevented successful seal formation.

The Nanion Port-a-patch device dispenses with the traditional microelectrode and replaces it with a glass chip to which cells/organelles are directly added. This simplicity involves minimal manipulation and by varying the size of the aperture in the glass chip, allows patching of small organelles such as lysosomes. Schieder *et al.* were the first to successfully obtain GΩ seals using this technology to patch vacuolin-swollen lysosomes. In data shown here, wild type lysosomes were nearly twice as likely to form a successful seal compared to lysosomes overexpressing HsTPC2 (success rates of 72.2 % to 30.2 % respectively). Interestingly, Schieder *et al.* also noticed a reduced seal yield in their cell line overexpressing MmTPC2.GFP (386); they commonly obtained up to

8 successful recordings from a wild type lysosome preparation whilst only 4/5 from the overexpressing lysosomes. This seems to suggest that the overexpression of the TPC2 protein inhibits the lysosomal membrane ability to interact with the glass chip, perhaps by altering membrane fluidity or fragility. The high levels of channel expression may also result in a large leak current which would also hinder strong seal formation.

Once seals were formed however, there was no difference in their quality as the majority of both wild type and HsTPC2 overexpressing lysosomes were within the GΩ range. The seals shown here seemed much more robust that those of Schieder *et al.*, with recordings lasting up to an hour with multiple buffer exchanges, whereas Schieder reports that they could only maintain seals for approximately 20 minutes (386) before they broke. This difference may be due to the higher purity of the lysosome purified by Fe-dextran chromatography over centrifugation, or the more physiologically relevant holding potential used (see below).

4.16.5 Lysosomal resting potential

Choosing the holding potential for these studies was not a trivial decision. The previous studies on patched lysosomes assumed the lysosomal membrane to be functionally equivalent to the PM and fixed the potentials at +80 mV (112, 387). They at least acknowledged the fact that the lysosomal lumen was more likely to resemble the extracellular milieu rather than the cytoplasm and conducted their experiments using an 'inside out' configuration.

The lysosomal membrane potential is comprised of two components: one is governed by the membrane impermeant contents of the lumen which gives a fixed potential; whilst the other component varies with ionic gradients (376). The fixed charge is known as the Donnan potential and is due to large anionic macromolecules within the lumen which cannot diffuse across the membrane; this results in an inside-negative potential ranging from -20 to -70 mV (96, 436). The negative charge provides a driving force for H^+ entry into acidic organelles (179, 240) as well as Cl^- clearance from the lumen (403, 404).

In the plant vacuole the resting potential is predicted to be inside negative ($\approx$ -30 mV) which may be due to a high permeability to Cl^- ions (352).

Moreover, in some studies, an inside-negative potential for lysosomes has been shown (164, 319), however these were conducted under non-physiological conditions

(in the absence of counterions and ATP) and the authors demonstrate that under more physiological conditions the potentials are more positive. In fact, looking at the table of predicted lysosomal potentials (table 4.1) they all show an inside-positive potential. This is because the Donnan potential is titrated as the lumen becomes more acidic (404) and the concentration of cations (Na^+, K^+ and Ca^{2+}) driven by the diffusion potential neutralise the negative charge and overcome it (384). This variable ion exchange is the second element in determining the lysosomal potential and is dependent on channel/transporter expression in the membrane.

Whilst table 4.1 suggests that definitive values of the lysosomal membrane potential have been determined, the variation among the results makes it difficult to pinpoint a value with certainty. The median centred around +40 mV which was assumed to be the physiologically relevant membrane potential.

This theoretical value was also confirmed in preliminary experiments on the Port-a-patch, whereby seals formed more quickly and remained more robust at positive potentials, especially +40 mV. Therefore, +40 mV was used as the holding potential throughout all the recordings shown. As mentioned above, this more physiological potential may explain why seals formed here were longer-lasting than those of Schieder *et al.* who held their lysosomes at +80 mV.

In a recent publication (May 2011) the lysosomal membrane potential was determined by FRET to be +19 mV (223). As FRET is a non-intrusive technique this value ought to be the closest prediction to the physiological membrane potential. Therefore even +40 mV was probably too high and future studies would need to consider this new result and conduct patch clamp at a lower holding potential.

4.16.6 Ionic composition of the lysosomal lumen

Another major concern regarded the native composition of ions within the lysosomal lumen. It was eventually decided that the preliminary experiments would simply use the solutions reported by Schieder *et al.*, as these had been previously shown to give successful NAADP-induced currents and would allow direct comparison of results. However, the physiological relevance of these solutions is debatable.

Whilst there have been many attempts to quantify the major constituent ions within the lysosomal lumen, there is yet to be a consensus on exact concentrations. Table 4.3 compiles the major studies conducted on lysosome-like organelles and the predicted

resting values of each constituent ion. The methodologies used to measure the lysosomal ion concentrations vary in their reliability and are comprehensively reviewed in a recent paper (Morgan *et al.* 2011 - in press).

Of course the solution used in this whole-lysosome patch clamp study was inherently unphysiological as two of the major ions (Na^+ and Cl^-) were deliberately omitted. The exclusion of Na^+ ions was made to simplify calculations of reversal potentials and to allow dissections of the K^+/Ca^+ permeability of the channel. Considering that the predicted Na^+ concentrations are lower than K^+ and that Ca^{2+} channels rarely discriminate between these two ions (65), the absence of Na^+ is compensated by an increase in K^+ from the predicted value of around 50 mM to 70 mM incorporating the $\approx$ 20 mM of Na^+ removed.

The absence of Cl^- may have more significant implications as Cl^- channels have been observed in the lysosomal membrane (113, 386, 387). This ion was therefore removed to try to eliminate competing channel conductances. Whilst this did not seem to affect recordings, concerns ought to be raised regarding the replacement anion. The acetate anion, $[CH_3COO]^-$, was used as the counter ion for all the cations present. In addition acetic acid was used to acidify the solution thus taking acetate concentrations to 192 mM within the lumen. The osmolarity of the solutions was adjusted with sucrose so that this high concentration did not affect the electrochemical gradient however, acetate is only a weak acid and whilst the anionic form is impermeable through most channels, the neutral protonated form can diffuse slowly across the membrane which would not only alter osmotic gradients but would also alkalinise the lumen by removing protons (198).

Finally, and most importantly is the concentration of Ca^{2+} ions used. The empirical data shown in table 4.3 suggests a luminal concentration of free Ca^{2+} to be in the 50 - 500 µM range. However, this is just the *free* Ca^{2+} which can be detected, it is likely that lysosomes have a large store of Ca^{2+} ions bound to buffering proteins such as calsequestrin. The analogous organelle in sea urchin eggs is the cortical granule which has been shown to contain a total $[Ca^{2+}]$ between 30 - 95 mM (154). This evidence may help justify the high luminal Ca^{2+} concentration (60 mM) used in the Port-a-patch experiments. This value was based on the solutions used by Schieder *et al.* as they had been shown to give measurable Ca^{2+} currents. Although Schieder *et al.* do not provide an explanation as to why they chose this value, such high concentrations were probably

Table 4.3: Ionic composition of the lysosomal lumen.

Ion	Organelle	Cell type	Resting value	Method	Reference
Na^+	Lysosome	RAW264.7 macrophage	20.6 mM	Null-point titration	(409)
	Chromaffin granule	Bovine adrenal chromaffin	17 - 36 mM	Null-point titration	(170)
K^+	Lysosome	RAW264.7 macrophage	50 - 62 mM	Null-point titration	(409)
	Lysosome	Rat liver	50 mM	Atomic absorption spectrometry	(319)
	Chromaffin granule	Bovine adrenal chromaffin	30 - 42 mM	Null-point titration	(170)
	Endosome	Rat Liver	67 mM	Null-point titration	(436)
Ca^{2+}	Lysosome	Murine Macrophage	400 - 600 µM	Fura-2 and Oregon Green BAPTA dextran	(76)
	Lysosome	Human Fibroblast	550 µM	Endocytosed Rhod-dextran	(254)
	Endosome	Pancreatic Acinar cell	37 µM	Endocytosed Oregon green BAPTA-5N	(394)
	Endosome	3T3 Swiss Fibroblast	3 - 29 µM	Endocytosed Oregon green BAPTA-5N	(151)
	Trans-Golgi	HeLa	300 µM	Golgi-Aequorin	(345)
	Trans-Golgi	HeLa	130 µM	Golgi-D1cpv	(349)
Cl^-	Endosome	J744 & CHO	17 - 73 mM	Endocytosed BAC-dextran	(403)
	Late endosome	J744 & CHO	18 - 46 mM	Endocytosed BAC-dextran	(404)
	Late endosome	Murine hepatocyte	20 - 58 mM	Endocytosed BAC-macroglobulin	(173)

required to achieve a sufficient signal to noise ratio because HsTPC2 had been already shown to have a small Ca^{2+} conductance.

It must also be noted that the cytoplasmic Ca^{2+} concentration was also high at 2 mM and thus the 30-fold chemical gradient is actually lower than that predicted *in vivo*. For reference the bilayer Ca^{2+} solutions were 50 mM luminal and 15 µM on the cytoplasmic face, resulting in a 3000-fold gradient, which is nearer the scale of magnitude of the physiological gradient ($\approx$ 6000) (31).

4.16.7 Whole lysosome conductance

Whole-lysosome patch clamp provides a comparison for the NAADP-induced Ca^{2+} currents seen in the single-channel recordings of the lipid bilayer, although in whole-lysosome patch clamp the currents represent the flux of ions through a population of HsTPC2 channels which are present in the lysosomal patch. Thus the size of the current seen was much larger with the maximum amplitude evoked by 100 nM NAADP reaching $\approx$ 300 pA in overexpressing cells and by measuring the gradient of the I/V plots, the whole-lysosome conductance can be obtained, the maximum of which was $\approx$ 2000 pS.

The analogous study on MmTPC2 overexpressing cells never saw NAADP-induced currents greater than 60 pA, and a whole-lysosome conductance of $\approx$ 350 pS (387). This difference in lysosomal conductance could simply be explained by the level of channel expression in the lysosomal membrane, as a higher number of channels would inevitably give a larger current.

4.16.8 Channel density prediction

The number of HsTPC2 channels present in the lysosomal patch can be estimated combining data gathered here and in the bilayer recordings. Considering that the single-channel conductance of HsTPC2 was shown in chapter 3 to be 15 pS, the current expected to pass through a single channel at -100 mV can be calculated. If this is compared to the $\approx$ 300 pA currents seen in a lysosome patch (with 100 nM NAADP), this predicts that approximately 200 channels were present and open in the lysosome overexpressing HsTPC2 (the full calculation is shown in the appendix, page 319). The large variation in the currents seen was probably due to the fluctuations in channel

expression across different lysosomes, taking the maximal and minimal currents seen, they suggest a range of expression from 50 to 290 open channels.

To predict the total number of channels, the open probability needs to be considered. At 100 nM NAADP, the P_o was 8 % (Figure 3.26, page 126) which suggests a maximum of 2500 channels per lysosome, 92% of which remain closed.

Whilst this seems a large number, further calculations on the geometry of the lysosome and the size of the channel seem to justify this result. Basing the size of the HsTPC2 upon the closely related VCGG which has been determined by electron microscopy (306), it is predicted to be 20 x 10 x 9 nm, thus an assumed protein footprint of 200 nm^2 (445). Even on a non-swollen lysosome with a diameter of 1 µm, the membrane surface area could fit 15,700 channels, and as the sucrose swelling can achieve lysosomal diameters of > 2.5 µm, these could accommodate nearly 100,000 HsTPC2 channels. Therefore, there is plenty of space for the level of HsTPC2 over-expression calculated.

Another control can be made by looking at the wild type currents, as the wild type HEK293 cells express endogenous HsTPC2 it ought to be possible to predict the endogenous expression levels. However, wild type lysosomes gave very low levels of Ca^{2+} current in response to 100 nM NAADP thus the signal to noise ratio was very high. Nonetheless, a threshold resolution can be calculated and the maximum number of endogenous channel calculated (assuming endogenous channels have the same conductance). Taking the current at 100 nM NAADP as 4.2 pS, this suggests the wild type lysosomes contained ≈ 2.6 open HsTPC2 channels, which translates into a maximum ≈ 30 channels in total.

These predictions align nicely with the 275 $\pm$ 45-fold increase in HsTPC2 mRNA which was shown in this cell line over the wild type HEK293 cell (55), this further supports the reliability of these data.

(See appendix, page 319 for full calculations and further modelling).

4.16.9 Second messenger distinctions

In an attempt to confirm the purity of the lysosomal sample, the second messengers NAADP, cADPR and IP_3 were added to patched lysosomes. NAADP gave large current responses (> 200 pA) whilst cADPR and IP_3 did not. This result allowed two conclusions to be made: firstly, this confirmed the purity of the lysosomes, a lack of

response suggests a lack of channel contamination and therefore that the ER had been removed from the sample; secondly, this confirmed that neither cADPR nor IP_3 acted directly upon lysosomal channels.

However, a number of concerns regarding these results are worthy of discussion. Only one concentration of cADPR and IP_3 was tested (both 100 µM), whilst these ligands are optimally efficacious in other systems at these concentrations (129, 318) both ligands show a tightly regulated range of efficacy and other concentrations may stimulate channel opening. Furthermore, NAADP-induced currents were not seen on wild type lysosomes, and this was explained due to low levels of channel expression. If the IP_3R and RyR were present in this preparation their levels were possibly too low to be measured, yet the level of noise seemed to be increased in the presence of these ligands, especially cADPR. Average background noise, measured by the difference in channel activity induced by a solution change was $\approx 10 \pm 15$ pS, however, if this solution contained 100 µM cADPR the currents fluctuated around 42 ± 55 pS which may suggest low levels of endogenous RyR activity, which would support the notion of RyRs on acidic organelles proposed by Mitchell *et al.* (295), or may suggest that the low level of ER contamination seen in figure 4.28 contains functional channels.

4.16.10 Response to NAADP

It is remarkable that the two HsTPC2 concentration response curves shown in this thesis are so closely matched, comparing the bell-shaped curve seen in the bilayer (with an acidified *trans* chamber and high Ca^{2+}) shown in figure 3.26, page 126. The bilayer data gave a stimulatory EC_{50} of 5 nM, here in the lysosomal patch the EC_{50} was ≈ 11 nM. The bilayer seems to be slightly more sensitive to NAADP however, more concentrations are needed to fully resolve the curvature of the patch clamp concentration-response data.

As both studies gave a bell-shaped response, the inhibitory IC_{50} can also be calculated and this shows a larger difference between the two studies with the respective bilayer and lysosomal patch $IC_{50} \approx 100$ nM & 10 µM. This 10-fold difference in channel closure may be due to the fact that in a population of channels there will be variation in NAADP-sensitivity between individual channels according to their position in the lysosomal membrane and lipid/protein modulation. Therefore more of a range of responses were seen. In single-channel recordings there is likely to be less variation as

each channel is recorded under identical conditions. Most mammalian bell-shaped NAADP concentration-response curves that have been published were stimulatory at nM concentrations of NAADP and inhibitory at µM concentrations (304), these too were measured from populations of receptors in their native membranes and thus correlate more closely with the patch clamp data.

In wild type lysosomes, NAADP-induced currents were barely detectable, as discussed above, this is probably due to the low abundance of the endogenous HsTPC2 protein.

4.16.11 Desensitisation by mM NAADP

As had been shown in the lipid bilayer, mM concentrations of NAADP were inhibitory to Ca^{2+} release. In the whole lysosome patch clamp, this characteristic property was verified. Moreover, it is shown that this effect was irreversible within the timeframe of ≈ 5 minutes because washout of the high concentration and reapplication of stimulatory concentrations of 100 nM NAADP did not elicit Ca^{2+} currents. Rosen *et al.* have proposed that the NAADP receptor contains two NAADP binding sites, one which is inhibitory (370). This data supports this theory and further suggests that binding to the inhibitory site is prolonged.

4.16.12 Antagonism by Ned-19

Blockade of HsTPC2 channel activity in the patched lysosome was caused by 100 µM Ned-19. This is a very high concentration 100-fold higher than the inhibitory concentration used in the lipid bilayer. As was shown earlier (figure 3.28, page 129) nM concentrations of Ned-19 stimulated channel opening.

A Ned-19 agonist response has been seen in whole cell Ca^{2+} imaging studies on HEK293 cells overexpressing TPC2, where concentrations > 25 µM Ned-19 in the extracellular buffer elicited Ca^{2+} release (data not published). Human T-lymphocytes under similar conditions also showed Ca^{2+} release in response to 100 µM Ned-19 extracellularly. Ned-19 is a charged molecule, which is thought to enter the cytoplasm through passive uptake via an amino acid transporter and although exact intracellular concentrations are difficult to predict, the final concentrations are expected to be in the nM range (Dr Grant Churchill - personal communication). This would therefore

support the findings that low concentrations of Ned-19 are stimulatory for channel opening.

Contradicting this, the sea urchin egg homogenate responded to 100 µM Ned-19 to give Ca^{2+} release which could be partially blocked by pretreatment with NAADP (5 nM) or diltiazem (data not published). Therefore the exact pharmacology of this compound seems to vary across systems but experiments at lower concentrations of Ned-19 may begin to reveal the partial agonist properties of this ligand in whole lysosome patch.

4.16.13 Channel conductance and ion selectivity

As was discussed in chapter 3, there is a large discrepancy in the published results regarding the ion selectivity of TPC2. Lipid bilayer studies and patch clamp studies of HsTPC2 mistargeted to the PM both showed that HsTPC2 was permeable to monovalent cations (50, 348), but contradicting this, patch clamp on whole lysosomes overexpressing MmTPC2 showed a strong selectivity for Ca^{2+} ions, with K^+ permeability only seen in mutated forms (387).

Whilst a full bi-ionic analysis was not conducted here, crude assumptions can be made from the reverse potential measured. NAADP-induced currents had a reverse potential of 42.9 ± 5.1 mV which is remarkably close to the calculated reverse potential of Ca^{2+} in this system (43.2 mV). Such a tight correlation of the empirical and calculated reverse potential was surprising considering the presence of K^+ in both chambers and the conclusions from the bilayer studies that the HsTPC is non-selective. The calculated K^+ reversal potential in this system was -13.2 mV. If K^+ ions were conducting the current, the empirical reverse potential would be skewed towards this negative voltage. No other permeable ions were present in this system as acetate anions replaced Cl^- in all solutions, thus the data shown here supports the idea that HsTPC2 is a Ca^{2+}-selective channel. The intricacies of ion-selectivity in related proteins have already been discussed (page 135) so this section will attempt to explain why this discrepancy is seen.

The two studies which propose Ca^{2+} selectivity, this and Schieder *et al.*, were investigating different TPC2 isoforms, from different cell lines, in different laboratories but both using identical techniques. This begs the question whether it is the techniques employed which introduce the difference in ion selectivity.

Two potential explanations are presented: the channel was damaged during immunoprecipitation which destroyed the pore's selectivity filter; or ion concentrations used in the recording chambers were not high enough to maintain selectivity.

The first explanation is based on the understanding that ion selectivity is an inherent channel property, directly related to amino acid positioning in the pore region. This understanding is modelled on the well characterised K^+ channel selectivity filter, first determined in KcsA (115), and supported by site directed mutagenesis studies within the pore region which disrupt ion selectivity, like the one shown by Schieder *et al.* (311, 387). If the channel had been damaged by purification or could not reform the correct structure in the bilayer, the precise three-dimensional orientation of the selectivity filter would be lost and the channel become permeable to K^+ ions. Similarly the channel could have been stripped it of lipids or accessory proteins which could be essential in maintaining channel structure and thus Ca^{2+}-selectivity.

The second explanation is supported by analogy with the VGCCs, close relatives of HsTPC2. VGCCs are highly Ca^{2+}-selective under physiological conditions (65), but in the absence of divalent ions become non-selective and able to conduct monovalent ions such as Na^+ and large methylated cations such as tetramethylammonium (181, 316). Barrier models have been proposed to explain this phenomenon, whereby VGCCs possess a high affinity binding site for permeant divalent ions which when occupied prevent monovalent ions entering the mouth of the pore (92). If the concentration of divalent ions is reduced to below µM levels, monovalent ions become more effective at competing and can permeate the channel (184). In the Port-a-patch system, $[Ca^{2+}]$ on both sides of the membrane were in the mM range (2 mM cytoplasmic, 50 mM luminal) however in the bilayer 15 µM $[Ca^{2+}]_{free}$ was used for many of the K^+ measurements. It could be that at this concentration HsTPC2 becomes K^+ permeable.

4.16.14 Whole lysosome patch vs. lipid bilayer studies

The two methodologies used in this thesis to measure currents through HsTPC2 channels gave remarkably similar results, however, over a few issues they give conflicting results and this therefore raises the question whether whole lysosome patch clamp is more reliable than the bilayer or *vice versa*. This can be considered from two perspectives, the physiological relevance of the recording conditions and the practical limitations of the recording technique.

From the physiological perspective, the whole lysosome patch clamp is more authentic as this technique preserves the HsTPC2 in the native membrane without disruption to any luminal accessory/modulatory proteins until seal formation. By contrast, the immunoprecipitation of HsTPC2 for bilayer work required the solubilisation of the protein from the lysosomal membrane and relied on tight interactions between accessory proteins to maintain the relationship. Moreover, the final lipid composition of the bilayer was homogenous phosphatidyl ethanol amine, far removed from the complex array of phospho- and glycosphingolipids seen in the lysosomal membrane (165).

The importance of the membrane composition should not be overlooked as there are multiple examples of TPC-related channels being regulated by lipid interactions. For example, the presence of lysophospholipids have been shown to down regulate the gating of L-type VGCCs (22) and phosphoinositides have recently been implicated in the modulation of TRPML1 (113). Further afield, TRPV1 requires a lipid component of the PM in order to bind its cognate ligand capsaicin (35), whilst other TRPV and TRPC proteins are directly gated by lipids (23). Also pertinent to this study is the essential requirement for phospholipids in the binding of radiolabelled NAADP to its target protein in sea urchin egg homogenates (77). Removal of phospholipids resulted in a marked decrease in the apparent affinity of the target protein for NAADP. None of these studies directly relate lipid interactions to ion selectivity but they do show that an unphysiological membrane environment could drastically affect channel function and thus the native membranes in lysosome patch clamp ought to be more reliable.

Similar concerns are raised over the presence of accessory proteins however, no technique shown here is guaranteed to preserve protein-protein interactions, as the solutions on both sides of the membrane were exchanged and any proteins not tightly bound would have been washed away. Other concerns such as the most physiologically relevant holding potentials and ion compositions affect both techniques.

The empirical evidence that native membrane patch clamp studies are more reliable has been shown by investigating the IP_3R where lipid-bilayer studies and native membrane studies have been compared in this field for over a decade (129). In general, direct patch clamp on the ER membrane (contiguous with the nuclear envelope outer membrane) gave more repeatable results, with higher open probabilities and often with different gating kinetics and pharmacology (129). This suggests that future work to investigate HsTPC ought to be conducted by whole-lysosome patch clamp.

Practically however, single-channel data derived from the bilayer studies have a greater resolution than the population recordings in lysosome patch clamp and greater confidence that the currents recorded are due to the purified HsTPC2, rather than unknown proteins present in the uncharacterised lysosomal membrane. Thus biophysical properties of the channel are less likely to be altered by contaminating proteins/lipids.

Although the manufacturers of Port-a-patch claim that single-channel measurements on lysosomal membranes should be possible, the signal to noise ratio seen in this study would suggest otherwise. Thus to obtain detailed information regarding the subconductance states and coupled gating of HsTPC2 the lipid bilayer is the only feasible technique.

The lipid bilayer technique also allows a greater level of flexibility because proteins can be purified from transiently transfected cell lines and purified protein can be frozen and stored (albeit with a limited shelf-life). Whereas to ensure that lysosomes are expressing proteins for patch clamp, stable cell lines must be generated, and lysosomes must always be prepared on the day of the experiment as the fragility of the lysosomal membrane prevents storage.

Thus both methodologies have their advantages and disadvantages and to fully understand the biophysical properties of HsTPC2, these techniques should be used in parallel.

4.17 Conclusions

Conventional methods of lysosomal purification by differential centrifugation were shown to indeed purify lysosomes from a cell homogenate, but with a high level of contamination by markers of the PM, ER, Golgi and mitochondria.

Investigation of various methodologies and optimisation of cell homogenisation resulted in a protocol that produces a high yield of extremely pure lysosomes. This can be achieved by magnetic chromatography from cells which had endocytosed Fe-dextran, and were lysed under low pressure by the Balch homogeniser.

Preliminary experiments into the electrophysiological properties of these lysosomes were conducted using planar patch clamp techniques. These experiments confirm that many characteristic properties of NAADP signalling correlate with the over-expression of HsTPC2. This data supports findings by Schieder *et al.* investigating the properties of MmTPC2 using similar techniques as well as corroborating data from the lipid bilayer work in chapter 3.

4.18 Future prospects

To progress this work, experiments must be conducted using more physiological solutions, with particular consideration for Ca^{2+} concentrations. Whilst this study acts as a proof of principle showing that HsTPC2 acts as a Ca^{2+} permeable channel in the native lysosomal membrane, such high concentrations of Ca^{2+} on both sides of the membrane are likely to mask any potential Ca^{2+}-dependent modulation like that seen in the plant TPC1 (175).

The question of Ca^{2+} selectivity also requires more robust evidence, this could be achieved by conducting measurements in bi-ionic solutions which allows the separation of K^+/Ca^{2+} currents. The single point mutation in MmTPC2 which caused loss of selectivity could also be replicated in HsTPC2, along with other conserved amino acids within the pore region which may play a role in Ca^{2+} selectivity.

The effect of luminal pH was not investigated here. Studies on MmTPC2 showed that a neutral luminal pH abolished all channel activity, whereas HsTPC2 in the lipid bilayer gave larger currents under neutral conditions. There is the potential that these differences are due to species variation but this discrepancy ought to be investigated on HsTPC2-expressing lysosomes as this may have physiological implications considering

the alkalinisation of the lysosomal lumen upon NAADP stimulation (303). The effects of counterion diffusion also need to be closely monitored, to ensure that membrane permeant acids (*e.g.* acetate) are not disrupting pH gradients.

Whole-lysosome patch clamp also provides a robust functional assay upon which to investigate the pharmacology of HsTPC2 populations. The mechanisms of the NAADP antagonists (PPADS, DHPs, Ned-19) may be elucidated, in particular the partial agonist effects of Ned-19. However, this work would need to be conducted in collaboration with single-channel studies to dissect out the synergy of Ned-19 and NAADP at their cognate binding sites (370).

An obvious next stage in TPC electrophysiology is to compare isoforms, although this may not be viable with human TPCs due to the disparate localisation of HsTPC1 on endosomes and lysosomes. Comparison of TPC2 channel activity across species would be a more feasible study. Towards this end, stable cell lines over-expressing the sea urchin SpTPC2 have already been made, and this isoform is also expressed in lysosomes (375). Whole-lysosome patch clamp on SpTPC2 would be the first study on non-mammalian TPC2 and would allow investigation of the intriguing channel gating properties seen in the sea urchin egg homogenate, such as sub-threshold desensitisation (1, 147).

In general, Port-a-patch could allow further characterisation of other lysosomal channels which may interact with TPC function, these include the chloride channels seen by Schieder *et al.* and the TRPML currents seen by Dong *et al.*. Whole-lysosome patch clamp is not a high-throughput assay but has potential to reveal a great deal about the channel properties of these inaccessible organelles.

Chapter 5

Results - Protein-protein interactions of HsTPCs

5.1 Summary

The preceding electrophysiological studies have highlighted the differences between native membrane expression and artificial bilayer environments on the channel properties of HsTPC2. These differences suggest that the *in situ* HsTPC2 may be subjected to a different regulatory regime and this is most likely to be through a series of accessory and modulatory proteins. One aim of this chapter was to elucidate the composition of the immunoprecipitated samples to detect whether particular interacting proteins could be identified.

Data shown earlier in the FPLC trace (figure 3.5, page 98) hinted that the solubilised HsTPC2 had a far larger molecular weight than expected ($>$ 600 kDa). This may have been due to a tightly interacting oligomeric complex. By analogy to other families of Ca^{2+} channels it is unlikely that HsTPC2 exists in isolation in the lysosomal membrane. For example, the VGCC family have four accessory subunits to their main α-pore ($\alpha_2, \beta, \gamma, \delta$) which regulate channel gating kinetics, trafficking and membrane stability respectively (64). The IP_3R interacts with proteins such as IRBIT (8) and chromogranins (423) which play a role in IP_3 sensitivity and pH-regulation of channel gating respectively, together with more standard regulatory proteins such as calmodulin, CaBP and RACK1 (129). Finally, the RyR channels have a host of modulators on either side of the membrane: cytoplasmic calmodulin (401) and FKBP12 (91)

which regulate channel gating, and luminal calsequestrin, junctin, triadin (167) which modulate RyR in response to luminal [Ca^{2+}].

The other key aim of this chapter was to determine whether the HsTPCs dimerise to form the putative 24-TM channel pore seen in closely related VGCC α-subunit, and TRP tetramers. Furthermore to establish whether any dimerisation could be seen between the isoforms to create HsTPC1/HsTPC2 heterodimers. As with the TRP family, heteromeric channels could be a basis of channel regulation and may have important physiological consequences.

To resolve these queries, the immunoprecipitated HsTPC2 complex was analysed by western blot and mass spectrometry. Interaction between HsTPC1 and HsTPC2 was then further assessed by coimmunoprecipitation, colocalisation and FRET studies. The implications of these findings are discussed in the context of channel function.

5.2 Presence of other putative NAADP receptors

As a reminder, in chapter 3, overexpressed HA-tagged HsTPC2 was successfully purified by immunoprecipitation using two different antibodies. Immunopurification of HsTPC2 via the HA epitope gave a non-functional channel, whereas purification against epitopes in the HsTPC2 protein gave a NAADP-regulated Ca^{2+} channel. In order to rule out the suggestion that the Ca^{2+} currents seen could be due to the contamination of the sample by the most likely NAADP receptor candidate TRPML1, a western blot was conducted on the immunoprecipitated complex

TRPML1 could associate with HsTPC2 as they are also colocated in the same membrane. A recent publication showed that TRPML1 (and to some extent TRPML3) could be coimmunoprecipitated with HsTPC2 purified from cells *overexpressing* both proteins (457). Here, only HsTPC2 was overexpressed and figure 5.1 shows an anti-TRPML western blot which demonstrates that *endogenous* TRPML was not coimmunoprecipitated.

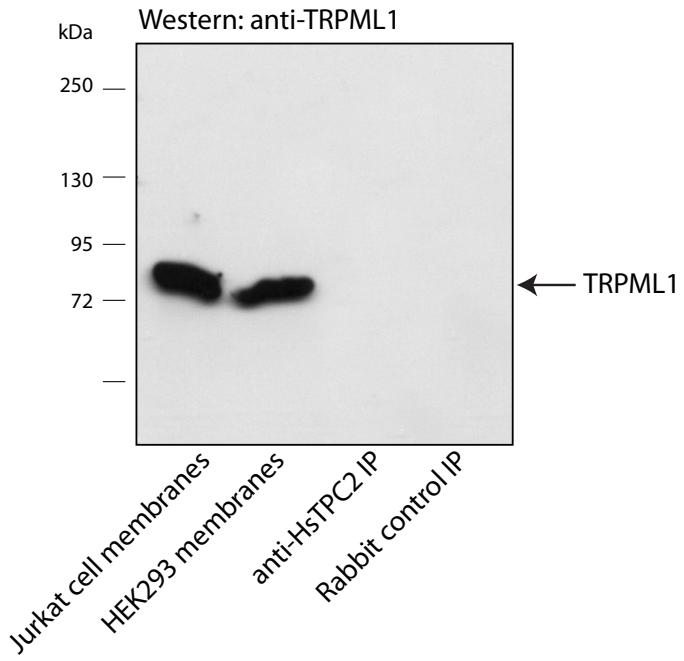


Figure 5.1: Western blot against TRP-ML1. Anti-TRP-ML1 western blot, probed with a rabbit polyclonal antibody (Santa Cruz H75) and relevant secondary antibody. Solubilised Jurkat cell membranes were used as a positive control. Solubilised HEK293 membranes demonstrate the presence of TRP-ML1; however, neither the anti-HsTPC2 immunoprecipitation nor the control rabbit serum immunoprecipitation show TRP-ML1 contamination.

5.3 Mass spectrometry analysis of IP complexes

Western blotting cannot identify interactions with unknown proteins. Therefore to dissect the protein content of purified samples, the immunopurified HsTPC2 complex was run on SDS-PAGE and treated with a Coomassie protein stain. Visible bands could then be excised and analysed by mass spectrometry.

5.3.1 Proteins coimmunoprecipitated by anti-HA

First, the anti-HA immunoprecipitation was investigated and figure 5.2 shows the Coomassie stain aligned to an anti-HA western blot of identical samples run on the same gel. A distinct band around 90 kDa correlates with the immunoreactive band on the western blot and is likely to be the purified HsTPC2. It is clear that this is not the only protein present with distinct bands revealing at least seven other proteins present at detectable levels (> 8 ng). The control rat IgG precipitation did not yield any proteins detectable by Coomassie.

The identity of these proteins was assessed by excision of the visible band and analysis by mass spectrometry. Each band was cut from the gel in both the anti-HA and rat IgG control lanes (regions marked on figure 5.2), the acrylamide was dissolved and the protein digested with trypsin to form a mixture of peptide fragments. This mixture was subsequently ionised by matrix-assisted laser desorption/ionization (MALDI) and the peptide masses determined by a Time of Flight (TOF) mass spectrometer. The mass of a peptide reveals its putative primary sequence, which can then be cross referenced against a protein database to identify potential proteins which were predicted to contain this precise sequence.

Initial attempts analysing individual bands identified nothing more than contaminant proteins present in both the specific and control elutions. This was probably due to the sensitivity of MALDI-TOF where the concentration of proteins of interest in each band was too low for detection. The acrylamide to protein ratio was also very high and this can sometimes inhibit the activity of the trypsin enzyme.

In collaboration with the Oxford University Central Proteomics Facility, a new method was devised to maximise protein retention and to reduce blockade of the trypsin digest by excess acrylamide, this simply involved running a concentrated sample of the HsTPC2 immunopurified complex on SDS PAGE for just 10 minutes to remove salts

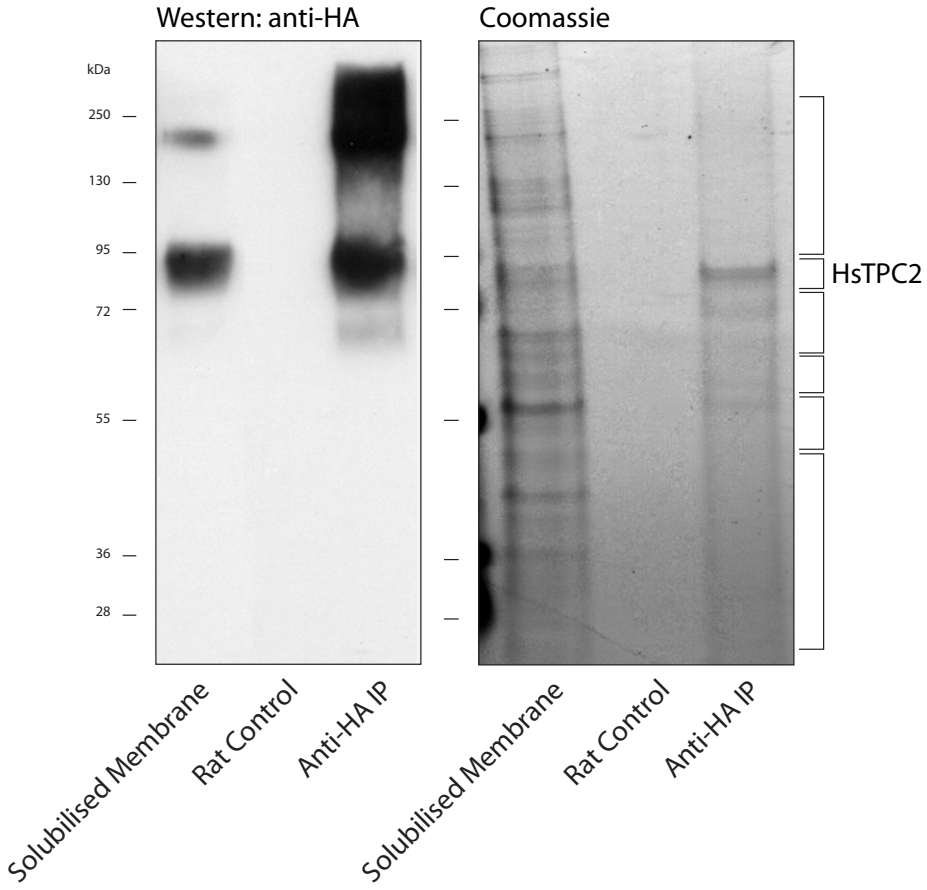


Figure 5.2: The protein composition of the anti-HA immunoprecipitated complex. The immunoprepitiation was carried out as optimised in section 3.5.1. The left hand panel contains an anti-HA western blot. The input of solubilised membranes acts as a positive control and shows the two characteristic bands for HsTPC2. 'Rat Control' contains the elution from beads coupled to non-immune rat IgGs whilst 'Anti-HA IP' contains the eluted complex from the anti-HA immunoprecipitation. The right panel shows identical samples of the two immunoprecipitated lanes which were run on the same SDS-PAGE gel and stained with Imperial blue protein stain (Pierce). The two panels are aligned according the molecular weight markers run adjacent to both samples. Excised regions are outlined on the right.

and the detergent. The entire lane was excised and digested but was then further purified by an additional separation by liquid chromatography (LC) before ionisation, this protocol of LCMS allowed the mass spectrometer to detect lower concentrations and thus resolve more peptide sequences.

Figure 5.3 shows the anti-HA western blot that was used to confirm the immunoprecipitation was successful, the rest of the sample was run on the same gel excised and sent for analysis by mass spectrometry. The results of the mass spectrometry are displayed in table 5.1. Contaminants such a keratin, which were present in the control were removed from this list.

Table 5.1: Proteins present in the HsTPC2 immunoprecipitate. LC-MS results predicted the presence of the 13 proteins listed. The threshold for inclusion was $p < 0.01$ and mascot score of > 60.
HNR = Heterogeneous nuclear ribonucleoprotein.

Protein	Gene	Known or presumed function	Peptides	Score
Two-Pore Channel 2	TPCN2	Putative NAADP receptor - Lysosomal Ca^{2+}channel	2	72
Two-Pore Channel 1	TPCN1	Putative NAADP receptor - Lysosomal Ca^{2+}channel	2	127
V-type ATPase subunit A	ATP6V1A	Subunit of V-type ATPase, the enzyme responsible for intracellular organelle acidification	2	102
Na^+/K^+ ATPase subunit	ATP1A2	Subunit of P-type ATPase - Na^+/K^+ exchanger	2	72
Flotillin-1	FLOT1	Integral membrane protein involved in vesicular trafficking	4	66
Cytoplasmic Actin-1	ACTB	Non-muscle cytoskeletal protein	4	114
Myosin-9	MYH9	Non-muscle cytoskeletal protein	1	77
Immunoglobulin Kappa	IGKV2-30	Antibody light chain	1	76
T-complex protein 1-δ	CCT4	Protein folding chaperone	3	84
HNR A3	HNRNPA3	mRNA binding protein	1	90
HNR M	HNRNPM	mRNA binding protein	4	109
Elongation factor 1-α 2	EEF1A2	tRNA binding protein	2	84
Histone H2A.V	H2AFV	DNA binding protein which forms the core of the nucleosome	2	71

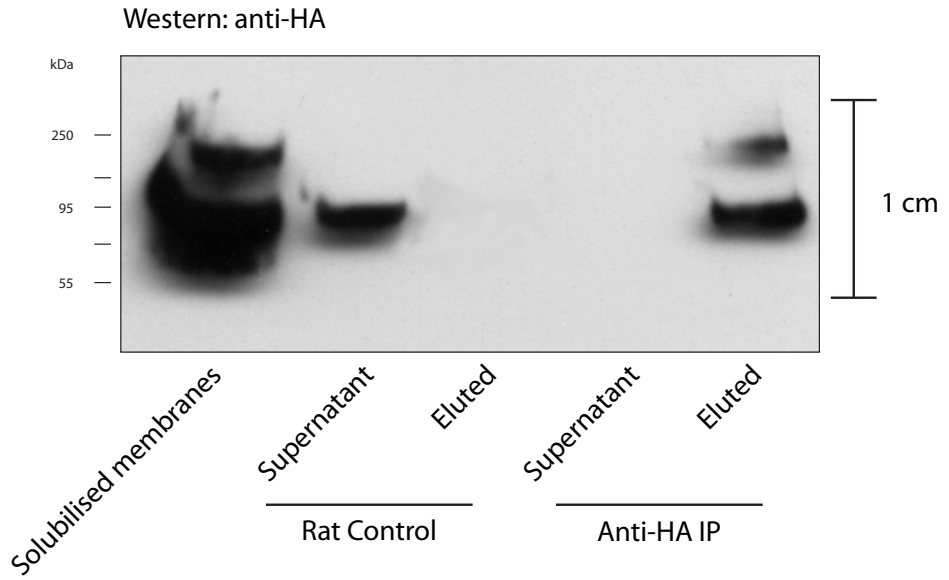


Figure 5.3: Anti-HA immunoprecipitation sent for mass spectrometry analysis. Anti-HA western blot of a 10 µl sample taken from an anti-HA immunoprecipitation, the rest of the sample was run on the same gel excised and sent for analysis by mass spectrometry. Solubilised membranes provide a positive control demonstrating HsTPC2 in the sample. 'Rat Control' contains the elution from beads coupled to non-immune rat IgGs whilst 'Anti-HA IP' contains the eluted complex from the anti-HA immunoprecipitation. 'Supernatant' refers to the solution once the beads have been removed. 'Eluted' refers to the complex that is released when beads are treated with 50 µg/ml HA peptide.

Reassuringly HsTPC2 was identified as a major constituent of the protein complex, which confirms the successful immunoprecipitation. A surprising finding of this analysis was the presence of the homologous isoform HsTPC1. Whilst it has been previously shown that HsTPC2 form homodimers (478), this is the first evidence that the two isoforms may come together to form HsTPC heterodimers and acted as a basis for many of the experiments shown later in this chapter (sections 5.4, 5.8, 5.10).

Also coimmunoprecipitated was the catalytic subunit of the V-type proton ATPase, which is responsible for the acidification of the lysosome (415). Two other subunits of this ATPase (A & B) were detected at lower levels, with too few peptide matches to meet the reliability threshold set here, but taken together these three lines of evidence are mutually confirmatory. A specific interaction between HsTPC2 and the V-type ATPase may allow modulation of channel or ATPase activity which could play a feedback role in the pH dependent regulation of the HsTPC2 channel as discussed in section 3.7.8 (page 125).

The α subunit of the Na^+/K^+ P-type ATPase was also detected by mass spectrometry. This is the catalytic component responsible for the hydrolysis of ATP coupled to the exchange of sodium and potassium ions but is usually associated with the plasma membrane. However, endosomal activity of this ATPase has been shown (130) where the electrogenic exchange inhibits the luminal acidification by altering the membrane potential. If a similar inhibition is seen in the lysosome this could feedback on HsTPC2 at the level of luminal pH, as above.

The structural proteins seen, such as flotillin-1, actin and myosin, could be contamination or may represent a role of HsTPC2 in lysosomal trafficking and structure. The TRP channels which are homologous to the TPCs have been shown to have a close association with scaffolding proteins and lipid raft domains (256). Flotillin in particular is an interesting candidate as it is involved in vesicular dynamics, membrane trafficking and phagocytosis (12).

Although a recent publication has associated the heterogenous nuclear ribonucleoprotein (HNRP1) with IP_3R-mediated Ca^{2+} release in Zebrafish (285), the presence of HNR proteins in the HsTPC2 complex is likely to be due to contamination. This assertion is based on the presence of HNR proteins in the rat IgG control immunoprecipitation, which suggests the interaction is non-specific.

Contamination by nucleic acid binding proteins was probably caused by nuclear disruption during homogenisation. This may be due to excessive forces exerted on the cell by the Dounce homogeniser and perhaps use of the Balch homogeniser or the inclusion of DNase would reduce this contamination in future studies.

5.3.2 Proteins coimmunoprecipitated by anti-HsTPC2

The anti-HA study revealed many putative protein associations but there is a major concern that these results do not reflect the physiological interactions of the HsTPC2 complex as the HsTPC2 purified by this technique never yielded functional channels in the lipid bilayer. Whilst this monoclonal anti-HA antibody gives a relatively clean preparation, it should be compared to an analysis of the protein purified by the anti-HsTPC2 polyclonal serum which would be more significant as it was this complex which yielded the lipid bilayer channel data in chapter 3.

As with the HA immunopurified complex, the polyclonal-purified HsTPC2 yielded an array of proteins which were coimmunoprecipitated. The Coomassie stain is shown in figure 5.4 and shows a sharp band which aligns with the immunoreactive band of HsTPC2 in the anti-HA western blot alongside. However, there were many more bands seen in this purification compared to the anti-HA immunoprecipitation, this may be due to the greater proportion of non-specific interactions shown by polyclonal antibodies compared to monoclonal antibodies.

The mass spectrometry was conducted as with the HA-purified complex, with the entire band being excised from just 1 cm of acrylamide gel. As predicted, the polyclonal serum gave a 'dirtier' set of results. Mass spectrometry analysis of a scaled up (5-fold) immunoprecipitation yielded over 300 proteins that were present in the HsTPC2 elution but not the rabbit control. HsTPC2 was present as a major constituent of the preparation being matched to four unique peptides.

Many of the 300 proteins were identified on the basis of just one unique peptide hit, this included the endogenous HsTPC1 which despite this low detection rate was predicted with 99.6 % certainty as this single peptide provided 14.6 % coverage of the amino acids present in the full protein. Once again this suggests that perhaps the two isoforms are interacting.

A summarised list of proteins detected ($>$ 3 unique peptides) is shown in table 5.2. The two HsTPC isoforms were not the only proteins to be seen in both mass spec-

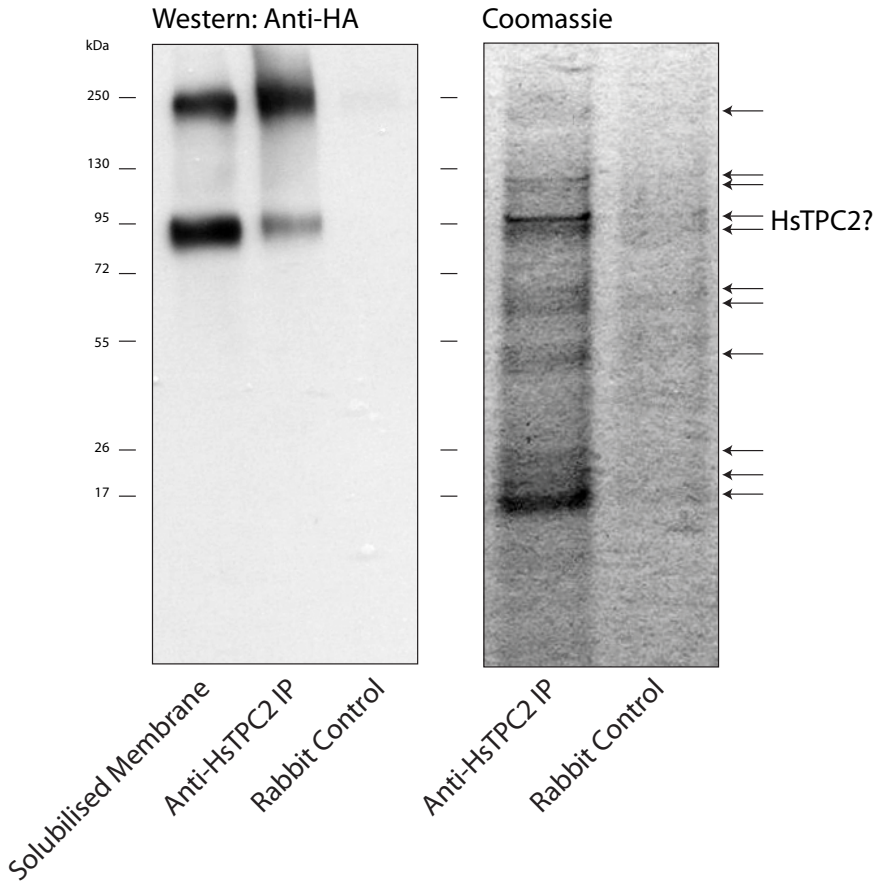


Figure 5.4: The protein composition of the anti-HsTPC2 immunoprecipitated complex. The left hand panel depicts an anti-HA western blot similar to that in figure 3.15, the input of solubilised membranes acts as a positive control and shows the characteristic HsTPC2 doublet. The second lane contains the eluted complex from the anti-HsTPC2 immunoprecipitation. The third lane contains the eluted complex from the immunoprecipitation using beads coupled to non-immune rabbit serum, HsTPC2 is not present. The right panel shows identical samples of the two immunoprecipitated lanes which were run on the same SDS-PAGE gel and stained with Imperial blue protein stain (Pierce). The two panels are aligned according the molecular weight markers run adjacent to both samples.

trometry predictions, a subunit of the Na^+/K^+ ATPase was also seen in the HsTPC2 purification which re-enforces the likelihood of an interaction between these two proteins.

A potential regulatory protein was seen in the guise of the insulin receptor substrate 4 (IRS4), this belongs to a family of cytoplasmic proteins known to be involved in protein phosphorylation, which is usually a key mechanism for channel regulation. IRS4 is usually phosphorylated by the insulin receptor tyrosine kinase upon receptor stimulation but in some cell lines this association is uncoupled (389). Downstream effects of activated IRS4 are still largely unknown, however, this protein has been shown to interact with the proto-oncogene p38 (211) and also has been associated by coimmunoprecipitation and mass spectrometry analysis with a imidazoline binding protein, IRAS (380). NAADP contains an imidazoline ring within the adenine base, this interaction could potentially have implications for the NAADP binding properties of HsTPC2.

Other proteins worthy of discussion, include a strong signal seen for an isoform of the Ca^{2+}-ATPase (ATP2A2) which is usually found in the ER. Lysosomal Ca^{2+}uptake is still unknown and this pump is not mentioned in the lysosomal proteosome (390), however it could have reached the lysosomal membrane by some heterotypic fusion event and may even act to regulate the Ca^{2+}-sensitive HsTPC2.

A mitochondrial protein known to be a catalytic subunit of the ATP synthase (ATP5C1) gave three strong peptide matches. This protein utilises a proton gradient to generate ATP synthesis and as such the catalytic domain of this protein is homologous with the V-type ATPase which uses ATP to create a proton gradient (382). Although a tenuous suggestion, this subunit may have been moonlighting within the lysosomal ATPase.

This desperate proposal was partly inspired by the absence of the V-type ATPase, which gave a strong signal in the HA-purified preparation but was not seen when purified by HsTPC2. This may indicate that the initial finding was anomalous, or may suggest a dynamism within the lysosomal membrane whereby regulatory proteins are in a state of equilibrium, binding only when necessary.

It ought to be mentioned that the majority of the other proteins found were structural proteins such as actin, mysosin or DNA binding proteins like many of the heterogenous nuclear ribonucleoproteins and tRNA synthases. It is again likely that their pres-

Table 5.2: Proteins present in the HsTPC2 immunoprecipitate. LC-MS results predicted (> 3 unique peptide matches) the presence of the 13 proteins listed. The threshold for inclusion was $p < 0.01$ and mascot score of > 60. ∗ Only one unique peptide match shown for HsTPC1.

Protein	Gene	Known or presumed function
Two-Pore Channel 2	TPCN2	Putative NAADP receptor - Lysosomal Ca^{2+}channel
Sarcoplasmic/endoplasmic reticulum Ca^{2+}ATPase 2	ATP2A2	Intracellular Ca^{2+}pump localised to the ER/SR membrane
Na^+/K^+-transporting ATPase subunit $\beta 3$	ATP1B3	Responsible for establishing and maintaining the electrochemical gradients of Na^+ and K^+ ions across the plasma membrane.
Insulin receptor substrate 4	IRS4	Contains many potential tyrosine and serine/threonine phosphorylation sites, known to be phosphorylated by IRS4
ATP synthase subunit γ	ATP5C1	Catalytic subunit of mitochondrial ATP-synthase
Exosome complex exonuclease RRP4	EXOSC2	mRNA binding protein and nuclease
Heat shock 70 kDa protein	HSPA1L	Stabilises proteins against aggregation and assists protein folding
ATP-dependent RNA helicase DDX50	DDX50	Translation initiation, nuclear and mitochondrial splicing, and ribosome and spliceosome assembly
60S ribosomal protein	RPL21P19, RPL26L1	Cytoplasmic ribosomal protein
Splicing factor 3B subunit 1	SF3B1	Forms the U2 small nuclear ribonucleoproteins complex
Myb-binding protein 1A	MYBBP1A	
Fatty acid synthase	FASN	Catalyzes the synthesis of palmitate from acetyl-CoA and malonyl-CoA, in the presence of NADPH, into long-chain saturated fatty acids
Pre-mRNA-processing-splicing factor 8	PRPF8	Component of the splicosome
Gem-associated protein	GEMIN5	Assists the cytoplasmic assembly of small nuclear ribonucleoproteins
Cell division cycle 5-like protein	CDC5L	An essential component of a non-snRNA spliceosome
Xaa-Pro aminopeptidase 3	XPNPEP3	Remove the N-terminal amino acid from peptides with a proline residue in the penultimate position
Lamin-B1	LMNB1	Inner nuclear membrane structural protein
NAD(P) transhydrogenase	NNT	
Ras GTPase-activating-like protein	IQGAP1	Cytoskeletal protein
Dihydrolipoyllysine-residue acetyltransferase	DLAT	Component of pyruvate dehydrogenase complex
Isoform 1 of General transcription factor II	GTF2I	Multifunctional phosphoprotein with roles in transcription and signal transduction
Heterogeneous nuclear ribonucleoprotein A1	HNRPA1L3	mRNA binding protein
Double-stranded RNA-binding protein Staufen 1	STAU1	Transports mRNAs to different subcellular compartments and organelles
Dolichyl-diphosphooligosaccharide-protein glycosyltransferase subunit 2	RPN2	Part of an N-oligosaccharyl transferase complex in rER
Isoleucyl-, Arginyl- and Aspartyl-tRNA synthetase	IARS, RARS, DARS	Catalyzes the aminoacylation of tRNA
Bifunctional aminoacyl-tRNA synthetase	EPRS	Catalyzes the aminoacylation of glutamic acid and proline tRNA species
DNA replication licensing factors	MCM5, MCM3	Chromatin-binding proteins
Isoform 1 of RNA-binding protein 39	RBM39	Component of the splicosome
SDHA protein	SDHA	Subunit A of succinate dehydrogenase in the mitochondrial membrane
∗ Two-Pore Channel 1	TPCN1	Putative NAADP receptor - Lysosomal Ca^{2+}channel

ence is simply due to contamination by DNA or other cellular debris as very few could be shown to have any connection with known lysosomal function or Ca^{2+}-interactions.

5.4 Coimmunoprecipitation of HsTPCs

5.4.1 Endogenous HsTPC1 coimmunoprecipitation with HA.HsTPC2

The major finding of both mass spectrometry analyses that cannot be overlooked is the coimmunoprecipitation of HsTPC1 which gave a strong signal in both preparations. This is the first suggestion that the two isoforms may interact. To underpin the validity of mass spectrometry data, samples of HsTPC2 purified by HA-immunoprecipitation were subjected to western blots using antibodies against HsTPC1. Control western blots (not shown) against the HA-tag confirm that HsTPC2 was successfully purified and was present in the sample. Figure 5.5 demonstrates (by two separate polyclonal antibodies) that HsTPC1 was indeed also present in the purified sample but not in the rat IgG control immunoprecipitation. The specificity of the antibodies used will be discussed in section 5.6.

5.4.2 HA.HsTPC2 coimmunoprecipitation with endogenous HsTPC1

Whilst the rat IgG control eliminates the possibility of HsTPC1 interacting with the sepharose bead or rat IgG complex, HsTPC1 could be contaminating the preparation through a non-specific interaction with the rat monoclonal HA-antibody. To eliminate this possibility and to confirm an interaction between HsTPC1 and the overexpressed HA.HsTPC2, an immunoprecipitation was conducted against the endogenous HsTPC1, followed by a western blot probing for the presence of the HA tagged-HsTPC2.

Figure 5.6 depicts a strong presence of HA.HsTPC2 in cell lysate, as would be expected in this overexpressing cell line. More importantly, HA.HsTPC2 was seen in the endogenous-HsTPC1 immunoprecipitate and not the rabbit control. This confirmed that low levels of HsTPC1 coimmunoprecipitated the overexpressed protein and that the interaction could occur with either isoform acting as the target for precipitation.

These experiments were confined to a single cell line overexpressing HsTPC2 roughly 250-fold (supplementary data of (55)). It could be argued that with such an unphysiological amplification some of this protein may be mistargeted and any heterodimeric interactions are simply due to hydrophobic interactions with a very abundant protein.

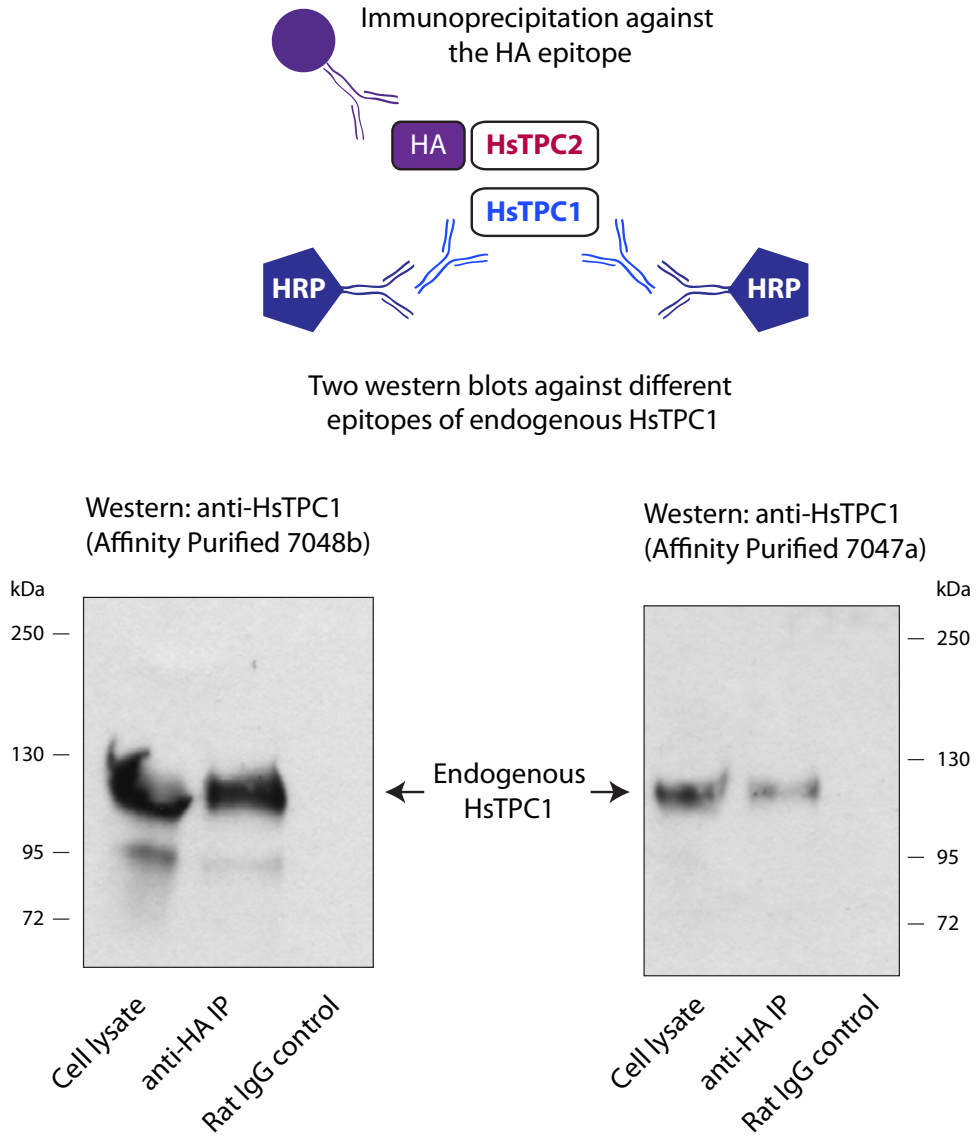


Figure 5.5: Endogenous HsTPC1 is coimmunoprecipitated with HA.HsTPC2. **Top:** Schematic depiction of the antibodies used: the immunoprecipitation was targeted against the HA tag, whilst the western blots were probed with anti-HsTPC1 rabbit polyclonals (affinity purified 7048b and 7047a) followed by an anti-rabbit IgG HRP conjugate. **Bottom:** Anti-HsTPC1 western blots depicting the presence of endogenous HsTPC1 in whole cell lysate, the HA immunoprecipitate, but not the rat IgG control.

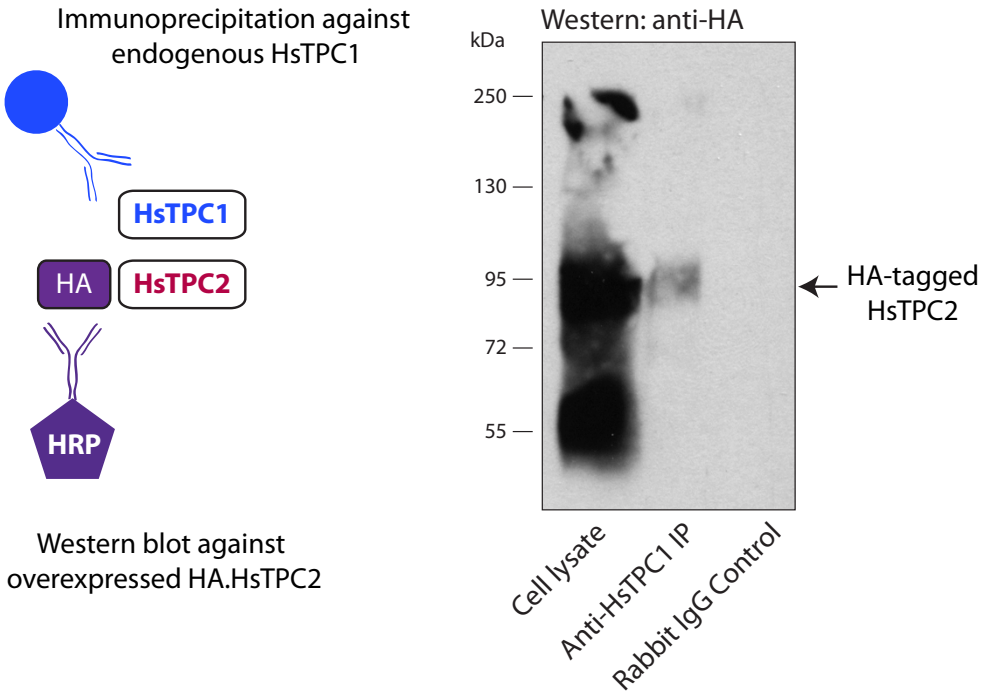


Figure 5.6: Overexpressed HsTPC2 is coimmunoprecipitated with endogenous HsTPC1. Left: Schematic depiction of the antibodies used: the immunoprecipitation was targeted against two epitopes on HsTPC1 (see antibody 7047 on table B.3), whilst the western blots were probed with an anti-HA HRP conjugate. **Right:** Anti-HA western blot depicting the presence of overexpressed HA.HsTPC2 in whole cell lysate, the immunoprecipitate, but not the rabbit IgG control.

Ideally, the coimmunoprecipitation experiment would be conducted on the endogenous HsTPCs, however, section 5.4.5 will explain why this was not possible. An alternative strategy to achieve a greater confidence was to repeat these coimmunoprecipitations in a separate cell line to investigate whether a heterodimeric interaction could still be seen.

5.4.3 HsTPC1.His coimmunoprecipitation with endogenous HsTPC2

The interaction of HsTPC1 and HsTPC2 was further investigated using a cell line which overexpressed HsTPC1 labelled with a tag of six histidine residues (His_6) at the carboxy terminus (introduced in figure 3.3, page 93)

Firstly an immunoprecipitation was conducted directed against epitopes in HsTPC2 (as was optimised in section 3.6). This immunoprecipitated the low levels of endogenous HsTPC2 and figure 5.7 reveals that the His-tagged HsTPC1 was specifically coimmunoprecipitated. Therefore, confirming that the heterodimeric interaction was retained in this separate stable cell line.

Interestingly this interaction was not seen on membrane samples which had been frozen at $-20\,^{\circ}C$, which suggests that the interaction is lost by freezing. All immunoprecipitations were thus conducted on freshly harvested membrane preparations.

5.4.4 Endogenous HsTPC2 coimmunoprecipitation with HsTPC1.His

The reverse experiment whereby the HsTPC1.His protein was immunoprecipitated and the western probed for endogenous HsTPC2 was hampered by a lack of good antibodies against HsTPC2 for western blots. Figure 5.8 shows the best result obtained, which although depicting a signal at the correct size in the immunoprecipitated lane, the cell lysate which is used as a positive control throughout all immunoprecipitation reactions, did not show a signal. The positive control western of the same samples probed with the His tag (not shown) confirmed presence of HsTPC1.His in both the cell lysate and the immunoprecipitation, but not in the mouse control.

5.4.5 Antibody limitations

The best possible control experiment to rule out the potential effects of protein overexpression would be to investigate the interaction of both endogenous proteins in a

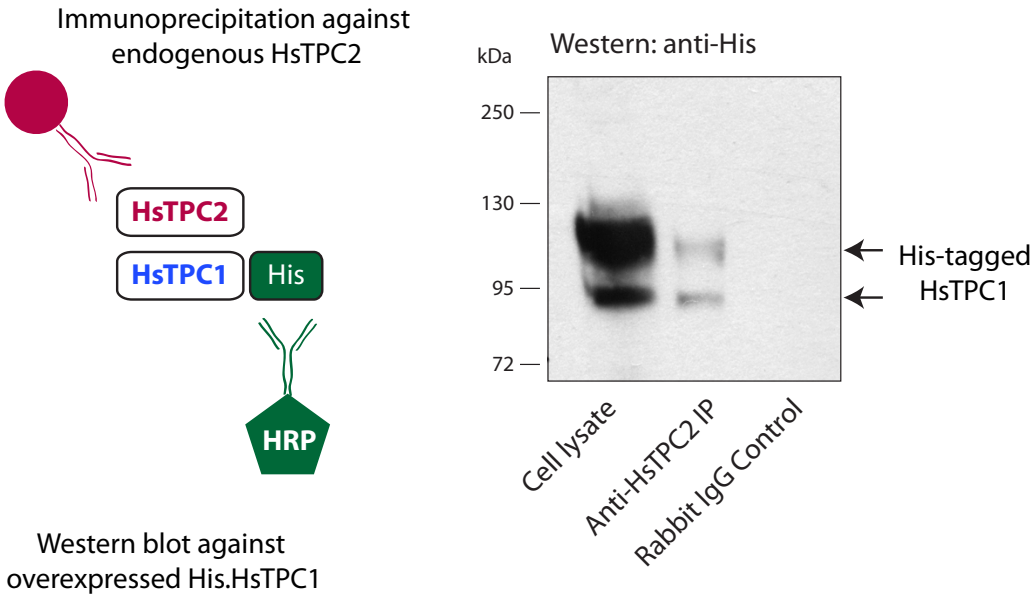


Figure 5.7: Overexpressed HsTPC1 is coimmunoprecipitated with endogenous HsTPC2. Left: Schematic depiction of the antibodies used: the immunoprecipitation was targeted against the two epitopes on HsTPC2 (see antibody 7049 on table B.3), whilst the western blots were probed with anti-rabbit HRP conjugate. **Right:** Anti-His western blot depicting the presence of overexpressed HsTPC1.His in the cell lysate and the HsTPC2 immunoprecipitate, but not rabbit IgG control.

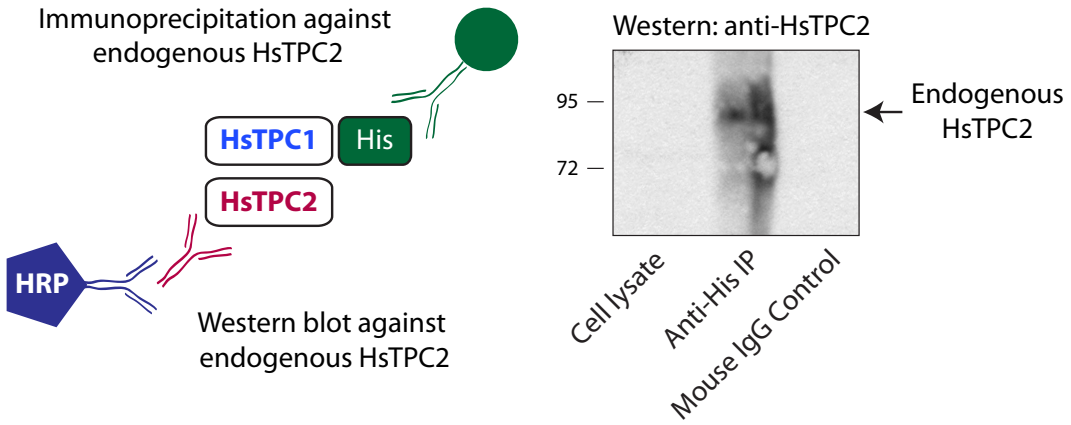


Figure 5.8: Endogenous HsTPC2 is coimmunoprecipitated with overexpressed His.HsTPC1. Left: Schematic depiction of the antibodies used: the immunoprecipitation was targeted against His tag, whilst the western blots were probed with an anti-HsTPC2 rabbit polyclonal (7050, see antibody table B.3) followed by an anti-rabbit IgG HRP conjugate. **Right:** Anti-HsTPC2 western blot depicting the presence of endogenous HsTPC2 in the immunoprecipitate, but not detected in the rat IgG control and cell lysate.

wild type cell. All immunoprecipitations had been optimised for both the endogenous HsTPC1 and HsTPC2 using in-house polyclonal rabbit antibodies. This proved problematic when investigating the endogenous interaction as rabbit antibodies used in the immunoprecipitation often contaminated the eluted samples and were subsequently recognised by the secondary anti-rabbit IgG antibody on the western blot.

This signal from contaminating IgGs masked any specific signals as can be seen in figure 5.9 which shows an example western blot where the cell lysate gave a clean endogenous HsTPC1 signal, but the IP elution was contaminated by IgG ($\approx$ 150 kDa).

Many attempts were made to overcome this problem. Covalently coupling the antibodies to the sepharose beads using DMT reduced the contamination to some extent, but dissociated IgGs were still present in the eluted sample. Commercially available secondary antibodies that were guaranteed to target only the rabbit light chain (25 kDa) were used to detect the primary antibody whilst any contaminating light chain IgG was run off the gel, however no signal was seen using this secondary (data not shown). Another brand claimed to only recognise the native rabbit IgG of the primary antibody, whilst not interacting with the contaminant that ought to have been

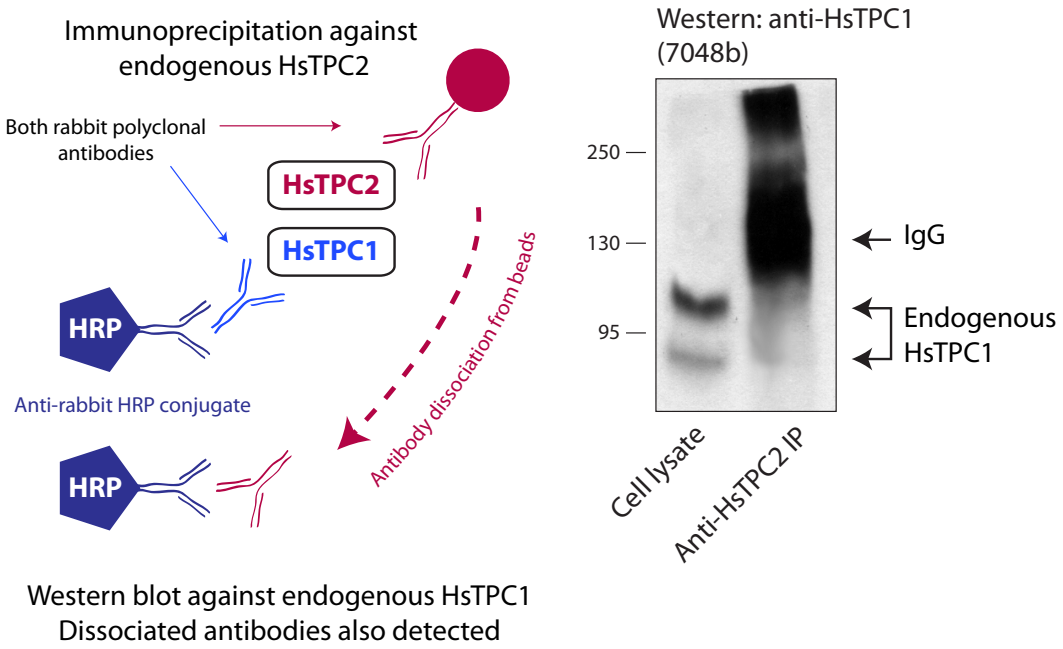


Figure 5.9: Antibody cross-reactivity masks endogenous signals. Left: Schematic depiction of the antibodies used: the immunoprecipitation was targeted against the two epitopes on HsTPC2 (7049), whilst the western blots were probed with an anti-HsTPC1 rabbit polyclonal (affinity purified 7048b) followed by an anti-rabbit IgG HRP conjugate. **Right:** Anti-HsTPC1 western blot depicting the presence of endogenous HsTPC1 in whole cell lysate, the HsTPC1 signal in the immunoprecipitate is obscured by IgG contamination.

denatured during SDS-PAGE, this gave non-specific bands in the control and a high background (data not shown). One alternative that was not tried was the biotinylation of the primary antibody probed with streptavadin HRP conjugate, this may provide a way of dissecting the specific band and reduce background.

This failure to distinguish endogenous HsTPCs gave the impetus to design new constructs with easily recognisable tags.

5.5 HsTPC constructs created for further analysis

All experiments thus far have been reliant on the stable cell lines (Zhu laboratory) and antibodies generated by the Galione group in Oxford. However, limitations in antibody specificity and requirements for localisation studies made it necessary to generate new HsTPC2 constructs which were tagged with the red fluorescent protein mCherry. Constructs were made to express the tagged protein at the carboxy terminus, as this ensures that the presence of the tag corresponds to the full-length expression of the HsTPC protein.

With this factor in mind and the fact that the Zhu constructs of HsTPC1.His and HA.HsTPC2 were in different expression vectors, new constructs were also made for both isoforms expressing the HA-tag at the caboxy terminus in the pcDNA5TO vector for consistency.

Constructs were based on the available IMAGE clones of HsTPCs (see methods section 2.16.1), there is one amino acid difference between the Zhu construct and the IMAGE HsTPC2 isoform (L484M). This is a minor substitution of two similarly sized amino acids, however the methionine introduces an additional thioether (-S-) group into the IMAGE construct which may result in a slightly altered protein structure.

These new constructs were confirmed by DNA sequencing and their expression checked by transiently transfecting the constructs into HEK293T cells. After 24 hours of expression, membranes were purified and solubilised. These were run on western blots to confirm the size of the protein matched the predicted molecular weight. Figure 5.10 depicts these western blots alongside membranes purified from cells transfected with the control vectors.

All constructs shown are of the correct molecular weight and the control vectors showed no signal. The larger bands in the HA western blot are due to glycosylation as

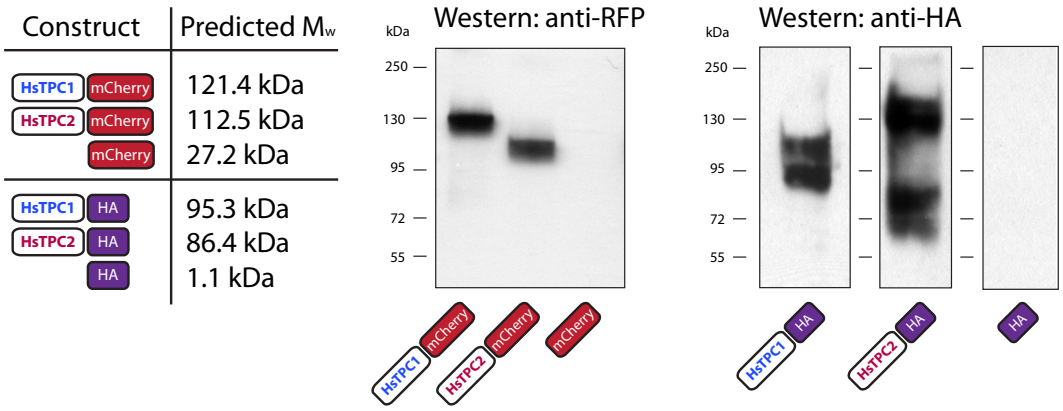


Figure 5.10: The mCherry- and HA-tagged HsTPC constructs. Left: The table lists the predicted sizes of the tagged-proteins which can be compared to the western blots. **Right:** Western blots of carboxy-tagged HsTPC constructs with mCherry and HA tags probed against RFP and HA respectively.

discussed in section 3.2, higher bands were also seen in longer exposures of the mCherry western blot (see figure 5.14).

5.6 Validating serum specificity

With these new constructs it was possible to conduct an essential control experiment to check that the in-house rabbit antibodies were able to distinguish between the two isoforms and that detection of coimmunoprecipitated HsTPCs was not simply due to antibody crossreactivity. To do this, it was essential to obtain a pure sample of each HsTPC and test every antibody on each isoform. Immunoprecipitation reactions were conducted using commercial anti-HA beads (Roche) against solubilised membranes from HEK293T cells expressing each HA-tagged isoform. Western blots were prepared from samples eluted with a harsh denaturing and reducing buffer (Laemmli buffer with 100 µM DTT) and the affinity purified antibodies were used to probe the blots.

Figure 5.11 depicts this procedure and the blots obtained. These demonstrate clearly that each anti-TPC antibody is highly specific for a single isoform as no immunoreactive bands can be seen when probing the alternative isoform.

Whilst this experiment confirms the specificity of the antibodies, it introduces a contradiction as it suggests that under these conditions there is no coimmunoprecipi-

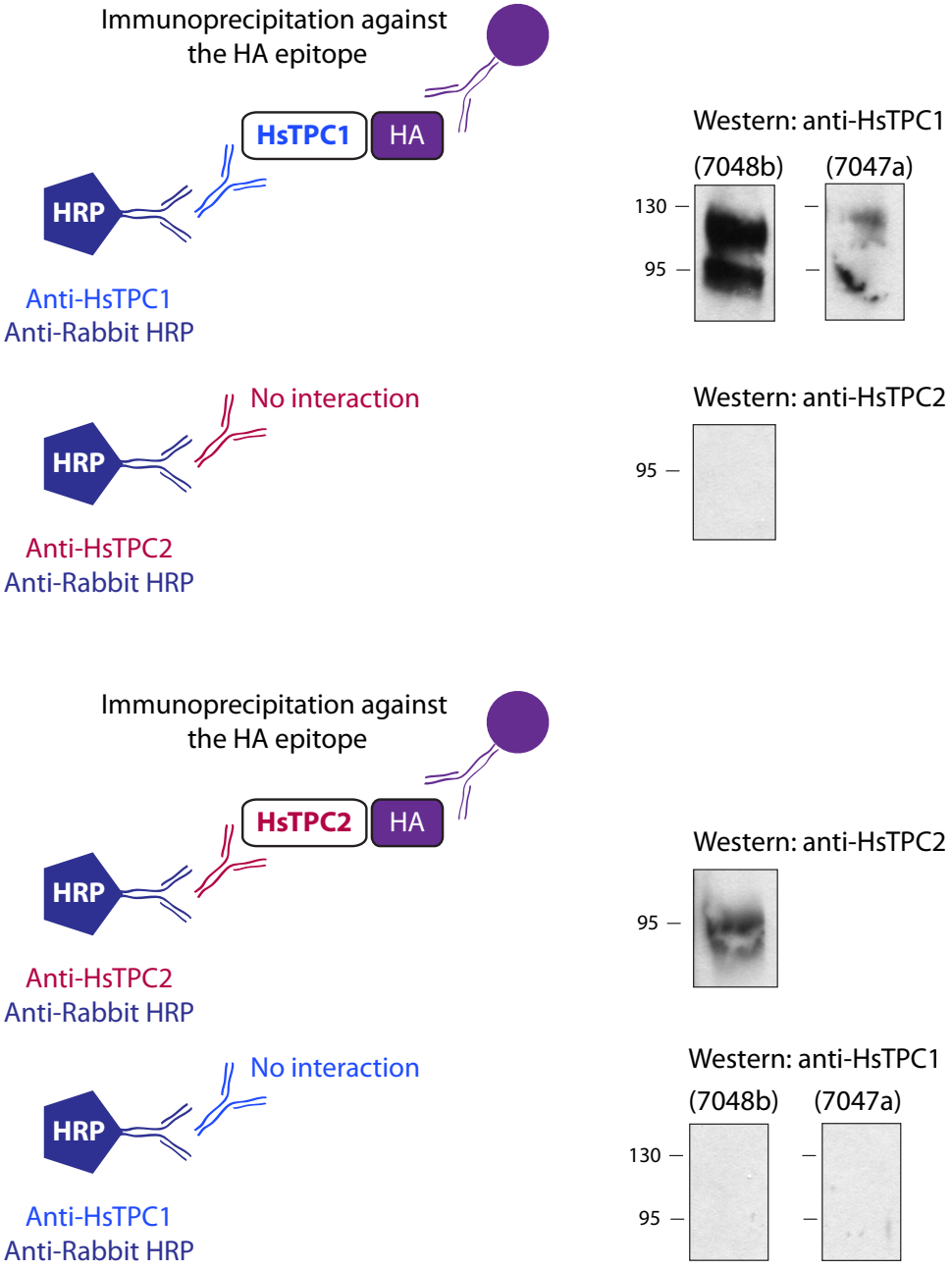


Figure 5.11: HsTPC antibodies are isoform specific for western blotting. Top: Immunoprecipitation against the HA tag on HsTPC1 and western blots against both isoforms. Left: Schematic depiction of the antibodies used. Right: Positive signals seen by both anti-HsTPC1 antibodies but not by anti-HsTPC2 antibody.
Bottom: Immunoprecipitation against the HA tag on HsTPC2 and western blots against both isoforms. Left: Schematic depiction of the antibodies used. Right: Positive signals seen by anti-HsTPC2 antibodies but not by the anti-HsTPC1 antibodies. All westerns were loaded with the total elutate (50 µl) from commercial HA beads treated with a denaturing buffer.

tation of the endogenous HsTPCs which are present in the cell line. This discrepancy can be explained by a difference in abundance. The new constructs are based in the pcDNA5TO expression vector which contains the SV-40 promoter. By transiently transfecting this construct into the HEK293T cell line which stably overexpresses the large T-antigen, these two components come together to encourage episomal replication of the vector DNA. More vector DNA results in more mRNA and thus large quantities of protein. The purification methodology for this experiment was also biased towards maximal protein yield rather than retention of complexes as the washes and elutions were more harsh. This resulted in vastly more HA-tagged HsTPC present than any coimmunoprecipitated endogenous protein, and hence the western blots easily detected the expressed protein but could not distinguish any endogenous protein.

5.6.1 Dimerisation of cotransfected constructs.

The variety of tags also allowed further studies into the coimmunoprecipitation of homodimeric interactions as each HsTPC isoform could be cotransfected with two differently tagged constructs: mCherry and HA. If homodimers formed then the immunoprecipitation of one tag would yield the presence of the opposite tag in the eluted complex. This was tried with all combinations of homodimers depicted in figure 5.12 and all combinations of heterodimers presented in figure 5.13.

The homodimerisation of both HsTPC1 and HsTPC2 was seen to be successful in every variant tried. Figure 5.12 shows three immunoprecipitations conducted on cells cotransfected with the mCherry-tagged and HA-tagged constructs of the same isoform. The elutions from these immunoprecipitations were probed by two western blots either against the HA tag or mCherry. Hence figure 5.12 contains both a positive control where one tag was the target of both the immunoprecipitation and the western, together with evidence of homodimerisation where an HA tag appeared in a mCherry immunoprecipitation and *vice versa*. The anti-HsTPC2 immunoprecipitation gave a positive signal for both tags.

Each immunoprecipitation was conducted alongside the relevant IgG control of a non-immune antibody from the same species as the specific antibody *i.e.* HA was controlled with a rat IgG, mCherry a mouse IgG and the HsTPC sera controlled with the pre-immune rabbit serum. It is worth noting that the antibody used to immunoprecipitate the mCherry constructs was a mouse monoclonal against DsRed (see appendix

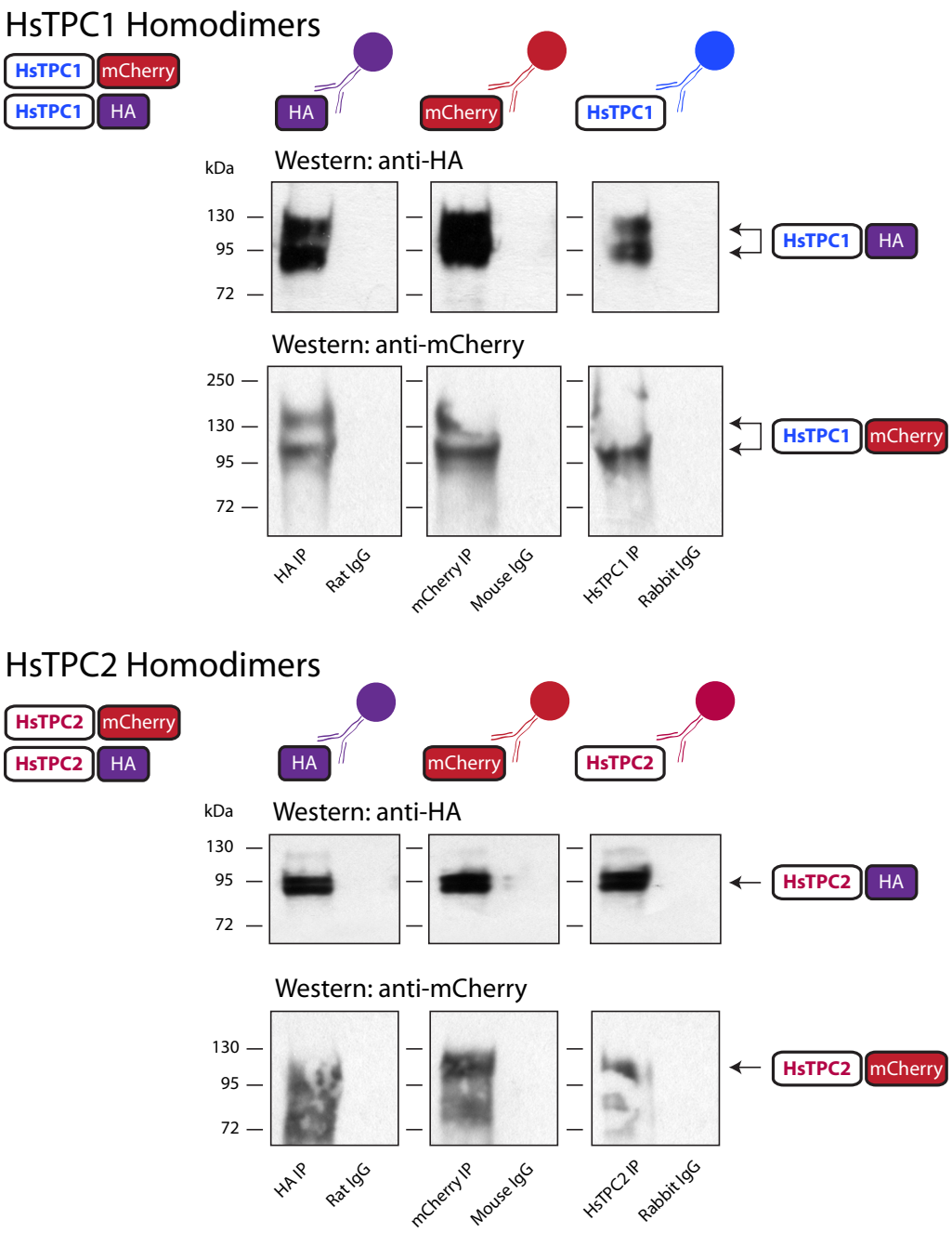


Figure 5.12: Immunoprecipitation and western blot of HsTPC homodimers. Anti-HA, anti-mCherry and anti-HsTPC immunoprecipitations conducted on transiently transfected cells, each with the relevant IgG control, probed for the HA-tag or mCherry by western blot. All IP-western combinations gave positive results. **Top:** Cells overexpressing mCherry-tagged HsTPC1 and HA-tagged HsTPC1. **Bottom:** Cells overexpressing mCherry-tagged HsTPC2 and HA-tagged HsTPC2.

table B.3), whereas the mCherry western blot was conducted using a rat monoclonal developed and kindly donated by Rottach *et al.* (373). This prevented antibody cross reactivity in the western blot.

Figure 5.13 shows the various coimmunoprecipitation-western results for putative heterodimers. As was seen in the stable cell lines, immunoprecipitations against one HsTPC invariably brought the other isoform with it. This data further confirms the conclusions made from coimmunoprecipitation from the stable cells lines (section 5.4) that heterodimers do form.

These results were reproducible to the extent that all combinations gave a positive coimmunoprecipitation-western signal (n = 3). However, quantitive comparison between western blots is difficult due to variation in exposure time and differences in antibody affinity. This makes it impossible to predict from these results whether homodimerisation or heterodimerisation is the more physiological combination.

Nonetheless this data confirms with two different tags that HsTPC2 forms homodimers, and is the first study to show homodimerisation in HsTPC1. Moreover, by various combinations of coimmunoprecipitation this data shows evidence of HsTPC1/HsTPC2 heterodimers which refutes suggestions by Zong *et al.* that the HsTPCs do not heterodimerise (478).

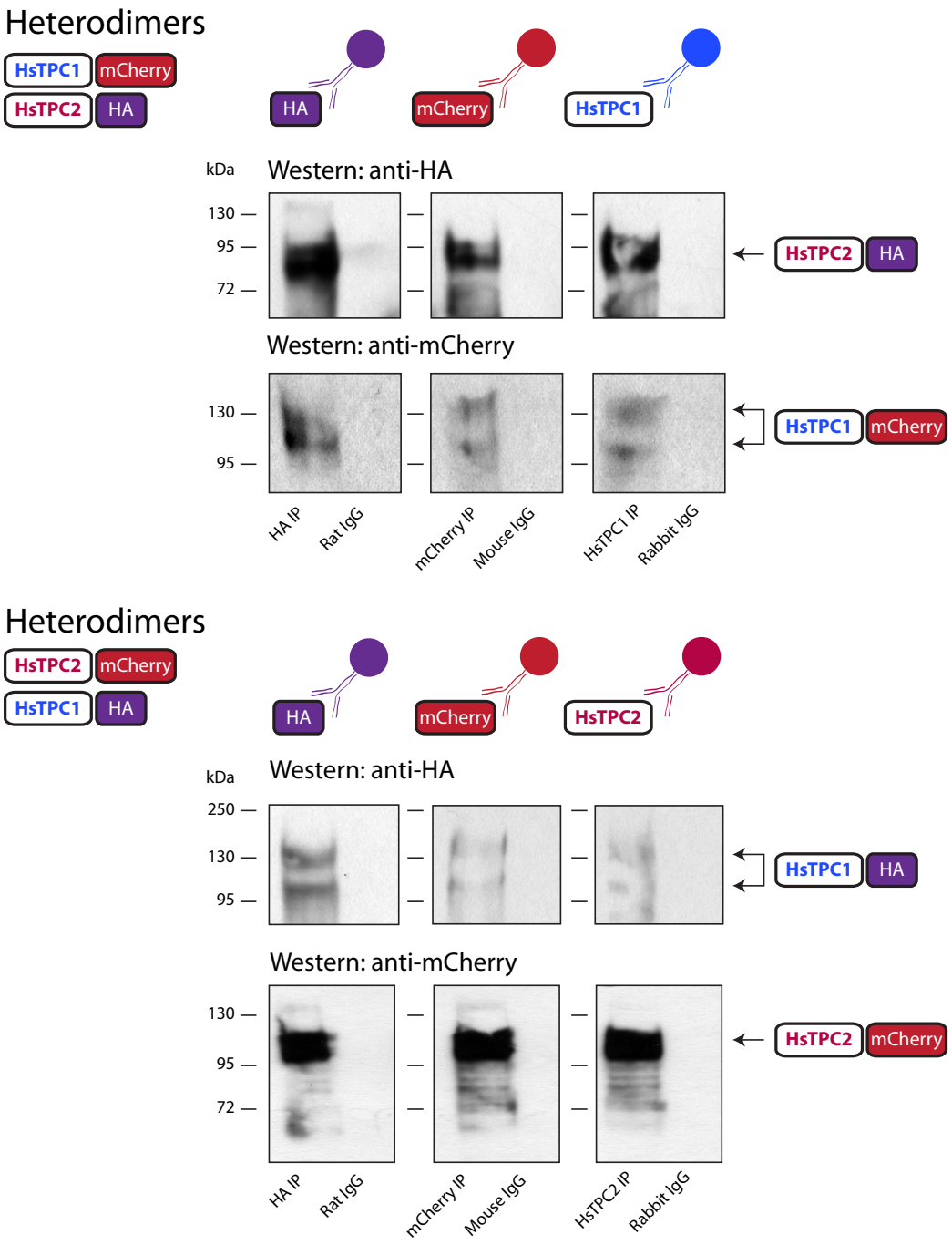


Figure 5.13: Immunoprecipitation and western blot of HsTPC heterodimers. Anti-HA, anti-mCherry and anti-HsTPC immunoprecipitations conducted on transiently transfected cells, each with the relevant IgG control, probed for the HA-tag or mCherry by western blot. All IP-western combinations gave positive results. **Top:** Cells overexpressing mCherry-tagged HsTPC1 and HA-tagged HsTPC2. **Bottom:** Cells overexpressing mCherry-tagged HsTPC2 and HA-tagged HsTPC1.

5.7 Dissecting the HsTPC western blot

An observation throughout the various western blots conducted on both isoforms of HsTPC was the frequent presence of an upper band approximately twice the size of the predicted molecular weight. When this was first seen, it was attributed to a non-specific aggregate due to the high hydrophobicity of the HsTPCs, and that the highly denaturing and reducing conditions of SDS-PAGE ought to have disrupted any dimer interactions. Figure 5.14 shows example blots of this higher band in long exposed western blots of both mCherry and HA tagged HsTPCs. These recent predictions of dimerisation between HsTPCs prompted an investigation into whether this band could perhaps be due to a robust HsTPC dimer.

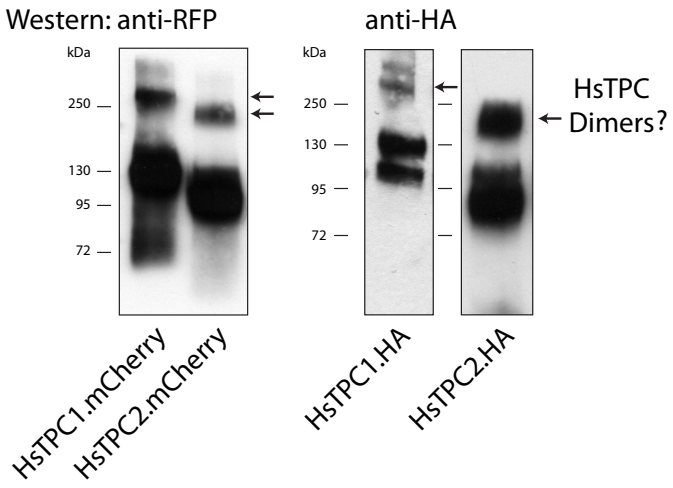


Figure 5.14: Higher molecular weight bands suggest dimerisation. Two western blots against tagged-HsTPCs demonstrating the presence of a high molecular band which may correspond to a HsTPC dimer. **Left:** mCherry-tagged HsTPCs probed with an anti-RFP antibody (see table B.3) and subsequent anti-rat HRP conjugate. **Right:** HA-tagged HsTPCs probed with anti-HA HRP conjugate.

A non-specific aggregate ought to show a generic molecular weight as the exact composition would be irrelevant. It is therefore intriguing that in figure 5.14 the high bands for HsTPC1 and HsTPC2 could be resolved with distinctly different masses, each of which corresponded with twice the mass of the respective monomer. This would strongly suggest that these bands were due to the presence of HsTPC dimers. Several attempts to break this possible interaction were made, however, prolonged treatment

with the reducing agent DTT did not affect these top band and boiling the samples magnified their intensity which suggests that they were simply due to aggregation upon denaturation.

From the conclusions made above, co-expression of both HsTPC1 and HsTPC2 would predict a western blot with three bands: the largest being a HsTPC1 homodimer, the smallest being a HsTPC2 homodimer and inbetween a HsTPC1/HsTPC2 heterodimer. This hypothesis was tested using a non-denaturing gel to preserve putative dimer interactions.

Figure 5.15 shows a series of western blots from samples run on PFO PAGE, where PFO (Perfluoro-octanoic acid) is a non-denaturing detergent which replaces SDS. The samples consisted of solubilised membranes from cells expressing the HA-tagged HsTPCs either alone or in combination. This resulted in just a single high band being seen in each sample, no 'monomer' bands were seen. As there still seems to be a distinction in the molecular masses seen in HsTPC1 and HsTPC2 this may suggest strict homodimerisation; however this would imply that two homodimer signals ought to be seen in the coexpressed cells, which they were not.

These results remain ambiguous and protein biochemistry cannot rule out with certainty that the observed dimers do not result from non-specific interactions due to methodological limitations. Therefore experiments were focused on cell biological and biophysical approaches to study the extent of isoform interactions. To investigate the possibilities of an *in situ* interaction, the subcellular localisation of the fluorescently labelled HsTPCs was compared.

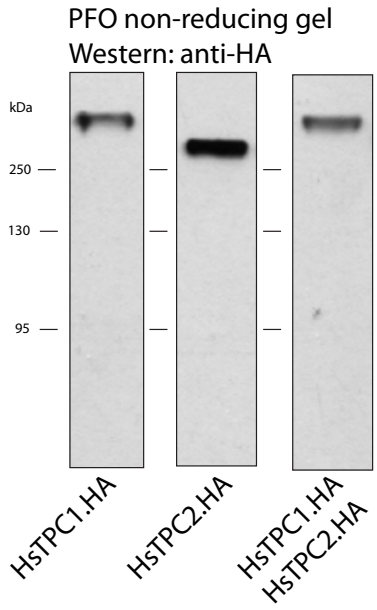


Figure 5.15: Non-denaturing gel does not distinguish multiple dimer bands. Western blots conducted against the HA tag on samples expressing both HsTPC isoforms singularly or combined. All blots show a high molecular weight band above the resolution of the protein ladder. Normal monomer bands were not seen.

5.8 Subcellular localisation of HsTPCs

Many studies have already been conducted on the localisation of the TPCs from various species and in various cell lines. The results of these studies are summarised in table 5.3. However, it was essential to check the localisation with these new constructs and to express both the HsTPC1 and HsTPC2 under directly comparable conditions. HEK293 cells were cotransfected with an mCherry-tagged HsTPC along with one of the following GFP-tagged organelle markers: LAMP1, a marker for the lysosome (122); early endosome antigen 1 (EEA1), which identifies the early endosome (27); the transferrin receptor (TfR1) which identifies recycling endosomes (116); and KDEL, a four amino-acid motif which targets proteins to the ER (427).

An array of images was taken by confocal microscopy and the colocalisation determined for each cell by the Pearson coefficient for mCherry overlaping with GFP. Figure 5.16 displays a representative example image for each marker construct coexpressed with mCherry-tagged HsTPC1. These images show that whilst there is some overlap with the marker proteins, HsTPC1 does not seem to be confined to one organelle in particular. Figure 5.16 also shows the scatter plots of all the cells analysed and the mean colocalisation coefficient. From these plots, HsTPC1 seems to be prevalently located to the recycling endosome or lysosome.

This result correlates with the work in the SKBR3 cells (47) and HEK293 cells (55) where HsTPC1 was shown to have a disparate existence being present in both endosomes and lysosomes to a substantial degree. This confirms that the disparate localisation of the mCherry-tagged HsTPC1 construct is a common occurrence and reinforces data regarding the endo-lysosomal targeting of HsTPC1.

The HsTPC2 localisation was more distinct, with a strong overlap with the lysosomal marker LAMP1 in almost all cells whilst significantly lower levels of overlap with the other markers. Figure 5.17 depicts representative examples of confocal images and combines the colocalisation coefficients for multiples cells into a scatter plot. Again this correlates with previously reported data which show substantial overlap with both LAMP1 and LAMP2 in HEK293 cells and SKBR3 (47, 55).

Species	Isoform	Tag	Cell line	Expression	Marker used	Organelle	Colocalisation	Reference
Hs	1	GFP	SKBR3	Transient transfection	KDEL	ER	–	(47)
Hs	1	mRFP	Xl Oocytes	Microinjection	RFC	Plasma membrane	–	(47)
Hs	1	GFP	Xl Oocytes	Microinjection	RhoB	Endosomes	✓	(47)
Hs	1	GFP	Xl Oocytes	Microinjection	LAMP1	Late endosomes & Lysosomes	✓	(47)
Hs	1	GFP or His	HEK293	Stable	LAMP2	Late endosomes & Lysosomes	✓✓	(55)
Hs	1	GFP or His	HEK293	Stable	M6PR	Late endosomes	✓✓	(55)
Hs	1	GFP or His	HEK293	Stable	EEA1	Early endosomes	✓✓	(55)
Hs	1	GFP or His	HEK293	Stable	TfR1	Recycling endosomes	✓✓✓	(55)
Hs	1	GFP	SKBR3	Transient transfection	LAMP1	Late endosomes & Lysosomes	✓✓✓	(47)
Hs	1	mRFP	SKBR3	Transient transfection	Endo	Early & Late endosomes	✓✓✓	(47)
Mm	1	EGFP	HEK293	Transient transfection		Plasma membrane & nuclei	✓	(478)
Sp	1	GFP/mCherry	SKBR3/HEK293	Transient transfection	LysoTracker	Acidic stores	✓✓✓	(49, 375)
Sp	1	GFP	Xl Oocytes	Microinjection			Intracellular	(49)
Hs	2	mRFP	Xl Oocytes	Microinjection	RFC	Plasma membrane	–	(47)
Hs	2	GFP	SKBR3	Transient transfection	KDEL	ER	–	(47)
Hs	2	mRFP	SKBR3	Transient transfection	Endo	Early & Late endosomes	–	(47)
Hs	2	mRFP	SKBR3	Transient transfection	RFC	Plasma membrane	–	(50)
Hs	2	HA	HEK293	Stable	EEA1	Early endosomes	–	(55)
Hs	2	HA	HEK293	Stable	DPI	ER	–	(55)
Hs	2	HA	HEK293	Stable	GM130	Golgi apparatus	–	(55)
Hs	2	HA	HEK293	Stable	CytC	Mitochondria	–	(55)
Hs	2	HA	HEK293	Stable	M6PR	Late endosomes	✓	(55)
Hs	2	GFP	Xl Oocytes	Microinjection	LysoTracker	Acidic stores	✓✓✓	(333)
Hs	2	HA	HEK293	Stable	LysoTracker	Acidic stores	✓✓✓	(55)
Hs	2	-	HEK293	Endogenous	LAMP2	Late endosomes & Lysosomes	✓✓✓	(55)
Hs	2	GFP	SKBR3	Transient transfection	LAMP1	Late endosomes & Lysosomes	✓✓✓	(47)
Hs	2	HA	HEK293	Stable	LAMP2	Late endosomes & Lysosomes	✓✓✓	(55)
Mm	2	-	COS-7	Transient transfection	Mitotracker	Mitochondria	–	(478)
Mm	2	EGFP	HEK293	Transient transfection		Plasma membrane & nuclei	–	(478)
Mm	2	-	COS-7	Transient transfection	Calnexin	ER	✓	(478)
Mm	2	HA	HEK293	Stable	LysoTracker	Late endosomes & Lysosomes	✓✓✓	(55)
Mm	2	HA	HEK293	Stable	LAMP1	Late endosomes & Lysosomes	✓✓✓	(55)
Mm	2	HA	HEK293	Stable	LAMP2	Late endosomes & Lysosomes	✓✓✓	(55)
Mm	2	-	COS-7	Transient transfection	LAMP1	Late endosomes & Lysosomes	✓✓✓	(478)
Sp	2	GFP/mCherry	SKBR3/HEK293	Transient transfection	LysoTracker	Acidic stores	✓✓✓	(49, 375)
Sp	2	GFP	SKBR3	Transient transfection	LAMP1	Late endosomes & Lysosomes	✓✓✓	(49)
Sp	2	GFP	Xl Oocytes	Microinjection			Intracellular	(49)
Sp	3	GFP/mCherry	SKBR3/HEK293	Transient transfection	LysoTracker	Acidic stores	✓✓✓	(49, 375)
Sp	3	GFP	Xl Oocytes	Microinjection			Intracellular	(49)
Gg	3	GFP	HEK293	Stable	LAMP2	Late endosomes & Lysosomes	✓	(55)
Gg	3	GFP	HEK293	Stable	M6PR	Late endosomes	✓	(55)

Table 5.3: Summary of published TPC localisation. Localisation determined by intrinsic fluorescence of protein tags and markers or by immunocytochemistry. Table sorted by isoform and by species: Hs - *Homo sapiens*, Mm - *Mus musculus*, Sp - *Strongylocentrotus purpuratus*, Gg - *Gallus gallus*, Xl - *Xenopus laevis*.

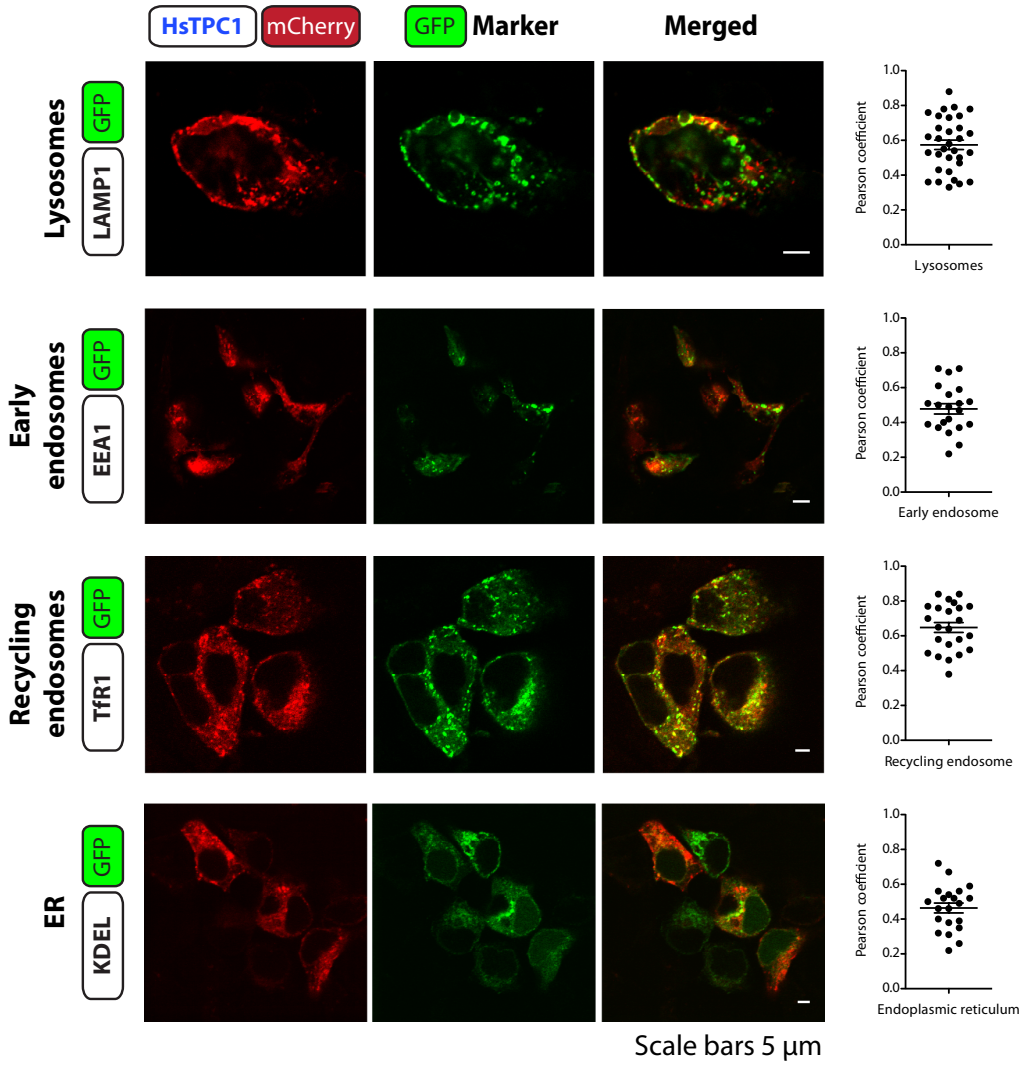


Figure 5.16: Colocalisation of HsTPC1 with GFP-tagged organelle markers. Representative confocal microscope images from fixed cells transiently coexpressing mCherry-tagged HsTPC1 (red) and GFP-tagged LAMP1, EEA1, TrR1 and KDEL (green). The merged images (yellow) give an indication as to the extent of colocalisation. The scatter plots beside the images depict the extent of colocalisation (Pearson). Each point represents one cell (n = 21 - 32).

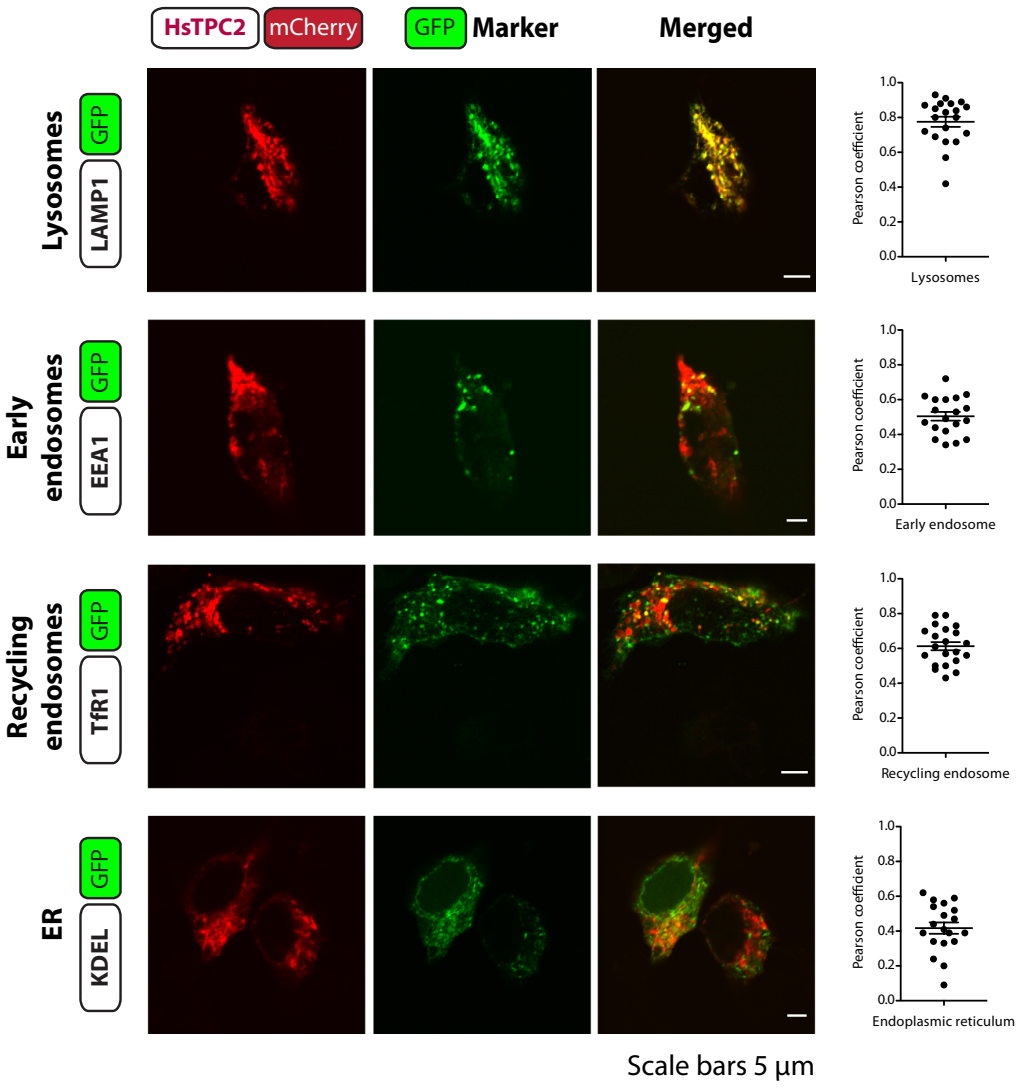


Figure 5.17: Colocalisation of HsTPC2 with GFP-tagged organelle markers. Representative confocal microscope images from fixed cells transiently coexpressing mCherry-tagged HsTPC2 (red) and GFP-tagged LAMP1, EEA1, TrR1 and KDEL (green). The merged images (yellow) give an indication as to the extent of colocalisation. Scatter plots beside the images depict the extent of colocalisation (Pearson). Each point represents one cell (n = 18 - 21).

5.9 Colocalisation of HsTPCs

As both HsTPCs show some element of lysosomal localisation, the question arises at to whether both isoforms are expressed in the same lysosomes or are divided into distinct vesicles. If the theory of heterodimerisation is to be upheld there ought to be an element of HsTPC1/HsTPC2 overlap.

HA-tagged and mCherry tagged HsTPCs were coexpressed in HEK293 cells, which were then fixed and treated for immunofluorescence against the HA epitope (labelled green). Both combinations were tried, with each HA-tagged and mCherry-tagged HsTPC being expressed with the opposite isoform with the opposite tag. The results showed huge variation, so for each combination two images are shown in figure 5.18 to give an example of a strong and weak overlap. The colocalisation coefficient chart for each combination is depicted alongside and demonstrates the extent of the variation.

Such heterogenous colocalisation may reflect the dynamic nature of the endoslysosomal system, whereby vesicles are perpetually fusing and hybridising (260, 346). Whilst HsTPC2 seems resolutely in the lysosomal domain, HsTPC1 can be seen within the membranes of a range of vesicles and therefore must face constant relocation which will inevitably dictate the relationship with HsTPC2 and this may result in distinctive functional roles.

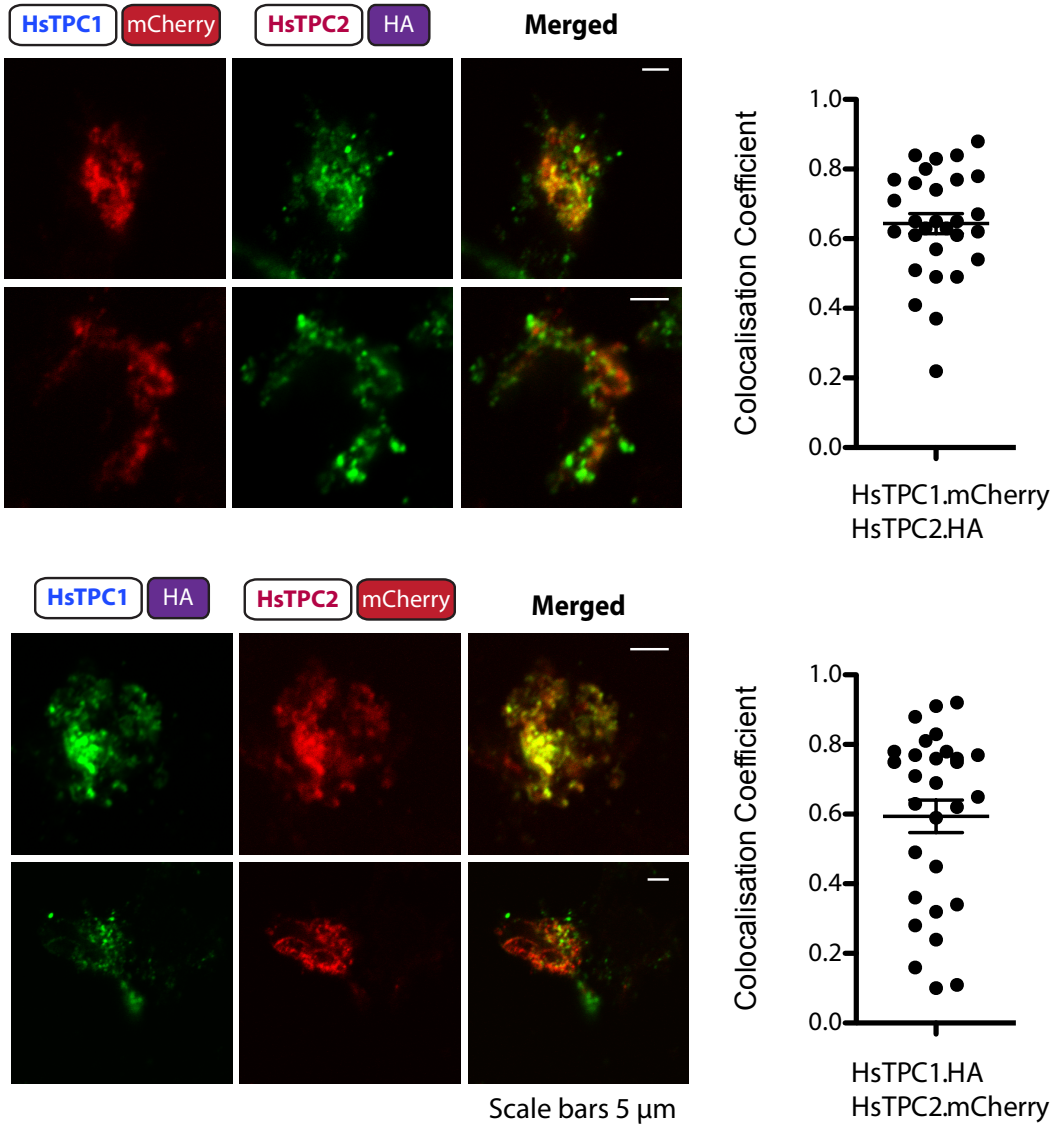


Figure 5.18: Colocalisation of tagged HsTPCs. Top: Confocal images depicting the variation seen across cells coexpressed with mCherry-tagged HsTPC1 (red) and HA-tagged HsTPC2 (green). The scatter plot compiles the colocalisation coefficients of all cells (n = 29) to give a mean coefficient of 0.64 ± 0.03. **Bottom:** As above but with the constructs expressing the opposite tags *i.e* HA-tagged HsTPC1 (green) and mCherry-tagged HsTPC2. The mean coefficient for this combination was 0.59 ± 0.05, (n = 29). HA-constructs were localised by an anti-HA rat monoclonal followed by an anti-rat alexa 488 conjugate. All cells were fixed with 0.01 % paraformaldehyde.

5.10 FRET

To dissect out those HsTPCs that are directly interacting *in situ*, microscopy techniques based on fluorescence/Förster resonance energy transfer (FRET) were conducted on fluorescently tagged HsTPCs. This technique has a greater resolution than immunofluorescence and differentiates between proteins which are present together in the same membrane from those which are within the same quaternary complex.

Constructs were made which tagged HsTPCs with two variants of the green fluorescent protein, the cyan-fluorescent and yellow-fluorescent proteins (CFP and YFP) (430). These two proteins function as a donor-acceptor pair, whereby the emission spectrum of the donor molecule (CFP) overlaps with the absorption spectrum of the acceptor (YFP). The excitation and emission spectra of CFP and YFP are superimposed in figure 5.19 with the shaded region depicting the overlap between the the CFP emission and YFP excitation; it is this overlap which allows FRET to take place. Provided that the HsTPC proteins are in close enough proximity for energy transfer to occur (< 10 nm) this would result in the excitation of the donor protein causing an emission from the acceptor protein.

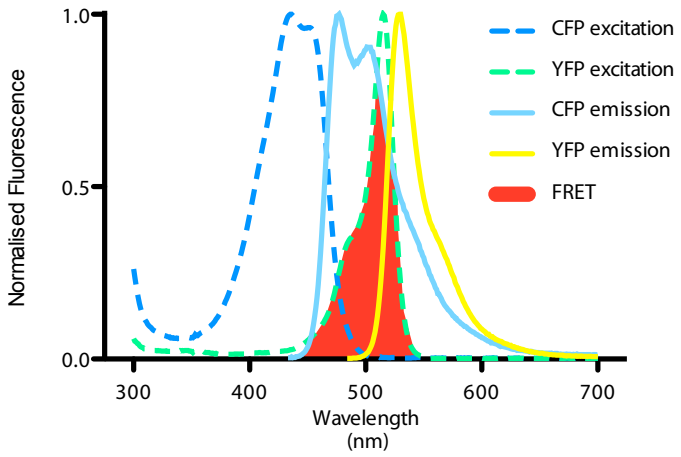


Figure 5.19: The excitation and emission spectra of CFP and YFP. Superimposed traces of CFP and YFP excitation (dashed lines - blue and green respectively) and emission (solid lines - cyan and yellow respectively). Where the CFP emission overlaps the YFP excitation this region is shaded red. This overlap allows energy transfer from CFP to YFP hence FRET.

FRET is a commonly used technique to monitor protein-protein interactions (350) and was hoped to confirm an interaction between the HsTPC isoforms. Constructs were made to express the FRET pair proteins at either the amino- or carboxy- terminus, this allowed various combinations of interaction to study the orientation of potential homo- and heterodimers. These constructs were verified by DNA sequencing which resulted in all four tag-variations of the HsTPC2 being successful; however, the full set of constructs is lacking the amino-tagged HsTPC1 with CFP as subcloning failed after multiple attempts. Figure 5.20 depicts the construct configuration and predicted molecular weight, alongside western blots from purified and solubilised HEK293T membranes transiently transfected to express these constructs.

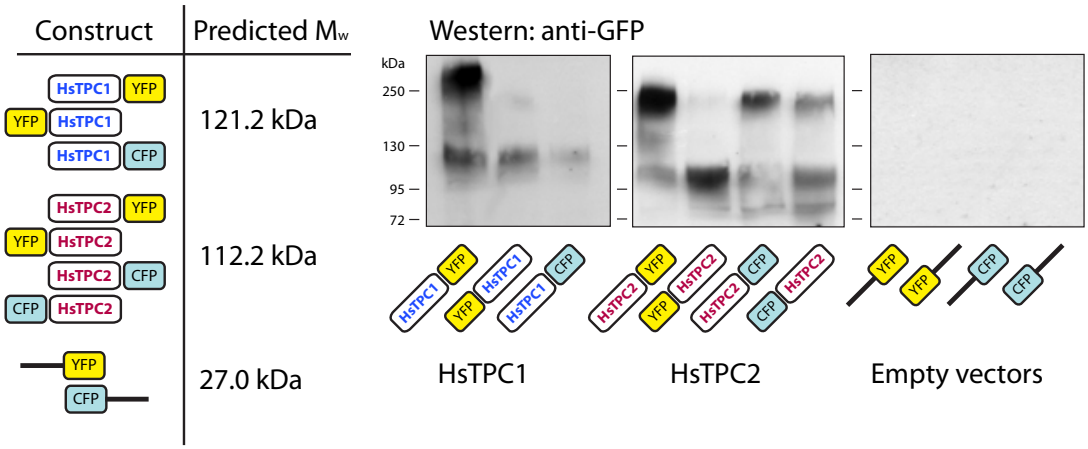


Figure 5.20: CFP- and YFP-tagged HsTPC constructs. Left: The table lists the predicted sizes of the tagged-proteins which can be compared to the western blots. **Right:** Western blots of amino- and carboxy-tagged HsTPC constructs with CFP and YFP tags probed with a GFP HRP-conjugate antibody.

Whilst there is a reasonably high level of background these westerns confirm that the tag-HsTPC fusion proteins were expressed at the correct size with some demonstrating a potential high molecular weight dimer band.

5.10.1 The orientation of dimerisation

There are two orientations possible in the formation of HsTPC dimers: either the two partners interact 'head-to-tail' with the carboxy-terminus of one HsTPC interacting

with the amino-terminus of the dimer partner (rotational symmetry of two); alternatively they arrange 'head-to-head' and both HsTPCs effectively mirror their partner.

For the studies on HsTPCs it was assumed that the head-to-tail, rotational symmetry orientation was most likely and thus for FRET to occur the fluorescent proteins would need to be on opposite ends *i.e.* the amino-terminus of one HsTPC protein and the carboxy-terminus of the other. This assumption was based on the structure of VGCC which show rotational symmetry (64).

5.10.2 Localisation of CFP and YFP constructs

Before progressing with direct FRET measurement, the localisation of the new CFP/YFP constructs was verified by treating cells transiently expressing the tagged HsTPCs and measuring colocalisation with LysoTracker red (a marker for acidic stores). From previous studies, lysosomal HsTPC2 ought to localise tightly with this marker, whilst endosomal HsTPC1 ought to partially overlap (table 5.3).

Figure 5.21 depicts the three HsTPC1 constructs all of which show a punctate distribution, but these punctae show little overlap with the LysoTracker signal. The population data scatter chart shows that the mean colocalisation was significantly lower than HsTPC1 overlap with the GFP-LAMP1 marker (0.57 $\pm$0.03) for both the carboxy-terminal tagged constructs (CFP: 0.25 $\pm$ 0.05, YFP: 0.37 $\pm$ 0.05), whilst the amino-terminal YFP construct averaged slightly higher than anticipated (0.71 $\pm$ 0.04). This may be due to mistargeting of the carboxy-terminal tagged HsTPC1 or simply due to variations in HsTPC1 localisation which seems to be the more dynamic isoform.

HsTPC2 gave a more reliable overlap across all constructs, showing punctate distribution (Figure 5.22) and colocalisation coefficients comparable to the mCherry/LAMP1 study in figure 5.17 (0.76 $\pm$0.03). The mean across all CFP/YFP constructs was 0.72 $\pm$ 0.02 (n = 70). This reliably confirms that these constructs are mainly localised to the lysosome.

5.10.3 Sensitised FRET

Sensitised Emission FRET involves simple measurements of fluorescence intensity in three channels which measure the CFP emission, the YFP emission and the FRET emission. To measure the CFP emission, the proteins were excited using a laser at 458 nm, emission was detected between 473 - 612 nm, for the YFP emission the laser

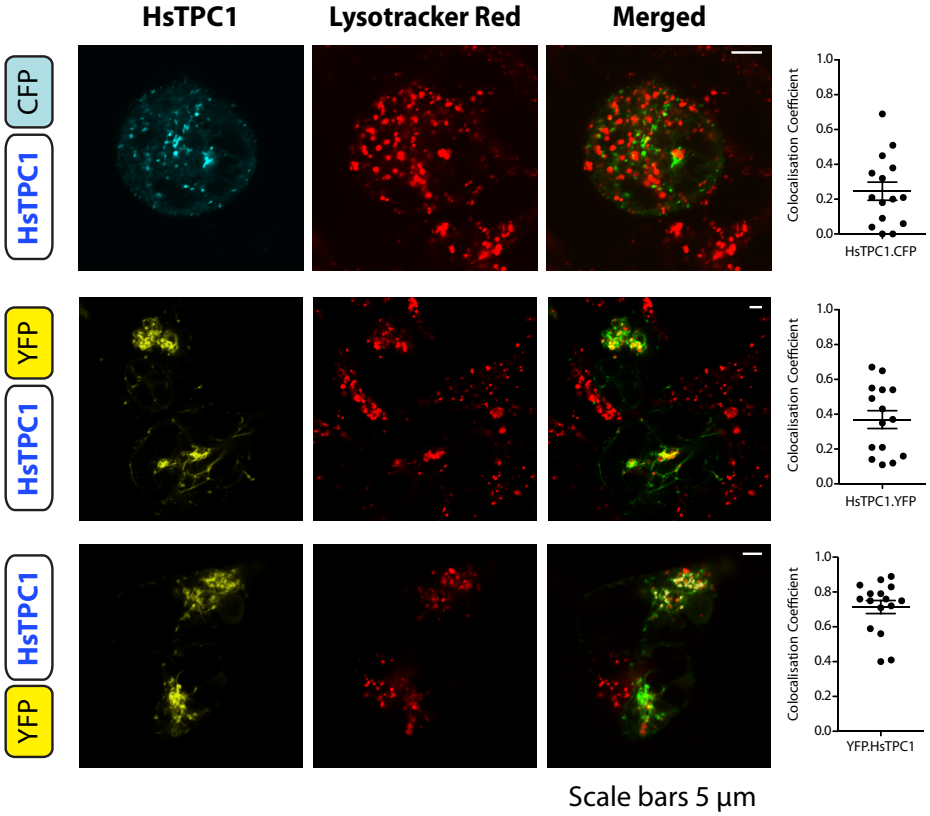


Figure 5.21: Colocalisation of HsTPC1 constructs with LysoTracker. Example images and scatter plots showing the extent of colocalisation with fluorescently tagged-HsTPC1. CFP-tagged (blue) and YFP-tagged (yellow) constructs are displayed in the left hand column, LysoTracker red localisation (red) in the central column and the merged channel is on the right. Both CFP/YFP are depicted as green in the merged channel and yellow when colocalised with LysoTracker. Scatter plots display the mean colocalisation coefficient ± S.E.M. These were: HsTPC1.CFP = 0.25 ± 0.05, HsTPC1.YFP = 0.37 ± 0.05, YFP.HsTPC1 = 0.71 ± 0.04. (n = 15 - 16).

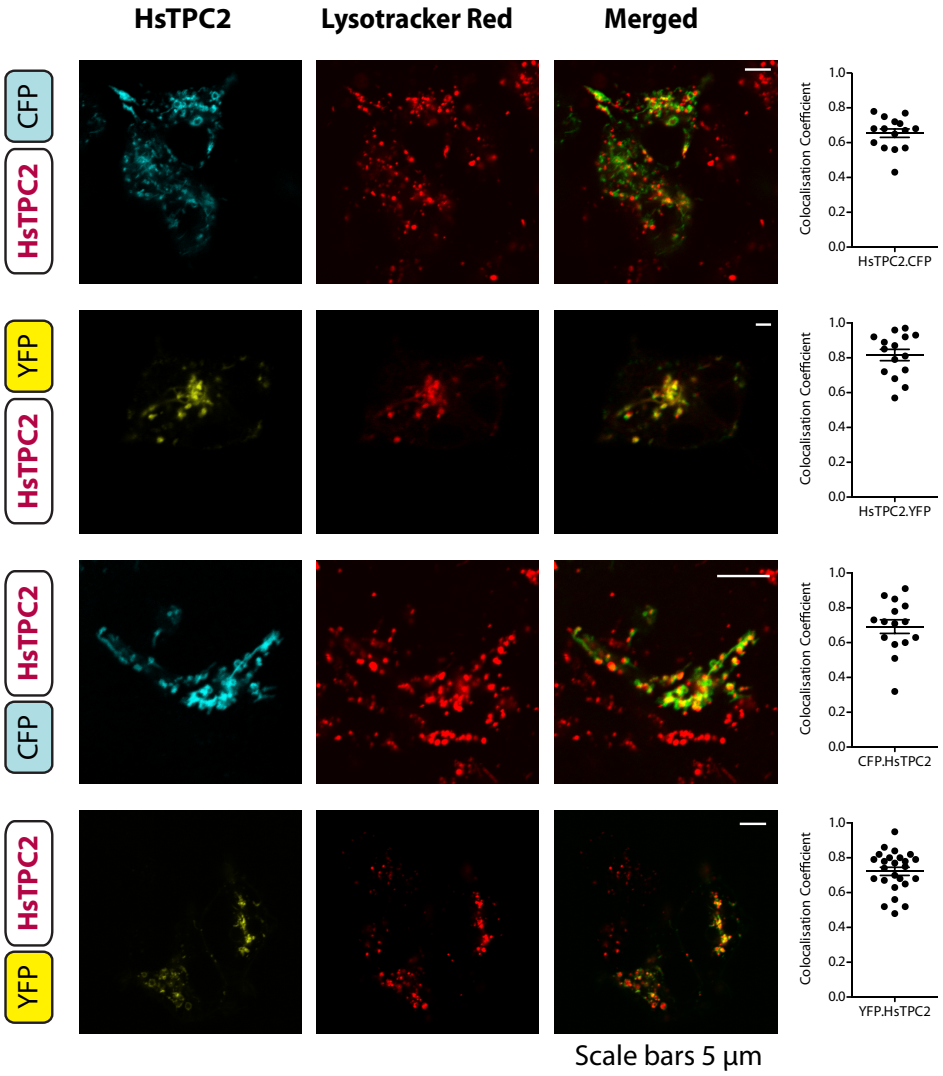


Figure 5.22: Colocalisation of HsTPC2 constructs with LysoTracker. Example images and scatter plots showing the extent of colocalisation with fluorescently tagged-HsTPC2. CFP-tagged (blue) and YFP-tagged (yellow) constructs are displayed in the left hand column, LysoTracker red localisation (red) in the central column and the merged channel is on the right. Both CFP/YFP are depicted as green in the merged channel and yellow when colocalised with LysoTracker. Scatter plots display the mean colocalisation coefficient ± S.E.M. These were: HsTPC2.CFP = 0.65 ± 0.02, HsTPC2.YFP = 0.81 ± 0.03, YFP.HsTPC2 = 0.72 ± 0.02, CFP.HsTPC2 = 0.69 ± 0.04.

used was 514 nm and detection between 530 - 600 nm. The FRET channel involved the excitation of CFP and the emission of YFP, hence this was excited with the 458 nm laser but the detection range was widened to collect more signal (> 505 nm). Figure 5.23 displays this information on three spectral plots.

Before FRET measurements were recorded, the extent of channel bleedthrough needed determining. This was achieved by measuring fluorescence intensities in all three channels on cells that either expressed CFP-only or YFP-only. There was an inevitable low level of bleedthrough seen in the FRET channel in both cell types, the ratio of bleedthrough to true signal could be calculated and later subtracted from any FRET measurement.

Figure 5.24 depicts example images and describes how these calculations were made. Coefficient A reflects the CFP bleedthrough into the FRET channel as a proportion of the total CFP signal and was determined in CFP-only cells (n = 13). This gave the coefficient of CFP bleedthrough as 0.25 $\pm$0.11. Coefficient B reflects the ratio of YFP bleedthrough into the FRET channel compared to total YFP signal in YFP-only cells (n = 8), this was 0.18 $\pm$0.04. Previous reports prescribe successful FRET measurements for values of coefficient A $<$ 0.2 and coefficient B between 0.1 - 0.4 (158), so here the CFP bleedthough is marginally higher than recommended. Attempts to reduce the amount of bleedthrough included a shift in the FRET detection range to slightly higher wavelengths, however this resulted in drastically reduced FRET measurements and it was decided that the bleedthrough was less detrimental to the results.

To calculate the normalised FRET signal (FRETN), the average intensity of the FRET channel needed to be corrected for the contributions from CFP and YFP bleedthrough. This signal was then normalised across all cells for the concentrations of CFP and YFP expressed.

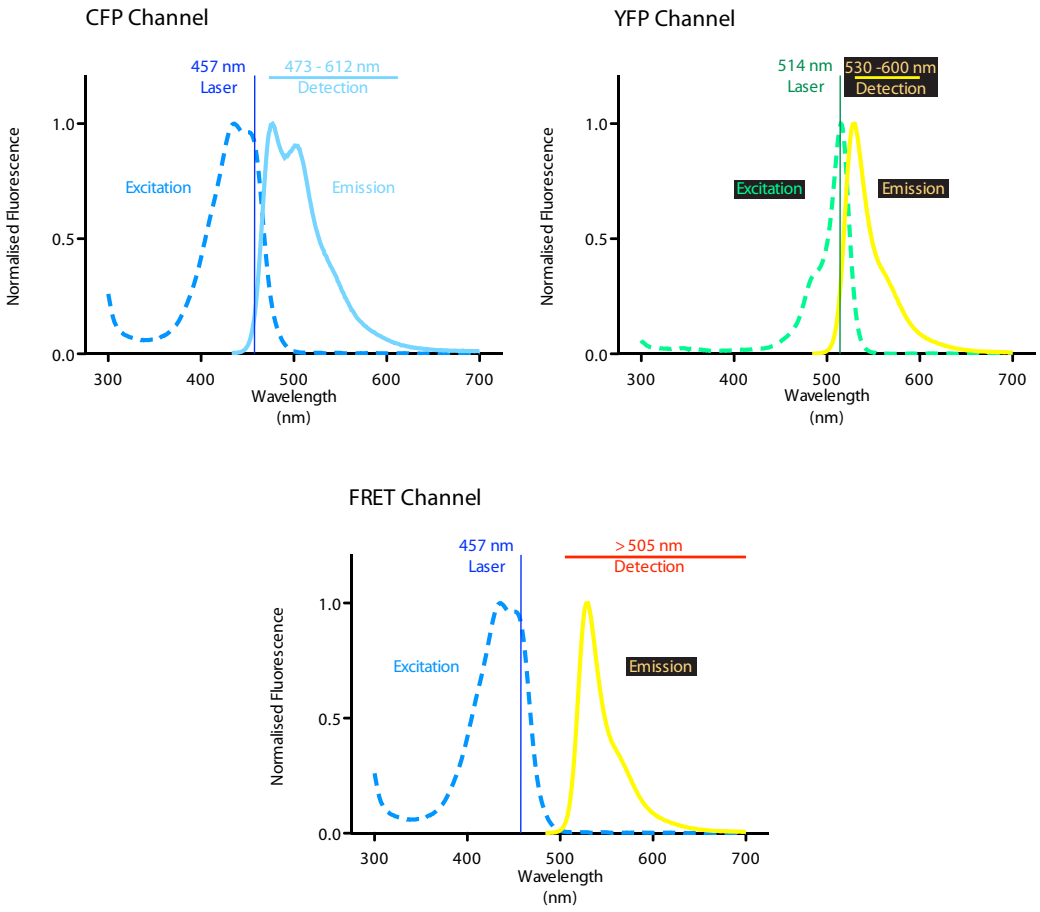


Figure 5.23: Parameters for FRET measurements. Three channels used to record FRET measurements, excitation laser and detection range superimposed on CFP/YFP excitation and emission spectra. **Top Left:** CFP Channel: excited by the 457 nm laser line and detected between 473 - 612 nm. **Top Right:** YFP Channel: excited by the 514 nm laser line and detected between 530 - 600 nm. **Bottom:** FRET Channel: CFP excited by the 457 nm laser line, YFP emission detected $>$ 505nm.

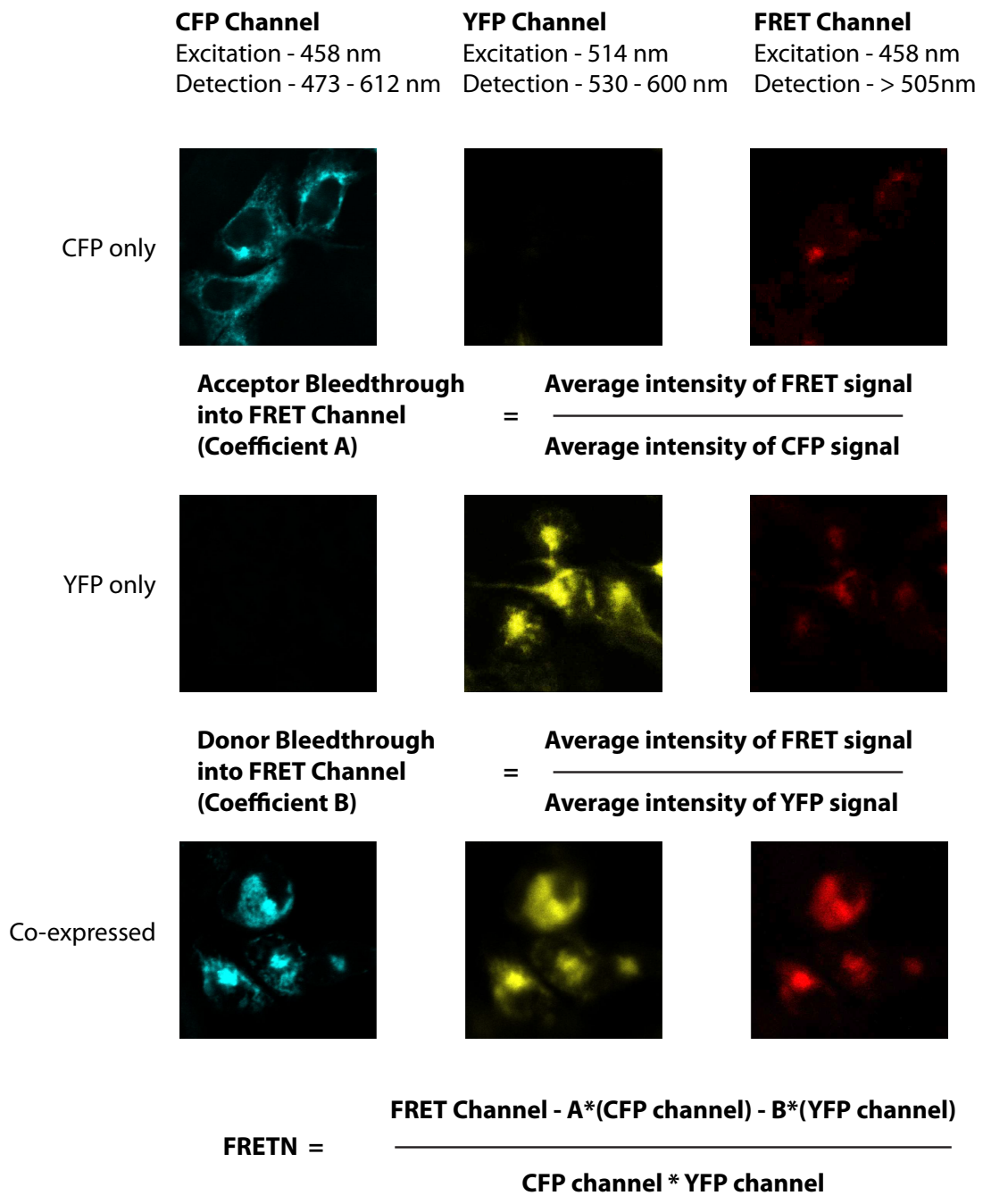


Figure 5.24: FRETN - sensitized FRET measurement. Example images from the three channels portraying the calculations required for FRETN. Average intensity refers to the arbitrary intensity value per pixel and is the average per cell.

5.10.4 HsTPC homodimers

Analysis of FRETN signals were conducted with two separate cotransfections and included 6 - 8 cells for each combination of constructs. All graphs are accompanied by a schematic depiction of the assumed HsTPC conformation formed by the cotransfected constructs, these are aligned beneath the FRETN signal seen for that conformation.

Looking initially at FRET between homodimers, the results of HsTPC1 interactions are shown in figure 5.25. The fact that a significant FRETN signal was seen positively confirms an interaction between two HsTPC1 proteins, where one expresses the YFP-tag and the other the CFP-tag, hence HsTPC1 homodimers do form. Moreover, the stronger FRETN signal was seen in cells expressing the FRET-pair on opposite ends of the HsTPC1 protein. Whereas if the FRET-pair were both on the same end of the HsTPC1 (carboxy-terminus) negligible signal was seen. This supports the 'head-to-tail' orientation of HsTPC1 in dimer formation.

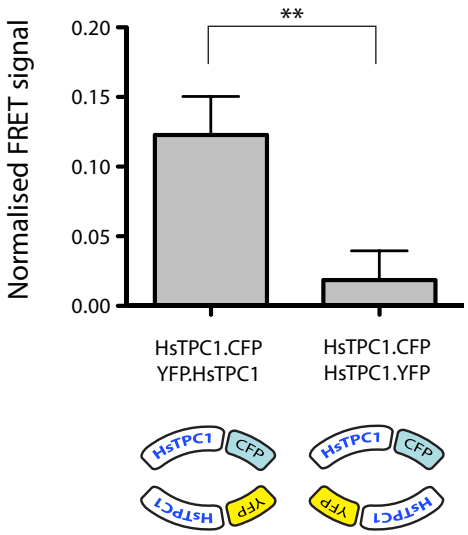


Figure 5.25: Population data of sensitised FRET in HsTPC1 homodimers. Two combinations of HsTPC1 constructs representing the two possible orientations of the fluorescent tags in homodimers. (n = 13 - 15). ** $p < 0.01$.

This result was further confirmed by analysis of the HsTPC2 FRETN signals. Those positive conformations gave a higher absolute level of FRET (almost double the HsTPC1 signal), perhaps suggesting a stronger tendency for HsTPC2 to dimerise,

due to the more consistent localisation. The array of HsTPC2 constructs allows four combinations to investigate dimer orientation, these are depicted in figure 5.26. Statistics were conducted comparing each CFP construct with a pair of YFP constructs tagged at alternate ends.

If the CFP/YFP pair was expressed on opposite ends of the HsTPC2, a FRET signal was seen, whereas if they were at the same end on both proteins no interaction was seen. This result also suggests that HsTPC2 forms a closed loop as FRET is seen when the CFP/YFP pair is expressed on either the amino- or caboxy-termini of either HsTPC2.

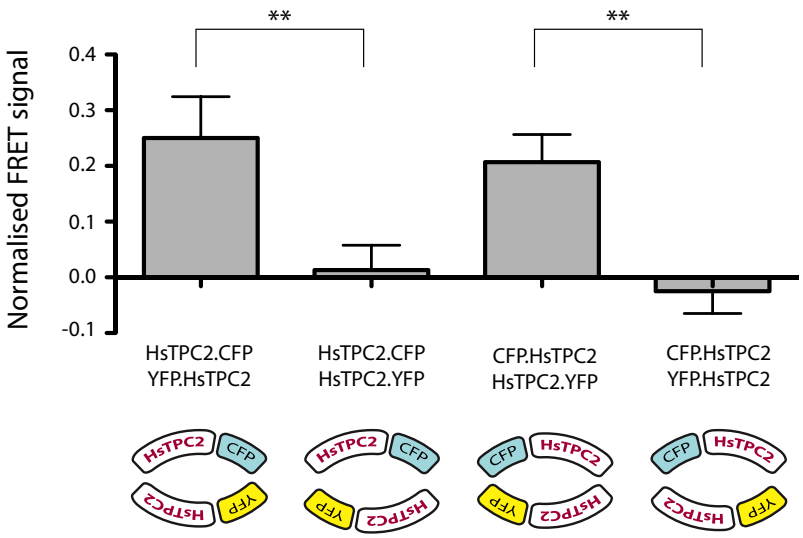


Figure 5.26: Population data of sensitised FRET in HsTPC2 homodimers. Four combinations of HsTPC2 constructs representing the two possible orientations of the fluorescent tags in homodimers. (n = 15 - 16). ** $p < 0.01$.

5.10.5 HsTPC heterodimers

The obvious next question was to cotransfect a combination of HsTPC1 and HsTPC2 labelled with the FRET pair to determine the extent of heterodimerisation. Six different combinations were possible, half of which would form heterodimers expressing the FRET pair on opposite ends and half on the same end. The results are shown in figure 5.27 and analysed with respect to the CFP construct. FRET was not seen in

the majority of combinations, just one combination produced a significant FRET signal, albeit 4-fold lower than the HsTPC2 signals. This positive combination, however, followed the same orientation prediction as with the homodimers, whereby the FRET pair were on opposite ends which supports a head-to-tail orientation.

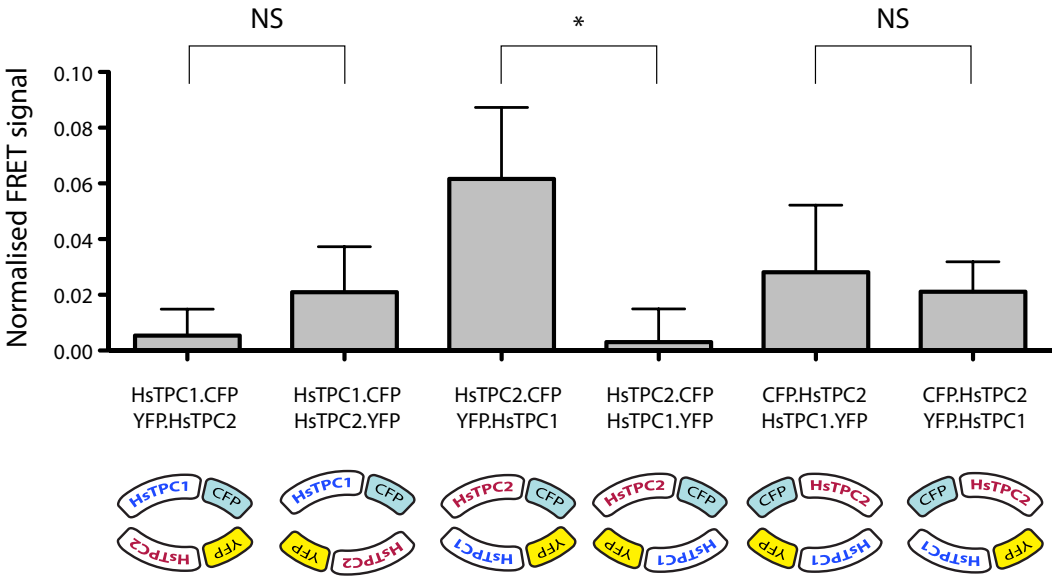


Figure 5.27: Population data of sensitised FRET in heterodimers. Six combinations of HsTPC1 and HsTPC2 constructs representing the two possible orientations of the fluorescent tags in heterodimers.(n = 12 - 15). $*$ $p < 0.05$, NS - not statistically significant.

5.10.6 Potential pitfalls

This simple FRET study predicts that not only do HsTPC1 and HsTPC2 proteins form homodimers, there is a suggestion of heterodimerisation too. One of the reasons that so few of the heterodimer combinations produced FRET signals was perhaps due to the lack of predicted colocalisation; the carboxy-tagged CFP and YFP HsTPC1 variants showed vary little overlap with LysoTracker, whilst all HsTPC2 variants showed a strong lysosomal localisation - if these proteins are in different organelle membranes then there should be no FRET signals. Thus the only heterodimeric interaction suggested was with the YFP.HsTPC1 which showed a strong lysosomal localisation. This would allow significant interaction with HsTPC2 and the potential for dimerisation.

The fact that all FRET signals were only seen when the CFP/YFP pair were expressed on opposite ends gives a reasonable indication of the orientation of any dimers formed. Assuming a lack of flexibility in the HsTPC tail regions, this would mean that the carboxy-terminus and amino-teminus of the two proteins interact, and the easiest way for this to occur would be that the two proteins form a loop. This fits with models of the VGCCs where the four domains wrap into a circle (64), and the two domains in each HsTPC replicate this and come together to form a homologous pore.

Whilst FRET can only occur where proteins interact with a separation of < 10 nm, it would be a useful control to check that these FRET signals are indeed due to dimerisation rather than simply a tight interaction of clustered channels within the lysosomal membrane. CFP/YFP variants of a known lysosomal protein *e.g.* LAMP1 should not give FRET signals when coexpressed with CFP/YFP HsTPCs, and this control would add strength to these results.

Another method to determine the reliability of these FRETN signals was to conduct acceptor photobleaching on these FRET pairs.

5.11 Acceptor photobleaching FRET

Sensitized and normalised FRET is a heavily processed measurement, with each stage accumulating errors. As a means of checking FRETN results acceptor photobleaching can be used to confirm interactions. This involves the denaturation of the acceptor molecule (YFP) by intensive stimulation, to destroy its fluorescence. By photobleaching the acceptor fluorophore, this has the effect of dequenching the donor (CFP) fluorescence, and as it can no longer transfer energy to the acceptor it must emit the energy as additional fluorescence (296). This method (119) was straightforward to implement and involved very few controls and little image processing. The FRET signal was recorded under static conditions and was expressed as a percentage of the CFP emission after acceptor bleach. Figure 5.28 shows an example experiment and the calculations required to obtain FRET efficiency.

5.11.1 CFP photobleaching

CFP/YFP constructs were transfected as before with the various combinations of constructs. Images were taken of the cell before and after a harsh photobleaching regime

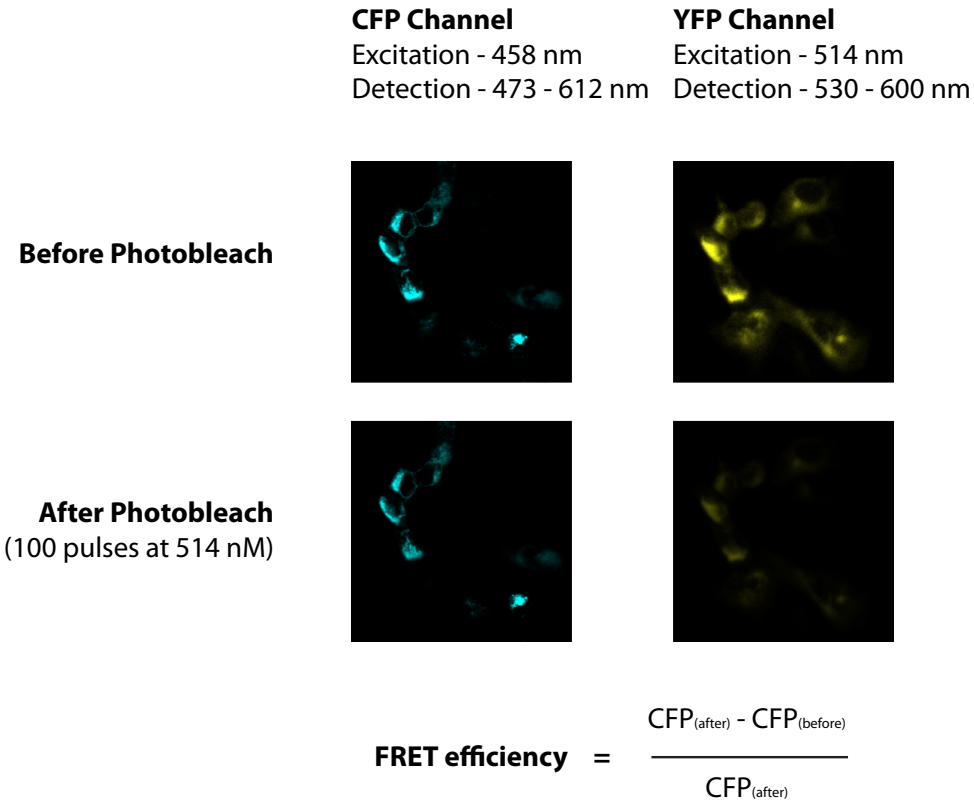


Figure 5.28: Acceptor photobleaching in cells coexpressing YFP/CFP-tagged HsTPCs. Example images demonstrating the effects of photobleaching on typical cells and portraying the calculations required in the measurement of FRET photobleaching. CFP_{before} and CFP_{after} refer to the average CFP fluorescence intensity per cell, before and after photobleaching respectively. Photobleaching consisted of 100 pulses of the 514 nm laser at 100% power.

of 100x scans of the 514 nm laser at maximum power. This resulted in acceptor photobleaching which eliminated an average of 92.6 ± 5.3% of YFP emission (n = 88). Whilst this should not have considerably affected the CFP signal, there is a small overlap of the CFP excitation spectrum with the 514 nm laser and some photobleaching was noted in the CFP channel. Whilst a reduction in the number of 514 nm pulses reduced this CFP-bleaching, it never fully abolished the YFP signal.

The control cells expressing CFP-only were subjected to the photobleaching regime and showed a mean diminished signal of 33.4 ± 11.2% (n = 8). However, the data shown in subsequent graphs (figures 5.29 to 5.31) demonstrate that this CFP bleaching was inconsistent across the constructs, perhaps due to differences in protein expression level or the subcellular localisation affecting the spectral properties of CFP.

5.11.2 HsTPC dimers

Figure 5.29 depicts the levels of FRET determined by photobleaching in HsTPC1 expressing cells. Where the CFP/YFP pair was expressed on opposite ends, an increase in CFP fluorescence was seen, however with the other orientation extensive CFP-photobleaching was seen.

It is worth mentioning that the CFP photobleaching was exaggerated by an initially low CFP signal whereby a small change results in a large percentage change. This is further augmented by the way in which FRET efficiency by acceptor photobleaching is calculated (figure 5.28). The standard calculation normalises data by dividing by the CFP intensity *after* photobleaching. If CFP is photobleached this number becomes smaller, therefore the resulting efficiency becomes larger.

Notwithstanding these concerns, the results of the HsTPC2 constructs are depicted in figure 5.30. Those combinations which gave strong sensitized FRET signals resulted in a positive increase in CFP fluorescence after YFP-photobleaching, whilst those thought not to interact closely enough have reduced fluorescence. The difference is significant and in concordance with the FRETN data.

Finally, the heterodimer studies again show the most variation with most combinations giving insignificant differences between combinations. Once again only one combination seems to suggest the occurrence of FRET and this contains the YFP.HsTPC1 construct which suggested a high level of lysosomal localisation.

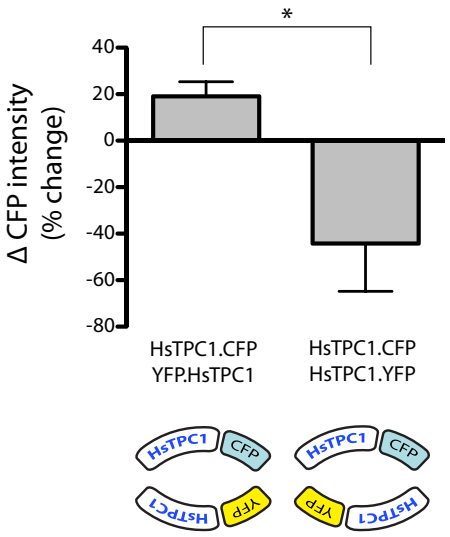


Figure 5.29: Population data of HsTPC1 acceptor-photobleached FRET. Two combinations of HsTPC1 constructs representing the two possible orientations of the fluorescent tags in homodimers. (n = 8 - 9). $*$ p < 0.05.

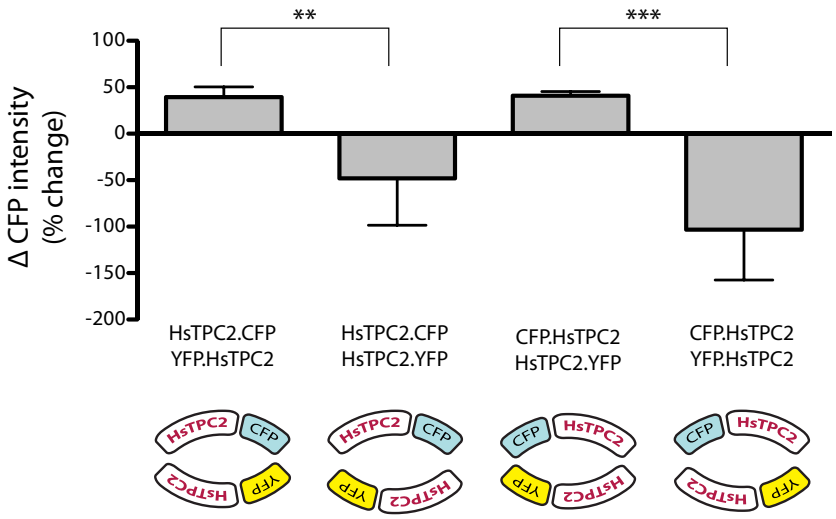


Figure 5.30: Population data of HsTPC2 acceptor-photobleached FRET. Four combinations of HsTPC2 constructs representing the two possible orientations of the fluorescent tags in homodimers. (n = 6 - 11). $**$ p < 0.01, $***$ p < 0.001.

All statistical analysis shown compares each CFP construct with the two YFP constructs of opposite orientations. However, as YFP.HsTPC1 is thought to be a factor in governing the positive signal in this heterodimer configuration, the analysis can be swapped to compare the YFP construct with the two CFP constructs with opposite orientations. In this case, there is still a significant difference with a p value < 0.01.

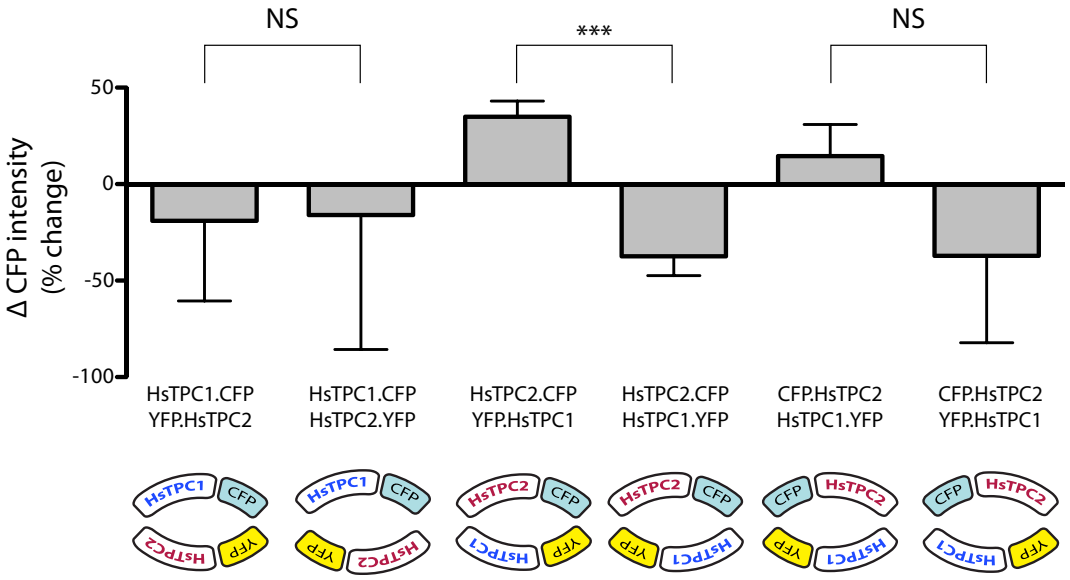


Figure 5.31: Population data of HsTPC1 and HsTPC2 acceptor-photobleached FRET. Six combinations of HsTPC1 and HsTPC2 constructs representing the two possible orientations of the fluorescent tags in heterodimers.(n = 5 - 9). *** $p < 0.001$, NS - not statistically significant.

5.11.3 Controls and concerns

The photobleach study has many concerns. The extent of CFP photobleaching, although exaggerated by the scale of the numbers, should not be occurring. Further optimisation of the photobleaching regime, perhaps with a lower laser power, or altered filter set may help to reduce CFP bleaching. These results were also recorded on 8-bit images, which intrinsically gives greater variation in intensity measurements, future studies ought to be recorded with 12-bit images, as this would give more consistent and reliable data.

Another control that ought to be included is the concomitant recording of YFP-photobleaching with the increased CFP fluorescence. During the photobleaching regime the extent of CFP recovery ought to linearly correlate with decaying YFP fluorescence. In these experiments photobleaching of the CFP was seen, which means that this correlation evidently could not have been occurring. However, it seems that any increase in fluorescence due to FRET outweighed the bleaching effect.

This photobleaching protocol requires more troubleshooting and optimisation of conditions, however these preliminary results back up the data shown in sensitised FRET and further supports the existence of HsTPC2 homodimer and potential heterodimer formation.

5.12 Discussion

Taken together the data here strongly suggests that an interaction exists between two HsTPC proteins to form a dimeric channel, as predicted. Caveats were highlighted in each methodology used, and if taken individually the coimmunoprecipitation, colocalisation and FRET studies cannot definitively rule out that the observed dimers do not simply result from technical imperfections. However, three separate studies resulting in the same conclusions, strengthen the hypothesis.

5.12.1 Homodimerisation

Predictions based on the channel homology with VGCCs have suggested homodimerisation of TPCs when TPC1 was first cloned from rat kidney (199). The first empirical evidence that homodimers of HsTPC2 could form was shown by coimmunoprecipitating overexpressed HsTPC2 with two different epitope tags (478).

Data shown here confirmed this interaction by immunoprecipitation of HsTPC2 with two different tags in a different stable cell lines. Furthermore, HsTPC1 homodimers have been proposed. FRET analysis supports these conclusions and suggests that homodimerisation is preferred over heterodimerisation as stronger FRET signals were seen.

Related proteins also show homo-multimerisation of protein subunits to form the ubiquitous 24-TM domain channel pore. The best example of this is seen in the TRP family where most mammalian TRP proteins form homomeric tetramers (4x 6-TM domains) (381). However, this is not exclusive, with many of the TRP family forming tight hetero-tetrameric interactions within their subgroup. The only channel so far shown to be exclusively made of one subtype is the TRPC2 (381) as this still shows channel activity when co-expressed with dominant-negative subunits and cannot be seen to coimmunoprecipitate with other isoforms (186). A strong preference towards homomers is also seen in many of the TRPV family, with TRPV3 and TRPV4 only showing weak coimmunoprecipitation with other isoforms in overexpressing cells (178)

Further afield, there is also a preference for homo-tetramerisation of RyR (405) and IP_3R (139, 307), with most native proteins composed of four same isoform subunits. However, these channels have also been shown to form heteromeric channels (301, 450).

5.12.2 Heterodimerisation

The heteromeric interaction between HsTPC1 and HsTPC2 isoforms was proven by two separate immunoprecipitations analysed by mass spectrometry. This was supported by consistent coimmunoprecipitations analysed by western blot and in one case FRET signals were seen between the two tagged-isoforms. On the other hand, poor colocalisation of the two HsTPC isoforms would suggest only limited interaction, and the majority of coexpressed constructs showed insubstantial FRET signals. There is also the doubt seeded by the fact that Zong *et al.* did not see coimmunoprecipition in their cell line (478). Taken together this suggests that an interaction is possible, but not common.

Hetero-multimerisation can be seen in most Ca^{2+} channels and in some cases (CNG (392) & CatSper (357) channels) is preferred. However, studies investigating the interaction of channel subunit isoforms often lack physiological relevance, due to high levels of overexpression in cells which would not normally coexpress both isoforms. Authors frequently admit that whilst heteromultimerisation can be seen, it is probably not the native channel state (178, 248). HsTPCs are likely to conform to this theory, as the separate subcellular localisation suggests that whilst heterodimers can form, homodimers are probably more relevant *in vivo*.

The most closely related protein to the TPCs is the CatSper isoform 2 (84) (see figure 1.12, page 29). CatSper2 is composed of a single pore 6-TM domain (364) and is thought to form a functional channel by tetramerising with the three other CatSper isoforms (1, 3 & 4 together with accessory proteins Catsperβ, γ, δ) (255). Intriguingly these channels seem to be exclusively heteromeric and require all four isoforms present (357). Although the other CatSper isoforms are more distantly related, their interactions with CatSper2 may allude to mechanisms of multimer formation in HsTPCs (100).

Another useful comparison is that of the TRPMLs which not only are related to TPCs but also expressed in the lysosomal membrane (85). TRPML1 has been shown to form both homotetramers and heterotetramers with TRPML2 and TRPML3 (100, 440). This has been shown to govern the conductance state of the final TRP channel (100) with current amplitudes following the pattern: heteromers containing 1&2 > 1&1 > 1&3.

Ryanodine receptor heterotetramers also showed an altered conductance state when in heteromeric configurations, this was shown by introducing a mutant RyR1 isoform which showed negligible Ca^{2+} conductance and loss of cation selectivity. Heteromeric channels exhibited intermediate channel properties and reduced Ca^{2+} selectivity over wild type (451).

Another salient feature of heterodimers relevant to the HsTPCs is shown in the IP_3R (205, 301, 317), where each subunit individually contributes to the overall receptor ligand-affinity (200), thus the heteromeric composition of the channel determines the concentration-response relationship.

The cyclic nucleotide gated (CNG) channels are more closely related to TPCs than IP_3Rs, because the CNG channels contain the homologous 6-TM pore domain. Whilst some CNG channels can form homomeric channels (CNGA1,2 & 3) all subunits preferentially form heterotetramers (337, 474). The permutations of various subunit combinations produce heteromeric channels with different biophysical and pharmacological properties. These differences include: cyclic nucleotide affinities; ion-selectivity; and regulation by Ca^{2+} (213, 283).

Taken together, these studies suggest that formation of HsTPC heterodimers may play a role in channel regulation by altering channel conductance, ion selectivity or even ligand sensitivity.

5.12.3 Orientation of interaction

Based on the homology with the voltage gated Ca^{2+}channels (64), which is turn is based on the known structure of the voltage gated K^+ channel (201), the channel pore of a 24-TM channel is assumed to have four degrees of rotational symmetry. This would suggest the TPCs interact head-to-tail.

Homology can also be seen in the single domain TRP channels, which are known to tetramerise to form the pore (381). Whilst most studies assume a rotational symmetry (131, 248, 388), a few suggest that tetramerisation is governed by interaction via carboxy-terminus tails (142, 186). A study into the carboxy-terminal kinase-like domain of TRPM7 was the first substructure of a TRP channel fragment that has been crystallized and solved (456). This fragment was shown to form dimers which would require the rotational symmetry of channel to be abandoned in this domain. These studies either suggest that the TRP channels have a range of conformations,

or they possess a flexible carboxy tail which allows the pore forming regions to maintain a rotational symmetry whilst the carboxy-tails twist and interact with a different symmetry.

The CNG channels also highlight an interesting structural property relevant to the TPCs. As mentioned above, each subunit of these channels has the 6-TM pore domain common to VGCC-family; electron microscopy of purified CNG channel from bovine retina revealed that the four domains present in each channel form two distinct 12-TM domains reminiscent of the structure of TPC (183). Therefore the final CNG channel structure is a dimer of dimers (183). This symmetry seems to have been lost at the level of the 24-TM VGCCs (306), but TPCs may sit as an intermediate between the CNG structure and full channel structure.

Furthermore, investigation into the interaction of CNG dimers shows that these channels preferentially interact head-to-tail, with the carboxy terminus of one subunit interacting with the amino terminus of the next (371, 439). This would support the FRET study result whereby HsTPCs only gave FRET signals when the fluorescent tags were on opposite ends of the two subunits.

5.12.4 HsTPC-HsTPC interaction

Analogy to other channels may also help predict how the TPCs are interacting to form dimers. In TRP channels most evidence so far points to important roles of the N and C terminal tails (67, 120, 142), however, some studies also show interaction via transmembrane motifs (178, 452).

N-terminal ankyrin repeats have been proposed in TRPV6 as a putative subunit 'zipper', and fragments of N-terminal tails have been shown to interrupt tetramer formation and knock out channel function (120). Whereas in TRPV1, yeast two-hybrid and pull-down studies implicate the C-terminal tail subunit interaction (142). Also TRP channels show transmembrane interactions modelled on parallel structures in K^+ channels (KcsA, Kir-Bac 1.1 and K_VAP) which have shown large inter-subunit contacts via pore loops and TM segments (178, 452).

Bioinformatic analysis of the CatSper family have identified alpha-helical coiled coil structural motifs on the C-terminal tails of the channel subunits, and these are thought to be essential in tetramerisation (255). This assumption is based upon the heterotetrameric core structure of the SNARE complex (121).

Investigating the tail regions of the HsTPCs, no discernible motifs known to be associated with protein-protein interaction could be identified, in fact, these regions showed high levels of intrinsic disorder. This may suggest an accessory protein is required to stabilise these tails as has been proposed for the CatSper channels (255).

5.12.5 Dynamic assembly

Considering the different subcellular locations of HsTPC1 and HsTPC2, it is difficult to understand how these isoforms may be coming together to form a functioning heterodimeric channel. However, the endo-lysosomal system is in continuous flux, so one explanation is that the interaction is dynamic and heterodimers form in response to a certain stimulus. Inter-organelle channel regulation can be seen in the plasma membrane Orai channel whereby channel gating requires an interaction with the ER-membrane protein STIM. Ca^{2+} depletion of the ER causes STIM protein to cluster and migrate to the PM-adjacent regions (438). ER-PM junctions are then thought to form where STIM induces dimerisation of Orai dimers to give the functioning store operated Ca^{2+} channel (338).

As HsTPCs need to interact to form the channel, they would need to sit within the same membrane. This could be feasible as endosome-lysosome fusion is a common physiological event in most cells (261, 262). This would bring the endosomal HsTPC1 together with lysosomal HsTPC2 and resulting hybrid organelle may then show an altered HsTPC channel function due to the formation of heterodimers. This may play a part in the endocytotic pathway, which is tightly regulated by Ca^{2+}-release events (260, 356).

5.12.6 Biological relevance of heterodimers

Until we know whether the association of HsTPC1 and HsTPC2 alters the channel properties shown in the previous two chapters, it is impossible to resolve the full implications of any heterodimerisation. However, using the TRP channels as an example, the effects of heteromeric channel assembly have been proposed to confer biologically important functions including: regulation of basal channel activity; activation/inactivation properties; channel selectivity and conductance; subcellular targeting of channels; and in some TRP channels a subunit may have dominant negative properties which effectively disable ion conductance (381).

Interestingly, in the sea urchin TPC isoforms, the transient expression of SpTPC3 in HEK293 cells had an inhibitory effect on NAADP-evoked Ca^{2+} release. Inhibition was seen on both the endogenous activity and in cells overexpressing SpTPC2 which usually augmented Ca^{2+} release in response to NAADP (375). This suggests a dominant negative role of this isoform, and further supports the premise of TPC heteromeric interactions between isoforms. Whilst there is no TPC3 isoform in humans, HsTPC1 may play an inhibitory role and thus may alter channel activity. This hypothesis could explain the presence of the 70 % subconductance state seen in the lipid bilayer (section 3.7.2).

5.12.7 Other interactions

From the mass spectrometry data shown at the beginning of this chapter, other proteins may interact with the HsTPCs. The results were briefly discussed when first shown but some of the key interactions are worth reiterating here.

HsTPC2 putatively interacts with the Na^+/K^+ ATPase as this protein was identified in the coimmunoprecipitated complex, with both anti-HA and anti-HsTPC2 antibodies. This ATPase is normally associated with the plasma membrane where it establishes the membrane potential by pumping Na^+ out of the cell in exchange for K^+ ($3Na^+ : 2K^+$); however it is also expressed on intracellular organelles where its electrogenic activity generates an inside-positive potential which acts as a break on acidification (130, 169). Given the regulation of HsTPC2 by luminal pH, this interaction may allow a feedback mechanism correlating Ca^{2+}-release activity with pH via the Na^+/K^+ ATPase. Alternatively, K^+ ions have been shown to play a crucial role in NAADP binding to its receptor (108), thus the local concentration of cytoplasmic K^+ could affect the NAADP concentration-response relationship. By tightly associating with a Na^+/K^+ ATPase, HsTPC2 could provide its own local source of K^+ ions. An interesting comparison is provided by the IP_3R, where all three isoforms have been shown to interact with the catalytic subunit of the Na^+/K^+ ATPase (471). The exact mechanism and outcome of this interaction is still to be elucidated, however, disruption of the $IP_3R/Na^+/K^+$ ATPase complex leads to defective Ca^{2+} release in response to ATP (69).

Another significant finding was the interaction with the V-type ATPase which was seen in the anti-HA immunopurified HsTPC2 complex, but not in the anti-HsTPC2

immunopurified complex. As this is the primary route of lysosomal acidification, the V-type ATPase is essential in setting the lysosomal membrane potential. Being a large 910 kDa complex, the V-type ATPase is composed of 14 different subunits (128), of which the catalytic subunits A and B were seen to be associated with the HsTPC2 complex. This could implicate HsTPC2 as a regulatory protein governing lysosomal pH which would feedback upon its own channel function.

Finally, another ATPase was also coimmunoprecipitated with the HsTPC2 complex, this was an isoform of the ER Ca^{2+}-ATPase. A lysosomal localisation of this pump family is not unknown as Ca^{2+}-ATPases have been reported in acidic organelles from human platelets (257). Given the luminal-[Ca^{2+}] modulation of HsTPC2 sensitivity to NAADP, this could again be the source of channel feedback or a means of replenishing the lysosomal Ca^{2+} stores after activation.

Other proteins of interest were also coimmunoprecipitated, these included the IRS4 which could be postulated as a potential NAADP-binding protein, and flotillin-1 which implicates HsTPC2 with lysosomal trafficking. With these proteins and the ATPases discussed above, coimmunopreciptitation would need to be confirmed by western blot before further conclusions could be made.

A recent publication shows that TRPML1 directly associates with HsTPCs by coimmunoprecipitation (457), but from experiments shown earlier in this chapter, neither mass spectrometry nor western blots from two different immunoprecipitation reactions revealed an interaction. Nevertheless, if an interaction were to take place this could be occurring at two levels: either the TRPML1 subunits show enough homology with HsTPCs to interact with a stoichiometry of 1 HsTPC : 2 TRPML1 to complete the 24-TM pore forming channel, or two complete channels (HsTPC dimer & TRPML tetramer) are associated. Whilst the latter hypothesis seems unlikely considering the size of a full channel, the HsTPC/TRPML complex would be small compared to RyR and yet RyRs intrinsically organise themselves into a neat lattice array (462). If similar quaternary interactions are seen in the lysosomal membrane this may explain why these two channels were thought to associate.

5.13 Conclusions

This final results chapter summarises the fundamental properties of the HsTPC complex. Since the discovery that HsTPC1 was coimmunoprecipitated with HsTPC2 in the mass spectrometry analysis, it has allowed a greater understanding of how these proteins exist within the cell and how they may interact.

From coimmunoprecipitation studies analysed by mass spectrometry and western blotting, the HsTPCs have been shown to form both homo- and heterodimers in overexpressing cells. This confirms predictions based on homology with the VGCCs, CatSpers and the TRP channels. The localisation of fluorescently-tagged HsTPCs showed that HsTPC2 was mainly localised to the lysosome, whereas HsTPC1 showed a more disparate subcellular localisation from endosomes to lysosomes. This separation suggested that if heterodimerisation were occurring it could only be within a subset of the HsTPCs where they were colocalised on the lysosomes. FRET analysis supported the homomeric association of HsTPCs, and further enforced that heterodimerisation only occurred where HsTPC1 was mainly localised to the lysosome. The physiological relevance of this data is ambiguous, but may suggest a dynamic interaction between these two isoforms.

Preliminary evidence also identifies other proteins involved in the HsTPC complex, many of which could have crucial feedback roles and may explain some of the characteristic features of NAADP-evoked Ca^{2+} release.

5.14 Future prospects

The dimerisation of HsTPCs has long been predicted, but this was the first study to comprehensively investigate their interaction. However, the mechanisms and protein motifs involved in this interaction are still unknown and future studies would need to dissect out these molecular components of the HsTPCs. As a starting reference the TRP channel amino- and carboxy-terminal interactions provide a homologous system in which these experiments have been successful. Truncated tails may independently interact without need for the pore-forming TM domains and to this end GST-tagged tail regions of mammalian TPCs are being prepared for these studies. An understanding of how the HsTPCs interact with each other may allow specific pharmacological intervention or point mutations to disrupt channel function *in vivo*.

The biophysical properties of the potential HsTPC dimer combinations could also be compared and preliminary experiments have already begun to concatenate combinations of HsTPC1 and HsTPC2 onto a single strand of mRNA and thus a single protein. This would emulate the structure of the VGCC and the channel properties could be measured as with HsTPC2 in the artifical bilayer system or indeed in the optimised lysosome patch. Ca^{2+}release properties of cells expressing concatenated-dimer HsTPCs could also be investigated by Ca^{2+}imaging techniques upon addition of membrane permeant NAADP, as has been conducted in other isoforms (375). Concatenated subunits of TRPV5/6 have been made and greatly progressed the functional characterisation of heteromeric TRP channels (381).

Concatenation of subunits would also allow investigation into the potential role of SpTPC3 as a dominant negative subunit. Although humans do not express this isoform, structure-function studies on SpTPC3 may reveal homologous domains in the HsTPCs which govern channel conductance or gating. Preliminary work has already begun and HsTPC1/HsTPC2 concatemers have been subcloned into the pcDNA5TO vector and are awaiting functional analysis.

The inherent structure of the HsTPC dimer governs the basic biophysical properties of the channel however, interaction with accessory proteins is likely to be essential for physiological NAADP responses and Ca^{2+} release. Preliminary mass spectrometry evidence has suggested a few potential components of the HsTPC complex but the interactions seen need to be confirmed by western blot to verify whether the interaction was specific. Clarification is also required regarding any discrepancies between the composition of the two immunoprecipitations, one which yielded a functional Ca^{2+} channel complex and the other which did not. Further mass spectrometry experiments would be needed.

Finally and most importantly the identity of the NAADP binding protein needs elucidating. Whether NAADP binds directly to TPCs or via an accessory protein is under discussion, and further analysis by mass spectrometry and N-terminal sequencing will hopefully identify putative candidates. Once the binding protein has been found this will allow a greater manipulation of NAADP pharmacology and a better understanding of the physiology behind this pathway.

Chapter 6

Discussion

As the direct conclusions and implications of the results have already been discussed, this chapter will focus on how the programme of work applies to the wider field of Ca^{2+} signalling and the effects that the HsTPCs could have on cell physiology.

6.1 HsTPCs as NAADP-gated Ca^{2+} channels

This thesis has investigated some of the fundamental properties of the HsTPCs and was the first study to show NAADP-gated Ca^{2+} currents through a TPC channel. This was confirmed by two separate techniques, lipid bilayer reconstitution of HsTPC2 and whole-lysosome patch clamp recordings. Both techniques produced a bell-shaped concentration-response curve for NAADP, over a range of concentrations which conform with those seen in endogenous tissues (4, 5, 25, 202, 282, 431).

Figure 6.1 shows a compilation of those studies which have reported bell-shaped concentration-response curves in mammalian cells and tissues. The methods used to administer NAADP vary across these studies, and of course the efficacy of NAADP will be different on a tissue sample compared to cultured cells. These variations notwithstanding, the NAADP concentration-response curves obtained in chapters 3 & 4 (drawn in bold) correlate with each other and sit within the spread of results in endogenous tissues. This correlation gives a greater confidence that the data shown here is physiologically relevant.

The mechanisms behind the reduced response to high concentrations of NAADP are largely unknown but thanks to techniques employed here, the HsTPC2 channel

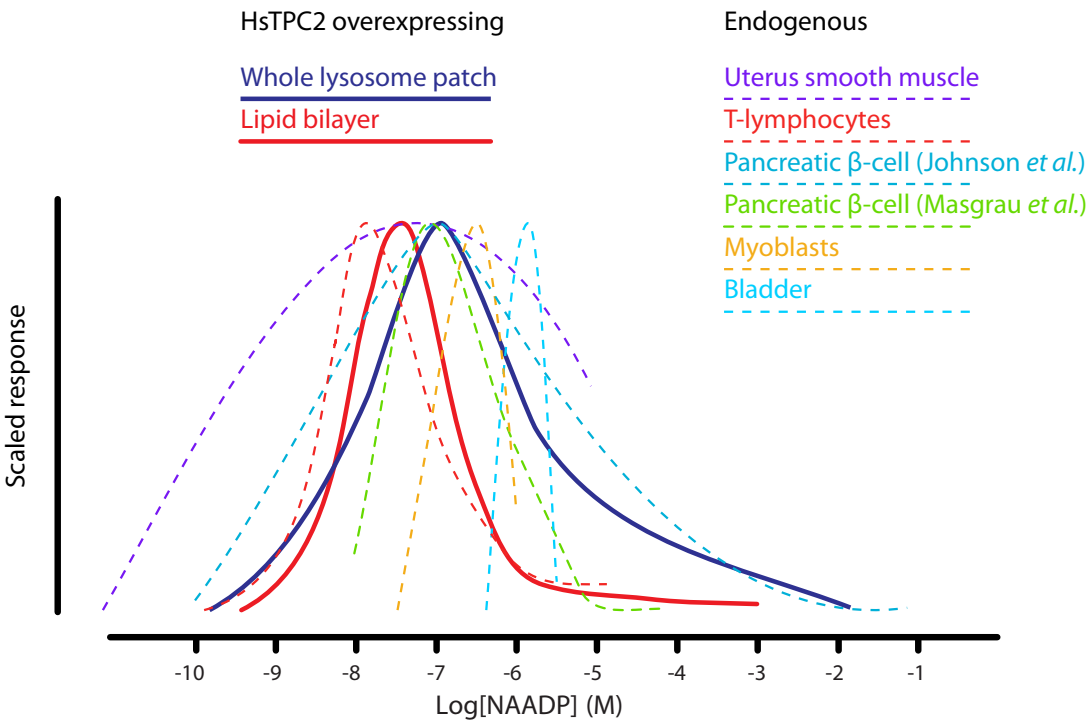


Figure 6.1: Compilation of bell-shaped NAADP concentration response curves. Curves traced and scaled from the various studies reporting bell-shaped responses to NAADP. The two solid curves in bold are those from purified HsTPC2 (Red - chapter 3) and HsTPC2-overexpressing lysosomes (Navy - chaper 4). Dashed lines are from endogenous tisses: Uterus smooth muscle (5), T-lymphocytes (25), Pancreatic β cells (202, 282), myoblasts (4) and bladder smooth muscle (431).

was shown to be directly involved. Thus a few speculative mechanisms can be eliminated. These include suggestions that the bell-shaped curve is due to increased NAADP metabolism at high concentrations, and that changes in membrane potential may inactivate HsTPC2. The basis of elimination would be that fact that the immunopurified HsTPC2 in the bilayer, and purified lysosomes would be free of the enzymes involved in NAADP metabolism, and that both studies showed no voltage regulation of HsTPC2.

The most likely mechanism is that high concentrations of NAADP bind to, and directly inactivate HsTPC2 without apparent receptor activation. A mechanism for this subtle regulation has not been elucidated but dissection with various analogues of Ned-19 on sea urchin egg homogenates have predicted that the TPCs may possess a high affinity activatory NAADP binding site and a low affinity inactivatory binding site (370). If only the high-affinity site binds NAADP the channel can open but if both sites are occupied the channel will remain closed. The functional relevance of this inhibition by high concentration of NAADP is unknown as the concentration of endogenous NAADP is yet to be accurately measured.

6.2 Interaction with other Ca^{2+}-signalling pathways

It was not just the sensitivity to NAADP which remained consistent between the bilayer and whole lysosome patch; the biophysical channel properties were also comparable. Both studies showed an ohmic Ca^{2+} channel, which was not gated by voltage. However, in the two studies, response to NAADP was measured by two different parameters: in the bilayer the P_o was recorded; and in the patch clamp it was the current amplitude. It was assumed that the increased current amplitude in the lysosome was due to an increased frequency of channel opening, rather than an increase in Ca^{2+} conductance. Therefore with a low abundance and low conductance the NAADP-evoked Ca^{2+} currents from endogenous HsTPCs would result in a small and highly localised Ca^{2+} signal which seems contradictory to the role that NAADP plays on a global scale.

In fact, it is precisely this small and localised Ca^{2+} signal which gives the HsTPCs such a versatile role in Ca^{2+} signalling. The position of HsTPCs within the dynamic endo-lysosomal system enables these small signals to be targeted in the vicinity of Ca^{2+}-regulated effectors which can amplify and propagate the signal.

Three modes of HsTPC-mediated Ca^{2+} signalling mechanisms are shown in figure 6.2 and are discussed in the following sections. These include the amplification and globalisation of a HsTPC-mediated Ca^{2+} trigger via the ER, the direct and indirect regulation of Ca^{2+}-activated channels in the PM, and finally the role of HsTPC1 and HsTPC2 in governing lysosomal and endosomal interactions, fusion and trafficking.

6.3 HsTPCs and the ER

The first evidence that the ER may play a role in NAADP signalling was shown by Cancela *et al.* in 1999, long before the discovery of TPCs. They proposed the trigger effect, whereby a small NAADP-induced Ca^{2+} release from lysosomes elicits a greater global signal via CICR on the ER (chapter 1, figure 1.13) (57).

The HsTPCs have been directly implicated in this phenomenon but different laboratories show contrasting results.

6.3.1 HsTPC2-mediated trigger

In HEK293 cells overexpressing HsTPC2, NAADP evoked a biphasic Ca^{2+} transient (55). This was thought to be due to a small Ca^{2+} increase from the acidic stores which triggered a larger release from the ER. Pharmacological intervention with bafilomycin A1 knocked out both phases of the response because bafilomycin A1 inhibits the V-type ATPase and thus prevents Ca^{2+} release from acidic stores (55). Without this initial response, the ER cannot be triggered and therefore neither transient was seen. This was confirmed by treatment with the SERCA blocker, thapsigargin, which only abolished the larger CICR phase without altering this initial Ca^{2+} release, consistent with this secondary phase being ER-derived.

This biphasic response was due to the overexpression of HsTPC2 as it was not seen in wild type HEK293 cells, and furthermore shRNA knock-down of HsTPC2 could abolish the response (55, 57). As was discussed in chapter 4, there is a large difference in the Ca^{2+}-currents seen in HsTPC2 overexpressing lysosomes compared to wild type lysosomes. Perhaps this reflects a high threshold of CICR activation in the HEK293 cells which can only be triggered by overexpressed channel activity.

One explanation of this is could be due to the relationship between HsTPCs and the ER Ca^{2+}-release channels. Experiments in pulmonary arterial smooth muscle have

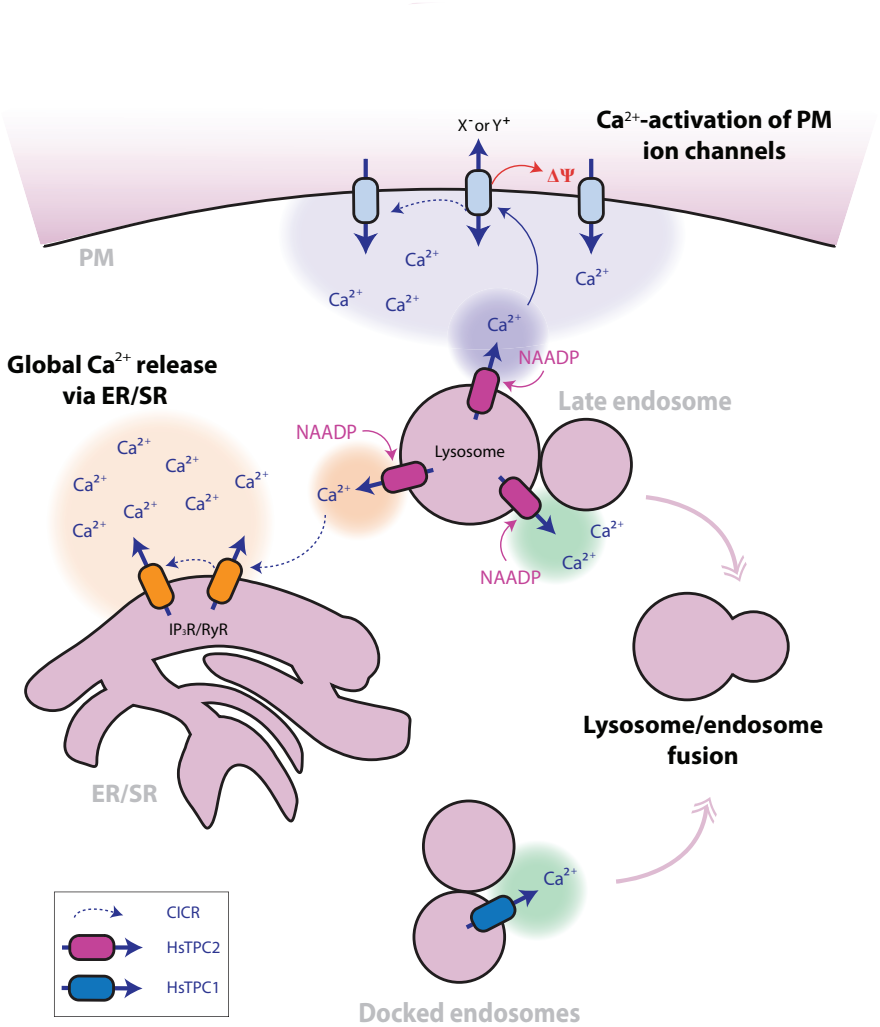


Figure 6.2: Three modes of HsTPC-mediated Ca^{2+} signalling. Left: NAADP-induced Ca^{2+} release via HsTPC2 in the lysosome acts as a local trigger for CICR amplification and globalisation by inducing Ca^{2+} release from the ER/SR. **Top:** Lysosomes positioned near the PM may regulate membrane excitability (excitable cells) or ion fluxes (nonexcitable cells) by regulating Ca^{2+}-activated plasma membrane channels. These could conduct anions (X^-) or cations (Y^+). Ion flux may result in change in membrane potential ($\Delta\Psi$) which could further activate voltage-gated channels such as the VGCCs. Ca^{2+}-influx could then stimulate a global signal via CICR. **Right:** Local Ca^{2+} release from HsTPC2 in lysosomes or HsTPC1 in endosomes may regulate vesicular fusion and trafficking in the endo-lysosomal pathway.

also shown the triggering of global Ca^{2+}signals by NAADP-evoked, local Ca^{2+} release, moreover, these were associated with RyR and inhibition of IP_3R had no effect (46, 218). This result was contradicted in the HsTPC2-overexpressing HEK293 cells which do not express functional RyR (9), and where the biphasic response was inhibited by the IP_3R antagonist heparin (55). Discrepancies of this kind could be due to differences in channel interaction between cell type or could be a direct result of the overexpression of HsTPC2 miscoupling to the IP_3R in the absence of RyR.

A comparison can be seen in NAADP-induced Ca^{2+} release in HEK293 cells transiently transfected with MmTPC2 (478). As above, bafilomycin A1 was shown to inhibit Ca^{2+} transients in response to intracellular dialysis of NAADP, however depletion of the ER by thapsigargin had no effect on the response. Therefore in these cells, as with wild type HEK293 cells, NAADP did not trigger global Ca^{2+} release from the ER. This discrepancy can be reconciled by the Ca^{2+} release via MmTPC2 not meeting the threshold for CICR. As was discussed in chapter 4, the lysosomal current data obtained for MmTPC2-overexpressing lysosomes from the same group (387) was 5-fold lower compared to HsTPC2-overexpressing lysosomes tested here. Therefore a smaller trigger via MmTPC2 is less likely to stimulate CICR from the IP_3R.

It would be an interesting comparison to see whether a similar discrepancy would be seen in a cell line which did express RyR, as this may have a lower Ca^{2+} threshold.

6.3.2 HsTPC1-mediated trigger

The subcellular localisation of HsTPC1 shown in chapter 5 gave a disparate distribution of this channel across lysosomes, early and recycling endosomes, and the ER. With such an errant existence, it is difficult to see how HsTPC1 could be involved in the tight coupling of a trigger mechanism. NAADP-evoked Ca^{2+} transients seen in HsTPC1 overexpressing HEK293 cells confirmed this apprehension, as there was no evidence of global ER-derived Ca^{2+} release, just a small spatially restricted Ca^{2+} transient (supplementary data of (55)). This lack of coupling could not be due to the magnitude of Ca^{2+}-release as discussed above, because the transients seen were of equal size to those in HsTPC2 overexpressing cells which had been treated with thapsigargin or heparin. This suggests that HsTPC1-derived Ca^{2+} signals may function in a local domain to specifically regulate endosomal function without affecting global Ca^{2+} signals, perhaps due to the lack of endosome-ER junctions (475).

Again, however, this data is contradicted by measurements made in a different cell line. Transient expression of HsTPC1 in the human breast cancer cell line, SKBR3, resulted in global Ca^{2+} responses to 10 nM of NAADP administered by microinjection (47). This global signal was attenuated by both bafilomycin A1 and ryanodine, which suggested that NAADP was triggering Ca^{2+} release via HsTPC1 and this signal was amplified by RyR on the ER, triggered by CICR. Various explanations could explain the difference in these results. Firstly, the transiently transfected HsTPC1 in SKBR3 showed a stronger lysosomal localisation than the stably overexpressing HEK293 cells, therefore conforming with the model of trigger hypothesis model based on Ca^{2+} derived from the lysosome (47, 55). Secondly, levels of expression seemed to be higher in the transiently transfected cells, this would result in a larger Ca^{2+} trigger. Thirdly, the coupling of ER may be different in SKBR3 to HEK293 cells, with a closer ER interaction with endosomes. Fourthly and most importantly, SKBR3 cells express endogenous RyR (11), which have been shown to be the preferential partner in NAADP-evoked CICR (218, 219).

Although work here has not investigated the Ca^{2+} conducting properties of HsTPC1, the techniques which have been optimised for HsTPC2 in the bilayer and whole-lysosome patch could be applied to HsTPC1 measurements. The biophysical properties of the channel may assist in the dissections of these trigger events.

Similarly, work in this thesis may be relevant in the interpretation of the discrepancies across cell types. All overexpression studies have assumed that HsTPC-mediated Ca^{2+} release has been via homodimeric channels; perhaps these differences in coupling efficiency are caused by an altered proportion of heterodimers as discussed in chapter 5.

6.3.3 Trigger zones

The trigger hypothesis is based on the assumption that the lysosome and the ER have a close interaction. This communication between organelles via local Ca^{2+} microdomains is not a new concept, with the close association of mitochondria and ER essential in the regulation of mitochondrial metabolism and apoptosis via the ER-located IP_3R and RyR (99, 366). The protein mitofusin 2 has even been suggested as the tether which holds the adjacent organelles together (102).

In pulmonary arterial smooth muscle, both NAADP and the vasoconstrictor hormone endothelin-1 stimulated Ca^{2+} release from lysosomes, which was then amplified

by the recruitment of RyRs on the SR. The interaction was so tight that lysosome-SR junctions were proposed and lysosomes were shown to colocalise with RyR on the SR to form a "trigger zone" of less than 100 nm (218). As the TPCs are located within the lysosomal membrane, the coimmunoprecipitation of HsTPC2 with the structural proteins actin-1, mysosin-9 and flotillin-1, as seen in chapter 5, may be crucial in maintaining this close juxtaposition of lysosome-ER.

6.4 HsTPCs and the plasma membrane

The ER is not the only site where the HsTPCs can propagate Ca^{2+} signals. Local NAADP-evoked Ca^{2+} signals derived from lysosomes in the vicinity of the plasma membrane (PM) have been shown to open Ca^{2+}-activated channels in several different cell types.

This was first shown by the patch clamp of pancreatic acinar cells, where NAADP was introduced via the patch pipette or uncaged by photolysis (57). NAADP first released Ca^{2+} from the NAADP-sensitive store which stimulated activation of unidentified plasma membrane currents (57). One hypothesis suggests that these currents may play a role in acinar cell fluid secretion (134).

Depolarisation of the PM has also been associated with lysosome-derived Ca^{2+} in neurones from the rat medulla oblongata (51). In these cells diffusion of membrane-permeant NAADP-AM activated Ca^{2+} release from acidic stores, which resulted in global Ca^{2+} signals propagated via the ER, but also local Ca^{2+} signals near the PM which activated non-selective cation channels on the cell surface and caused the depolarisation (51).

Finally, in pancreatic β cells, the NAADP antagonist Ned-19 was used to demonstrate a role of NAADP in glucose-mediated depolarisation and insulin secretion (310). This was thought to be due to the activation of Ca^{2+} channels in the PM by NAADP. Although there was no evidence of PM expression of either HsTPC isoform in the localisation study in chapter 5. This β cell evidence may suggest a role of TPCs in the PM or lysosomes that are closely coupled to PM channels which could be triggered like IP_3R and RyR. The requirement for TPCs is further supported by work in the β cells derived from $TPC2^{-/-}$ knock-out mice which do not show the stimulation-secretion coupling profile of the wild type (55).

The mechanisms of TPC interaction with the PM are still unknown, but given the dynamic nature of the endo-lysosomal system and especially the localisation of HsTPC1 to recycling endosomes (chapter 5) it is possible that HsTPC1 may facilitate NAADP-induced Ca^{2+} currents across the plasma membrane. The coimmunoprecipitation of HsTPC2 with the Na^+/K^+ ATPase, shown in chapter 5, may also suggest an association with the PM.

A recent publication reports the presence of STIM1 and STIM2 in the membrane of acidic Ca^{2+} stores in human platelets (464). Depletetion of the stores by bafilomycin A1 enhanced the association of these stores with Orai1 in the PM. This may provide one mechanism by which HsTPC-containing organelles migrate to the PM.

6.5 HsTPCs in lysosomal function

This thesis has focused on many of the protein properties of the HsTPCs, however it is worth putting this data in the context of lysosomal function.

The lysosome is the primary site of cellular degradation, *i.e.* defective lipids, proteins, organelles *etc.* are trafficked to the lysosome, where they are broken down and recycled (159, 280). The proteolytic function of the lysosome is assisted by the acidic luminal conditions, and many of the lysosomal enzymes work best at a low pH, for example, glucocerebrosidase activity drops to negligible levels > pH 5 (437). The regulation of HsTPC2 by luminal pH as shown in the lipid bilayer study in chapter 3 could feedback on the degradative function of the lysosome. It was shown that when the luminal pH was 7.2, HsTPC2 had a 10-fold higher open probability (P_o) than at pH 4.8, and seemed to bind irreversibly to NAADP (figures 3.22 & 3.26). Such high channel activity would lead to store depletion of Ca^{2+}, which may be beneficial for lysosomal re-acidification, as an empty store has a lower electrochemical gradient against which the V-type ATPase must pump. Moreover, the lower P_o and reversible binding of NAADP seen at pH 4.8 (figure 3.26, page 126) may help maintain the acidity of the lumen. It has been shown that NAADP-induced Ca^{2+} release causes alkalinisation of the lysosomal lumen (303), if this proton leak is via HsTPC2, by ensuring a low P_o the extent of alkalisation could be limited. The reversibility of NAADP also provides a quick *off* mechanism to prevent prolonged stimulation.

Luminal [Ca^{2+}] was also shown to govern HsTPC2 sensitivity to NAADP, reducing the EC_{50} from 500 nM to 5 nM NAADP when the Ca^{2+} concentration was raised from 10 µM to 200 µM (figure 3.24, page 123). This may act as a negative control mechanism, whereby the HsTPC2 channel is only sensitised to open when the store is sufficiently replete with Ca^{2+}. This preservation of lysosomal Ca^{2+} stores may be crucial in the role of lysosomes in fusion with endosomes, as both luminal Ca^{2+} and calmodulin are required for the completion of late-endosome/lysosome fusion (262) and lysosome reformation (260) associated with autophagy and phagocytosis (356).

The importance of pH and Ca^{2+} regulation, which HsTPC2 has demonstrated, is particularly highlighted when it is disrupted. Aberrant overexpression of SpTPCs in HEK293 cells resulted in profound changes in lysosomal trafficking, lysosome size and distribution (375). These morphological changes are more commonly observed in certain lysosomal storage diseases, such as Niemann-Pick as will be discussed below (254). These symptoms of TPC overexpression could be remedied by treatment with the NAADP antagonist Ned-19.

The work presented in chapter 4 optimised a method of lysosomal purification in order to conduct HsTPC2 electrophysiological studies. However, this purification procedure could also be used to further investigate the physiology and function of isolated lysosomes and the proteins present in the lysosomal membrane. Therefore although focus here has been on HsTPC2, this thesis also provides a basis for further work on TRPML1, TRPM2 and other related channels.

6.5.1 HsTPCs in autophagy

Macroautophagy is the process by which large cytosolic macromolecules and organelles are degraded and recycled. This occurs via the autophagosome, a double membraned organelle, which forms around the target region in the cytoplasm and engulfs the material to be catabolised (227). Mature autophagosomes fuse with lysosomes for further breakdown of the luminal contents (226).

A recent publication has linked HsTPCs to the regulation of autophagy in cultured astrocytes (339). Microinjection of NAADP directly into the astocyte cytoplasm, induced Ca^{2+}-release in a bell-shaped concentration-response relationship, and this response was potentiated by overexpression of HsTPCs. NAADP also induced increased formation of acidic vesicles similar to the autophagosome as they expressed autophagic

markers LC3II and beclinI. Furthermore, levels of LC3II were reduced in astrocytes which expressed a dominant-negative HsTPC2 construct. This data suggests a role for NAADP and HsTPCs in autophagy.

Further work on the channel properties and heteromerisation of HsTPCs may help elucidate how these distinct roles of HsTPC-mediated Ca^{2+} release are differentiated.

6.6 HsTPCs in endosomal function

Although HsTPC2 is almost exclusively confined to the lysosome, HsTPC1 is more widely distributed within endo-lysosomal compartments and may play a role in the regulation of the endosomal pathway. The crucial function of endosomes is the trafficking of endocytosed materials and the sorting of membrane bound proteins either to be recycled to the PM or degraded by the lysosome (355). This trafficking requires many membrane fusion events, commonly initiated by Ca^{2+} transients (263), which could be mediated by HsTPC1 Ca^{2+} release from the lumen.

Figure 5.16 showed a proportion of HsTPC1 located on the membrane of recycling endosomes, these organelles are essential in receptor recycling and trafficking to and from the plasma membrane. A role in trafficking would put the HsTPCs in a pivotal role in cellular physiology, because the rate at which receptors are recycled to the membrane governs how sensitive a cell can be to external stimuli (377, 442). Experiments with bafilomycin A1 have shown cell type-specific responses, potentially involving TPCs. In HeLa cells, bafilomycin A1 prevented transport of receptors from endosomes to lysosomes (17), but not recycling back to the PM. Whereas in CHO cells, bafilomycin A1 reduced the rate of receptor recycling (203, 353). These effects may due to the lack of TPC mediated Ca^{2+} fusion events as bafilomycin A1 depletes the acidic stores of Ca^{2+}, the differences in cell type response maybe due to different localisation or isoform expression of TPCs.

Although limited to lysosomal patch-clamp, work shown here could be further adapted to investigate these phenomena. Much of the work on membrane fusion was conducted on isolated yeast vacuoles (53), which are analogous organelles to lysosomes. Chapter 4 outlines the optimal preparation of isolated lysosomes and therefore provides a perfect system for investigating these Ca^{2+}-mediated lysosomal fusion events. A simple observation from figure 4.2 already provides preliminary evidence that the presence

of high cytosolic Ca^{2+} (8 mM) alone causes aggregation of lysosomes, but seemingly cannot induce fusion. Experiments like this could be expanded.

An understanding of the mechanisms regulating endo-lysosomal fusion might lead to the deliberate homotypic fusion of lysosomes for patch clamp studies and eliminate the chemical interventions required to enlarge lysosomes (section 4.5).

6.7 HsTPCs in lysosome-related organelles

HsTPCs may also play a role in more specific organelles within the lysosomal family, such as melanosomes, which are responsible for the delivery of melanin to keratinocytes (385). Again, membrane fusion events, which govern melanosome function, are thought to be regulated by Ca^{2+} transients (206). A direct role of HsTPC2 has already been shown to play a part in this system as two coding variants were shown to determine brown or blonde hair colour in an Icelandic population (section 1.9.7) (413, 414). The difference could be due to mistrafficking of melanosomes, or defective Ca^{2+}-dependent fusion because of altered channel function of HsTPC2.

This would also be a very feasible hypothesis to confirm using the methods optimised in chapter 4. Differences in the channel function of these two HsTPC2 coding variants could be studied by their expression in lysosomes and subsequent purification and patch clamp.

6.8 HsTPCs in disease

Having discussed the potential roles that HsTPCs play in healthy cells, this section will consider how atypical HsTPC function may result in disease.

A number of diseases have been associated with lysosomal dysfunction, these manifest themselves by altered lysosomal morphology, defective enzyme activity and accumulation of undegraded material (330). It is for this last reason they are referred to as lysosomal storage disorders (LSDs). Defective HsTPC function could be implicated in Gaucher's disease (472), an LSD characterised by accumulation of glucosylceramide and distinctive cell morphology (Gaucher cell), with swollen, striated cytoplasm. Evidence for this link is the fact that Gaucher patient-derived fibroblasts were partially recovered by treatment with VGCC blockers, diltiazem and verapamil (305), both known

antagonists of NAADP-mediated Ca^{2+}-release via TPCs (149, 475). Considering the discussion above regarding HsTPC2 and the pH regulation of glucocerebrosidase (the enyzme responsible for the breakdown of glucosylceramide) this further suggests an involvement of HsTPCs. It would be interesting to see whether Ned-19 could recover Gaucher cells to normal as this is a specific antagonist of HsTPC2 as shown in figures 3.28 & 4.40.

Niemann-Pick type C1 (NPC1) disease is a neurodegenerative LSD, characterised by excessive lysosomal accumulation of sphingosine, glycosphingolipids, sphingomyelin and cholesterol (412). In a drug induced model of NPC1, sphingosine storage in the lysosomal lumen disrupted normal Ca^{2+} homeostasis, resulting in a depleted Ca^{2+} store (254). This depletion was demonstrated by a 70 % reduction in NAADP-mediated Ca^{2+} release. Which in turn prevented Ca^{2+}-dependent fusion and trafficking in the endo-lysosomal pathway, therefore cholesterol and sphingolipids could not be recycled to the PM and they were accumulated in the lysosome to give the pathological NPC1 phenotype.

Whilst the underlying cause of NPC1 is still unknown, it would be interesting to investigate the effects of sphingosine, cholesterol, sphingomyelin, glycosphingolipids on HsTPC2 channel activity to determine whether this channel plays a role in the dysregulation of Ca^{2+} homeostasis. Using methods from this thesis, two separate studies could be conducted. Purified HsTPC2 could be incorporated into an artificial lipid bilayer containing deliberately high concentrations of sphingosine or cholesterol and channel activity could then be measured. Alternatively, lysosomes could be purified from NPC1 cells (drug induced or from the NPC1 mouse (254)) and whole lysosome patch clamp could then investigate how Ca^{2+} currents pass across the whole lysosome membrane.

Deafness and audio impairment is one of the common symptoms identified in LSDs such as Guachers and Hunter syndrome (56, 210, 320). HsTPC2 may play a pathophysiological role in these disorders. It was mentioned in the introduction (section 1.9.7) that there exists a direct pathological link between TPCN2 (the gene for HsTPC2) and a hereditary hearing impairment (209, 216). This autosomal recessive nonsyndromic deafness is caused by changes at the human chromosomal locations 11q13.2-q13.4, where TPCN2 is encoded with 12 other genes and no disease causing mutations have been shown (209). One potential hypothesis is that increased levels of HsTPC2 can confer exaggerated mechanosensitivity to a cell (475). This evidence combined with the

fact that the disruption of mechanotransduction in hair cells causes deafness in mouse models (163), suggest that it may be the expression levels of HsTPC2 resulting in the deafness rather than any defects in channel activity. If overexpression of HsTPC2 is the underlying cause of the disease, channel antagonists such as Ned-19 could play a therapeutic role to reduce excessive channel activity. Furthermore using techniques of lipid bilayer and whole lysosome patch, the pharmacology of HsTPC2 could be further investigated and could be a basis for the development and testing of novel chemical modulators of channel activity which could be used to therapeutically.

6.9 Final conclusions

This chapter has briefly discussed the potential roles that HsTPCs may play in cell physiology and how the techniques developed and used here could further elucidate those roles.

The spatio-temporal regulation of Ca^{2+} is proving more and more important in understanding how a ubiquitous Ca^{2+} signal can encode such specificity. The coordination of HsTPCs in small dynamic vesicles produces a flexible and versatile signalling apparatus whereby localised Ca^{2+} signals can be targeted to trigger key physiological responses. Extracellular stimuli which are selectively coupled to NAADP, can therefore produce distinct patterns of Ca^{2+} signals which result in a specific response.

Through a closer understanding of the HsTPCs as endolysosomal proteins and Ca^{2+} channels, their role in producing such specific patterns can be determined. This thesis has investigated the regulation of HsTPCs at various levels: gating by NAADP, modulation by luminal pH and [Ca^{2+}], *in situ* regulation by native lipids and finally the protein-protein interaction and potential dimer interactions which could govern channel activity. By establishing these key characteristics of the HsTPCs and their role within the endolysosomal system, this leads to a better understanding of the mechanisms of cellular Ca^{2+} signals in physiological and pathophysiological processes.

Appendices

Appendix A

Supplementary figures

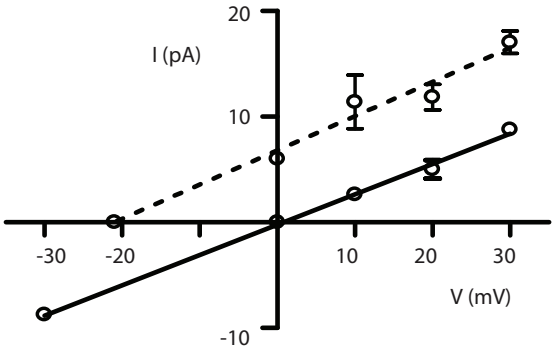


Figure A.1: Current-Voltage relationship with K^+ as the permeant ion. The *cis* chamber was held at various potentials with respect to the fixed potential *trans* chamber and current amplitude across the bilayer measured in the presence of 10 µM NAADP. The solid line represents the relationship when both chambers contained symmetrical 210 mM KCl; pH 7.2. The dashed line represents the relationship in the presence of a KCl gradient (*cis*: 510 mM, *trans*: 210 mM).

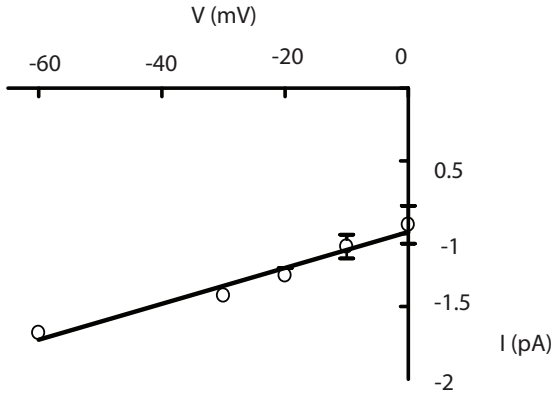


Figure A.2: Current-Voltage relationship with Ca^{2+} as the permeant ion. The *cis* chamber was held at various potentials with respect to the fixed potential *trans* chamber and current amplitude across the bilayer measured in the presence of 10 µM NAADP.

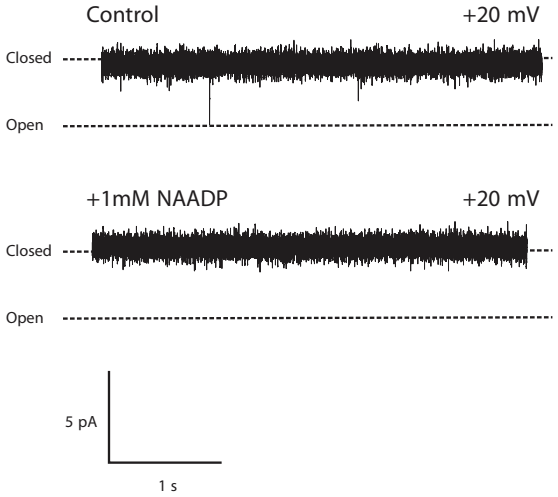


Figure A.3: High concentrations of NAADP block channel activity. Representative traces demonstrating HsTPC2 activity in the presence of mM NAADP without previous incubation with activating concentrations. K^+ was the conducting ion; both chambers were symmetrical at pH 7.2. The top trace shows a typical experiment with basal HsTPC2 activity of brief channel openings in the absence of NAADP. $P_o = 0.0003 \pm 0.0002$ (n = 3, S.D.). Subsequent addition of a high concentration of NAADP (1 mM) completely abolished channel openings, $P_o = 0$ (n = 5).

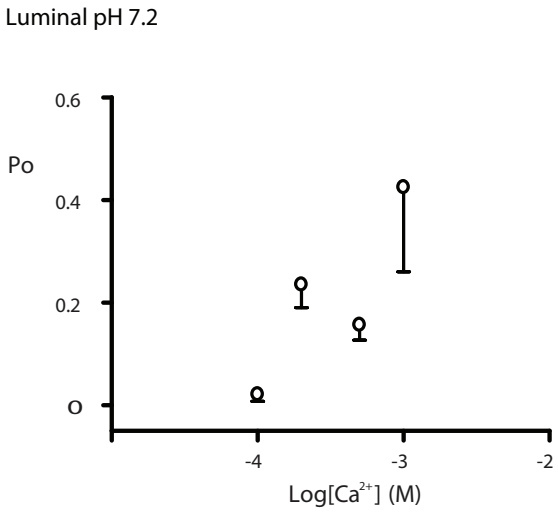


Figure A.4: The effect of luminal Ca^{2+} concentration on HsTPC2 P_o. The relationship between the P_o in the continued presence of 10 nM cytosolic NAADP and the *trans* chamber (luminal) Ca^{2+} concentration. K^+ was the conducting ion; both chambers were at pH 7.2. Data are mean values (n = 3, S.D.)

A. SUPPLEMENTARY FIGURES

Appendix B

Methods tables

Table B.1: A list of media used to grow cell lines.

Cell type	Medium	Selective Antibiotic
Wild Type HEK293 HEK293T	DMEM 10 % FBS 50 U/ml Penicillin 50 U/ml Streptamycin 2 mM L-Glutamine	None
HsTPC1 Stable cell line (C-terminal His_6 Tag)	DMEM 10 % FBS 50 U/ml Penicillin 50 U/ml Streptamycin 2 mM L-Glutamine	100 µg/ml Hygromycin
HsTPC2 Stable cell line (N-terminal 2x HA Tag)	DMEM 10 % FBS 50 U/ml Penicillin 50 U/ml Streptamycin 2 mM L-Glutamine	500 µg/ml Geneticin (Neomycin analogue)

Suppliers

DMEM = Dulbecco's Modified Eagle Medium (Invitrogen), FBS = Fetal Bovine Serum (BioSera), Geneticin (Invivogen), Hygromycin (Autogen Bioclear), Penicillin/Streptomycin (Sigma), L-Glutamine (Sigma).

Table B.2: Vector constructs. Human TPCs with various tags were subcloned into pcDNA5TO or a Clontech vector already expressing YFP/CFP and expressed in HEK293 cells by transient transfection

Vector	Provider	cDNA	Tag	Terminus	Expression system
pcDNA5/TO	Invitrogen	HsTPC1	HA	carboxy	HEK293T
		HsTPC1	mCherry		
		HsTPC2	HA		
		HsTPC2	mCherry		
pEYFP-N	Clontech	HsTPC1	YFP	carboxy	HEK293
		HsTPC2			
pEYFP-C		HsTPC1		amino	
		HsTPC2			
pECFP-N		HsTPC1	CFP	carboxy	
		HsTPC2			
pECFP-C		HsTPC2	CFP	amino	

Table B.3: Antibodies used for immunolocalization studies and western blotting.

Name	Antibody type	Epitope	Origin	HRP	Secondary
α-HA	Rat monoclonal	YPYDVPDYA	Roche clone 3F10	✓	N/A
α-His_5	Mouse monoclonal	penta-histadine	Qiagen QIAexpress	✓	N/A
α-GFP	Rabbit polyclonal	Full length GFP	Santa Cruz FL	✓	N/A
α-RFP	Rat monoclonal	multiple full length RFPs	Rottach *et al.* (373)		α-Rat
α-DsRed	Mouse monoclonal	Full length DsRed	Clontech		α-Mouse
α-TRPML1	Goat polyclonal	Internal peptide fragment	Santa Cruz L 15		α-Goat
α-TRPML1	Rabbit polyclonal	Residues 106-180 HsTRPML1	Santa Cruz H 75		α-Rabbit
α-LAMP2	Mouse monoclonal	H4B4 - adherent spleen cells	Santa Cruz H4B4		α-Mouse
α-Calnexin	Rabbit polyclonal	Residues 573-592 HsCNX	Sigma (SAB4503258)		α-Rabbit
α-Ryanodine Receptor	Mouse monoclonal	Non-isoform specific	Sigma (R129)		α-Mouse
α-HsTPC2	Rabbit polyclonal	Residues 240 - 254	In-house		α-Rabbit
(7049 and 7050)		Residues 408 - 422			
α-HsTPC1	Rabbit polyclonal	Residues 776 - 792	In-house		α-Rabbit
(7047 and 7048)		Residues 798 - 816			

Appendix C

Calculations

Reverse potentials

The reverse potentials quoted in section 4.16.13 were calculated using the Nernst equation as below:

$$\begin{aligned} \text{E} &= \frac{RT}{zF} \times ln\frac{[ion]_{outside}}{[ion]_{inside}} \\ \text{For } Ca^{2+}: & \\ &= \frac{8.314 \times 295}{2 \times 96485} \times ln\frac{60}{2} \\ &= 43.2 \text{ mV} \\ \text{For } K^{+}: & \\ &= \frac{8.314 \times 295}{1 \times 96485} \times ln\frac{70}{120} \\ &= -13.2 \text{ mV} \end{aligned}$$

Where R is the universal gas constant (R = 8.314 J K^{-1} mol^{-1}), T is the temperature of the system (°K), z is the charge on the ion (Ca^{2+} = 2, K^{+} = 1), F is the Faraday constant (F = 96485 × 10^4 C mol^{-1}). $[ion]_{outside}$ refers to the ion concentration in the cytoplasmic buffer, $[ion]_{inside}$ is the concentration in the luminal buffer.

Predicted number of HsTPC2 channels

Comparing the single channel conductance of HsTPC2 predicted in the lipid bilayer, with the whole lysosome currents seen in the patch clamp study it is possible to predict the number of open channels per lysosome. As given in section 4.16.8

$$\begin{aligned} 1 \text{ Amp} &= 6.24 \times 10^{18} \text{ charge/second} \\ Ca^{2+} \text{ is divalent} &\Rightarrow 3.12 \times 10^{18} \ Ca^{2+}\text{/second} \end{aligned}$$

Empirical evidence from chapter 4 (page 208) showed that in the whole lysosome over-expressing HsTPC2 at -100 mV, 100 nM NAADP induced a current of $\approx$ 300 pA.

$$\begin{aligned} \text{Amplitude} \times Ca^{2+}\text{/second} &= Ca^{2+} \text{ flux per lysosome} \\ 300 \times 10^{-12} \times 3.12 \times 10^{18} &= 9.36 \times 10^{8} \ Ca^{2+}\text{/second/lysosome} \end{aligned}$$

Given the single channel conductance of a HsTPC2 was predicted to be 15 pS (page 118), the current per channel could be calculated at -100 mV:

$$\begin{aligned} \text{Where I (current)} &= \text{V (voltage)} \times \text{S (conductance)} \\ &= 100 \times 10^{-3} \times 15 \times 10^{-12} \\ &= 1.5 \times 10^{-12} \text{ Amps} \end{aligned}$$

Converting to Ca^{2+}/second:

$$\begin{aligned} &= 1.5 \times 10^{-12} \times 3.12 \times 10^{18} \\ &= 4.68 \times 10^{6} \ Ca^{2+}\text{/second/HsTPC2 channel} \end{aligned}$$

Dividing whole lysosome Ca^{2+} flux by single channel Ca^{2+} flux:

$$\begin{aligned} \text{Number of channels} &= 9.36 \times 10^{8} / 4.68 \times 10^{6} \\ &= 200 \text{ channels/lysosome} \end{aligned}$$

Similar mathematics can be used to predict the maximum (290) and minimum (50) number of open channels over the range of currents seen. Furthermore endogenous HsTPC2 expression on wild type lysosomes can be predicted by this method (2.6 open channels per lysosome).

To give the hypothetical total number of channels (including those that remained closed) this number can be divided by the open probability at this concentration which from figure pHplot (page 126) was $\approx$ 0.08, this would give 2500 channels in the HsTPC2-overexpressing lysosome, and 30 endogenous HsTPC2 channels in wild type lysosomes.

Lysosomal depletion

Using these numbers and a predicted value for lysosomal [Ca^{2+}] it ought to be possible to predict how long it would take to deplete a lysosome of Ca^{2+}.

Assuming the lysosome to be a sphere of 1 µm diameter

$$\begin{aligned}\text{Volume of a lysosome} &= \tfrac{4}{3}\pi r^3 \\ &= \tfrac{4}{3}\pi \times \left(0.5 \times 10^{-6}\right)^3 \\ &= 5.2 \times 10^{-19}\ \text{m}^3 \\ &= 5.2 \times 10^{-16}\ \text{litres}\end{aligned}$$

The predicted concentration of Ca^{2+} ions in the lysosome is 250 µM
(Median value - page 222)

$$\begin{aligned}\text{Moles of } Ca^{2+} &= \text{concentration} \times \text{volume} \\ &= 250 \times 10^{-6} \times 5.2 \times 10^{-16} \\ &= 1.3 \times 10^{-19}\ \text{moles}\end{aligned}$$

Multiplied by Avogadro's number:

$$\begin{aligned}\text{Total \# } Ca^{2+} \text{ ions} &= 1.3 \times 10^{-19} \times 6.02 \times 10^{23} \\ &= 7.88 \times 10^{4}\ Ca^{2+}\ \text{ions/lysosome}\end{aligned}$$

Remembering the single channel conductance:

$$\text{HsTPC2 conductance} = 4.7 \times 10^{6}\ Ca^{2+}/\text{second/channel}$$

Time taken to fully empty the lysosome of Ca^{2+}:

(assuming just one HsTPC2 channel)

$$\begin{aligned}\frac{\text{Total } Ca^{2+}}{\text{HsTPC2 conductance}} &= \tfrac{7.88\times10^4}{4.7\times10^6} \\ &= 1.67 \times 10^{-2}\ \text{seconds} \\ &= 16.7\ \text{ms}\end{aligned}$$

(assuming 200 open HsTPC2 channels)

$$= 0.08\ \text{ms}$$

Geometry of HsTPC2 expression

Basing the size of the HsTPC2 channel on the VGCCs as determined by electron microscopy (306), it is predicted to be 20 x 10 x 9 nm, thus an assumed protein footprint of 200 nm^2 (445).

The maximum number of HsTPC2 channels which could physically fit onto a lysosome can be predicted. Again assuming the diameter of a non-swollen lysosome to be 1 µm, the surface area of a lysosome is:

$$\begin{aligned}
\text{Surface area of a Lysosome} &= 4\pi r^2 \\
&= 4 \times \pi \times (0.5 \times 10^{-6})^2 \\
&= 3.14 \times 10^{-12}\ \text{m}^2 \\
\text{In nanometers:} & \\
&= 3.14 \times 10^{6}\ \text{nm}^2 \\
\\
\text{Number of channels} &= \text{Total area / area of HsTPC2 footprint} \\
&= 3.14 \times 10^{6}/200 \\
&= 15,700 \text{ channels}
\end{aligned}$$

Where r is the radius of the lysosome (0.5 µm).

Distribution on the surface of a sphere

The approximate distance between channels on the surface of the sphere (assuming even distribution) is simply the square root of the surface area divided by the number of channels, defined by the equation (24):

$$\text{Distance between channels} = \sqrt{\frac{4\pi r^2}{N}}$$

Taking a lysosome of 1 µm diameter:

and assuming 2500 channels per lysosome:

$$= \sqrt{\frac{4\pi \times (0.5 \times 10^{-6})^2}{2500}}$$

$$= 35.4 \text{ nm between channels}$$

Where r is the radius of the lysosome (0.5 µm). N is the number of channels.

This distance suggests that FRET did not occur due to overpacking in the membrane. Each channel is separated by $\approx$ 30 nm, which is greater than the $<$ 10 nm distances required for FRET.

Conductance through the surface of a sphere

The biophysical properties of a sphere can be modelled, assuming a even distribution of equally sized conducting pores. The conductance through a sphere is defined by the equation (24):

$$\frac{I}{I_0} = \frac{1}{1+(\pi r/Na)}$$

Where I is the current through the membrane, I_0 is the maximum current possible, a is the radius of the channel, N is the number of channels in the membrane and r is the radius of the sphere. This relationship is plotted in figure C.1.

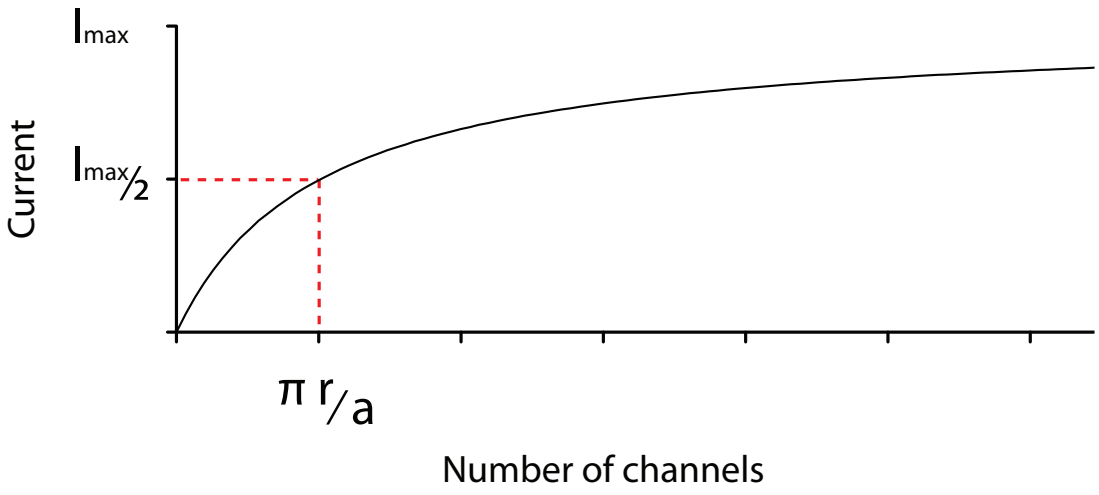


Figure C.1: The relationship between number of channels and current through the surface of a sphere. I_{max} is the maximum current possible, πr/a is the fraction of channels required to achieve half maximal current.

The number of channels required to achieve half maximal current amplitude ($I_{max}/2$) is therefore:

$$\begin{aligned} \frac{I}{I_0} = \frac{1}{1+(\pi r/Na)} &= 0.5 \\ 1 &= 0.5 + \pi r/2Na \\ 2Na &= Na + \pi r \\ N &= \pi r/a \end{aligned}$$

In this system:

At $I_{max}/2$:

$$\begin{aligned} \text{Number of channels} &= \pi r/a \\ &= \pi \times 0.5 \times 10^{-6}/5 \times 10^{-9} \\ &= 314 \text{ channels} \end{aligned}$$

For a sphere the size of a lysosome, with pores the putative size of HsTPC2, 314 channels would allow the most dynamic control whereby a small change in N gives a large change in I.
200 channels gives 38% of the maximum current, and 2.6 channels gives $> 1\%$.

References

[1] R Aarhus, D M Dickey, R M Graeff, K R Gee, T F Walseth, and H C Lee. **Activation and inactivation of Ca^{2+} release by $NAADP^{+}$**. *J Biol Chem*, **271**(15):8513–8516, Apr 1996. 22, 146, 232

[2] R. Aebersold and M. Mann. **Mass spectrometry-based proteomics**. *Nature*, **422**(6928):198–207, 2003. 73

[3] G.P. Ahern, P.R. Junankar, and A.F. Dulhunty. **Subconductance states in single-channel activity of skeletal muscle ryanodine receptors after removal of FKBP12**. *Biophysical Journal*, **72**(1):146 – 162, 1997. 115

[4] P K Aley, A M Mikolajczyk, B Munz, G C Churchill, A Galione, and F Berger. **Nicotinic acid adenine dinucleotide phosphate regulates skeletal muscle differentiation via action at two-pore channels**. *Proc Natl Acad Sci U S A*, **107**(46):19927–19932, Nov 2010. 23, 27, 295, 296

[5] P K Aley, H J Noh, X Gao, A A Tica, E Brailoiu, and G C Churchill. **A functional role for nicotinic acid adenine dinucleotide phosphate in oxytocin-mediated contraction of uterine smooth muscle from rat**. *J Pharmacol Exp Ther*, **333**(3):726–735, Jun 2010. 23, 27, 139, 295, 296

[6] G J Allen, S R Muir, and D Sanders. **Release of Ca^{2+} from individual plant vacuoles by both $InsP_3$ and cyclic ADP-ribose**. *Science*, **268**(5211):735–737, May 1995. 214

[7] K Anderson, F A Lai, Q Y Liu, E Rousseau, H P Erickson, and G Meissner. **Structural and functional characterization of the purified cardiac ryanodine receptor-Ca^{2+} release channel complex**. *J Biol Chem*, **264**(2):1329–1335, Jan 1989. 134

[8] H Ando, A Mizutani, H Kiefer, D Tsuzurugi, T Michikawa, and K Mikoshiba. **IRBIT suppresses IP_3 receptor activity by competing with IP_3 for the common binding site on the IP_3 receptor**. *Mol Cell*, **22**(6):795–806, Jun 2006. 11, 233

[9] M Aoyama, A Yamada, J Wang, S Ohya, S Furuzono, T Goto, S Hotta, Y Ito, T Matsubara, K Shimokata, S R Chen, Y Imaizumi, and S Nakayama. **Requirement of ryanodine receptors for pacemaker Ca^{2+} activity in ICC and HEK293 cells**. *J Cell Sci*, **117**(Pt 13):2813–2825, Jun 2004. 300

[10] K Arai, T Kanaseki, and S Ohkuma. **Isolation of highly purified lysosomes from rat liver: identification of electron carrier components on lysosomal membranes**. *J Biochem*, **110**(4):541–547, Oct 1991. 151

[11] E A Ariazi, E Brailoiu, S Yerrum, H A Shupp, M J Slifker, H E Cunliffe, M A Black, A L Donato, J B Arterburn, T I Oprea, E R Prossnitz, N J Dun, and V C Jordan. **The G protein-coupled receptor GPR30 inhibits proliferation of estrogen receptor-positive breast cancer cells**. *Cancer Res*, **70**(3):1184–1194, Feb 2010. 301

[12] T Babuke and R Tikkanen. **Dissecting the molecular function of reggie/flotillin proteins**. *Eur J Cell Biol*, **86**(9):525–532, Sep 2007. 240

[13] J Bak, R A Billington, and A A Genazzani. **Effect of luminal and extravesicular Ca^{2+} on NAADP binding and release properties**. *Biochem Biophys Res Commun*, **295**(4):806–811, Jul 2002. 23, 27

[14] J Bak, P White, G Timár, L Missiaen, A A Genazzani, and A Galione. **Nicotinic acid adenine dinucleotide phosphate triggers Ca^{2+} release from brain microsomes**. *Curr Biol*, **9**(14):751–754, Jul 1999. 23, 27

[15] A C Bakker, P Webster, W A Jacob, and N W Andrews. **Homotypic fusion between aggregated lysosomes triggered by elevated $[Ca^{2+}]i$ in fibroblasts**. *J Cell Sci*, **110 (Pt 18)**:2227–2238, Sep 1997. 151

[16] W E Balch and J E Rothman. **Characterization of protein transport between successive compartments of the Golgi apparatus: asymmetric properties of donor and acceptor activities in a cell-free system**. *Arch Biochem Biophys*, **240**(1):413–425, Jul 1985. 179

[17] G Baravalle, D Schober, M Huber, N Bayer, R F Murphy, and R Fuchs. **Transferrin recycling and dextran transport to lysosomes is differentially affected by bafilomycin, nocodazole, and low temperature**. *Cell Tissue Res*, **320**(1):99–113, Apr 2005. 305

[18] R Bargal, N Avidan, E Ben-Asher, Z Olender, M Zeigler, A Frumkin, A Raas-Rothschild, G Glusman, D Lancet, and G Bach. **Identification of the gene causing mucolipidosis type IV**. *Nat Genet*, **26**(1):118–123, Sep 2000. 30

[19] B D Beaumelle, A Gibson, and C R Hopkins. **Isolation and preliminary characterization of the major membrane boundaries of the endocytic pathway in lymphocytes**. *J Cell Biol*, **111**(5 Pt 1):1811–1823, Nov 1990. 179

[20] T. Beccari, S. Stinchi, and A. Orlacchio. **Biochemical Roles of Eukaryotic Cell Surface Macromolecules-MINI REVIEWS-Lysosomal aD-mannosidase**. *Bioscience Reports-Short Papers and Reviews in Molecular and Cellular Biology*, **19**(3):157–162, 1999. 189

[21] A Beck, M Kolisek, L A Bagley, A Fleig, and R Penner. **Nicotinic acid adenine dinucleotide phosphate and cyclic ADP-ribose regulate TRPM2 channels in T lymphocytes**. *FASEB J*, **20**(7):962–964, May 2006. 31

REFERENCES

[22] G Ben-Zeev, M Telias, and I Nussinovitch. **Lysophospholipids modulate voltage-gated calcium channel currents in pituitary cells; effects of lipid stress**. *Cell Calcium*, **47**(6):514–524, Jun 2010. 229

[23] C D Benham, J B Davis, and A D Randall. **Vanilloid and TRP channels: a family of lipid-gated cation channels**. *Neuropharmacology*, **42**(7):873–888, Jun 2002. 229

[24] H.C. Berg. *Random walks in biology*. Princeton Univ Pr, 1993. 323, 324

[25] I Berg, B V Potter, G W Mayr, and A H Guse. **Nicotinic acid adenine dinucleotide phosphate ($NAADP^+$) is an essential regulator of T-lymphocyte Ca^{2+}-signaling**. *J Cell Biol*, **150**(3):581–588, Aug 2000. 23, 207, 295, 296

[26] Jeremy M. Berg. **Biochemistry**. *W. H. FREEMAN AND COMPANY*, **Vol. 11. 5th ed.**, 2002. 94

[27] T Bergeland, L Haugen, O J Landsverk, H Stenmark, and O Bakke. **Cell-cycle-dependent binding kinetics for the early endosomal tethering factor EEA1**. *EMBO Rep*, **9**(2):171–178, Feb 2008. 262

[28] G Berridge, R Cramer, A Galione, and S Patel. **Metabolism of the novel Ca^{2+}-mobilizing messenger nicotinic acid-adenine dinucleotide phosphate via a 2'-specific Ca^{2+}-dependent phosphatase**. *Biochem J*, **365**(Pt 1):295–301, Jul 2002. 16

[29] G Berridge, G Dickinson, J Parrington, A Galione, and S Patel. **Solubilization of receptors for the novel Ca^{2+}-mobilizing messenger, nicotinic acid adenine dinucleotide phosphate**. *J Biol Chem*, **277**(46):43717–43723, Nov 2002. 28, 89, 95, 97

[30] M J Berridge, M D Bootman, and H L Roderick. **Calcium signalling: dynamics, homeostasis and remodelling**. *Nat Rev Mol Cell Biol*, **4**(7):517–529, Jul 2003. 1, 2, 4, 8, 10

[31] M J Berridge, P Lipp, and M D Bootman. **The versatility and universality of calcium signalling**. *Nat Rev Mol Cell Biol*, **1**(1):11–21, Oct 2000. 3, 4, 8, 223

[32] V Bertagnolo, M Mazzoni, D Ricci, C Carini, L M Neri, M Previati, and S Capitani. **Identification of PI-PLC beta 1, gamma 1, and delta 1 in rat liver: subcellular distribution and relationship to inositol lipid nuclear signalling**. *Cell Signal*, **7**(7):669–678, Sep 1995. 10

[33] A Bertl, H Bihler, C Kettner, and C L Slayman. **Electrophysiology in the eukaryotic model cell Saccharomyces cerevisiae**. *Pflügers Arch*, **436**(6):999–1013, Nov 1998. 214, 215

[34] A Bertl, E Blumwald, R Coronado, R Eisenberg, G Findlay, D Gradmann, B Hille, K Köhler, H A Kolb, and E MacRobbie. **Electrical measurements on endomembranes**. *Science*, **258**(5084):873–874, Nov 1992. 200

[35] S Bevan, S Hothi, G Hughes, I F James, H P Rang, K Shah, C S Walpole, and J C Yeats. **Capsazepine: a competitive antagonist of the sensory neurone excitant capsaicin**. *Br J Pharmacol*, **107**(2):544–552, Oct 1992. 229

[36] D Beyhl, S Hörtensteiner, E Martinoia, E E Farmer, J Fromm, I Marten, and R Hedrich. **The fou2 mutation in the major vacuolar cation channel TPC1 confers tolerance to inhibitory luminal calcium**. *Plant J*, **58**(5):715–723, Jun 2009. 141

[37] I Bezprozvanny and B E Ehrlich. **Inositol (1,4,5)-trisphosphate ($InsP_3$)-gated Ca channels from cerebellum: conduction properties for divalent cations and regulation by intraluminal calcium**. *J Gen Physiol*, **104**(5):821–856, Nov 1994. 118, 122, 132, 141

[38] I Bezprozvanny, J Watras, and B E Ehrlich. **Bell-shaped calcium-response curves of $Ins(1,4,5)P_3$- and calcium-gated channels from endoplasmic reticulum of cerebellum**. *Nature*, **351**(6329):751–754, Jun 1991. 11, 12

[39] R A Billington and A A Genazzani. **Characterization of $NAADP^+$ binding in sea urchin eggs**. *Biochem Biophys Res Commun*, **276**(1):112–116, Sep 2000. 89

[40] R A Billington and A A Genazzani. **PPADS is a reversible competitive antagonist of the NAADP receptor**. *Cell Calcium*, **41**(6):505–511, Jun 2007. 24, 32

[41] R A Billington, A Ho, and A A Genazzani. **Nicotinic acid adenine dinucleotide phosphate (NAADP) is present at micromolar concentrations in sea urchin spermatozoa**. *J Physiol*, **544**(Pt 1):107–112, Oct 2002. 17

[42] R A Billington, J W Thuring, S J Conway, L Packman, A B Holmes, and A A Genazzani. **Production and characterization of reduced NAADP (nicotinic acid-adenine dinucleotide phosphate)**. *Biochem J*, **378**(Pt 1):275–280, Feb 2004. 16

[43] B. Bjellqvist, B. Basse, E. Olsen, and J.E. Celis. **Reference points for comparisons of two-dimensional maps of proteins from different human cell types defined in a pH scale where isoelectric points correlate with polypeptide compositions**. *Electrophoresis*, **15**(1):529–539, 1994. 50

[44] D Boehning, S K Joseph, D O Mak, and J K Foskett. **Single-channel recordings of recombinant inositol trisphosphate receptors in mammalian nuclear envelope**. *Biophys J*, **81**(1):117–124, Jul 2001. 216

[45] D Boehning, D O Mak, J K Foskett, and S K Joseph. **Molecular determinants of ion permeation and selectivity in inositol 1,4,5-trisphosphate receptor Ca^{2+} channels**. *J Biol Chem*, **276**(17):13509–13512, Apr 2001. 216

[46] F X Boittin, A Galione, and A M Evans. **Nicotinic acid adenine dinucleotide phosphate mediates Ca^{2+} signals and contraction in arterial smooth muscle via a two-pool mechanism**. *Circ Res*, **91**(12):1168–1175, Dec 2002. 14, 300

[47] E Brailoiu, D Churamani, X Cai, M G Schrlau, G C Brailoiu, X Gao, R Hooper, M J Boulware, N J Dun, J S Marchant, and S Patel. **Essential requirement for two-pore channel 1 in NAADP-mediated calcium signaling**. *J Cell Biol*, **186**(2):201–209, Jul 2009. 27, 33, 34, 35, 37, 90, 94, 147, 262, 263, 301

[48] E Brailoiu, J L Hoard, C M Filipeanu, G C Brailoiu, S L Dun, S Patel, and N J Dun. **Nicotinic acid adenine dinucleotide phosphate potentiates neurite outgrowth**. *J Biol Chem*, **280**(7):5646–5650, Feb 2005. 19

[49] E Brailoiu, R Hooper, X Cai, G C Brailoiu, M V Keebler, N J Dun, J S Marchant, and S Patel. **An ancestral deuterostome family of two-pore channels mediates nicotinic acid adenine dinucleotide phosphate-dependent calcium release from acidic organelles**. *J Biol Chem*, **285**(5):2897–2901, Jan 2010. 42, 43, 263

[50] E Brailoiu, T Rahman, D Churamani, D L Prole, G C Brailoiu, R Hooper, C W Taylor, and S Patel. **An NAADP-gated two-pore channel targeted to the plasma membrane uncouples triggering from amplifying Ca^{2+} signals**. *J Biol Chem*, **285**(49):38511–38516, Dec 2010. 37, 133, 137, 139, 140, 142, 144, 227, 263

[51] G C Brailoiu, E Brailoiu, R Parkesh, A Galione, G C Churchill, S Patel, and N J Dun. **NAADP-mediated channel 'chatter' in neurons of the rat medulla oblongata**. *Biochem J*, **419**(1):91–97, Apr 2009. 302

[52] G C Brailoiu, B Gurzu, X Gao, R Parkesh, P K Aley, D I Trifa, A Galione, N J Dun, M Madesh, S Patel, G C Churchill, and E Brailoiu. **Acidic NAADP-sensitive calcium stores in the endothelium: agonist-specific recruitment and role in regulating blood pressure**. *J Biol Chem*, **285**(48):37133–37137, Nov 2010. 27

[53] R D Burgoyne and M J Clague. **Calcium and calmodulin in membrane fusion**. *Biochim Biophys Acta*, **1641**(2-3):137–143, Aug 2003. 305

[54] J K Burkhardt, F A Wiebel, S Hester, and Y Argon. **The giant organelles in beige and Chediak-Higashi fibroblasts are derived from late endosomes and mature lysosomes**. *J Exp Med*, **178**(6):1845–1856, Dec 1993. 217

[55] P J Calcraft, M Ruas, Z Pan, X Cheng, A Arredouani, X Hao, J Tang, K Rietdorf, L Teboul, K T Chuang, P Lin, R Xiao, C Wang, Y Zhu, Y Lin, C N Wyatt, J Parrington, J Ma, A M Evans, A Galione, and M X Zhu. **NAADP mobilizes calcium from acidic organelles through two-pore channels**. *Nature*, **459**(7246):596–600, May 2009. 34, 35, 36, 38, 44, 45, 49, 51, 90, 94, 95, 105, 107, 120, 124, 133, 147, 224, 248, 262, 263, 298, 300, 301, 302

[56] P E Campbell, C M Harris, C M Harris, T Sirimanna, and A Vellodi. **A model of neuronopathic Gaucher disease**. *J Inherit Metab Dis*, **26**(7):629–639, 2003. 307

[57] J M Cancela, G C Churchill, and A Galione. **Coordination of agonist-induced Ca^{2+}-signalling patterns by NAADP in pancreatic acinar cells**. *Nature*, **398**(6722):74–76, Mar 1999. 23, 27, 32, 120, 124, 126, 139, 298, 302

[58] E Carafoli. **Plasma membrane calcium pump: structure, function and relationships**. *Basic Res Cardiol*, **92 Suppl 1**:59–61, 1997. 2

[59] E Carafoli. **The calcium-signalling saga: tap water and protein crystals**. *Nat Rev Mol Cell Biol*, **4**(4):326–332, Apr 2003. 1

[60] E Carafoli and M Brini. **Calcium pumps: structural basis for and mechanism of calcium transmembrane transport**. *Curr Opin Chem Biol*, **4**(2):152–161, Apr 2000. 4

[61] E Carafoli, F Kessler, R Falchetto, R Heim, M Quadroni, J Krebs, E E Strehler, and T Vorherr. **The molecular basis of the modulation of the plasma membrane calcium pump by calmodulin**. *Ann N Y Acad Sci*, **671**:58–68, Nov 1992. 2

[62] E Carafoli, L Santella, D Branca, and M Brini. **Generation, control, and processing of cellular calcium signals**. *Crit Rev Biochem Mol Biol*, **36**(2):107–260, Apr 2001. 1, 3

[63] W A Catterall. **Functional subunit structure of voltage-gated calcium channels**. *Science*, **253**(5027):1499–1500, Sep 1991. 5

[64] W A Catterall. **Structure and regulation of voltage-gated Ca^{2+} channels**. *Annu Rev Cell Dev Biol*, **16**:521–555, 2000. 5, 233, 270, 279, 287

[65] W A Catterall, E Perez-Reyes, T P Snutch, and J Striessnig. **International Union of Pharmacology. XLVIII. Nomenclature and structure-function relationships of voltage-gated calcium channels**. *Pharmacol Rev*, **57**(4):411–425, Dec 2005. 136, 137, 221, 228

[66] J Cerny, Y Feng, A Yu, K Miyake, B Borgonovo, J Klumperman, J Meldolesi, P L McNeil, and T Kirchhausen. **The small chemical vacuolin-1 inhibits Ca^{2+}-dependent lysosomal exocytosis but not cell resealing**. *EMBO Rep*, **5**(9):883–888, Sep 2004. 63, 151, 174, 216

[67] Q Chang, E Gyftogianni, S F van de Graaf, S Hoefs, F A Weidema, R J Bindels, and J G Hoenderop. **Molecular determinants in TRPV5 channel assembly**. *J Biol Chem*, **279**(52):54304–54311, Dec 2004. 288

[68] A Chattopadhyay and K G Harikumar. **Dependence of critical micelle concentration of a zwitterionic detergent on ionic strength: implications in receptor solubilization**. *FEBS Lett*, **391**(1-2):199–202, Aug 1996. 95

[69] Y Chen, T Cai, C Yang, D A Turner, D R Giovannucci, and Z Xie. **Regulation of inositol 1,4,5-trisphosphate receptor-mediated calcium release by the Na^+/K^+-ATPase in cultured renal epithelial cells**. *J Biol Chem*, **283**(2):1128–1136, Jan 2008. 290

[70] H Cheng, W J Lederer, and M B Cannell. **Calcium sparks: elementary events underlying excitation-contraction coupling in heart muscle**. *Science*, **262**(5134):740–744, Oct 1993. 8

[71] X Cheng. **Characterisation and identification of the NAADP receptor.** *DPhil thesis*, 2009. 97

[72] R Chenna, H Sugawara, T Koike, R Lopez, T J Gibson, D G Higgins, and J D Thompson. **Multiple sequence alignment with the Clustal series of programs**. *Nucleic Acids Res*, **31**(13):3497–3500, Jul 2003. 29, 40

REFERENCES

[73] L L Ching, A J Williams, and R Sitsapesan. **Evidence for Ca^{2+} activation and inactivation sites on the luminal side of the cardiac ryanodine receptor complex**. *Circ Res*, **87**(3):201–206, Aug 2000. 141

[74] E N Chini and T P Dousa. **Nicotinate-adenine dinucleotide phosphate-induced Ca^{2+}-release does not behave as a Ca^{2+}-induced Ca^{2+}-release system**. *Biochem J*, **316 (Pt 3)**:709–711, Jun 1996. 23

[75] E I Christensen and A B Maunsbach. **Effects of dextran on lysosomal ultrastructure and protein digestion in renal proximal tubule**. *Kidney Int*, **16**(3):301–311, Sep 1979. 168

[76] K A Christensen, J T Myers, and J A Swanson. **pH-dependent regulation of lysosomal calcium in macrophages**. *J Cell Sci*, **115**(Pt 3):599–607, Feb 2002. 4, 222

[77] D Churamani, G D Dickinson, and S Patel. **NAADP binding to its target protein in sea urchin eggs requires phospholipids**. *Biochem J*, **386**(Pt 3):497–504, Mar 2005. 229

[78] G C Churchill and A Galione. **NAADP induces Ca^{2+} oscillations via a two-pool mechanism by priming IP_3- and cADPR-sensitive Ca^{2+} stores**. *EMBO J*, **20**(11):2666–2671, Jun 2001. 18

[79] G C Churchill and C F Louis. **Roles of Ca^{2+}, inositol trisphosphate and cyclic ADP-ribose in mediating intercellular Ca^{2+} signaling in sheep lens cells**. *J Cell Sci*, **111 (Pt 9)**:1217–1225, May 1998. 8

[80] G C Churchill, Y Okada, J M Thomas, A A Genazzani, S Patel, and A Galione. **NAADP mobilizes Ca^{2+} from reserve granules, lysosome-related organelles, in sea urchin eggs**. *Cell*, **111**(5):703–708, Nov 2002. 4, 18, 19, 27

[81] G C Churchill, J S O'Neill, R Masgrau, S Patel, J M Thomas, A A Genazzani, and A Galione. **Sperm deliver a new second messenger: NAADP**. *Curr Biol*, **13**(2):125–128, Jan 2003. 17

[82] D E Clapham. **Intracellular calcium. Replenishing the stores**. *Nature*, **375**(6533):634–635, Jun 1995. 1, 11

[83] D E Clapham. **TRP channels as cellular sensors**. *Nature*, **426**(6966):517–524, Dec 2003. 5

[84] D E Clapham and D L Garbers. **International Union of Pharmacology. L. Nomenclature and structure-function relationships of CatSper and two-pore channels**. *Pharmacol Rev*, **57**(4):451–454, Dec 2005. 286

[85] D E Clapham, D Julius, C Montell, and G Schultz. **International Union of Pharmacology. XLIX. Nomenclature and structure-function relationships of transient receptor potential channels**. *Pharmacol Rev*, **57**(4):427–450, Dec 2005. 286

[86] D E Clapham, L W Runnels, and C Strübing. **The TRP ion channel family**. *Nat Rev Neurosci*, **2**(6):387–396, Jun 2001. 30

[87] D L Clapper, T F Walseth, P J Dargie, and H C Lee. **Pyridine nucleotide metabolites stimulate calcium release from sea urchin egg microsomes desensitized to inositol trisphosphate**. *J Biol Chem*, **262**(20):9561–9568, Jul 1987. 18

[88] M.G. Claros and G. Heijne. **TopPred II: an improved software for membrane protein structure predictions**. *Computer applications in the biosciences: CABIOS*, **10**(6):685, 1994. 50

[89] L Cocco, N M Maraldi, S Capitani, A M Martelli, and F A Manzoli. **Nuclear localization and signalling activity of inositol lipids**. *Ital J Anat Embryol*, **106**(2 Suppl 1):31–43, 2001. 10

[90] Z A Cohn and B A Ehrenreich. **The uptake, storage, and intracellular hydrolysis of carbohydrates by macrophages**. *J Exp Med*, **129**(1):201–225, Jan 1969. 174

[91] J H Collins. **Sequence analysis of the ryanodine receptor: possible association with a 12K, FK506-binding immunophilin/protein kinase C inhibitor**. *Biochem Biophys Res Commun*, **178**(3):1288–1290, Aug 1991. 12, 233

[92] B Corry, T W Allen, S Kuyucak, and S H Chung. **A model of calcium channels**. *Biochim Biophys Acta*, **1509**(1-2):1–6, Dec 2000. 228

[93] F Cosker, N Cheviron, M Yamasaki, A Menteyne, F E Lund, M J Moutin, A Galione, and J M Cancela. **The ecto-enzyme CD38 is a NAADP synthase which couples receptor activation to Ca^{2+} mobilization from lysosomes in pancreatic acinar cells**. *J Biol Chem*, Sep 2010. 14, 16

[94] T L Cover and S R Blanke. **Helicobacter pylori VacA, a paradigm for toxin multifunctionality**. *Nat Rev Microbiol*, **3**(4):320–332, Apr 2005. 217

[95] L. Coyaud, A. Kurkdjian, R. Kado, and R. Hedrich. **Ion channels and ATP-driven pumps involved in ion transport across the tonoplast of sugar-beet vacuoles**. *Biochimica et Biophysica Acta (BBA)-Biomembranes*, **902**(2):263–268, 1987. 214

[96] H Cretin. **The proton gradient across the vacuolysosomal membrane of lutoids from the latex of Hevea brasiliensis. I. Further evidence for a proton-translocating ATPase on the vacuolysosomal membrane of intact lutoids**. *J Membr Biol*, **65**(3):175–184, 1982. 219

[97] M Csala, G Bánhegyi, L Braun, R Szirmai, A Burchell, B Burchell, A Benedetti, and J Mandl. **Beta-glucuronidase latency in isolated murine hepatocytes**. *Biochem Pharmacol*, **59**(7):801–805, Apr 2000. 157

[98] M Cserzö, E Wallin, I Simon, G von Heijne, and A Elofsson. **Prediction of transmembrane alpha-helices in prokaryotic membrane proteins: the dense alignment surface method**. *Protein Eng*, **10**(6):673–676, Jun 1997. 50

[99] G Csordás, A P Thomas, and G Hajnóczky. **Calcium signal transmission between ryanodine receptors and mitochondria in cardiac muscle**. *Trends Cardiovasc Med*, **11**(7):269–275, Oct 2001. 301

[100] C Curcio-Morelli, P Zhang, B Venugopal, F A Charles, M F Browning, H F Cantiello, and S A Slaugenhaupt. **Functional multimerization of mucolipin channel proteins**. *J Cell Physiol*, **222**(2):328–335, Feb 2010. 286

[101] J L Daiss and T F Roth. **Isolation of coated vesicles: comparative studies**. *Methods Enzymol*, **98**:337–349, 1983. 179

[102] O M de Brito and L Scorrano. **Mitofusin 2 tethers endoplasmic reticulum to mitochondria**. *Nature*, **456**(7222):605–610, Dec 2008. 174, 301

[103] K DeCourcy and B Storrie. **Osmotic swelling of endocytic compartments induced by internalized sucrose is restricted to mature lysosomes in cultured mammalian cells**. *Exp Cell Res*, **192**(1):52–60, Jan 1991. 63, 174, 218

[104] O Dellis, S G Dedos, S C Tovey, Taufiq-Ur-Rahman, S J Dubel, and C W Taylor. **Ca^{2+} entry through plasma membrane IP_3 receptors**. *Science*, **313**(5784):229–233, Jul 2006. 11

[105] O Dellis, A M Rossi, S G Dedos, and C W Taylor. **Counting functional inositol 1,4,5-trisphosphate receptors into the plasma membrane**. *J Biol Chem*, **283**(2):751–755, Jan 2008. 11

[106] N Demaurex. **pH Homeostasis of cellular organelles**. *News Physiol Sci*, **17**:1–5, Feb 2002. 125

[107] B Dewald and O Touster. **A new alpha-D-mannosidase occurring in Golgi membranes**. *J Biol Chem*, **248**(20):7223–7233, Oct 1973. 160

[108] G D Dickinson and S Patel. **Modulation of NAADP (nicotinic acid-adenine dinucleotide phosphate) receptors by K^+ ions: evidence for multiple NAADP receptor conformations**. *Biochem J*, **375**(Pt 3):805–812, Nov 2003. 290

[109] C Dickson, V Fantl, C Gillett, S Brookes, J Bartek, R Smith, C Fisher, D Barnes, and G Peters. **Amplification of chromosome band 11q13 and a role for cyclin D1 in human breast cancer**. *Cancer Lett*, **90**(1):43–50, Mar 1995. 43

[110] O Diettrich, K Mills, A W Johnson, A Hasilik, and B G Winchester. **Application of magnetic chromatography to the isolation of lysosomes from fibroblasts of patients with lysosomal storage disorders**. *FEBS Lett*, **441**(3):369–372, Dec 1998. 65

[111] C Dingwall and R Laskey. **The nuclear membrane**. *Science*, **258**(5084):942–947, Nov 1992. 4, 11, 215

[112] X P Dong, X Cheng, E Mills, M Delling, F Wang, T Kurz, and H Xu. **The type IV mucolipidosis-associated protein TRPML1 is an endolysosomal iron release channel**. *Nature*, **455**(7215):992–996, Oct 2008. 30, 151, 193, 202, 212, 213, 216, 219

[113] X P Dong, D Shen, X Wang, T Dawson, X Li, Q Zhang, X Cheng, Y Zhang, L S Weisman, M Delling, and H Xu. **$PI(3,5)P_2$ controls membrane trafficking by direct activation of mucolipin Ca^{2+} release channels in the endolysosome**. *Nat Commun*, **1**:38–38, 2010. 31, 213, 216, 221, 229

[114] P Donoso, H Prieto, and C Hidalgo. **Luminal calcium regulates calcium release in triads isolated from frog and rabbit skeletal muscle**. *Biophys J*, **68**(2):507–515, Feb 1995. 141

[115] D A Doyle, J Morais Cabral, R A Pfuetzner, A Kuo, J M Gulbis, S L Cohen, B T Chait, and R MacKinnon. **The structure of the potassium channel: molecular basis of K+ conduction and selectivity**. *Science*, **280**(5360):69–77, Apr 1998. 228

[116] A Doyotte, A Mironov, E McKenzie, and P Woodman. **The Bro1-related protein HD-PTP/PTPN23 is required for endosomal cargo sorting and multivesicular body morphogenesis**. *Proc Natl Acad Sci U S A*, **105**(17):6308–6313, Apr 2008. 262

[117] M Duvvuri and J P Krise. **A novel assay reveals that weakly basic model compounds concentrate in lysosomes to an extent greater than pH-partitioning theory would predict**. *Mol Pharm*, **2**(6):440–448, Nov-Dec 2005. 65

[118] B E Ehrlich and J Watras. **Inositol 1,4,5-trisphosphate activates a channel from smooth muscle sarcoplasmic reticulum**. *Nature*, **336**(6199):583–586, Dec 1988. 114, 118

[119] M G Erickson, B A Alseikhan, B Z Peterson, and D T Yue. **Preassociation of calmodulin with voltage-gated Ca^{2+} channels revealed by FRET in single living cells**. *Neuron*, **31**(6):973–985, Sep 2001. 279

[120] I Erler, D Hirnet, U Wissenbach, V Flockerzi, and B A Niemeyer. **Ca^{2+}-selective transient receptor potential V channel architecture and function require a specific ankyrin repeat**. *J Biol Chem*, **279**(33):34456–34463, Aug 2004. 288

[121] J A Ernst and A T Brunger. **High resolution structure, stability, and synaptotagmin binding of a truncated neuronal SNARE complex**. *J Biol Chem*, **278**(10):8630–8636, Mar 2003. 288

[122] J M Falcón-Pérez, R Nazarian, C Sabatti, and E C Dell'Angelica. **Distribution and dynamics of Lamp1-containing endocytic organelles in fibroblasts deficient in BLOC-3**. *J Cell Sci*, **118**(Pt 22):5243–5255, Nov 2005. 262

[123] P FATT and B L GINSBORG. **The ionic requirements for the production of action potentials in crustacean muscle fibres**. *J Physiol*, **142**(3):516–543, Aug 1958. 63

[124] A L Ferris, J C Brown, R D Park, and B Storrie. **Chinese hamster ovary cell lysosomes rapidly exchange contents**. *J Cell Biol*, **105**(6 Pt 1):2703–2712, Dec 1987. 174, 218

[125] C D Ferris, R L Huganir, S Supattapone, and S H Snyder. **Purified inositol 1,4,5-trisphosphate receptor mediates calcium flux in reconstituted lipid vesicles**. *Nature*, **342**(6245):87–89, Nov 1989. 11

[126] C D Ferris and S H Snyder. **Inositol 1,4,5-trisphosphate-activated calcium channels**. *Annu Rev Physiol*, **54**:469–488, 1992. 6

REFERENCES

[127] E A Finch, T J Turner, and S M Goldin. **Calcium as a coagonist of inositol 1,4,5-trisphosphate-induced calcium release**. *Science*, **252**(5004):443–446, Apr 1991. 12

[128] M Forgac. **Vacuolar ATPases: rotary proton pumps in physiology and pathophysiology**. *Nat Rev Mol Cell Biol*, **8**(11):917–929, Nov 2007. 291

[129] J K Foskett, C White, K H Cheung, and D O Mak. **Inositol trisphosphate receptor Ca^{2+} release channels**. *Physiol Rev*, **87**(2):593–658, Apr 2007. 11, 12, 135, 136, 137, 215, 216, 225, 229, 233

[130] R Fuchs, S Schmid, and I Mellman. **A possible role for Na^+,K^+-ATPase in regulating ATP-dependent endosome acidification**. *Proc Natl Acad Sci U S A*, **86**(2):539–543, Jan 1989. 240, 290

[131] Y Fujiwara and D L Minor. **X-ray crystal structure of a TRPM assembly domain reveals an antiparallel four-stranded coiled-coil**. *J Mol Biol*, **383**(4):854–870, Nov 2008. 287

[132] T Furuichi, I C Mori, K Takahashi, and S Muto. **Sugar-induced increase in cytosolic Ca^{2+} in *Arabidopsis thaliana* whole plants**. *Plant Cell Physiol*, **42**(10):1149–1155, Oct 2001. 35, 41

[133] J Gaburjakova and M Gaburjakova. **Effect of luminal Ca^{2+} on the stability of coupled gating between ryanodine receptors from the rat heart**. *Acta Physiol (Oxf)*, **193**(3):219–227, Jul 2008. 137, 138

[134] A Galione. **NAADP receptors**. *Cold Spring Harb Perspect Biol*, **3**(1), Jan 2011. 302

[135] A Galione, A M Evans, J Ma, J Parrington, A Arredouani, X Cheng, and M X Zhu. **The acid test: the discovery of two-pore channels (TPCs) as NAADP-gated endolysosomal Ca^{2+} release channels**. *Pflügers Arch*, **458**(5):869–876, Sep 2009. 31, 34

[136] A Galione, H C Lee, and W B Busa. **Ca^{2+}-induced Ca^{2+} release in sea urchin egg homogenates: modulation by cyclic ADP-ribose**. *Science*, **253**(5024):1143–1146, Sep 1991. 12

[137] A Galione and O H Petersen. **The NAADP receptor: new receptors or new regulation?** *Mol Interv*, **5**(2):73–79, Apr 2005. 19

[138] A Galione and M Ruas. **NAADP receptors**. *Cell Calcium*, **38**(3-4):273–280, Sep-Oct 2005. 20, 21

[139] D L Galvan, E Borrego-Diaz, P J Perez, and G A Mignery. **Subunit oligomerization, and topology of the inositol 1,4, 5-trisphosphate receptor**. *J Biol Chem*, **274**(41):29483–29492, Oct 1999. 285

[140] G Gambara, R A Billington, M Debidda, A D'Alessio, F Palombi, E Ziparo, A A Genazzani, and A Filippini. **NAADP-induced Ca^{2+} signaling in response to endothelin is via the receptor subtype B and requires the integrity of lipid rafts/caveolae**. *J Cell Physiol*, **216**(2):396–404, Aug 2008. 33

[141] S Gansauge, F Gansauge, M Ramadani, H Stobbe, B Rau, N Harada, and H G Beger. **Overexpression of cyclin D1 in human pancreatic carcinoma is associated with poor prognosis**. *Cancer Res*, **57**(9):1634–1637, May 1997. 43

[142] N García-Sanz, A Fernández-Carvajal, C Morenilla-Palao, R Planells-Cases, E Fajardo-Sánchez, G Fernández-Ballester, and A Ferrer-Montiel. **Identification of a tetramerization domain in the C terminus of the vanilloid receptor**. *J Neurosci*, **24**(23):5307–5314, Jun 2004. 287, 288

[143] E. Gasteiger, A. Gattiker, C. Hoogland, I. Ivanyi, R.D. Appel, and A. Bairoch. **ExPASy: the proteomics server for in-depth protein knowledge and analysis**. *Nucleic Acids Research*, **31**(13):3784, 2003. 50

[144] E. Gasteiger, C. Hoogland, A. Gattiker, S. Duvaud, M.R. Wilkins, R.D. Appel, and A. Bairoch. **Protein identification and analysis tools on the ExPASy server**. *The proteomics protocols handbook*, pages 571–607, 2005. 50

[145] L Y Geer, S P Markey, J A Kowalak, L Wagner, M Xu, D M Maynard, X Yang, W Shi, and S H Bryant. **Open mass spectrometry search algorithm**. *J Proteome Res*, **3**(5):958–964, Sep-Oct 2004. 74

[146] A A Genazzani. ***Psammechinus miliaris* egg homogenate as a model to investigate Ca^{2+}-release mechanisms**. *Journal of the Marine Biological Association of the United Kingdom*, **79**:323–326, 1999. 22

[147] A A Genazzani, R M Empson, and A Galione. **Unique inactivation properties of NAADP-sensitive Ca^{2+} release**. *J Biol Chem*, **271**(20):11599–11602, May 1996. 22, 23, 25, 146, 232

[148] A A Genazzani and A Galione. **Nicotinic acid-adenine dinucleotide phosphate mobilizes Ca^{2+} from a thapsigargin-insensitive pool**. *Biochem J*, **315 (Pt 3)**:721–725, May 1996. 18, 19, 23

[149] A A Genazzani, M Mezna, D M Dickey, F Michelangeli, T F Walseth, and A Galione. **Pharmacological properties of the Ca^{2+}-release mechanism sensitive to NAADP in the sea urchin egg**. *Br J Pharmacol*, **121**(7):1489–1495, Aug 1997. 20, 22, 23, 27, 307

[150] J V Gerasimenko, Y Maruyama, K Yano, N J Dolman, A V Tepikin, O H Petersen, and O V Gerasimenko. **NAADP mobilizes Ca^{2+} from a thapsigargin-sensitive store in the nuclear envelope by activating ryanodine receptors**. *J Cell Biol*, **163**(2):271–282, Oct 2003. 32, 140, 151

[151] J V Gerasimenko, A V Tepikin, O H Petersen, and O V Gerasimenko. **Calcium uptake via endocytosis with rapid release from acidifying endosomes**. *Curr Biol*, **8**(24):1335–1338, Dec 1998. 222

[152] C L German and C L Howe. **Preparation of biologically active subcellular fractions using the Balch homogenizer**. *Anal Biochem*, **394**(1):117–124, Nov 2009. 179

[153] D Gillespie and M Fill. **Intracellular calcium release channels mediate their own countercurrent: the ryanodine receptor case study**. *Biophys J*, **95**(8):3706–3714, Oct 2008. 135

[154] I Gillot, B Ciapa, P Payan, and C Sardet. **The calcium content of cortical granules and the loss of calcium from sea urchin eggs at fertilization**. *Dev Biol*, **146**(2):396–405, Aug 1991. 221

[155] Flyion Gmbh. *Fully automated patch clamp robot*, 2009. 193

[156] M W Goldberg and T D Allen. **The nuclear pore complex: three-dimensional surface structure revealed by field emission, in-lens scanning electron microscopy, with underlying structure uncovered by proteolysis**. *J Cell Sci*, **106 (Pt 1)**:261–274, Sep 1993. 215

[157] S M Gollin. **Chromosomal alterations in squamous cell carcinomas of the head and neck: window to the biology of disease**. *Head Neck*, **23**(3):238–253, Mar 2001. 43

[158] G W Gordon, G Berry, X H Liang, B Levine, and B Herman. **Quantitative fluorescence resonance energy transfer measurements using fluorescence microscopy**. *Biophys J*, **74**(5):2702–2713, May 1998. 273

[159] D Gozuacik and A Kimchi. **Autophagy as a cell death and tumor suppressor mechanism**. *Oncogene*, **23**(16):2891–2906, Apr 2004. 46, 303

[160] R Graeff, Q Liu, I A Kriksunov, Q Hao, and H C Lee. **Acidic residues at the active sites of CD38 and ADP-ribosyl cyclase determine nicotinic acid adenine dinucleotide phosphate (NAADP) synthesis and hydrolysis activities**. *J Biol Chem*, **281**(39):28951–28957, Sep 2006. 16

[161] R M Graeff, R J Podein, R Aarhus, and H C Lee. **Magnesium ions but not ATP inhibit cyclic ADP-ribose-induced calcium release**. *Biochem Biophys Res Commun*, **206**(2):786–791, Jan 1995. 12

[162] J M Graham. **Isolation of lysosomes from tissues and cells by differential and density gradient centrifugation**. *Curr Protoc Cell Biol*, **Chapter 3**, May 2001. 151

[163] L Grant and P A Fuchs. **Auditory transduction in the mouse**. *Pflügers Arch*, **454**(5):793–804, Aug 2007. 308

[164] S Grinstein and W Furuya. **The electrochemical H^+ gradient of platelet secretory alpha-granules. Contribution of a H^+ pump and a Donnan potential**. *J Biol Chem*, **258**(12):7876–7882, Jun 1983. 219

[165] S K Gross, P F Daniel, J E Evans, and R H McCluer. **Lipid composition of lysosomal multilamellar bodies of male mouse urine**. *J Lipid Res*, **32**(1):157–164, Jan 1991. 229

[166] R. Gupta, E. Jung, and S. Brunak. **Prediction of N-glycosylation sites in human proteins**. *preparation. The web tool is located at http://www. cbs. dtu. dk/services/NetNGlyc*, 2002. 50, 92

[167] I Györke, N Hester, L R Jones, and S Györke. **The role of calsequestrin, triadin, and junctin in conferring cardiac ryanodine receptor responsiveness to luminal calcium**. *Biophys J*, **86**(4):2121–2128, Apr 2004. 141, 142, 234

[168] S Györke and D Terentyev. **Modulation of ryanodine receptor by luminal calcium and accessory proteins in health and cardiac disease**. *Cardiovasc Res*, **77**(2):245–255, Jan 2008. 97

[169] D J Hackam, O D Rotstein, W J Zhang, N Demaurex, M Woodside, O Tsai, and S Grinstein. **Regulation of phagosomal acidification. Differential targeting of Na^+/H^+ exchangers, Na^+/K^+-ATPases, and vacuolar-type H^+-ATPases.** *J Biol Chem*, **272**(47):29810–29820, Nov 1997. 290

[170] J R Haigh, R Parris, and J H Phillips. **Free concentrations of sodium, potassium and calcium in chromaffin granules**. *Biochem J*, **259**(2):485–491, Apr 1989. 222

[171] T Haller, P Dietl, P Deetjen, and H Völkl. **The lysosomal compartment as intracellular calcium store in MDCK cells: a possible involvement in $InsP_3$-mediated Ca^{2+} release**. *Cell Calcium*, **19**(2):157–165, Feb 1996. 4

[172] Y Hara, M Wakamori, M Ishii, E Maeno, M Nishida, T Yoshida, H Yamada, S Shimizu, E Mori, J Kudoh, N Shimizu, H Kurose, Y Okada, K Imoto, and Y Mori. **LTRPC2 Ca^{2+}-permeable channel activated by changes in redox status confers susceptibility to cell death**. *Mol Cell*, **9**(1):163–173, Jan 2002. 31

[173] M Hara-Chikuma, B Yang, N D Sonawane, S Sasaki, S Uchida, and A S Verkman. **ClC-3 chloride channels facilitate endosomal acidification and chloride accumulation**. *J Biol Chem*, **280**(2):1241–1247, Jan 2005. 222

[174] P Harikumar and J P Reeves. **The lysosomal proton pump is electrogenic**. *J Biol Chem*, **258**(17):10403–10410, Sep 1983. 202

[175] R. Hedrich, UI Flugge, and JM Fernandez. **Patch-clamp studies of ion transport in isolated plant vacuoles**. *FEBS letters*, **204**(2):228–232, 1986. 214, 231

[176] R Hedrich and I Marten. **TPC1 - SV Channels Gain Shape**. *Mol Plant*, Mar 2011. 41, 134, 136, 146

[177] R. Hedrich and E. Neher. **Cytoplasmic calcium regulates voltage-dependent ion channels in plant vacuoles**. *Nature*, **329**:833 – 836, 1987. 214

[178] N Hellwig, N Albrecht, C Harteneck, G Schultz, and M Schaefer. **Homo- and heteromeric assembly of TRPV channel subunits**. *J Cell Sci*, **118**(Pt 5):917–928, Mar 2005. 285, 286, 288

[179] R Henning. **pH gradient across the lysosomal membrane generated by selective cation permeability and Donnan equilibrium**. *Biochim Biophys Acta*, **401**(2):307–316, Aug 1975. 219

[180] A Herrmann-Frank, E Darling, and G Meissner. **Functional characterization of the Ca^{2+}-gated Ca^{2+} release channel of vascular smooth muscle sarcoplasmic reticulum**. *Pflügers Arch*, **418**(4):353–359, May 1991. 134

REFERENCES

[181] P Hess and R W Tsien. **Mechanism of ion permeation through calcium channels**. *Nature*, **309**(5967):453–456, May 1984. 228

[182] C Hidalgo and P Donoso. **Luminal calcium regulation of calcium release from sarcoplasmic reticulum**. *Biosci Rep*, **15**(5):387–397, Oct 1995. 124

[183] M K Higgins, D Weitz, T Warne, G F Schertler, and U B Kaupp. **Molecular architecture of a retinal cGMP-gated channel: the arrangement of the cytoplasmic domains**. *EMBO J*, **21**(9):2087–2094, May 2002. 288

[184] Bertil Hille. *Ion Channels of Excitable Membranes*. Sinauer Associates Inc., third edition, 2001. 228

[185] K. Hofmann and W. Stoffel. **TMbase-A database of membrane spanning proteins segments**. *Biol Chem HoppeSeyler*, **347**, 1993. 50

[186] T Hofmann, M Schaefer, G Schultz, and T Gudermann. **Subunit composition of mammalian transient receptor potential channels in living cells**. *Proc Natl Acad Sci U S A*, **99**(11):7461–7466, May 2002. 285, 287

[187] M Hohenegger, J Suko, R Gscheidlinger, H Drobny, and A Zidar. **Nicotinic acid-adenine dinucleotide phosphate activates the skeletal muscle ryanodine receptor**. *Biochem J*, **367**(Pt 2):423–431, Oct 2002. 32, 140, 151

[188] R Hooper, D Churamani, E Brailoiu, C W Taylor, and S Patel. **Membrane topology of NAADP-sensitive two-pore channels and their regulation by N-linked glycosylation**. *J Biol Chem*, Dec 2010. 163

[189] J H Horne and T Meyer. **Luminal calcium regulates the inositol trisphosphate receptor of rat basophilic leukemia cells at a cytosolic site**. *Biochemistry*, **34**(39):12738–12746, Oct 1995. 124

[190] X Huang, T E Godfrey, W E Gooding, K S McCarty, and S M Gollin. **Comprehensive genome and transcriptome analysis of the 11q13 amplicon in human oral cancer and synteny to the 7F5 amplicon in murine oral carcinoma**. *Genes Chromosomes Cancer*, **45**(11):1058–1069, Nov 2006. 43

[191] X Huang and A Madan. **CAP3: A DNA sequence assembly program**. *Genome Res*, **9**(9):868–877, Sep 1999. 80

[192] C Huynh and N W Andrews. **The small chemical vacuolin-1 alters the morphology of lysosomes without inhibiting Ca^{2+}-regulated exocytosis**. *EMBO Rep*, **6**(9):843–847, Sep 2005. 151, 174, 216, 218

[193] J.I. Hwang, Y.S. Oh, K.J. Shin, H. Kim, S.H. Ryu, and P.G. Suh. **Molecular cloning and characterization of a novel phospholipase C, PLC-η**. *Biochemical Journal*, **389**(Pt 1):181, 2005. 10

[194] M Inui and S Fleischer. **Purification of Ca^{2+} release channel (ryanodine receptor) from heart and skeletal muscle sarcoplasmic reticulum**. *Methods Enzymol*, **157**:490–505, 1988. 97

[195] M Inui, A Saito, and S Fleischer. **Isolation of the ryanodine receptor from cardiac sarcoplasmic reticulum and identity with the feet structures**. *J Biol Chem*, **262**(32):15637–15642, Nov 1987. 89, 97, 107

[196] M Inui, A Saito, and S Fleischer. **Purification of the ryanodine receptor and identity with feet structures of junctional terminal cisternae of sarcoplasmic reticulum from fast skeletal muscle**. *J Biol Chem*, **262**(4):1740–1747, Feb 1987. 89

[197] L Ionescu, K H Cheung, H Vais, D O Mak, C White, and J K Foskett. **Graded recruitment and inactivation of single $InsP_3$ receptor Ca^{2+}-release channels: implications for quantal [corrected] Ca^{2+}release**. *J Physiol*, **573**(Pt 3):645–662, Jun 2006. 215

[198] M Irwin. **THE EFFECT OF ACETATE BUFFER MIXTURES, ACETIC ACID, AND SODIUM ACETATE, ON THE PROTOPLASM, AS INFLUENCING THE RATE OF PENETRATION OF CRESYL BLUE INTO THE VACUOLE OF NITELLA**. *J Gen Physiol*, **11**(2):111–121, Nov 1927. 221

[199] K Ishibashi, M Suzuki, and M Imai. **Molecular cloning of a novel form (two-repeat) protein related to voltage-gated sodium and calcium channels**. *Biochem Biophys Res Commun*, **270**(2):370–376, Apr 2000. 35, 43, 44, 285

[200] M Iwai, T Michikawa, I Bosanac, M Ikura, and K Mikoshiba. **Molecular basis of the isoform-specific ligand-binding affinity of inositol 1,4,5-trisphosphate receptors**. *J Biol Chem*, **282**(17):12755–12764, Apr 2007. 11, 287

[201] Y Jiang, A Lee, J Chen, V Ruta, M Cadene, B T Chait, and R MacKinnon. **X-ray structure of a voltage-dependent K^+ channel**. *Nature*, **423**(6935):33–41, May 2003. 287

[202] J D Johnson and S Misler. **Nicotinic acid-adenine dinucleotide phosphate-sensitive calcium stores initiate insulin signaling in human beta cells**. *Proc Natl Acad Sci U S A*, **99**(22):14566–14571, Oct 2002. 23, 139, 295, 296

[203] L S Johnson, K W Dunn, B Pytowski, and T E McGraw. **Endosome acidification and receptor trafficking: bafilomycin A1 slows receptor externalization by a mechanism involving the receptor's internalization motif**. *Mol Biol Cell*, **4**(12):1251–1266, Dec 1993. 305

[204] L.R. Jones and S.E. Cala. **Biochemical evidence for functional heterogeneity of cardiac sarcoplasmic reticulum vesicles.** *Journal of Biological Chemistry*, **256**(22):11809, 1981. 13

[205] S K Joseph, C Lin, S Pierson, A P Thomas, and A R Maranto. **Heteroligomers of type-I and type-III inositol trisphosphate receptors in WB rat liver epithelial cells**. *J Biol Chem*, **270**(40):23310–23316, Oct 1995. 287

[206] P G Joshi, N Nair, G Begum, N B Joshi, V P Sinkar, and S Vora. **Melanocyte-keratinocyte interaction induces calcium signalling and melanin transfer to keratinocytes**. *Pigment Cell Res*, **20**(5):380–384, Oct 2007. 306

[207] Y Kadota, T Goh, H Tomatsu, R Tamauchi, K Higashi, S Muto, and K Kuchitsu. **Cryptogein-induced initial events in tobacco BY-2 cells: pharmacological characterization of molecular relationship among cytosolic Ca^{2+} transients, anion efflux and production of reactive oxygen species**. *Plant Cell Physiol*, **45**(2):160–170, Feb 2004. 41

[208] E J Kaftan, B E Ehrlich, and J Watras. **Inositol 1,4,5-trisphosphate ($InsP_3$) and calcium interact to increase the dynamic range of $InsP_3$ receptor-dependent calcium signaling**. *J Gen Physiol*, **110**(5):529–538, Nov 1997. 12

[209] E Kalay, R Caylan, A F Kiroglu, T Yasar, R W Collin, J G Heister, J Oostrik, C W Cremers, H G Brunner, A Karaguzel, and H Kremer. **A novel locus for autosomal recessive nonsyndromic hearing impairment, DFNB63, maps to chromosome 11q13.2-q13.4**. *J Mol Med*, **85**(4):397–404, Apr 2007. 43, 44, 307

[210] J H Kamphoven, M M de Ruiter, L P Winkel, H M Van den Hout, J Bijman, C I De Zeeuw, H L Hoeve, B A Van Zanten, A T Van der Ploeg, and A J Reuser. **Hearing loss in infantile Pompe's disease and determination of underlying pathology in the knockout mouse**. *Neurobiol Dis*, **16**(1):14–20, Jun 2004. 44, 307

[211] M Karas, A P Koval, Y Zick, and D LeRoith. **The insulin-like growth factor I receptor-induced interaction of insulin receptor substrate-4 and Crk-II**. *Endocrinology*, **142**(5):1835–1840, May 2001. 243

[212] N N Kasri, K Török, A Galione, C Garnham, G Callewaert, L Missiaen, J B Parys, and H De Smedt. **Endogenously bound calmodulin is essential for the function of the inositol 1,4,5-trisphosphate receptor**. *J Biol Chem*, **281**(13):8332–8338, Mar 2006. 215

[213] U.B. Kaupp and R. Seifert. **Cyclic nucleotide-gated ion channels**. *Physiological reviews*, **82**(3):769, 2002. 287

[214] T Kawano, T Kadono, K Fumoto, F Lapeyrie, M Kuse, M Isobe, T Furuichi, and S Muto. **Aluminum as a specific inhibitor of plant TPC1 Ca^{2+} channels**. *Biochem Biophys Res Commun*, **324**(1):40–45, Nov 2004. 41

[215] A Keller, J Eng, N Zhang, X J Li, and R Aebersold. **A uniform proteomics MS/MS analysis platform utilizing open XML file formats**. *Mol Syst Biol*, **1**:2005–2005, 2005. 74

[216] S Y Khan, S Riazuddin, M Tariq, S Anwar, M I Shabbir, S A Riazuddin, S N Khan, T Husnain, Z M Ahmed, T B Friedman, and S Riazuddin. **Autosomal recessive nonsyndromic deafness locus DFNB63 at chromosome 11q13.2-q13.3**. *Hum Genet*, **120**(6):789–793, Feb 2007. 43, 307

[217] B J Kim, K H Park, C Y Yim, S Takasawa, H Okamoto, M J Im, and U H Kim. **Generation of nicotinic acid adenine dinucleotide phosphate and cyclic ADP-ribose by glucagon-like peptide-1 evokes Ca^{2+} signal that is essential for insulin secretion in mouse pancreatic islets**. *Diabetes*, **57**(4):868–878, Apr 2008. 14

[218] N P Kinnear, F X Boittin, J M Thomas, A Galione, and A M Evans. **Lysosome-sarcoplasmic reticulum junctions. A trigger zone for calcium signaling by nicotinic acid adenine dinucleotide phosphate and endothelin-1**. *J Biol Chem*, **279**(52):54319–54326, Dec 2004. 17, 19, 33, 300, 301, 302

[219] N P Kinnear, C N Wyatt, J H Clark, P J Calcraft, S Fleischer, L H Jeyakumar, G F Nixon, and A M Evans. **Lysosomes co-localize with ryanodine receptor subtype 3 to form a trigger zone for calcium signalling by NAADP in rat pulmonary arterial smooth muscle**. *Cell Calcium*, **44**(2):190–201, Aug 2008. 33, 301

[220] Y Kirichok, G Krapivinsky, and D E Clapham. **The mitochondrial calcium uniporter is a highly selective ion channel**. *Nature*, **427**(6972):360–364, Jan 2004. 3

[221] K Kiselyov, J Chen, Y Rbaibi, D Oberdick, S Tjon-Kon-Sang, N Shcheynikov, S Muallem, and A Soyombo. **TRP-ML1 is a lysosomal monovalent cation channel that undergoes proteolytic cleavage**. *J Biol Chem*, **280**(52):43218–43223, Dec 2005. 139

[222] K Kiselyov, G A Mignery, M X Zhu, and S Muallem. **The N-terminal domain of the IP_3 receptor gates store-operated hTrp3 channels**. *Mol Cell*, **4**(3):423–429, Sep 1999. 11

[223] M Koivusalo, B E Steinberg, D Mason, and S Grinstein. ***In situ* measurement of the electrical potential across the lysosomal membrane using FRET**. *Traffic*, May 2011. 202, 220

[224] M Kolisek, A Beck, A Fleig, and R Penner. **Cyclic ADP-ribose and hydrogen peroxide synergize with ADP-ribose in the activation of TRPM2 channels**. *Mol Cell*, **18**(1):61–69, Apr 2005. 31

[225] P G Kostyuk, O A Krishtal, and V I Pidoplichko. **Effect of internal fluoride and phosphate on membrane currents during intracellular dialysis of nerve cells**. *Nature*, **257**(5528):691–693, Oct 1975. 200

[226] G. Kroemer and M. Jäättelä. **Lysosomes and autophagy in cell death control**. *Nature Reviews Cancer*, **5**(11):886–897, 2005. 304

[227] G. Kroemer and B. Levine. **Autophagic cell death: the story of a misnomer**. *Nature Reviews Molecular Cell Biology*, **9**(12):1004–1010, 2008. 304

[228] F A Lai, K Anderson, E Rousseau, Q Y Liu, and G Meissner. **Evidence for a Ca^{2+} channel within the ryanodine receptor complex from cardiac sarcoplasmic reticulum**. *Biochem Biophys Res Commun*, **151**(1):441–449, Feb 1988. 13

[229] F A Lai, H P Erickson, E Rousseau, Q Y Liu, and G Meissner. **Purification and reconstitution of the calcium release channel from skeletal muscle**. *Nature*, **331**(6154):315–319, Jan 1988. 13, 132, 133

REFERENCES

[230] R L Lamason, M A Mohideen, J R Mest, A C Wong, H L Norton, M C Aros, M J Jurynec, X Mao, V R Humphreville, J E Humbert, S Sinha, J L Moore, P Jagadeeswaran, W Zhao, G Ning, I Makalowska, P M McKeigue, D O'donnell, R Kittles, E J Parra, N J Mangini, D J Grunwald, M D Shriver, V A Canfield, and K C Cheng. **SLC24A5, a putative cation exchanger, affects pigmentation in zebrafish and humans**. *Science*, **310**(5755):1782–1786, Dec 2005. 44

[231] I Lange, S Yamamoto, S Partida-Sanchez, Y Mori, A Fleig, and R Penner. **TRPM2 functions as a lysosomal Ca^{2+}-release channel in beta cells**. *Sci Signal*, **2**(71), 2009. 31

[232] M F Langhorst, N Schwarzmann, and A H Guse. **Ca^{2+} release via ryanodine receptors and Ca^{2+} entry: major mechanisms in NAADP-mediated Ca^{2+} signaling in T-lymphocytes**. *Cell Signal*, **16**(11):1283–1289, Nov 2004. 32

[233] J T Lanner, D K Georgiou, A D Joshi, and S L Hamilton. **Ryanodine receptors: structure, expression, molecular details, and function in calcium release**. *Cold Spring Harb Perspect Biol*, **2**(11), Nov 2010. 13

[234] A B Lansley and M J Sanderson. **Regulation of airway ciliary activity by Ca^{2+}: simultaneous measurement of beat frequency and intracellular Ca^{2+}**. *Biophys J*, **77**(1):629–638, Jul 1999. 8

[235] J M LaPlante, J Falardeau, M Sun, M Kanazirska, E M Brown, S A Slaugenhaupt, and P M Vassilev. **Identification and characterization of the single channel function of human mucolipin-1 implicated in mucolipidosis type IV, a disorder affecting the lysosomal pathway**. *FEBS Lett*, **532**(1-2):183–187, Dec 2002. 134, 139

[236] D Laver. **The power of single channel recording and analysis: its application to ryanodine receptors in lipid bilayers**. *Clin Exp Pharmacol Physiol*, **28**(8):675–686, Aug 2001. 142

[237] D R Laver. **Luminal Ca^{2+} activation of cardiac ryanodine receptors by luminal and cytoplasmic domains**. *Eur Biophys J*, **39**(1):19–26, Dec 2009. 141

[238] D R Laver, K R Eager, L Taoube, and G D Lamb. **Effects of cytoplasmic and luminal pH on Ca^{2+}release channels from rabbit skeletal muscle**. *Biophys J*, **78**(4):1835–1851, Apr 2000. 32, 140

[239] D R Laver, E R O'Neill, and G D Lamb. **Luminal Ca^{2+}-regulated Mg^{2+} inhibition of skeletal RyRs reconstituted as isolated channels or coupled clusters**. *J Gen Physiol*, **124**(6):741–758, Dec 2004. 141

[240] D Lebel, G Grondin, and J Paquette. **In vitro stability of pancreatic zymogen granules: roles of pH and calcium**. *Biol Cell*, **63**(3):343–353, 1988. 219

[241] C P Leckie, M R McAinsh, G J Allen, D Sanders, and A M Hetherington. **Abscisic acid-induced stomatal closure mediated by cyclic ADP-ribose**. *Proc Natl Acad Sci U S A*, **95**(26):15837–15842, Dec 1998. 214

[242] H C Lee. **Physiological functions of cyclic ADP-ribose and NAADP as calcium messengers**. *Annu Rev Pharmacol Toxicol*, **41**:317–345, 2001. 12, 14

[243] H C Lee. **Nicotinic acid adenine dinucleotide phosphate (NAADP)-mediated calcium signaling**. *J Biol Chem*, **280**(40):33693–33696, Oct 2005. 14

[244] H C Lee and R Aarhus. **A derivative of NADP mobilizes calcium stores insensitive to inositol trisphosphate and cyclic ADP-ribose**. *J Biol Chem*, **270**(5):2152–2157, Feb 1995. 14, 18, 20

[245] H C Lee and R Aarhus. **Functional visualization of the separate but interacting calcium stores sensitive to NAADP and cyclic ADP-ribose**. *J Cell Sci*, **113 Pt 24**:4413–4420, Dec 2000. 18

[246] H C Lee, R Aarhus, K R Gee, and T Kestner. **Caged nicotinic acid adenine dinucleotide phosphate. Synthesis and use**. *J Biol Chem*, **272**(7):4172–4178, Feb 1997. 124

[247] G Lennon, C Auffray, M Polymeropoulos, and M B Soares. **The I.M.A.G.E. Consortium: an integrated molecular analysis of genomes and their expression**. *Genomics*, **33**(1):151–152, Apr 1996. 74

[248] P K Lepage and G Boulay. **Molecular determinants of TRP channel assembly**. *Biochem Soc Trans*, **35**(Pt 1):81–83, Feb 2007. 132, 286, 287

[249] A M Lewis, R Masgrau, S R Vasudevan, M Yamasaki, J S O'Neill, C Garnham, K James, A Macdonald, M Ziegler, A Galione, and G C Churchill. **Refinement of a radioreceptor binding assay for nicotinic acid adenine dinucleotide phosphate**. *Anal Biochem*, **371**(1):26–36, Dec 2007. 16, 60

[250] C W Lin, M Sasaki, M L Orcutt, H Miyayama, and R M Singer. **Plasma membrane localization of alkaline phosphatase in HeLa cells**. *J Histochem Cytochem*, **24**(5):659–667, May 1976. 160

[251] A R Lindsay, S D Manning, and A J Williams. **Monovalent cation conductance in the ryanodine receptor-channel of sheep cardiac muscle sarcoplasmic reticulum**. *J Physiol*, **439**:463–480, Aug 1991. 134

[252] A R Lindsay and A J Williams. **Functional characterisation of the ryanodine receptor purified from sheep cardiac muscle sarcoplasmic reticulum**. *Biochim Biophys Acta*, **1064**(1):89–102, Apr 1991. 118, 124

[253] P Lipp and E Niggli. **Submicroscopic calcium signals as fundamental events of excitation–contraction coupling in guinea-pig cardiac myocytes**. *J Physiol*, **492 (Pt 1)**:31–38, Apr 1996. 8

[254] E Lloyd-Evans, A J Morgan, X He, D A Smith, E Elliot-Smith, D J Sillence, G C Churchill, E H Schuchman, A Galione, and F M Platt. **Niemann-Pick disease type C1 is a sphingosine storage disease that causes deregulation of lysosomal calcium**. *Nat Med*, **14**(11):1247–1255, Nov 2008. 43, 124, 222, 304, 307

[255] A Lobley, V Pierron, L Reynolds, L Allen, and D Michalovich. **Identification of human and mouse CatSper3 and CatSper4 genes: characterisation of a common interaction domain and evidence for expression in testis**. *Reprod Biol Endocrinol*, **1**:53–53, Aug 2003. 286, 288, 289

[256] T P Lockwich, X Liu, B B Singh, J Jadlowiec, S Weiland, and I S Ambudkar. **Assembly of Trp1 in a signaling complex associated with caveolin-scaffolding lipid raft domains**. *J Biol Chem*, **275**(16):11934–11942, Apr 2000. 240

[257] J J López, C Camello-Almaraz, J A Pariente, G M Salido, and J A Rosado. **Ca^{2+} accumulation into acidic organelles mediated by Ca^{2+}- and vacuolar H^+-ATPases in human platelets**. *Biochem J*, **390**(Pt 1):243–252, Aug 2005. 4, 291

[258] T Lübke, P Lobel, and D E Sleat. **Proteomics of the lysosome**. *Biochim Biophys Acta*, **1793**(4):625–635, Apr 2009. 151

[259] V Lukyanenko, I Györke, and S Györke. **Regulation of calcium release by calcium inside the sarcoplasmic reticulum in ventricular myocytes**. *Pflügers Arch*, **432**(6):1047–1054, Oct 1996. 122, 124

[260] J P Luzio, N A Bright, and P R Pryor. **The role of calcium and other ions in sorting and delivery in the late endocytic pathway**. *Biochem Soc Trans*, **35**(Pt 5):1088–1091, Nov 2007. 37, 266, 289, 304

[261] J P Luzio, S R Gray, and N A Bright. **Endosome-lysosome fusion**. *Biochem Soc Trans*, **38**(6):1413–1416, Dec 2010. 158, 187, 289

[262] J P Luzio, V Poupon, M R Lindsay, B M Mullock, R C Piper, and P R Pryor. **Membrane dynamics and the biogenesis of lysosomes**. *Mol Membr Biol*, **20**(2):141–154, Apr-Jun 2003. 161, 189, 289, 304

[263] J P Luzio, P R Pryor, and N A Bright. **Lysosomes: fusion and function**. *Nat Rev Mol Cell Biol*, **8**(8):622–632, Aug 2007. 158, 187, 305

[264] F.J.M. Maathuis and D. Sanders. **Patch-clamping plant cells**. *Methods in cell biology*, **49**:293–302, 1995. 214

[265] F.J.M. Maathuis, A.R. Taylor, S.M. Assmann, and D. Sanders. **Seal-promoting solutions and pipette perfusion for patch clamping plant cells**. *The Plant Journal*, **11**(4):891–896, 1997. 214

[266] A Macgregor, M Yamasaki, S Rakovic, L Sanders, R Parkesh, G C Churchill, A Galione, and D A Terrar. **NAADP controls cross-talk between distinct Ca^{2+} stores in the heart**. *J Biol Chem*, **282**(20):15302–15311, May 2007. 23, 33

[267] N Maeda, T Kawasaki, S Nakade, N Yokota, T Taguchi, M Kasai, and K Mikoshiba. **Structural and functional characterization of inositol 1,4,5-trisphosphate receptor channel from mouse cerebellum**. *J Biol Chem*, **266**(2):1109–1116, Jan 1991. 11

[268] D O Mak and J K Foskett. **Single-channel inositol 1,4,5-trisphosphate receptor currents revealed by patch clamp of isolated *Xenopus* oocyte nuclei**. *J Biol Chem*, **269**(47):29375–29378, Nov 1994. 11

[269] D O Mak and J K Foskett. **Effects of divalent cations on single-channel conduction properties of *Xenopus* IP_3 receptor**. *Am J Physiol*, **275**(1 Pt 1):179–188, Jul 1998. 11

[270] D O Mak, S McBride, and J K Foskett. **ATP regulation of recombinant type 3 inositol 1,4,5-trisphosphate receptor gating**. *J Gen Physiol*, **117**(5):447–456, May 2001. 216

[271] D O Mak, S McBride, and J K Foskett. **Regulation by Ca^{2+} and inositol 1,4,5-trisphosphate ($InsP_3$) of single recombinant type 3 $InsP_3$ receptor channels. Ca^{2+} activation uniquely distinguishes types 1 and 3 $InsP_3$ receptors**. *J Gen Physiol*, **117**(5):435–446, May 2001. 216

[272] D O Mak, S M McBride, N B Petrenko, and J K Foskett. **Novel regulation of calcium inhibition of the inositol 1,4,5-trisphosphate receptor calcium-release channel**. *J Gen Physiol*, **122**(5):569–581, Nov 2003. 216

[273] D O Mak, J E Pearson, K P Loong, S Datta, M Fernández-Mongil, and J K Foskett. **Rapid ligand-regulated gating kinetics of single inositol 1,4,5-trisphosphate receptor Ca^{2+} release channels**. *EMBO Rep*, **8**(11):1044–1051, Nov 2007. 216

[274] F Malavasi, S Deaglio, A Funaro, E Ferrero, A L Horenstein, E Ortolan, T Vaisitti, and S Aydin. **Evolution and function of the ADP ribosyl cyclase/CD38 gene family in physiology and pathology**. *Physiol Rev*, **88**(3):841–886, Jul 2008. 14

[275] M Mándi and J Bak. **Nicotinic acid adenine dinucleotide phosphate (NAADP) and Ca^{2+} mobilization**. *J Recept Signal Transduct Res*, **28**(3):163–184, 2008. 120

[276] M Mándi, B Tóth, G Timár, and J Bak. **Ca^{2+} release triggered by NAADP in hepatocyte microsomes**. *Biochem J*, **395**(2):233–238, Apr 2006. 23

[277] S M Mane, L Marzella, D F Bainton, V K Holt, Y Cha, J E Hildreth, and J T August. **Purification and characterization of human lysosomal membrane glycoproteins**. *Arch Biochem Biophys*, **268**(1):360–378, Jan 1989. 152

[278] M Manzoni, E Monti, R Bresciani, A Bozzato, S Barlati, M T Bassi, and G Borsani. **Overexpression of wild-type and mutant mucolipin proteins in mammalian cells: effects on the late endocytic compartment organization**. *FEBS Lett*, **567**(2-3):219–224, Jun 2004. 30

[279] S M Marchenko, V V Yarotskyy, T N Kovalenko, P G Kostyuk, and R C Thomas. **Spontaneously active and $InsP_3$-activated ion channels in cell nuclei from rat cerebellar Purkinje and granule neurones**. *J Physiol*, **565**(Pt 3):897–910, Jun 2005. 141

[280] G Mariño and C López-Otín. **Autophagy: molecular mechanisms, physiological functions and relevance in human pathology**. *Cell Mol Life Sci*, **61**(12):1439–1454, Jun 2004. 303

REFERENCES

[281] S O Marx, K Ondrias, and A R Marks. **Coupled gating between individual skeletal muscle Ca^{2+} release channels (ryanodine receptors)**. *Science*, **281**(5378):818–821, Aug 1998. 115, 137

[282] R Masgrau, G C Churchill, A J Morgan, S J Ashcroft, and A Galione. **NAADP: a new second messenger for glucose-induced Ca^{2+} responses in clonal pancreatic beta cells**. *Curr Biol*, **13**(3):247–251, Feb 2003. 17, 23, 27, 139, 207, 295, 296

[283] K. Matulef and W.N. Zagotta. **Cyclic nucleotide-gated ion channels**. *Annual review of cell and developmental biology*, **19**(1):23–44, 2003. 287

[284] D McHugh, R Flemming, S Z Xu, A L Perraud, and D J Beech. **Critical intracellular Ca^{2+} dependence of transient receptor potential melastatin 2 (TRPM2) cation channel activation**. *J Biol Chem*, **278**(13):11002–11006, Mar 2003. 31

[285] W. Mei, K.W. Lee, F.L. Marlow, A.L. Miller, and M.C. Mullins. **hnRNP I is required to generate the Ca^{2+} signal that causes egg activation in zebrafish**. *Development*, **136**(17):3007, 2009. 240

[286] G Meissner. **Monovalent ion and calcium ion fluxes in sarcoplasmic reticulum**. *Mol Cell Biochem*, **55**(1):65–82, 1983. 12

[287] G Meissner. **Ryanodine receptor/Ca^{2+} release channels and their regulation by endogenous effectors**. *Annu Rev Physiol*, **56**:485–508, 1994. 13, 134, 137

[288] A Menteyne, A Burdakov, G Charpentier, O H Petersen, and J M Cancela. **Generation of specific Ca^{2+} signals from Ca^{2+} stores and endocytosis by differential coupling to messengers**. *Curr Biol*, **16**(19):1931–1937, Oct 2006. 33

[289] H Miedema, A H de Boer, and O Pantoja. **The gating kinetics of the slow vacuolar channel. A novel mechanism for SV channel functioning?** *J Membr Biol*, **194**(1):11–20, Jul 2003. 41

[290] B F Miller, T Aiba, F P Keyes, P W Curreri, and A W Branwood. **Beta-glucuronidase activity and its variation with pH in human atherosclerotic arteries**. *J Atheroscler Res*, **6**(4):352–358, Jul-Aug 1966. 157

[291] C Miller. **Open-state substructure of single chloride channels from *Torpedo electroplax***. *Philos Trans R Soc Lond B Biol Sci*, **299**(1097):401–411, Dec 1982. 61

[292] C Miller and R L Rosenberg. **A voltage-gated cation conductance channel from fragmented sarcoplasmic reticulum. Effects of transition metal ions**. *Biochemistry*, **18**(7):1138–1145, Apr 1979. 61

[293] R J Miller. **Mitochondria - the Kraken wakes!** *Trends Neurosci*, **21**(3):95–97, Mar 1998. 3

[294] L Missiaen, L Raeymaekers, L Dode, J Vanoevelen, K Van Baelen, J B Parys, G Callewaert, H De Smedt, S Segaert, and F Wuytack. **SPCA1 pumps and Hailey-Hailey disease**. *Biochem Biophys Res Commun*, **322**(4):1204–1213, Oct 2004. 4

[295] K J Mitchell, F A Lai, and G A Rutter. **Ryanodine receptor type I and nicotinic acid adenine dinucleotide phosphate receptors mediate Ca^{2+} release from insulin-containing vesicles in living pancreatic beta-cells (MIN6)**. *J Biol Chem*, **278**(13):11057–11064, Mar 2003. 32, 225

[296] A Miyawaki and R Y Tsien. **Monitoring protein conformations and interactions by fluorescence resonance energy transfer between mutants of green fluorescent protein**. *Methods Enzymol*, **327**:472–500, 2000. 279

[297] F Moccia, D Lim, K Kyozuka, and L Santella. **NAADP triggers the fertilization potential in starfish oocytes**. *Cell Calcium*, **36**(6):515–524, Dec 2004. 23

[298] A Mojzisová, O Krizanová, L Záciková, V Komínková, and K Ondrias. **Effect of nicotinic acid adenine dinucleotide phosphate on ryanodine calcium release channel in heart**. *Pflügers Arch*, **441**(5):674–677, Feb 2001. 32, 140, 151

[299] Areles Molleman. *Patch Clamping - an Introductory Guide to Patch Clamp Electrophyisology*. John Wiley & Sons, Ltd., 2002. 202

[300] S. Moller, M.D.R. Croning, and R. Apweiler. **Evaluation of methods for the prediction of membrane spanning regions**. *Bioinformatics*, **18**(1):218–218, 2002. 50

[301] T Monkawa, A Miyawaki, T Sugiyama, H Yoneshima, M Yamamoto-Hino, T Furuichi, T Saruta, M Hasegawa, and K Mikoshiba. **Heterotetrameric complex formation of inositol 1,4,5-trisphosphate receptor subunits**. *J Biol Chem*, **270**(24):14700–14704, Jun 1995. 285, 287

[302] I Moreschi, S Bruzzone, N Bodrato, C Usai, L Guida, R A Nicholas, M U Kassack, E Zocchi, and A De Flora. **$NAADP^{+}$ is an agonist of the human $P2Y_{11}$ purinergic receptor**. *Cell Calcium*, **43**(4):344–355, Apr 2008. 32

[303] A J Morgan and A Galione. **NAADP induces pH changes in the lumen of acidic Ca^{2+} stores**. *Biochem J*, **402**(2):301–310, Mar 2007. 125, 126, 140, 232, 303

[304] A J Morgan and A Galione. **Investigating cADPR and NAADP in intact and broken cell preparations**. *Methods*, **46**(3):194–203, Nov 2008. 23, 27, 120, 226

[305] T W Mu, D M Fowler, and J W Kelly. **Partial restoration of mutant enzyme homeostasis in three distinct lysosomal storage disease cell lines by altering calcium homeostasis**. *PLoS Biol*, **6**(2), Feb 2008. 306

[306] K. Murata, N. Odahara, A. Kuniyasu, Y. Sato, H. Nakayama, and K. Nagayama. **Asymmetric arrangement of auxiliary subunits of skeletal muscle voltage-gated L-type Ca^{2+} channel**. *Biochemical and biophysical research communications*, **282**(1):284–291, 2001. 224, 288, 322

[307] S Nakade, S K Rhee, H Hamanaka, and K Mikoshiba. **Cyclic AMP-dependent phosphorylation of an immunoaffinity-purified homotetrameric inositol 1,4,5-trisphosphate receptor (type I) increases Ca^{2+} flux in reconstituted lipid vesicles**. *J Biol Chem*, **269**(9):6735–6742, Mar 1994. 285

[308] Y Nakanishi, I Yabe, and M Maeshima. **Patch clamp analysis of a H^+ pump heterologously expressed in giant yeast vacuoles**. *J Biochem*, **134**(4):615–623, Oct 2003. 214

[309] L Navazio, M A Bewell, A Siddiqua, G D Dickinson, A Galione, and D Sanders. **Calcium release from the endoplasmic reticulum of higher plants elicited by the NADP metabolite nicotinic acid adenine dinucleotide phosphate**. *Proc Natl Acad Sci U S A*, **97**(15):8693–8698, Jul 2000. 23

[310] E Naylor, A Arredouani, S R Vasudevan, A M Lewis, R Parkesh, A Mizote, D Rosen, J M Thomas, M Izumi, A Ganesan, A Galione, and G C Churchill. **Identification of a chemical probe for NAADP by virtual screening**. *Nat Chem Biol*, **5**(4):220–226, Apr 2009. 24, 25, 27, 90, 127, 129, 302

[311] P H Nelson. **A permeation theory for single-file ion channels: One- and two-step models**. *J Chem Phys*, **134**(16):165102–165102, Apr 2011. 228

[312] C L Newton, G A Mignery, and T C Südhof. **Co-expression in vertebrate tissues and cell lines of multiple inositol 1,4,5-trisphosphate ($InsP_3$) receptors with distinct affinities for $InsP_3$**. *J Biol Chem*, **269**(46):28613–28619, Nov 1994. 11

[313] T Nguyen, W C Chin, and P Verdugo. **Role of Ca^{2+}/K^+ ion exchange in intracellular storage and release of Ca^{2+}**. *Nature*, **395**(6705):908–912, Oct 1998. 135

[314] B Nilius and T Voets. **TRP channels: a TR(I)P through a world of multifunctional cation channels**. *Pflügers Arch*, **451**(1):1–10, Oct 2005. 136

[315] N Noguchi, S Takasawa, K Nata, A Tohgo, I Kato, F Ikehata, H Yonekura, and H Okamoto. **Cyclic ADP-ribose binds to FK506-binding protein 12.6 to release Ca^{2+} from islet microsomes**. *J Biol Chem*, **272**(6):3133–3136, Feb 1997. 12, 133

[316] W Nonner, D P Chen, and B Eisenberg. **Anomalous mole fraction effect, electrostatics, and binding in ionic channels**. *Biophys J*, **74**(5):2327–2334, May 1998. 228

[317] F C Nucifora, A H Sharp, S L Milgram, and C A Ross. **Inositol 1,4,5-trisphosphate receptors in endocrine cells: localization and association in hetero- and homotetramers**. *Mol Biol Cell*, **7**(6):949–960, Jun 1996. 287

[318] O A Ogunbayo, Y Zhu, D Rossi, V Sorrentino, J Ma, M X Zhu, and A M Evans. **Cyclic adenosine diphosphate ribose activates ryanodine receptors, whereas NAADP activates two-pore domain channels**. *J Biol Chem*, **286**(11):9136–9140, Mar 2011. 225

[319] S Ohkuma, Y Moriyama, and T Takano. **Electrogenic nature of lysosomal proton pump as revealed with a cyanine dye**. *J Biochem*, **94**(6):1935–1943, Dec 1983. 202, 219, 222

[320] K K Ohlemiller, A K Hennig, J M Lett, A F Heidbreder, and M S Sands. **Inner ear pathology in the mucopolysaccharidosis VII mouse**. *Hear Res*, **169**(1-2):69–84, Jul 2002. 307

[321] K Ondrias and A Mojzisová. **Coupled gating between individual cardiac ryanodine calcium release channels**. *Gen Physiol Biophys*, **21**(1):73–84, Mar 2002. 137

[322] F O'Rourke, K Soons, R Flaumenhauft, J Watras, C Baio-Larue, E Matthews, and M B Feinstein. **Ca^{2+} release by inositol 1,4,5-trisphosphate is blocked by the K^+-channel blockers apamin and tetrapentylammonium ion, and a monoclonal antibody to a 63 kDa membrane protein: reversal of blockade by K^+ ionophores nigericin and valinomycin and purification of the 63 kDa antibody-binding protein**. *Biochem J*, **300 (Pt 3)**:673–683, Jun 1994. 135

[323] R D Page. **TreeView: an application to display phylogenetic trees on personal computers**. *Comput Appl Biosci*, **12**(4):357–358, Aug 1996. 50

[324] P Palade. **The hunt for an alternate way to generate NAADP. Focus on "NAADP as a second messenger: neither CD38 nor base-exchange reaction are necessary for in vivo generation of NAADP in myometrial cells"**. *Am J Physiol Cell Physiol*, **292**(1):4–7, Jan 2007. 14

[325] C P Palmer, X L Zhou, J Lin, S H Loukin, C Kung, and Y Saimi. **A TRP homolog in *Saccharomyces cerevisiae* forms an intracellular Ca^{2+}-permeable channel in the yeast vacuolar membrane**. *Proc Natl Acad Sci U S A*, **98**(14):7801–7805, Jul 2001. 214, 215

[326] V Pandey, C C Chuang, A M Lewis, P K Aley, E Brailoiu, N J Dun, G C Churchill, and S Patel. **Recruitment of NAADP-sensitive acidic Ca^{2+} stores by glutamate**. *Biochem J*, **422**(3):503–512, Sep 2009. 17

[327] E Papini, M Bugnoli, M De Bernard, N Figura, R Rappuoli, and C Montecucco. **Bafilomycin A1 inhibits *Helicobacter pylori*-induced vacuolization of HeLa cells**. *Mol Microbiol*, **7**(2):323–327, Jan 1993. 217

[328] I Parker, J Choi, and Y Yao. **Elementary events of $InsP_3$-induced Ca^{2+} liberation in *Xenopus* oocytes: hot spots, puffs and blips**. *Cell Calcium*, **20**(2):105–121, Aug 1996. 8

[329] I Parker and Y Yao. **Ca^{2+} transients associated with openings of inositol trisphosphate-gated channels in *Xenopus* oocytes**. *J Physiol*, **491 (Pt 3)**:663–668, Mar 1996. 8

[330] E Parkinson-Lawrence, M Fuller, J J Hopwood, P J Meikle, and D A Brooks. **Immunochemistry of lysosomal storage disorders**. *Clin Chem*, **52**(9):1660–1668, Sep 2006. 306

[331] S Patel, G C Churchill, and A Galione. **Unique kinetics of nicotinic acid-adenine dinucleotide phosphate (NAADP) binding enhance the sensitivity of NAADP receptors for their ligand**. *Biochem J*, **352 Pt 3**:725–729, Dec 2000. 89

[332] S Patel and R Docampo. **Acidic calcium stores open for business: expanding the potential for intracellular Ca^{2+} signaling**. *Trends Cell Biol*, **20**(5):277–286, May 2010. 214

[333] S Patel, J S Marchant, and E Brailoiu. **Two-pore channels: Regulation by NAADP and customized roles in triggering calcium signals**. *Cell Calcium*, **47**(6):480–490, Jun 2010. 35, 41, 263

[334] R L Patterson, D B van Rossum, R K Barrow, and S H Snyder. **RACK1 binds to inositol 1,4,5-trisphosphate receptors and mediates Ca^{2+} release**. *Proc Natl Acad Sci U S A*, **101**(8):2328–2332, Feb 2004. 11

[335] B M Pearse. **Isolation of coated vesicles**. *Methods Enzymol*, **98**:320–326, 1983. 179

[336] E Peiter, F J Maathuis, L N Mills, H Knight, J Pelloux, A M Hetherington, and D Sanders. **The vacuolar Ca^{2+}-activated channel TPC1 regulates germination and stomatal movement**. *Nature*, **434**(7031):404–408, Mar 2005. 35, 41, 214

[337] C. Peng, E.D. Rich, and M.D. Varnum. **Subunit configuration of heteromeric cone cyclic nucleotide-gated channels**. *Neuron*, **42**(3):401–410, 2004. 287

[338] A Penna, A Demuro, A V Yeromin, S L Zhang, O Safrina, I Parker, and M D Cahalan. **The CRAC channel consists of a tetramer formed by Stim-induced dimerization of Orai dimers**. *Nature*, **456**(7218):116–120, Nov 2008. 289

[339] G.J.S. Pereira, H. Hirata, G.M. Fimia, L.G. do Carmo, C. Bincoletto, S.W. Han, R.S. Stilhano, R.P. Ureshino, D. Bloor-Young, G. Churchill, et al. **Nicotinic acid adenine dinucleotide phosphate (NAADP) regulates autophagy in cultured astrocytes**. *Journal of Biological Chemistry*, 2011. 304

[340] V Pérez, T Wherrett, S Shabala, J Muñiz, O Dobrovinskaya, and I Pottosin. **Homeostatic control of slow vacuolar channels by luminal cations and evaluation of the channel-mediated tonoplast Ca^{2+} fluxes *in situ***. *J Exp Bot*, **59**(14):3845–3855, 2008. 41

[341] C M Perez-Terzic, E N Chini, S S Shen, T P Dousa, and D E Clapham. **Ca^{2+} release triggered by nicotinate adenine dinucleotide phosphate in intact sea urchin eggs**. *Biochem J*, **312 (Pt 3)**:955–959, Dec 1995. 20, 21

[342] A L Perraud, A Fleig, C A Dunn, L A Bagley, P Launay, C Schmitz, A J Stokes, Q Zhu, M J Bessman, R Penner, J P Kinet, and A M Scharenberg. **ADP-ribose gating of the calcium-permeable LTRPC2 channel revealed by Nudix motif homology**. *Nature*, **411**(6837):595–599, May 2001. 31

[343] A L Perraud, C Schmitz, and A M Scharenberg. **TRPM2 Ca^{2+} permeable cation channels: from gene to biological function**. *Cell Calcium*, **33**(5-6):519–531, May-Jun 2003. 31

[344] O H Petersen, O V Gerasimenko, J V Gerasimenko, H Mogami, and A V Tepikin. **The calcium store in the nuclear envelope**. *Cell Calcium*, **23**(2-3):87–90, Feb-Mar 1998. 4

[345] P Pinton, T Pozzan, and R Rizzuto. **The Golgi apparatus is an inositol 1,4,5-trisphosphate-sensitive Ca^{2+} store, with functional properties distinct from those of the endoplasmic reticulum**. *EMBO J*, **17**(18):5298–5308, Sep 1998. 4, 6, 10, 189, 222

[346] R C Piper and J P Luzio. **CUPpling calcium to lysosomal biogenesis**. *Trends Cell Biol*, **14**(9):471–473, Sep 2004. 266

[347] S J Pitt, T Funnell, M Sitsapesan, E Venturi, K Rietdorf, M Ruas, A Ganesan, R Gosain, G C Churchill, M X Zhu, J Parrington, A Galione, and R Sitsapesan. **TPC2 is a novel NAADP-sensitive Ca^{2+}-release channel, operating as a dual sensor of luminal pH and Ca^{2+}**. *J Biol Chem*, **285**:35039 – 35046, Aug 2010. 32, 36

[348] S J Pitt, K H Park, M Nishi, T Urashima, S Aoki, D Yamazaki, J Ma, H Takeshima, and R Sitsapesan. **Charade of the SR K^+-channel: two ion-channels, TRIC-A and TRIC-B, masquerade as a single K^+-channel**. *Biophys J*, **99**(2):417–426, Jul 2010. 115, 227

[349] P Pizzo, V Lissandron, and T Pozzan. **The trans-golgi compartment: A new distinct intracellular Ca^{2+}store**. *Commun Integr Biol*, **3**(5):462–464, Sep 2010. 222

[350] B A Pollok and R Heim. **Using GFP in FRET-based applications**. *Trends Cell Biol*, **9**(2):57–60, Feb 1999. 269

[351] I Pottosin, T Wherrett, and S Shabala. **SV channels dominate the vacuolar Ca^{2+} release during intracellular signaling**. *FEBS Lett*, **583**(5):921–926, Mar 2009. 41, 141

[352] I I Pottosin and G Schönknecht. **Vacuolar calcium channels**. *J Exp Bot*, **58**(7):1559–1569, 2007. 35, 41, 141, 219

[353] J F Presley, S Mayor, T E McGraw, K W Dunn, and F R Maxfield. **Bafilomycin A1 treatment retards transferrin receptor recycling more than bulk membrane recycling**. *J Biol Chem*, **272**(21):13929–13936, May 1997. 305

[354] A J Proctor, L M Coombs, J P Cairns, and M A Knowles. **Amplification at chromosome 11q13 in transitional cell tumours of the bladder**. *Oncogene*, **6**(5):789–795, May 1991. 43

[355] P R Pryor and J P Luzio. **Delivery of endocytosed membrane proteins to the lysosome**. *Biochim Biophys Acta*, **1793**(4):615–624, Apr 2009. 305

[356] P R Pryor, B M Mullock, N A Bright, S R Gray, and J P Luzio. **The role of intraorganellar Ca^{2+} in late endosome-lysosome heterotypic fusion and in the reformation of lysosomes from hybrid organelles**. *J Cell Biol*, **149**(5):1053–1062, May 2000. 158, 289, 304

[357] H Qi, M M Moran, B Navarro, J A Chong, G Krapivinsky, L Krapivinsky, Y Kirichok, I S Ramsey, T A Quill, and D E Clapham. **All four CatSper ion channel proteins are required for male fertility and sperm cell hyperactivated motility**. *Proc Natl Acad Sci U S A*, **104**(4):1219–1223, Jan 2007. 286

[358] O S Qureshi, A Paramasivam, J C Yu, and R D Murrell-Lagnado. **Regulation of $P2X_4$ receptors by lysosomal targeting, glycan protection and exocytosis**. *J Cell Sci*, **120**(Pt 21):3838–3849, Nov 2007. 32

[359] S Y Rah, M Mushtaq, T S Nam, S H Kim, and U H Kim. **Generation of cyclic ADP-ribose and nicotinic acid adenine dinucleotide phosphate by CD38 for Ca^{2+} signaling in interleukin-8-treated lymphokine-activated killer cells**. *J Biol Chem*, **285**(28):21877–21887, Jul 2010. 14

[360] M Ramjeesingh, L J Huan, E Garami, and C E Bear. **Novel method for evaluation of the oligomeric structure of membrane proteins**. *Biochem J*, **342 (Pt 1)**:119–123, Aug 1999. 54

[361] S Ranf, P Wünnenberg, J Lee, D Becker, M Dunkel, R Hedrich, D Scheel, and P Dietrich. **Loss of the vacuolar cation channel, AtTPC1, does not impair Ca^{2+} signals induced by abiotic and biotic stresses**. *Plant J*, **53**(2):287–299, Jan 2008. 41

[362] G Raposo, M S Marks, and D F Cutler. **Lysosome-related organelles: driving post-Golgi compartments into specialisation**. *Curr Opin Cell Biol*, **19**(4):394–401, Aug 2007. 44

[363] M K Raychowdhury, S González-Perrett, N Montalbetti, G A Timpanaro, B Chasan, W H Goldmann, S Stahl, A Cooney, E Goldin, and H F Cantiello. **Molecular pathophysiology of mucolipidosis type IV: pH dysregulation of the mucolipin-1 cation channel**. *Hum Mol Genet*, **13**(6):617–627, Mar 2004. 134, 135, 139, 141

[364] D Ren, B Navarro, G Perez, A C Jackson, S Hsu, Q Shi, J L Tilly, and D E Clapham. **A sperm ion channel required for sperm motility and male fertility**. *Nature*, **413**(6856):603–609, Oct 2001. 286

[365] Liquids Research. *Dextran Ferrofluid datasheet*, 2009. 213

[366] R Rizzuto, P Pinton, W Carrington, F S Fay, K E Fogarty, L M Lifshitz, R A Tuft, and T Pozzan. **Close contacts with the endoplasmic reticulum as determinants of mitochondrial Ca^{2+} responses**. *Science*, **280**(5370):1763–1766, Jun 1998. 301

[367] L D Robb-Gaspers and A P Thomas. **Coordination of Ca^{2+} signaling by intercellular propagation of Ca^{2+} waves in the intact liver**. *J Biol Chem*, **270**(14):8102–8107, Apr 1995. 8

[368] J M Rodriguez-Paris, K V Nolta, and T L Steck. **Characterization of lysosomes isolated from *Dictyostelium discoideum* by magnetic fractionation**. *J Biol Chem*, **268**(12):9110–9116, Apr 1993. 168

[369] T B Rogers, G Inesi, R Wade, and W J Lederer. **Use of thapsigargin to study Ca^{2+} homeostasis in cardiac cells**. *Biosci Rep*, **15**(5):341–349, Oct 1995. 18

[370] D Rosen, A M Lewis, A Mizote, J M Thomas, P K Aley, S R Vasudevan, R Parkesh, A Galione, M Izumi, A Ganesan, and G C Churchill. **Analogues of the nicotinic acid adenine dinucleotide phosphate (NAADP) antagonist Ned-19 indicate two binding sites on the NAADP receptor**. *J Biol Chem*, **284**(50):34930–34934, Dec 2009. 22, 127, 142, 226, 232, 297

[371] T Rosenbaum and S E Gordon. **Dissecting intersubunit contacts in cyclic nucleotide-gated ion channels**. *Neuron*, **33**(5):703–713, Feb 2002. 288

[372] B. Rost, G. Yachdav, and J. Liu. **The predictprotein server**. *Nucleic acids research*, **32**(suppl 2):W321, 2004. 50

[373] A Rottach, E Kremmer, D Nowak, H Leonhardt, and M C Cardoso. **Generation and characterization of a rat monoclonal antibody specific for multiple red fluorescent proteins**. *Hybridoma (Larchmt)*, **27**(5):337–343, Oct 2008. 257, 317

[374] E Rousseau, J S Smith, J S Henderson, and G Meissner. **Single channel and $^{45}Ca^{2+}$ flux measurements of the cardiac sarcoplasmic reticulum calcium channel**. *Biophys J*, **50**(5):1009–1014, Nov 1986. 12

[375] M Ruas, K Rietdorf, A Arredouani, L C Davis, E Lloyd-Evans, H Koegel, T M Funnell, A J Morgan, J A Ward, K Watanabe, X Cheng, G C Churchill, M X Zhu, F M Platt, G M Wessel, J Parrington, and A Galione. **Purified TPC Isoforms Form NAADP Receptors with Distinct Roles for Ca^{2+} Signaling and Endolysosomal Trafficking**. *Curr Biol*, **20**(8):703–709, Mar 2010. 42, 43, 127, 133, 232, 263, 290, 293, 304

[376] S L Rybak, F Lanni, and R F Murphy. **Theoretical considerations on the role of membrane potential in the regulation of endosomal pH**. *Biophys J*, **73**(2):674–687, Aug 1997. 219

[377] L Sadowski, I Pilecka, and M Miaczynska. **Signaling from endosomes: location makes a difference**. *Exp Cell Res*, **315**(9):1601–1609, May 2009. 305

[378] M Saito, P I Hanson, and P Schlesinger. **Luminal chloride-dependent activation of endosome calcium channels: patch clamp study of enlarged endosomes**. *J Biol Chem*, **282**(37):27327–27333, Sep 2007. 31, 217

[379] F. Sanger and A.R. Coulson. **A rapid method for determining sequences in DNA by primed synthesis with DNA polymerase 1**. *Journal of Molecular Biology*, **94**(3):441–446, 1975. 80

[380] H Sano, S C Liu, W S Lane, J E Piletz, and G E Lienhard. **Insulin receptor substrate 4 associates with the protein IRAS**. *J Biol Chem*, **277**(22):19439–19447, May 2002. 243

[381] M Schaefer. **Homo- and heteromeric assembly of TRP channel subunits**. *Pflügers Arch*, **451**(1):35–42, Oct 2005. 285, 287, 289, 293

[382] G Schäfer and M Meyering-Vos. **F-type or V-type? The chimeric nature of the archaebacterial ATP synthase**. *Biochim Biophys Acta*, **1101**(2):232–235, Jul 1992. 243

[383] J B Schenkman and D L Cinti. **Preparation of microsomes with calcium**. *Methods Enzymol*, **52**:83–89, 1978. 64, 158

[384] D Scherman, J Nordmann, and J P Henry. **Existence of an adenosine 5'-triphosphate dependent proton translocase in bovine neurosecretory granule membrane**. *Biochemistry*, **21**(4):687–694, Feb 1982. 220

[385] M V Schiaffino. **Signaling pathways in melanosome biogenesis and pathology**. *Int J Biochem Cell Biol*, **42**(7):1094–1104, Jul 2010. 306

[386] M Schieder, K Rötzer, A Brüggemann, M Biel, and C Wahl-Schott. **Planar patch clamp approach to characterize ionic currents from intact lysosomes**. *Sci Signal*, **3**(151), 2010. 158, 199, 202, 212, 216, 218, 219, 221

[387] M Schieder, K Rötzer, A Brüggemann, M Biel, and C A Wahl-Schott. **Characterization of two-pore channel 2 (TPCN2)-mediated Ca^{2+} currents in isolated lysosomes**. *J Biol Chem*, **285**(28):21219–21222, Jul 2010. 36, 64, 70, 90, 136, 139, 140, 146, 150, 151, 152, 158, 199, 202, 216, 219, 221, 223, 227, 228, 300

[388] W P Schilling and M Goel. **Mammalian TRPC channel subunit assembly**. *Novartis Found Symp*, **258**:18–30, 2004. 287

[389] S Schreyer, D Ledwig, I Rakatzi, I Klöting, and J Eckel. **Insulin receptor substrate-4 is expressed in muscle tissue without acting as a substrate for the insulin receptor**. *Endocrinology*, **144**(4):1211–1218, Apr 2003. 243

[390] B A Schröder, C Wrocklage, A Hasilik, and P Saftig. **The proteome of lysosomes**. *Proteomics*, **10**(22):4053–4076, Nov 2010. 243

[391] G M Shaik, L Dráberová, P Heneberg, and P Dráber. **Vacuolin-1-modulated exocytosis and cell resealing in mast cells**. *Cell Signal*, **21**(8):1337–1345, Aug 2009. 217

[392] M S Shapiro and W N Zagotta. **Stoichiometry and arrangement of heteromeric olfactory cyclic nucleotide-gated ion channels**. *Proc Natl Acad Sci U S A*, **95**(24):14546–14551, Nov 1998. 286

[393] D Shental-Bechor and Y Levy. **Folding of glycoproteins: toward understanding the biophysics of the glycosylation code**. *Curr Opin Struct Biol*, **19**(5):524–533, Oct 2009. 94

[394] M W Sherwood, I A Prior, S G Voronina, S L Barrow, J D Woodsmith, O V Gerasimenko, O H Petersen, and A V Tepikin. **Activation of trypsinogen in large endocytic vacuoles of pancreatic acinar cells**. *Proc Natl Acad Sci U S A*, **104**(13):5674–5679, Mar 2007. 222

[395] J W Shuai and P Jung. **Optimal intracellular calcium signaling**. *Phys Rev Lett*, **88**(6):068102–068102, Feb 2002. 141

[396] R Sitsapesan, R A Montgomery, K T MacLeod, and A J Williams. **Sheep cardiac sarcoplasmic reticulum calcium-release channels: modification of conductance and gating by temperature**. *J Physiol*, **434**:469–488, Mar 1991. 60, 61

[397] R Sitsapesan and A J Williams. **Gating of the native and purified cardiac SR Ca^{2+}-release channel with monovalent cations as permeant species**. *Biophys J*, **67**(4):1484–1494, Oct 1994. 115, 122, 124

[398] R Sitsapesan and A J Williams. **Cyclic ADP-ribose and related compounds activate sheep skeletal sarcoplasmic reticulum Ca^{2+} release channel**. *Am J Physiol*, **268**(5 Pt 1):1235–1240, May 1995. 12

[399] G D Smith and T J Peters. **Analytical subcellular fractionation of rat liver with special reference to the localisation of putative plasma membrane marker enzymes**. *Eur J Biochem*, **104**(1):305–311, Feb 1980. 160

[400] J S Smith, T Imagawa, J Ma, M Fill, K P Campbell, and R Coronado. **Purified ryanodine receptor from rabbit skeletal muscle is the calcium-release channel of sarcoplasmic reticulum**. *J Gen Physiol*, **92**(1):1–26, Jul 1988. 12, 13, 114, 132, 134, 135

[401] J S Smith, E Rousseau, and G Meissner. **Calmodulin modulation of single sarcoplasmic reticulum Ca^{2+}-release channels from cardiac and skeletal muscle**. *Circ Res*, **64**(2):352–359, Feb 1989. 233

[402] S Soares, M Thompson, T White, A Isbell, M Yamasaki, Y Prakash, F E Lund, A Galione, and E N Chini. **NAADP as a second messenger: neither CD38 nor base-exchange reaction are necessary for in vivo generation of NAADP in myometrial cells**. *Am J Physiol Cell Physiol*, **292**(1):227–239, Jan 2007. 14, 17

[403] N D Sonawane, J R Thiagarajah, and A S Verkman. **Chloride concentration in endosomes measured using a ratioable fluorescent Cl- indicator: evidence for chloride accumulation during acidification**. *J Biol Chem*, **277**(7):5506–5513, Feb 2002. 219, 222

[404] N D Sonawane and A S Verkman. **Determinants of [Cl^-] in recycling and late endosomes and Golgi complex measured using fluorescent ligands**. *J Cell Biol*, **160**(7):1129–1138, Mar 2003. 219, 220, 222

[405] V Sorrentino and P Volpe. **Ryanodine receptors: how many, where and why?** *Trends Pharmacol Sci*, **14**(3):98–103, Mar 1993. 6, 285

[406] A A Soyombo, S Tjon-Kon-Sang, Y Rbaibi, E Bashllari, J Bisceglia, S Muallem, and K Kiselyov. **TRP-ML1 regulates lysosomal pH and acidic lysosomal lipid hydrolytic activity**. *J Biol Chem*, **281**(11):7294–7301, Mar 2006. 30

[407] S P Srinivas, A Ong, L Goon, L Goon, and J A Bonanno. **Lysosomal Ca^{2+} stores in bovine corneal endothelium**. *Invest Ophthalmol Vis Sci*, **43**(7):2341–2350, Jul 2002. 4

[408] M Steen, T Kirchberger, and A H Guse. **NAADP mobilizes calcium from the endoplasmic reticular Ca^{2+} store in T-lymphocytes**. *J Biol Chem*, **282**(26):18864–18871, Jun 2007. 32, 140, 151

[409] B E Steinberg, K K Huynh, A Brodovitch, S Jabs, T Stauber, T J Jentsch, and S Grinstein. **A cation counterflux supports lysosomal acidification**. *J Cell Biol*, **189**(7):1171–1186, Jun 2010. 135, 222

[410] B E Steinberg, N Touret, M Vargas-Caballero, and S Grinstein. ***in situ* measurement of the electrical potential across the phagosomal membrane using FRET and its contribution to the proton-motive force**. *Proc Natl Acad Sci U S A*, **104**(22):9523–9528, May 2007. 202

[411] E E Strehler and D A Zacharias. **Role of alternative splicing in generating isoform diversity among plasma membrane calcium pumps**. *Physiol Rev*, **81**(1):21–50, Jan 2001. 2

[412] S L Sturley, M C Patterson, W Balch, and L Liscum. **The pathophysiology and mechanisms of NP-C disease**. *Biochim Biophys Acta*, **1685**(1-3):83–87, Oct 2004. 307

[413] P Sulem, D F Gudbjartsson, S N Stacey, A Helgason, T Rafnar, M Jakobsdottir, S Steinberg, S A Gudjonsson, A Palsson, G Thorleifsson, S Pálsson, B Sigurgeirsson, K Thorisdottir, R Ragnarsson, K R Benediktsdottir, K K Aben, S H Vermeulen, A M Goldstein, M A Tucker, L A Kiemeney, J H Olafsson, J Gulcher, A Kong, U Thorsteinsdottir, and K Stefansson. **Two newly identified genetic determinants of pigmentation in Europeans**. *Nat Genet*, **40**(7):835–837, Jul 2008. 43, 44, 306

[414] P Sulem, D F Gudbjartsson, S N Stacey, A Helgason, T Rafnar, K P Magnusson, A Manolescu, A Karason, A Palsson, G Thorleifsson, M Jakobsdottir, S Steinberg, S Pálsson, F Jonasson, B Sigurgeirsson, K Thorisdottir, R Ragnarsson, K R Benediktsdottir, K K Aben, L A Kiemeney, J H Olafsson, J Gulcher, A Kong, U Thorsteinsdottir, and K Stefansson. **Genetic determinants of hair, eye and skin pigmentation in Europeans**. *Nat Genet*, **39**(12):1443–1452, Dec 2007. 44, 306

[415] G H Sun-Wada and Y Wada. **Vacuolar-type proton pump ATPases: roles of subunit isoforms in physiology and pathology**. *Histol Histopathol*, **25**(12):1611–1620, Dec 2010. 240

[416] S Supattapone, P F Worley, J M Baraban, and S H Snyder. **Solubilization, purification, and characterization of an inositol trisphosphate receptor**. *J Biol Chem*, **263**(3):1530–1534, Jan 1988. 89, 97, 99, 107, 133

[417] P Szepetowski, V Ollendorff, J Grosgeorge, A Courseaux, D Birnbaum, C Theillet, and P Gaudray. **DNA amplification at 11q13.5-q14 in human breast cancer**. *Oncogene*, **7**(12):2513–2517, Dec 1992. 43

[418] W X Tang, Y F Chen, A P Zou, W B Campbell, and P L Li. **Role of FKBP12.6 in cADPR-induced activation of reconstituted ryanodine receptors from arterial smooth muscle**. *Am J Physiol Heart Circ Physiol*, **282**(4):1304–1310, Apr 2002. 110

[419] C W Taylor. **Store-operated Ca^{2+} entry: A STIMulating stOrai**. *Trends Biochem Sci*, **31**(11):597–601, Nov 2006. 6

[420] C W Taylor, A A Genazzani, and S A Morris. **Expression of inositol trisphosphate receptors**. *Cell Calcium*, **26**(6):237–251, Dec 1999. 11

[421] U Terpitz, D Raimunda, M Westhoff, V L Sukhorukov, L Beaugé, E Bamberg, and D Zimmermann. **Electrofused giant protoplasts of Saccharomyces cerevisiae as a novel system for electrophysiological studies on membrane proteins**. *Biochim Biophys Acta*, **1778**(6):1493–1500, Jun 2008. 214

[422] J D Thompson, D G Higgins, and T J Gibson. **CLUSTAL W: improving the sensitivity of progressive multiple sequence alignment through sequence weighting, position-specific gap penalties and weight matrix choice**. *Nucleic Acids Res*, **22**(22):4673–4680, Nov 1994. 49

[423] E C Thrower, C U Choe, S H So, S H Jeon, B E Ehrlich, and S H Yoo. **A functional interaction between chromogranin B and the inositol 1,4,5-trisphosphate receptor/Ca^{2+} channel**. *J Biol Chem*, **278**(50):49699–49706, Dec 2003. 233

[424] A P Timerman, H Onoue, H B Xin, S Barg, J Copello, G Wiederrecht, and S Fleischer. **Selective binding of FKBP12.6 by the cardiac ryanodine receptor**. *J Biol Chem*, **271**(34):20385–20391, Aug 1996. 12

[425] A Tinker and A J Williams. **Divalent cation conduction in the ryanodine receptor channel of sheep cardiac muscle sarcoplasmic reticulum**. *J Gen Physiol*, **100**(3):479–493, Sep 1992. 118

[426] B Tomlins, A J Williams, and R A Montgomery. **The characterization of a monovalent cation-selective channel of mammalian cardiac muscle sarcoplasmic reticulum**. *J Membr Biol*, **80**(2):191–199, 1984. 61

[427] N Touret, P Paroutis, M Terebiznik, R E Harrison, S Trombetta, M Pypaert, A Chow, A Jiang, J Shaw, C Yip, H P Moore, N van der Wel, D Houben, P J Peters, C de Chastellier, I Mellman, and S Grinstein. **Quantitative and dynamic assessment of the contribution of the ER to phagosome formation**. *Cell*, **123**(1):157–170, Oct 2005. 262

[428] C Toyoshima and G Inesi. **Structural basis of ion pumping by Ca^{2+}-ATPase of the sarcoplasmic reticulum**. *Annu Rev Biochem*, **73**:269–292, 2004. 3

[429] L M Traub, S I Bannykh, J E Rodel, M Aridor, W E Balch, and S Kornfeld. **AP-2-containing clathrin coats assemble on mature lysosomes**. *J Cell Biol*, **135**(6 Pt 2):1801–1814, Dec 1996. 218

[430] R Y Tsien. **The green fluorescent protein**. *Annu Rev Biochem*, **67**:509–544, 1998. 268

[431] N Tugba Durlu-Kandilci, M Ruas, K T Chuang, A Brading, J Parrington, and A Galione. **TPC2 proteins mediate nicotinic acid adenine dinucleotide phosphate (NAADP)- and agonist-evoked contractions of smooth muscle**. *J Biol Chem*, **285**(32):24925–24932, Aug 2010. 23, 27, 295, 296

[432] D R Tulsiani, D J Opheim, and O Touster. **Purification and characterization of alpha-D-mannosidase from rat liver golgi membranes**. *J Biol Chem*, **252**(10):3227–3233, May 1977. 160

[433] G.E. Tusnady and I. Simon. **Principles governing amino acid composition of integral membrane proteins: application to topology prediction1**. *Journal of Molecular Biology*, **283**(2):489–506, 1998. 50

REFERENCES

[434] A Untergasser, H Nijveen, X Rao, T Bisseling, R Geurts, and J A Leunissen. **Primer3Plus, an enhanced web interface to Primer3**. *Nucleic Acids Res*, **35**(Web Server issue):71–74, Jul 2007. 86

[435] A van der Spoel, E Bonten, and A d'Azzo. **Processing of lysosomal beta-galactosidase. The C-terminal precursor fragment is an essential domain of the mature enzyme**. *J Biol Chem*, **275**(14):10035–10040, Apr 2000. 152

[436] R W Van Dyke and J D Belcher. **Acidification of three types of liver endocytic vesicles: similarities and differences**. *Am J Physiol*, **266**(1 Pt 1):81–94, Jan 1994. 202, 219, 222

[437] S van Weely, M van den Berg, J A Barranger, M C Sa Miranda, J M Tager, and J M Aerts. **Role of pH in determining the cell-type-specific residual activity of glucocerebrosidase in type 1 Gaucher disease**. *J Clin Invest*, **91**(3):1167–1175, Mar 1993. 303

[438] P Várnai, L Hunyady, and T Balla. **STIM and Orai: the long-awaited constituents of store-operated calcium entry**. *Trends Pharmacol Sci*, **30**(3):118–128, Mar 2009. 289

[439] M D Varnum and W N Zagotta. **Interdomain interactions underlying activation of cyclic nucleotide-gated channels**. *Science*, **278**(5335):110–113, Oct 1997. 288

[440] K Venkatachalam, T Hofmann, and C Montell. **Lysosomal localization of TRPML3 depends on TRPML2 and the mucolipidosis-associated protein TRPML1**. *J Biol Chem*, **281**(25):17517–17527, Jun 2006. 286

[441] R Vennekens, G Owsianik, and B Nilius. **Vanilloid transient receptor potential cation channels: an overview**. *Curr Pharm Des*, **14**(1):18–31, 2008. 31

[442] M von Zastrow and A Sorkin. **Signaling on the endocytic pathway**. *Curr Opin Cell Biol*, **19**(4):436–445, Aug 2007. 305

[443] S G Voronina, M W Sherwood, O V Gerasimenko, O H Petersen, and A V Tepikin. **Visualizing formation and dynamics of vacuoles in living cells using contrasting dextran-bound indicator: endocytic and nonendocytic vacuoles**. *Am J Physiol Gastrointest Liver Physiol*, **293**(6):1333–1338, Dec 2007. 168

[444] T F Walseth, R Aarhus, J A Kerr, and H C Lee. **Identification of cyclic ADP-ribose-binding proteins by photoaffinity labeling**. *J Biol Chem*, **268**(35):26686–26691, Dec 1993. 12

[445] M.C. Wang, R.F. Collins, R.C. Ford, N.S. Berrow, A.C. Dolphin, and A. Kitmitto. **The three-dimensional structure of the cardiac L-type voltage-gated calcium channel**. *Journal of Biological Chemistry*, **279**(8):7159, 2004. 224, 322

[446] S Wang, A Lukinius, Y Zhou, P Stålberg, A Gobl, K Oberg, and B Skogseid. **Subcellular distribution of phospholipase C isoforms in rodent pancreas and gastric mucosa**. *Endocrinology*, **141**(7):2589–2593, Jul 2000. 10

[447] J M Ward and J I Schroeder. **Calcium-Activated K^+ Channels and Calcium-Induced Calcium Release by Slow Vacuolar Ion Channels in Guard Cell Vacuoles Implicated in the Control of Stomatal Closure**. *Plant Cell*, **6**(5):669–683, May 1994. 136, 137

[448] J.R. Whitaker and P.E. Granum. **An absolute method for protein determination based on difference in absorbance at 235 and 280 nm**. *Analytical Biochemistry*, **109**(1):156–159, 1980. 53

[449] A J Williams, D J West, and R Sitsapesan. **Light at the end of the Ca^{2+}-release channel tunnel: structures and mechanisms involved in ion translocation in ryanodine receptor channels**. *Q Rev Biophys*, **34**(1):61–104, Feb 2001. 110

[450] B Xiao, H Masumiya, D Jiang, R Wang, Y Sei, L Zhang, T Murayama, Y Ogawa, F A Lai, T Wagenknecht, and S R Chen. **Isoform-dependent formation of heteromeric Ca^{2+} release channels (ryanodine receptors)**. *J Biol Chem*, **277**(44):41778–41785, Nov 2002. 285

[451] L Xu, Y Wang, N Yamaguchi, D A Pasek, and G Meissner. **Single channel properties of heterotetrameric mutant RyR1 ion channels linked to core myopathies**. *J Biol Chem*, **283**(10):6321–6329, Mar 2008. 287

[452] X Z Xu, H S Li, W B Guggino, and C Montell. **Coassembly of TRP and TRPL produces a distinct store-operated conductance**. *Cell*, **89**(7):1155–1164, Jun 1997. 288

[453] I Yabe, K Horiuchi, K Nakahara, T Hiyama, T Yamanaka, P C Wang, K Toda, A Hirata, Y Ohsumi, R Hirata, Y Anraku, and I Kusaka. **Patch clamp studies on V-type ATPase of vacuolar membrane of haploid Saccharomyces cerevisiae. Preparation and utilization of a giant cell containing a giant vacuole**. *J Biol Chem*, **274**(49):34903–34910, Dec 1999. 214

[454] S Yagodin, N B Pivovarova, S B Andrews, and D B Sattelle. **Functional characterization of thapsigargin and agonist-insensitive acidic Ca^{2+} stores in *Drosophila melanogaster* S2 cell lines**. *Cell Calcium*, **25**(6):429–438, Jun 1999. 19

[455] H Yamada, H Hayashi, and Y Natori. **A simple procedure for the isolation of highly purified lysosomes from normal rat liver**. *J Biochem*, **95**(4):1155–1160, Apr 1984. 151

[456] H Yamaguchi, M Matsushita, A C Nairn, and J Kuriyan. **Crystal structure of the atypical protein kinase domain of a TRP channel with phosphotransferase activity**. *Mol Cell*, **7**(5):1047–1057, May 2001. 287

[457] S Yamaguchi, A Jha, Q Li, A A Soyombo, G D Dickinson, D Churamani, E Brailoiu, S Patel, and S Muallem. **TRPML1 and two-pore channels are functionally independent organellar ion channels**. *J Biol Chem*, May 2011. 31, 234, 291

[458] M Yamasaki, R Masgrau, A J Morgan, G C Churchill, S Patel, S J Ashcroft, and A Galione. **Organelle selection determines agonist-specific Ca^{2+} signals in pancreatic acinar and beta cells**. *J Biol Chem*, **279**(8):7234–7240, Feb 2004. 19, 27

[459] M Yamasaki, J M Thomas, G C Churchill, C Garnham, A M Lewis, J M Cancela, S Patel, and A Galione. **Role of NAADP and cADPR in the induction and maintenance of agonist-evoked Ca^{2+} spiking in mouse pancreatic acinar cells**. *Curr Biol*, **15**(9):874–878, May 2005. 17

[460] J Yang, S McBride, D O Mak, N Vardi, K Palczewski, F Haeseleer, and J K Foskett. **Identification of a family of calcium sensors as protein ligands of inositol trisphosphate receptor Ca^{2+} release channels**. *Proc Natl Acad Sci U S A*, **99**(11):7711–7716, May 2002. 216

[461] M Yazawa, T Vorherr, P James, E Carafoli, and K Yagi. **Binding of calcium by calmodulin: influence of the calmodulin binding domain of the plasma membrane calcium pump**. *Biochemistry*, **31**(12):3171–3176, Mar 1992. 2

[462] C C Yin, L G D'Cruz, and F A Lai. **Ryanodine receptor arrays: not just a pretty pattern?** *Trends Cell Biol*, **18**(4):149–156, Apr 2008. 291

[463] S P Yu and D W Choi. **Na^{+}-Ca^{2+} exchange currents in cortical neurons: concomitant forward and reverse operation and effect of glutamate**. *Eur J Neurosci*, **9**(6):1273–1281, Jun 1997. 2

[464] H. Zbidi, I. Jardin, G.E. Woodard, J.J. Lopez, A. Berna-Erro, G.M. Salido, and J.A. Rosado. **STIM1 and STIM2 are located in the acidic Ca^{2+} stores and associates with Orai1 upon depletion of the acidic stores in human platelets**. *Journal of Biological Chemistry*, **286**(14):12257, 2011. 303

[465] F Zhang, S Jin, F Yi, and P L Li. **TRP-ML1 functions as a lysosomal NAADP-sensitive Ca^{2+} release channel in coronary arterial myocytes**. *J Cell Mol Med*, **13**(9B):3174–3185, Sep 2009. 30, 134, 137, 139

[466] F Zhang and P L Li. **Reconstitution and characterization of a nicotinic acid adenine dinucleotide phosphate (NAADP)-sensitive Ca^{2+} release channel from liver lysosomes of rats**. *J Biol Chem*, **282**(35):25259–25269, Aug 2007. 30

[467] F Zhang, M Xu, W Q Han, and P L Li. **Reconstitution of lysosomal NAADP-TRP-ML1 signalling pathway and its function in TRP-ML1$^{-/-}$ cells**. *Am J Physiol Cell Physiol*, May 2011. 30, 139

[468] F Zhang, G Zhang, A Y Zhang, M J Koeberl, E Wallander, and P L Li. **Production of NAADP and its role in Ca^{2+} mobilization associated with lysosomes in coronary arterial myocytes**. *Am J Physiol Heart Circ Physiol*, **291**(1):274–282, Jul 2006. 32

[469] J.J. Zhang, A.J. Williams, and R. Sitsapesan. **Evidence for novel caffeine and Ca^{2+} binding sites on the lobster skeletal ryanodine receptor**. *British journal of pharmacology*, **126**(4):1066–1074, 1999. 115

[470] L Zhang, J Kelley, G Schmeisser, Y M Kobayashi, and L R Jones. **Complex formation between junctin, triadin, calsequestrin, and the ryanodine receptor. Proteins of the cardiac junctional sarcoplasmic reticulum membrane**. *J Biol Chem*, **272**(37):23389–23397, Sep 1997. 97

[471] S Zhang, S Malmersjö, J Li, H Ando, O Aizman, P Uhlén, K Mikoshiba, and A Aperia. **Distinct role of the N-terminal tail of the Na^{+},K^{+}-ATPase catalytic subunit as a signal transducer**. *J Biol Chem*, **281**(31):21954–21962, Aug 2006. 290

[472] H Zhao and G A Grabowski. **Gaucher disease: Perspectives on a prototype lysosomal disease**. *Cell Mol Life Sci*, **59**(4):694–707, Apr 2002. 306

[473] L Zhen, M E Rusiniak, and R T Swank. **The beta-glucuronidase propeptide contains a serpin-related octamer necessary for complex formation with egasyn esterase and for retention within the endoplasmic reticulum**. *J Biol Chem*, **270**(20):11912–11920, May 1995. 157

[474] J. Zheng and W.N. Zagotta. **Stoichiometry and assembly of olfactory cyclic nucleotide-gated channels**. *Neuron*, **42**(3):411–421, 2004. 287

[475] M X Zhu, J Ma, J Parrington, P J Calcraft, A Galione, and A M Evans. **Calcium signaling via two-pore channels: local or global, that is the question**. *Am J Physiol Cell Physiol*, **298**(3):430–441, Mar 2010. 300, 307

[476] A V Zima, D J Bare, G A Mignery, and L A Blatter. **IP_3-dependent nuclear Ca^{2+} signalling in the mammalian heart**. *J Physiol*, **584**(Pt 2):601–611, Oct 2007. 6, 10

[477] B Zimmermann and B Walz. **The mechanism mediating regenerative intercellular Ca^{2+} waves in the blowfly salivary gland**. *EMBO J*, **18**(12):3222–3231, Jun 1999. 8

[478] X Zong, M Schieder, H Cuny, S Fenske, C Gruner, K Rötzer, O Griesbeck, H Harz, M Biel, and C Wahl-Schott. **The two-pore channel TPCN2 mediates NAADP-dependent Ca^{2+}-release from lysosomal stores**. *Pflügers Arch*, **458**(5):891–899, Sep 2009. 34, 36, 240, 257, 263, 285, 286, 300

The page numbers upon which the reference appears are included after the reference entry.

These are hyperlinked on the digital copy.

Statement of Authorship

This thesis is approximately 48,000 words long; exclusive of bibliography, appendices, diagrams and tables.

All raw data recorded from the artificial bilayer were collected by Dr Samantha Pitt at the University of Bristol, using HsTPC2 protein that I purified in Oxford.

This data can be seen in chapter 3, section 3.7.



Tim Funnell
June 2011